frontiers | Research Topics

Novel mechanisms involved in urinary bladder control: Advances in neural, humoral and local factors underlying function and disease, volume II

Edited by
Monica Akemi Sato, Laurival Antonio De Luca, Patrik Aronsson and Russ Chess-Williams

Published in
Frontiers in Physiology

ISSN 1664-8714
ISBN 978-2-83251-474-0
DOI 10.3389/978-2-83251-474-0

About Frontiers

Frontiers is more than just an open access publisher of scholarly articles: it is a pioneering approach to the world of academia, radically improving the way scholarly research is managed. The grand vision of Frontiers is a world where all people have an equal opportunity to seek, share and generate knowledge. Frontiers provides immediate and permanent online open access to all its publications, but this alone is not enough to realize our grand goals.

Frontiers journal series

The Frontiers journal series is a multi-tier and interdisciplinary set of open-access, online journals, promising a paradigm shift from the current review, selection and dissemination processes in academic publishing. All Frontiers journals are driven by researchers for researchers; therefore, they constitute a service to the scholarly community. At the same time, the *Frontiers journal series* operates on a revolutionary invention, the tiered publishing system, initially addressing specific communities of scholars, and gradually climbing up to broader public understanding, thus serving the interests of the lay society, too.

Dedication to quality

Each Frontiers article is a landmark of the highest quality, thanks to genuinely collaborative interactions between authors and review editors, who include some of the world's best academicians. Research must be certified by peers before entering a stream of knowledge that may eventually reach the public - and shape society; therefore, Frontiers only applies the most rigorous and unbiased reviews. Frontiers revolutionizes research publishing by freely delivering the most outstanding research, evaluated with no bias from both the academic and social point of view. By applying the most advanced information technologies, Frontiers is catapulting scholarly publishing into a new generation.

What are Frontiers Research Topics?

Frontiers Research Topics are very popular trademarks of the *Frontiers journals series*: they are collections of at least ten articles, all centered on a particular subject. With their unique mix of varied contributions from Original Research to Review Articles, Frontiers Research Topics unify the most influential researchers, the latest key findings and historical advances in a hot research area.

Find out more on how to host your own Frontiers Research Topic or contribute to one as an author by contacting the Frontiers editorial office: frontiersin.org/about/contact

Novel mechanisms involved in urinary bladder control: Advances in neural, humoral and local factors underlying function and disease, volume II

Topic editors

Monica Akemi Sato — Faculdade de Medicina do ABC, Brazil
Laurival Antonio De Luca — Departamento de Fisiologia e Patologia da Faculdade de Odontologia da Universidade Estadual Paulista, Brazil
Patrik Aronsson — University of Gothenburg, Sweden
Russ Chess-Williams — Bond University, Australia

Citation

Sato, M. A., De Luca, L. A., Aronsson, P., Chess-Williams, R., eds. (2023). *Novel mechanisms involved in urinary bladder control: Advances in neural, humoral and local factors underlying function and disease, volume II*. Lausanne: Frontiers Media SA. doi: 10.3389/978-2-83251-474-0

Table of contents

frontiers | Frontiers in Physiology

TYPE Editorial
PUBLISHED 17 October 2022
DOI 10.3389/fphys.2022.1056316

OPEN ACCESS

EDITED AND REVIEWED BY
Geoffrey A. Head,
Baker Heart and Diabetes Institute, Australia

*CORRESPONDENCE
Monica A. Sato,
monica.akemi.sato@gmail.com

SPECIALTY SECTION
This article was submitted to Exercise Physiology, a section of the journal Frontiers in Physiology

RECEIVED 28 September 2022
ACCEPTED 03 October 2022
PUBLISHED 17 October 2022

CITATION
Sato MA, De Luca LA Jr, Chess-Williams R and Aronsson P (2022), Editorial: Novel mechanisms involved in urinary bladder control: Advances in neural, humoral and local factors underlying function and disease, volume II. *Front. Physiol.* 13:1056316. doi: 10.3389/fphys.2022.1056316

Editorial: Novel mechanisms involved in urinary bladder control: Advances in neural, humoral and local factors underlying function and disease, volume II

Monica A. Sato[1]*, Laurival A. De Luca Jr[2], Russ Chess-Williams[3] and Patrik Aronsson[4]

[1]Department of Morphology and Physiology, Faculdade de Medicina do ABC, Centro Universitario FMABC, Santo Andre, Brazil, [2]Department of Physiology and Pathology, Faculty of Dentistry, São Paulo State University, Araraquara, Brazil, [3]Faculty of Health Sciences & Medicine, Bond University, Gold Coast, QLD, Australia, [4]Department of Pharmacology, Institute of Neuroscience and Physiology, University of Gothenburg, Sahlgrenska Academy, Gothenburg, Sweden

KEYWORDS

urinary bladder, overactive bladder, diabetes mellitus, purinergic, angiotensin-(1-7) [Ang-(1-7)], urofacial syndrome, HPSE2, brain network

Editorial on the Research Topic
Novel mechanisms involved in urinary bladder control: Advances in neural, humoral and local factors underlying function and disease, volume II

This second volume of a Research Topic devoted to the investigation of the control of urinary bladder in physiological and pathological conditions reiterates its relevance. As a subject with several "facets" (Sato et al., 2020), not surprisingly, it brings new contributions of several researchers, thereby advancing further our knowledge about such control. The attentive reader will also see that the many facets continue to embrace a complete range of questions ranging from local organ mechanisms to those dependent on high brain functions. We are glad that both volumes, in addition to complete each other, also match in this respect.

The urine storage and voiding from the bladder are mediated by both central and peripheral mechanisms, nevertheless they still remain to be fully elucidated. Interestingly, Lamy et al. have shown that Angiotensin-(1–7) administrated intravenously or topically (*in situ*) onto the urinary bladder (UB) elicits an increase in the intravesical pressure. The authors also demonstrated that Mas receptors for Angiotensin-(1–7) and ACE-2, an enzyme required for Angiotensin-(1–7) synthesis, are expressed in the bladder. Therefore,

they suggested that this peptide acts in the UB to increase the IP and can be also locally synthesized in the UB.

The review of Pang et al. presented in this topic shows previous functional imaging studies and combines them with brain regions involved in bladder control, demonstrating interactions between these regions, and brain networks, as well as changes in brain function in diseases affecting the urinary bladder. Pang et al. extend the working model proposed by Griffiths et al. (2015) about the brain network, and provide insights for current and future bladder-control research.

Several bladder diseases arise due to abnormal contractions (Chapple et al., 2018), and Phelps et al. aimed to identify the possible similarities in extracellular Ca2+ requirements between muscarinic, histamine, 5-hydroxytryptamine (5-HT), neurokinin-A (NKA), prostaglandin E2 (PGE2), and angiotensin II (ATII) receptors for mediating contractile activity of the urinary bladder (urothelium and lamina propria). Despite the finding that the specific requirement of Ca2+ on contractile responses varies depending on the receptor, Phelps et al. suggested that extracellular Ca2+ has a key role in mediating G protein-coupled receptor contractions of the urothelium and lamina propria.

Two of the studies examined purinergic mechanisms that operate within the bladder. The first investigated the role of purine metabolism in purinergic mechanisms. Earlier studies have shown that adenosine 5′-triphosphate (ATP) released from the urothelium has a prominent role in bladder mechanotransduction (Birder and Andersson, 2013; Takezawa et al., 2016). Urothelial ATP regulates the micturition cycle by activation of purinergic receptors, which are expressed in many cell types in the lamina propria (LP), including afferent neurons, and have been implicated in the direct mechanosensitive signaling between urothelium and detrusor (Cockayne et al., 2000; Vlaskovska et al., 2001; Burnstock, 2014). Aresta Branco et al. investigated possible mechanosensitive mechanisms of ATP hydrolysis in the LP at the anti-luminal side of nondistended (empty) or distended (full) murine (C57BL/6J) detrusor-free bladder model. The authors demonstrated that mechanosensitive degradation of ATP and ADP by membrane-bound and soluble nucleotidases in the LP reduces the availability of excitatory purines in the LP at the end of bladder filling. Hence, they suggested a possible safeguard mechanism to prevent overexcitability of the bladder, in which adequate proportions of excitatory and inhibitory purines in the bladder wall are determined by distention-associated purine release and purine metabolism.

The second purinergic study examined the role of P2X7 receptors in the bladder. The purinergic P2X7 receptor (P2X7R) is expressed abundantly on the bladder urothelium and its role in inflammation and cell death has been increasingly recognized (Vial and Evans, 2000; Menzies et al., 2003; Svennersten et al., 2015). It is well known that chemotherapy with cyclophosphamide can induce cystitis in the patients due to excretion of a toxic metabolite called acrolein. Cystitis is an inflammation of the bladder that is associated with damage to the integrity of the urothelial barrier. Taidi et al. investigated the role of P2X7R in acrolein-induced inflammatory damage in primary cultured porcine bladder urothelial cells. The authors demonstrated that acrolein induced a significant reduction in urothelial cell viability and barrier function, which was protected by the presence of P2X7R antagonist. Thereby, Taidi et al. suggested that P2X7R blockade may be a possible therapy in patients with bladder cystitis evoked by cyclophosphamide treatment.

The dysregulation in neurotransmission has been implicated in several lower urinary bladder conditions, however the mechanisms underlying the neurotransmitter release in the bladder still require elucidation. Carew et al. investigated the expression of myosin 5a (Myo5a), which is a motor protein that facilitates the directed motion of synaptic vesicles along actin fibers, in the regulation of excitatory neurotransmission in the bladder. The authors demonstrated that Myo5a is localized in cholinergic nerve fibers in the bladder and identified several Myo5a splice variants in the detrusor and suggested that the abundance of each is likely critical for efficient synaptic vesicle transport and neurotransmission in the bladder.

High glucose levels can induce changes in the urinary bladder. Oliveira et al. has shown that the treatment of mice with methylglyoxal (MGO), which is a compound generated during glycolysis and present in high levels in the plasma of patients with diabetes mellitus (Kilhovd et al., 2003; Han et al., 2009), induces detrusor overactivity through the formation of advanced glycation end products (AGE) that bind to RAGE receptors. These receptors are members of the immunoglobulin superfamily of cell surface receptors, responsible for recognizing endogenous ligands (Kim et al., 2021). Oliveira et al. also demonstrated that MGO treatment increased reactive oxygen species (ROS) production, which was markedly higher in the detrusor muscle than in the urothelium. They suggested that MGO accumulation increases AGE formation, which activates the RAGE-ROS signaling and consequent Rho kinase-induced muscle sensitization, which leads to detrusor overactivity.

Despite the urinary bladder is markedly enlarged in the streptozotocin-induced type 1 diabetes mellitus in rats, which may contribute to the frequent diabetic uropathy, very little is known about the bladder changes in type 2 diabetes models. Diabetic polyuria has been proposed as the pathophysiological mechanism behind bladder enlargement. In the review of Yesilyurt et al., bladder weight and blood glucose from 16 studies were evaluated and concluded that the presence and extent of bladder enlargement varied markedly depending on the diabetes models. The authors also suggest that particularly in type 2 diabetes models, the bladder enlargement is primarily driven by glucose levels/glucosuria.

Overactive bladder (OAB) has been accepted as an idiopathic disorder defined by urinary urgency, increased daytime urinary frequency and/or nocturia, with or without urinary incontinence. This clinical syndrome is characterized clinically by an absence of other organic diseases, including urinary tract infection. However, a growing body of evidence has shown that a significant proportion of OAB patients have active bladder infection. The review of Mansfield et al. discusses the findings of recent laboratory and clinical studies, providing the relationship between urinary tract infection, bladder inflammation, and the pathophysiology of OAB. The authors suggest that urinary tract infection may be an underappreciated contributor to the pathophysiology of some OAB patients who are resistant to standard treatments.

Urinary bladder function can also be affected by chronic psychological stress leading to an exacerbated lower urinary tract dysfunction as in OAB or interstitial cystitis-bladder pain syndrome (Macaulay et al., 1987; Lutgendorf et al., 2001; Rothrock et al., 2001; McVary et al., 2005; Fan et al., 2008; Zhang et al., 2013; Bradley et al., 2014; Lai et al., 2015a, 2015b). The review of Gao and Rodriguez highlights recent findings about stress-related animal models as water avoidance stress, social stress, early life stress, repeated variable stress, chronic variable stress, intermittent restraint stress and others, demonstrating that different types of chronic stress induce relatively distinguished changes at multiple levels of the micturition pathway.

This topic also brings a novelty showed by Beaman et al. about a rare disease called urofacial syndrome (UFS), which is an autosomal recessive congenital disorder of the urinary bladder characterized by voiding dysfunction and a grimace upon smiling (Elejalde, 1979; Ochoa 2004; Newman and Woolf, 2018; Osorio et al., 2021). Biallelic variants of the HPSE2 gene that encodes the secreted protein heparanase-2 have been described in about half of the families studied with UFS (McKenzie et al., 2000; Newman and Woolf, 2018; McKenzie 2020). Bladder autonomic neurons emerge from pelvic ganglia, in which resident neural cell bodies derive from migrating neural crest cells. Beaman et al. demonstrated in normal embryos that heparanase-2 and immunoglobulin like domains 2 (LRIG2) are expressed in neural like cells with a migratory phenotype, postulated to be pelvic ganglia precursors. Thereby, Beaman et al. suggested that biallelic variants of LRIG2 should be also implicated in the rare UFS.

In conclusion, this Research Topic encompasses a broad range of studies from basic science to clinical and certainly challenges researchers to further investigate unsolved questions. We trust that the valuable lessons learnt about the urinary bladder will be useful further for the development of novel therapeutic approaches upon the growing number of patients with bladder dysfunctions worldwide.

Author contributions

MS drafted the first manuscript and LD, RC-W and PA contributed equally to manuscript revision. All authors have read and approved the submitted version.

Acknowledgments

We would like to thank all contributing authors for their time and effort. We also thank the Frontiers in Physiology editorial team for all the support.

Conflict of interest

The authors declare that the research was conducted in the absence of any commercial or financial relationships that could be construed as a potential conflict of interest.

Publisher's note

References

Birder, L., and Andersson, K.-E. (2013). Urothelial signaling. *Physiol. Rev.* 93 (2), 653–680. doi:10.1152/physrev.00030.2012

Bradley, C. S., Nygaard, I. E., Torner, J. C., Hillis, S. L., Johnson, S., and Sadler, A. G. (2014). Overactive bladder and mental health symptoms in recently deployed female veterans. *J. Urol.* 191, 1327–1332. doi:10.1016/j.juro.2013.11.100

Burnstock, G. (2014). Purinergic signalling in the urinary tract in health and disease. *Purinergic Signal.* 10 (1), 103–155. doi:10.1007/s11302-013-9395-y

Chapple, C. R., Osman, N. I., Birder, L., Dmochowski, R., Drake, M. J., van Koeveringe, G., et al. (2018). Terminology report from the international continence society (ICS) working group on underactive bladder (UAB). *Neurourol. Urodyn.* 37 (8), 2928–2931. doi:10.1002/nau.23701

Cockayne, D. A., Hamilton, S. G., Zhu, Q.-M., Dunn, P. M., Zhong, Y., Novakovic, S., et al. (2000). Urinary bladder hyporeflexia and reduced pain-related behaviour in P2X3-deficient mice. *Nature* 407 (6807), 1011–1015. doi:10.1038/35039519

Elejalde, B. R., and Gorlin, R. J. (1979). Genetic and diagnostic considerations in three families with abnormalities of facial expression and congenital urinary obstruction: "The Ochoa syndrome. *Am. J. Med. Genet.* 3, 97–108. doi:10.1002/ajmg.1320030114

Fan, Y. H., Lin, A. T., Wu, H. M., Hong, C. J., and Chen, K. K. (2008). Psychological profile of Taiwanese interstitial cystitis patients. *Int. J. Urol.* 15, 416–418. doi:10.1111/j.1442-2042.2008.02020.x

Griffiths, D. (2015). Neural control of micturition in humans: A working model, *Nat. Rev. Urol.* 12, 695–705. doi:10.1038/nrurol.2015.266

Han, Y., Randell, E., Vasdev, S., Gill, V., Curran, M., Newhook, L. A., et al. (2009). Plasma advanced glycation endproduct, methylglyoxal-derived hydroimidazolone is elevated in young, complication-free patients with type 1 diabetes. *Clin. Biochem.* 42, 562–569. doi:10.1016/j.clinbiochem.2008.12.016

Kilhovd, B. K., Giardino, I., Torjesen, P. A., Birkeland, K. I., Berg, T. J., Thornalley, P. J., et al. (2003). Increased serum levels of the specific AGE-compound methylglyoxal-derived hydroimidazolone in patients with type 2 diabetes. *Metabolism.* 52, 163–167. doi:10.1053/meta.2003.50035

Kim, H. J., Jeong, M. S., and Jang, S. B. (2021). Molecular characteristics of RAGE and Advances in small-molecule inhibitors. *Int. J. Mol. Sci.* 22, 6904. doi:10.3390/ijms22136904

Lai, H., Gardner, V., Vetter, J., and Andriole, G. L. (2015a). Correlation between psychological stress levels and the severity of overactive bladder symptoms. *BMC Urol.* 15, 14. doi:10.1186/s12894-015-0009-6

Lai, H., Gereau, R. W. I. V., Luo, Y., O'Donnell, M., Rudick, C. N., Pontari, M., et al. (2015b). Animal models of urologic chronic pelvic pain syndromes: Findings from the multidisciplinary approach to the study of chronic pelvic pain research network. *Urology* 85, 1454–1465. doi:10.1016/j.urology.2015.03.007

Lutgendorf, S. K., Kreder, K. J., Rothrock, N. E., Ratliff, T. L., and Zimmerman, B. (2001). A laboratory stress model for examining stress and symptomatology in interstitial cystitis patients. *Urology* 57, 122. doi:10.1016/s0090-4295(01)01076-7

Macaulay, A. J., Stern, R. S., Holmes, D. M., and Stanton, S. L. (1987). Micturition and the mind: Psychological factors in the aetiology and treatment of urinary symptoms in women. *Br. Med. J. Clin. Res. Ed.* 294, 540–543. doi:10.1136/bmj.294.6571.540

McKenzie, E. (2020). Hpa2 gene cloning. *Adv. Exp. Med. Biol.* 1221, 787–805. doi:10.1007/978-3-030-34521-1_34

McKenzie, E., Tyson, K., Stamps, A., Smith, P., Turner, P., Barry, R., et al. (2000). Cloning and expression profiling of Hpa2, a novel mammalian heparanase family member. *Biochem. Biophys. Res. Commun.* 276, 1170–1177. doi:10.1006/bbrc.2000.3586

McVary, K. T., Rademaker, A., Lloyd, G. L., and Gann, P. (2005). Autonomic nervous system overactivity in men with lower urinary tract symptoms secondary to benign prostatic hyperplasia. *J. Urol.* 174 (4 Pt 1), 1327–1433. doi:10.1097/01.ju.0000173072.73702.64

Menzies, J., Paul, A., and Kennedy, C. (2003). P2X7 subunit-like immunoreactivity in the nucleus of visceral smooth muscle cells of the Guinea pig. *Auton. Neurosci.* 106, 103–109. doi:10.1016/s1566-0702(03)00078-x

Newman, W. G., and Woolf, A. S. (20131993–2022). "Urofacial syndrome," in *GeneReviews® [internet]*. M. P. Adam, H. H. Ardinger, R. A. Pagon, S. E. Wallace, L. J. H. Bean, and K. W. Gripp. Editors (Seattle (WA): University of Washington, Seattle

Ochoa, B. (2004). Can a congenital dysfunctional bladder Be diagnosed from a smile? The Ochoa syndrome updated. *Pediatr. Nephrol.* 19, 6–12. doi:10.1007/s00467-003-1291-1

Osorio, S., Rivillas, N. D., and Martinez, J. A. (2021). Urofacial (Ochoa) syndrome: A literature review. *J. Pediatr. Urol.* 17, 246–254. doi:10.1016/j.jpurol.2021.01.017

Rothrock, N. E., Lutgendorf, S. K., Kreder, K. J., Ratliff, T., and Zimmerman, B. (2001). Stress and symptoms in patients with interstitial cystitis: A life stress model. *Urology* 57, 422–427. doi:10.1016/s0090-4295(00)00988-2

Sato, M. A., De Luca, L. A., Jr, Aronsson, P., and Chess-Williams, R. (2020). Editorial: Novel mechanisms involved in urinary bladder control: Advances in neural, humoral and local factors underlying function and disease. *Front. Physiol.* 11, 606265. doi:10.3389/fphys.2020.606265

Svennersten, K., Hallén-Grufman, K., De Verdier, P. J., Wiklund, N. P., and Poljakovic, M. (2015). Localization of P2X receptor subtypes 2, 3 and 7 in human urinary bladder. *BMC Urol.* 15, 81. doi:10.1186/s12894-015-0075-9

Takezawa, K., Kondo, M., Nonomura, N., and Shimada, S. (2016). Urothelial ATP signaling: What is its role in bladder sensation? *Neurourol. Urodyn.* 36 (4), 966–972. doi:10.1002/nau.23099

Vial, C., and Evans, R. J. (2000). P2X receptor expression in mouse urinary bladder and the requirement of P2X1 receptors for functional P2X receptor responses in the mouse urinary bladder smooth muscle. *Br. J. Pharmacol.* 131, 1489–1495. doi:10.1038/sj.bjp.0703720

Vlaskovska, M., Kasakov, L., Rong, W., Bodin, P., Bardini, M., Cockayne, D. A., et al. (2001). P2X3Knock-Out mice reveal a major sensory role for urothelially released ATP. *J. Neurosci.* 21 (15), 5670–5677. doi:10.1523/jneurosci.21-15-05670.2001

Zhang, C., Hai, T., Yu, L., Liu, S., Li, Q., Zhang, X., et al. (2013). Association between occupational stress and risk of overactive bladder and other lower urinary tract symptoms: A cross-sectional study of female nurses in China. *Neurourol. Urodyn.* 32, 254–260. doi:10.1002/nau.22290

frontiers in Physiology

REVIEW
published: 21 March 2022
doi: 10.3389/fphys.2022.818993

The Effect of Chronic Psychological Stress on Lower Urinary Tract Function: An Animal Model Perspective

*Yunliang Gao[1] and Larissa V. Rodríguez[2]**

[1] Department of Urology, The Second Xiangya Hospital of Central South University, Changsha, China, [2] Department of Urology, Keck School of Medicine, University of Southern California, Los Angeles, CA, United States

Chronic psychological stress can affect urinary function and exacerbate lower urinary tract (LUT) dysfunction (LUTD), particularly in patients with overactive bladder (OAB) or interstitial cystitis–bladder pain syndrome (IC/BPS). An increasing amount of evidence has highlighted the close relationship between chronic stress and LUTD, while the exact mechanisms underlying it remain unknown. The application of stress-related animal models has provided powerful tools to explore the effect of chronic stress on LUT function. We systematically reviewed recent findings and identified stress-related animal models. Among them, the most widely used was water avoidance stress (WAS), followed by social stress, early life stress (ELS), repeated variable stress (RVS), chronic variable stress (CVS), intermittent restraint stress (IRS), and others. Different types of chronic stress condition the induction of relatively distinguished changes at multiple levels of the micturition pathway. The voiding phenotypes, underlying mechanisms, and possible treatments of stress-induced LUTD were discussed together. The advantages and disadvantages of each stress-related animal model were also summarized to determine the better choice. Through the present review, we hope to expand the current knowledge of the pathophysiological basis of stress-induced LUTD and inspire robust therapies with better outcomes.

Keywords: chronic psychological stress, lower urinary tract dysfunction, bladder, animal model, mechanism, treatment

OPEN ACCESS

Edited by:
Monica Akemi Sato, Faculdade de Medicina do ABC, Brazil

Reviewed by:
Dale E. Bjorling, University of Wisconsin-Madison, United States
Muriel Larauche, University of California, Los Angeles, United States

****Correspondence:***
Larissa V. Rodríguez
lrodriguez@med.usc.edu

Specialty section:
This article was submitted to Integrative Physiology, a section of the journal Frontiers in Physiology

Received: *20 November 2021*
Accepted: *18 February 2022*
Published: *21 March 2022*

Citation:
Gao Y and Rodríguez LV (2022) The Effect of Chronic Psychological Stress on Lower Urinary Tract Function: An Animal Model Perspective. Front. Physiol. 13:818993. doi: 10.3389/fphys.2022.818993

INTRODUCTION

Stress is an adaptive reaction of the organism in response to the effects of different external and internal adverse events (or stressors) (Chrousos, 2009). Psychological stress in humans can be regarded as a chain of events that disrupt homeostasis due to the direct effect of stress on the mind (Schneiderman et al., 2005). Short-term psychological stress can act as a strong motivator

Abbreviations: COX-2, cyclooxygenase-2; CRF, corticotropin-releasing factor; CVS, chronic variable stress; ELS, early life stress; FSS, foot shock stress; HPA, hypothalamic pituitary adrenocortical axis; NFAT, nuclear factor of activated T-cells; NGF, nerve growth factor; PACAP, pituitary adenylate cyclase-activating polypeptide; PMC, pontine micturition center; PVN, paraventricular nucleus; RVS, repeated variable stress; SAS, sympathetic-adrenal system; SS, social stress; TRPV1, transient receptor potential vanilloid type 1; TRPV4, transient receptor potential vanilloid type 4; WAS, water avoidance stress.

to perform better. However, chronic psychological stress may lead to maladaptive adjustments in homeostasis, which includes pathological effects on metabolism, vascular function, nerve system, and others (Wingfield and Sapolsky, 2003). In particular, chronic psychological stress has been perceived clinically as a potential risk factor that affects urinary function and exacerbates the symptoms of patients with lower urinary tract (LUT) dysfunction (LUTD), most profoundly in overactive bladder (OAB) and interstitial cystitis–bladder pain syndrome (IC/BPS) (Macaulay et al., 1987; Lutgendorf et al., 2001; Rothrock et al., 2001; McVary et al., 2005; Fan et al., 2008; Zhang et al., 2013; Bradley et al., 2014; Lai et al., 2015a, 2016). For example, multiple studies have found that adults with LUTDs display a positive relation to affective disorders such as anxiety and depression (Rothrock et al., 2001; Coyne et al., 2009). Similarly, children with LUTDs commonly report psychological symptoms and disorders (Oliver et al., 2013). The causative effects of psychological stress on LUTD can be further supported by the findings from veterans, who with psychiatric comorbidities were significantly more likely to have a LUTD diagnosis (Klausner et al., 2009; Bradley et al., 2014, 2017; Breyer et al., 2014). Therefore, chronic psychological stress may play a role in both the development and exacerbation of bladder symptoms.

Despite the findings from clinical studies, the pathophysiological mechanisms of chronic psychological stress-induced LUTD have still not been clearly defined. Instead of the inherent limitations (e.g., legal, ethical, and moral limitations) of clinical studies, the application of stress-related animal models facilitates further exploration and acknowledgement of the interplay of psychological stress and LUTD. These animal models appear to share multiple key characteristics of LUTDs such as increased voiding frequency (Smith et al., 2011), enhanced bladder pain (Lee et al., 2015), or bladder distension (Chang et al., 2009). Currently, a substantial number of animal models have been developed to study stress-induced LUTD, and the commonly used models include water avoidance stress (WAS) (Cetinel et al., 2005; Saglam et al., 2006; Robbins et al., 2007; Zeybek et al., 2007; Okasha and Bayomy, 2010; Smith et al., 2011; McGonagle et al., 2012; Yamamoto et al., 2012; Bazi et al., 2013; Lee et al., 2015; Ackerman et al., 2016; Gao et al., 2017; Matos et al., 2017; Dias et al., 2019; Kullmann et al., 2019; Holschneider et al., 2020a,b; Sanford et al., 2020; West et al., 2021), social stress (Chang et al., 2009; Wood et al., 2009, 2012, 2013; Mann et al., 2015; Mingin et al., 2015; Weiss et al., 2015; Wang et al., 2017; Butler et al., 2018; West et al., 2020; Yang et al., 2020), early life stress (ELS) (Chaloner and Greenwood-Van Meerveld, 2013; Mohammadi et al., 2016; Pierce et al., 2016, 2018; Fuentes et al., 2017, 2021; Fuentes and Christianson, 2018; Ligon et al., 2018), and repeated variable stress (RVS) (Hammack et al., 2009; Merrill et al., 2013; Merrill and Vizzard, 2014; Hattori et al., 2019; Girard et al., 2020). As shown by the findings from these models, chronic stress could induce functional and histopathological changes at multiple levels of the micturition pathway, providing insight into the underlying mechanisms and potential treatments of LUTD.

However, different psychological stressors have their own natures and likely stimulate separate brain regions to elicit appropriate responses (Scharf and Schmidt, 2012). Due to this stressor-dependent effect, stress animal models have presented varied LUTD-related results, which in some cases are conflicting. Additionally, a stress model frequently mimics only limited aspects of LUTD in humans and is tailored to answer a specific experimental theory. Moreover, each stress animal model has its own advantages and disadvantages, which should be discussed in detail. Therefore, the aim of our study is to provide a state-of-the-art overview of stress-related animal models, hoping to obtain mechanistic insights, facilitate model choices and propose novel treatment strategies for LUTD.

METHODS

A comprehensive electronic literature search was conducted using the PubMed database to identify publications related to chronic psychological stress-induced LUTDs. The keywords included the following terms: "stress," "animal model," "bladder," "lower urinary tract," "pain," "voiding," "micturition," "micturition frequency," "urinary frequency," or "frequency," using single or combination of words. The search was restricted to studies published between January 2000 and August 2021. Each article's title and abstract were reviewed for their appropriateness and relevance to the topic. The reference lists from the articles identified by this search strategy were also examined to find additional sources.

BASIC ASSESSMENT METHODS FOR CHRONIC STRESS-RELATED ANIMAL MODELS

Lower urinary tract dysfunction, such as OAB or IC/BPS, is commonly a symptom-based diagnosis, and symptoms are associated with urine storage and voiding phases. The hallmark symptoms appear to be urinary frequency and bladder-related pain. Due to the subjective nature of symptoms, the animal cannot communicate intent or relate their urinary symptoms to researchers. Therefore, it is necessary to apply surrogate markers for the symptoms of LUTD instead of intentional acts. Several technical methods have been developed to quantify the voiding activities and bladder nociception on the basis of feasibility and physiological relevance (Lai et al., 2015b).

Assessment of Voiding Activities

Three common methods have been applied to assess voiding activities, which include micturition cage, urine blotting patterns, and cystometry. In the approach of the micturition cage, a single animal will be placed into a micturition cage to record voiding frequency, interval, and volume, as well as water intake in real time (Wood et al., 2001). For the approach of urine blotting patterns, a blotting paper is laid on the bottom of the cage (below the mesh floor) to absorb the urine, and voiding activities are quantified as urine spots visualized under UV lamp or by methylene blue staining (Boudes et al., 2011). Cystometry allows the quantification of various urodynamic parameters during

bladder infusion, such as voiding pressure, contraction duration, intercontraction intervals (ICIs), and non-voiding contractions. Cystometry serves as a standardized methodology and can be combined with visceromotor response (VMR) measurement.

Assessment of Bladder Nociception in Animal Models

Two main methods have been developed to determine bladder nociception in animals. VMR, a pseudo-affective reflex, is considered to be a reliable and reproducible marker to quantify pain sensation and study analgesic agents (Ness et al., 2001; Pierce et al., 2016; Gao et al., 2017). It is recorded as electromyogram responses of the abdominal external oblique musculature to graded bladder distention in anesthetized animals. VMR threshold pressure is defined as the bladder pressure evoking VMR and used to assess the visceral pain sensitization. Other indicators are also used to evaluate VMR, including amplitude, duration, and area under the curve (AUC) (Ness and Elhefni, 2004; Gao et al., 2017). VMR could be inhibited by analgesics or augmented by the presence of stress or inflammation (Castroman and Ness, 2001).

Alternatively, von Frey suprapubic hyperalgesia is used to be a surrogate metric for assessing referred bladder hyperalgesia. It is measured by response to suprapubic mechanical stimuli with a calibrated series of nylon Von Frey monofilaments (Rudick et al., 2007; Lee et al., 2015).

ANIMAL MODELS OF CHRONIC STRESS-INDUCED LOWER URINARY TRACT DYSFUNCTION

A wide range of animal models have been developed to study the close link between chronic psychological stress and LUTD (**Figure 1**). It seems inconceivable to use a single animal model to replicate all the facets of LUTD in humans. It is better to carefully select certain species and stress paradigms before the experiments. The functional and histopathological changes are mainly decided by stressors *via* particular mechanisms (**Table 1**).

Model of Water Avoidance Stress

It is common to all investigations on this WAS model to place a single rodent on a platform centered in the middle of a water-filled basin. The rodent will try to avoid the adverse stimulus (water) by staying on the platform, causing potent psychological stress. WAS has previously been shown to be associated with increased anxiety-like behavior in rodents and visceral hyperalgesia in their guts (Bradesi et al., 2005). Currently, it is also used to replicate chronic stress-induced LUTD in rodents. The WAS model is found to present high construct and face validity to bladder hypersensitive syndromes.

However, the choices of rodent species, gender, and stress paradigm vary in different studies. Selecting the rodent species apparently limits the selection of specific strains based on their own characteristics. Wistar-Kyoto (WKY) rats are genetically predisposed to elevated levels of anxiety (Pare, 1992), commonly regarded as a standard model animal for testing visceral nociception. Sprague-Dawley (SD) rats are generally considered to be a low or moderate anxiety strain, and their use for stress protocols seems controversial due to two different studies with opposite results (Robbins et al., 2007; Bazi et al., 2013). Mice are seldom used for WAS paradigms, despite a certain report of successful application (McGonagle et al., 2012). When referring to gender, female rodents are usually chosen on account of the greater illness severity of female voiding disorders in women (Stewart et al., 2003; Lifford and Curhan, 2009). A diverse duration exists for WAS model establishment by different research groups. Most investigators, including our group, have subjected rodents to WAS 1 h per day for 10 consecutive days (Robbins et al., 2007; Smith et al., 2011; Ackerman et al., 2016; Gao et al., 2017). However, the stress paradigm could be low to 5 (Cetinel et al., 2005) or 7 (Bazi et al., 2013) days if rodents are exposed to WAS for 2 h daily.

Functionally, WAS exposure in rats potently produces a phenotype characterized by increased anxiety-like behaviors, urinary frequency, and bladder hyperalgesia (Smith et al., 2011; Bazi et al., 2013; Lee et al., 2015; Ackerman et al., 2016). Using micturition cage analysis, we first reported that female WKY rats with WAS exposure developed nearly double the voiding frequency and nearly half the voiding interval as the controls (Smith et al., 2011). These voiding alterations persisted for approximately 1 month after WAS exposure. Similarly, Yamamoto et al. (2012) and Bazi et al. (2013) demonstrated increased voiding frequency and decreased ICI and volume in WAS SD rats compared to the controls. Additionally, a lower bladder pressure can trigger the voiding phase in WAS WKY rats, which suggests the appearance of WAS-induced bladder hypersensitivity (Gao et al., 2017; Wang et al., 2017). Most importantly, exposure of WKY rats to WAS produced sensitized and enhanced bladder nociceptive responses. They can manifest as early appearing and vigorous VMRs to graded (Robbins et al., 2007; Gao et al., 2017) or continuous (Lee et al., 2015; Gao et al., 2017) bladder distension, and also significant tactile hindpaw allodynia and suprapubic hyperalgesia to von Frey filament testing (Lee et al., 2015). Furthermore, once established, the increased tactile allodynia and bladder hyperalgesia could last over 1 month without continued stress exposure, possibly due to involvement of central augmentation and peripheral neuroplasticity (Lee et al., 2015).

Additionally, WAS could also result in different kinds of histopathological changes in rat bladder. Harvested bladder tissue from stressed rats showed inflammatory conditions, which include ulcerated areas, edema, vascular congestion, inflammatory cell infiltration, increased angiogenesis, and an increased number of mast cells in the mucosa (Cetinel et al., 2005; Saglam et al., 2006; Okasha and Bayomy, 2010; Smith et al., 2011; Bazi et al., 2013; Matos et al., 2017). Meanwhile, under electron microscopy, vacuole formation, dilated perinuclear cisternae, and dilatation in the intercellular spaces were also observed in the urothelium of WAS rats (Cetinel et al., 2005; Saglam et al., 2006; Okasha and Bayomy, 2010). Moreover, WAS exposure altered the mitochondrial function of urothelial cells and led to secondary impairment of urothelial function (Kullmann et al., 2019). Based

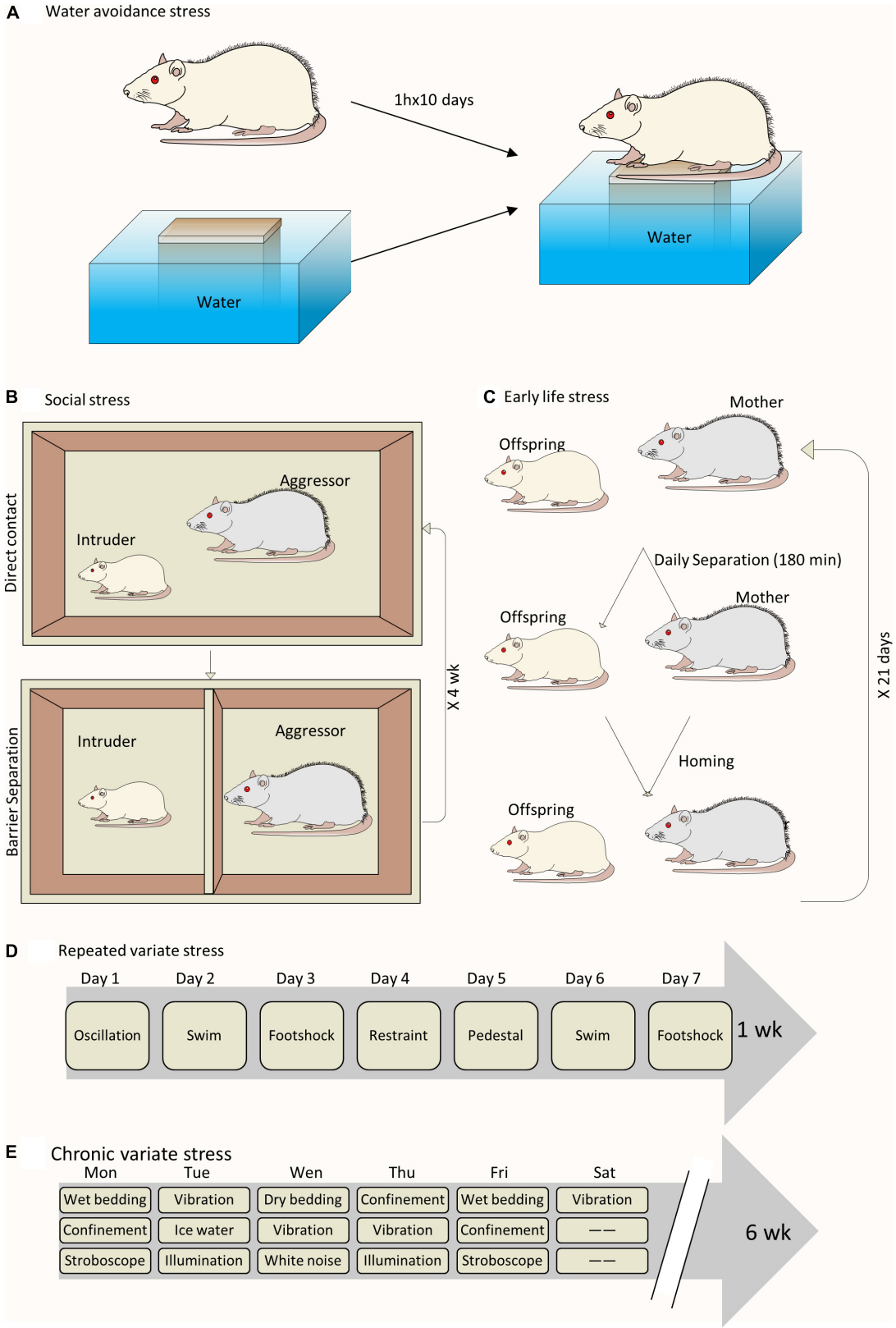

FIGURE 1 | Schematic drawing of different animal models to study chronic psychological stress-induced bladder dysfunction. **(A)** A sample of WAS model. **(B)** A sample of social stress model. **(C)** A sample of ELS model. **(D)** A sample of RVS model. **(E)** A sample of chronic variable stress model.

TABLE 1 | Animal models of chronic psychological stress-induced bladder dysfunction.

Model	References	Species	Sex	Micturition frequency	Bladder hyperalgesia	Main advantage	Best translational research use
Water avoidance stress	Yamamoto et al., 2012; Bazi et al., 2013	Sprague-Dawley rats	Female or male	↑	-	Well and easily established, economic, objective, reproducible	Studying of psychological stress-induced voiding dysfunctions like interstitial cystitis or bladder pain syndrome or overactive bladder phenotype
	Robbins et al., 2007; Smith et al., 2011; Lee et al., 2015; Ackerman et al., 2016; Gao et al., 2017; Matos et al., 2017; Kullmann et al., 2019; Holschneider et al., 2020b; Sanford et al., 2020	Wistar-Kyoto rats	Female	↑	↑		
	Cetinel et al., 2005; Saglam et al., 2006; Zeybek et al., 2007; Okasha and Bayomy, 2010	Wistar albino rats	Female	-	-		
	Dias et al., 2019	Wistar rats	Female	↑	-		
	McGonagle et al., 2012	Swiss-Webster mice	Male	↓	-		
	West et al., 2021	C57BL/6J mice	Female	↑	-		
Social stress	Long et al., 2014; Weiss et al., 2015; Butler et al., 2018	Swiss-Webster mice	Male	↓	-	Ethological relevant, reproducible	Studying of psychological stress-induced voiding dysfunctions, particularly urinary retention
	Wood et al., 2009, 2012, 2013	Sprague-Dawley rat	Male	↓	-		
	Mingin et al., 2014; Yang et al., 2020	FVB mice	Male	↑ or ↓	-		
	Mann et al., 2015; Mingin et al., 2015; West et al., 2020	C57BL/6 mice	Male	↑ or ↓	-		
Early life stress	Pierce et al., 2016; Fuentes et al., 2017, 2021; Pierce et al., 2018	C57BL/6 mice	Female or male	↑	↑	Ethological relevant	Studying of adult bladder dysfunction after early psychological stress exposure
	Mohammadi et al., 2016; Ligon et al., 2018	Long-Evans rats	Female	↑	↑		
Repeated variable stress	Merrill et al., 2013; Merrill and Vizzard, 2014	Wistar rats	Male	↑	-	Reproducible, lack of habituation	Studying of different daily stress-induced voiding dysfunctions
	Hattori et al., 2019	Sprague-Dawley rats	Female	↑	-		
	Girard et al., 2020	Transgenic mice	Female	↑	↑		
Chronic variable stress	Yoon et al., 2010; Han et al., 2015	Sprague-Dawley rats	Female	↑	-	Lack of habituation	Study of bladder functional changes under long-term stressful condition
Intermittent restraint stress	Ihara et al., 2019	C57BL/6 mice	Male	↑	-	Easily established, economic, reproducible	Study of stress-induced nocturia

on the above evidence, several investigators have tried to explore potential drugs to reverse these degenerative changes in stressed rat bladders. Cetinel et al. (2005) first reported the protective effect of melatonin on WAS-induced bladder degeneration in Wistar albino rats. After melatonin treatment, the impaired integrity of urothelial morphology and the increased number of mast cells in the mucosa were ameliorated in WAS rats. Saglam et al. (2006) noted that aqueous garlic extract protected the urothelium by preserving the urothelial mucous layer and reducing the number and degranulation of mast cells. Since then, several other drugs have also been tested to treat WAS-induced bladder degeneration in rats, which include taurine (Zeybek et al., 2007), quercetin (Okasha and Bayomy, 2010), epigallocatechin gallate (Bazi et al., 2013), cyclooxygenase-2 (COX-2) inhibitor (Yamamoto et al., 2012), silodosin (α-1 adrenoceptor antagonist) (Matos et al., 2017), and guanethidine (an adrenergic neuron blocking agent) (Kullmann et al., 2019). These studies have suggested certain possible and effective treatment options for chronic stress-related LUTD.

Based on these functional and histological findings, plenty of mechanisms were proposed to explain the pathophysiological basis of WAS-induced LUTD. Yamamoto et al. speculated that upregulated bladder COX-2 gene expression contributed to WAS-induced voiding frequency (Yamamoto et al., 2012). Dias et al. (2019). demonstrated significantly increased serum and urinary levels of nerve growth factor (NGF) in stressed rats, and blocking its high-affinity receptor tropomyosin-related kinase subtype A (Trk A) prevented WAS-induced voiding changes. NGF is a well-known molecule that contributes to the bladder afferent hypersensitization and hyperexcitability (Yoshimura et al., 2014). Specifically, the role of sensitized C-fiber afferents in bladder hypersensitivity was demonstrated in our previous study, in which WAS WKY rats showed a low threshold but enhanced VMR response to bladder cold saline infusion in comparison with the controls (Gao et al., 2017). Moreover, the exaggerated activity of the peripheral sympathetic nervous system may also contribute to bladder dysfunction and pain in WAS rats, possibly suppressed by the administration of silodosin (Matos et al., 2017) and guanethidine (Kullmann et al., 2019). Beyond these peripheral mechanisms, WAS-induced bladder hyperalgesia was correlated with increased spinal glutamate neurotransmission attributable to the downregulation of glial glutamate transporter 1 (Glt-1) receptors (Ackerman et al., 2016). Exogenous Glt1 upregulation *via* ceftriaxone treatment attenuated hyperalgesia and voiding dysfunction after WAS exposure (Ackerman et al., 2016; Holschneider et al., 2020a). Our brain mapping results showed greater activation in cerebral regions of the micturition circuit responsive to urgency, viscerosensory perception, and its relay to motor regions coordinating imminent bladder contraction, in particular the pontine micturition center (PMC), periaqueductal gray (PAG), thalamus, cingulate, and insula (Gao et al., 2017; Wang et al., 2017). Voluntary exercise or ceftriaxone administration could diminish bladder hypersensitivity and attenuate brain regions related to nociceptive and micturition circuits (Holschneider et al., 2020a,b; Sanford et al., 2020).

Of note, WAS exposure in mice results in different types of voiding dysfunction. In West's study, female C57BL/6 mice were exposed to WAS for 1 h per day for 10 days, which produces an OAB phenotype with increased voiding frequency and enhanced bladder contractile responses (West et al., 2021). In contrast, McGonagle et al. (2012) applied the WAS protocol (1 h daily for 4 weeks) in male Swiss Webster mice and reported an altered voiding phenotype with a decreased voiding frequency and increased average voided volumes, seemingly attributable to the alteration of the calcineurin–nuclear factor of activated T-cells (NFAT) pathway in the bladder.

Accordingly, WAS is a less expensive but more objective means to study underlying mechanisms of chronic stress-induced LUTD and evaluate the impact of pharmacological agents. This WAS-induced voiding phenotype is much close to physiological condition without bladder irritants or directly inflicting bladder inflammation. The technique is easily done and outcomes are highly reproducible. One limitation of the WAS model seems to be restricted to certain rat strains such as anxiety-prone ones. Wistar albino rats have also been chosen in some WAS protocols, while none of them have reported bladder hyperalgesia after WAS exposure (Cetinel et al., 2005; Saglam et al., 2006; Zeybek et al., 2007). Altogether, these considerations can demonstrate that rodents—particularly the anxiety-prone ones—provide multiple accesses to effectively mimic the key features of human LUTD.

Model of Social Stress

Social stress (or social defeat), usually mimicking bullying–childhood violence, has been shown to induce distinct voiding dysfunction in rodents. In the common social stress paradigm, the subordination of one male by another larger and more aggressive male could increase the risk of anxiety and depression (West et al., 2020). Male mice are the most frequently employed mice to explore this stress-related LUTD. This could be exemplified by Chang et al.'s study, in which a single submissive FVB mouse was repeatedly exposed (4 weeks) to an aggressive male C57BL/6 mouse for 1 h a day followed by 23 h of barrier separation (Chang et al., 2009). Several other investigators conducted similar paradigms to induce social stress (Long et al., 2014; Mingin et al., 2014, 2015; Weiss et al., 2015; Yang et al., 2020). Alternatively, the duration of social stress in the study Mann et al. (2015) was reduced to 2 weeks, and the direct daily exposure of male mice to aggressive ones was reduced to 10 min. In West's study, pairs of male C57BL/6 mice were exposed to an aggressor for 1 h/day for 10 days (West et al., 2020). Instead of mice, Wood et al. (2009) exposed a male SD rat to a larger Long-Evans resident for a 30-min session with direct or indirect contact on 7 consecutive days.

After social stress exposure, rodents develop micturition alterations resembling partial bladder outlet obstruction in many ways. Chang et al. (2009). showed that socially stressed FVB mice had a lower voiding frequency, a greater voiding volume, and an increased threshold than matched controls, which suggests a social stress-induced urinary retention. Long et al. similarly determined that socially stressed C57BL/6 mice could present a single, large void pattern (Mann et al., 2015). Apart from mice, such social stress-related urinary LUTD was also noted in a rat model, and only stressed rats presented numerous non-micturition-related contractions (Wood et al., 2009). Several

other studies also corroborated the above findings of stress-induced urinary LUTD (Wood et al., 2013; Long et al., 2014; Mingin et al., 2014).

Furthermore, social stress leads to hypertrophy and remodeling of the rodent bladder (Chang et al., 2009; Wood et al., 2009, 2012). Chang et al. (2009) demonstrated a 2-fold increase in the bladder-to-body mass index in socially stressed FVB mice. In this study, stressed bladders showed alterations in myosin heavy chain isoform expression and DNA synthesis mediating bladder wall reconstruction (Chang et al., 2009). Mann et al. (2015) also found that social stress induced a higher bladder-to-body mass index and thicker bladder wall. Moreover, the occurrence of bladder inflammation was evidenced by increased bladder NGF and histamine protein expression in socially stressed FVB mice (Mingin et al., 2014). In contrast, Mann et al. (2015) demonstrated an intact urothelial barrier and normal vascularity in socially stressed C57BL/6 bladders.

These aforementioned studies shed some light on potential mechanistic pathways linking social stress to LUTD from peripheral involvement to central participation. One of them involved a clear-cut change in the bladder calcineurin–NFAT pathway, the inhibition of which by cyclosporine A resulted in amelioration of the post-stressed abnormal voiding phenotype (Long et al., 2014; Weiss et al., 2015). A recent study showed that a social stress-altered voiding phenotype was associated with desensitized bladder sensory nerves by greater urothelial acetylcholine release and purinergic responses (West et al., 2020). Additionally, corticotropin-releasing factor (CRF), a stress-related neuropeptide, may be intrinsically involved in this type of LUTD. Social stress increased the number of CRF-immunoreactive neurons and the expression of CRF mRNA in Barrington's nucleus (PMC), which possibly leads to subsequent bladder dysfunction (Wood et al., 2009). This CRF mRNA expression in Barrington's nucleus remained elevated after 1 month of recovery from social stress, correlated with persistent voiding dysfunction (Butler et al., 2018). Administration of a CRF1 antagonist or shRNA targeting CRF in Barrington's nucleus could improve social stress-induced retention (Wood et al., 2013). Another elevated neuropeptide brain-derived neurotrophic factor was also noted in rodent serum after social stress exposure, and a short-term subanesthetic dose of ketamine reduced its expression and reverse the trend of stress-related infrequent voiding (Yang et al., 2020).

In addition, the effect of social stress on the bladder seems context- and duration-dependent. After social stress, increased voiding frequency can occur first (Mingin et al., 2014, 2015) but voiding frequency decreases later with enhanced stress intensity (Mingin et al., 2014). Mingin et al. (2015) observed decreased ICI, voided volume, bladder capacity, and elevated transient receptor potential vanilloid 1 (TRPV1) expression in socially stressed C57BL/6 mice. Inhibiting TRPV1 was able to significantly restore bladder overactivity and reduce afferent bladder nerve activity in stressed mice (Mingin et al., 2015). Moreover, TRPV1 knockout mice also showed no social stress-induced bladder dysfunction (Tykocki et al., 2018). TRPV1 has emerged as a key regulator of bladder sensory processes and as a potential therapeutic target for LUTD (Vanneste et al., 2021).

In contrast to other stressors, social stress is ethologically relevant and suitable to create more innovative and effective management for children presenting voiding dysfunction with bullying or childhood violence history. Context- and duration-dependent effects are typical features of the social stress paradigm. However, an apparent limitation comes from its uneconomic process, such as essential single cage housing to avoid developing social rank hierarchies even among sibling littermates. In addition, another compelling issue is whether social stress can exert an effect on female rodents because current reports are all focused on males.

Model of Early Life Stress

Early life stress, or early adverse events, has been shown to serve as a strong predictor of a painful voiding phenotype later in life. Several translational studies have tried to examine the impact of ELS on the bladder using two main types of animal models, namely neonatal maternal separation (NMS) (Pierce et al., 2016, 2018; Fuentes et al., 2017) and neonatal odor-shock conditioning (NOSC) (Mohammadi et al., 2016; Ligon et al., 2018). To produce NMS, mouse pups are removed from their dam for 3 h/day from postnatal days 1 to 21 (Pierce et al., 2016, 2018; Fuentes et al., 2017). NMS could also be combined with acute WAS as adults to imitate ELS with later adult trauma (Pierce et al., 2016; Fuentes et al., 2017). Pierce et al. (2016) provided evidence that NMS in female C57BL/6 mice was capable of inducing bladder hypersensitivity, manifested as a significantly increased VMR to bladder distension. Exposure to adult WAS further increased bladder sensitivity and micturition rate in these NMS mice, strongly suggestive of the necessity of additional stress for induction of painful LUTD phenotype (Pierce et al., 2016). Further molecular evidence from this study demonstrated neurogenic bladder inflammation and disruption of the proper hypothalamic–pituitary–adrenal (HPA) axis function after NMS. The HPA axis is well known to regulate stress response and affect the perception of pain (Habib et al., 2001). Pierce's later study proved that voluntary exercise could attenuate NMS-induced behavioral outcomes in female C57BL/6 mice (Pierce et al., 2018), quite similar to the findings in WAS rats with voluntary exercise (Holschneider et al., 2020b; Sanford et al., 2020). Beyond female mice, male mice could also exhibit NMS-induced bladder hypersensitivity (Fuentes et al., 2017), urologic chronic pelvic pain, and mast cell degranulation in the bladder (Fuentes et al., 2021), all of which could also be ameliorated by voluntary exercise (Fuentes et al., 2021). Compared to mouse species, SD rat pups subjected to 6 h of daily NMS presented intermittent urinary retention with delayed withdrawal of the immature perigenital-bladder reflex (Wu and de Groat, 2006).

The NOSC model was initially developed to mimic attachment to an abusive caregiver. Mohammadi et al. (2016) utilized this model to condition male and female Long-Evans pups on postnatal days 8–12 to predictable odor-shock, unpredictable odor-shock, or odor-only treatment. In adulthood, female rats with unpredictable NOSC presented a significantly increased urine voiding volume and decreased detrusor contractile responses. Conversely, male rats showed no difference in voiding behavior or detrusor muscle activity after stress exposure,

indicative of a female predominance of NOSC on urinary bladder function. Mohammadi's recent study demonstrated that linaclotide, a guanylate cyclase-C agonist, could significantly reduce NOSC-induced bladder hypersensitivity (Ligon et al., 2018). In contrast to the NMS model, bladder inflammation was not found in this NOSC model.

The main advantage of the ELS model is to initiate adult physiological changes by a childhood psychological intervention, which expands our knowledge of how ELS predisposes an individual to develop LUTD during adulthood. This model has both face validity and construct validity, as well as incorporation of a non-invasive induction. Given that NMS dramatically affects the function of the HPA axis, it is important to control environmental stimuli during both the neonatal and adult periods.

Model of Repeated Variable Stress

To mimic the variety of life stressors experienced by humans on a daily basis, an RVS model is established to elucidate the connection between stress and voiding dysfunction (Merrill et al., 2013; Merrill and Vizzard, 2014). Generally, rodents assigned to RVS are exposed to a 7-day stress protocol with a single stressor daily, which includes oscillation, swim, footshock, restraint, pedestal, swim, and footshock. After RVS exposure, both male Wistar rats (Merrill et al., 2013; Merrill and Vizzard, 2014) and female transgenic mice (Girard et al., 2020) exhibited increased voiding frequency and somatic sensitivity similar to IC/BPS. Elevated inflammatory markers (NGF, histamine, myeloperoxidase, and chemokines) have been found in stressed bladder tissue (Merrill et al., 2013; Girard et al., 2020), which is indicative of an RVS-induced inflammatory milieu of the bladder. Conversely, Hattori et al. (2019) examined the effect of RVS on female SD rats and found a significantly decreased micturition frequency and ICI in conscious and unconscious cystometry, respectively.

Several plausible mechanisms were offered for the RVS-induced voiding alterations. Merrill and Vizzard (2014) identified significantly increased TRPV4 expression in the urothelium of RVS rats and the intravesical TRPV4 antagonist HC067047 attenuated this RVS-induced bladder dysfunction. Notably, a more recent study by this research group reported a change in pituitary adenylate cyclase-activating polypeptide (PACAP) receptor signaling in lumbosacral dorsal root ganglions and spinal cord but not in the urinary bladder (Girard et al., 2020). PACAP, a type of neuropeptide, is expressed in neural and non-neural components of LUT and exhibits neuroplastic changes under pathological conditions that include psychological stress, inflammation, and neuron injury (Girard et al., 2017). Intravesical administration of a PACAP receptor antagonist could contribute to decreased voiding frequency and pelvic sensitivity following RVS exposure (Girard et al., 2020). Moreover, administration of the α1-adrenoceptor antagonist naftopidil orally could partly prolong ICI in female SD rats subjected to RVS (Hattori et al., 2019).

The main advantage of the RVS protocol is that it is well-established, reproducible, and more relevant to human daily life stressors. Also, novel stressor exposure on a daily basis could lead to a lack of habituation.

Model of Chronic Variable Stress

Chronic variable stress (CVS), or the chronic mild stress model, was initially utilized in the psychological research field for studies on depression. Similar to RVS, CVS included a series of stressors. In Yoon's protocol, female SD rats were exposed to scheduled stress environments that include starvation, low temperatures (4°C), immobilization, and changes in the diurnal rhythm for 7, 14, and 28 days (Yoon et al., 2010). In this study, voiding frequency in stressed rats significantly increased with the prolonged duration of stress exposure, possibly related to higher bladder contractility caused by higher expression of Rho-kinase (one of the major mediators for muscle contraction and relaxation responses) in the bladder tissue. CVS also induced increased expression of types I and III collagen in bladder tissue, which suggests bladder fibrosis for bladder stability–overactivity (Yoon et al., 2010). Additionally, Han et al. (2015) applied a modified CVS protocol with a series of stressors for 6 weeks, such as confinement in a small cage, white noise during the dark phase, stroboscope, light on at night, intruder sound, and food and water deprivation. In Han's study, stressed female SD rats also showed bladder hypersensitivity in cystometry such as increased micturition frequency and decreased micturition volume and ICI. Consistent with Yoon's study above, Han's further evaluation demonstrated increased RhoA/Rho-kinase expression and decreased neuronal nitric oxide synthase expression in the stressed bladder wall, which indicates a hyperactive bladder with a lower relaxation capacity (Han et al., 2015).

The pivotal feature of the CVS model is to utilize various unpredictable stressors to investigate the micturition pattern alterations reflecting long-term stressful human life events. Different stressors may contribute to the absence of adaptation. While obviously, establishing the CVS model needs much more time and total experimental cost.

Intermittent Restraint Stress

Intermittent restraint stress (IRS), a notable psychological stressor to rodents, is also applied to study stress-induced LUTD. In Ihara's study, male C57BL/6 mice were subjected to IRS during zeitgeber times 4–6 for 2 h/day for 5 consecutive days and exhibited higher voiding frequency and smaller urine volume or voiding in the light (sleep) phase (Ihara et al., 2019). This voiding phenotype such as nocturia may be pertinent to changes in circadian bladder function due to the dysregulation of clock genes such as Per2. Amending the circadian rhythm by Per2 inhibition could reduce voiding frequency and increase bladder capacity during the light phase in IRS mice. Mann's reports, however, demonstrated that water-restraint stress (9 a.m. to 1 p.m., 4 h/day for 21 days), another type of restraint stress, could not produce functional or histopathological changes in the bladder of the male C57BL/6 mice (Mann et al., 2015). These differences between the findings of Ihara and Mann were possibly related to the differences in restraint stress type, stress duration,

and daily stress schedule. The IRS model seems relatively cost-effective and straightforward to implement, but it carries some caveats including stress habituation or a lack of ecological relevance (Koolhaas et al., 2006). The voiding phenotypes may be influenced by different IRS protocols.

Others

Other stressors such as intraspecies emotional communication (IEC) and foot shock stress (FSS) are also applied to explore the mechanisms underlying stress-induced LUTDs. IEC produced purely psychological stress without physical stress intervention (Gomita et al., 1989). Male WKY rats with IEC 2 h/day for 7 days developed greater micturition frequency and voided volume per day, which probably results from IEC reinforced muscarinic receptor 3-mediated contractions *via* CRF1 pathway (Seki et al., 2019). FSS was a readily controlled physical stressor to produce behavioral and neurochemical changes (Kant et al., 1983; Rivier and Vale, 1987; Henry et al., 2006). FSS-stressed female SD rats displayed bladder hypersensitivity, which could be significantly alleviated by blocking spinal CRF2 (Robbins and Ness, 2008) or oxytocin systematic treatment (Black et al., 2009). Acute stressors such as acute immobilization (Boucher et al., 2002, 2010) and acute FSS (Robbins et al., 2011; DeBerry et al., 2015; Ness et al., 2018) can also induce LUTDs, which are not discussed detailly in this study.

SEX- AND STRAIN-SPECIFIC DIFFERENCES IN ANIMAL MODELS

Various epidemiological studies have demonstrated that gender bias in human LUTD is apparent and that women are more vulnerable to the development of LUTD (Stewart et al., 2003; Lifford and Curhan, 2009). Therefore, as described above, female rodents are usually employed to study stress-related LUTDs. However, one important point should be taken into account: the animal's sex and hormones may contribute to the alterations in micturition following chronic stress exposure. For instance, male or female mice with WAS exposure showed significant differences in voiding frequency (McGonagle et al., 2012; West et al., 2021). Similar results can be found in the male or female rats in response to NOSC exposure (Mohammadi et al., 2016). Several hypotheses attempt to explain the sexually dimorphic effects of chronic stress on micturition. One hypothesis is the involvement of estrous influences. Estrogen is well known to be effective on female bladder contractility and stability in both humans and animals (see review Hanna-Mitchell et al., 2016). Moreover, estrogen could also be affected by chronic stress. For example, female SD rats with CVS exposure presented significant increases in voiding frequency and bladder contraction, together with a significant decrease in estrogen. Another hypothesis is the sex-specific effects of stress exposure on the HPA axis. As shown by Sterrenburg's study, CVS could induce sex-specific differences in methylation and expression of the CRF gene in animal brains (Sterrenburg et al., 2011).

Another point that should be noted is that the results of lower urinary function tests vary among strains. As mentioned above, WKY rats are more genetically predisposed to anxiety than SD rats. Robbins's study reported that chronic psychological stress (WAS) significantly enhanced bladder nociceptive responses only in WKY rats rather than SD rats (Robbins et al., 2007). Similarly, WAS exposure induced different voiding results obtained from two mouse strains (C57BL/6 and Swiss Webster) (McGonagle et al., 2012; West et al., 2021). These differences in urinary function tests may be related to strain-specific bladder physiology or behavioral factors. Other non-stress-related studies have been also demonstrated the strain-specific effect on urinary function (Yu et al., 2014; Bjorling et al., 2015).

However, more studies are necessary to determine the sex- and strain-specific differences in stress-related LUTD models.

IMPLICATIONS FOR INTEGRATED MECHANISMS

As mentioned above, various studies on different chronic psychological stress models have yielded incremental pieces of evidence for stress-induced LUTDs. However, the results from them appeared to be disparate for a definite conclusion. By integrating the evidence together, we could create a reasonable picture of the pathophysiology of stress-induced LUTDs (**Figure 2**). The possible mechanisms are roughly divided into two main classes as follows.

Central Stress Mechanisms

Limbic–hypothalamic–pituitary–adrenal axis is crucial to coordinate behavioral, physiological, and molecular responses to chronic psychological stressors (Pacák, 2000; Ulrich-Lai and Herman, 2009; Ullmann et al., 2020). In particular, the paraventricular nucleus (PVN) of the hypothalamus is generally recognized as the main center regulating responses to stress (Pacák, 2000; Herman et al., 2008). PVN could secrete CRF, project into different sites (hypothalamus, brainstem, etc.), and stimulate adrenocorticotropic hormone secretion from the pituitary (Kalantaridou et al., 2010). CRF could mediate general responses to stress and other responses such as visceral hyperalgesia (Elman and Borsook, 2016; Chess-Williams et al., 2021; Huang et al., 2021). Other stress response-relevant brain regions include the prefrontal cortex, amygdala, and hippocampus (Kalantaridou et al., 2010). The disruption of the HPA axis has been reported in ELS rodents (Pierce et al., 2016). The functional alterations in these mentioned brain regions, together with other key areas (cingulate, insula, thalamus, etc.), were identified in WAS rats by brain mapping analysis (Wang et al., 2017; Holschneider et al., 2020a; Sanford et al., 2020) and in patients with LUTD by fMRI studies (Kleinhans et al., 2016). Additionally, aberrant expression and function of CRF in PMC were also noted in rodents subjected to WAS or social stress (Wood et al., 2009; Wang et al., 2017). Recently, Shimizu et al. (2021) postulated several brain molecules related to the stress-induced LUTDs, which include bombesin, angiotensin II, nicotinic acetylcholine receptor, nitric oxide, and H_2S. Hence, psychological stress could significantly affect the cerebral

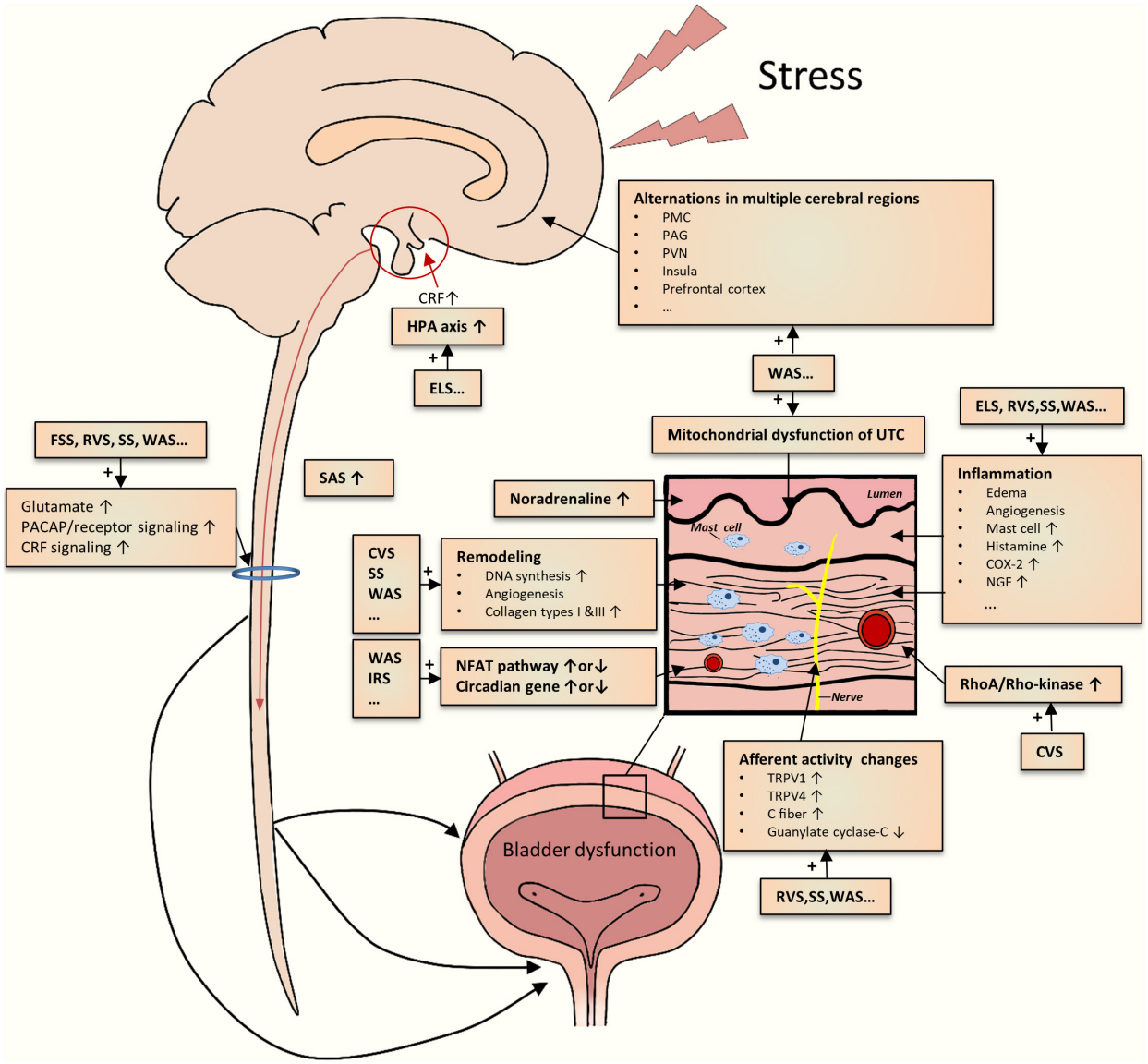

FIGURE 2 | Schematic drawing of the summarization of possible mechanisms underlying the chronic psychological stress-induced LUTD. The current studies demonstrate multiple central and peripheral alterations contributing to bladder dysfunction.

regions related to stress responses and micturition circuit, which contributes to the development of LUTDs.

The sympathetic-adrenal system (SAS), another classic pathway for initiation and coordination of stress responses, appears to be involved in stress-induced LUTDs. SAS mainly consists of central (locus coeruleus and noradrenaline system) and peripheral (sympathetic nervous system and adrenal medulla) elements (Nargund, 2015). Activated by CRF *via* different approaches (Harris, 2015; Tache et al., 2018), SAS participates in multiple processes including micturition, mechanical hyperalgesia maintenance, and induction of viscrosensory hypersensitivity (Charrua et al., 2015). Activation of the SAS was partly proved by the results from the WAS and RVS models. Blocking SAS by the administration silodosin (Matos et al., 2017), guanethidine (Kullmann et al., 2019), or naftopidil (Hattori et al., 2019) could mitigate urinary dysfunctions after chronic stress exposure. These preclinical results were in line with the clinical studies, which confirmed the existence of SAS activation (Charrua et al., 2015).

Apart from these supraspinal mechanisms, spinal ones may also be engaged in stress-induced LUTDs. Chronic stress seems to enhance spinal signaling transductions, as evidenced by increased spinal glutamate neurotransmission (Ackerman et al., 2016; Holschneider et al., 2020a), PACAP (Girard et al., 2020), and CRF2 (Robbins and Ness, 2008) signaling transduction. Dorsal root ganglions may positively participate in these enhanced signal transductions (Girard et al., 2020). Spinal sensitization has been identified in other non-stressed animal models

(Zvarova and Vizzard, 2006; Arms et al., 2013; Chen et al., 2016; Girard et al., 2016; Ozaki et al., 2018).

Local Bladder Stress Mechanism

One theory for stress-induced LUTDs is the occurrence of bladder afferent hyperexcitability after chronic stress exposure. As mentioned above, stressed rodents commonly exhibited greater voiding frequency but lower pressure threshold and VMR threshold, which suggests bladder hypersensitivity and hyperalgesia. The activation of bladder C-fiber afferents (Gao et al., 2017) or TRPV1-sensitive bladder afferents (Mingin et al., 2015) may be involved in the stress-induced afferent hyperexcitability. Other candidates, such as TRPV4 pathway (Merrill and Vizzard, 2014), guanylate cyclase-C pathway (Ligon et al., 2018), and various inflammatory pathways (COX-2,NGF, histamine, myeloperoxidase, chemokines, etc.) (Yamamoto et al., 2012; Merrill et al., 2013; Mingin et al., 2014; Dias et al., 2019; Girard et al., 2020), may also be responsible for bladder afferent hyperexcitability.

In addition, chronic stress caused other functional and structural changes in the bladder tissues, particularly detrusor muscle and urothelium. Both *in vivo* and *in vitro* methods have demonstrated an enhanced detrusor contraction in stressed rodents (Yoon et al., 2010; Seki et al., 2019; West et al., 2021), partly related to bladder remodeling (Chang et al., 2009; Wood et al., 2009, 2012). The alteration in the urothelium, such as abnormal mitochondrial function, may contribute to increased bladder signal input (Kullmann et al., 2019). Particularly, chronic stress can bring about increased bladder inflammation that includes edema, inflammatory cell infiltration, and angiogenesis (Chess-Williams et al., 2021).

CONCLUSION

Chronic psychological stress can impact LUT function with or without pathological consequences. This study provided a comprehensive overview of stress-related animal models for the study of LUTD and summarized the compensatory mechanisms underlying the emergence of LUTD. Variations in stress duration, the nature of chronic stressors, and differences in animal species, strains, and sex may contribute to different effects on the bladder. Based on the findings from these models, a variety of possible mechanisms and potential treatments have been demonstrated. Future studies should provide experimental means to improve the scientific basis for this common clinical problem, with the hope of ultimately expanding the therapeutic options for those patients with functional bladder disorders.

AUTHOR CONTRIBUTIONS

YG: data collection, analysis, and manuscript preparation. LR: project design and manuscript review. Both authors contributed to the article and approved the submitted version.

FUNDING

This study was supported by grants from the National Natural Science Foundation of China (grant no. 81800669) and the Natural Science Foundation of Hunan Province (grant no. 2021JJ40829) to YG.

REFERENCES

Ackerman, A. L., Jellison, F. C., Lee, U. J., Bradesi, S., and Rodriguez, L. V. (2016). The Glt1 glutamate receptor mediates the establishment and perpetuation of chronic visceral pain in an animal model of stress-induced bladder hyperalgesia. *Am. J. Physiol. Renal Physiol.* 310, F628–F636. doi: 10.1152/ajprenal.00297.2015

Arms, L., Girard, B. M., Malley, S. E., and Vizzard, M. A. (2013). Expression and function of CCL2/CCR2 in rat micturition reflexes and somatic sensitivity with urinary bladder inflammation. *Am. J. Physiol. Renal Physiol.* 305, F111–F122. doi: 10.1152/ajprenal.00139.2013

Bazi, T., Hajj-Hussein, I. A., Awwad, J., Shams, A., Hijaz, M., and Jurjus, A. (2013). A modulating effect of epigallocatechin gallate (EGCG), a tea catechin, on the bladder of rats exposed to water avoidance stress. *Neurourol. Urodyn.* 32, 287–292. doi: 10.1002/nau.22288

Bjorling, D. E., Wang, Z., Vezina, C. M., Ricke, W. A., Keil, K. P., Yu, W., et al. (2015). Evaluation of voiding assays in mice: impact of genetic strains and sex. *Am. J. Physiol. Renal Physiol.* 308, F1369–F1378. doi: 10.1152/ajprenal.00072.2015

Black, L. V., Ness, T. J., and Robbins, M. T. (2009). Effects of oxytocin and prolactin on stress-induced bladder hypersensitivity in female rats. *J. Pain* 10, 1065–1072. doi: 10.1016/j.jpain.2009.04.007

Boucher, W. S., Letourneau, R., Huang, M., Kempuraj, D., Green, M., Sant, G. R., et al. (2002). Intravesical sodium hyaluronate inhibits the rat urinary mast cell mediator increase triggered by acute immobilization stress. *J. Urol.* 167, 380–384.

Boucher, W., Kempuraj, D., Michaelian, M., and Theoharides, T. C. (2010). Corticotropin-releasing hormone-receptor 2 is required for acute stress-induced bladder vascular permeability and release of vascular endothelial growth factor. *BJU Int.* 106, 1394–1399. doi: 10.1111/j.1464-410X.2010.09237.x

Boudes, M., Uvin, P., Kerselaers, S., Vennekens, R., Voets, T., and De Ridder, D. (2011). Functional characterization of a chronic cyclophosphamide-induced overactive bladder model in mice. *Neurourol. Urodyn.* 30, 1659–1665. doi: 10.1002/nau.21180

Bradesi, S., Schwetz, I., Ennes, H. S., Lamy, C. M., Ohning, G., Fanselow, M., et al. (2005). Repeated exposure to water avoidance stress in rats: a new model for sustained visceral hyperalgesia. *Am. J. Physiol. Gastrointest. Liver Physiol.* 289, G42–G53. doi: 10.1152/ajpgi.00500.2004

Bradley, C. S., Nygaard, I. E., Hillis, S. L., Torner, J. C., and Sadler, A. G. (2017). Longitudinal associations between mental health conditions and overactive bladder in women veterans. *Am. J. Obstet. Gynecol.* 217:430.e1–e8. doi: 10.1016/j.ajog.2017.06.016

Bradley, C. S., Nygaard, I. E., Torner, J. C., Hillis, S. L., Johnson, S., and Sadler, A. G. (2014). Overactive bladder and mental health symptoms in recently deployed female veterans. *J. Urol.* 191, 1327–1332. doi: 10.1016/j.juro.2013.11.100

Breyer, B. N., Cohen, B. E., Bertenthal, D., Rosen, R. C., Neylan, T. C., and Seal, K. H. (2014). Lower urinary tract dysfunction in male Iraq and Afghanistan war veterans: association with mental health disorders: a population-based cohort study. *Urology* 83, 312–319. doi: 10.1016/j.urology.2013.08.047

Butler, S., Luz, S., McFadden, K., Fesi, J., Long, C., Spruce, L., et al. (2018). Murine social stress results in long lasting voiding dysfunction. *Physiol. Behav.* 183, 10–17. doi: 10.1016/j.physbeh.2017.09.020

Castroman, P., and Ness, T. J. (2001). Vigor of visceromotor responses to urinary bladder distension in rats increases with repeated trials and stimulus intensity. *Neurosci. Lett.* 306, 97–100.

Cetinel, S., Ercan, F., Cikler, E., Contuk, G., and Sener, G. (2005). Protective effect of melatonin on water avoidance stress induced degeneration of the bladder. *J. Urol.* 173, 267–270. doi: 10.1097/01.ju.0000145891.35810.56

Chaloner, A., and Greenwood-Van Meerveld, B. (2013). Sexually dimorphic effects of unpredictable early life adversity on visceral pain behavior in a rodent model. *J. Pain* 14, 270–280. doi: 10.1016/j.jpain.2012.11.008

Chang, A., Butler, S., Sliwoski, J., Valentino, R., Canning, D., and Zderic, S. (2009). Social stress in mice induces voiding dysfunction and bladder wall remodeling. *Am. J. Physiol. Renal Physiol.* 297, F1101–F1108. doi: 10.1152/ajprenal.90749.2008

Charrua, A., Pinto, R., Birder, L. A., and Cruz, F. (2015). Sympathetic nervous system and chronic bladder pain: a new tune for an old song. *Transl. Androl. Urol.* 4, 534–542. doi: 10.3978/j.issn.2223-4683.2015.09.06

Chen, Z., Du, S., Kong, C., Zhang, Z., and Mokhtar, A. D. (2016). Intrathecal administration of TRPA1 antagonists attenuate cyclophosphamide-induced cystitis in rats with hyper-reflexia micturition. *BMC Urol.* 16:33. doi: 10.1186/s12894-016-0150-x

Chess-Williams, R., McDermott, C., Sellers, D. J., West, E. G., and Mills, K. A. (2021). Chronic psychological stress and lower urinary tract symptoms. *Low. Urin. Tract. Symptoms* 13, 414–424. doi: 10.1111/luts.12395

Chrousos, G. P. (2009). Stress and disorders of the stress system. *Nat. Rev. Endocrinol.* 5, 374–381.

Coyne, K. S., Kaplan, S. A., Chapple, C. R., Sexton, C. C., Kopp, Z. S., Bush, E. N., et al. (2009). Risk factors and comorbid conditions associated with lower urinary tract symptoms: EpiLUTS. *BJU Int.* 103(Suppl. 3), 24–32. doi: 10.1111/j.1464-410X.2009.08438.x

DeBerry, J. J., Robbins, M. T., and Ness, T. J. (2015). The amygdala central nucleus is required for acute stress-induced bladder hyperalgesia in a rat visceral pain model. *Brain Res.* 1606, 77–85. doi: 10.1016/j.brainres.2015.01.008

Dias, B., Serrão, P., Cruz, F., and Charrua, A. (2019). Effect of water avoidance stress on serum and urinary NGF levels in rats: diagnostic and therapeutic implications for BPS/IC patients. *Sci. Rep.* 9:14113. doi: 10.1038/s41598-019-50576-4

Elman, I., and Borsook, D. (2016). Common brain mechanisms of chronic pain and addiction. *Neuron* 89, 11–36. doi: 10.1016/j.neuron.2015.11.027

Fan, Y. H., Lin, A. T., Wu, H. M., Hong, C. J., and Chen, K. K. (2008). Psychological profile of Taiwanese interstitial cystitis patients. *Int. J. Urol.* 15, 416–418. doi: 10.1111/j.1442-2042.2008.02020.x

Fuentes, I. M., and Christianson, J. A. (2018). The influence of early life experience on visceral pain. *Front. Syst. Neurosci.* 12:2. doi: 10.3389/fnsys.2018.00002

Fuentes, I. M., Jones, B. M., Brake, A. D., Pierce, A. N., Eller, O. C., Supple, R. M., et al. (2021). Voluntary wheel running improves outcomes in an early life stress-induced model of urologic chronic pelvic pain syndrome in male mice. *Pain* 162, 1681–1691. doi: 10.1097/j.pain.0000000000002178

Fuentes, I. M., Pierce, A. N., Di Silvestro, E. R., Maloney, M. O., and Christianson, J. A. (2017). Differential influence of early life and adult stress on urogenital sensitivity and function in male mice. *Front. Syst. Neurosci.* 11:97. doi: 10.3389/fnsys.2017.00097

Gao, Y., Zhang, R., Chang, H. H., and Rodriguez, L. V. (2017). The role of C-fibers in the development of chronic psychological stress induced enhanced bladder sensations and nociceptive responses: a multidisciplinary approach to the study of urologic chronic pelvic pain syndrome (MAPP) research network study. *Neurourol. Urodyn.* 37, 673–680. doi: 10.1002/nau.23374

Girard, B. M., Campbell, S. E., Beca, K. I., Perkins, M., Hsiang, H., May, V., et al. (2020). Intrabladder PAC1 receptor antagonist, PACAP(6-38), reduces urinary bladder frequency and pelvic sensitivity in mice exposed to repeated variate stress (RVS). *J. Mol. Neurosci.* 71, 1575–1588. doi: 10.1007/s12031-020-01649-x

Girard, B. M., Malley, S., May, V., and Vizzard, M. A. (2016). Effects of CYP-Induced Cystitis on Growth Factors and Associated Receptor Expression in Micturition Pathways in Mice with Chronic Overexpression of NGF in Urothelium. *Journal of Molecular Neuroscience* 59, 531–543. doi: 10.1007/s12031-016-0774-z

Girard, B. M., Tooke, K., and Vizzard, M. A. (2017). PACAP/Receptor system in urinary bladder dysfunction and pelvic pain following urinary bladder inflammation or stress. *Front. Syst. Neurosci.* 11:90. doi: 10.3389/fnsys.2017.00090

Gomita, Y., Yamori, M., Furuno, K., and Araki, Y. (1989). Influences of psychological stress produced by intraspecies emotional communication on nicorandil plasma levels in rats. *Pharmacology* 38, 388–396. doi: 10.1159/000138562

Habib, K. E., Gold, P. W., and Chrousos, G. P. (2001). Neuroendocrinology of stress. *Endocrinol. Metab. Clin. North Am.* 30, 695–728; vii–viii. doi: 10.1016/s0889-8529(05)70208-5

Hammack, S. E., Cheung, J., Rhodes, K. M., Schutz, K. C., Falls, W. A., Braas, K. M., et al. (2009). Chronic stress increases pituitary adenylate cyclase-activating peptide (PACAP) and brain-derived neurotrophic factor (BDNF) mRNA expression in the bed nucleus of the stria terminalis (BNST): roles for PACAP in anxiety-like behavior. *Psychoneuroendocrinology* 34, 833–843. doi: 10.1016/j.psyneuen.2008.12.013

Han, D. Y., Jeong, H. J., and Lee, M. Y. (2015). Bladder hyperactivity induced by chronic variable stress in rats. *Low. Urin. Tract. Symptoms* 7, 56–61. doi: 10.1111/luts.12048

Hanna-Mitchell, A. T., Robinson, D., Cardozo, L., Everaert, K., and Petkov, G. V. (2016). Do we need to know more about the effects of hormones on lower urinary tract dysfunction? ICI-RS 2014. *Neurourol. Urodyn.* 35, 299–303. doi: 10.1002/nau.22809

Harris, R. B. (2015). Chronic and acute effects of stress on energy balance: are there appropriate animal models? *Am. J. Physiol. Regul. Integr. Comp. Physiol.* 308, R250–R265. doi: 10.1152/ajpregu.00361.2014

Hattori, T., Sugaya, K., Nishijima, S., Kadekawa, K., Ueda, T., and Yamamoto, H. (2019). Emotional stress facilitates micturition reflex: possible inhibition by an α1-adrenoceptor blocker in the conscious and anesthetized state. *Int. Neurourol. J.* 23, 100–108. doi: 10.5213/inj.1836284.142

Henry, B., Vale, W., and Markou, A. (2006). The effect of lateral septum corticotropin-releasing factor receptor 2 activation on anxiety is modulated by stress. *J. Neurosci.* 26, 9142–9152. doi: 10.1523/jneurosci.1494-06.2006

Herman, J. P., Flak, J., and Jankord, R. (2008). Chronic stress plasticity in the hypothalamic paraventricular nucleus. *Prog. Brain Res.* 170, 353–364. doi: 10.1016/s0079-6123(08)00429-9

Holschneider, D. P., Wang, Z., Chang, H., Zhang, R., Gao, Y., Guo, Y., et al. (2020a). Ceftriaxone inhibits stress-induced bladder hyperalgesia and alters cerebral micturition and nociceptive circuits in the rat: a multidisciplinary approach to the study of urologic chronic pelvic pain syndrome research network study. *Neurourol. Urodyn.* 39, 1628–1643. doi: 10.1002/nau.24424

Holschneider, D. P., Wang, Z., Guo, Y., Sanford, M. T., Yeh, J., Mao, J. J., et al. (2020b). Exercise modulates neuronal activation in the micturition circuit of chronically stressed rats: a multidisciplinary approach to the study of urologic chronic pelvic pain syndrome (MAPP) research network study. *Physiol. Behav.* 215, 112796. doi: 10.1016/j.physbeh.2019.112796

Huang, S. T., Song, Z. J., Liu, Y., Luo, W. C., Yin, Q., and Zhang, Y. M. (2021). BNST $_{AV}$ ^{GABA}-PVN ^{CRF} circuit regulates visceral hypersensitivity induced by maternal separation in Vgat-Cre mice. *Front. Pharmacol.* 12:615202. doi: 10.3389/fphar.2021.615202

Ihara, T., Nakamura, Y., Mitsui, T., Tsuchiya, S., Kanda, M., Kira, S., et al. (2019). Intermittent restraint stress induces circadian misalignment in the mouse bladder, leading to nocturia. *Sci. Rep.* 9:10069. doi: 10.1038/s41598-019-46517-w

Kalantaridou, S. N., Zoumakis, E., Makrigiannakis, A., Lavasidis, L. G., Vrekoussis, T., and Chrousos, G. P. (2010). Corticotropin-releasing hormone, stress and human reproduction: an update. *J. Reprod. Immunol.* 85, 33–39. doi: 10.1016/j.jri.2010.02.005

Kant, G. J., Mougey, E. H., Pennington, L. L., and Meyerhoff, J. L. (1983). Graded footshock stress elevates pituitary cyclic AMP and plasma beta-endorphin, beta-LPH corticosterone and prolactin. *Life Sci.* 33, 2657–2663. doi: 10.1016/0024-3205(83)90350-8

Klausner, A. P., Ibanez, D., King, A. B., Willis, D., Herrick, B., Wolfe, L., et al. (2009). The influence of psychiatric comorbidities and sexual trauma on lower urinary tract symptoms in female veterans. *J. Urol.* 182, 2785–2790. doi: 10.1016/j.juro.2009.08.035

Kleinhans, N. M., Yang, C. C., Strachan, E. D., Buchwald, D. S., and Maravilla, K. R. (2016). Alterations in connectivity on functional magnetic resonance imaging with provocation of lower urinary tract symptoms: a MAPP research network feasibility study of urological chronic pelvic pain syndromes. *J. Urol.* 195, 639–645. doi: 10.1016/j.juro.2015.09.092

Koolhaas, J. M., de Boer, S. F., and Buwalda, B. (2006). Stress and adaptation: toward ecologically relevant animal models. *Curr. Direct. Psychol. Sci.* 15, 109–112.

Kullmann, F. A., McDonnell, B. M., Wolf-Johnston, A. S., Kanai, A. J., Shiva, S., Chelimsky, T., et al. (2019). Stress-induced autonomic dysregulation of mitochondrial function in the rat urothelium. *Neurourol. Urodyn.* 38, 572–581. doi: 10.1002/nau.23876

Lai, H. H., Rawal, A., Shen, B., and Vetter, J. (2016). The relationship between anxiety and overactive bladder or urinary incontinence symptoms in the clinical population. *Urology* 98, 50–57. doi: 10.1016/j.urology.2016.07.013

Lai, H., Gardner, V., Vetter, J., and Andriole, G. L. (2015a). Correlation between psychological stress levels and the severity of overactive bladder symptoms. *BMC Urol.* 15:14. doi: 10.1186/s12894-015-0009-6

Lai, H., Gereau, R. W. IV, Luo, Y., O'Donnell, M., Rudick, C. N., Pontari, M., et al. (2015b). Animal models of urologic chronic pelvic pain syndromes: findings from the multidisciplinary approach to the study of chronic pelvic pain research network. *Urology* 85, 1454–1465. doi: 10.1016/j.urology.2015.03.007

Lee, U. J., Ackerman, A. L., Wu, A., Zhang, R., Leung, J., Bradesi, S., et al. (2015). Chronic psychological stress in high-anxiety rats induces sustained bladder hyperalgesia. *Physiol. Behav.* 139, 541–548. doi: 10.1016/j.physbeh.2014.11.045

Lifford, K. L., and Curhan, G. C. (2009). Prevalence of painful bladder syndrome in older women. *Urology* 73, 494–498. doi: 10.1016/j.urology.2008.01.053

Ligon, C., Mohammadi, E., Ge, P., Hannig, G., Higgins, C., and Greenwood-Van Meerveld, B. (2018). Linaclotide inhibits colonic and urinary bladder hypersensitivity in adult female rats following unpredictable neonatal stress. *Neurogastroenterol. Motil.* 30:e13375. doi: 10.1111/nmo.13375

Long, C. J., Butler, S., Fesi, J., Frank, C., Canning, D. A., and Zderic, S. A. (2014). Genetic or pharmacologic disruption of the calcineurin-nuclear factor of activated T-cells axis prevents social stress-induced voiding dysfunction in a murine model. *J. Pediatr. Urol.* 10, 598–604. doi: 10.1016/j.jpurol.2014.04.002

Lutgendorf, S. K., Kreder, K. J., Rothrock, N. E., Ratliff, T. L., and Zimmerman, B. (2001). A laboratory stress model for examining stress and symptomatology in interstitial cystitis patients. *Urology* 57(6 Suppl. 1):122. doi: 10.1016/s0090-4295(01)01076-7

Macaulay, A. J., Stern, R. S., Holmes, D. M., and Stanton, S. L. (1987). Micturition and the mind: psychological factors in the aetiology and treatment of urinary symptoms in women. *Br. Med. J. (Clin. Res. Ed.)* 294, 540–543.

Mann, E. A., Alam, Z., Hufgard, J. R., Mogle, M., Williams, M. T., Vorhees, C. V., et al. (2015). Chronic social defeat, but not restraint stress, alters bladder function in mice. *Physiol. Behav.* 150, 83–92. doi: 10.1016/j.physbeh.2015.02.021

Matos, R., Serrao, P., Rodriguez, L., Birder, L. A., Cruz, F., and Charrua, A. (2017). The water avoidance stress induces bladder pain due to a prolonged alpha1A adrenoceptor stimulation. *Naunyn Schmiedebergs Arch. Pharmacol.* 390, 839–844. doi: 10.1007/s00210-017-1384-1

McGonagle, E., Smith, A., Butler, S., Sliwoski, J., Valentino, R., Canning, D., et al. (2012). Water avoidance stress results in an altered voiding phenotype in male mice. *Neurourol. Urodyn.* 31, 1185–1189. doi: 10.1002/nau.22207

McVary, K. T., Rademaker, A., Lloyd, G. L., and Gann, P. (2005). Autonomic nervous system overactivity in men with lower urinary tract symptoms secondary to benign prostatic hyperplasia. *J. Urol.* 174(4 Pt 1), 1327–1433.

Merrill, L., and Vizzard, M. A. (2014). Intravesical TRPV4 blockade reduces repeated variate stress-induced bladder dysfunction by increasing bladder capacity and decreasing voiding frequency in male rats. *Am. J. Physiol. Regul. Integr. Comp. Physiol.* 307, R471–R480. doi: 10.1152/ajpregu.00008.2014

Merrill, L., Malley, S., and Vizzard, M. A. (2013). Repeated variate stress in male rats induces increased voiding frequency, somatic sensitivity, and urinary bladder nerve growth factor expression. *Am. J. Physiol. Regul. Integr. Comp. Physiol.* 305, R147–R156. doi: 10.1152/ajpregu.00089.2013

Mingin, G. C., Heppner, T. J., Tykocki, N. R., Erickson, C. S., Vizzard, M. A., and Nelson, M. T. (2015). Social stress in mice induces urinary bladder overactivity and increases TRPV1 channel-dependent afferent nerve activity. *Am. J. Physiol. Regul. Integr. Comp. Physiol.* 309, R629–R638. doi: 10.1152/ajpregu.00013.2015

Mingin, G. C., Peterson, A., Erickson, C. S., Nelson, M. T., and Vizzard, M. A. (2014). Social stress induces changes in urinary bladder function, bladder NGF content, and generalized bladder inflammation in mice. *Am. J. Physiol. Regul. Integr. Comp. Physiol.* 307, R893–R900. doi: 10.1152/ajpregu.00500.2013

Mohammadi, E., Prusator, D. K., Healing, E., Hurst, R., Towner, R. A., Wisniewski, A. B., et al. (2016). Sexually dimorphic effects of early life stress in rat pups on urinary bladder detrusor muscle contractility in adulthood. *Biol. Sex Differ.* 7:8. doi: 10.1186/s13293-016-0062-1

Nargund, V. H. (2015). Effects of psychological stress on male fertility. *Nat. Rev. Urol.* 12, 373–382. doi: 10.1038/nrurol.2015.112

Ness, T. J., and Elhefni, H. (2004). Reliable visceromotor responses are evoked by noxious bladder distention in mice. *J. Urol.* 171, 1704–1708. doi: 10.1097/01.ju.0000116430.67100.8f

Ness, T. J., DeWitte, C., DeBerry, J. J., and Randich, A. (2018). Neonatal bladder inflammation alters the role of the central amygdala in hypersensitivity produced by Acute Footshock stress in adult female rats. *Brain Res.* 1698, 99–105. doi: 10.1016/j.brainres.2018.06.030

Ness, T. J., Lewis-Sides, A., and Castroman, P. (2001). Characterization of pressor and visceromotor reflex responses to bladder distention in rats: sources of variability and effect of analgesics. *J. Urol.* 165, 968–974.

Okasha, E. F., and Bayomy, N. A. (2010). Protective role of quercetin (Phytochemical) against water avoidance stress induced interstitial cystitis of adult female albino rats light and electron microscopic study. *Egypt. J. Histol.* 33, 649–658.

Oliver, J. L., Campigotto, M. J., Coplen, D. E., Traxel, E. J., and Austin, P. F. (2013). Psychosocial comorbidities and obesity are associated with lower urinary tract symptoms in children with voiding dysfunction. *J. Urol.* 190(Suppl. 4), 1511–1515. doi: 10.1016/j.juro.2013.02.025

Ozaki, T., Matsuoka, J., Tsubota, M., Tomita, S., Sekiguchi, F., Minami, T., et al. (2018). Zinc deficiency promotes cystitis-related bladder pain by enhancing function and expression of Cav3.2 in mice. *Toxicology* 393, 102–112. doi: 10.1016/j.tox.2017.11.012

Pacák, K. (2000). Stressor-specific activation of the hypothalamic-pituitary-adrenocortical axis. *Physiol. Res.* 49(Suppl. 1), S11–S17.

Pare, W. P. (1992). Learning behavior, escape behavior, and depression in an ulcer susceptible rat strain. *Integr. Physiol. Behav. Sci.* 27, 130–141.

Pierce, A. N., Di Silvestro, E. R., Eller, O. C., Wang, R., Ryals, J. M., and Christianson, J. A. (2016). Urinary bladder hypersensitivity and dysfunction in female mice following early life and adult stress. *Brain Res.* 1639, 58–73. doi: 10.1016/j.brainres.2016.02.039

Pierce, A. N., Eller-Smith, O. C., and Christianson, J. A. (2018). Voluntary wheel running attenuates urinary bladder hypersensitivity and dysfunction following neonatal maternal separation in female mice. *Neurourol. Urodyn.* 37, 1623–1632. doi: 10.1002/nau.23530

Rivier, C., and Vale, W. (1987). Diminished responsiveness of the hypothalamic-pituitary-adrenal axis of the rat during exposure to prolonged stress: a pituitary-mediated mechanism. *Endocrinology* 121, 1320–1328. doi: 10.1210/endo-121-4-1320

Robbins, M. T., and Ness, T. J. (2008). Footshock-induced urinary bladder hypersensitivity: role of spinal corticotropin-releasing factor receptors. *J. Pain* 9, 991–998. doi: 10.1016/j.jpain.2008.05.006

Robbins, M. T., Deberry, J., Randich, A., and Ness, T. J. (2011). Footshock stress differentially affects responses of two subpopulations of spinal dorsal horn neurons to urinary bladder distension in rats. *Brain Res.* 1386, 118–126. doi: 10.1016/j.brainres.2011.02.081

Robbins, M., DeBerry, J., and Ness, T. (2007). Chronic psychological stress enhances nociceptive processing in the urinary bladder in high-anxiety rats. *Physiol. Behav.* 91, 544–550. doi: 10.1016/j.physbeh.2007.04.009

Rothrock, N. E., Lutgendorf, S. K., Kreder, K. J., Ratliff, T., and Zimmerman, B. (2001). Stress and symptoms in patients with interstitial cystitis: a life stress model. *Urology* 57, 422–427.

Rudick, C. N., Chen, M. C., Mongiu, A. K., and Klumpp, D. J. (2007). Organ cross talk modulates pelvic pain. *Am. J. Physiol. Regul. Integr. Comp. Physiol.* 293, R1191–R1198. doi: 10.1152/ajpregu.00411.2007

Saglam, B., Cikler, E., Zeybek, A., Cetinel, S., Sener, G., and Ercan, F. (2006). An aqueous garlic extract alleviates water avoidance stress-induced degeneration of the urinary bladder. *BJU Int.* 98, 1250–1254. doi: 10.1111/j.1464-410X.2006.06511.x

Sanford, M. T., Yeh, J. C., Mao, J. J., Guo, Y., Wang, Z., Zhang, R., et al. (2020). Voluntary exercise improves voiding function and bladder hyperalgesia in an animal model of stress-induced visceral hypersensitivity: a multidisciplinary approach to the study of urologic chronic pelvic pain syndrome research network study. *Neurourol. Urodyn.* 39, 603–612. doi: 10.1002/nau.24270

Scharf, S. H., and Schmidt, M. V. (2012). Animal models of stress vulnerability and resilience in translational research. *Curr. Psychiatry Rep.* 14, 159–165. doi: 10.1007/s11920-012-0256-0

Schneiderman, N., Ironson, G., and Siegel, S. (2005). Stress and health: psychological, behavioral, and biological determinants. *Annu. Rev. Clin. Psychol.* 1, 607–628. doi: 10.1146/annurev.clinpsy.1.102803.144141

Seki, M., Zha, X. M., Inamura, S., Taga, M., Matsuta, Y., Aoki, Y., et al. (2019). Role of corticotropin-releasing factor on bladder function in rats with psychological stress. *Sci. Rep.* 9:9828. doi: 10.1038/s41598-019-46267-9

Shimizu, T., Shimizu, S., Higashi, Y., and Saito, M. (2021). Psychological/mental stress-induced effects on urinary function: possible brain molecules related to psychological/mental stress-induced effects on urinary function. *Int. J. Urol.* 28, 1093–1104. doi: 10.1111/iju.14663

Smith, A. L., Leung, J., Kun, S., Zhang, R., Karagiannides, I., Raz, S., et al. (2011). The effects of acute and chronic psychological stress on bladder function in a rodent model. *Urology* 78:967.e1–e7. doi: 10.1016/j.urology.2011.06.041

Sterrenburg, L., Gaszner, B., Boerrigter, J., Santbergen, L., Bramini, M., Elliott, E., et al. (2011). Chronic stress induces sex-specific alterations in methylation and expression of corticotropin-releasing factor gene in the rat. *PLoS One* 6:e28128. doi: 10.1371/journal.pone.0028128

Stewart, W. F., Van Rooyen, J. B., Cundiff, G. W., Abrams, P., Herzog, A. R., Corey, R., et al. (2003). Prevalence and burden of overactive bladder in the United States. *World J. Urol.* 20, 327–336. doi: 10.1007/s00345-002-0301-4

Tache, Y., Larauche, M., Yuan, P. Q., and Million, M. (2018). Brain and Gut CRF signaling: biological actions and role in the gastrointestinal tract. *Curr. Mol. Pharmacol.* 11, 51–71. doi: 10.2174/1874467210666170224095741

Tykocki, N. R., Heppner, T. J., Erickson, C. S., van Batavia, J., Vizzard, M. A., Nelson, M. T., et al. (2018). Development of stress-induced bladder insufficiency requires functional TRPV1 channels. *Am. J. Physiol. Renal Physiol.* 315, F1583–F1591. doi: 10.1152/ajprenal.00231.2018

Ullmann, E., Chrousos, G., Perry, S. W., Wong, M.-L., Licinio, J., Bornstein, S. R., et al. (2020). Offensive behavior, striatal glutamate metabolites, and limbic–hypothalamic–pituitary–adrenal responses to stress in chronic anxiety. *Int. J. Mol. Sci.* 21:7440. doi: 10.3390/ijms21207440

Ulrich-Lai, Y. M., and Herman, J. P. (2009). Neural regulation of endocrine and autonomic stress responses. *Nat. Rev. Neurosci.* 10, 397–409. doi: 10.1038/nrn2647

Vanneste, M., Segal, A., Voets, T., and Everaerts, W. (2021). Transient receptor potential channels in sensory mechanisms of the lower urinary tract. *Nat. Rev. Urol.* 18, 139–159. doi: 10.1038/s41585-021-00428-6

Wang, Z., Chang, H. H., Gao, Y., Zhang, R., Guo, Y., Holschneider, D. P., et al. (2017). Effects of water avoidance stress on peripheral and central responses during bladder filling in the rat: a multidisciplinary approach to the study of urologic chronic pelvic pain syndrome (MAPP) research network study. *PLoS One* 12:e0182976. doi: 10.1371/journal.pone.0182976

Weiss, D. A., Butler, S. J., Fesi, J., Long, C. J., Valentino, R. J., Canning, D. A., et al. (2015). Putting the past behind us: social stress-induced urinary retention can be overcome. *J. Pediatr. Urol.* 11, 188–194. doi: 10.1016/j.jpurol.2015.04.018

West, E. G., Sellers, D. J., Chess-Williams, R., and McDermott, C. (2021). Bladder overactivity induced by psychological stress in female mice is associated with enhanced bladder contractility. *Life Sci.* 265, 118735. doi: 10.1016/j.lfs.2020.118735

West, E. G., Sellers, D. J., Chess-Williams, R., and McDermott, C. (2020). Voiding behavior and efferent bladder function altered in mice following social defeat but not witness trauma. *Front. Physiol.* 11:247. doi: 10.3389/fphys.2020.00247

Wingfield, J. C., and Sapolsky, R. M. (2003). Reproduction and resistance to stress: when and how. *J. Neuroendocrinol.* 15, 711–724. doi: 10.1046/j.1365-2826.2003.01033.x

Wood, R., Eichel, L., Messing, E. M., and Schwarz, E. (2001). Automated noninvasive measurement of cyclophosphamide-induced changes in murine micturition frequency and volume and demonstration of pharmacologic sensitivity. *Urology* 57(6 Suppl. 1), 115–116. doi: 10.1016/s0090-4295(01)01059-7

Wood, S. K., Baez, M. A., Bhatnagar, S., and Valentino, R. J. (2009). Social stress-induced bladder dysfunction: potential role of corticotropin-releasing factor. *Am. J. Physiol. Regul. Integr. Comp. Physiol.* 296, R1671–R1678. doi: 10.1152/ajpregu.91013.2008

Wood, S. K., McFadden, K. V., Grigoriadis, D., Bhatnagar, S., and Valentino, R. J. (2012). Depressive and cardiovascular disease comorbidity in a rat model of social stress: a putative role for corticotropin-releasing factor. *Psychopharmacology (Berl.)* 222, 325–336. doi: 10.1007/s00213-012-2648-6

Wood, S. K., McFadden, K., Griffin, T., Wolfe, J. H., Zderic, S., and Valentino, R. J. (2013). A corticotropin-releasing factor receptor antagonist improves urodynamic dysfunction produced by social stress or partial bladder outlet obstruction in male rats. *Am. J. Physiol. Regul. Integr. Comp. Physiol.* 304, R940–R950. doi: 10.1152/ajpregu.00257.2012

Wu, H.-Y., and de Groat, W. C. (2006). Maternal separation uncouples reflex from spontaneous voiding in rat pups. *J. Urol.* 175, 1148–1151. doi: 10.1016/s0022-5347(05)00321-6

Yamamoto, K., Takao, T., Nakayama, J., Kiuchi, H., Okuda, H., Fukuhara, S., et al. (2012). Water avoidance stress induces frequency through cyclooxygenase-2 expression: a bladder rat model. *Int. J. Urol.* 19, 155–162. doi: 10.1111/j.1442-2042.2011.02905.x

Yang, S. S., Chang, H. H., and Chang, S. J. (2020). Does ketamine ameliorate the social stress-related bladder dysfunction in mice? *Neurourol. Urodyn.* 39, 935–944. doi: 10.1002/nau.24324

Yoon, H., Lee, D., Chun, K., Yoon, H., and Yoo, J. (2010). Effect of stress on the expression of rho-kinase and collagen in rat bladder tissue. *Korean J. Urol.* 51, 132–138. doi: 10.4111/kju.2010.51.2.132

Yoshimura, N., Oguchi, T., Yokoyama, H., Funahashi, Y., Yoshikawa, S., Sugino, Y., et al. (2014). Bladder afferent hyperexcitability in bladder pain syndrome/interstitial cystitis. *Int. J. Urol.* 21(Suppl. 1), 18–25. doi: 10.1111/iju.12308

Yu, W., Ackert-Bicknell, C., Larigakis, J. D., MacIver, B., Steers, W. D., Churchill, G. A., et al. (2014). Spontaneous voiding by mice reveals strain-specific lower urinary tract function to be a quantitative genetic trait. *Am. J. Physiol. Renal Physiol.* 306, F1296–F1307. doi: 10.1152/ajprenal.00074.2014

Zeybek, A., Saglam, B., Cikler, E., Cetinel, S., Ercan, F., and Sener, G. (2007). Taurine ameliorates stress-induced degeneration of the urinary bladder. *Acta Histochem.* 109, 208–214. doi: 10.1016/j.acthis.2006.12.001

Zhang, C., Hai, T., Yu, L., Liu, S., Li, Q., Zhang, X., et al. (2013). Association between occupational stress and risk of overactive bladder and other lower urinary tract symptoms: a cross-sectional study of female nurses in China. *Neurourol. Urodyn.* 32, 254–260. doi: 10.1002/nau.22290

Zvarova, K., and Vizzard, M. A. (2006). Changes in galanin immunoreactivity in rat micturition reflex pathways after cyclophosphamide-induced cystitis. *Cell Tissue Res.* 324, 213–224. doi: 10.1007/s00441-005-0114-z

Conflict of Interest: The authors declare that the research was conducted in the absence of any commercial or financial relationships that could be construed as a potential conflict of interest.

frontiers in Physiology

ORIGINAL RESEARCH
published: 28 March 2022
doi: 10.3389/fphys.2022.860342

Enhanced RAGE Expression and Excess Reactive-Oxygen Species Production Mediates Rho Kinase-Dependent Detrusor Overactivity After Methylglyoxal Exposure

*Akila L. Oliveira[1], Matheus L. Medeiros[1], Mariana G. de Oliveira[1], Caio Jordão Teixeira[2], Fabíola Z. Mónica[1] and Edson Antunes[1]**

[1]Department of Pharmacology, University of Campinas (UNICAMP), Campinas, Brazil, [2]Department of Physiology and Biophysics, Institute of Biomedical Science, University of Sao Paulo, Sao Paulo, Brazil

OPEN ACCESS

Edited by:
Russ Chess-Williams, Bond University, Australia

Reviewed by:
Maryrose Sullivan, Harvard Medical School, United States
José Eduardo Da Silva Santos, Federal University of Santa Catarina, Brazil

***Correspondence:**
Edson Antunes
eantunes@unicamp.br

Specialty section:
This article was submitted to Integrative Physiology, a section of the journal Frontiers in Physiology

Received: *22 January 2022*
Accepted: *11 March 2022*
Published: *28 March 2022*

Citation:
Oliveira AL, Medeiros ML, de Oliveira MG, Teixeira CJ, Mónica FZ and Antunes E (2022) Enhanced RAGE Expression and Excess Reactive-Oxygen Species Production Mediates Rho Kinase-Dependent Detrusor Overactivity After Methylglyoxal Exposure. Front. Physiol. 13:860342. doi: 10.3389/fphys.2022.860342

Methylglyoxal (MGO) is a highly reactive dicarbonyl compound implicated in diabetes-associated diseases. In vascular tissues, MGO induces the formation of advanced glycation end products (AGEs) that bounds its receptor RAGE, initiating the downstream tissue injury. Outside the cardiovascular system, MGO intake produces mouse voiding dysfunction and bladder overactivity. We have sought that MGO-induced bladder overactivity is due to activation of AGE-RAGE-reactive-oxygen species (ROS) signaling cascade, leading to Rho kinase activation. Therefore, female mice received 0.5% MGO orally for 12 weeks, after which *in vitro* bladder contractions were evaluated in the presence or not of superoxide dismutase (PEG-SOD) or the Rho kinase inhibitor Y27632. Treatment with MGO significantly elevated the serum levels of MGO and fluorescent AGEs, as well as the RAGE immunostaining in the urothelium, detrusor, and vascular endothelium. RAGE mRNA expression in the bladder was also higher in the MGO group. Methylglyoxal significantly increased the ROS production in both urothelium and detrusor smooth muscle, with the increases in detrusor markedly higher than urothelium. The bladder activity of superoxide dismutase (SOD) was significantly reduced in the MGO group. Gene expressions of L-type Ca^{2+} channels, RhoA, ROCK-1, and ROCK-2 in bladder tissues were significantly elevated in the MGO group. Increased bladder contractions to electrical-field stimulation, carbachol α,β-methylene ATP, and extracellular Ca^{2+} were observed after MGO exposure, which was significantly reduced by prior incubation with either PEG-SOD or Y27632. Overall, our data indicate serum MGO accumulation elevates the AGEs levels and activates the RAGE-ROS signaling leading to Rho kinase-induced muscle sensitization, ultimately leading to detrusor overactivity.

Keywords: advanced glycation end products, rage, urothelium, Y27632, superoxide dismutase, L-type Ca^{2+} channels

INTRODUCTION

Methylglyoxal (MGO) is a highly reactive dicarbonyl compound generated during glycolysis in the presence of high glucose levels (Rabbani and Thornalley, 2015). High levels of MGO are found in the plasma of patients with diabetes mellitus (Kilhovd et al., 2003; Han et al., 2009), and this high glucose-mediated increase of MGO production is believed to account for the cell damage in diabetes-associated pathological conditions (Liu et al., 2012). MGO modifies lysine, arginine, and cysteine residues in peptides or proteins to yield irreversible advanced glycation end products (AGEs), leading to cross-linking and denaturation of proteins (Liu et al., 2012). AGEs bound its receptor RAGE, which is a member of the immunoglobulin superfamily of cell surface receptors that can recognize endogenous ligands (Kim et al., 2021). Upon activation, RAGE triggers multiple intracellular signaling pathways, including the activation of NADPH oxidase, producing excess reactive-oxygen species (ROS) levels (Nowotny et al., 2015; Rabbani and Thornalley, 2015; Mey and Haus, 2018).

RhoA/Rho-kinase activation by different GPCR agonist plays a critical role in the regulation of actin cytoskeleton dynamics and generation of actin-myosin contractility in vascular and non-vascular smooth muscles (Peters et al., 2006; Shimokawa et al., 2016). Rho kinase is a serine/threonine kinase with a molecular weight of 160 kDa, and comprises two isoforms, ROCK1 and ROCK2 (Nunes and Webb, 2020). The activity of RhoA is controlled by the guanine nucleotide exchange factors (GEFs) that catalyze the exchange of the inactive Rho-GDP for the active Rho-GTP state, which interacts with the downstream effector Rho kinase, ultimately leading to Ca^{2+} sensitization and contraction (Nunes and Webb, 2020). The smooth muscle contraction involves a balance between myosin light chain kinase (MLCK) and myosin light chain phosphatase (MLCP), where the MLC phosphorylation enhances the contractile mechanism. MLCP enzyme consists of three subunits, namely, the catalytic subunit PP1cδ, the regulatory subunit MYPT1, and a 20 kDa subunit. MYPT1 modulates Ca^{2+}-dependent phosphorylation of MLC by MLCK. Activation of Rho-kinase regulates the phosphorylation level of MLC by directly phosphorylating this enzyme and by inactivating MLCP through phosphorylation of MYPT1 at Thr697 and Thr855, thus enhancing the MLC phosphorylation (MacDonald and Walsh, 2018). In addition, the RhoA/Rho kinase pathway is one of the major intracellular pathways that enhance the expressions of molecules for oxidative stress (Hobbs et al., 2014; Strassheim et al., 2019). Previous studies showed that reactive-oxygen species (ROS) enhances the Rho-GTPase activity (Heo and Campbell, 2005; Aghajanian et al., 2009). In pulmonary vascular smooth muscle under chronic hypoxia, ROS generation was shown to mediate the Ca^{2+} sensitization and vasoconstriction through upregulation of RhoA/ROCK signaling (MacKay et al., 2017; Yan et al., 2020). The impairment of corpus cavernosum relaxations diabetic mice were associated with upregulation of the RhoA/Rho-kinase signaling pathway and increased oxidative stress (Li et al., 2012; Priviero et al., 2016). In isolated cells, Rho kinase activation also increase the ROS production (Lu et al., 2013; Fujimoto et al., 2017; Cap et al., 2020).

Metabolic diseases are clinically characterized by elevated blood glucose levels that are associated with complications such as kidney and heart disease, and microvascular and macrovascular alterations. Outside the cardiovascular system, metabolic factors play important roles in the development of overactive bladder syndrome (OAB), urinary incontinence, and other lower urinary tract symptoms (LUTS) (Lai et al., 2019; Wittig et al., 2019), which may be due to alterations at the level of the detrusor smooth muscle, urothelium and neuronal innervation (Daneshgari et al., 2017). In animal models of diabetes, micturition dysfunction is characterized by increases in void number, volume, and capacity, despite conflicting data have been obtained depending on the model used (Gasbarro et al., 2010; Leiria et al., 2011; Leiria et al., 2012; Wu et al., 2016; Ellenbroek et al., 2018; Yang et al., 2019; Kim et al., 2020). More recently, we have reported a model of bladder dysfunction induced by 4- and 12-weeks intake of MGO to healthy male mice (de Oliveira et al., 2020; Oliveira et al., 2021), which differs from the classical diabetic animals in that MGO is not generated from the endogenous glucose metabolism and therefore does not affect the glucose levels and insulin sensitivity (Medeiros et al., 2020). Urodynamic evaluation of MGO-treated mice revealed significant increases of micturition frequency and the number of non-voiding contractions (NVCs), along with enhanced *in vitro* bladder contractility to muscarinic and P2X1 receptor activation. We tested here the hypothesis that MGO-induced bladder overactivity is a consequence of the activation of the AGE-RAGE-ROS axis, ultimately leading to upregulation of the Rho kinase system in detrusor smooth muscle. Therefore, in intact or mucosa-denuded mouse bladder strips, we carried out molecular and biochemical assays for RAGE, ROS, L-type Ca^{2+} channels, and Rho kinase expressions and evaluated the *in vitro* contractile responses in the presence of superoxide dismutase (SOD) and the Rho kinase inhibitor Y27632.

MATERIALS AND METHODS

Animals and Treatment With MGO

Five-week-old female C57BL/6 mice weighing 18 ± 0.30 g at the beginning of the study were housed in cages (three mice per cage) made of polypropylene with dimensions 30 × 20 × 13 cm) located in a ventilated cage shelters with a constant humidity of 55 ± 5% and temperature of 24 ± 1°C under a 12 h light-dark cycle. The animals were acclimated for 7 days before starting the treatments. Animals received standard food *ad libitum* and filtered water. Animal procedures and experimental protocols were approved by Ethics Committee in Animal Use, State University of Campinas (CEUA-UNICAMP; Protocol No. 5443-1/2019). The animals were randomly assigned using a number randomization calculator (available at https://www.graphpad.com). Animals received 0.5% MGO (Sigma Aldrich, Missouri, United States) in the drinking water for 12 weeks, whereas control mice received tap water alone. The doses and route of administration of MGO used were chosen according to a previous study in mice (Medeiros et al., 2020). Body weights, water consumption, and food consumption were assessed weekly in all groups. Animal studies are reported in compliance with the ARRIVE guidelines.

Measurements of Levels of MGO, Fluorescent AGEs and Glucose

Peripheral blood (0.5 ml) was collected by the intracardiac puncture. Blood was centrifuged at 5,000 × g for 10 min at 4°C and serum was transferred to microcentrifuge tubes. To measure MGO levels in serum, the samples were deproteinized using Deproteinizing Sample Preparation Kit - TCA (Abcam ab204708) according to the manufacturer's instructions. Serum levels of MGO were measured using ELISA competitive kit for OxiSelect™ Methylglyoxal (Catalog No. STA-811, Cell Biolabs, San Diego, CA, United States). F-AGEs in serum were measured diluting the samples 1:2 in phosphate-buffered saline (PBS, pH 7.4), and transferred to black 96-well plates, 200 µl total per well. Fluorescence spectra were recorded in duplicate on a fluorometer (SynergyTM H1 Hybrid Reader, Biotek, United States). The excitation and emission wavelengths were 360 and 447 nm, respectively, and the PBS solution was used as blank. Individual concentrations were normalized by blank fluorescence. The fluorescence intensity was expressed in arbitrary units (a.u.). To assess glucose concentration, animals fasted for 8 h, blood from the tail vein was collected and glucose was measured using ACCUCHECK Blood Glucose (Monitoring System®, Roche Diagnostics, Indianapolis, United States).

Measurements of Superoxide Dismutase Activity in Bladder Tissue

For the measurement of SOD activity, bladder tissue was homogenized following the manufacturer's protocol, and bladder homogenate (supernatant) was used for measurement of enzymatic SOD assay kit (Cayman Chemical, Catalog No 706002, Ann Arbor, MI, United States).

Bladder Histology

The animals were weighed and anesthetized with isoflurane in a concentration greater than 5% and cervical dislocation was performed to confirm the euthanasia. The bladder was removed and weighed wet for determination of the relative bladder weight (bladder to body ratio). The bladder was fixed with 10% phosphate-buffered formalin for 24 h, dehydrated in ethanol, and embedded in paraffin. Tissues were sliced (5-µm sections) on a microtome (Leica, Wetzlar, Germany), dewaxed in xylene, rehydrated in gradient alcohol, and stained with Haematoxylin & Eosin (H&E) and Masson trichrome for light microscopy examination. Digital images were obtained with a microscope Eclipse 80i (Nikon, Tokyo, Japan) equipped with a digital camera (DS-U3, Nikon). The thickness of urothelium and detrusor smooth muscle, and the collagen content were evaluated using the Fiji version of the ImageJ Software (Version 1.46r), according to a previous study (Oliveira et al., 2021).

Immunohistochemistry for RAGE

Bladder immunoperoxidase reactions were processed based on previous studies (Medeiros et al., 2021). Briefly, bladder samples were removed, immersed in 10% formalin fixative solution for 48 h, and embedded in paraffin. Five-micron sections were mounted onto aminopropyltriethoxysilane-coated glass slides. Sections were deparaffinized, rehydrated, and washed with 0.05 M Tris buffer solution (TBS) at pH 7.4. Subsequently, for antigen retrieval, sections were treated with 0.01 M Tris-EDTA buffer containing 0.05% Tween-20 (pH 9.0) for 24 min at 98°C. Endogenous peroxidase activity was inhibited with 0.3% hydrogen peroxide (H_2O_2) solution. For blocking the non-specific sites, a 5% bovine serum albumin (BSA) solution containing 0.1% Tween-20 for 60 min was used. Sections were incubated with mouse monoclonal anti-RAGE primary antibody (1:70; Cat. No. ab54741, Abcam, Cambridge, United Kingdom) diluted in TBS containing 3% BSA overnight at 4°C. Subsequently, sections were washed, and incubated with biotinylated goat anti-mouse IgG, avidin and biotinylated HRP (1:20; Cat. No. EXTRA2, Sigma Aldrich, St Louis, MO, United States) following all the manufacturer's instructions. For detection of the immunostained area with RAGE, a 3.3′ diaminobenzidine solution (DAB; cat. no. D4293, Sigma Aldrich) was employed. As a negative control, a section was used in parallel to primary antibody omission. As a positive control, sections of mouse lungs were used (Medeiros et al., 2021). All slides were counterstained with hematoxylin and mounted for observation by microscopy. Representative images were acquired using a light microscope Leica DM 5000B (Leica Microsystems Inc., Buffalo Grove, IL, United States) equipped with a digital camera under a ×40 objective.

Measurement of ROS Levels in Bladder Tissues

The oxidative fluorescent dye dihydroethidium (DHE) was used to evaluate *in situ* ROS generation. The bladders were embedded in a freezing medium and transverse sections (12-µm) were obtained on a cryostat, collected in glass slides, equilibrated for 10 min in Hank's solution (1.6 mM $CaCl_2$, 1.0 mM $MgSO_4$, 145.0 mM NaCl, 5.0 KCl, 0.5 mM NaH_2PO_4, 10.0 mM Glucose, 10.0 HEPES, pH 7.4). Fresh Hank's DHE solution (2 µM) was applied to each tissue section, and the slides were incubated in a light-protected humidified chamber at 37°C for 30 min. Images were obtained with a microscope (Eclipse 80i, Nikon, Tokyo, Japan) equipped for epifluorescence (excitation at 488 nm; emission at 610 nm) and a digital camera (DS-U3, Nikon). Fluorescence was detected with a 585 nm long-pass filter. The number of nuclei labeled with ethidium bromide was automatically counted in separated detrusor smooth muscle and urothelium using ImageJ software (NIH, Maryland, United States), and expressed as labeled nuclei per square millimeter.

Quantitative Real-Time RT-PCR (qPCR) for RAGE, L-type Ca^{2+} Channels (Cacn1), RhoA, ROCK1 and ROCK2

Total RNA was extracted from freshly dissected bladders using TRIzol® reagent (Invitrogen, MS, United States), according to

TABLE 1 | Primer sequences used for real-time PCR amplifications.

Gene	Forward	Reverse
RAGE (IDT Integrated DNA Tecnhologies)	5′-CTGAACTCACAGCCAGTGTCCC-3′	5′-CCCTGACTCGGAGTT-3′
Cacn1 (Exxtend Oligo Solutions)	5′-ACCCTCCTCCGTCGAATTC-3′	5′-GTGTGCCATCGCTGTTCAGA-3′
RHOA (Exxtend Oligo Solutions)	5′-CCTTCGGAATGACGAGCAC-3′	5′-AGATGAGGCACCCAGACTTTT-3′
ROCK1 (Exxtend Oligo Solutions)	5′-ACCCACCATCTGGCTTTGTC-3′	5′-CGGTTTATCAGGTAGCATCCC-3′
ROCK 2 (Exxtend Oligo Solutions)	5′-GATGGTTGTCATTGCCTGTGC-3′	5′-TGCTCTTTATCTTGTTCGCTGT-3′
ACTB (Qiagen Quantitec Primers Assays)	QT00095242	NM_007,393

the manufacturer's protocol. Dnase treated RNA samples were then transcribed with High-Capacity Reverse Transcription Kit® (Applied Biosystems, CA, United States). cDNA samples concentrations were quantified using a spectrophotometer (Nanodrop Lite®, Thermo Scientific, Massachusetts, United States). Synthetic oligonucleotide primers (**Table 1**) were obtained from Integrated DNA Technologies (Iowa, United States), Exxtend Oligo Solutions (Brazil) and Qiagen Quantitec Primeras Assays (Germany). The reactions were performed with 10 ng cDNA, 6 µl SYBR Green Master Mix® (Life Technologies, CA, United States), and the optimal primer concentration in a total volume of 12 µl. Real-time PCR was performed in the equipment StepOne-Plus® Real Time PCR System (Applied Biosystems). The reaction program was 95°C for 10 min, followed by 40 cycles of 95°C for 15 s then 60°C for 1 min. At the end of a normal amplification, a degradation time was added, during which the temperature increased gradually from 60 to 95°C. Threshold cycle (Ct) was defined as the point at which the fluorescence rises appreciably above the background fluorescence. To determine the specificity of the amplification, the melting curve analysis of the PCR products was performed to ensure that only one fragment was amplified. To determine the specificity of the amplification, the melting curve analysis of the PCR products was performed to ensure that only one fragment was amplified. The $2^{-\Delta\Delta Ct}$ method was utilized to analyze the results, which were expressed by the difference between Ct values of chosen genes and the housekeeping gene β–actin. The signal strength for β–actin did not differ between groups (Ct: 19.06 ± 0.33 and 18.95 ± 0.24 for control and MGO respectively).

Bladder Preparation and Organ Bath Set-up

The animals were weighed and anesthetized with isoflurane in a concentration greater than 5% and cervical dislocation was performed to confirm the euthanasia. The bladder was removed and weighed wet for determination of the relative bladder weight (bladder to body ratio), after which it was carefully divided into 2 strips. In one bladder strip, the urothelium with the lamina propria was carefully removed using fine-tip forceps whereas the other strip remained with the mucosa intact. Strips were mounted in 10 ml organ baths containing Krebs–Henseleit solution (117 mM NaCl, 4.7 mM KCl, 2.5 mM $CaCl_2$, 1.2 mM $MgSO_4$, 1.2 mM KH_2PO_4, 25 mM $NaHCO_3$ and 11 mM Glucose, pH 7.4) continuously bubbled with a mixture of 95% O_2 and 5% CO_2. Tissues were allowed to equilibrate for 45 min under resting tension and then adjusted for 5 mN. Changes in isometric force were recorded using a PowerLab system (ADInstruments Inc., Sydney, AU).

Bladder Contractions Induced by Electrical-Field Stimulation

EFS was applied to intact and mucosa-denuded bladder strips placed between two platinum ring electrodes connected to a stimulator (Grass Technologies, Rodhe Island, United States). EFS was conducted at 80 V, 1 ms pulse width, and trains of stimuli lasting 10 s at varying frequencies (1–32 Hz) with 2 min intervals between stimulations. In a separate set of experiments of mucosa-denuded bladders, strips were preincubated (30 min) with either the Rho-kinase inhibitor Y27632 (1 µM) (Catalog No Y0503, Sigma-Aldrich, United States) or superoxide dismutase-polyethylene glycol (PEG-SOD; 87 IU/ml; Catalog No S9549, Sigma-Aldrich, United States) prior to application of EFS. The contractile responses were expressed as mN/mg.

Concentration-Response Curves to Carbachol and α,β-Methylene ATP

Cumulative concentration-response curves to the muscarinic receptor agonist carbachol (1 nM–100 µM; Sigma Aldrich, Missouri, United States) were constructed in both intact and mucosa-denuded preparations. In the mucosa-denuded strips, Y27632 (1 µM) or PEG-SOD (87 IU/ml) was preincubated (30 min) prior to construction of concentration-response curves to carbachol. Non-linear regression analysis to determine the potency (pEC_{50}) of carbachol was carried out using GraphPad Prism (GraphPad Software, Inc., California, United States) with the constraint that F = 0. Concentration-response data were fitted to a log dose-response function with a variable slope in the form: E = Emax/([1 + (10c/10x) n] + F), where E is the effect of above basal, Emax is the maximum response produced by agonists; c is the logarithm of the pEC_{50}, the concentration of drug that produces a half maximal response; x is the logarithm of the concentration of the drug; the exponential term, *n*, is a curve-fitting parameter that defines the slope of the concentration–response line, and F is the response observed in the absence of added drug.

In separate bladder strips, non-cumulative curves to the P2X1 purinergic agonist α,β-methylene ATP (1, 3 and 10 µM; Sigma Aldrich, Missouri, United States) were constructed in intact and

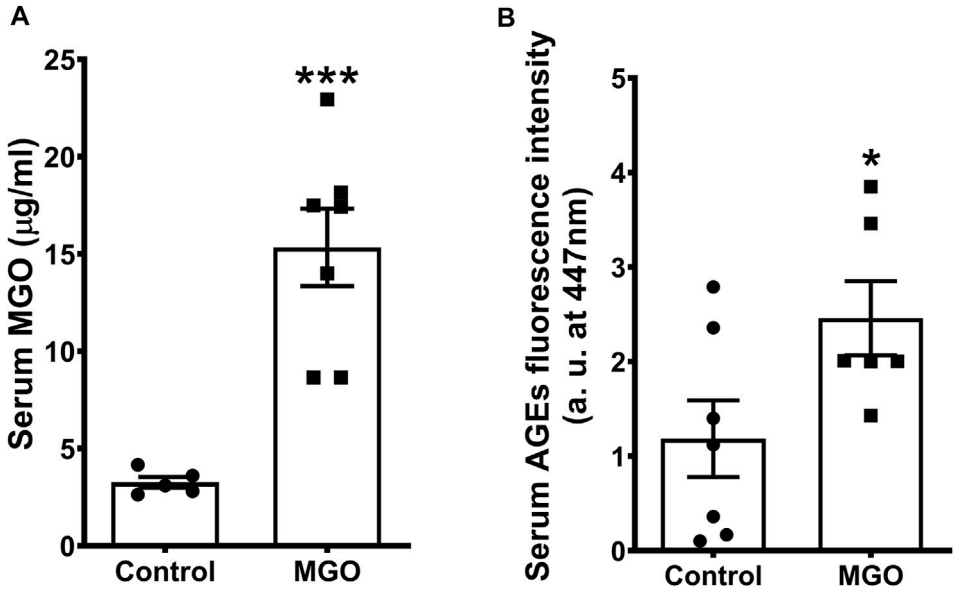

FIGURE 1 | Serum levels of methylglyoxal (MGO) **(A)** and fluorescent advanced glycation end products (F-AGEs **(B)** in mice receiving or not 0.5% MGO for 12 weeks in the drinking water. Data are expressed as mean ± SEM (n = 5–7). *p < 0.05, ***p < 0.001 compared with control group (unpaired t-test).

mucosa-denuded bladder strips using 20-min intervals between concentrations to avoid tachyphylaxis. The contractile responses were expressed as mN per milligram of wet tissue (mN/mg). To verify the viability of the preparations, 80 mM KCl solution was added to the baths at the end of equilibration time.

Pharmacological Evaluation of Bladder Contraction to Extracellular Ca^{2+} Influx

Cumulative concentration-response curves to extracellular $CaCl_2$ (10 μM–100 mM) in intact and mucosa-denuded bladder strips were constructed according to a previous study (Leiria et al., 2011). Briefly, tissues were equilibrated for 45 min in 10 mL-organ baths containing Krebs-Henseleit solution, after which the bath solution was removed and replaced by a Ca^{2+}-free Krebs solution containing EGTA (1 mM) to sequester Ca^{2+} ions. The preparations were contracted with KCl (80 mM) followed by contractions with carbachol (10 μM) to deplete intracellular Ca^{2+}. Next, preparations were incubated with cyclopiazonic acid (CPA; 10 μM) for 30 min to block sarcoplasmic reticulum Ca^{2+} stores. Concentration-responses curves to $CaCl_2$ were then constructed. Mucosa-denuded bladder strips were preincubated (30 min) with either Y27632 (1 μM) or PEG-SOD (87 IU/ml) before construction of concentration-response curves to $CaCl_2$.

Statistical Analysis

Data were expressed as the mean ± standard error of the mean (SEM) of 23 mice (bladder measures) or 5 to 8 (other parameters) per group. The GraphPad Prism Version 6 Software (GraphPad Software Inc.) was used for all statistical analysis. Statistical difference between groups was determined by ANOVA and Tukey's post-test. Student's unpaired t-test was used when appropriate. $p < 0.05$ was accepted as significant.

RESULTS

Levels of Methylglyoxal, F-AGEs and Glucose

The serum MGO concentration after 12-weeks oral dose of 0.5% MGO was 4.8-fold higher than control mice ($p < 0.01$; **Figure 1A**). Serum levels of F-AGEs were also significantly increased in MGO compared with control group ($p < 0.05$; **Figure 1B**). The levels of fasting glucose (86.8 ± 5.43 mg/dl), water consumption (2.45 ± 0.22 ml/day) and food intake (3.4 ± 0.11 g/day) in MGO group did not differ significantly from control group (89.7 ± 4.63 mg/dl, 2.61 ± 0.09 ml/day, and 3.2 ± 0.11 g/day, respectively; n = 7).

Bladder Measures and Histology

The body weight did not significantly differ between control and MGO groups (**Figure 2A**), but the bladder weight and relative bladder weight were increased by about of 20% ($p < 0.05$) in MGO-treated mice (**Figures 2B,C**). Histological analysis of bladders by hematoxylin and eosin (HE) and Masson's trichrome stains (**Figures 2D,E**) revealed that MGO exposure caused small (despite significant at $p < 0.05$) increases of the thickness of both urothelium and detrusor smooth muscle layers as well as of the collagen content (**Figures 2F–H**).

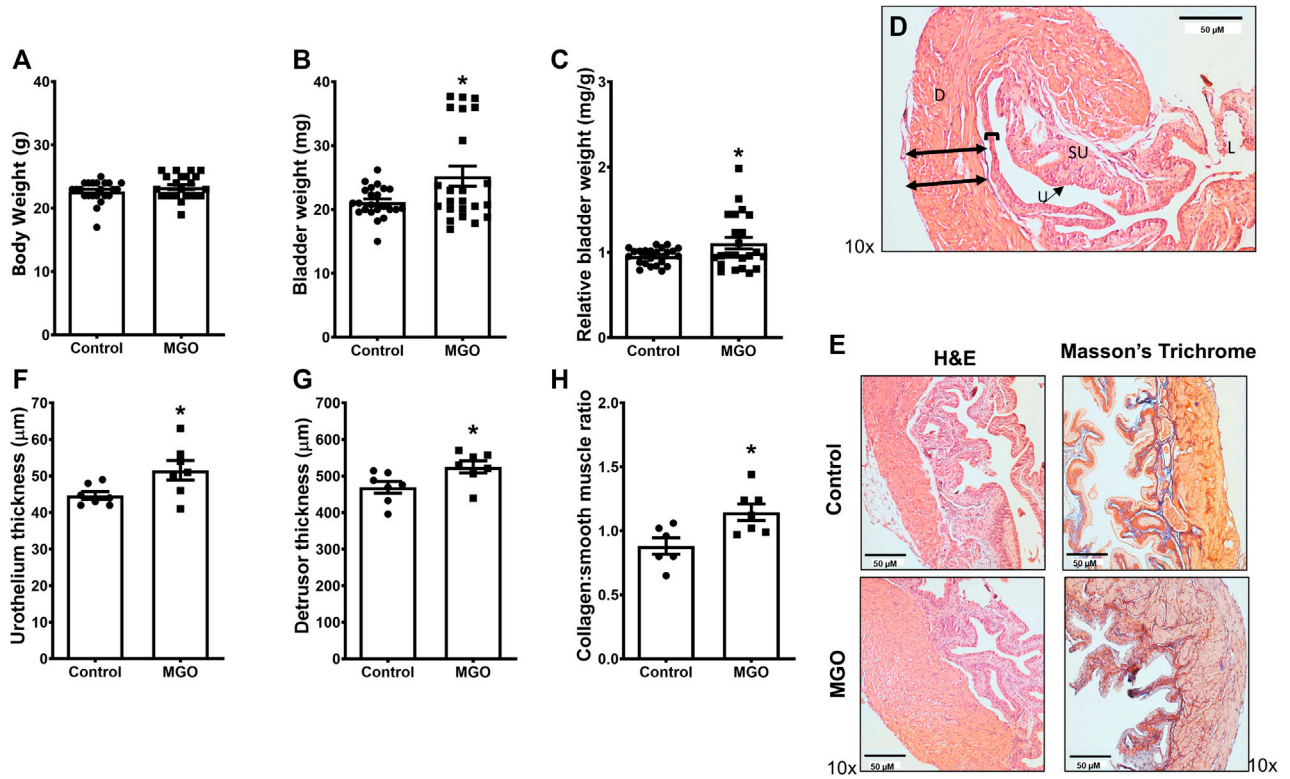

FIGURE 2 | Bladder measures and histological evaluation of methylglyoxal (MGO)-treated mice in comparison with control animals. Panels **(A–C)** show body weight, bladder weight and relative bladder weight, respectively, in control and MGO groups. Panel **(D)** shows a histological image of a bladder from control mice indicating the urothelium and detrusor smooth muscle with double-black arrows indicating the limits of quantification in detrusor and brackets indicating limits of quantification in urothelium. Panel **(E)** shows representative histological images of bladders of control and MGO groups using cross-section hematoxylin and eosin (HE) and Masson's trichrome staining. Panels **(F–H)** show quantifications of urothelium thickness, detrusor thickness and collagen content, respectively. Data are expressed as mean ± SEM (n = 23 for body weights; n = 7 for urothelium thickness, detrusor thickness and collagen content). *$p < 0.05$ compared with control group (unpaired t-test). **D**, detrusor smooth muscle; **SU,** suburothelium, **U**, urothelium; **L,** lumen. Black bars in panels **D** and **E** represent a scale of 50 µm (×10 objective).

Enhanced RAGE Expression in Bladders by MGO Exposure

Immunohistochemistry for RAGE was evaluated in lungs of healthy mice (as positive control) and bladders of untreated and MGO-exposed mice. Mouse lungs clearly immunostained for RAGE as detected mainly in peribronchiolar and perivascular regions of the lung (**Figure 3A**). In bladders of control group, RAGE immunoreactivity was observed in urothelium only (**Figure 3C**) whereas in MGO group an intense RAGE immunoreactivity was observed in both urothelium and detrusor, as well as in the vascular endothelium supplying the detrusor and lamina propria (**Figure 3D**). Analysis of mRNA expressions of RAGE in bladder tissues revealed a significantly higher expression in MGO in comparison with control group ($p < 0.01$; **Figure 3E**).

Enhanced ROS Levels and Decreased SOD Activity in Bladders by MGO Exposure

The ROS levels in both urothelium and detrusor smooth muscle were measured using the fluorescent dye DHE in frozen bladder sections (**Figure 4A**). In the control group, the basal ROS levels were 70% higher in the urothelium than detrusor ($p < 0.001$). Exposure to MGO significantly increased the ROS levels in the urothelium and detrusor smooth muscle compared with the control group, but the increases were higher in detrusor (108%, $p < 0.001$) than urothelium 25% ($p < 0.05$) (**Figures 4B,C**). The analysis of SOD activity showed a 40% reduction in MGO compared with control group ($p < 0.01$; **Figure 4E**).

MGO Exposure Increases mRNA Expression of L-type Ca^{2+} Channels (Cacn1) and Rho-Kinase System in Bladders

qPCR analysis of bladders revealed that MGO exposure significantly increased the mRNA expressions of L-type Ca^{2+} channels, RhoA, ROCK1 and ROCK2 when compared to the control group ($p < 0.05$; **Figures 5A–D**).

Contractile Responses of Intact and Mucosa-Denuded Bladders

For the functional assays, the bladder mucosa was maintained intact or mechanically removed. **Figure 6A** shows that mechanical mucosa

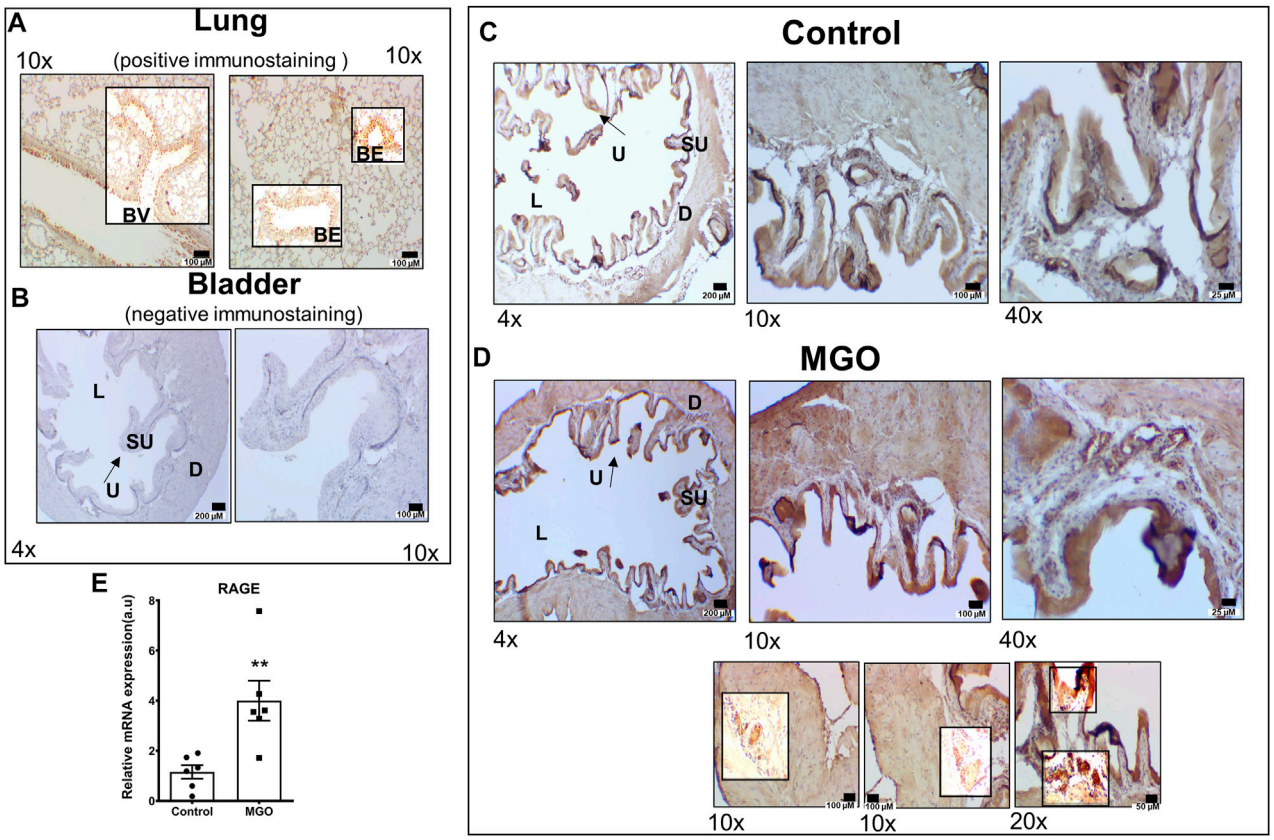

FIGURE 3 | RAGE Immunostaining and mRNA expression in control and MGO-treated mice. Panel **(A)** shows RAGE immunohistochemistry in lungs of healthy mice (brown staining) as positive control, detailing the bronchial epithelium (BE) and blood vessels (BV). Panel **(B)** shows negative control (omission of antibody) in mouse bladder, detailing the urothelium (U), suburothelium (SU), lumen (L) and detrusor smooth muscle (D). Panel **(C,D)** show, respectively, RAGE immunoreactivity of bladder images of control groups MGO groups. The three sub-panels in panel **(D)** (MGO group) detail the immunostaining for RAGE in vessels supplying the detrusor and urothelium, as well as in the superficial layer of urothelium and vessels in sub-urothelium. In the bladder of control mice, RAGE immunoreactivity was observed in urothelium only, whereas in MGO group, a strong RAGE immunoreactivity was observed in urothelium, detrusor and vascular endothelium. Panel E shows RAGE mRNA expressions in bladder tissues with data expressed as mean ± SEM of arbitrary units (a. u.; $^{**}p < 0.01$ compared with control, n = 6). Black bars in panels A to D represent scales of 200 μm (×4 objective), 100 μm (×10 objective), 50 μm (×20 objective) and 25 μm (×40 objective).

removal produced no gross damage to the detrusor layer. We then evaluated the contractile responses to electrical-field stimulation (EFS; 1–32 Hz), muscarinic agonist carbachol (0.001–100 μM0, P2X receptor agonist α,β-methylene ATP (1–10 μM), and extracellular Ca^{2+} (0.01–100 mM) in both intact and mucosa-denuded bladder strips from control and MGO-exposed mice.

In the control group, the mucosa removal did not significantly affect the bladder contractile responses to EFS at any frequency. In the MGO group, the contractile responses to EFS were greater than the control group irrespective of whether the mucosa was intact or removed ($p < 0.05$; **Figure 6B**).

In the control group, the mucosa removal did not significantly affect carbachol-induced bladder contractions. Exposure to MGO did not significantly change the carbachol-induced contractions in mucosa-intact preparations, but it markedly increased the contractions in mucosa-denuded tissues ($p < 0.01$; **Figure 6C**). The potency value for carbachol was significantly reduced in mucosa-denuded tissues (5.79 ± 0.11; $p < 0.05$) in comparison with the other groups (6.16 ± 0.13, 6.12 ± 0.14 and 6.27 ± 0.15 for control-intact, MGO-intact, and control-denuded strips, respectively).

Exposure to MGO significantly increased the contractile responses to α,β-methylene ATP, as observed in both intact and mucosa-denuded bladder strips ($p < 0.05$; **Figure 6D**).

In the control group, mucosa removal significantly enhanced the bladder contractions to extracellular Ca^{2+}. MGO exposure increased the $CaCl_2$-induced contractions in the intact bladder preparations ($p < 0.05$), but it did not further increase the contractions in the mucosa-denuded preparations (**Figure 6E**).

Y27632 and PEG-SOD Normalizes the Contractility of Mucosa-Denuded Bladder Strips in MGO

The possibility that the increased bladder contractions in MGO-exposed mice reflect enhanced ROS production and Rho kinase activation in the detrusor smooth muscle was investigated in mucosa-denuded preparations preincubated (30 min) with either

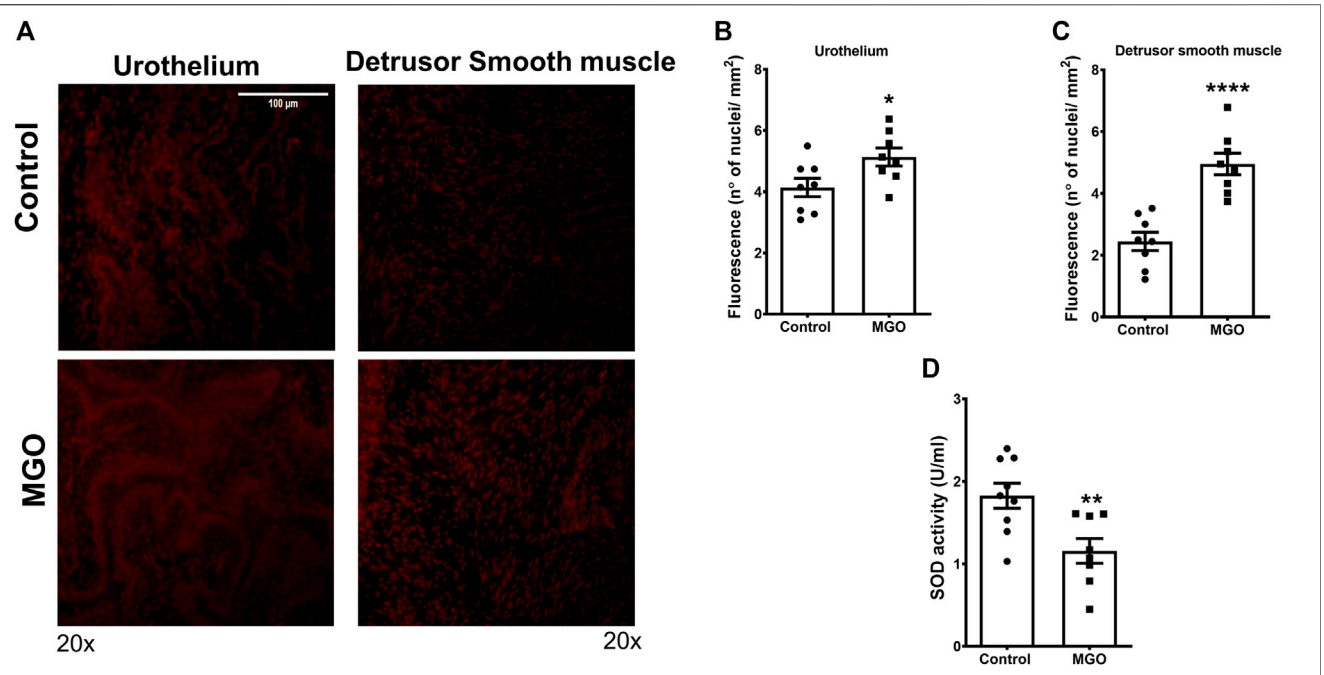

FIGURE 4 | Methylglyoxal (MGO) treatment increases the reactive-oxygen species (ROS) levels in urothelium and detrusor smooth muscle and decreases SOD activity in bladders. Panel **(A)** shows representative images of ROS measurement through dye dihydroethidium-induced fluorescence in urothelium and detrusor smooth muscle in control and MGO groups (20×). Panels **(B,C)** show quantitative ROS levels in urothelium and detrusor smooth muscle, respectively. Panel **(D)** shows superoxide dismutase (SOD) activity ($n = 8$). Data are expressed as mean ± SEM. $^{*}p < 0.05$, $^{**}p < 0.01$, $^{****}p < 0.0001$ compared with control group. White bar in panel A represents a scale of 100 um (×20 objective).

PEG-SOD (87 IU/ml) or the Rho kinase inhibitor Y27632 (1 μM). In the control group, at the concentrations employed, neither SOD nor Y27632 affected the contractions induced by EFS, carbachol, α,β-methylene ATP, and $CaCl_2$ (**Figures 7A,C,E,G**). However, in the MGO group, preincubation with SOD or Y27632 nearly prevented the bladder contractions to EFS, carbachol, and α,β-methylene ATP (**Figures 7B,D,F**). In the MGO group, the increased $CaCl_2$-induced contraction was not affected by SOD preincubation, but it was normalized by Y27632 (**Figure 7H**).

DISCUSSION

The present study demonstrates that oral intake with 0.5% MGO for 12 weeks in female mice increases the serum levels of AGEs and the bladder expressions of RAGE, ROS, RhoA, ROCK1, ROCK2 and L-type Ca^{2+} channels. MGO treatment increased the bladder contraction to EFS, carbachol, and α,β-methylene-ATP, an effect prevented by prior incubation with either SOD or Y27632. Overall, activation of AGE-RAGE-ROS signaling in bladder tissues may be responsible for the resulting MGO-induced detrusor overactivity.

In the present study, we administered 0.5% MGO for 12 weeks in female mice, after which MGO and F-AGEs were measured in serum. Similar to male mice (Oliveira et al., 2021), higher levels of MGO and F-AGEs were found in MGO-exposed mice. No changes in glucose levels (this study) or insulin resistance (Medeiros et al., 2020) were observed in the MGO-treated mice, confirming that elevated serum MGO was indeed generated by the oral intake of MGO rather than by the endogenous glucose metabolism, as observed in diabetes-associated diseases (Yamagishi et al., 2012). Histological analysis of the bladders showed that MGO treatment caused small increases (despite significant) in bladder weight, urothelium thickness, detrusor thickness and collagen content. In bladders of male mice receiving MGO (Oliveira et al., 2021), we detected a similar increase of the urothelium thickness, despite no alteration in the detrusor thickness was observed. With respect to the collagen content, the increases in bladder of males (Oliveira et al., 2021) were markedly higher than the females (this study). We are uncertain about the reasons that explain the histological differences in bladders of male and females, but that may rely on the bioavailability of MGO and formation of AGEs, as well as on the ability of the glyoxalase system to detoxify MGO in each mouse sex.

It is well established that accumulation of MGO causes the so-called dicarbonyl stress, which is defined as the abnormal accumulation of dicarbonyl reactive metabolites leading to protein glycation and hence tissue injury (Rabbani and Thornalley, 2015). AGEs bound its cell receptor RAGE in vascular endothelial, initiating tissue injury that may involve increased ROS production (Delbin et al., 2012). Cells have evolved a balanced system to neutralize the extra ROS that consist of enzymatic antioxidants such as SOD, and studies show that antioxidant activity of SOD may be impaired upon ROS excess, thereby dysregulating many physiological processes (He et al., 2017). Except of bladder cancer (Khorramdelazad et al., 2015)

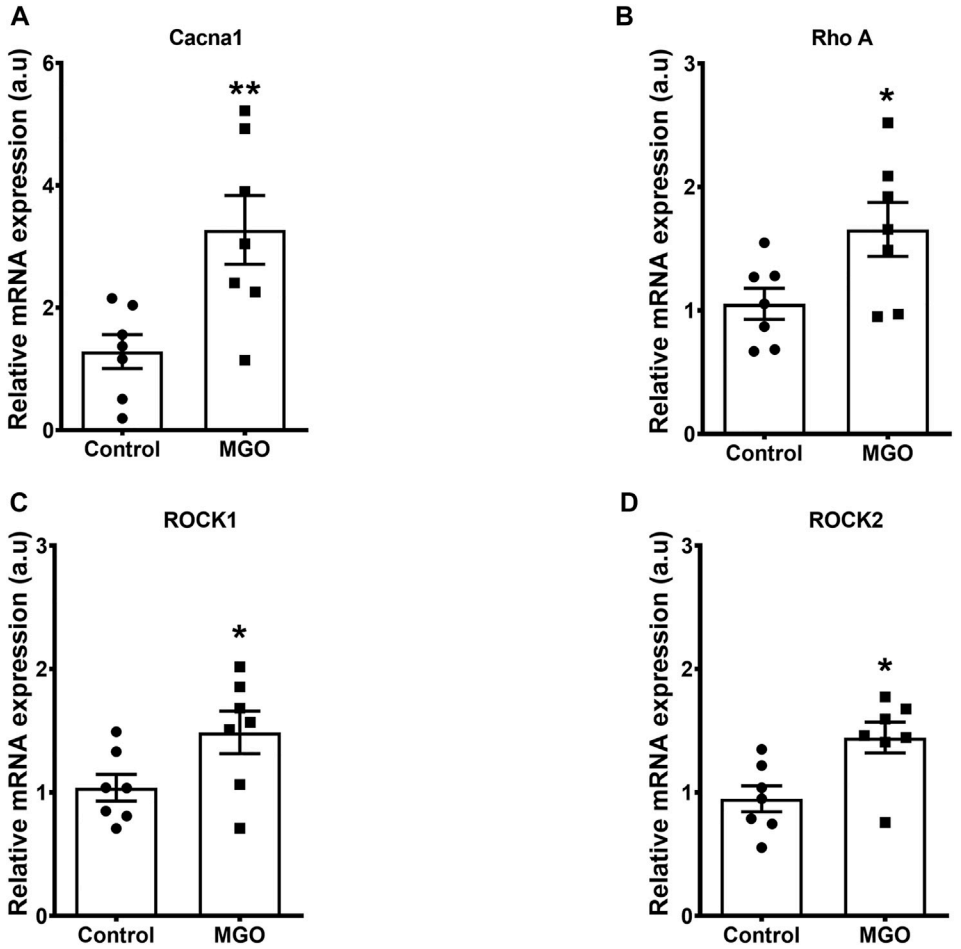

FIGURE 5 | Methylglyoxal (MGO) treatment increases the mRNA expressions of L-type Ca^{2+} channels **(A)**, RhoA **(B)**, ROCK1 **(C)** and ROCK 2 **(D)** in intact bladder tissues. Data are expressed as mean ± SEM for $n = 7$. $^{*}p < 0.05$ compared with control group.

and mouse cystitis (Roundy et al., 2013; Hiramoto et al., 2020), no previous study explored the RAGE expression in bladders. Compared to control mice, RAGE immunostaining was higher in both urothelium and detrusor of MGO-treated mice, as well as in the vascular endothelium supplying the detrusor and lamina propria. Analysis of mRNA expressions of RAGE also revealed a higher RAGE expression in bladder tissues of the MGO group. Additionally, using the fluorescent dye DHE in frozen bladder sections, MGO treatment significantly increased the ROS levels in both urothelium and detrusor smooth muscle (despite higher levels were found in the detrusor), which was accompanied by reduced SOD activity in the bladder. Therefore, like vascular tissues, the activation of AGE-RAGE-ROS signaling may be implicated in MGO-induced detrusor overactivity (**Figure 8**).

Acetylcholine *via* muscarinic M3 receptors is the principal excitatory transmitter at the parasympathetic nerve terminals in detrusor smooth muscle, whereas ATP, *via* P2X1 receptors, mediates the atropine-resistant neurogenic bladder contractions and may be involved in some types of bladder dysfunction (Abrams et al., 2006; Yoshimura et al., 2008). Bladder contractions in response to EFS reflect mainly the release of both acetylcholine and ATP (Leiria et al., 2011). In our study, the bladder contractions induced by EFS were significantly higher in MGO group, as observed both in intact and mucosa-denuded preparations. The contractions induced by the full muscarinic agonist carbachol did not differ between control and MGO groups in intact bladders, but the mucosa removal largely increased the contractions in MGO-treated animals. In addition, the P2X1 agonist α,β-methylene ATP induced higher contractile responses in bladders of MGO group, irrespective if mucosa was removed or not. Of note, our findings that presence of mucosa impairs the bladder contractions by carbachol activation (but not by α,β-methylene ATP) indicates that MGO treatment also affects the urothelium, which under muscarinic receptor activation may releases relaxing factors that counteracts the contractions. Under physiological conditions, the muscarinic and purinergic-mediated bladder smooth muscle contractions depend on extracellular Ca^{2+} influx secondary to L-type Ca^{2+} channel opening (Rapp et al., 2005; Leiria et al., 2011; Yu, 2022). Compared with control animals, in intact bladder preparations of MGO-treated mice we found a higher mRNA expression of L-type Ca^{2+} channels, and that the cumulative addition of extracellular Ca^{2+} in nominally Ca^{2+}-free solution produced significantly higher bladder contractions. Interestingly,

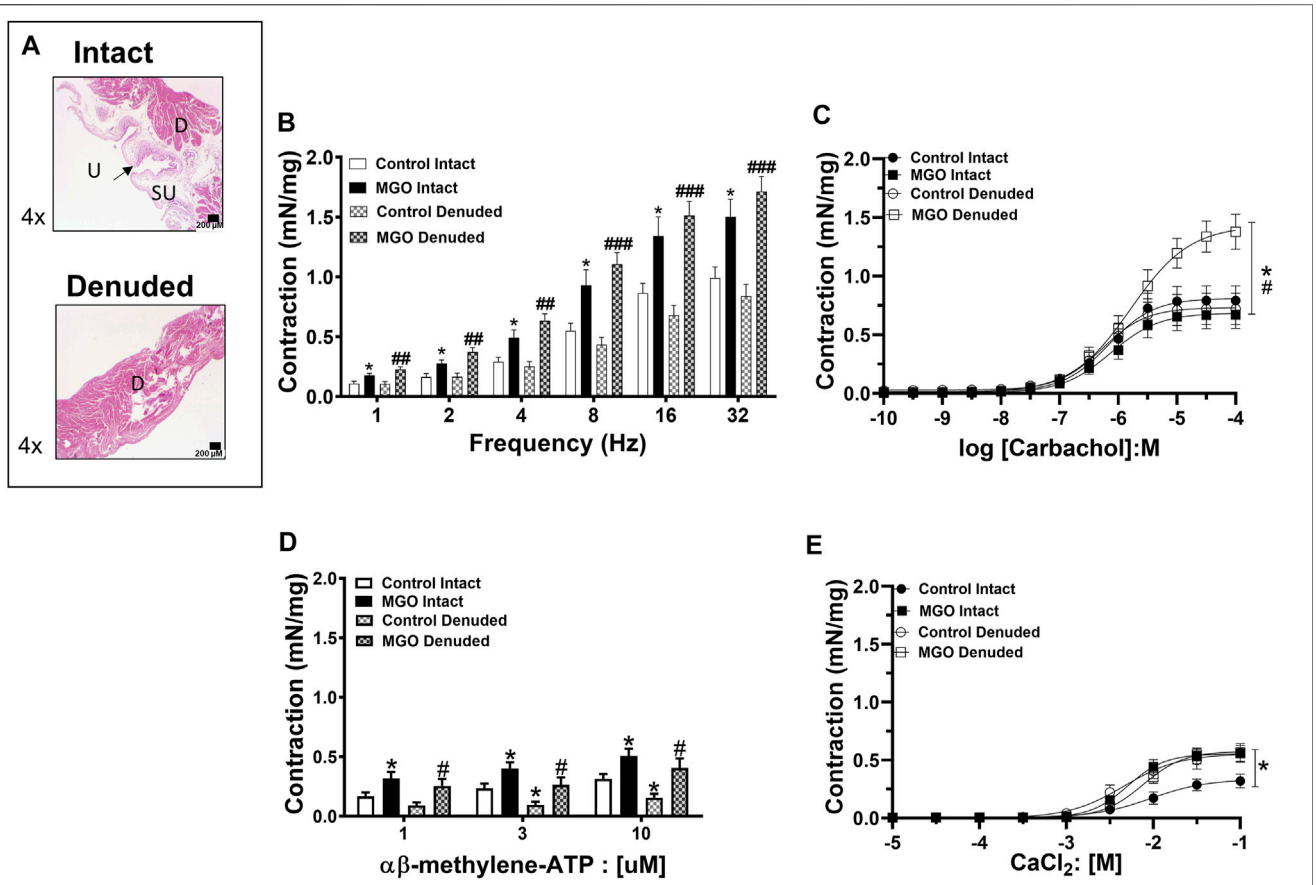

FIGURE 6 | The effects of methylglyoxal (MGO) treatment in intact and mucosa-denuded bladder contractions. Panel **(A)** shows representative images of intact bladders indicating the presence of urothelium, suburothelium and detrusor smooth muscle whereas in denuded bladder only the detrusor can be observed. Panels **(B–E)** show the contractions induced by electrical-field stimulation (EFS; 1–32 Hz), carbachol (0.1–100 µM), α,β-methylene-ATP (1–10 µM) and extracellular Ca^{2+} (10 µM–100 mM), respectively. Data are expressed as mean ± SEM (6–10 mice per group). $^{*}p < 0.05$ compared with respective control-intact groups; $^{\#}p < 0.05$, $^{\#\#}p < 0.05$, $^{\#\#\#}p < 0.001$ compared with respective control-denuded groups. In panel **A**, urothelium, suburothelium and detrusor smooth muscle are designated as U, SU, and D, respectively. Black bars in panel A represent a scale of 200 µm (×4 objective).

when the bladder mucosa was removed, MGO failed to increase the contractions above the control levels, suggesting that extracellular Ca^{2+} entry in mucosa favors the release of relaxing mediators that act to reduce the muscle contraction. Urothelium is reported to release inhibitory mediators that modulate the relaxant responses of the bladder (Sellers et al., 2018), including nitric oxide (NO), prostanoids (Guan et al., 2017) and hydrogen peroxide (H_2S; d'Emmanuele di Villa Bianca et al., 2016), amongst others. Urothelium also expresses β-adrenoceptors, which modulates the relaxant responses to β-adrenoceptor agonists, possibly *via* the release of urothelium-derived factors (Otsuka et al., 2008; Moro et al., 2013). In our study, whether the increased bladder contractions by prolonged intake of MGO is also accompanied by an impairment of urothelium-mediated relaxant responses remain to be investigated.

The Rho kinase pathway is reported to regulate the sensitivity of the Ca^{2+} dependent regulatory system (Wegener et al., 2004). Dysregulation of the Rho kinase system has been implicated in detrusor overactivity in animal models of acetic acid-induced cystitis, stretch-induced bladder contractions, and chronic bladder ischemia (Peters et al., 2006; Shimizu et al., 2013; Shiomi et al., 2013; Wróbel and Rechberger, 2017; Akaihata et al., 2018). Moreover, *in vitro* biochemical assays and *in vitro* studies in vascular smooth muscle have shown an association between increased oxidative stress and upregulation of the RhoA/Rho-kinase system (Heo and Campbell, 2005; Aghajanian et al., 2009; Priviero et al., 2016; MacKay et al., 2017). Accordingly, our findings show higher mRNA expressions of L-type Ca^{2+} channels, RhoA, ROCK1, and ROCK2 in the bladder tissues of the MGO group. We then performed functional assays in mucosa-denuded bladder strips in the absence and in the presence of either SOD or Y27632. At the concentrations employed here, in the control group, both compounds had no effects on EFS-, carbachol- and α,β-methylene ATP-induced contractions. However, in MGO-treated mice, SOD or Y27632 significantly reduced the contractile responses, clearly indicating a major role for superoxide and Rho kinase in the detrusor overactivity (**Figure 8**). This is consistent with previous studies in pulmonary vascular smooth muscle under chronic hypoxia (MacKay et al., 2017; Yan et al., 2020) and corpus cavernosum of diabetic mice (Li et al., 2012; Priviero et al., 2016) where ROS generation through upregulation of RhoA/ROCK signaling mediated the pulmonary

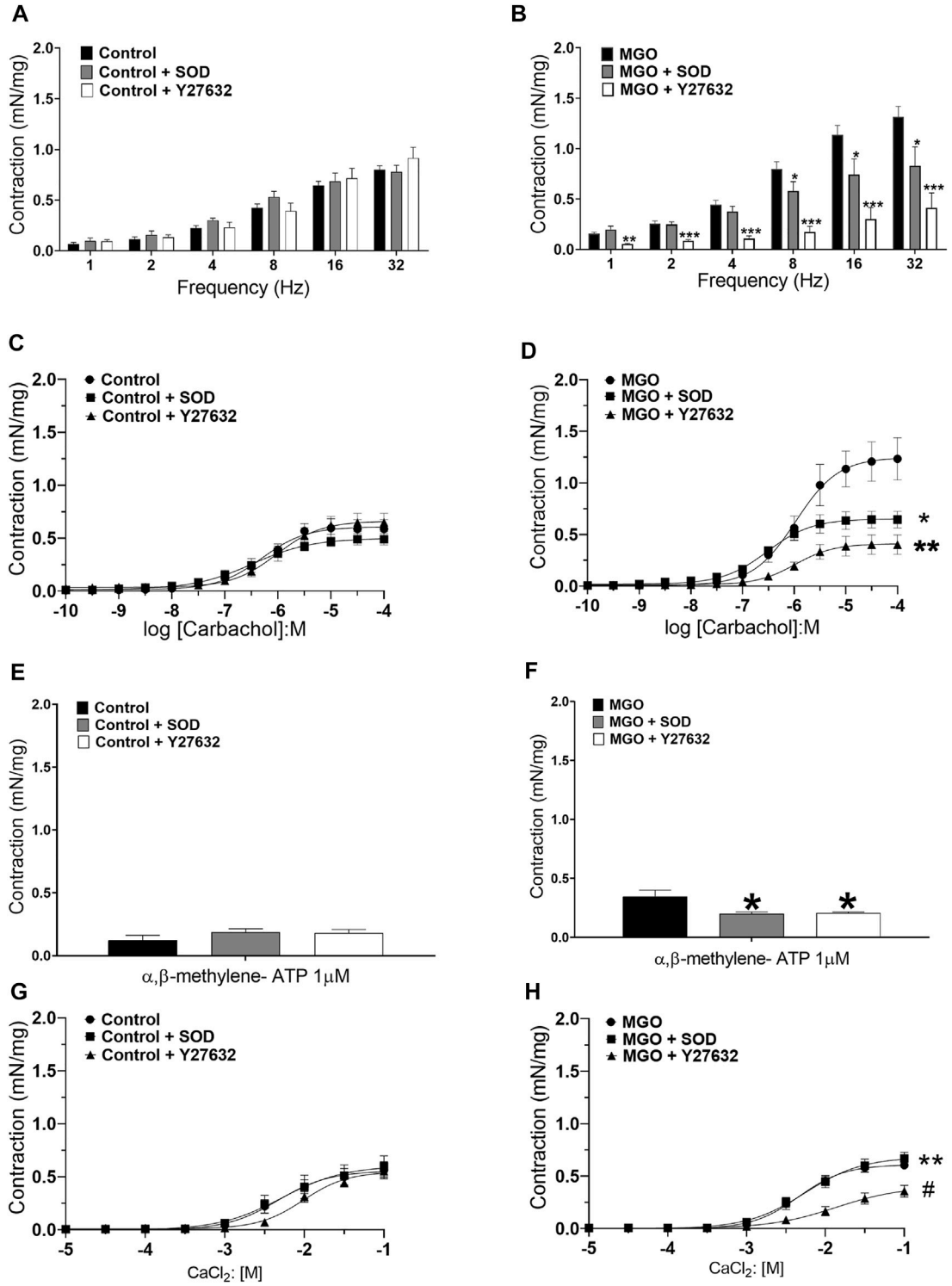

FIGURE 7 | Incubation of mucosa-denuded bladder preparations with superoxide dismutase (PEG-SOD; 87 IU/ml) or the Rho kinase inhibitor Y27632 (1 μM) reduces the enhanced detrusor smooth muscle contractions in mice treated with methylglyoxal (MGO) in comparison with control mice. Panels **(A,C,D and E)** shows the contractions induced by electrical-field stimulation (frequency), carbachol, α,β-methylene-ATP (1–10 μM) and extracellular Ca^{2+} in control mice, respectively. Panels **(B,D,F and H)** shows the contractions induced by the same stimuli in MGO-treated mice. Data are expressed as mean ± SEM (n = 5-6 per group). $^{*}p < 0.05$, $^{**}p < 0.01$, $^{***}p < 0.001$ compared with untreated preparations. $^{\#}p < 0.05$ compared with MGO + SOD group.

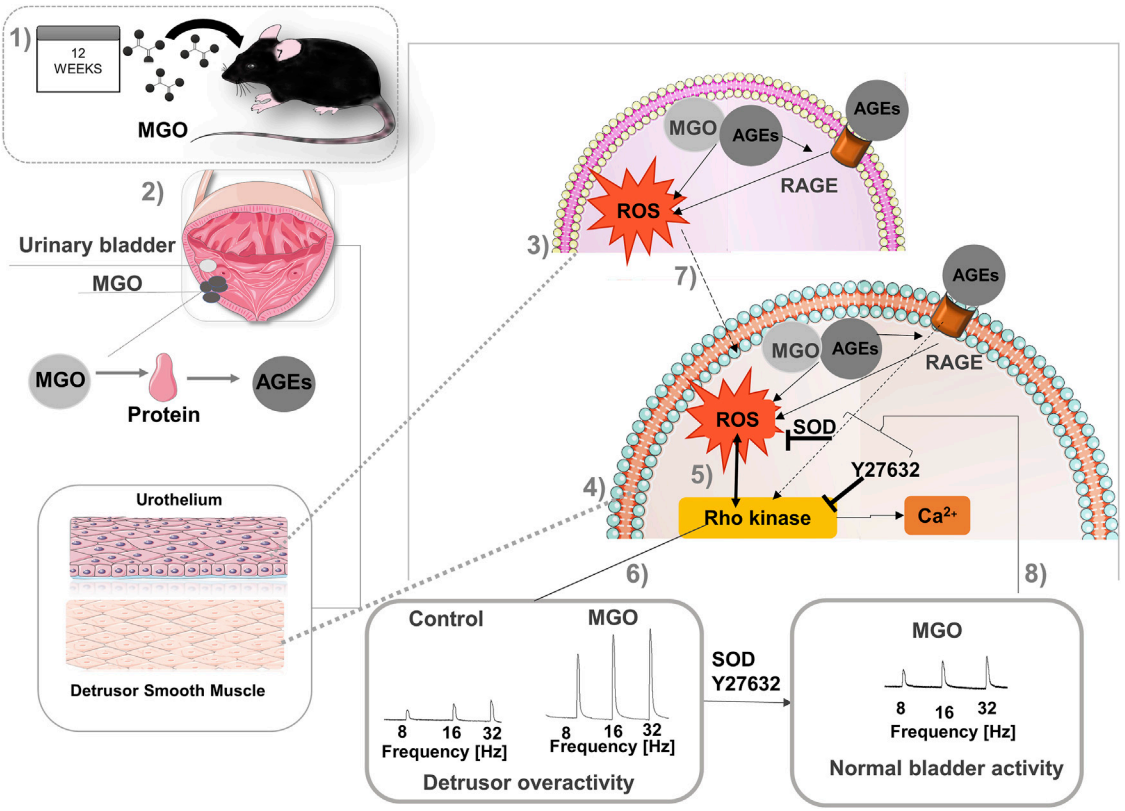

FIGURE 8 | Proposal of mechanisms involved in detrusor overactivity induced prolonged intake of methylglyoxal (MGO) in female mice. Methylglyoxal was given at 0.5% in the drinking water of female mice for 12 weeks (1). In urinary bladder (2), MGO generates advanced glycation end products (AGEs) that interacts with its cell surface receptor, RAGE, in both urothelium (3) and detrusor smooth muscle (4), leading to excess of reactive-oxygen species (ROS) generation in both layers. In detrusor smooth muscle cells, ROS activates the Rho kinase system (5), ultimately leading to Ca^{2+} sensitization and detrusor overactivity (6). Alternatively, RAGE activation may directly activate Rho kinase further elevating the ROS levels. ROS produced in urothelium (7) may also diffuse to detrusor cells amplifying the smooth muscle contraction. Bladder incubation with superoxide dismutase (SOD) or the Rho kinase inhibitor Y27632 significantly reduce the detrusor overactivity, normalizing the bladder activity (8). This image was produced with the assistance of Servier Medical Art (https://smart.servier.com) licensed by a Creative Commons Attribution 3.0 Unported License.

vasoconstriction and impaired cavernosal relaxations. However, in isolated cells, Rho kinase inhibitors like Y27632 can also reduce the ROS production (Lu et al., 2013; Fujimoto et al., 2017). Recently, the ROS-mediated increases of RhoA levels in a murine macrophage cell line were shown to amplify the superoxide production through ROCK phosphorylation of p47phox, maintaining a positive feedback loop for superoxide generation (Cap et al., 2020). Therefore, in our study, additional approaches would be required to elucidate if upregulation of Rho kinase in bladders of MGO-treated mice also amplify the ROS production in positive feedback way. With respect to the contractile responses induced by extracellular Ca^{2+} in mucosa-denuded bladder strips of MGO group, we found that SOD preincubation had no effect, whereas Y27632 rather restored the contractions to control levels. This finding suggests that the resulting bladder contraction due to extracellular Ca^{2+} influx through L-type Ca^{2+} channels is not under the influence of the upstream superoxide anion production in detrusor, but itself can increase the sensitivity to Rho kinase.

In terms of study limitation, MGO here was administered to healthy female mice in the drinking water at 0.5% for 12 weeks, after which plasma and bladder were collected and used for the biochemical, molecular, and functional assays. This model greatly differs from the classical diabetic animal model in that MGO is not generated from the endogenous glucose metabolism but rather exogenously supplied to animals. Despite high serum levels of MGO and AGEs (this study) along with reduced glyoxalase-1 expression and activity (Oliveira et al., 2021) are observed in mice orally taking MGO, which suggest a true dicarbonyl stress (Rabbani and Thornalley, 2015), caution should be taken when comparing our present model with those involving endogenous generations of dicarbonyl species.

CONCLUSION

Prolonged MGO intake in mice leads to serum accumulation of MGO and F-AGES, which triggers the activation of RAGE-ROS signaling in the bladder wall, leading to detrusor overactivity, which is normalized by SOD or the Rho kinase inhibitor Y27631 (**Figure 8**). It is possible that overactive bladder syndrome in diabetes-associated diseases reflects by accumulation of MGO in circulating blood.

DATA AVAILABILITY STATEMENT

The raw data supporting the conclusions of this article will be made available by the authors, without undue reservation.

ETHICS STATEMENT

The animal study was reviewed and approved by the Ethics Committee in Animal Use, State University of Campinas (CEUA-UNICAMP; Protocol No. 5443-1/2019).

AUTHOR CONTRIBUTIONS

AO, MM, MO and CT carried out the experiments. AO, FM and EA analyzed the experimental results. AO and EA designed the experiments and wrote the manuscript.

FUNDING

We gratefully acknowledge São Paulo Research Foundation (FAPESP; Grant Nos 2017/15175-1, 2018/09765-3).

REFERENCES

Abrams, P., Andersson, K.-E., Buccafusco, J. J., Chapple, C., de Groat, W. C., Fryer, A. D., et al. (2006). Muscarinic Receptors: Their Distribution and Function in Body Systems, and the Implications for Treating Overactive Bladder. *Br. J. Pharmacol.* 148, 565–578. doi:10.1038/sj.bjp.0706780

Aghajanian, A., Wittchen, E. S., Campbell, S. L., and Burridge, K. (2009). Direct Activation of RhoA by Reactive Oxygen Species Requires a Redox-Sensitive Motif. *PLoS One* 4, e8045. doi:10.1371/journal.pone.0008045

Akaihata, H., Nomiya, M., Matsuoka, K., Koguchi, T., Hata, J., Haga, N., et al. (2018). Protective Effect of a Rho-Kinase Inhibitor on Bladder Dysfunction in a Rat Model of Chronic Bladder Ischemia. *Urology* 111, e7. doi:10.1016/j.urology.2017.10.007

Cap, K. C., Kim, J.-G., Hamza, A., and Park, J.-B. (2020). P-Tyr42 RhoA GTPase Amplifies Superoxide Formation through P47phox, Phosphorylated by ROCK. *Biochem. Biophys. Res. Commun.* 523, 972–978. doi:10.1016/j.bbrc.2020.01.001

Daneshgari, F., Liu, G., and Hanna-Mitchell, A. T. (2017). Path of Translational Discovery of Urological Complications of Obesity and Diabetes. *Am. J. Physiol. Renal Physiol.* 312, F887–F896. doi:10.1152/ajprenal.00489.2016

de Oliveira, M. G., Medeiros, M. L. d., Tavares, E. B. G., Mónica, F. Z., and Antunes, E. (2020). Methylglyoxal, a Reactive Glucose Metabolite, Induces Bladder Overactivity in Addition to Inflammation in Mice. *Front. Physiol.* 11, 290. doi:10.3389/fphys.2020.00290

Delbin, M. A., Davel, A. P. C., Couto, G. K., de Araújo, G. G., Rossoni, L. V., Antunes, E., et al. (2012). Interaction between Advanced Glycation End Products Formation and Vascular Responses in Femoral and Coronary Arteries from Exercised Diabetic Rats. *PLoS One* 7, e53318. doi:10.1371/journal.pone.0053318

d'Emmanuele di Villa Bianca, R., Mitidieri, E., Fusco, F., Russo, A., Pagliara, V., Tramontano, T., et al. (2016). Urothelium Muscarinic Activation Phosphorylates CBSSer227 via cGMP/PKG Pathway Causing Human Bladder Relaxation through H2S Production. *Sci. Rep.* 6, 31491. doi:10.1038/srep31491

Ellenbroek, J. H., Arioglu Inan, E., and Michel, M. C. (2018). A Systematic Review of Urinary Bladder Hypertrophy in Experimental Diabetes: Part 2. Comparison of Animal Models and Functional Consequences. *Neurourol. Urodyn.* 37, 2346–2360. doi:10.1002/nau.23786

Fujimoto, T., Inoue, T., Ohira, S., Awai-Kasaoka, N., Kameda, T., Inoue-Mochita, M., et al. (2017). Inhibition of Rho Kinase Induces Antioxidative Molecules and Suppresses Reactive Oxidative Species in Trabecular Meshwork Cells. *J. Ophthalmol.* 2017, 1–23. doi:10.1155/2017/7598140

Gasbarro, G., Lin, D. L., Vurbic, D., Quisno, A., Kinley, B., Daneshgari, F., et al. (2010). Voiding Function in Obese and Type 2 Diabetic Female Rats. *Am. J. Physiol. Renal Physiol.* 298, F72–F77. doi:10.1152/ajprenal.00309.2009

Guan, N. N., Gustafsson, L. E., and Svennersten, K. (2017). Inhibitory Effects of Urothelium-Related Factors. *Basic Clin. Pharmacol. Toxicol.* 121, 220–224. doi:10.1111/bcpt.12785

Han, Y., Randell, E., Vasdev, S., Gill, V., Curran, M., Newhook, L. A., et al. (2009). Plasma Advanced Glycation Endproduct, Methylglyoxal-Derived Hydroimidazolone Is Elevated in Young, Complication-free Patients with Type 1 Diabetes. *Clin. Biochem.* 42, 562–569. doi:10.1016/j.clinbiochem.2008.12.016

He, L., He, T., Farrar, S., Ji, L., Liu, T., and Ma, X. (2017). Antioxidants Maintain Cellular Redox Homeostasis by Elimination of Reactive Oxygen Species. *Cell Physiol. Biochem.* 44, 532–553. doi:10.1159/000485089

Heo, J., and Campbell, S. L. (2005). Mechanism of Redox-Mediated Guanine Nucleotide Exchange on Redox-Active Rho GTPases. *J. Biol. Chem.* 280, 31003–31010. doi:10.1074/jbc.M504768200

Hiramoto, S., Tsubota, M., Yamaguchi, K., Okazaki, K., Sakaegi, A., Toriyama, Y., et al. (2020). Cystitis-Related Bladder Pain Involves ATP-dependent HMGB1 Release from Macrophages and its Downstream H2S/Cav3.2 Signaling in Mice. *Cells* 9, 1748. doi:10.3390/cells9081748

Hobbs, G. A., Zhou, B., Cox, A. D., and Campbell, S. L. (2014). Rho GTPases, Oxidation, and Cell Redox Control. *Small GTPases* 5, e28579. doi:10.4161/sgtp.28579

Khorramdelazad, H., Bagheri, V., Hassanshahi, G., Karami, H., Moogooei, M., Zeinali, M., et al. (2015). S100A12 and RAGE Expression in Human Bladder Transitional Cell Carcinoma: a Role for the Ligand/RAGE axis in Tumor Progression? *Asian Pac. J. Cancer Prev.* 16, 2725–2729. doi:10.7314/apjcp.2015.16.7.2725

Kilhovd, B. K., Giardino, I., Torjesen, P. A., Birkeland, K. I., Berg, T. J., Thornalley, P. J., et al. (2003). Increased Serum Levels of the Specific AGE-Compound Methylglyoxal-Derived Hydroimidazolone in Patients with Type 2 Diabetes. *Metabolism* 52, 163–167. doi:10.1053/meta.2003.50035

Kim, A. K., Hamadani, C., Zeidel, M. L., and Hill, W. G. (2020). Urological Complications of Obesity and Diabetes in Males and Females of Three Mouse Models: Temporal Manifestations. *Am. J. Physiol. Renal Physiol.* 318, F160–F174. doi:10.1152/ajprenal.00207.2019

Kim, H. J., Jeong, M. S., and Jang, S. B. (2021). Molecular Characteristics of RAGE and Advances in Small-Molecule Inhibitors. *Int. J. Mol. Sci.* 22, 6904. doi:10.3390/ijms22136904

Lai, H. H., Helmuth, M. E., Smith, A. R., Wiseman, J. B., Gillespie, B. W., and Kirkali, Z. (2019). Relationship between Central Obesity, General Obesity, Overactive Bladder Syndrome and Urinary Incontinence Among Male and Female Patients Seeking Care for Their Lower Urinary Tract Symptoms. *Urology* 123, 34–43. doi:10.1016/j.urology.2018.09.012

Leiria, L., Mónica, F., Carvalho, F., Claudino, M., Franco-Penteado, C., Schenka, A., et al. (2011). Functional, Morphological and Molecular Characterization of Bladder Dysfunction in Streptozotocin-Induced Diabetic Mice: Evidence of a Role for L-type Voltage-Operated Ca2+channels. *Br. J. Pharmacol.* 163, 1276–1288. doi:10.1111/j.1476-5381.2011.01311.x

Leiria, L. O., Sollon, C., Calixto, M. C., Lintomen, L., Mónica, F. Z., Anhê, G. F., et al. (2012). Role of PKC and CaV1.2 in Detrusor Overactivity in a Model of Obesity Associated with Insulin Resistance in Mice. *PLoS One* 7, e48507. doi:10.1371/journal.pone.0048507

Li, M., Zhuan, L., Wang, T., Rao, K., Yang, J., Yang, J., et al. (2012). Apocynin Improves Erectile Function in Diabetic Rats through Regulation of NADPH Oxidase Expression. *J. Sex. Med.* 9, 3041–3050. doi:10.1111/j.1743-6109.2012.02960.x

Liu, J., Mak, T. C.-P., Banigesh, A., Desai, K., Wang, R., and Wu, L. (2012). Aldolase B Knockdown Prevents High Glucose-Induced Methylglyoxal Overproduction and Cellular Dysfunction in Endothelial Cells. *PLoS One* 7, e41495. doi:10.1371/journal.pone.0041495

Lu, Y., Li, H., Jian, W., Zhuang, J., Wang, K., Peng, W., et al. (2013). The Rho/Rho-Associated Protein Kinase Inhibitor Fasudil in the protection of Endothelial Cells against Advanced Glycation End Products through the Nuclear Factor κB Pathway. *Exp. Ther. Med.* 6, 310–316. doi:10.3892/etm.2013.1125

MacDonald, J. A., and Walsh, M. P. (2018). Regulation of Smooth Muscle Myosin Light Chain Phosphatase by Multisite Phosphorylation of the Myosin Targeting Subunit, MYPT1. *Cardiovasc. Hematol. Disord. Drug Targets* 18, 4–13. doi:10.2174/1871529X18666180326120638

MacKay, C. E., Shaifta, Y., Snetkov, V. V., Francois, A. A., Ward, J. P. T., and Knock, G. A. (2017). ROS-dependent Activation of RhoA/Rho-Kinase in Pulmonary Artery: Role of Src-Family Kinases and ARHGEF1. *Free Radic. Biol. Med.* 110, 316–331. doi:10.1016/j.freeradbiomed.2017.06.022

Medeiros, M. L., de Oliveira, M. G., Tavares, E. G., Mello, G. C., Anhê, G. F., Mónica, F. Z., et al. (2020). Long-term Methylglyoxal Intake Aggravates Murine Th2-Mediated Airway Eosinophil Infiltration. *Int. Immunopharmacol.* 81, 106254. doi:10.1016/j.intimp.2020.106254

Medeiros, M. L., Oliveira, A. L., de Oliveira, M. G., Mónica, F. Z., and Antunes, E. (2021). Methylglyoxal Exacerbates Lipopolysaccharide-Induced Acute Lung Injury via RAGE-Induced ROS Generation: Protective Effects of Metformin. *J. Inflamm. Res.* 14, 6477–6489. doi:10.2147/JIR.S337115

Mey, J. T., and Haus, J. M. (2018). Dicarbonyl Stress and Glyoxalase-1 in Skeletal Muscle: Implications for Insulin Resistance and Type 2 Diabetes. *Front. Cardiovasc. Med.* 5, 117. doi:10.3389/fcvm.2018.00117

Moro, C., Tajouri, L., and Chess-Williams, R. (2013). Adrenoceptor Function and Expression in Bladder Urothelium and Lamina Propria. *Urology* 81, 211. doi:10.1016/j.urology.2012.09.011

Nowotny, K., Jung, T., Höhn, A., Weber, D., and Grune, T. (2015). Advanced Glycation End Products and Oxidative Stress in Type 2 Diabetes Mellitus. *Biomolecules* 5, 194–222. doi:10.3390/biom5010194

Nunes, K. P., and Webb, R. C. (2020). New Insights into RhoA/Rho-Kinase Signaling: a Key Regulator of Vascular Contraction. *Small GTPases* 12, 458–469. doi:10.1080/21541248.2020.1822721

Oliveira, A. L., de Oliveira, M. G., Medeiros, M. L., Mónica, F. Z., and Antunes, E. (2021). Metformin Abrogates the Voiding Dysfunction Induced by Prolonged Methylglyoxal Intake. *Eur. J. Pharmacol.* 910, 174502. doi:10.1016/j.ejphar.2021.174502

Otsuka, A., Shinbo, H., Matsumoto, R., Kurita, Y., and Ozono, S. (2008). Expression and Functional Role of β-adrenoceptors in the Human Urinary Bladder Urothelium. *Naunyn-Schmied Arch. Pharmacol.* 377, 473–481. doi:10.1007/s00210-008-0274-y

Peters, S. L. M., Schmidt, M., and Michel, M. C. (2006). Rho Kinase: a Target for Treating Urinary Bladder Dysfunction? *Trends Pharmacol. Sci.* 27, 492–497. doi:10.1016/j.tips.2006.07.002

Priviero, F. B. M., Toque, H. A. F., Nunes, K. P., Priolli, D. G., Teixeira, C. E., and Webb, R. C. (2016). Impaired Corpus Cavernosum Relaxation Is Accompanied by Increased Oxidative Stress and Up-Regulation of the Rho-Kinase Pathway in Diabetic (Db/Db) Mice. *PLoS One* 11, e0156030. doi:10.1371/journal.pone.0156030

Rabbani, N., and Thornalley, P. J. (2015). Dicarbonyl Stress in Cell and Tissue Dysfunction Contributing to Ageing and Disease. *Biochem. Biophys. Res. Commun.* 458, 221–226. doi:10.1016/j.bbrc.2015.01.140

Rapp, D. E., Lyon, M. B., Bales, G. T., and Cook, S. P. (2005). A Role for the P2X Receptor in Urinary Tract Physiology and in the Pathophysiology of Urinary Dysfunction. *Eur. Urol.* 48, 303–308. doi:10.1016/j.eururo.2005.04.019

Roundy, L. M., Jia, W., Zhang, J., Ye, X., Prestwich, G. D., and OottamasathienQ, S. (2013). LL-37 Induced Cystitis and the Receptor for Advanced Glycation End-Products (RAGE) Pathway. *ABB* 04, 1–8. doi:10.4236/abb.2013.48a2001

Sellers, D., Chess-Williams, R., and Michel, M. C. (2018). Modulation of Lower Urinary Tract Smooth Muscle Contraction and Relaxation by the Urothelium. *Naunyn-Schmiedeberg Arch. Pharmacol.* 391, 675–694. doi:10.1007/s00210-018-1510-8

Shimizu, N., De Velasco, M. A., Umekawa, T., Uemura, H., and Yoshikawa, K. (2013). Effects of the Rho Kinase Inhibitor, Hydroxyfasudil, on Bladder Dysfunction and Inflammation in Rats with HCl-Induced Cystitis. *Int. J. Urol.* 20, 1136–1143. doi:10.1111/iju.12119

Shimokawa, H., Sunamura, S., and Satoh, K. (2016). RhoA/Rho-Kinase in the Cardiovascular System. *Circ. Res.* 118, 352–366. doi:10.1161/CIRCRESAHA.115.306532

Shiomi, H., Takahashi, N., Kawashima, Y., Ogawa, S., Haga, N., Kushida, N., et al. (2013). Involvement of Stretch-Induced Rho-Kinase Activation in the Generation of Bladder Tone. *Neurourol. Urodyn.* 32, 1019–1025. doi:10.1002/nau.22360

Strassheim, D., Gerasimovskaya, E., Irwin, D., Dempsey, E. C., Stenmark, K., and Karoor, V. (2019). RhoGTPase in Vascular Disease. *Cells* 8, 551. doi:10.3390/cells8060551

Wegener, J. W., Schulla, V., Lee, T. S., Koller, A., Feil, S., Feil, R., et al. (2004). An Essential Role of Ca V 1.2 L-type Calcium Channel for Urinary Bladder Function. *FASEB J.* 18, 1159–1161. doi:10.1096/fj.04-1516fje

Wittig, L., Carlson, K. V., Andrews, J. M., Crump, R. T., and Baverstock, R. J. (2019). Diabetic Bladder Dysfunction:A Review. *Urology* 123, 1–6. doi:10.1016/j.urology.2018.10.010

Wróbel, A., and Rechberger, T. (2017). The Influence of Rho-Kinase Inhibition on Acetic Acid-Induced Detrusor Overactivity. *Neurourol. Urodynam.* 36, 263–270. doi:10.1002/nau.22918

Wu, L., Zhang, X., Xiao, N., Huang, Y., Kavran, M., Elrashidy, R. A., et al. (2016). Functional and Morphological Alterations of the Urinary Bladder in Type 2 Diabetic FVBdb/db Mice. *J. Diabetes Complications* 30, 778–785. doi:10.1016/j.jdiacomp.2016.03.003

Yamagishi, S.-i., Maeda, S., Matsui, T., Ueda, S., Fukami, K., and Okuda, S. (2012). Role of Advanced Glycation End Products (AGEs) and Oxidative Stress in Vascular Complications in Diabetes. *Biochim. Biophys. Acta Gen. Sub.* 1820, 663–671. doi:10.1016/j.bbagen.2011.03.014

Yan, S., Resta, T. C., and Jernigan, N. L. (2020). Vasoconstrictor Mechanisms in Chronic Hypoxia-Induced Pulmonary Hypertension: Role of Oxidant Signaling. *Antioxidants* 9, 999. doi:10.3390/antiox9100999

Yang, X. F., Wang, J., Rui-Wang, R., Xu, Y. F., Chen, F. j., Tang, L. Y., et al. (2019). Time-dependent Functional, Morphological, and Molecular Changes in Diabetic Bladder Dysfunction in Streptozotocin-induced Diabetic Mice. *Neurourol. Urodyn.* 38, 1266–1277. doi:10.1002/nau.24008

Yoshimura, N., Kaiho, Y., Miyazato, M., Yunoki, T., Tai, C., Chancellor, M. B., et al. (2008). Therapeutic Receptor Targets for Lower Urinary Tract Dysfunction. *Naunyn-Schmied Arch. Pharmacol.* 377, 437–448. doi:10.1007/s00210-007-0209-z

Yu, W. (2022). Reviving Cav1.2 as an Attractive Drug Target to Treat Bladder Dysfunction. *FASEB J.* 36, e22118. doi:10.1096/fj.202101475R

Conflict of Interest: The authors declare that the research was conducted in the absence of any commercial or financial relationships that could be construed as a potential conflict of interest.

Publisher's Note: All claims expressed in this article are solely those of the authors and do not necessarily represent those of their affiliated organizations, or those of the publisher, the editors and the reviewers. Any product that may be evaluated in this article, or claim that may be made by its manufacturer, is not guaranteed or endorsed by the publisher.

frontiers in Physiology

ORIGINAL RESEARCH
published: 31 March 2022
doi: 10.3389/fphys.2022.841181

The Dependence of Urinary Bladder Responses on Extracellular Calcium Varies Between Muscarinic, Histamine, 5-HT (Serotonin), Neurokinin, Prostaglandin, and Angiotensin Receptor Activation

*Charlotte Phelps, Russ Chess-Williams and Christian Moro**

Centre for Urology Research, Faculty of Health Sciences and Medicine, Bond University, Robina, QLD, Australia

With many common bladder diseases arising due to abnormal contractions, a greater understanding of the receptor systems involved may aid the development of future treatments. The aim of this study was to identify any difference in the involvement of extracellular calcium (Ca^{2+}) across prominent contractile-mediating receptors within cells lining the bladder. Strips of porcine urothelium and lamina propria were isolated from the urinary bladder dome and mounted in isolated tissue baths containing Krebs-bicarbonate solution, perfused with carbogen gas at 37°C. Tissue contractions, as well as changes to the frequency and amplitude of spontaneous activity were recorded after the addition of muscarinic, histamine, 5-hydroxytryptamine, neurokinin-A, prostaglandin E2, and angiotensin II receptor agonists in the absence and presence of 1 μM nifedipine or nominally zero Ca^{2+} solution. The absence of extracellular Ca^{2+} influx after immersion into nominally zero Ca^{2+} solution, or the addition of nifedipine, significantly inhibited the contractile responses ($p < 0.05$ for all) after stimulation with carbachol (1 μM), histamine (100 μM), 5-hydroxytryptamine (100 μM), neurokinin-A (300 nM), prostaglandin E2 (10 μM), and angiotensin II (100 nM). On average, Ca^{2+} influx from extracellular sources was responsible for between 20–50% of receptor-mediated contractions. This suggests that although the specific requirement of Ca^{2+} on contractile responses varies depending on the receptor, extracellular Ca^{2+} plays a key role in mediating G protein-coupled receptor contractions of the urothelium and lamina propria.

Keywords: bladder mucosa, G protein-coupled receptor (GCPR), l-type calcium channel, lamina propria, spontaneous activity, underactive bladder, muscularis mucosae

OPEN ACCESS

Edited by:
Nick Spencer,
Flinders University, Australia

Reviewed by:
Betty Exintaris,
Monash University, Australia
Sang Don Koh,
University of Nevada, Reno, United States

****Correspondence:***
Christian Moro
cmoro@bond.edu.au

Specialty section:
This article was submitted to Integrative Physiology, a section of the journal Frontiers in Physiology

Received: *22 December 2021*
Accepted: *14 March 2022*
Published: *31 March 2022*

Citation:
Phelps C, Chess-Williams R and Moro C (2022) The Dependence of Urinary Bladder Responses on Extracellular Calcium Varies Between Muscarinic, Histamine, 5-HT (Serotonin), Neurokinin, Prostaglandin, and Angiotensin Receptor Activation. Front. Physiol. 13:841181. doi: 10.3389/fphys.2022.841181

1 INTRODUCTION

While strong and sustained bladder contractions are vital for urinary voiding, during the filling stage abnormal and spontaneous contractions can result in bladder dysfunction. One common presentation is underactive bladder, characterized by a slow urinary stream, hesitancy and straining to void, with or without a feeling of incomplete bladder emptying, and sometimes with storage symptoms (Chapple et al., 2018). Normally, voiding commences when M3 muscarinic

receptors in the smooth muscle of the bladder wall are stimulated by neuronally derived acetylcholine. However, recent research has identified a number of other receptor systems on cells within the bladder wall which may also modulate bladder contractions (Stromberga et al., 2019; Stromberga et al., 2020b). Of particular interest are those linked to $G_{q/11}$ proteins, with their stimulation often resulting in strong tissue contractions. With many common bladder diseases arising as a result of abnormal contractions, an understanding of the potential receptor systems involved in this response is vital for the development of new and upcoming treatments for those affiliated with bladder dysfunctions.

A continuing interest has developed into the potential role of histamine (Stromberga et al., 2019), prostaglandins (Stromberga et al., 2020b), angiotensin (Lim et al., 2021), adrenergic (Moro et al., 2013), neurokinin (Grundy et al., 2018), muscarinic (Moro et al., 2011), and 5-hydroxytryptamine (Moro et al., 2016) receptors in influencing contractions of the urothelium and lamina propria (U&LP) layers. This layer has been observed to modulate overall bladder activity through the release of chemical mediators (Moro et al., 2011), as well as other pacemaking functions via the presence of the muscularis mucosae in the underlying connective tissue layer (Fry et al., 2007). The U&LP (also referred to as the bladder mucosa) may also play a key role in the mechanisms of action for current therapeutics (Moro et al., 2011), such as the parasympathomimetic bethanechol, which is one of the more commonly prescribed first-line treatments in the pharmaceutical management of underactive bladder (Kim, 2017). However, aside from this focus on the M3 muscarinic receptor, there is also a growing interest in combination therapies where, for example, administering both muscarinic agonists and alpha-adrenoceptor antagonists concurrently demonstrated greater success when compared to monotherapy in the management of underactive bladder (Yamanishi et al., 2004). This potential for alternative therapeutic options is important, as many patients who are administered muscarinic-acting pharmaceuticals in the management of bladder contractile disorders cease the regimen due to adverse side effects or lower than expected treatment outcomes (Yeowell et al., 2018). This is a growing area of research, with more work to be done regarding the potential benefits or harms from using parasympathomimetics in the management of underactive bladder (Moro et al., 2021).

Although the detrusor smooth muscle layer of the bladder has been the traditional target for research and therapeutic development, in recent years the importance of the U&LP in the maintenance of normal bladder function has been highlighted. The bladder generates spontaneous contractions, which can be altered in cases such as outlet obstruction or nerve injury (Kushida and Fry, 2016). The role of this spontaneous activity in the intact bladder is unclear (Fry and McCloskey, 2019), but may be mediated by signals originating in the U&LP, suggesting mechanisms where this tissue might underlie bladder contractile disorders (Fry and Vahabi, 2016). Calcium (Ca^{2+}) and membrane potential transients commence in the lamina propria and spread towards the detrusor. In addition, the U&LP can release mediators, such as acetylcholine during stretching (Moro et al., 2011), which can induce increased spontaneous contractions in the detrusor (Kanai, 2007). A number of cells within the tissue may induce this spontaneous activity, as well as generate spontaneous Ca^{2+} transients, such as myofibroblasts (Sui et al., 2008), pericytes (Lee et al., 2016; Hashitani et al., 2018), interstitial-like cells (Fry and McCloskey, 2019) or muscularis mucosae (Heppner et al., 2011; Kushida and Fry, 2016). These cells remain highly sensitive to Ca^{2+}, and there is value in identifying sources of Ca^{2+} influx into the tissue from extracellular fluids. Of note, however, is the potential for species differences in the generation and activity of phasic contractions. For example, the spontaneous activity of the bladder urothelium and lamina propria in the pig appears to predominantly arise from the muscularis mucosae, although there is evidence that this is not the case across all species (Mitsui et al., 2020).

With stimulation of the G protein-coupled receptors (GPCRs) resulting in contractions of the urinary bladder U&LP, identifying any common mechanisms of action between them is important. One primary function of the GPCRs in the urinary bladder may be the modulation of Ca^{2+} channels in the cell membranes, accommodating an influx of Ca^{2+} from extracellular fluids, and mediating a variety of physiological responses, from bladder contractions to increased pacemaker activity (Wuest et al., 2007). This study aims to identify similarities in extracellular Ca^{2+} requirements between muscarinic, histamine, 5-hydroxytryptamine (5-HT), neurokinin-A (NKA), prostaglandin E2 (PGE2), and angiotensin II (ATII) receptors for mediating contractile activity of the urinary bladder U&LP.

2 MATERIALS AND METHODS

2.1 Tissue Collection

Urinary bladders from Large White-Landrace-Duroc pigs (6 months old, 80 kg live weight) were used as the tissue in this study. All bladders were obtained from the local abattoir after slaughter for the routine commercial provision of food with no animals bred, harmed, culled, interfered, or interacted with as part of this research project. As such, animal ethics approval was not required (Business Queensland, 2015). Only female bladders were used in this study. After collection from the abattoir, tissues were transported in a portable cooler in cold Krebs-Henseleit bicarbonate solution (NaCl 118.4 mM, $NaHCO_3$ 24.9 mM, D-glucose 11.7 mM, KCl 4.6 mM, $MgSO_4$ 2.41 mM, $CaCl_2$ 1.9 mM, and KH_2PO_4 1.18 mM) maintained at 4 °C to the University research facilities and used within 3 hours of the animal's slaughter.

2.2 Tissue Preparation

A single 4 cm strip was taken longitudinally from the bladder wall at the midpoint between the trigone and the bladder apex. Tissue strips were continually washed with a cold Krebs-Henseleit bicarbonate solution during the preparation and dissection stage. The white-coloured detrusor smooth muscle was dissected away from the pink-coloured urothelium and lamina propria using fine scissors. Histological assessment is known to effectively separate the two layers (Moro et al.,

2012). After dissection and preparation, this single strip was cut in the middle, resulting in 2 × 2 cm strips which were mounted and suspended in 10 ml isolated tissue baths (Labglass, Brisbane, Australia) containing warmed Krebs solution at 37°C and perfused with carbogen gas (95% oxygen and 5% carbon dioxide). A maximum of two 4 cm strips were taken from each unique porcine bladder across the experiments. Throughout this manuscript, n values quoted are from paired tissue strips, and as such, the number of animals (N) used can be calculated using $n \div 2$. After mounting, tissue tension was manually adjusted to 2 g using each transducer positioner's fine adjustment knob. Each bath was washed with warmed Krebs a total of three times prior to the start of experimentation. At the conclusion of each experiment, tissue weight was measured on a scale to an accuracy of 0.001 g. The mean weight of porcine U&LP tissues was 0.22 ± 0.01 g (n = 208).

2.3 Pharmaceutical Agents

Krebs-Henseleit bicarbonate solution ingredients were obtained from Sigma-Aldrich (Missouri, U.S.). Carbamylcholine chloride (carbachol) and histamine dihydrochloride (histamine) were obtained from Sigma-Aldrich (Missouri, U.S.), nifedipine and NKA were from Tocris Bioscience (Bristol, U.K.), 5-HT was from Toronto Research Centre (Toronto, CA), and ATII and PGE2 were obtained from Cayman Chemicals (Michigan, U.S.). Nifedipine and PGE2 were dissolved in 100% ethanol, while all other pharmaceutical agents were soluble in distilled water. Concentrations chosen for the agonists and antagonists were selected based on their selectivity at each receptor and consistent with concentrations used in previous studies. In each case, the agonist concentration used induced a submaximal contraction (with an aim to achieve around 80% of peak receptor-induced contraction).

2.4 Measurements and Data Collection

In the nifedipine studies, a vehicle control of 100% ethanol was added to control tissues or nifedipine (1 μM) was added to the experimental tissues and left to equilibrate for 30 min. Nifedipine was kept in darkness until the final application in the organ bath and experiments were concluded within 30 min to ensure no adverse light impacts. In the Ca^{2+}-free studies, control tissues were washed with Krebs solution as normal, whereas the experimental tissues were washed three times with a nominally Ca^{2+}-free Krebs solution. This also ensured that any excess Ca^{2+} on the tissue, or Ca^{2+} leaking out from intracellular sources, was cleared from the bath. Tissues were then left to equilibrate for 3 min in nominally zero Ca^{2+} solution before agonists were added. A single dose of a select GPCR agonist was added to both the control and experimental tissues after equilibration. Tension, frequency, and amplitude of spontaneous contractions were measured with an isometric force transducer (MCT050/D, ADInstruments, Castle Hill, Australia) and recorded on a Powerlab system using Labchart v7 software (ADInstruments). Although a threshold was not applied, in all cases each spontaneous contraction exceeded 0.4 g.

2.5 Statistical Analysis

Changes in tension and amplitude were measured in grams (g), where amplitude was measured from the lowest point of spontaneous phasic contraction to peak. Frequency was expressed as the number of spontaneous phasic contractions per minute (cpm). All data was analysed using GraphPad Prism version 9 (San Diego, CA), and results were presented as mean ± standard error of the mean (SEM). A paired t-test was used to analyse tissue responses before and after the addition of agonist. A paired Student's two-tailed t-test was used to analyse the significance of results when comparing tissues with direct controls, as per previous studies (Stromberga et al., 2020a). A one-way ANOVA with Tukey post-test was also undertaken to compare the means where more than two variables were assessed. For all statistical analysis, $p < 0.05$ was considered statistically significant.

2.6 Preliminary Results Related to the Omission of Extracellular Ca^{2+}

There is variation in the literature surrounding methods to remove extracellular Ca^{2+} from an isolated tissue bath. Firstly, this may involve the omission of calcium chloride (CaCl) from Krebs-Henseleit bicarbonate solution (Poyser, 1984). Secondly, the addition of Ca^{2+} chelating agents ethylenediaminetetraacetic acid (EDTA, 1–5 mM) (Maggi et al., 1989) or glycoletherdiaminetetraacetic acid (EGTA, 0.5 mM) solution (Yoshimura and Yamaguchi, 1997) have been proposed. However, EGTA may have impacts on other ions (Wheeler and Weiss, 1979) or other mechanisms within the tissue (Poyser, 1984), as well as potentially destabilise cell membranes, leading to increased Ca^{2+} permeability (Guan et al., 1988). To assess this feasibility of using Ca^{2+} chelators, we observed that compared to the simple omission of CaCl, the addition of 1 mM EDTA or 0.5 mM EGTA had no effect on contractile responses to our agonists (e.g., carbachol 1 μM). Thirdly, in some studies, the removal of Ca^{2+} appeared to result in a hypovolemic solution, and in order to rectify this, the concentration of other ions was altered. In our pilot studies, when incorporating additional Mg^{2+} to substitute for omitted Ca^{2+}, there was no significant effect on contractions (n = 8). As such, no additional magnesium was added to replace the omission of the Ca^{2+} divalent cation. Fourthly, there is the potential for Ca^{2+} to enter the Ca^{2+}-free bath solution from the cytoplasm, or via the activation of other cellular pumps/exchangers. To minimise the impact of this, after mounting in the bath, tissues were washed three times over 5 min in warmed Ca^{2+}-free Krebs. As a final check, before and after contractions, the extracellular buffer was collected and checked with spectrophotometric assessments (Pacific Laboratory Products, Victoria, Australia), with no Ca^{2+} detected on this assay. This provided confidence in a nominally zero Ca^{2+} solution. As there were no observable or significant impacts to any contractions from adjusting for the methods listed above, the decision was made to henceforth solely remove Ca^{2+} from the Krebs solution and not alter anything else, as this was the path of least manipulation.

TABLE 1 | Summary of U&LP tissue spontaneous phasic activity. Tension, frequency, and amplitude recorded in response to receptor agonists. Data presented as mean ± SEM.

Agonist	Conc	Δ Tension (g)	Δ Frequency (cpm)	Δ Amplitude (g)	*n*
Carbachol	1 μM	3.77 ± 0.31***	1.15 ± 0.20***	–0.27 ± 0.10*	22
Histamine	100 μM	1.54 ± 0.20***	0.64 ± 0.24*	–0.08 ± 0.07	16
5-HT	100 μM	6.23 ± 0.64***	2.15 ± 0.64**	–0.37 ± 0.09***	17
NKA	300 nM	2.50 ± 0.25***	0.11 ± 0.24	–0.12 ± 0.06	17
PGE2	10 μM	2.43 ± 0.22***	–0.05 ± 0.34	–0.03 ± 0.04	16
ATII	100 nM	1.50 ± 0.18***	0.20 ± 0.08*	–0.22 ± 0.06**	16

*p < *0.05*, **p < *0.01*, ***p < *0.001 (paired* t*-test).*

3 RESULTS

3.1 Influence of GCPR Agonists in U&LP

In the absence of stimulation from any agonist, U&LP tissue strips developed spontaneous phasic contractions at a frequency of 3.65 ± 0.08 cpm with an amplitude of 0.73 ± 0.04 g (n = 104). When receptor agonists carbachol (1 μM), histamine (100 μM), 5-HT (100 μM), NKA (300 nM), PGE2 (10 μM), and ATII (100 nM) were added to the tissues, U&LP baseline tension increased significantly for all activated receptors ($p < 0.001$, **Table 1**). In addition, the frequency of spontaneous phasic contractions increased for carbachol ($p < 0.001$), histamine ($p < 0.05$), 5-HT ($p < 0.01$), and ATII ($p < 0.05$), but not NKA or PGE2. Amplitude was reduced by all the agonists, but the changes were statistically significant for only carbachol ($p < 0.05$), 5-HT ($p < 0.001$), and ATII ($p < 0.01$).

3.2 Influence of Nifedipine on U&LP Contractions

When nifedipine (1 μM) or vehicle control (totaling 0.035% ethanol) were added to tissues at the start of the 30 min equilibration period, there were no immediate changes to baseline tension, frequency, or amplitude for any of the agonists.

3.2.1 Effect of Nifedipine on Baseline Tensions

After activation of the muscarinic, histamine, 5-HT, NKA, PGE2 and ATII receptors, the baseline tension of the U&LP tissue increased, and the increases were similar for all the agonists (**Figure 1**). In the presence of nifedipine (1 μM), the contractions were inhibited as follows (paired Student's two-tailed t-tests): carbachol by 54% (1μM, n = 11, $p < 0.01$); histamine by 45% (100μM, n = 8, $p < 0.05$); 5-HT by 28% (100μM, n = 8, $p < 0.01$); NKA by 49% (300nM, n = 8, $p < 0.001$); PGE2 by 29% (10μM, n = 8, $p < 0.05$); and ATII by 47% (100nM, n = 8, $p < 0.05$). The impact of nifedipine was relatively consistent after the activation of each agonist, with no significant differences found between any of the responses (p = NSD, ANOVA with Tukey post-test for this final statistical assessment only).

3.2.2 Effect of Nifedipine on Frequency and Amplitude of Phasic Contractions

The frequencies and amplitudes of spontaneous phasic contractions produced by the U&LP tissues were investigated in the absence and presence of nifedipine for each of the receptor agonists (**Table 2**). No significant differences in the contractile frequency or amplitude were observed between the presence and absence of nifedipine (1 μM) for responses to carbachol, histamine, 5-HT, or NKA. Contractions for PGE2 (10μM, n = 8, $p < 0.01$) and ATII (100nM, n = 8, $p < 0.05$) exhibited a reduction in the amplitude of spontaneous phasic contractions in the presence of nifedipine, and when compared to the response in the absence of nifedipine, was a statistically significant difference.

3.3 Influence of Nominally Zero Ca^{2+} Solution on U&LP Contractions

3.3.1 Effect of Nominally Zero Ca^{2+} Solution on Baseline Tensions

U&LP contractions for all receptor agonists in the presence of nominally zero Ca^{2+} solution were significantly inhibited compared to the control group in normal Krebs solution. In the absence of any extracellular Ca^{2+} sources, the contractions of the U&LP were impaired (paired Student's two-tailed t-test, **Figure 2**). Contractions were inhibited as follows: carbachol by 39% (1μM, n = 11, $p < 0.01$); histamine by 46% (100 μM, n = 8, $p < 0.05$); 5-HT by 28% (100 μM, n = 8, $p < 0.05$); NKA by 22% (300 nM, n = 9, $p < 0.05$); PGE2 by 32% (10 μM, n = 8, $p < 0.05$); and ATII by 43% (100 nM, n = 8, $p < 0.01$). Across all receptors, there were no significant differences between the averaged responses (p = NSD, ANOVA with Tukey post-test).

3.3.2 Effect of Nominally Zero Ca^{2+} Solution on Frequency and Amplitude of Phasic Contractions

Tissues exposed to a Ca^{2+}-free extracellular environment had no alterations to their frequency or amplitude of spontaneous phasic contractions during responses to receptor agonists carbachol (1 μM), histamine (100 μM), 5-HT (100 μM), NKA (300 nM) or PGE2 (10 μM). Although the activation of all receptors induced increases to baseline tensions, only ATII (100 nM) also resulted in the significant decrease in the frequency of spontaneous phasic contractions in the presence of nominally zero Ca^{2+} solution (**Table 3**).

3.4 Overall Impact of Extracellular Ca^{2+} on Baseline Tension Contractions

In this study, two different methods were applied to assess the impact of extracellular Ca^{2+}: the immersion of the tissue in nominally zero Ca^{2+} solution; or through Ca^{2+} channel antagonism with nifedipine (1 μM). Both methods significantly inhibited contractile activity changes in response to the assessed agonists. Overall, when looking at the impact of either nifedipine or nominally zero Ca^{2+} solution, there were no significant differences (Student's two-tailed unpaired t-tests for each) between the effectiveness of inhibitions of tension, frequency,

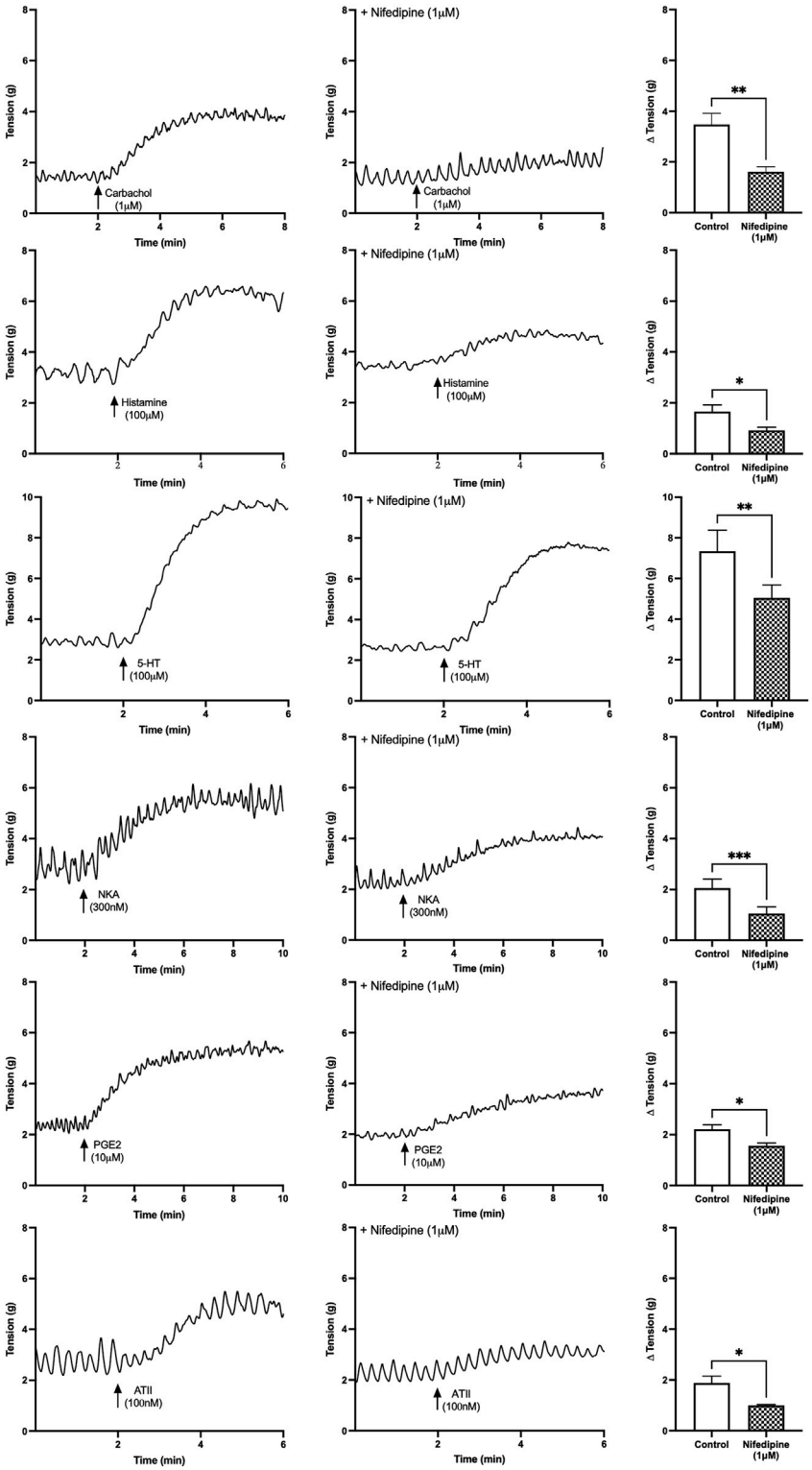

FIGURE 1 | U&LP baseline tension responses to receptor agonists carbachol (1 μM), histamine (100 μM), 5-HT (100 μM), NKA (300 nM), PGE2 (10 μM), and ATII (100 nM) in the absence of (left) and the presence of (right) nifedipine (1 μM). *$p < 0.05$, **$p < 0.01$, ***$p < 0.001$ (paired Student's two-tailed *t*-test).

TABLE 2 | U&LP change in frequency and amplitude responses to receptor agonists in the absence (control) and presence of nifedipine (1 μM). There were no significant differences between the average frequency changes between the absence and presence of nifedipine for any of the agonists. Data presented as mean ± SEM.

		Δ Frequency (cpm)			
Agonist	**Conc**	**Control**	**+ Nifedipine**	***p*-value**	***n***
Carbachol	1 μM	0.92 ± 0.17***	1.20 ± 0.44*	0.58	11
Histamine	100 μM	0.76 ± 0.28*	0.83 ± 0.33*	0.88	8
5-HT	100 μM	2.58 ± 0.95*	3.67 ± 1.66	0.26	8
NKA	300 nM	0.44 ± 0.40	0.50 ± 0.59	0.91	8
PGE2	10 μM	-0.23 ± 0.38	-0.41 ± 0.41	0.78	8
ATII	100 nM	0.06 ± 0.17	0.24 ± 0.18	0.45	8
		Δ Amplitude (g)			
Carbachol	1 μM	−0.51 ± 0.17*	−0.18 ± 0.06*	0.07	11
Histamine	100 μM	−0.03 ± 0.05	−0.07 ± 0.04	0.54	8
5-HT	100 μM	−0.25 ± 0.10*	−0.28 ± 0.08**	0.70	9
NKA	300 nM	−0.23 ± 0.08*	−0.18 ± 0.07*	0.48	8
PGE2	10 μM	−0.04 ± 0.04	−0.16 ± 0.03***	0.01**	8
ATII	100 nM	−0.32 ± 0.08**	−0.16 ± 0.06**	0.05*	8

*p < 0.05, **p < 0.01, ***p < 0.001 (paired t-test) after the addition of each agonist (listed to the left) in the absence and presence of nifedipine (1 μM). p-values (paired Student's two-tailed t-test) in the right column denote the differences between the responses to agonist in the absence of and the responses to agonist in the presence of nifedipine.

or amplitude after the addition of carbachol (1 μM), histamine (100 μM), 5-HT (100 μM), NKA (300 nM), PGE2 (10 μM), and ATII (100nM, p = NSD for all).

4 DISCUSSION

The extent of influence that either extracellular or intracellular Ca^{2+} has on smooth muscle contraction varies throughout the body, promoting a specific interest towards identifying the prominent sources of Ca^{2+} influx across different organs. Ca^{2+} has a clear role in mediating the contractile activity of the bladder (Ikeda and Kanai, 2008), but the specific source of the Ca^{2+} in the urothelium and lamina propria tissue layer has never been investigated. Extracellular Ca^{2+} is of particular interest as it plays an essential role in many physiologic functions throughout the human body, and stimulates not only contraction, but also key underlying Ca^{2+} -dependent systems, which could be altered in bladder disorders (de Groat, 2004). As such, identifying the potential mechanisms involved in receptor-mediated contractions can support the development of new and novel pharmaceuticals, as well as develop a greater understanding of potential mechanisms underlying bladder dysfunction.

This study has identified prominent extracellular Ca^{2+} influences on muscarinic, histamine, 5-HT, neurokinin-A, prostaglandin E2 and angiotensin-II receptor mechanisms of action. Each of these receptor systems are G protein-coupled receptors of the G_{q11} class. Particular subtypes of interest have been previously identified as the M3 muscarinic (Moro et al., 2011), H1 histamine (Stromberga et al., 2019), 5-HT_{2A} serotonergic (Moro et al., 2016), neurokinin (Grundy et al., 2018), EP1 prostaglandin (Stromberga et al., 2020b), and AT_1 angiotensin II (Lim et al., 2021) receptors. This broad presence of GPCRs in the U&LP constitutes the majority of surface receptors in the bladder, and many can be activated through neurotransmitters, hormones, and external stimuli that elicit a variety of cellular responses to stimulate downstream signalling activities (Mizuno and Itoh, 2009). Both inhibition of the L-type Ca^{2+} channels with nifedipine or inhibiting Ca^{2+} influx from extracellular fluids showed similar influences towards impairing GPCR contractions, inhibiting 20–50% of the contractile responses. These results are consistent with the finding by Heppner et al. (2011) where the inhibition of L-type voltage-gated Ca^{2+} channels reduced carbachol-induced contractions of human tissue by 74%, 18% in pig and 27% in mouse tissue. The additional finding that spontaneous phasic activity is not affected by the addition of nifedipine suggests that the overall conductance which generates the spontaneous contractions does not appear to have a relation with the L-type Ca^{2+} channels.

In this study, the response of each of the GPCRs to nifedipine has supported the presence of L-type voltage-gated Ca^{2+} channels in the U&LP of the urinary bladder. Lining the bladder lumen, the urothelium not only has an integral role in acting as the highly resistant physical barrier between urine and the underlying tissues, but also responds to stimuli and can transfer information to underlying cells (Birder and Andersson, 2013). Heppner et al. (2011) also observed the bladder U&LP of guinea pig tissue to exhibit dependence on Ca^{2+} influx through L-type Ca^{2+} channels, with spontaneous contractions significantly inhibited by nifedipine. However, clear evidence is lacking on the location of the L-type Ca^{2+} channels within these tissue layers. The lamina propria, a layer of highly innervated connective tissue located between the basement membrane of the urothelium and luminal surface of the detrusor, has demonstrated an essential role in signalling functions (Andersson and McCloskey, 2014; Heppner et al., 2017). In particular, its role in Ca^{2+} signalling may be of importance to the maintenance of normal bladder function and may present as a core site of extracellular Ca^{2+} influence. This could be through myofibroblasts, which have been identified to contribute to spontaneous activity through extracellular sources, and also express muscarinic and purinergic receptors that could assist in propagating signals to the urothelium (Heppner et al., 2011). Moreover, it has been suggested that the muscularis mucosae found within the underlying lamina propria of some species may also be impacted by the entry of extracellular Ca^{2+} (Heppner et al., 2011). In addition, interstitial cells of Cajal-like cells, located within the lamina propria layers, have also demonstrated firing activity of Ca^{2+} transients (Hashitani et al., 2004; Johnston et al., 2008), and there is some influence on the activity of pericytes surrounding blood vessels within the tissue (Mitsui and Hashitani, 2020).

The partial reduction (20–50%) in GPCR-mediated contractions of the U&LP by nifedipine may indicate additional sources of Ca^{2+} entry. This could include other voltage-gated channels such as T-type or P-type Ca^{2+} channels, previously identified in the urinary bladder (Deng

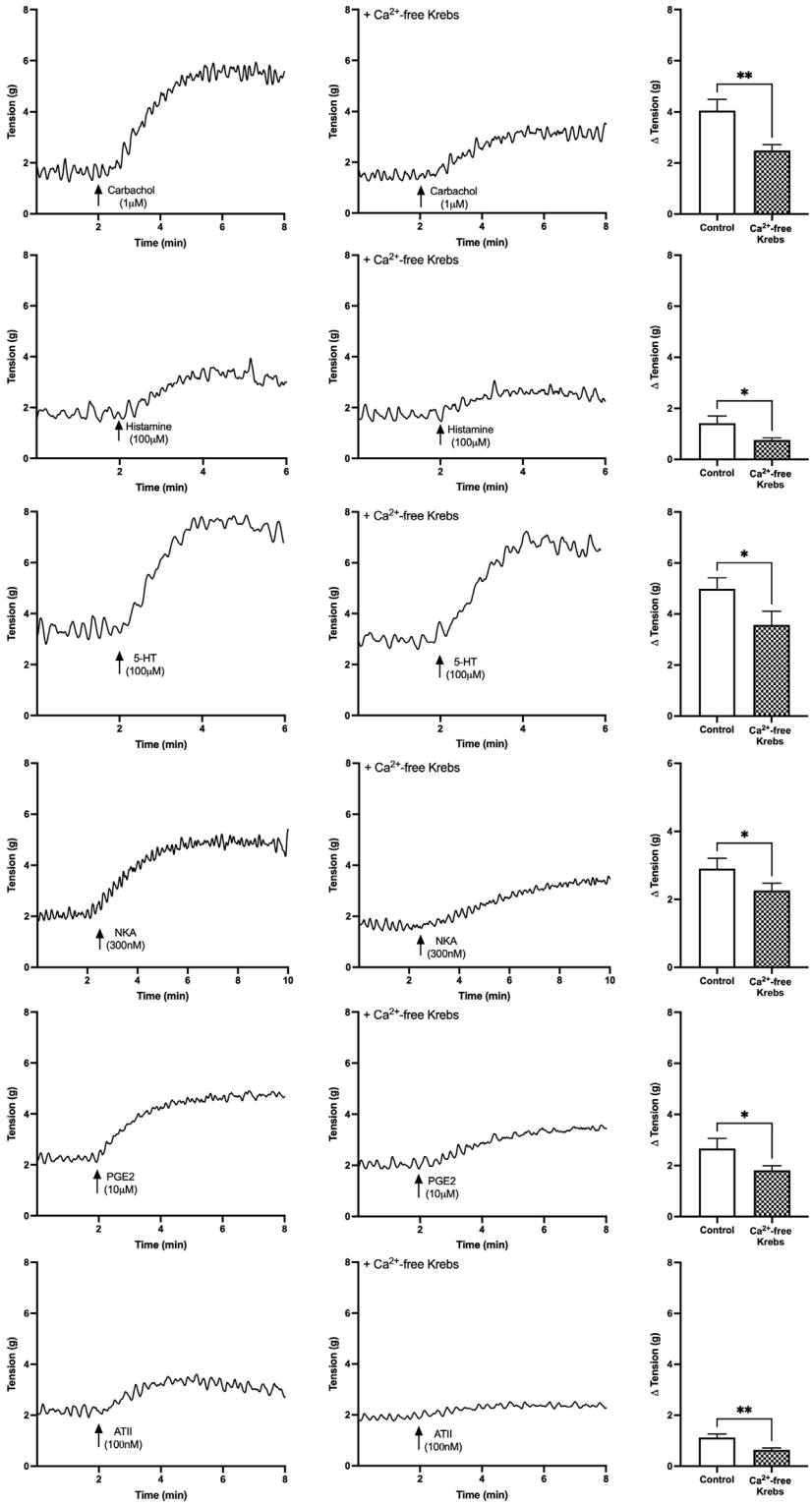

FIGURE 2 | U&LP baseline tension responses to receptor agonists carbachol (1 μM), histamine (100 μM), 5-HT (100 μM), NKA (300 nM), PGE2 (10 μM), and ATII (100 nM) as controls in the normal Krebs (left) and in nominally zero Ca^{2+} solution (right). *$p < 0.05$, **$p < 0.01$, ***$p < 0.001$ (paired Student's two-tailed *t*-test).

TABLE 3 | U&LP change in frequency and amplitude responses to receptor agonists in the absence (control) and presence of nominally zero Ca^{2+} solution. No significant differences between the average amplitude changes between the absence and presence of nominally zero Ca^{2+} solution for any of the agonists. Data presented as mean ± SEM.

Agonist	Conc	Control	+ Ca^{2+}-free Krebs	*p*-value	*n*
Δ Frequency (cpm)					
Carbachol	1 μM	1.38 ± 0.36**	1.88 ± 0.84*	0.48	11
Histamine	100 μM	0.74 ± 0.27*	0.93 ± 0.70	0.52	6
5-HT	100 μM	2.44 ± 0.77*	2.68 ± 1.31	0.83	8
NKA	300 nM	0.01 ± 0.24	1.93 ± 0.47	0.09	9
PGE2	10 μM	0.14 ± 0.59	0.63 ± 0.45	0.49	8
ATII	100 nM	0.22 ± 0.09*	−0.32 ± 0.16	0.02*	8
Δ Amplitude (g)					
Carbachol	1 μM	−0.02 ± 0.05	0.02 ± 0.05	0.58	11
Histamine	100 μM	−0.13 ± 0.12	−0.19 ± 0.07*	0.71	8
5-HT	100 μM	−0.51 ± 0.14**	−0.22 ± 0.22	0.17	8
NKA	300 nM	−0.01 ± 0.07	−0.05 ± 0.05	0.63	9
PGE2	10 μM	−0.02 ± 0.08	−0.08 ± 0.08	0.66	8
ATII	100 nM	−0.12 ± 0.08	0.04 ± 0.11	0.32	8

*$p < 0.05$, **$p < 0.01$ (paired t-test) after the addition of each agonist (listed to the left) in the absence and presence of Ca^{2+}-free Krebs. p-values (paired Student's two-tailed t-test) in the right column denote the differences between the responses to agonist in the absence of and the responses to agonist in the presence of nominally zero Ca^{2+} solution.*

et al., 2012). In addition, this partial reduction which was maintained in a Ca^{2+} -free environment suggests internal stores of Ca^{2+}, such as from the sarcoplasmic reticulum, or other signalling pathways activated by $G_{q/11}$ receptor proteins, may play a role in mediating contractile activity of the U&LP.

4.1 Clinical Relevance

Antimuscarinics and parasympathomimetics have shown success for the management of bladder contractile disorders, and currently sit as first-line pharmaceutical treatments for overactive bladder and underactive bladder, respectively. However, most patients cease treatment regimens due to lower than expected benefits and adverse side effects. Recent success has been found with combination therapies and there is increasing interest in the identification of alternative receptors systems that may be involved in contraction, and hence future targets for therapeutic treatments. This study's identification of similarities between receptors mediating and modulating contraction in the urinary bladder may present future therapeutic targets or provide insights into mechanisms that may be dysfunctional in overactive or underactive bladder. Of particular interest was this study's finding that histamine, neurokinin-A and angiotensin II are highly dependent on extracellular Ca^{2+}, warranting further investigation into their clinical use for the management of bladder dysfunction.

4.2 Limitations and Future Direction

A limitation of this study was the use of single-dose applications of receptor agonists to examine changes in frequencies and amplitudes of phasic contractions over 30-min time periods. It should be noted that in detrusor studies of carbachol-induced bladder contractions, human tissue responded to inhibited extracellular Ca^{2+} to a greater extent than pig tissue (Wuest et al., 2007), however, this has not been demonstrated in urothelial and lamina propria studies. Future studies could investigate the potential role of ageing in influencing receptor responses to extracellular contractions, such as histamine (Stromberga et al., 2020a), as well as explore the influence of other GPCRs and the influence of Ca^{2+} on their responses.

5 CONCLUSION

This study identified a prominent role of extracellular Ca^{2+} for urinary bladder contractile activity. The responses obtained from muscarinic, histamine, 5-HT, neurokinin-A, prostaglandin E2 and angiotensin II receptor activation are highly sensitive to extracellular Ca^{2+}, presenting a potential mechanism underlying bladder dysfunction.

DATA AVAILABILITY STATEMENT

The raw data supporting the conclusion of this article will be made available by the authors, without undue reservation.

AUTHOR CONTRIBUTIONS

Data was collected by CP. The study design, analysis of data, and preparation of manuscript received equal contribution from all authors CP, RC-W, and CM.

FUNDING

CP was supported by an Australian Government Research Training Program Scholarship.

REFERENCES

Andersson, K. E., and McCloskey, K. D. (2014). Lamina Propria: the Functional center of the Bladder? *Neurourol. Urodynam.* 33 (1), 9–16. doi:10.1002/nau.22465

Birder, L., and Andersson, K.-E. (2013). Urothelial Signaling. *Physiol. Rev.* 93 (2), 653–680. doi:10.1152/physrev.00030.2012

Business Queensland (2015). Using Animals for Scientific Purposes. Queensland Government. [Online] Available at: https://www.business.qld.gov.au/industries/farms-fishing-forestry/agriculture/livestock/animal-welfare/animals-science/using-animals (Accessed March 3, 2021).

Chapple, C. R., Osman, N. I., Birder, L., Dmochowski, R., Drake, M. J., van Koeveringe, G., et al. (2018). Terminology Report from the International Continence Society (ICS) Working Group on Underactive Bladder (UAB). *Neurourol. Urodynam.* 37 (8), 2928–2931. doi:10.1002/nau.23701

de Groat, W. C. (2004). The Urothelium in Overactive Bladder: Passive Bystander or Active Participant? *Urology* 64 (6), 7–11. doi:10.1016/j.urology.2004.08.063

Deng, J., He, P., Zhong, X., Wang, Q., Li, L., and Song, B. (2012). Identification of T-type Calcium Channels in the Interstitial Cells of Cajal in Rat Bladder. *Urology* 80 (6), e1–13891387. doi:10.1016/j.urology.2012.07.031

Fry, C. H., and McCloskey, K. D. (2019). Spontaneous Activity and the Urinary Bladder. *Adv. Exp. Med. Biol.* 1124, 121–147. doi:10.1007/978-981-13-5895-1_5

Fry, C. H., Sui, G.-P., Kanai, A. J., and Wu, C. (2007). The Function of Suburothelial Myofibroblasts in the Bladder. *Neurourol. Urodyn.* 26 (6), 914–919. doi:10.1002/nau.20483

Fry, C. H., and Vahabi, B. (2016). The Role of the Mucosa in normal and Abnormal Bladder Function. *Basic Clin. Pharmacol. Toxicol.* 119, 57–62. doi:10.1111/bcpt.12626

Grundy, L., Chess-Williams, R., Brierley, S. M., Mills, K., Moore, K. H., Mansfield, K., et al. (2018). NKA Enhances Bladder-Afferent Mechanosensitivity via Urothelial and Detrusor Activation. *Am. J. Physiology-Renal Physiol.* 315 (4), F1174–f1185. doi:10.1152/ajprenal.00106.2018

Hashitani, H., Mitsui, R., Miwa-Nishimura, K., and Lam, M. (2018). Role of Capillary Pericytes in the Integration of Spontaneous Ca2+ Transients in the Suburothelial Microvasculature *In Situ* of the Mouse Bladder. *J. Physiol.* 596 (16), 3531–3552. doi:10.1113/jp275845

Hashitani, H., Yanai, Y., and Suzuki, H. (2004). Role of Interstitial Cells and gap Junctions in the Transmission of Spontaneous Ca2+signals in Detrusor Smooth Muscles of the guinea-pig Urinary Bladder. *J. Physiol.* 559, 567–581. doi:10.1113/jphysiol.2004.065136

Heppner, T. J., Hennig, G. W., Nelson, M. T., and Vizzard, M. A. (2017). Rhythmic Calcium Events in the Lamina Propria Network of the Urinary Bladder of Rat Pups. *Front. Syst. Neurosci.* 11, 87. doi:10.3389/fnsys.2017.00087

Heppner, T. J., Layne, J. J., Pearson, J. M., Sarkissian, H., and Nelson, M. T. (2011). Unique Properties of Muscularis Mucosae Smooth Muscle in guinea Pig Urinary Bladder. *Am. J. Physiology-Regulatory, Integr. Comp. Physiol.* 301 (2), R351–R362. doi:10.1152/ajpregu.00656.2010

Ikeda, Y., and Kanai, A. (2008). Urotheliogenic Modulation of Intrinsic Activity in Spinal Cord-Transected Rat Bladders: Role of Mucosal Muscarinic Receptors. *Am. J. Physiology-Renal Physiol.* 295 (2), F454–F461. doi:10.1152/ajprenal.90315.2008

Johnston, L., Carson, C., Lyons, A. D., Davidson, R. A., and McCloskey, K. D. (2008). Cholinergic-induced Ca2+ Signaling in Interstitial Cells of Cajal from the guinea Pig Bladder. *Am. J. Physiology-Renal Physiol.* 294 (3), F645–F655. doi:10.1152/ajprenal.00526.2007

Kanai, A., Roppolo, J., Ikeda, Y., Zabbarova, I., Tai, C., Birder, L., et al. (2007). Origin of Spontaneous Activity in Neonatal and Adult Rat Bladders and its Enhancement by Stretch and Muscarinic Agonists. *Am. J. Physiology-Renal Physiol.* 292, F1065–F1072. doi:10.1152/ajprenal.00229.2006

Kim, D. K. (2017). Current Pharmacological and Surgical Treatment of Underactive Bladder. *Investig. Clin. Urol.* 58, S90–S98. doi:10.4111/icu.2017.58.S2.S90

Kushida, N., and Fry, C. H. (2016). On the Origin of Spontaneous Activity in the Bladder. *BJU Int.* 117 (6), 982–992. doi:10.1111/bju.13240

Lee, K., Mitsui, R., Kajioka, S., Naito, S., and Hashitani, H. (2016). Role of PTHrP and Sensory Nerve Peptides in Regulating Contractility of Muscularis Mucosae and Detrusor Smooth Muscle in the guinea Pig Bladder. *J. Urol.* 196 (4), 1287–1294. doi:10.1016/j.juro.2016.04.082

Lim, I., Mitsui, R., Kameda, M., Sellers, D. J., Chess-Williams, R., and Hashitani, H. (2021). Comparative Effects of Angiotensin II on the Contractility of Muscularis Mucosae and Detrusor in the Pig Urinary Bladder. *Neurourol. Urodynam.* 40 (1), 102–111. doi:10.1002/nau.24548

Maggi, C. A., Santicioli, P., Geppetti, P., Parlani, M., Astolfi, M., Bianco, E. D., et al. (1989). The Effect of Calcium Free Medium and Nifedipine on the Release of Substance P-like Immunoreactivity and Contractions Induced by Capsaicin in the Isolated guinea-pig and Rat Bladder. *Gen. Pharmacol. Vasc. Syst.* 20 (4), 445–456. doi:10.1016/0306-3623(89)90194-8

Mitsui, R., and Hashitani, H. (2020). Synchrony of Spontaneous Ca2+ Activity in Microvascular Mural Cells. *J. Smooth Muscle Res.* 56 (0), 1–18. doi:10.1540/jsmr.56.1

Mitsui, R., Lee, K., Uchiyama, A., Hayakawa, S., Kinoshita, F., Kajioka, S., et al. (2020). Contractile Elements and Their Sympathetic Regulations in the Pig Urinary Bladder: a Species and Regional Comparative Study. *Cell Tissue Res* 379 (2), 373–387. doi:10.1007/s00441-019-03088-6

Mizuno, N., and Itoh, H. (2009). Functions and Regulatory Mechanisms of Gq-Signaling Pathways. *Neurosignals* 17 (1), 42–54. doi:10.1159/000186689

Moro, C., Edwards, L., and Chess-Williams, R. (2016). 5-HT2A Receptor Enhancement of Contractile Activity of the Porcine Urothelium and Lamina Propria. *Int. J. Urol.* 23 (11), 946–951. doi:10.1111/iju.13172

Moro, C., Leeds, C., and Chess-Williams, R. (2012). Contractile Activity of the Bladder Urothelium/lamina Propria and its Regulation by Nitric Oxide. *Eur. J. Pharmacol.* 674 (2-3), 445–449. doi:10.1016/j.ejphar.2011.11.020

Moro, C., Phelps, C., Veer, V., Clark, J., Glasziou, P., Tikkinen, K. A. O., et al. (2021). The Effectiveness of Parasympathomimetics for Treating Underactive Bladder: A Systematic Review and Meta-analysis. *Neurourology and Urodynamics* 41 (1), 127–139. doi:10.1002/nau.24839

Moro, C., Tajouri, L., and Chess-Williams, R. (2013). Adrenoceptor Function and Expression in Bladder Urothelium and Lamina Propria. *Urology* 81 (1), e1–211. doi:10.1016/j.urology.2012.09.011

Moro, C., Uchiyama, J., and Chess-Williams, R. (2011). Urothelial/lamina Propria Spontaneous Activity and the Role of M3 Muscarinic Receptors in Mediating Rate Responses to Stretch and Carbachol. *Urology* 78 (6), e9–1442. doi:10.1016/j.urology.2011.08.039

Poyser, N. L. (1984). Effect of Using Calcium-free Krebs' Solution on Basal and A23187-Stimulated Prostaglandin Output from the Day 15 guinea-pig Uterus Superfused *In Vitro*. *Prostaglandins, Leukot. Med.* 13 (3), 259–269. doi:10.1016/0262-1746(84)90038-6

Stromberga, Z., Chess-Williams, R., and Moro, C. (2020a). Alterations in Histamine Responses between Juvenile and Adult Urinary Bladder Urothelium, Lamina Propria and Detrusor Tissues. *Sci. Rep.* 10 (1), 1–9. doi:10.1038/s41598-020-60967-7

Stromberga, Z., Chess-Williams, R., and Moro, C. (2019). Histamine Modulation of Urinary Bladder Urothelium, Lamina Propria and Detrusor Contractile Activity via H1 and H2 Receptors. *Sci. Rep.* 9 (1), 3899. doi:10.1038/s41598-019-40384-1

Stromberga, Z., Chess-Williams, R., and Moro, C. (2020b). Prostaglandin E2 and F2alpha Modulate Urinary Bladder Urothelium, Lamina Propria and Detrusor Contractility via the FP Receptor. *Front. Physiol.* 11 (705), 1–11. doi:10.3389/fphys.2020.00705

Sui, G.-P., Wu, C., Roosen, A., Ikeda, Y., Kanai, A. J., and Fry, C. H. (2008). Modulation of Bladder Myofibroblast Activity: Implications for Bladder Function. *Am. J. Physiology-Renal Physiol.* 295 (3), F688–F697. doi:10.1152/ajprenal.00133.2008

Wuest, M., Hiller, N., Braeter, M., Hakenberg, O. W., Wirth, M. P., and Ravens, U. (2007). Contribution of Ca2+ Influx to Carbachol-Induced Detrusor Contraction Is Different in Human Urinary Bladder Compared to Pig and Mouse. *Eur. J. Pharmacol.* 565 (1-3), 180–189. doi:10.1016/j.ejphar.2007.02.046

Yamanishi, T., Yasuda, K., Kamai, T., Tsujii, T., Sakakibara, R., Uchiyama, T., et al. (2004). Combination of a Cholinergic Drug and an Alpha-Blocker Is More Effective Than Monotherapy for the Treatment of Voiding Difficulty in Patients with Underactive Detrusor. *Int. J. Urol.* 11 (2), 88–96. doi:10.1111/j.1442-2042.2004.00753.x

Yeowell, G., Smith, P., Nazir, J., Hakimi, Z., Siddiqui, E., and Fatoye, F. (2018). Real-world Persistence and Adherence to Oral Antimuscarinics and Mirabegron in Patients with Overactive Bladder (OAB): a Systematic Literature Review. *BMJ Open* 8 (11), e021889. doi:10.1136/bmjopen-2018-021889

Yoshimura, Y., and Yamaguchi, O. (1997). Calcium Independent Contraction of Bladder Smooth Muscle. *Int. J. Urol.* 4 (1), 62–67. doi:10.1111/j.1442-2042.1997.tb00142.x

Conflict of Interest: The authors declare that the research was conducted in the absence of any commercial or financial relationships that could be construed as a potential conflict of interest.

frontiers | Frontiers in Physiology

ORIGINAL RESEARCH
published: 12 April 2022
doi: 10.3389/fphys.2022.885545

Protective Effect of Purinergic P2X7 Receptor Inhibition on Acrolein-Induced Urothelial Cell Damage

Zhinoos Taidi[1], *Kylie J. Mansfield*[2], *Hafiz Sana-Ur-Rehman*[1], *Kate H. Moore*[3] *and Lu Liu*[1]*

[1]School of Medical Sciences, UNSW Sydney, Sydney, NSW, Australia, [2]Graduate School of Medicine, University of Wollongong, Wollongong, NSW, Australia, [3]St George Hospital, UNSW Sydney, Sydney, NSW, Australia

OPEN ACCESS

Edited by:
Patrik Aronsson,
University of Gothenburg, Sweden

Reviewed by:
Basu Chakrabarty,
University of Bristol, United Kingdom
Warren G. Hill,
Beth Israel Deaconess Medical Center and Harvard Medical School, United States

***Correspondence:**
Lu Liu
Lu.Liu@unsw.edu.au

Specialty section:
This article was submitted to Integrative Physiology, a section of the journal Frontiers in Physiology

Received: 28 February 2022
Accepted: 23 March 2022
Published: 12 April 2022

Citation:
Taidi Z, Mansfield KJ, Sana-Ur-Rehman H, Moore KH and Liu L (2022) Protective Effect of Purinergic P2X7 Receptor Inhibition on Acrolein-Induced Urothelial Cell Damage. Front. Physiol. 13:885545. doi: 10.3389/fphys.2022.885545

Patients undergoing chemotherapy with cyclophosphamide experience cystitis due to excretion of a toxic metabolite, acrolein. Cystitis, an inflammation of the bladder, is associated with damage to the integrity of the urothelial barrier. The purinergic P2X7 receptor (P2X7R) is increasingly recognized for its role in inflammation and cell death. P2X7R is expressed abundantly on the bladder urothelium. The aim of this study was to investigate the role of P2X7R in acrolein-induced inflammatory damage in primary cultured porcine bladder urothelial cells. Confluent urothelial cells in culture were treated with acrolein to induce damage; also, with the P2X7R selective antagonist, A804598. Cell viability assay, immunocytochemistry, and trans-epithelial electrical resistance (TEER) studies were carried out to investigate the effect of treatments on urothelial cell function. Acrolein induced a significant reduction in urothelial cell viability, which was protected by the presence of A804598 (10 μM). The urothelial barrier function, indicated by TEER values, was also significantly reduced by acrolein, whereas pre-incubation with P2X7R antagonist significantly protected the urothelial cell barrier from acrolein-induced TEER reduction. The structure of urothelial cell tight junctions was similarly impacted by acrolein treatment, showing the fragmentation of zona occludens-1 (ZO-1) immunoreactivity. Pre-treatment of cells with A804598 countered against the actions of acrolein and maintained ZO-1 expression level and cell structure. The damaging effect of acrolein on urothelial cells integrity could be impaired by inhibition of P2X7R, therefore P2X7R blockade may be a possible therapy in patients with bladder cystitis caused by cyclophosphamide treatment.

Keywords: acrolein, urothelium, interstitial cystitis, bladder inflammation, purinergic receptors, purinergic P2X7 receptor, urothelial permeability

Abbreviations: CYP, cyclophosphamide; IC/BPS, interstitial cystitis/bladder pain syndrome; P2X7R, P2X7 purinergic receptor; TEER, trans-epithelial electrical resistance; ZO-1, zona occludens-1.

INTRODUCTION

Cyclophosphamide (CYP) and its toxic urinary metabolite, acrolein, causes severe cystitis, inflammation of the bladder, in patients who undergo chemotherapy. CYP-induced cystitis is one of the most frequently used models to study inflammatory cystitis (Birder and Andersson, 2018) as it displays many features similar to conditions such as interstitial cystitis/bladder pain syndrome (IC/BPS). In patients with IC/BPS, inflammation leads to the loss of or severe damage to the urothelial layer (Liu et al., 2015), absence of tight junction proteins (Slobodov et al., 2004), and increased urothelial permeability (Graham and Chai, 2006). These changes are associated with increased production of inflammatory mediators (Lamale et al., 2006; Offiah et al., 2016), histamine (Sant and Theoharides, 1994; Rudick et al., 2008), and nitric oxide (Koskela et al., 2008), as well as infiltration of inflammatory cells such as neutrophils and eosinophils (Dodd and Tello, 1998).

During bladder filling, ATP released from the urothelium is believed to function as a signaling transmitter acting on purinergic P2X2 and P2X3 receptors located on bladder afferent nerves to facilitate the sensation of fullness (Burnstock, 1972). ATP released from urothelial cells has also been shown to be increased in patients with IC/BPS (Sun and Chai, 2006) and feline model of IC/BPS (Birder et al., 2003) as well as in CYP-induced cystitis in rats (Smith et al., 2005). Patients with IC/BPS experience enhanced pain on bladder filling, which is associated with enhanced ATP release and upregulated P2X2 and P2X3 receptor expression (Tempest et al., 2004). In addition to P2X2 and P2X3 receptors, the P2X7 receptor (P2X7R) is likely to play an important regulatory role in bladder inflammatory responses seen in cystitis (Taidi et al., 2019). P2X7R expression has been shown in different layers of the urinary bladder with P2X7R immunoreactivity abundant on both the urothelium and smooth muscle (Vial and Evans, 2000; Menzies et al., 2003; Svennersten et al., 2015). Upregulation of submucosal P2X7R was detected in a mouse model of CYP-induced cystitis. In this model, treatment with a P2X7R selective antagonist significantly reduced cystitis symptoms (Martins et al., 2012).

Sustained activation of P2X7R by high concentrations of extracellular ATP (>100 μM) is associated with apoptotic cell death (Li et al., 2014), triggered by the formation of large non-selective membrane pores. These pores allow larger molecules to pass through cells membranes (Karasawa et al., 2017), including the release of apoptotic factors to promote caspase activation, and cell death (Burnstock and Knight, 2018). Previous studies have shown that substantially enhanced ATP release in response to acrolein was seen in primary rat urothelial cells and human urothelial cell lines (RT4 and T24) under basal and stretched conditions (Nirmal et al., 2014; Mills et al., 2019), indicating that increased purinergic signalling may be associated with CYP-induced cystitis and pain. However, the role of P2X7R in terms of urothelial barrier integrity and permeability in cystitis has not been explored.

Using an *ex-vivo* porcine bladder model, we have recently reported that instillation of acrolein into the bladder lumen caused damage to the urothelial and suburothelial layers, along with diminished bladder contractility in response to acetylcholine stimulation. The addition of P2X7R antagonist significantly attenuated acrolein-induced damage to the bladder (Taidi et al., 2021). The aim of this study was to further investigate whether the P2X7R is involved in acrolein-induced changes in urothelial barrier structure and integrity at the cellular level. Using primary cultured porcine urothelial cells, we have studied the role of P2X7R in acrolein-induced changes in cell morphology and viability as well as the expression of tight junction protein, zona occludens-1 (ZO-1). We have also investigated the role of P2X7R in acrolein induced disturbance of urothelial monolayer integrity by measuring trans-epithelial electrical resistance (TEER), using our newly developed *in vitro* urothelial barrier model.

MATERIALS AND METHODS

Animal Samples

Adult female porcine bladders were harvested directly from a local abattoir and transported to the laboratory within 3 h. Upon receipt, bladders were rinsed twice with carbogenated Krebs-Henseleit solution (in mM, NaCl 118, KCl 4.7, $NaHCO_3$ 25, KH_2PO_4 1.2, $MgSO_4$ 1.2, $CaCl_2$ 2.5, and D-glucose 11.7, pH 7.4), supplemented with 1% of antibiotic-antimitotic solution (10,000 units/ml of penicillin, 10,000 μg/ml of streptomycin, and 25 μg/ml of amphotericin B Gibco, Cat# 15240062).

Primary Porcine Urothelial Cell Isolation and Culture

The urothelial cells were scraped off from the luminal surface of the porcine bladder using a scalpel blade and suspended in RPMI 1640 culture media (R5886, Sigma-Aldrich) including 10% foetal bovine serum (FBS) (10099141, Thermo Fisher Scientific) and 1% antibiotic-antimitotic, as reported previously (Bahadory et al., 2013). Trypsin-EDTA (0.25%, 25200072, Thermo Fisher Scientific) was added to the luminal side of the bladder to remove any residual urothelial cells. After 5 min incubation at 37°C, cells were scraped off into RPMI complete media and centrifuged at 750 g for 5 min. Urothelial cells were then plated into T75 flasks and incubated at 37°C in 5% CO_2 until they reach 70–80% confluence (approximately 7–10 days).

Cell Morphology and Viability

Once cells achieved 80% confluence, primary urothelial cells were passaged and plated (1×10^5) in a 24-well plate (Corning) and treated overnight at 37°C in 5% CO_2 with acrolein (12.5–100 μM, 110221, Sigma-Aldrich). Cells were also treated with acrolein (50 μM) plus P2X7R antagonist, A804598 (at 1 and 10 μM, 01617, Sigma-Aldrich). Cells were monitored for changes in morphology and pictures captured at 2 h post treatment as well as after overnight treatment. Following overnight treatment, cell viability was measured using resazurin (10%, 0.3 mg/ml, ab129732, Abcam) (Riss et al., 2016; Mills et al., 2019). The fluorescence signal was quantified by Fluostar plate reader (560 nm excitation/590 nm emission) at 3 h.

Development of *in vitro* Urothelial Barrier Model

To establish a reliable cell culture system for urothelial monolayer, we attempted to plate urothelial cells in different culture media. With some culture conditions, cells did not form high integrity barriers, or TEER values were too high to be disrupted by the application of TNFα and IL-β (both 100 ng/ml), which was used as a positive control in this study as these have been shown to markedly reduce TEER values in Caco-2 cells (Diezmos et al., 2018). A reliable system was eventually established using the following conditions: primary porcine urothelial cells were isolated and cultured in T75 flasks containing RPMI complete media until 70–80% confluence, as described above. Confluent urothelial cells were passaged and plated in permeable 12-well transwell inserts (Corning 3,413, 6.5 mm diameter inserts and 0.4 μm pore size) at 1×10^5 cells per insert and incubated at 37°C in 5% CO_2. DMEM culture media supplemented with 10% FBS, 1% antibiotic-antimitotic, and 1% glucose was used to replace RPMI. For each well, DMEM was added to both the apical (into transwell) and basal (into the well outside of the transwell) chamber. TEER or the electrical resistance of urothelial cells was measured using EVOM epithelial volt/ohm meter (EVOM, World precision instruments). TEER was monitored daily until the steady level was reached (achieved after 8–10 days in culture). The TEER value for urothelial cells was 7,390 ± 495 Ωcm^2 (mean ± SEM), which was higher than that of Caco-2 cells (925–2,500 Ωcm^2).

In vitro Model of Damaged Urothelial Monolayer by Acrolein

Once consistent TEER values at the desired level had been reached, acrolein (at 50 μM) was applied to the apical surface of the urothelial cell layer, to induce urothelial cell damage. Application to the apical surface was chosen to mimic the *in vivo* cytotoxic effects of acrolein present in the urine of patients treated with CYP (Takamoto et al., 2004; Haldar et al., 2014). To determine the effect of P2X7R antagonist, A804598 (10 μM) on acrolein-induced urothelial cell damage, the antagonist was added to both the apical and basal cell surfaces. The antagonist applied to only the apical side had also been tried, but the results were less optimal. Urothelial cells were pre-incubated with A804598 for 30 min prior to the addition of acrolein. Baseline TEER was measured at 0 h, then changes in TEER were followed at 2, 4, 24, and 48 h after treatment.

Immunofluorescence Staining

Immunocytochemical studies were conducted on porcine urothelial cells cultured on a glass coverslip in RPMI for 7–10 days. Confluent cells were fixed with 95% ethanol and 5% acetic acid solution for 10 min. Before use, cells were washed (3 × 10 min) with phosphate buffered saline (PBS 0.1 M, pH 7.4) followed by 30 min incubation in 10% goat or donkey serum to block nonspecific binding sites of a secondary antibody. To confirm that the primary cultured cells were of epithelial origin, cells were labelled with the cytokeratin marker AE1/AE3 antibody (1:200, M3515, Dako). To demonstrate the expression of P2X7R on isolated porcine urothelial cells, the cultured cells were incubated with primary P2X7R antibody (1:100, ab93354, Abcam) overnight at room temperature. Urothelial cell tight-junction proteins were labelled with anti-ZO-1 antibody (Invitrogen 61–7,300, 1:100) overnight at room temperature. Following incubation with primary antibodies, cells were washed (3 × 10 min) in tris-buffered saline (TBS) and tagged with a secondary fluorescent antibody for 1 h at room temperature [Alexa Fluor 594 (1:200, ab150080) for ZO-1; Alexa Fluor 488 (1:200, ab150105) for AE1/AE3, and Alexa Fluor 488 (1:200, ab150129) for P2X7R, all from Abcam]. Cells were then washed again with TBS (3 × 10 min) before the urothelial cell nuclei were stained with DAPI. Immunoreactive images were captured using Neurolucida microscope, 20/×40 objectives, and analysed using ImageJ software.

To determine the effect of the acrolein on ZO-1 expression, urothelial cells were incubated with 50 μM acrolein for 2 and 24 h in RPMI (as above) at 37°C in 5% CO_2 before being fixed for ZO-1 immunohistochemistry. To determine the effect of P2X7R selective antagonist A804598 on acrolein-induced changes in ZO-1 tight junction protein expression, urothelial cells were pre-incubated with A804598 (10 μM) for 30 min prior to the addition of acrolein.

Statistical Analysis

Data were analysed with GraphPad Prism 8 and expressed as mean ± standard error of the mean. One-way ANOVA followed by Bonferroni's multiple comparisons was applied to analyse cell viability results, and two-way ANOVA followed by Bonferroni's multiple comparisons was used to analyse the TEER results. p value <0.05 was set as statistical significance.

RESULTS

AE1/AE3 and P2X7R Immunofluorescence Staining

As shown in **Figure 1A**, all cultured porcine urothelial cells were positive immunoreactivity against AE1/AE3, verifying the epithelial origin of these cells. P2X7R immunoreactivity was demonstrated in the cytoplasm and membranes of most but not all primary cultured porcine urothelial cells (**Figure 1B**), confirming the expression of P2X7R on cultured urothelial cells.

Effect of P2X7R Inhibition on Acrolein-Induced Cytotoxicity

Acrolein markedly reduced the urothelial cell viability in a concentration-dependent manner (**Figure 2A**). As the concentration of acrolein increased to 25 and 50 μM there was an increasing cytotoxic effect seen by the reduction in cell viability ($p < 0.0001$). This appeared to plateau at 50 μM acrolein. Therefore, the effect of the P2X7R selective antagonist (A804598) was examined on cells treated with 50 μM acrolein (**Figure 2B**). The cytotoxic effect of acrolein was not significantly

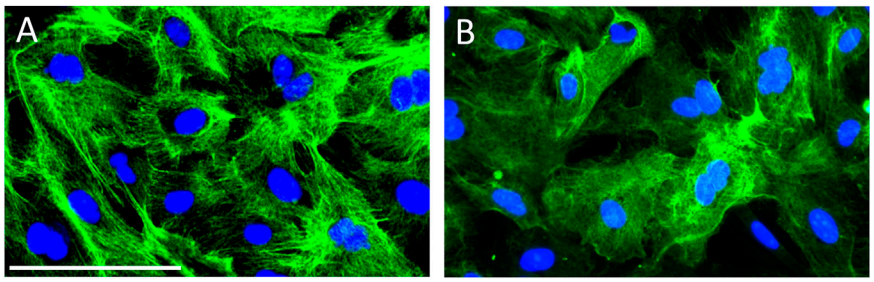

FIGURE 1 | Immunocytochemistry on porcine primary cultured urothelial cells. **(A)** All cultured cells uniformly expressed AE1/AE3 cytokeratin, the epithelial cell marker, indicating the pure identity of cultured porcine urothelial cells. **(B)** Cultured urothelial cells show an intense expression of P2X7R in the cytoplasm and membranes. The green color denotes AE/AE3 staining in panel A and P2X7R staining in panel B. The blue color shows the nuclei stained with DAPI. Magnification bar shows 50 μm.

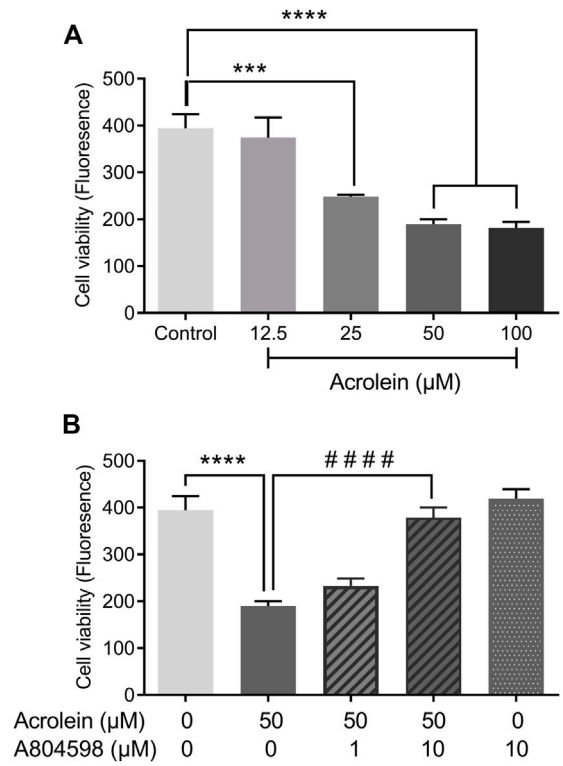

FIGURE 2 | Effects of P2X7R inhibition on acrolein-induced cytotoxicity as measured by oxidation of resazurin. **(A)** Acrolein reduced urothelial cell viability in a concentration-dependent manner (12.5–100 μM). **(B)** The reduced cell viability caused by acrolein (50 μM) was prevented by the addition of P2X7R antagonist A804598 at 10 μM, although the preventive effect was not significant at a lower concentration (1 μM). A804598 (10 μM) alone showed no different compared to the control. ***$p < 0.001$, ****$p < 0.0001$ compared to the control; ####$p < 0.0001$ compared to the acrolein treated group ($n = 6$ for all groups, one-way ANOVA followed by Bonferroni's multiple comparisons.

inhibited by the pre-treatment of cells with A804598 at 1 μM A804598 at 10 μM, however, showed a great impact on the cytotoxic effect of acrolein and significantly abolished the acrolein induced cytotoxicity ($p < 0.0001$). The result of A804598 alone was similar to that of the control group.

Effect of P2X7R Inhibition on Acrolein-Induced Changes in Cell Morphology

Urothelial cells freshly isolated from the luminal surface of the porcine urinary bladder were initially rounded in shape. After three to 4 days in culture, cells flattened and spread out. After 7–10 days in culture, cells appeared confluent with urothelial cells forming a well-connected monolayer of epithelial-like shaped cells with a typical cobble-stone morphology (Le et al., 2014) (**Figure 3A**).

Treatment of the cultured urothelial cells with 50 μM acrolein for 2 h resulted in obvious damage to the urothelial cell monolayer. Attached and well-connected urothelial cells became dissociated at several points within the monolayer (indicated by white arrows in **Figure 3B**). Further incubation overnight with 50 μM acrolein enhanced this dissociation, with cells losing their flattened, cobble-stone morphology, and becoming spherical or irregular in shape with more cells losing adherence, indicative of an increase in dead cells (**Figure 3C**). Incubation of the urothelial cells with the selective P2X7R antagonist, A804598 (10 μM) by itself, did not cause any changes in cell morphology (**Figure 3D**). Pre-incubation of urothelial cells with A804598 (10 μM) protected the urothelial monolayer from the disruptive effects of acrolein at 2 h (**Figure 3E**) and overnight (**Figure 3F**). Although minor dissociation was still seen on urothelial monolayer after 2 h incubation with acrolein (50 μM) following pre-treatment with A804598 (**Figure 3E**, white arrows), cells appeared to proliferate overnight and return to a normal cobble-stone morphology (**Figure 3F**).

Effect of P2X7R Inhibition on Acrolein-Induced Disruption to Urothelial Cell Integrity

Treatment of cultured porcine urothelial cells with 50 μM acrolein caused significant disruption to urothelial cell

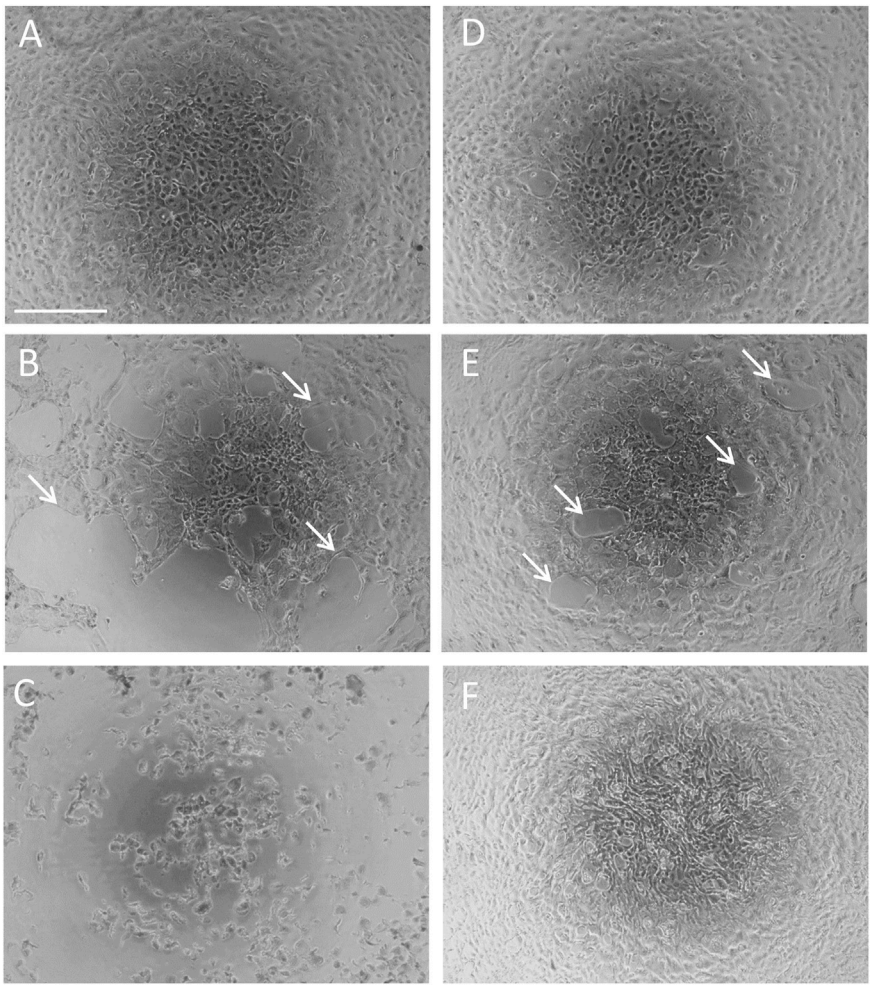

FIGURE 3 | Effect of P2X7R inhibition on acrolein-induced changes in cell morphology. Confluent primary cultured urothelial cells under normal culture conditions **(A)**. Cells were treated with acrolein (50 μM) for 2 h **(B)** or overnight **(C)**. Cells were treated with the selective P2X7R antagonist A804598 (10 μM) overnight **(D)**. Cells were pre-incubated with A804598 (10 μM) for half an hour and then treated with acrolein (50 μM) for 2 h **(E)** or overnight **(F)**. Magnification bar shows 100 μm. White arrows indicate the disruption of cell-cell adhesions.

integrity as indicated by a decrease in TEER values (**Figure 4**). After 24 h of acrolein treatment, there was a 60% reduction in trans-epithelial resistance. Pre-incubation of urothelial cells with the P2X7R antagonist A804598 (10 μM) showed protection against acrolein-induced disruption to urothelial cell integrity, as the TEER values returned to the control level, which was significantly different from that of the acrolein only group between 4 and 48 h. A804598 by itself did not lead to any significant changes in TEER compared to control.

Effect of P2X7R Inhibition on Acrolein-Induced Disruption to Urothelial Cell Tight Junction Protein ZO-1

The integrity of the urothelial cell monolayers formed after 8–10 days in culture was demonstrated by strong immunoreactivity of tight junction protein ZO-1 (**Figure 5A**). Acrolein induced cytotoxicity and disruption to the urothelial cell integrity was demonstrated by the reduction in ZO-1 immunoreactivity. ZO-1 immunoreactivity was clearly discontinuous and highly compromised in urothelial cells treated with acrolein (50 μM) for 4 h (**Figure 5C**) compared to controls. However, when cells were treated with both A804598 (10 μM) and acrolein (50 μM), the disruption to ZO-1 expression was inhibited (**Figure 5D**), indicating that A804598 protected urothelial cell monolayers from acrolein-induced damage. A804598 (10 μM) alone did not show any effect on ZO-1 expression (**Figure 5B**).

DISCUSSION

Interstitial cystitis and other inflammatory bladder conditions are associated with changes in the urothelial cell viability, integrity, and permeability. The current study has demonstrated that urothelial cell changes induced by acrolein are very similar to

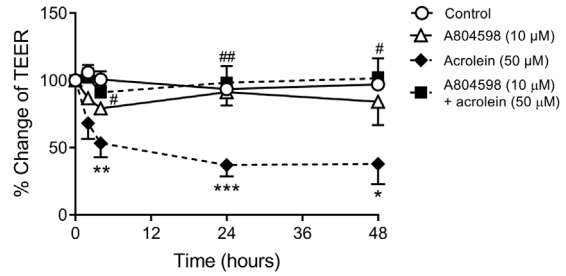

FIGURE 4 | Effect of P2X7R inhibition on acrolein-induced disruption to urothelial cell integrity measured by TEER. Data were expressed as the percentage change of TEER relative to pre-treatment of the same well. Two-way ANOVA analysis showed a highly significant reduction in TEER after urothelial cells were treated with acrolein (50 μM) up to 48 h (****$p < 0.0001$ compared to control). Acrolein induced TEER reduction was significantly prevented by co-incubation with P2X7R antagonist A804598 (10 μM) (#####$p < 0.0001$ compared to acrolein alone). A804598 alone did not show any effect on TEER values. Each condition was measured as duplicates of n = 8 animals. Two-way ANOVA followed by Bonferroni's multiple comparison tests show *$p < 0.05$, **$p < 0.01$, ***$p < 0.001$ compared to the same time point of the control group; #$p < 0.05$, ##$p < 0.01$ compared to the same time point of the acrolein alone group.

those demonstrated in patients with bladder conditions associated with IC/PBS. Importantly, this study has shown that these changes can be inhibited by the selective P2X7R antagonist, A804598.

The urothelium of the bladder from patients with IC/BPS is thinner, usually only 1 or 2 cells thick, compared to the urothelium from normal bladders, which is approximately 5 cells thick (Slobodov et al., 2004). Decreased urothelial cell viability and increased apoptotic cell death are common in cystitis. They have been demonstrated in IC/BPS (Shie and Kuo, 2011; Shie et al., 2012) and other type of urinary bladder cystitis including ketamine-induced cystitis (Lee et al., 2013). Increased urothelial cell apoptosis is also common in other bladder conditions, including bladder outlet obstruction, spinal cord injury, and recurrent urinary tract infection (Liu et al., 2015). As supported by the findings in the current study, acrolein is a well-known cytotoxic compound with effects on cell viability reported for doses between 5 μM (Suabjakyong et al., 2015) and 100 μM (Mills et al., 2019).

As well as decreases in urothelial cell viability, cystitis is associated with disruption to the integrity of the urothelial barrier. Absence of ZO-1 (Slobodov et al., 2004) and increased urothelial permeability (Graham and Chai, 2006) have been reported in patients with haemorrhagic cystitis and also in animal models of CYP-induced cystitis or intravesical instillation of acrolein (Martins et al., 2012). Similar findings have been reported in other tissues with decreased epithelial integrity and increased epithelial barrier permeability observed in *in-vitro* models of acrolein-treated vocal fold epithelial cells (Liu et al., 2016) and intestinal epithelial cells (Chen et al., 2017). The present study demonstrated the expression of tight junction protein, ZO-1, in cultured porcine urothelial cells and that acrolein treatment has led to the degradation of tight junction protein. Increased urothelial cells permeability as a result of damaged or lost tight junction proteins will eventually cause the pathophysiological condition in which normal cell homeostasis is disturbed. In the current study this was

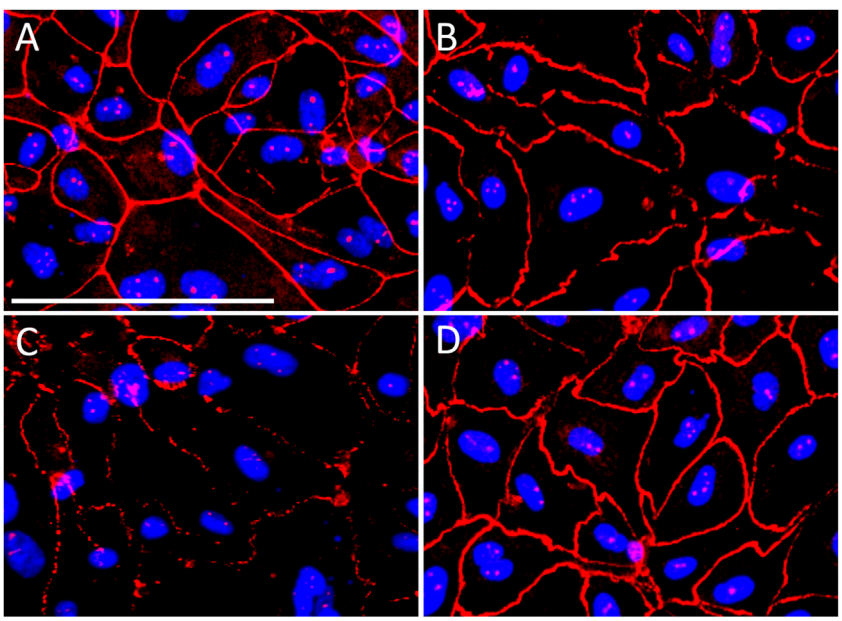

FIGURE 5 | Immunocytochemistry of tight junction protein zonula occludens-1 (ZO-1) (red) on primary cultured porcine bladder urothelial cells. ZO-1 immunoreactivity remained intact in **(A)** control cells and **(B)** cells treated with P2X7R antagonist A804598 (10 μM). Cells treated with acrolein (50 μM) for 4 h disrupted the integrity of ZO-1 immunoreactivity **(C)**. ZO-1 immunoreactivity remained intact in acrolein treated cells in the presence of A804598 (10 μM) **(D)**. The blue color shows the nuclei stained with DAPI. Magnification bar shows 100 μm.

demonstrated by a decrease in trans-epithelial resistance, indicating a disruption of the normal barrier functions of the urothelium.

Perhaps the most important finding of the current study was that the acrolein-induced changes in urothelial cell viability, integrity, and permeability were significantly inhibited by pre-treatment of urothelial cells with the selective P2X7R antagonist, A804598. This is the first report of the protective effect of P2X7R inhibition on acrolein-induced changes in urothelial cell permeability, although similar and comparable results have been reported previously in other models examining epithelial barrier integrity (Chen et al., 2014; Wu et al., 2017). This study is also the first to report the protective effect of A804598 on the expression of tight junction proteins in primary urothelial cells, which is in line with previous studies reported in other systems. For example, brilliant blue G, which is a selective non-competitive P2X7R antagonist, preserved the expression of both occludin and ZO-1 in the rat lung tissue in a model of neurogenic pulmonary edema (Chen et al., 2014). Also, in the model of sepsis-induced intestinal barrier disruption (Wu et al., 2017), P2X7R antagonist not only increased TEER but also showed a significant increase in expression of tight junction proteins, occludin, claudine-1, and ZO-1 (Wu et al., 2017). The same study showed that Bz-ATP (a purinergic agonist with potency for P2X7R) significantly decreased the expression of tight junction proteins and reduced TEER in the intestine (Wu et al., 2017).

The P2X7R antagonist, A804598, also protected against acrolein induced loss of cell viability. The effects of P2X7R on cell viability appears less clear cut in the literature. Although it is generally well received that P2X7R activation can cause apoptosis/necrosis and cell death due to the formation of large cytoplasmic pores, resulting in increased cell permeability (Schulze-Lohoff et al., 1998), there are reports showing that activation of P2X7R increases cell proliferation in lymphoid cells (Baricordi et al., 1999) and microglia cells (Bianco et al., 2006). The opposing roles of P2X7R in both cell proliferation and cell death are proposed to be dependent on the concentration of extracellular ATP. It is hypothesised that low concentrations of extracellular ATP lead to basal activity of P2X7R, which results in increased cell proliferation (Adinolfi et al., 2005); however, high extracellular ATP levels lead to apoptosis and cell death (Haanes et al., 2012). As mentioned previously, interstitial cystitis is associated with increased ATP release from urothelial cells (Sun and Chai, 2006). Therefore, in these conditions, blocking the P2X7R can protect urothelial cells from death. The second important consideration is that the P2X7R itself is an important regulator of extracellular ATP level (Brandao-Burch et al., 2012), leading to ATP-induced ATP release, via P2X7R and other ion channels, such as pannexin channels (Dahl, 2015; Ceriani et al., 2016). Therefore, P2X7R antagonism will not only inhibit urothelial cell apoptosis in the presence of high concentrations of extracellular ATP it will also prevent excessive ATP release into the extracellular space.

Taken together, the results of the current study indicate that acrolein decreases urothelial cell viability and disrupts the urothelial barrier integrity by damaging tight junction proteins, leading to increased urothelial barrier permeability. These changes, which are analogous to the changes seen in patients with interstitial cystitis, were inhibited by pre-treatment of urothelial cells with P2X7R antagonist, A804598. These findings are in line with our previously reported observations in our *ex-vivo* model of urothelial damage by direct instillation of acrolein into the whole porcine bladder lumen (Taidi et al., 2021) and provide further evidence for the potential of P2X7R antagonists in the treatment of IC/PBS.

Recently, many researchers have investigated the effect of P2X7R antagonists on lower urinary tract inflammatory diseases (Goncalves et al., 2006; Martins et al., 2012; Munoz et al., 2017). Martins and associates reported a decrease in the pain response in the CYP-treated animals following treatment with a P2X7R antagonist or genetic removal of P2X7R (Martins et al., 2012). They showed that the treatments result in decreased bladder inflammatory responses as well as reduced edema and hemorrhage (Martins et al., 2012). Another study has investigated the possible role of P2X7R in inflammatory pain in kidneys with unilateral ureteral obstruction. In P2X7R knockout mice, there was a reduction in inflammatory cell infiltration and a reduction in tubular apoptosis (Goncalves et al., 2006). Also, in a similar model of acute ischemic kidney injury in mice, the P2X7R antagonist A438079 reduced the expression of inflammatory chemokines (Yan et al., 2015). Likewise, in a murine colitis model, treatment with a P2X7R antagonist, A438079, reduced the production of inflammatory cytokines, TNF and IL-1β, in colon tissue (Wan et al., 2016). P2X7R antagonists have advanced to clinical trials as a treatment for a number of inflammatory diseases, including rheumatoid arthritis and inflammatory bowel disease (Park and Kim, 2017). The P2X7 antagonist AZD9056 has shown positive results in phase IIa trials, with improvement in pain related symptoms in patients with Crohn's disease (Eser et al., 2015).

Overall, the results of the current study have provided evidence for the therapeutic potential of P2X7R antagonists for inflammatory bladder diseases. Inhibition of P2X7R activity could be a pathway for the treatment of bladder inflammation and could potentially be co-administered with CYP in patients undergoing chemotherapy, thereby protecting them against treatment associated cystitis. Further studies should be conducted to investigate the effectiveness of different P2X7R antagonists. Our *in-vitro* barrier model developed using porcine urothelial cells can also be used to evaluate the effect of current treatments of IC/BPS on urothelial TEER, tight junction formation and viability to compare their efficacy in protecting urothelial integrity.

DATA AVAILABILITY STATEMENT

The raw data supporting the conclusion of this article will be made available by the authors, without undue reservation.

AUTHOR CONTRIBUTIONS

ZT: performed the research, analysed the data, and wrote the manuscript; KM: designed the research study and contributed to the writing of the manuscript; HS-U-R: developed *in vitro* urothelial barrier model; KHM: contributed to the writing of the manuscript and essential reagents; LL: designed the research study, contributed to the writing of the manuscript, and provided essential reagents and equipment.

FUNDING

This research was supported by UNSW Sydney (the University of New South Wales).

ACKNOWLEDGMENTS

The authors would like to thank the staff of the Picton Abattoir for the generous supply of pig bladders, Julie Bouza for bladder collection, and Irit Markus for technique support.

REFERENCES

Adinolfi, E., Callegari, M. G., Ferrari, D., Bolognesi, C., Minelli, M., Wieckowski, M. R., et al. (2005). Basal Activation of the P2X7 ATP Receptor Elevates Mitochondrial Calcium and Potential, Increases Cellular ATP Levels, and Promotes Serum-independent Growth. *MBoC* 16, 3260–3272. doi:10.1091/mbc.e04-11-1025

Bahadory, F., Moore, K. H., Liu, L., and Burcher, E. (2013). Gene Expression of Muscarinic, Tachykinin, and Purinergic Receptors in Porcine Bladder: Comparison with Cultured Cells. *Front. Pharmacol.* 4, 148. doi:10.3389/fphar.2013.00148

Baricordi, O. R., Melchiorri, L., Adinolfi, E., Falzoni, S., Chiozzi, P., Buell, G., et al. (1999). Increased Proliferation Rate of Lymphoid Cells Transfected with the P2X7 ATP Receptor. *J. Biol. Chem.* 274, 33206–33208. doi:10.1074/jbc.274.47.33206

Bianco, F., Ceruti, S., Colombo, A., Fumagalli, M., Ferrari, D., Pizzirani, C., et al. (2006). A Role for P2X7in Microglial Proliferation. *J. Neurochem.* 99, 745–758. doi:10.1111/j.1471-4159.2006.04101.x

Birder, L. A., Barrick, S. R., Roppolo, J. R., Kanai, A. J., De Groat, W. C., Kiss, S., et al. (2003). Feline Interstitial Cystitis Results in Mechanical Hypersensitivity and Altered ATP Release from Bladder Urothelium. *Am. J. Physiology-Renal Physiol.* 285, F423–F429. doi:10.1152/ajprenal.00056.2003

Birder, L., and Andersson, K.-E. (2018). Animal Modelling of Interstitial Cystitis/bladder Pain Syndrome. *Int. Neurourol J.* 22, S3–S9. doi:10.5213/inj.1835062.531

Brandao-Burch, A., Key, M. L., Patel, J. J., Arnett, T. R., and Orriss, I. R. (2012). The P2X7 Receptor Is an Important Regulator of Extracellular ATP Levels. *Front. Endocrin.* 3, 41. doi:10.3389/fendo.2012.00041

Burnstock, G. (1972). Purinergic Nerves. *Pharmacol. Rev.* 24, 509–581.

Burnstock, G., and Knight, G. E. (2018). The Potential of P2X7 Receptors as a Therapeutic Target, Including Inflammation and Tumour Progression. *Purinergic Signal.* 14, 1–18. doi:10.1007/s11302-017-9593-0

Ceriani, F., Pozzan, T., and Mammano, F. (2016). Critical Role of ATP-Induced ATP Release for Ca 2+ Signaling in Nonsensory Cell Networks of the Developing Cochlea. *Proc. Natl. Acad. Sci. U.S.A.* 113, E7194–e7201. doi:10.1073/pnas.1616061113

Chen, S., Zhu, Z., Klebe, D., Bian, H., Krafft, P. R., Tang, J., et al. (2014). Role of P2X Purinoceptor 7 in Neurogenic Pulmonary Edema after Subarachnoid Hemorrhage in Rats. *PLoS One* 9, e89042. doi:10.1371/journal.pone.0089042

Chen, W.-Y., Wang, M., Zhang, J., Barve, S. S., Mcclain, C. J., and Joshi-Barve, S. (2017). Acrolein Disrupts Tight junction Proteins and Causes Endoplasmic Reticulum Stress-Mediated Epithelial Cell Death Leading to Intestinal Barrier Dysfunction and Permeability. *Am. J. Pathol.* 187, 2686–2697. doi:10.1016/j.ajpath.2017.08.015

Dahl, G. (2015). ATP Release through Pannexon Channels. *Phil. Trans. R. Soc. B* 370, 20140191. doi:10.1098/rstb.2014.0191

Diezmos, E. F., Markus, I., Perera, D. S., Gan, S., Zhang, L., Sandow, S. L., et al. (2018). Blockade of Pannexin-1 Channels and Purinergic P2X7 Receptors Shows Protective Effects against Cytokines-Induced Colitis of Human Colonic Mucosa. *Front. Pharmacol.* 9, 865. doi:10.3389/fphar.2018.00865

Dodd, L. G., and Tello, J. (1998). Cytologic Examination of Urine from Patients with Interstitial Cystitis. *Acta Cytol.* 42, 923–927. doi:10.1159/000331969

Eser, A., Colombel, J.-F., Rutgeerts, P., Vermeire, S., Vogelsang, H., Braddock, M., et al. (2015). Safety and Efficacy of an Oral Inhibitor of the Purinergic Receptor P2X7 in Adult Patients with Moderately to Severely Active Crohn's Disease. *Inflamm. Bowel Dis.* 21, 1–2253. doi:10.1097/mib.0000000000000514

Gonçalves, R. G., Gabrich, L., Rosário, A., Jr., Takiya, C. M., Ferreira, M. L. L., Chiarini, L. B., et al. (2006). The Role of Purinergic P2X7 Receptors in the Inflammation and Fibrosis of Unilateral Ureteral Obstruction in Mice. *Kidney Int.* 70, 1599–1606. doi:10.1038/sj.ki.5001804

Graham, E., and Chai, T. C. (2006). Dysfunction of Bladder Urothelium and Bladder Urothelial Cells in Interstitial Cystitis. *Curr. Urol. Rep.* 7, 440–446. doi:10.1007/s11934-006-0051-8

Haanes, K. A., Schwab, A., and Novak, I. (2012). The P2X7 Receptor Supports Both Life and Death in Fibrogenic Pancreatic Stellate Cells. *PLoS One* 7, e51164. doi:10.1371/journal.pone.0051164

Haldar, S., Dru, C., and Bhowmick, N. A. (2014). Mechanisms of Hemorrhagic Cystitis. *Am. J. Clin. Exp. Urol.* 2, 199–208.

Karasawa, A., Michalski, K., Mikhelzon, P., and Kawate, T. (2017). The P2X7 Receptor Forms a Dye-Permeable Pore Independent of its Intracellular Domain but Dependent on Membrane Lipid Composition. *eLife* 6, e31186. doi:10.7554/eLife.31186

Koskela, L. R., Thiel, T., Ehrén, I., De Verdier, P. J., and Wiklund, N. P. (2008). Localization and Expression of Inducible Nitric Oxide Synthase in Biopsies from Patients with Interstitial Cystitis. *J. Urol.* 180, 737–741. doi:10.1016/j.juro.2008.03.184

Lamale, L. M., Lutgendorf, S. K., Zimmerman, M. B., and Kreder, K. J. (2006). Interleukin-6, Histamine, and Methylhistamine as Diagnostic Markers for Interstitial Cystitis. *Urology* 68, 702–706. doi:10.1016/j.urology.2006.04.033

Le, P. T., Pearce, M. M., Zhang, S., Campbell, E. M., Fok, C. S., Mueller, E. R., et al. (2014). IL22 Regulates Human Urothelial Cell Sensory and Innate Functions through Modulation of the Acetylcholine Response, Immunoregulatory Cytokines and Antimicrobial Peptides: Assessment of an *In Vitro* Model. *PLoS One* 9, e111375. doi:10.1371/journal.pone.0111375

Lee, C.-L., Jiang, Y.-H., and Kuo, H.-C. (2013). Increased Apoptosis and Suburothelial Inflammation in Patients with Ketamine-Related Cystitis: a Comparison with Non-ulcerative Interstitial Cystitis and Controls. *BJU Int.* 112, 1156–1162. doi:10.1111/bju.12256

Li, J., Chen, J., and Chen, G. (2014). P2X7 Receptor and Apoptosis. *Crit. Care Med.* 42, e804. doi:10.1097/ccm.0000000000000621

Liu, H.-T., Jiang, Y.-H., and Kuo, H.-C. (2015). Alteration of Urothelial Inflammation, Apoptosis, and junction Protein in Patients with Various Bladder Conditions and Storage Bladder Symptoms Suggest Common Pathway Involved in Underlying Pathophysiology. *Lower Urinary Tract Symptoms* 7, 102–107. doi:10.1111/luts.12062

Liu, X., Zheng, W., and Sivasankar, M. P. (2016). Acute Acrolein Exposure Induces Impairment of Vocal Fold Epithelial Barrier Function. *PLoS One* 11, e0163237. doi:10.1371/journal.pone.0163237

Martins, J., Silva, R., Coutinho-Silva, R., Takiya, C., Battastini, A., Morrone, F., et al. (2012). The Role of P2X7 Purinergic Receptors in Inflammatory and Nociceptive Changes Accompanying Cyclophosphamide-Induced Haemorrhagic Cystitis in Mice. *Br. J. Pharmacol.* 165, 183–196. doi:10.1111/j.1476-5381.2011.01535.x

Menzies, J., Paul, A., and Kennedy, C. (2003). P2X7 Subunit-like Immunoreactivity in the Nucleus of Visceral Smooth Muscle Cells of the guinea Pig. *Auton. Neurosci.* 106, 103–109. doi:10.1016/s1566-0702(03)00078-x

Mills, K. A., Chess-Williams, R., and Mcdermott, C. (2019). Novel Insights into the Mechanism of Cyclophosphamide-Induced Bladder Toxicity:

Chloroacetaldehyde's Contribution to Urothelial Dysfunction *In Vitro*. *Arch. Toxicol.* 93, 3291–3303. doi:10.1007/s00204-019-02589-1

Munoz, A., Yazdi, I. K., Tang, X., Rivera, C., Taghipour, N., Grossman, R. G., et al. (2017). Localized Inhibition of P2X7R at the Spinal Cord Injury Site Improves Neurogenic Bladder Dysfunction by Decreasing Urothelial P2X3R Expression in Rats. *Life Sci.* 171, 60–67. doi:10.1016/j.lfs.2016.12.017

Nirmal, J., Wolf-Johnston, A. S., Chancellor, M. B., Tyagi, P., Anthony, M., Kaufman, J., et al. (2014). Liposomal Inhibition of Acrolein-Induced Injury in Rat Cultured Urothelial Cells. *Int. Urol. Nephrol.* 46, 1947–1952. doi:10.1007/s11255-014-0745-7

Offiah, I., Didangelos, A., Dawes, J., Cartwright, R., Khullar, V., Bradbury, E. J., et al. (2016). The Expression of Inflammatory Mediators in Bladder Pain Syndrome. *Eur. Urol.* 70, 283–290. doi:10.1016/j.eururo.2016.02.058

Park, J.-H., and Kim, Y.-C. (2017). P2X7 Receptor Antagonists: a Patent Review (2010-2015). *Expert Opin. Ther. Patents* 27, 257–267. doi:10.1080/13543776.2017.1246538

Riss, T. L., Moravec, R. A., Niles, A. L., Duellman, S., Benink, H. A., Worzella, T. J., et al. (2016). "Cell Viability Assays," in *Assay Guidance Manual* (Bethesda: Eli Lilly & Company and the National Center for Advancing Translational Sciences). [Internet]. doi:10.1007/978-1-4939-6960-9

Rudick, C. N., Bryce, P. J., Guichelaar, L. A., Berry, R. E., and Klumpp, D. J. (2008). Mast Cell-Derived Histamine Mediates Cystitis Pain. *PLoS One* 3, e2096. doi:10.1371/journal.pone.0002096

Sant, G. R., and Theoharides, T. C. (1994). The Role of the Mast Cell in Interstitial Cystitis. *Urol. Clin. North America* 21, 41–53. doi:10.1016/s0094-0143(21)00590-5

Schulze-Lohoff, E., Hugo, C., Rost, S., Arnold, S., Gruber, A., Brüne, B., et al. (1998). Extracellular ATP Causes Apoptosis and Necrosis of Cultured Mesangial Cells via P2Z/P2X7receptors. *Am. J. Physiology-Renal Physiol.* 275, F962–F971. doi:10.1152/ajprenal.1998.275.6.F962

Shie, J.-H., and Kuo, H.-C. (2011). Higher Levels of Cell Apoptosis and Abnormal E-Cadherin Expression in the Urothelium Are Associated with Inflammation in Patients with Interstitial Cystitis/painful Bladder Syndrome. *BJU Int.* 108, E136–E141. doi:10.1111/j.1464-410X.2010.09911.x

Shie, J.-H., Liu, H.-T., and Kuo, H.-C. (2012). Increased Cell Apoptosis of Urothelium Mediated by Inflammation in Interstitial Cystitis/painful Bladder Syndrome. *Urology* 79, 484.e7-13. doi:10.1016/j.urology.2011.09.049

Slobodov, G., Feloney, M., Gran, C., Kyker, K. D., Hurst, R. E., and Culkin, D. J. (2004). Abnormal Expression of Molecular Markers for Bladder Impermeability and Differentiation in the Urothelium of Patients with Interstitial Cystitis. *J. Urol.* 171, 1554–1558. doi:10.1097/01.ju.0000118938.09119.a5

Smith, C. P., Vemulakonda, V. M., Kiss, S., Boone, T. B., and Somogyi, G. T. (2005). Enhanced ATP Release from Rat Bladder Urothelium during Chronic Bladder Inflammation: Effect of Botulinum Toxin A. *Neurochem. Int.* 47, 291–297. doi:10.1016/j.neuint.2005.04.021

Suabjakyong, P., Saiki, R., Van Griensven, L. J. L. D., Higashi, K., Nishimura, K., Igarashi, K., et al. (2015). Polyphenol Extract from Phellinus Igniarius Protects against Acrolein Toxicity *In Vitro* and Provides protection in a Mouse Stroke Model. *PLoS One* 10, e0122733. doi:10.1371/journal.pone.0122733

Sun, Y., and Chai, T. C. (2006). Augmented Extracellular ATP Signaling in Bladder Urothelial Cells from Patients with Interstitial Cystitis. *Am. J. Physiology-Cell Physiol.* 290, C27–C34. doi:10.1152/ajpcell.00552.2004

Svennersten, K., Hallén-Grufman, K., De Verdier, P. J., Wiklund, N. P., and Poljakovic, M. (2015). Localization of P2X Receptor Subtypes 2, 3 and 7 in Human Urinary Bladder. *BMC Urol.* 15, 81. doi:10.1186/s12894-015-0075-9

Taidi, Z., Mansfield, K. J., Bates, L., Sana-Ur-Rehman, H., and Liu, L. (2019). Purinergic P2X7 Receptors as Therapeutic Targets in Interstitial Cystitis/bladder Pain Syndrome; Key Role of ATP Signaling in Inflammation. *Bladder (San Franc)* 6, e38. doi:10.14440/bladder.2019.789

Taidi, Z., Zhou, T., Moore, K. H., Mansfield, K. J., and Liu, L. (2021). P2X7 Receptor Blockade Protects against Acrolein-Induced Bladder Damage: a Potential New Therapeutic Approach for the Treatment of Bladder Inflammatory Diseases. *Front. Pharmacol.* 12, 682520. doi:10.3389/fphar.2021.682520

Takamoto, S., Sakura, N., Namera, A., and Yashiki, M. (2004). Monitoring of Urinary Acrolein Concentration in Patients Receiving Cyclophosphamide and Ifosphamide. *J. Chromatogr. B* 806, 59–63. doi:10.1016/j.jchromb.2004.02.008

Tempest, H. V., Dixon, A. K., Turner, W. H., Elneil, S., Sellers, L. A., and Ferguson, D. R. (2004). P2X2 and P2X3 Receptor Expression in Human Bladder Urothelium and Changes in Interstitial Cystitis. *BJU Int.* 93, 1344–1348. doi:10.1111/j.1464-410X.2004.04858.x

Vial, C., and Evans, R. J. (2000). P2X Receptor Expression in Mouse Urinary Bladder and the Requirement of P2X1 Receptors for Functional P2X Receptor Responses in the Mouse Urinary Bladder Smooth Muscle. *Br. J. Pharmacol.* 131, 1489–1495. doi:10.1038/sj.bjp.0703720

Wan, P., Liu, X., Xiong, Y., Ren, Y., Chen, J., Lu, N., et al. (2016). Extracellular ATP Mediates Inflammatory Responses in Colitis via P2 × 7 Receptor Signaling. *Sci. Rep.* 6, 19108. doi:10.1038/srep19108

Wu, X., Ren, J., Chen, G., Wu, L., Song, X., Li, G., et al. (2017). Systemic Blockade of P2X7 Receptor Protects against Sepsis-Induced Intestinal Barrier Disruption. *Sci. Rep.* 7, 4364. doi:10.1038/s41598-017-04231-5

Yan, Y., Bai, J., Zhou, X., Tang, J., Jiang, C., Tolbert, E., et al. (2015). P2X7 Receptor Inhibition Protects against Ischemic Acute Kidney Injury in Mice. *Am. J. Physiology-Cell Physiol.* 308, C463–C472. doi:10.1152/ajpcell.00245.2014

Conflict of Interest: The authors declare that the research was conducted in the absence of any commercial or financial relationships that could be construed as a potential conflict of interest.

Publisher's Note: All claims expressed in this article are solely those of the authors and do not necessarily represent those of their affiliated organizations, or those of the publisher, the editors and the reviewers. Any product that may be evaluated in this article, or claim that may be made by its manufacturer, is not guaranteed or endorsed by the publisher.

frontiers | Frontiers in Physiology

ORIGINAL RESEARCH
published: 16 June 2022
doi: 10.3389/fphys.2022.918100

Mechanosensitive Hydrolysis of ATP and ADP in Lamina Propria of the Murine Bladder by Membrane-Bound and Soluble Nucleotidases

*Mafalda S. L. Aresta Branco, Alejandro Gutierrez Cruz, Jacob Dayton, Brian A. Perrino and Violeta N. Mutafova-Yambolieva**

Department of Physiology and Cell Biology, University of Nevada Reno School of Medicine, Reno, NV, United States

Prior studies suggest that urothelium-released adenosine 5′-triphosphate (ATP) has a prominent role in bladder mechanotransduction. Urothelial ATP regulates the micturition cycle through activation of purinergic receptors that are expressed in many cell types in the lamina propria (LP), including afferent neurons, and might also be important for direct mechanosensitive signaling between urothelium and detrusor. The excitatory action of ATP is terminated by enzymatic hydrolysis, which subsequently produces bioactive metabolites. We examined possible mechanosensitive mechanisms of ATP hydrolysis in the LP by determining the degradation of 1,N^6-etheno-ATP (eATP) at the anti-luminal side of nondistended (empty) or distended (full) murine (C57BL/6J) detrusor-free bladder model, using HPLC. The hydrolysis of eATP and eADP was greater in contact with LP of distended than of nondistended bladders whereas the hydrolysis of eAMP remained unchanged during filling, suggesting that some steps of eATP hydrolysis in the LP are mechanosensitive. eATP and eADP were also catabolized in extraluminal solutions (ELS) that were in contact with the LP of detrusor-free bladders, but removed from the organ chambers prior to addition of substrate. The degradation of both purines was greater in ELS from distended than from nondistended preparations, suggesting the presence of mechanosensitive release of soluble nucleotidases in the LP. The released enzyme activities were affected differently by Ca^{2+} and Mg^{2+}. The common nucleotidase inhibitors ARL67156, POM-1, PSB06126, and ENPP1 Inhibitor C, but not the alkaline phosphatase inhibitor (-)-p-bromotetramisole oxalate, inhibited the enzymes released during bladder distention. Membrane-bound nucleotidases were identified in tissue homogenates and in concentrated ELS from distended preparations by Wes immunodetection. The relative distribution of nucleotidases was ENTPD1 >> ENPP1 > ENTPD2 = ENTPD3 > ENPP3 = NT5E >> ENTPD8 = TNAP in urothelium and ENTPD1 >> ENTPD3 >> ENPP3 > ENPP1 = ENTPD2 = NT5E >> ENTPD8 = TNAP in concentrated

OPEN ACCESS

Edited by:
Patrik Aronsson, University of Gothenburg, Sweden

Reviewed by:
Shaun L. Sandow, University of the Sunshine Coast, Australia
Ping Lu, University of Massachusetts Medical School, United States

***Correspondence:**
Violeta N. Mutafova-Yambolieva
vmutafova@med.unr.edu

Specialty section:
This article was submitted to Integrative Physiology, a section of the journal Frontiers in Physiology

Received: *12 April 2022*
Accepted: *26 May 2022*
Published: *16 June 2022*

Citation:
Aresta Branco MSL, Gutierrez Cruz A, Dayton J, Perrino BA and Mutafova-Yambolieva VN (2022) Mechanosensitive Hydrolysis of ATP and ADP in Lamina Propria of the Murine Bladder by Membrane-Bound and Soluble Nucleotidases. Front. Physiol. 13:918100. doi: 10.3389/fphys.2022.918100

Abbreviations: ADO, adenosine; ADP, adenosine 5′-diphosphate; ALPL, alkaline phosphatase; AMP, adenosine 5′-monophosphate; ATP, adenosine 5′-triphosphate; cELS, concentrated extraluminal solution; DMSO, dimethyl sulfoxide; EL, extraluminal; ELS, extraluminal solutions; ENPPs, ectonucleotide pyrophosphatase/phosphodiesterases; ENTPDs, ectonucleoside triphosphate diphosphohydrolases; GPI, glycosylphosphatidylinositol; GPI-AP, GPI-anchored protein; HPLC-FLD, high-performance liquid chromatography with fluorescence detection; KBS, Krebs solution; LP, lamina propria; LDH, lactate dehydrogenase; mKBS, modified Krebs-bicarbonate solution; NT5E, 5′-nucleotidase; TNAP, tissue nonspecific alkaline phosphatase.

ELS, suggesting that regulated ectodomain shedding of membrane-bound nucleotidases possibly occurs in the LP during bladder filling. Mechanosensitive degradation of ATP and ADP by membrane-bound and soluble nucleotidases in the LP diminishes the availability of excitatory purines in the LP at the end of bladder filling. This might be a safeguard mechanism to prevent over-excitability of the bladder. Proper proportions of excitatory and inhibitory purines in the bladder wall are determined by distention-associated purine release and purine metabolism.

Keywords: urothelium, bladder, nucleotidases, purine nucleotides, ATP-adenosine triphosphate, ADP, lamina propria (LP), ATP hydrolysis

1 INTRODUCTION

The urinary bladder has two main functions: storage (continence) and voiding (micturition) of urine. Normal operation of these functions depends on proper detrusor excitability regulated by systemic (e.g., *via* the central and peripheral nervous systems) and local (e.g., *via* urothelial mediators and signal propagation in cell syncytium) mechanisms. While neural control of the bladder has been extensively investigated, local mechanisms of mechanotransduction from mucosa (urothelium) to nerves or detrusor during bladder filling have remained elusive (Dalghi et al., 2020). Adenosine 5′-triphosphate (ATP) has attracted much attention in urothelium biology after the seminal discovery in 1997 that ATP was released from rabbit bladder mucosa sheets mounted in Ussing chambers in response to hydrostatic pressure (Ferguson et al., 1997). In the following decades, studies have confirmed that ATP is released from bladder sheets of different species (Wang et al., 2005; Lewis and Lewis, 2006; Yu, 2015); from cultured urothelial cells upon hydrostatic pressure changes, stretch, hypotonicity-induced cell swelling, or drag forces (Matsumoto-Miyai et al., 2011; McLatchie and Fry, 2015); and, in bladder lumen at end of filling (Vlaskovska et al., 2001; Beckel et al., 2015; Durnin et al., 2016). We recently demonstrated that during bladder filling, ATP is not only released into the bladder lumen, but it is also released from the urothelium into the suburothelium/lamina propria (LP) (Durnin et al., 2019b). This finding provided more direct support to the assumption that ATP may be released in the LP to transmit information to the nervous and muscular systems during bladder filling (Birder and Andersson, 2013; Takezawa et al., 2016b). ATP increases the tone of the detrusor *via* stimulation of P2X and P2Y purinergic receptors on smooth muscle cells (Burnstock, 2014) and is proposed to activate the micturition reflex *via* stimulation of purinergic receptors in afferent neurons in the LP at the end of filling (Cockayne et al., 2000; Vlaskovska et al., 2001). Studies have suggested that release of ATP from the bladder urothelium might be enhanced in disease states such as inflammation, forms of overactive bladder, painful bladder syndrome, and cancer (Sun and Chai, 2006; Kumar et al., 2007; Silva-Ramos et al., 2013; Burnstock, 2014). Of particular importance is the finding that in addition to ATP, its metabolites adenosine 5′-diphosphate (ADP), adenosine 5′-monophosphate (AMP), and adenosine (ADO) are physiologically present in the LP during bladder filling (Durnin et al., 2019b). It is noteworthy to point out that ATP represents only ~5% of the purine pool available deep in the bladder wall at the end of bladder filling (Durnin et al., 2019b), suggesting that a significant degradation of ATP likely occurs in the LP during bladder filling. This would diminish the active concentrations of ATP in LP limiting the activation of $P2X_2/X_3$ receptors in afferent neurons and initiation of a voiding reflex. Therefore, understanding the mechanisms of ATP hydrolysis in the course of bladder filling becomes critically important for comprehending mechanotransduction mechanisms in the bladder wall. The study of purinergic receptors and their functions in regulation of bladder excitability is complicated by the presence at the cell surface of many enzymes—nucleotidases—that catabolize purine nucleotides into nucleosides. While hydrolysis of extracellular ATP terminates its direct action, it also generates ADP and ADO, both of which could affect bladder excitability. ADP is a potent agonist of $P2Y_1$, $P2Y_{12}$, and $P2Y_{13}$ purinergic receptors (Abbracchio et al., 2006) and stimulation of the $P2Y_{12}$ receptor results in detrusor contractions (Yu et al., 2014). ADO is a ligand for four ubiquitous G-protein coupled receptors (A1, A2A, A2B, and A3) (Fredholm et al., 2000), relaxes the bladder detrusor (Burnstock, 2014) and regulates the activity of sensory neurons in the bladder wall (Kitta et al., 2014). An effect thought to be due to ATP may, in fact, involve its hydrolysis products ADP or ADO. Significant amount of knowledge about extracellular nucleotide

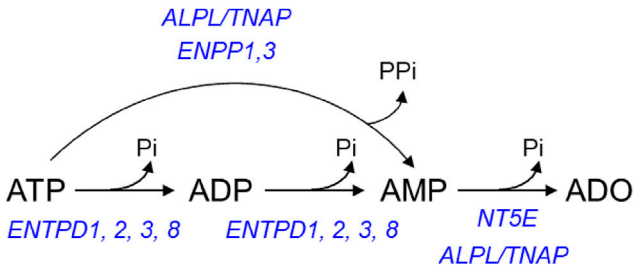

FIGURE 1 | Principal pathways of extracellular ATP hydrolysis. ATP is hydrolyzed to ADP and then ADP is hydrolyzed to AMP by ENTPD1, 2, 3, and 8. ATP can be degraded directly to AMP by alkaline phosphatase (ALPL/TNAP) and ENPP1 and 3. AMP, in turn, is degraded to ADO by NT5E and ALPL/TNAP.

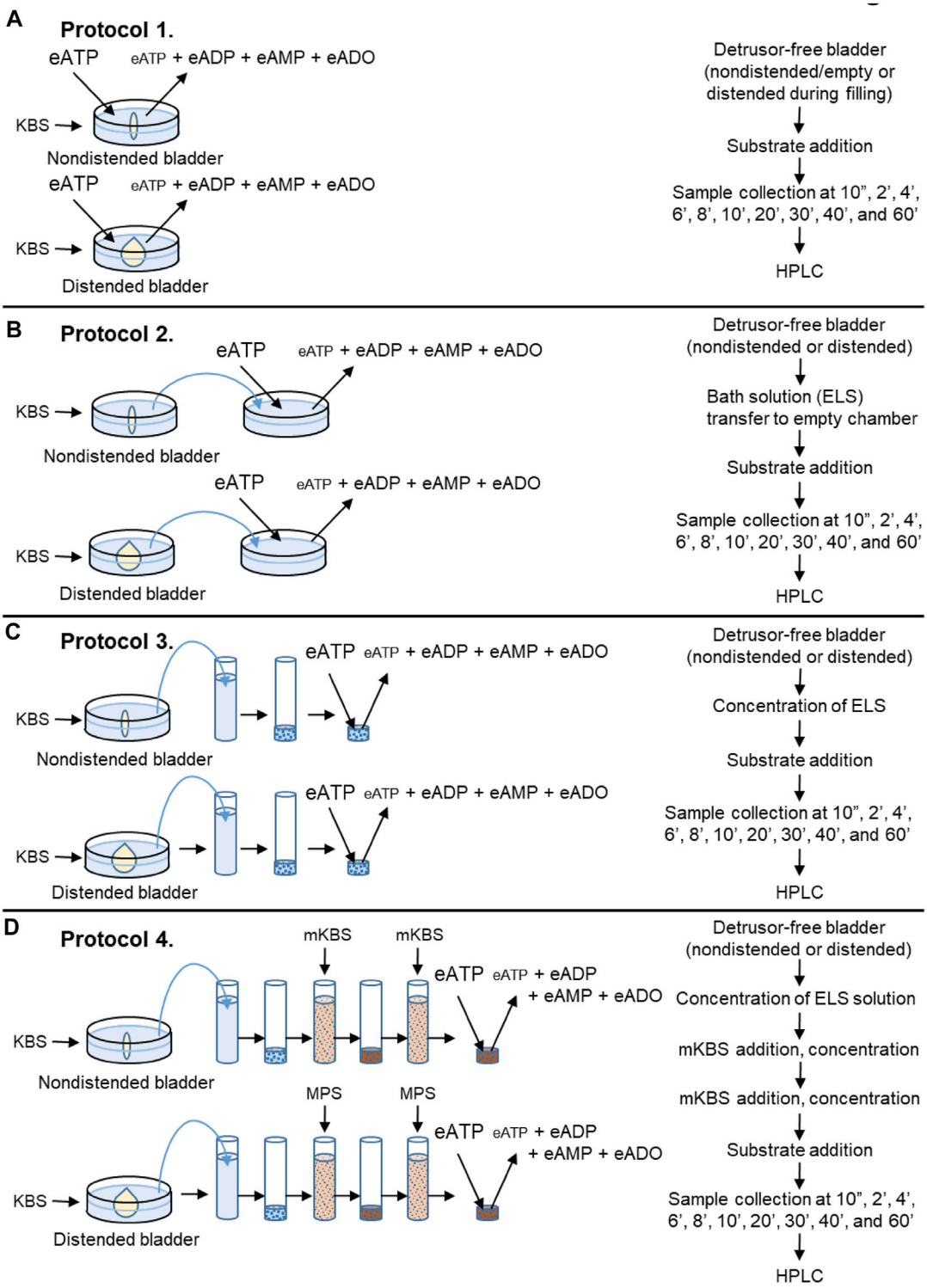

FIGURE 2 | Schematics of experimental procedures for evaluation of eATP degradation in extraluminal solutions from nondistended and distended detrusor-free bladder preparations. **(A)** Substrate (e.g., eATP or eADP) was added to KBS bathing the bladder preparation. Decrease of substrate and increase of product was measured using HPLC-FLD. **(B)** Bladder was incubated in KBS. After incubation time equivalent to the time for bladder filling, an aliquot of the bath solution (aka extraluminal solution, ELS) was transferred to an empty chamber. Substrate (e.g., eATP or eADP) was added to the transferred ELS and substrate hydrolysis was assessed by HPLC. **(C)** Bladder was incubated in KBS as described in panel **(B)**. Then an aliquot of ELS was placed in a filtration unit (MWCO 10 kDa) and centrifuged. The supernatant (aka concentrated ELS, cELS) was transferred to an Eppendorf tube to which the substrate was added and substrate decrease and product increase

(*Continued*)

FIGURE 2 | were evaluated using HPLC. **(D)** Bladder was incubated with KBS. Then, an aliquot of ELS was concentrated as described in panel **(C)**. Next, 2.9-ml of modified KBS (mKBS) (**Table 1**) was added in the centrifugal unit with EL supernatant in KBS and centrifuged. Then, 2.9-ml of mKBS was added to the centrifugal unit containing the EL supernatant in mKBS and centrifuged. The resulting supernatant was transferred to an Eppendorf tube and the volume of cELS was brought to 200 µl with mKBS (37°C). Substrate was added to the Eppendorf tube and substrate decrease and product increase was measured by HPLC.

metabolism in numerous systems has been accumulated in the past 20 years (Zimmermann et al., 2012; Zimmermann, 2021). However, the information about degradation of extracellular purines in the urinary bladder is surprisingly sparse (Lewis and Lewis, 2006; Yu et al., 2011; Yu, 2015).

The extracellular metabolism of ATP is remarkably complex (Zimmermann et al., 2012): ATP is degraded sequentially to ADP, AMP, and ADO in the extracellular space by ectonucleoside triphosphate diphosphohydrolases (ENTPDs), ecto-nucleotide pyrophosphatase/phosphodiesterases (ENPPs), alkaline phosphatase/tissue-nonspecific isozyme (TNAP), and 5′-nucleotidase (NT5E/CD73) (**Figure 1**). The contribution of nucleotidases in the degradation of urothelial ATP might be highly specialized (Yu et al., 2011; Yu, 2015). While release of ATP by mechanical stimulation of bladder mucosa or cultured urothelial cells has been reported, it is currently unknown whether mechanical stretch during bladder filling affects the degradation of ATP in the LP. Understanding of these mechanisms is important for comprehending the regulation of bladder excitability by excitatory and inhibitory purine mediators during different stages of bladder filling.

The present study was designed, therefore, to evaluate 1) how distention of the bladder wall during bladder filling affects the hydrolysis of ATP and other purines in the LP and 2) the possible involvement of membrane-bound and soluble enzymes in these processes.

2 MATERIALS AND METHODS

2.1 Animals

Adult (11–16 weeks) C57BL/6J male and female mice (Jackson Laboratory, Bar Harbor, MN) were used in this study. Mice were euthanized by sedation with isoflurane followed by cervical dislocation and exsanguination. The urinary bladder was removed and placed in oxygenated ice-cold Krebs-bicarbonate solution (KBS) with the following composition (mM): 118.5 NaCl, 4.2 KCl, 1.2 $MgCl_2$, 23.8 $NaHCO_3$, 1.2 KH_2PO_4, 11.0 dextrose, and 1.8 $CaCl_2$ (pH 7.4) and subject to further dissection.

TABLE 1 | Modified KBS solutions (mKBS) in which activities of released eATPase(s) were assayed.

	Ca^{2+} (1.8 mM)	Mg^{2+} (1.2 mM)	EGTA (5 mM)	EDTA (5 mM)
KBS	+	+	−	−
mKBS-A	+	−	−	−
mKBS-B	−	+	+	−
mKBS-C	−	−	+	−
mKBS-D	−	+	+	+
mKBS-E	−	−	+	+

2.2 Ethical Approval

Animals were maintained and experiments were performed in accordance with the National Institutes of Health Guide for the Care and Use of Laboratory Animals and the Institutional Animal Use and Care Committee at the University of Nevada.

2.3 *Ex vivo* Detrusor-Free Bladder Preparation

Ex vivo bladder preparations with detrusor smooth muscle removed were prepared as described previously (Durnin et al., 2019a; Durnin et al., 2019b). Briefly, the bladder was pinned to a Sylgard-covered dissecting dish filled with cold oxygenated KBS by the urethra, ureters, and bladder serosa at the apex. After cleaning the fat and connective tissue that surrounds the bladder and ureters, portions of the serosa with the muscle attached were pulled gently and cut with fine surgical scissors along the submucosal surface of the muscle layer without touching the urothelium. Once all the detrusor was removed, a PE-20 catheter was placed through the urethra and secured with 6-0 silk and 6-0 nylon sutures.

2.4 Evaluation of Nucleotidase Activities in Suburothelium/Lamina Propria of Detrusor-Free Bladder Preparations

2.4.1 General Protocol of Enzymatic Reactions

1,N^6-etheno-derivatives of ATP (eATP), ADP (eADP), and AMP (eAMP) (2 µM each) were used as substrates. Reactions were performed at 37°C either in the presence of bladder preparations or in solutions collected from baths that previously contained bladder preparations (called extraluminal solutions, ELS). Following addition of substrate (0 min), 20 µl samples were collected from the reaction solution at 10 s, 2, 4, 6, 8, 10, 20, 30, 40, and 60 min and diluted 10-fold in ice-cold citric phosphate buffer (pH 4.0) to stop the enzymatic reactions. Collected samples were compared with a 2 µM substrate in KBS that has not been in contact with enzyme (designated as "beaker" sample). All samples were stored at −20°C until final analysis. Substrate decrease and product increase was evaluated by ultrasensitive HPLC-FLD methodology as described in **Section 2.8** HPLC analysis of 1,N^6-etheno-nucleotides. Each e-purine was expressed as percent of total purines detected in each sample. Only one substrate was used in each bladder preparation.

2.4.2 Nucleotidase Activity in Lamina Propria in the Presence of Bladder Preparation (Protocol 1)

Detrusor-free bladder preparations were placed in 3-ml water jacketed chambers filled with KBS at 37°C, bubbled with 95% O_2/5% CO_2. After equilibration for 20 min, KBS in the chamber was

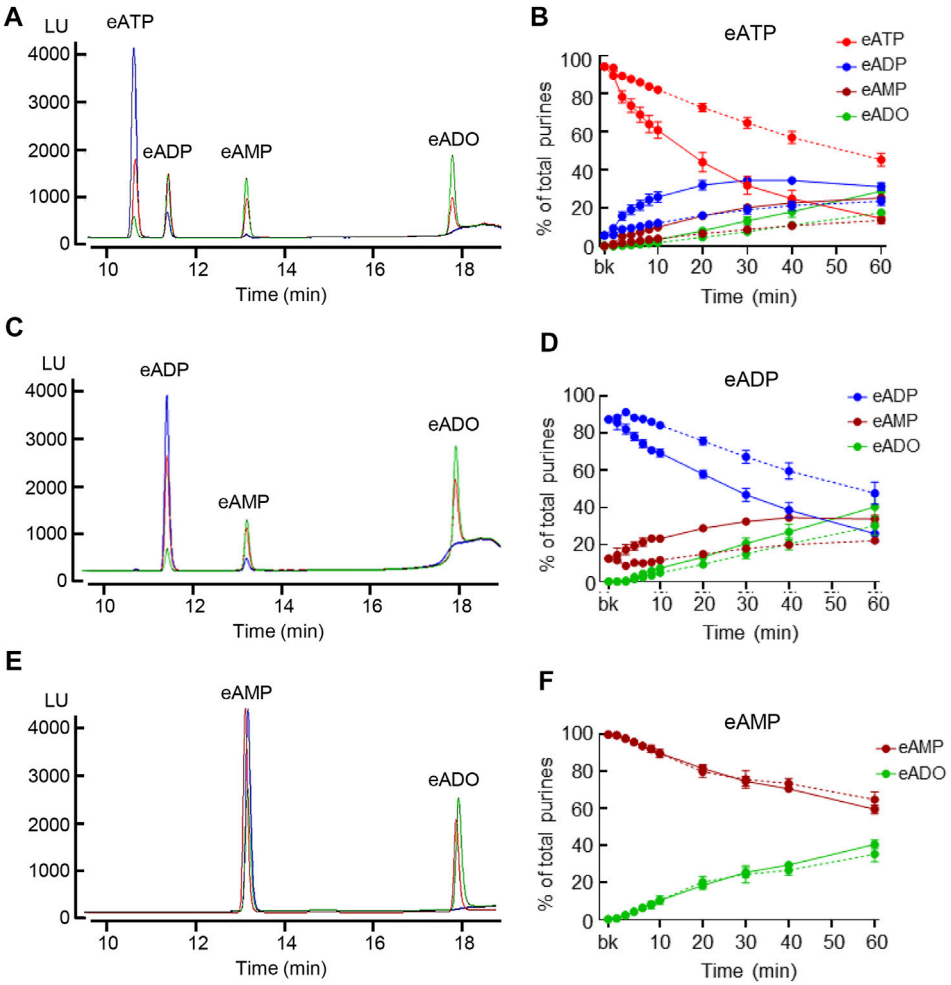

FIGURE 3 | Hydrolysis of eATP, eADP, and eAMP in contact with the LP of nondistended and distended detrusor-free bladders. **(A)** Original chromatograms of eATP in beaker (blue) and at 60 min of contact of eATP with the basolateral/anti-luminal side of nondistended (red) and distended (green) bladder preparations. Note the greater decrease of eATP and greater increase in eADP, eAMP, and eADO in distended than in nondistended preparations. **(B)** Summarized data showing the degradation of eATP in EL samples collected for 1 h after addition of eATP to ELS in the presence of bladder preparation (Protocol 1). eATP, eADP, eAMP, and eADO are presented as percentages of total purines (eATP + eADP + eAMP + eADO) present in ELS samples from nondistended (dotted connecting lines) and distended (solid connecting lines) preparations. **(C)** Original chromatograms of eADP in beaker (blue) and at 60 min of contact of eADP with the anti-luminal side of nondistended (red) and distended (green) bladder preparations. The chromatograms demonstrate greater decrease of eADP and greater increase in eAMP and eADO in distended than in nondistended preparations. **(D)** Summarized data showing the degradation of eADP in EL samples collected at different time points during 1 h after addition of eADP to ELS in the presence of bladder preparation (Protocol 1). eADP, eAMP, and eADO are presented as percentages of total purines (eADP + eAMP + eADO) present in ELS samples from nondistended (dotted connecting lines) and distended (solid connecting lines) preparations. **(E)** Original chromatograms of eAMP in beaker (blue) and at 60 min of contact of eAMP with the anti-luminal side of nondistended (red) and distended (green) bladder preparations. The chromatograms demonstrate similar decrease of eAMP and increase in eADO in distended and nondistended preparations. **(F)** Summarized data showing the degradation of eAMP in EL samples collected during 1 h after addition of eAMP in ELS in the presence of bladder preparation. eAMP and eADO are presented as percentages of total purines (eAMP + eADO) present in ELS samples from nondistended (dotted connecting lines) and distended (solid connecting lines preparations). Statistical significance is described in main text Results.

replaced with fresh KBS and the bladder was either left empty (nondistended condition) for the time equivalent to filling or filled at 15 µl/min with KBS *via* an infusion pump (Kent Scientific, Torrington, CT) to ~85–90% of bladder capacity determined at time of dissection (distended condition). Such filling volumes were similar to the volumes that were necessary to generate pre-voiding intravesical pressure (Durnin et al., 2019b), and were considered pre-voiding volumes. The degradation of eATP, eADP or eAMP was evaluated in the chamber containing 2.5 ml substrate solution in contact with nondistended or distended bladder preparations (**Figure 2A**, Protocol 1).

2.4.3 Soluble/Releasable Nucleotidase Activity in Lamina Propria (Protocols 2 and 3)

Following equilibration, the KBS in the chamber containing a bladder preparation was replaced with 3 ml of fresh KBS and the

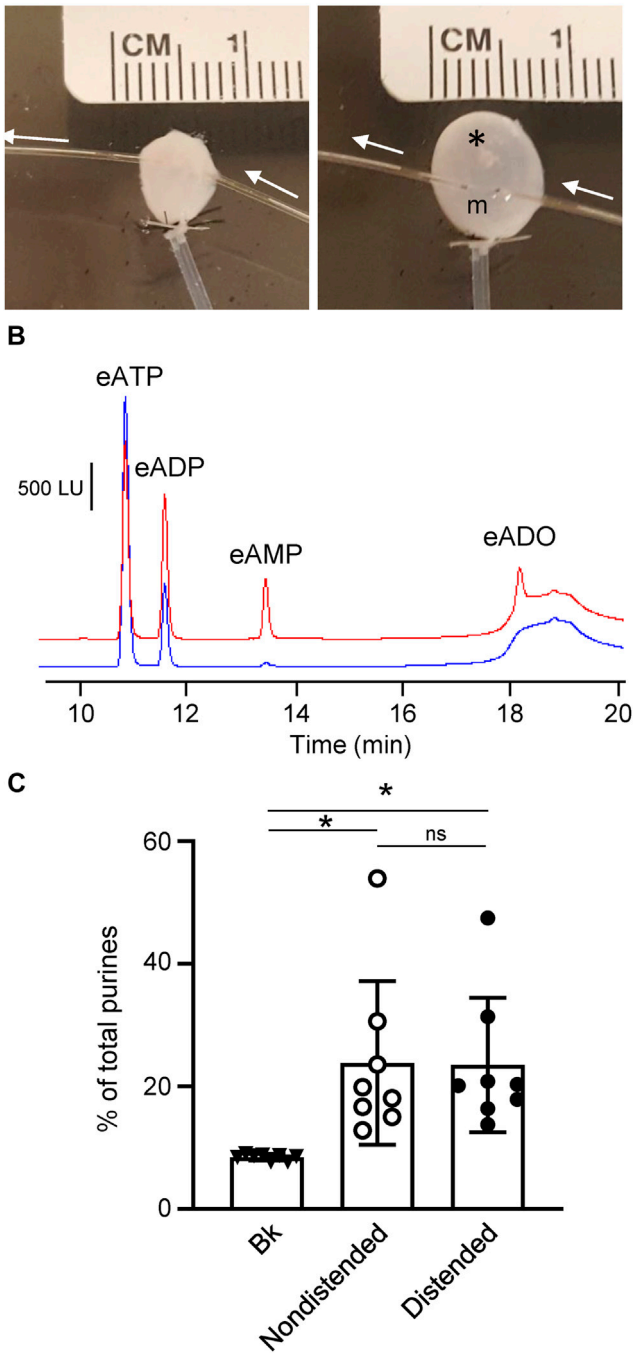

FIGURE 4 | Degradation of eATP in the suburothelium evaluated by microdialysis of the bladder wall. **(A)** Microdialysis probe implanted between suburothelium/LP and detrusor muscle of nondistended (left panel) and distended (right panel) mouse urinary bladder. m, microdialysis membrane outlined with black dots; white arrows show the direction of microdialysis perfusion. *, air bubbles inserted in bladder to show transparency of the wall. **(B)** Original chromatograms of eATP substrate in absence of tissue (beaker and blue) and in dialysate from nondistended bladder (red). Addition of eATP in the solution perfusing the microdialysis probe resulted in an eADP increase and the appearance of eAMP and eADO. (*Continued*)

FIGURE 4 | (C) Summarized data showing formation of product (eADP + eAMP + eADO) from eATP after microdialysis of nondistended and distended bladder preparations with eATP. Data are presented as percentages of total purines (eATP + eADP + eAMP + eADO) present in dialysate. *P < 0.05, ns, non-significant difference.

bladder was either left empty for the time equivalent to filling or filled at 15 µl/min with KBS to pre-voiding volume. Then, 2.4 ml of bathing solution (i.e., ELS) that was in contact with the bladder preparation was transferred to an empty water-jacketed chamber with an oxygen line. Substrate eATP, eADP or eAMP was added to the transferred solution at a final concentration of 2 µM and its degradation in the absence of tissue was evaluated for 1 h (**Figure 2B**, Protocol 2).

In a separate set of experiments, 2.9-ml of ELS was collected from nondistended or distended bladders and concentrated using 4-ml Amicon Ultra centrifugal filter units with a 10 kDa molecular weight cut-off pore size (Millipore Sigma, Burlington, MA, United States). Samples were concentrated by centrifugation at 4,000 × g for 25 min at 4°C using swing bucket rotor (ThermoFisher Scientific SorvallST 40R, Langenselbold, Germany). The concentrated EL solutions (cELS) were brought to 200 µl with oxygenated KBS and enzymatic reactions were performed at 37°C by adding substrate eATP, eADP or eAMP to the cEL sample (**Figure 2C**, Protocol 3).

2.4.4 Effects of Extracellular Ca^{2+} and Mg^{2+} on the Enzymatic Activities of Soluble (Released) Nucleotidases (Protocol 4)

Denuded bladder preparations were placed in water jacketed chambers filled with oxygenated KBS at 37°C. Following the equilibration, the KBS in the chamber was replaced with fresh KBS and the bladder was either left nondistended for the time equivalent to filling or it was filled (distended) at 15 µl/min with KBS to pre-voiding filling volume. This step ensured that soluble enzymes, if available, were released in regular KBS. Then, 2.9 ml of EL solution from nondistended or distended preparation was concentrated to approximately 80 µl using Amicon Ultra centrifugal filter units (10 kDa MWCO, 4-ml, and 25 min) as described in **Section 2.4.3** Soluble/Releasable Nucleotidase Activity in Lamina Propria (Protocol 3). In the next step, 2.9 ml of modified KBS (mKBS) that lacked Ca^{2+} and/or Mg^{2+} in the absence or presence of 5 mM EGTA and/or 5 mM EDTA (**Table 1**) was added to the centrifugal filter unit with cELS in KBS and was centrifuged at 4,000 × g for 15 min. To ensure complete replacement with mKBS, another 2.9-ml of mKBS was added to the centrifugal unit and concentrated at 4,000 × g for 25 min (**Figure 2D**, Protocol 4). The concentrated solutions containing enzymes in mKBS were brought up to 200 µl with mKBS and eATP substrate was added. eATP degradation was examined in: 1) nominally Mg^{2+}-free solution (*mKBS-A*), 2) Ca^{2+}-free KBS with 5 mM EGTA (*mKBS-B*), 3) Ca^{2+}-free and Mg^{2+}-free KBS with 5 mM EGTA (*mKBS-C*), 4) Ca^{2+}-free KBS with 5 mM EGTA and 5 mM EDTA (*mKBS-D*), and 5)

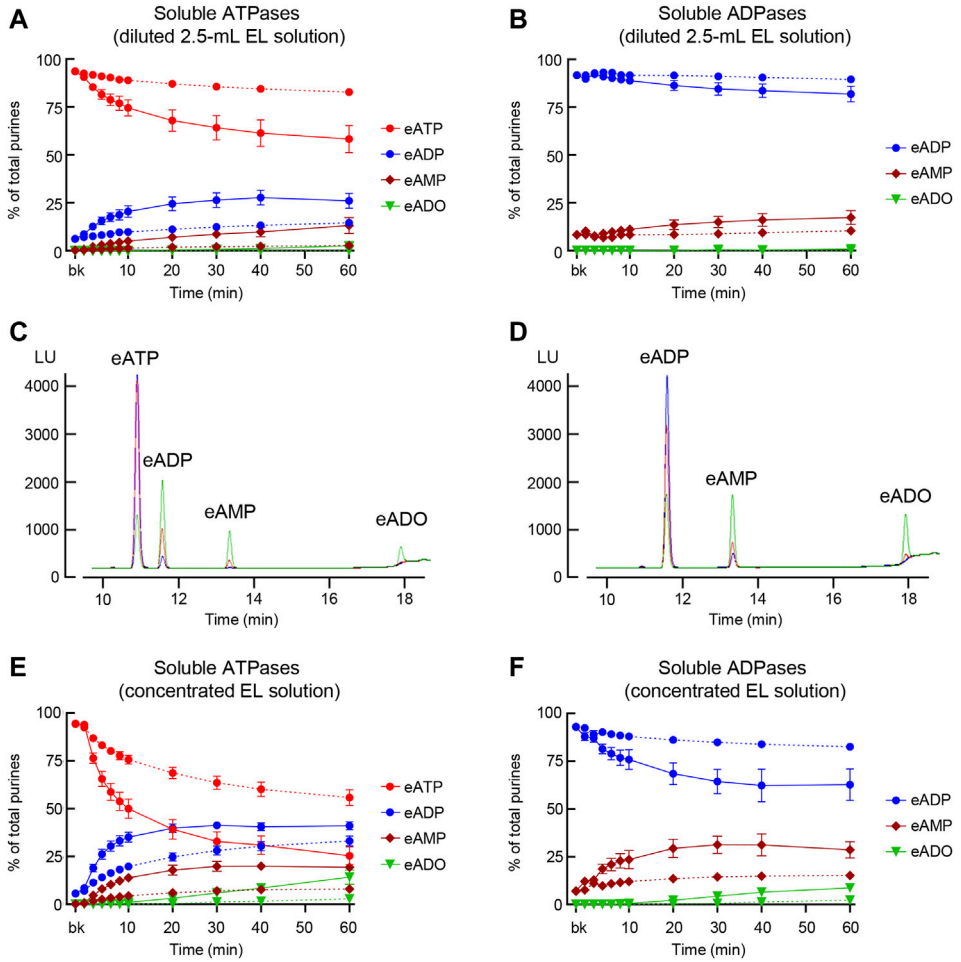

FIGURE 5 | Degradation of eATP and eADP by soluble enzymes released in the LP at rest and during bladder filling. **(A)** Summarized data showing the degradation of eATP in diluted (i.e., 2.5-ml) EL samples collected at different time points during 1 h after addition of eATP in the absence of bladder preparation (Protocol 2). eATP, eADP, eAMP, and eADO are presented as percentages of total purines (eATP + eADP + eAMP + eADO) present in EL solution samples from nondistended (dotted connecting lines) and distended (solid connecting lines) preparations. **(B)** Summarized data showing the degradation of eADP in diluted (i.e., 2.5-ml) EL samples collected at different time points during 1 h after addition of eADP in the absence of bladder preparation (Protocol 2). eADP, eAMP, and eADO are presented as percentages of total purines (eADP + eAMP + eADO) present in EL solution samples from nondistended (dotted connecting lines) and distended (solid connecting lines) preparations. **(C)** Original chromatograms of eATP in beaker (blue) and at 60 min of addition of eATP to concentrated EL samples (Protocol 3) collected from nondistended (red) and distended (green) bladder preparations. The chromatograms demonstrate greater decrease of eATP and increase in eADP, eAMP, and eADO in EL solutions from distended than from nondistended preparations. **(D)** Original chromatograms of eADP in beaker (blue) and at 60 min of addition of eADP to concentrated EL samples (Protocol 3) collected from nondistended (red) and distended (green) bladder preparations. The chromatograms demonstrate greater decrease of eADP and increase in eAMP and eADO in EL solutions from distended than from nondistended preparations. **(E)** Summarized data showing the degradation of eATP in EL samples collected at different time points during 1 h after addition of eATP in concentrated EL samples collected from nondistended (dotted connecting lines) and distended (solid connecting lines) (Protocol 3). eATP, eADP, eAMP, and eADO are presented as percentages of total purines (eATP + eADP + eAMP + eADO) present in the EL solution samples. **(F)** Summarized data showing the degradation of eADP in EL samples collected at different time points during 1 h after addition of eADP in concentrated EL samples collected from nondistended (dotted connecting lines) and distended (solid connecting lines) preparations (Protocol 3). eADP, eAMP, and eADO are presented as percentages of total purines (eADP + eAMP + eADO) present in the EL solution samples. Statistical significance is described in main text Results.

Ca^{2+}-free and Mg^{2+}-free KBS with EGTA and EDTA (5 mM each) (*mKBS-E*) (**Table 1**). Time-courses of enzymatic reactions following addition of eATP to reaction solutions were performed as described in **Section 2.4.1** General Protocol of Enzymatic Reactions. The hydrolysis of eATP in mKBS was compared with eATP hydrolysis in regular KBS processed in the same manner as concentrated mKBS. In some experiments, the hydrolysis of eADP was evaluated in mKBS that lacked Mg^{2+} (mKBS-A) or Ca^{2+} (mKBS-B and mKBS-E) and was compared with the eADP hydrolysis in regular KBS.

2.5 Pharmacological Characterization of Nucleotidase Activities

To assess the effects of nucleotidase inhibitors, enzymatic reactions were conducted as described in **Section 2.4** Evaluation of Nucleotidase Activities in Suburothelium/Lamina Propria of

Detrusor-Free Bladder Preparations either in the presence of vehicle (KBS or DMSO 0.1% in KBS) or of the following nucleotidase inhibitors: ARL67156 (100 μM in KBS; non-specific ENTPDase inhibitor), POM-1 (100 μM in KBS; non-specific ENTPDase inhibitor), ENPP1 Inhibitor C (50 μM in DMSO 0.1%), PSB06126 (10 μM in DMSO 0.1%; ENTPD3 inhibitor), and (-)-p-bromotetramisole oxalate (L-p-BT) (100 μM in DMSO 0.1%; TNAP inhibitor). Bladder preparations were incubated with the inhibitors throughout dissection, equilibration, nondistended and distended conditions and during the time-course reactions.

2.6 *Ex vivo* Microdialysis of Bladder Suburothelium

Ex vivo bladder preparations with intact detrusor smooth muscle were placed in a dissecting dish with oxygenated KBS and pinned by the serosa to the bottom of the dish. A PE-20 catheter was

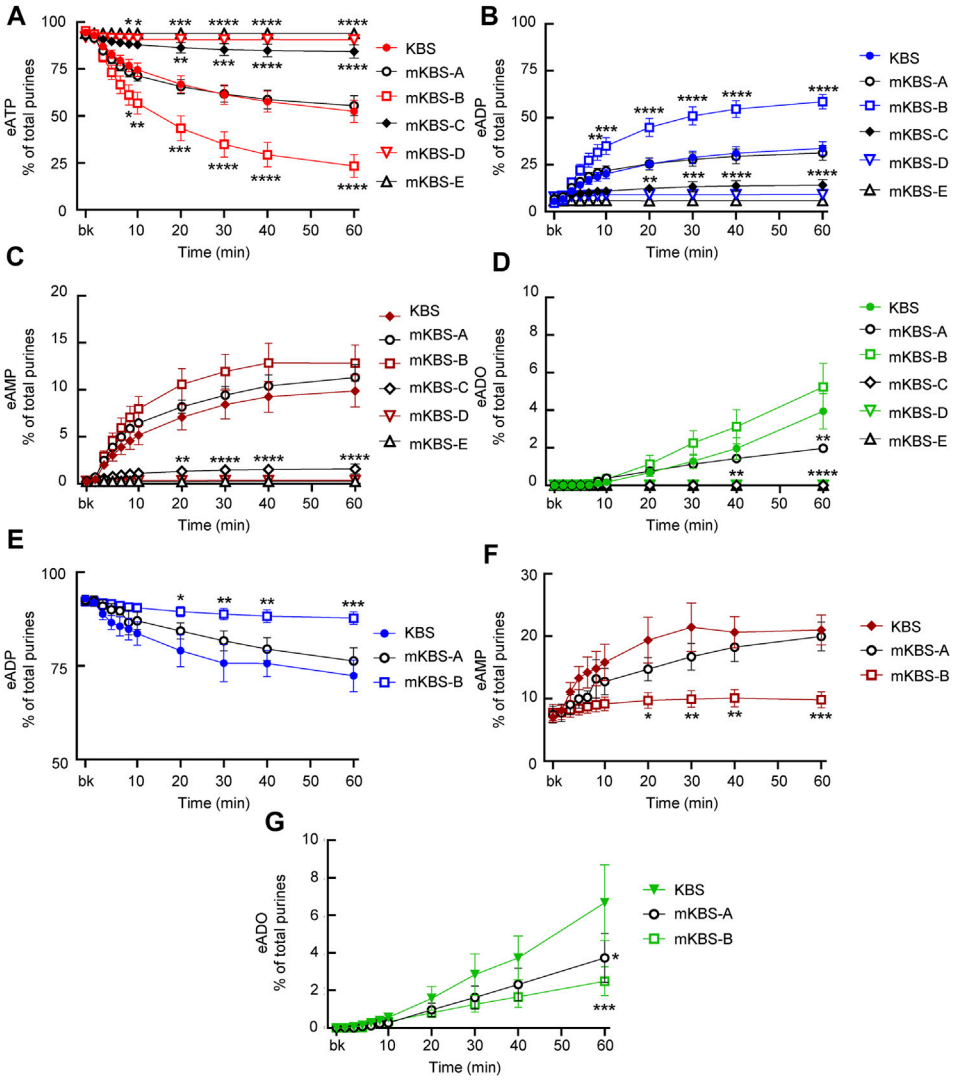

FIGURE 6 | Effects of extracellular Ca^{2+} and Mg^{2+} on activities of released ATPases and ADPases. **(A–D)** eATP hydrolysis by soluble enzymes in controls (KBS) and mKBS: panel **(A)** shows the decrease of eATP and panels **(B–D)** show the increase in eADP, eAMP, and eADO formed from eATP, respectively. **(E–G)** eADP hydrolysis by soluble enzymes in control (KBS) and mKBS: panel **(E)** shows eADP decrease and panels **(F,G)** show the increase in eAMP and eADO formed from eADP. KBS contains normal Ca^{2+} (1.8 mM) and Mg^{2+} (1.2 mM). mKBS-A contains normal Ca^{2+} (1.8 mM) and no Mg^{2+} (0 mM); mKBS-B contains 0 mM Ca^{2+}, normal Mg^{2+} (1.2 mM), and EGTA (5 mM); mKBS-C contains 0 mM Ca^{2+}, 0 mM Mg^{2+}, and EGTA (5 mM); mKBS-D contains 0 mM Ca^{2+}, normal Mg^{2+} (1.2 mM), EGTA (5 mM), and EDTA (5 mM); mKBS-E contains 0 mM Ca^{2+}, 0 mM Mg^{2+}, EGTA (5 mM), and EDTA (5 mM). Asterisks denote significant difference from controls (KBS). *$p < 0.05$, **$p < 0.01$, ***$p < 0.001$, ****$p < 0.0001$.

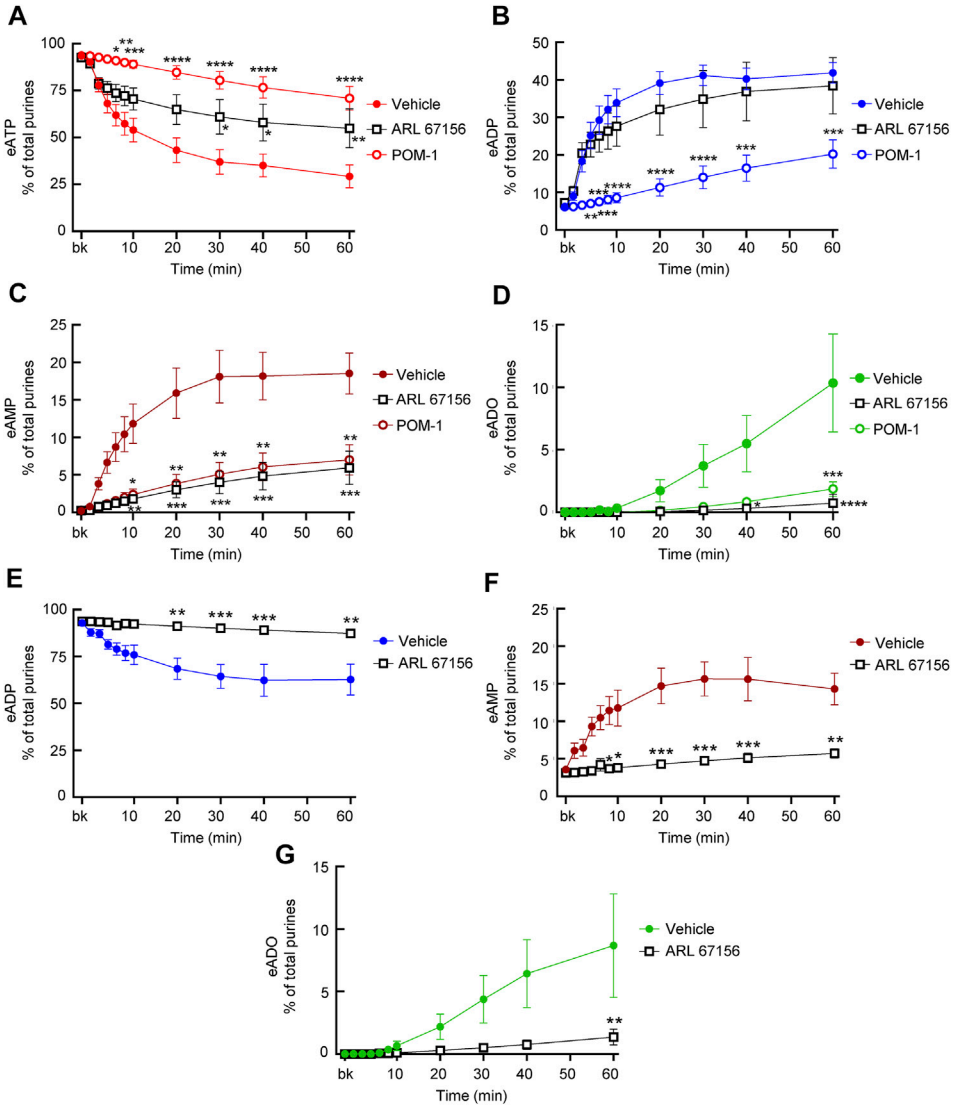

FIGURE 7 | Effects of ARL67156 and POM-1 on hydrolysis of eATP by soluble enzymes in LP. **(A–D)** eATP in the presence of vehicle (KBS) or ARL67156 (100 μM) or POM-1 (100 μM). **(E–G)** eADP hydrolysis by soluble enzymes in the presence of vehicle (KBS) or ARL67156 (100 μM). Asterisks denote significant difference from vehicle controls. *$p < 0.05$, **$p < 0.01$, ***$p < 0.001$, ****$p < 0.0001$.

placed through the urethra into the bladder lumen as described in **Section 2.3** *Ex vivo* Detrusor-Free Bladder Preparation. A linear probe for microdialysis (MD) with 2-mm dialysis membrane (CMA 30, Harvard Apparatus, Holliston, MA, United States or OP-X-Y, Amuza Inc., San Diego, CA, United States) was carefully implanted between the bladder mucosa and the detrusor (**Figure 4A**). The bladder preparation was then moved from the dissecting dish to a water-jacketed chamber filled with oxygenated KBS (pH 7.4 and 37°C). A syringe pump (Kent Scientific, Torrington, CT) was used to fill the bladder with oxygenated KBS through the intraluminal catheter. A second syringe pump was used to perfuse the MD probe with substrate solution. The MD probe was first perfused with KBS at 1 μl/min for 1 h to condition the probe, while the bladder preparation was kept empty. Equilibration was followed by perfusion of the MD probe at 1 μl/min with KBS containing 2 μM eATP. Dialysates were collected for 35 min while the bladder was either empty or was filled with KBS at 15 μl/min to a pre-voiding volume determined at time of dissection. After collecting each sample in ice-cold Eppendorf tube, citric buffer (pH 4.0) was added to the dialysate to preserve the purines in the collected sample. The samples were then processed for detection of eATP decrease and e-product increase by HPLC-FLD technique as described in HPLC analysis of 1,N^6-etheno-nucleotides. The location of the MD probe between detrusor and mucosa was verified at the end of each experiment. E-purines were expressed as percent of total purines detected in each sample.

2.7 Preparation of 1,N^6-Etheno-Nucleotides

1,N^6-etheno-ATP (eATP), 1,N^6-etheno-ADP (eADP), 1,N^6-etheno-AMP (eAMP), and 1,N^6-etheno-adenosine (eADO) were prepared according to a modified method of Levitt et al., 1984. Briefly, 180 µl of a citrate phosphate buffer (pH 4.0) containing 62 parts 0.1 M citric acid and 38 parts 0.2 M Na_2HPO_4, was added to 150 µl of 200 µM authentic purine (i.e., ATP, ADP, or AMP) in an Eppendorf tube. 2-Chloroacetaldehyde was synthesized according to a modified method of Levitt et al., 1984: equal amounts of 10-fold diluted H_2SO_4 in distilled H_2O and chloroacetaldehyde dimethyl acetal were added to a round bottom boiling flask. The mixture was distilled slowly under a fume hood and the distillate fraction containing approximately 1.0 M 2-chloroacetaldehyde was collected at 79–82°C. The reagent was stored at −20°C when not in use. Twenty µl 2-chloroacetaldehyde was added to the Eppendorf tube containing the mixture of authentic purine and citric buffer in a fume hood and then heated for 40 min at 80°C in a dry bath incubator (Fisher Scientific, United States) to produce 1,N^6-etheno-purine substrates and 1,N^6-etheno-purine standards (Bobalova et al., 2002).

2.8 HPLC Analysis of 1,N^6-Etheno-Nucleotides

A reverse phased gradient Agilent 1,200 liquid chromatography system equipped with a fluorescence detector (FLD) (Agilent Technologies, Wilmington, DE, United States) was used to detect 1,N^6-etheno-purines as described previously (Durnin et al., 2016; Durnin et al., 2019b). Briefly, the stationary phase consisted of a 25-cm by 4.5-mm (5 µm) silica reversed phase ODS-AM (C_{18}) column and a matching direct-connect guard column (YMC America, Inc., Devens, MA, United States). Gradient elution with 0.1 M KH_2PO_4 (pH 6.0) and increasing methanol (0–35% over 18 min) was employed. Column and autosampler temperatures were maintained at 25 and 4°C, respectively. Flow rate was 1 ml/min, run time was 20 min and post-run time was 5 min 1,N^6-etheno-derivatized purines were detected by fluorescence at an excitation wavelength of 230 nm and emission wavelength of 420 nm (Bobalova et al., 2002). ChemStation (v. B04-03) software (Agilent Technologies) was used to analyze areas under the peaks. The lower detection sensitivity for 1,N^6-etheno-derivatized purines was approximately 10 fmol. 1,N^6-etheno-derivatized purine standards (0.05–5 pmol) were processed with every set of samples.

2.9 Lactate Dehydrogenase Cell Toxicity Assay

Lactate dehydrogenase (LDH) activity (a marker of cell membrane integrity damage Radin et al., 2011) was measured in cELS prepared as described in **Section 2.4.3** Soluble/Releasable Nucleotidase Activity in Lamina Propria (Protocol 3) from distended detrusor-free or intact bladder preparations and from detrusor-free preparations treated with 1% Triton X-100 for 30 min (to induce cell lysis). LDH activity was determined using a colorimetric Lactate Dehydrogenase Assay Kit (Abcam, United States, Cat# ab102526). Absorbance was measured in 50 µl samples at optical density of 450 nm in a kinetic mode (every 3 min for 1 h) using Promega™ GloMax®-Multi Detection System (Promega, Madison, WI, United States). LDH activity in samples was compared with a NADH standard and the assay was validated using a positive LDH control provided by the manufacturer. LDH activity was calculated according to the manufacturer instructions, reported in mU/ml and plotted as mean ± SEM.

2.10 Automated Capillary Electrophoresis and Immunodetection With Wes Simple Western

For automated capillary electrophoresis and Western blotting by Wes (ProteinSimple, San Jose, CA, United States), mouse brain, urothelium tissue, and cELS were snap-frozen in liquid N_2, and stored at −80°C until processed (Li et al., 2018; Xie et al., 2018). cELS samples were prepared as described in **Section 2.4.3** Soluble/Releasable Nucleotidase Activity in Lamina Propria (Protocol 3). Urothelium and brain samples were homogenized in ice-cold lysis buffer (mM: 50 Tris–HCl pH 8.0, 60 β-glycerophosphate, 100 NaF, 2 EGTA, 25 sodium pyrophosphate, 1 DTT, 0.5% NP-40, 0.2% sodium dodecyl sulfate and protease inhibitors using a Bullet Blender) (one stainless steel bead per tube, speed 6, 5 min) (Bhetwal et al., 2011). The homogenates were then centrifuged at 16,000 × g, for 10 min at 4°C, and the supernatants stored at −80°C. The mouse brain homogenate was used as positive control. Protein concentrations of the supernatants were determined by the Bradford assay using bovine γ-globulin as standard. Protein levels were analyzed according to the Wes User Guide using a Wes Simple Western instrument from ProteinSimple (www.proteinsimple.com). The samples were mixed with the 5X Fluorescent Master Mix (containing 5X sample buffer, 5X fluorescent standard, and 200 mM DTT) and heated at 95°C for 5 min. The boiled samples, protein ladder, blocking buffer, primary antibodies, ProteinSimple horseradish peroxidase-conjugated anti-rabbit or anti-sheep (Invitrogen) secondary antibodies, luminol-peroxide, and wash buffer were loaded into the Wes plate (Wes 12–230 kDa Pre-filled Plates with Split Buffer, ProteinSimple). The plates and capillary cartridges were loaded into the Wes instrument, and protein separation, antibody incubation, and imaging were performed using default parameters. Compass software (ProteinSimple) was used to acquire the data, and to generate the virtual blot image reconstruction and chemiluminescence signal intensity electropherograms. The electropherogram shows the intensity detected along the length of the capillaries, and shows automatically detected peaks, that can be quantified by calculation of the area under the curve (AUC). The lane view is a virtual blot generated by the software from the actual data output, which takes the form of chemiluminescence signals versus apparent MW. Protein levels are expressed as the AUC of the peak chemiluminescence intensity.

2.10.1 Antibodies

The following primary antibodies were used for Wes analysis: from Cell Signaling Technology, rabbit anti-ENTPD1, and (E2X6B); rabbit anti-NT5E, (D7F9A); from ThermoFisher, sheep anti-ENTPD2, and (PA5-47777); rabbit anti-ENTPD3, (PA5-87888); rabbit anti-ENPP1, (PA5-17097); rabbit anti-ENPP3, (PA5-67955); from EpiGentek, rabbit anti-ENTPD8, and (A62482); from Abcam, rabbit anti-NT5C1A, and (ab190214); and, from Novus Biologicals, rabbit anti-TNAP, (SA40-00).

2.11 Drugs and Reagents

Adenosine, ATP, ADP, AMP, chloroacetaldehyde dimethyl acetal, dimethyl sulfoxide (DMSO), and Triton X-100 (Sigma-Aldrich, St. Louis, MO, United States), Ethylene glycol-bis(2-aminoethylether)-N,N,N′,N′-tetraacetic acid (EGTA) (ChemCruz Biomedicals, Dallas, TX, United States); N,N′-1,2-Ethanediylbis [N-(carboxymethyl)]glycine (EDTA) (Invitrogen, ThermoFisher Scientific), 6-[(3-aminophenyl)methyl]-N,N,5-trimethyl-[1,2,4]triazolo [1,5-a]pyrimidin-7-amine (ENPP1 Inhibitor C) (Cayman Chemicals, Ann Arbor, MI), (-)-p-bromotetramisole oxalate (L-p-BT) (MedChemExpress, Monmouth Junction, NJ, United States); 6-N,N-Diethyl-

D-β,γ-dibromomethyleneATP trisodium salt (ARL67156), sodium metatungstate (POM-1), and 1-Amino-4-(1-naphthyl) aminoanthraquinone-2-sulfonic acid sodium salt (PSB06126) (Bio-Techne Tocris, Minneapolis, MN)

2.12 Data Analysis

Data presented are means ± SEM. In some linear XY graphs, the data points are so similar that the symbols from individual points are superimposed. In some cases, the SEMs lie within the symbol. Scattered plot analysis was performed when appropriate. Means are compared by one-way ANOVA (Wes data) or two-way ANOVA (substrate degradation) for comparison of more than two groups followed by Dunnett's, Tukey's or Sidak's multiple comparisons tests per GraphPadPrism, v. 8.4.2., GraphPad Software, Inc., San Diego, CA. A probability value less than 0.05 was considered statistically significant.

3 RESULTS

3.1 The Detrusor-Free Bladder Preparation Does Not Display Abnormal Cell Damage of the Anti-Luminal Surface

LDH is a cytoplasmic enzyme present in most cells that is released upon damage of the cytoplasmatic membrane. We tested the LDH activity in cELS collected from detrusor-free preparations and from preparations with intact bladder walls as commonly used in bladder research. We compared the cell damage (measured as LDH activity) of the two types of preparations with cELS collected from detrusor-free bladders that were treated with Triton-X to induce a significant cell damage. The LDH activity was 186.39 ± 41.88 mU/ml in samples from Triton-X-treated preparations and 12.92 ± 2.69 and 50.53 ± 10.9 mU/ml in samples from distended detrusor-free and intact preparations, respectively (n = 4 and P = 0.9638). The LDH activity was 7.04 ± 0.47% and 30.97 ± 10.95% in cELS of detrusor-free and intact preparations ($p > 0.05$) when compared with the LDH activity in Triton-X treated samples taken as 100%. This data suggests that the detrusor-free bladder preparation does not display greater cell damage than effects that normally occur in commonly-used *ex vivo* bladder dissection.

3.2 The degradation of eATP and eADP in the Lamina Propria of filled bladders exceeds the degradation of eATP and eADP in the Lamina Propria of empty bladders

3.2.1 Protocol 1

To determine the degradation of eATP, eADP, and eAMP in contact with the LP, each substrate was added to the bath containing nondistended or distended detrusor-free bladder preparation. As shown in **Figure 3**, each substrate was progressively reduced and the corresponding products were progressively increased during the contact of substrate and bladder preparations (n = 5 in each group). In nondistended preparations, eATP comprised 94.19 ± 1.13% of total purines in beaker (0 min) and reached 45.39 ± 3.33% at 60 min ($p < 0.0001$) of reaction. In distended preparations, a significant decrease of eATP was observed at earlier time points than in nondistended preparations: eATP was reduced from 94.39 ± 0.9% of total purines in beaker to 14.55 ± 2.87% at 60 min ($p < 0.0001$) of reaction, 2wayANOVA with Dunnett's multiple comparisons test. The eATP decrease in nondistended preparations reached statistical significance at 8 min, whereas in distended preparations the decrease of eATP was statistically significant at 2 min of reaction ($p < 0.05$). The eATP decrease was significantly greater in distended than in nondistended preparations for the entire time of reaction starting at 4 min (P = 0.0170), 2way ANOVA Sidak's multiple comparisons test. The increase of the eATP products eADP, eAMP, and eADO was also greater in distended than in nondistended preparations. Thus, at 60 min of reaction, eADP was 23.54 ± 2.29% and 31.23 ± 2.03% (P = 0.0637); eAMP was 13.56 ± 0.98% and 25.31 ± 1.27% ($p < 0.0001$), and eADO was 17.5 ± 1.28% and 28.9 ± 4.09% ($p < 0.0001$) in nondistended and distended preparations, respectively; 2way ANOVA Sidak's multiple comparisons test.

Similar results were obtained with eADP as substrate (**Figures 3C,D**). eADP was decreased from 87.57 ± 1.14% in beaker to 47.7 ± 6.02% at 60 min ($p < 0.0001$) of reaction in nondistended preparations and from 87.56 ± 1.14% in beaker to 25.86 ± 4.4% at 60 min ($p < 0.0001$) of reaction in distended preparations, 2way ANOVA, Tukey multiple comparisons test. The eADP decrease was statistically significant at 10 min and at 30 min of reaction in distended and non-distended preparations, respectively ($p < 0.05$ vs. 0 min). The eADP decrease was greater in distended than in nondistended preparations during the enzymatic reaction starting at 6 min (P = 0.0153), n = 4 in each group, 2way ANOVA with Sidak's multiple comparisons test. The increase

of the eADP products eAMP and eADO was also greater in distended than in nondistended preparations. Thus, at 60 min of reaction, eAMP was 22.18 ± 1.29% and 33.79 ± 2.05% in nondistended and distended preparations, respectively ($p < 0.0001$) whereas eADO was 30.12 ± 5.19% and 40.35 ± 5.93% in nondistended and distended bladders, respectively ($P = 0.0277$).

The eAMP substrate (**Figures 3E,F**) was decreased from 99.78 ± 0.07% in beaker to 64.71 ± 4.17% and 59.45 ± 2.32% at 60 min of reaction in nondistended and distended preparations respectively, $n = 4$ in each group, $p < 0.0001$ vs. 0 min, 2way ANOVA Tukey's multiple comparisons test. No significant differences were observed in eAMP decrease or eADO increase between nondistended and distended preparations at all time points of reaction ($p > 0.05$), 2way ANOVA Sidak's multiple comparisons test.

3.3 Application of eATP in the Suburothelium *via* Microdialysis Results in eATP Hydrolysis

To determine whether eATP degradation occurs in the LP in the presence of detrusor, we applied the eATP substrate (2 μM) in the suburothelium using a MD probe inserted between urothelium and detrusor and examined whether an eATP decrease and product increase can be detected in dialysate (**Figure 4**). eATP was decreased from 91.56 ± 0.18% of total purines in beaker to 76.83 ± 4.84% ($P = 0.0361$) in dialysate from nondistended preparations ($n = 8$). eADP was 8.085 ± 0.18% and 12.87 ± 1.92% in beaker and dialysate, respectively ($P = 0.0839$) whereas eAMP was increased from 0.36 ± 0.002% in beaker to 6.88 ± 2.34% in dialysate ($P = 0.0478$). eADO was also significantly increased from 0% in beaker to 4.057 ± 0.596% of total purines in dialysate from nondistended preparations ($p < 0.0005$); one-way ANOVA with Dunnett's multiple comparisons test. We also measured the degradation of eATP during microdialysis of a bladder that was filled with KBS at 15 μl/min. Similar to nondistended preparations, eATP degradation was observed in dialysates from distended preparations: thus, eATP was reduced to 77.58 ± 4.15% ($P = 0.0237$) and eADP, eAMP, and eADO were increased to 13.13 ± 1.65% ($P = 0.0403$), 6.66 ± 1.94% (0.0253), and 3.71 ± 0.41% (<0.0001), respectively, of total purines in dialysates. The total product formation in dialysate was significantly greater than the total eATP product in beaker. There was no significant difference in product formation in dialysates from nondistended and distended preparations, $p > 0.05$ (**Figure 4C**), One-way ANOVA with Tuckey's multiple comparisons test. This data confirmed the key observation in detrusor-free bladder preparations signifying that ATP is hydrolyzed in the suburothelium to ADP, AMP, and ADO.

3.4 Enzymes That Hydrolyze eATP and eADP are Released in the Lamina Propria in a Stretch-Dependent Manner

3.4.1 Protocol 2

To determine whether soluble enzymes contribute to distention-dependent hydrolysis of eATP and eADP in the LP, the substrate was added to large-volume EL solutions that were transferred from chambers containing nondistended or distended bladders to empty chambers. The final volume of ELS plus substrate was 2.5 ml. Substrate decrease and product increase was measured for 1 h following addition of substrate. As shown in **Figure 5A**, eATP was significantly decreased in solutions collected from distended preparations, but not in solutions collected from nondistended preparations ($n = 12$ in each group). Thus, at 60 min of reaction, eATP was 93.63 ± 0.61% in beaker, 82.81 ± 1.93% in solutions from nondistended preparations ($P = 0.4125$) and 58.29 ± 7.09% in solutions from distended preparations ($p < 0.0001$), 2way ANOVA with Tukey's multiple comparisons test. The decrease of eATP was greater in solutions from distended than from nondistended preparations at 10–60 min ($p < 0.05$), 2way ANOVA with Sidak's multiple comparisons test. Likewise, the formation of eADP at 6–60 min, of eAMP at 30–60 min, and of eADO at 60 min was significantly greater ($p < 0.05$) in solutions collected from distended than from nondistended detrusor-free preparations.

When eADP was used as substrate in 2.5 ml ELS (**Figure 5B**), a significant decrease of eADP from beaker was observed at 40 min ($P = 0.0406$) and 60 min ($P = 0.0044$) of enzymatic reaction in ELS from distended but not from nondistended preparations ($n = 4$, 2way ANOVA with Tukey's multiple comparisons test). The difference of eADP decrease in ELS from nondistended and distended bladders was significant at 40 min ($P = 0.0486$) and 60 min ($P = 0.0197$) of reaction, 2way ANOVA with Sidak's multiple comparisons test.

3.4.2 Protocol 3

Prominent eATP or eADP substrate decrease and product increase was revealed in 12.5-fold concentrated ELS (cELS) from both nondistended and distended preparations (**Figures 5C–F**). In cELS from nondistended bladders (**Figure 5E**), a significant decrease of eATP was observed in 8–60 min ($p < 0.05$) as compared with eATP in beaker. In cELS from distended preparations, however, a significant decrease of eATP ($p < 0.05$) was observed at all time points except at 10 s ($n = 15$, 2way ANOVA Tuckey multiple comparisons tests). The decrease of eATP was significantly greater in cELS from distended than from nondistended preparations at 4–60 min of reaction ($p < 0.05$), 2way ANOVA Sidak's multiple comparisons test. The formation of eADP and eAMP from eATP was significantly greater in cELS from distended than from nondistended preparations at 4–60 min and 6–60 min, respectively ($p < 0.05$ and 2way ANOVA Sidak's multiple comparisons test). The increase in eADO was significant at 30–60 min ($p < 0.05$) of reaction in cELS from distended preparations, but it did not reach significance at all time points in cELS from nondistended preparations, 2way ANOVA Tukey's multiple comparisons test (**Figure 5E**).

eADP was not significantly degraded in cELS from nondistended preparations (**Figures 5D,F**). In cELS from distended preparations, however, a significant decrease of eADP was observed from 92.88 ± 0.62% in beaker to 62.7 ± 8.23% at 60 min of reaction ($p < 0.0001$), $n = 4$, 2way ANOVA,

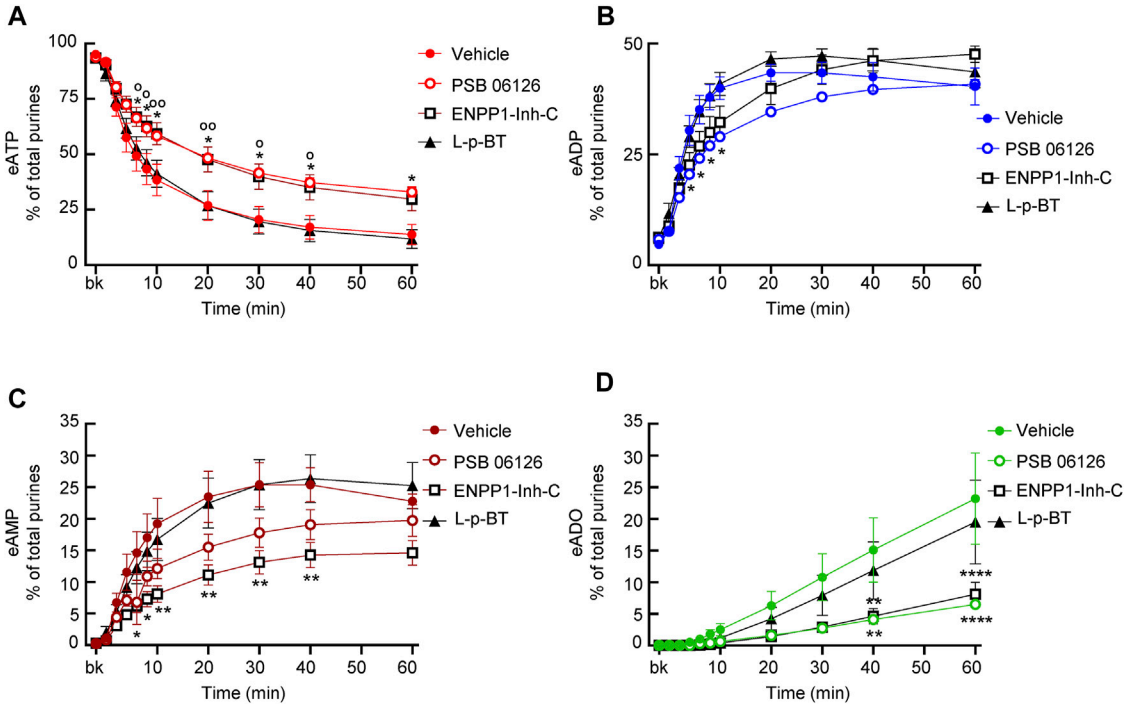

FIGURE 8 | Effects of PSB06126, ENPP1-Inh-C and L-p-bromotetramisole (L-p-BT) on hydrolysis of eATP by soluble enzymes in LP. **(A–D)** eATP hydrolysis by soluble enzymes in the presence of vehicle (0.1% DMSO) or PSB06126 (10 μM), ENPP1-Inh-C (50 μM) or L-p-bromotetramisole (L-p-BT) (100 μM). Asterisks denote significant difference of eATP decrease in the presence of ENPP1-Inh-C from vehicle controls. *$p < 0.05$, **$p < 0.01$, ****$p < 0.0001$. Open circles denote significant difference of eATP decrease in the presence of PSB06126 and vehicle control (panel **A**). °P<0.05, °°P<0.01.

and Sidak's multiple comparisons tests. The eADP decrease was statistically significant at 20–60 min. Significant increase of eAMP and eADO was observed at 6–60 min and 30–60 min, respectively ($p < 0.0001$ at 60 min for both products), $n = 4$, 2way ANOVA Sidak's multiple comparisons tests (**Figure 5F**).

3.5 Activities of Released Nucleotidases Depend Differentially on Extracellular Ca^{2+} and Mg^{2+}

3.5.1 Protocol 4

To determine how activities of enzymes released in the LP during bladder distention depend on Ca^{2+} and Mg^{2+}, we examined the eATP and eADP hydrolysis in mKBS that contained soluble enzymes but lacked Ca^{2+} or Mg^{2+}, in the presence of EGTA or EGTA + EDTA (**Table 1**). Replacement of regular KBS with mKBS required additional centrifugation of ELS prior to performing the enzymatic reactions. The control ELS (KBS) subjected to additional centrifugations retained nucleotidase activities as demonstrated by the substrate decrease and product increase after addition of eATP or eADP (**Figures 6A,B**).

In control ELS (KBS) from distended preparations (**Figure 6A**), the substrate eATP was decreased from 94.4 ± 0.24% in beaker to 52.44 ± 5.97% at 60 min ($p < 0.0001$) of reaction ($n = 9$ and 2way ANOVA with Tukey's, multiple comparisons test). The decrease of eATP remained unchecked in mKBS-A that contained normal Ca^{2+}, but lacked Mg^{2+}($n = 3$) (**Figure 6A**). However, in mKBS-B that contained normal Mg^{2+} but lacked Ca^{2+} ($n = 5$), the decrease of eATP was significantly enhanced at 8–60 min of reaction when compared with KBS controls (**Figure 6A**). Complete absence of Ca^{2+} in this solution was ensured by addition of 5 mM EGTA that specifically chelates Ca^{2+} (see Discussion). Removal of Mg^{2+} and Ca^{2+} in the presence of EGTA (mKBS-C and $n = 4$) almost completely inhibited the eATP decrease (**Figure 6A**). eATP hydrolysis was abolished in mKBS to which the non-specific chelator EDTA (5 mM) was added (e.g., mKBS-D and mKBS-E, each $n = 3$), **Figure 6A**.

The increase of eADP formed from eATP in mKBS followed similar patterns: the eADP increase was not affected by removal of Mg^{2+} alone, was enhanced in the absence of Ca^{2+} plus EGTA, and was abolished in the absence of both Ca^{2+} and Mg^{2+} and addition of EDTA (**Figure 6B**). The increase of eAMP formed from eATP (**Figure 6C**) was inhibited in the absence of both Ca^{2+} and Mg^{2+} in the presence of EDTA and/or EGTA, but the eAMP increase was not affected by the absence of either Ca^{2+} or Mg^{2+} alone. eADO formation (**Figure 6D**) reached statistically significant values at 40 and 60 min of reaction. The eADO increase was reduced at 60 min in the absence of Mg^{2+}, but was not changed in Ca^{2+}-free solution with EGTA (mKBS-B). As with the other e-products, the formation of eADO from eATP was abolished when both Ca^{2+} and Mg^{2+} were removed or EDTA was added (i.e., mKBS-C, mKBS-D, and mKBS-E) (**Figure 6D**).

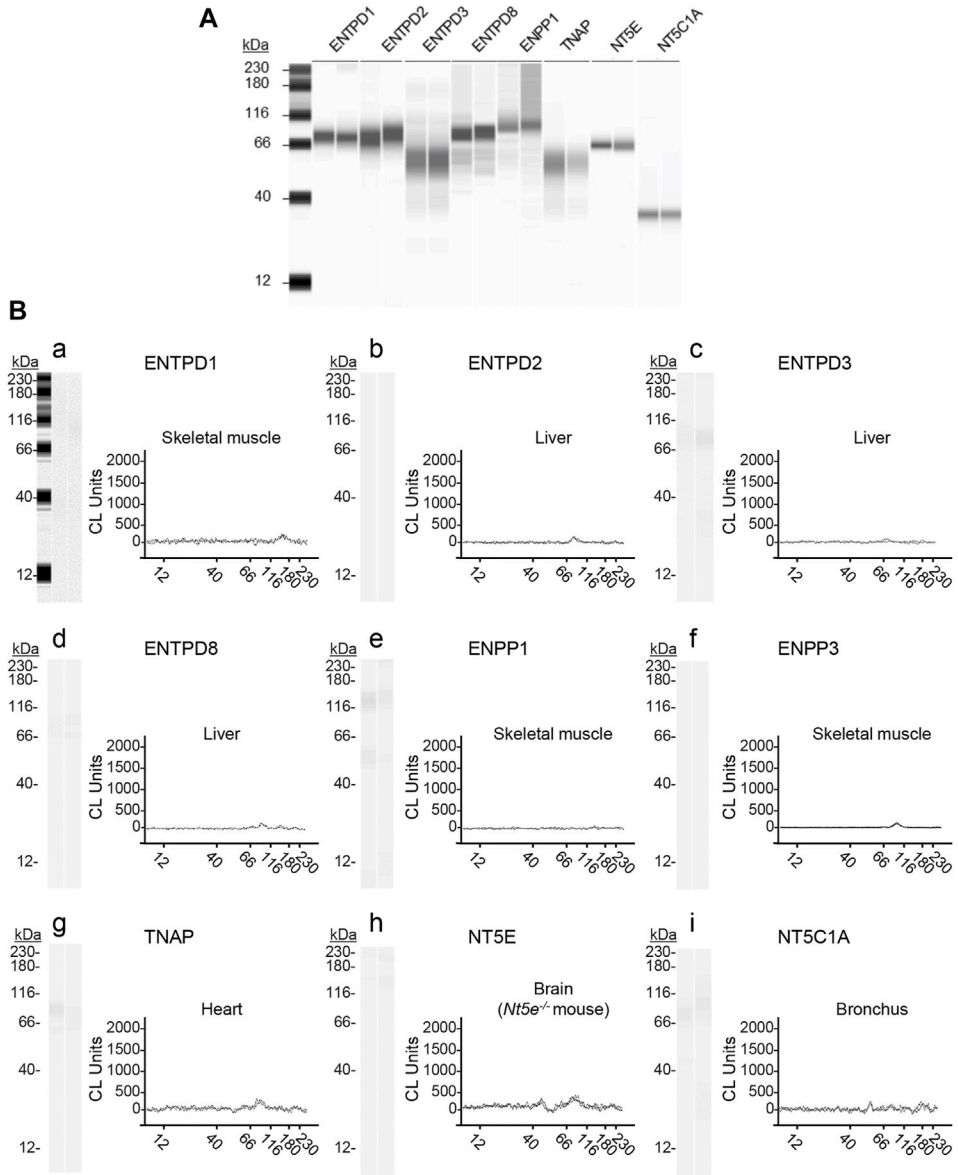

FIGURE 9 | Validation of anti-nucleotidase antibodies used for enzyme identification. ProteinSimple Wes was used to specifically detect the indicated nucleotidases in **(A)** mouse brain homogenates (positive controls) and in **(B)** mouse tissue homogenates in which the indicated nucleotidase has not been detected (negative controls). Panel **(Ba–Bi)** show representative blot images (left) and immunoelectropherograms (right) of negative control tissue homogenates. Each antibody was tested in duplicate. The antibodies, dilutions, corresponding amounts of homogenate per well, and expected molecular weight (from vendor) used were: rabbit anti-ENTPD1 (1:200, 15 µg, and 80 kDa), sheep anti-ENTPD2 (1:500, 7.5 µg, and 80 kDa); rabbit anti-ENTPD3 (1:500, 3.0 µg, and 80 kDa); rabbit anti-ENTPD8 (1:200, 15 µg, and 60 kDa); rabbit anti-ENPP1 (1:500, 15 µg, and 100 kDa); rabbit anti-ENPP3 (1:500, 15 µg, and 100 kDa); rabbit anti-NT5E (1:500, 15 µg, 7and 0 kDa); rabbit anti-TNAP (1:200, 30 µg, and 60 kDa; rabbit anti-NT5C1A (1:100, 30 µg, and 40 kDa)).

When eADP was used as substrate, it did not decrease significantly in EL solutions collected from nondistended preparations (data not shown). However, in cELS from distended preparations (KBS controls, n = 5, **Figure 6E**), eADP decreased from 92.99 ± 0.78% in beaker to 72.34 ± 4.23% at 60 min ($p < 0.0001$) of reaction. The decrease of eADP was accompanied with an increase of eAMP from 7.01 ± 0.78% in beaker to 20.99 ± 2.39% at 60 min ($p < 0.0001$) of reaction (**Figure 6F**). The formation of eADO from eADP was significantly increased from 0 ± 0% in beaker to 6.67 ± 2.02% at 60 min ($p < 0.0001$) (**Figure 6G**). Similar to the eATP substrate, removal of Mg^{2+} alone (mKBS-A) did not affect significantly the degradation of eADP. In contrast to eATP, however, removal of Ca^{2+} and addition of EGTA (i.e., mKBS-B) significantly inhibited the decrease of eADP substrate (**Figure 6E**). The formation of eAMP from eADP appeared to be reduced in nominally Mg^{2+}-free solution (mKBS-A); however, this effect did not reach statistical

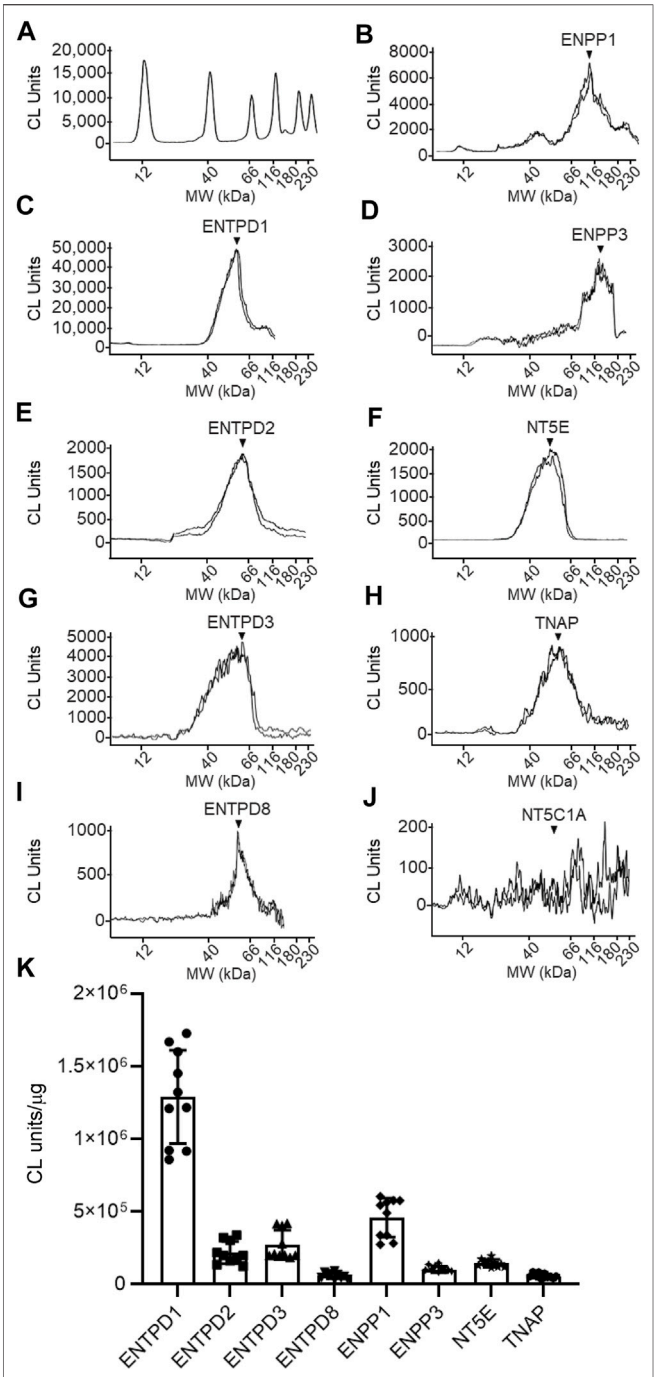

FIGURE 10 | Protein expression levels in urothelium homogenates prepared from detrusor-free bladder preparations. Representative immunoelectropherograms (duplicates) of nucleotidases detected in urothelium using ProteinSimple Wes **(A–J)**. Each antibody was diluted 100-fold and each well contained 6 µg of urothelium homogenate sample. The antibodies used are described in **Figure 9** and in main text Antibodies. **(K)** Scatter plots of AUC of chemiluminescence (CL) signals normalized per µg loaded urothelium sample. Each symbol represents a single loading from 5 urothelium samples, loaded in triplicates. Statistical significance is described in main text Results.

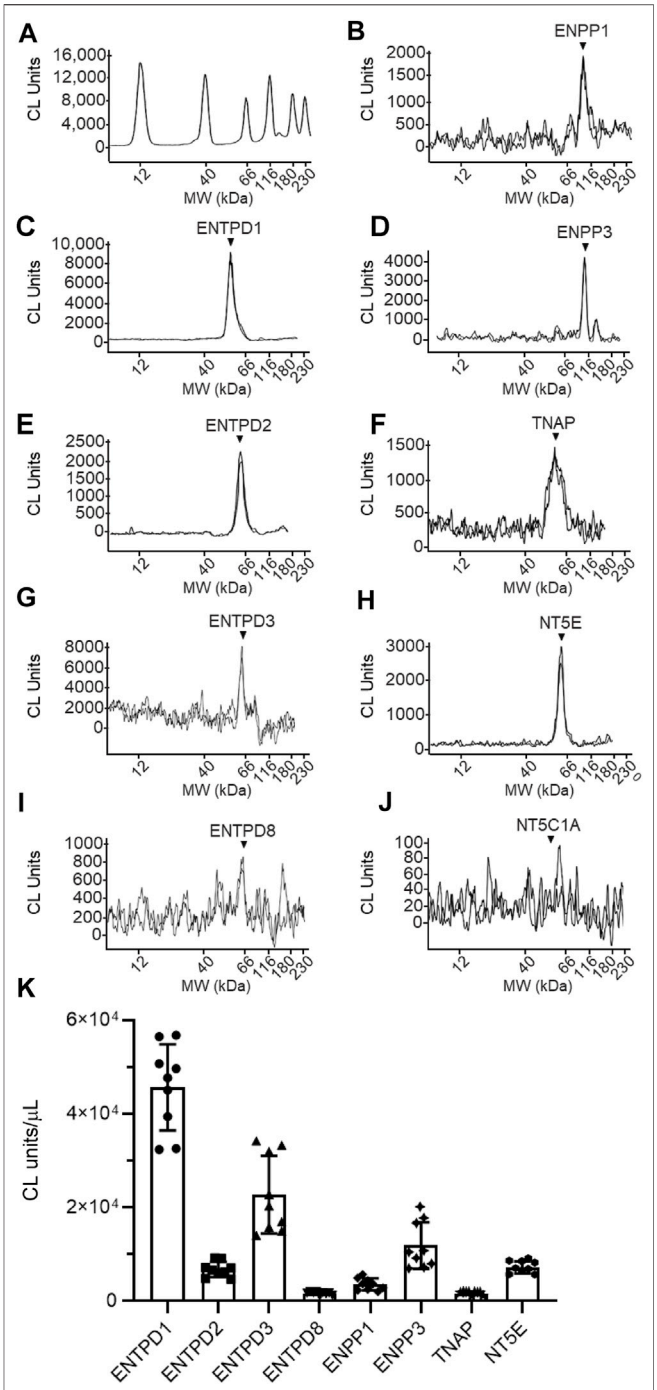

FIGURE 11 | Protein expression levels in cELS collected from distended detrusor-free bladder preparations. Representative immunoelectropherograms (duplicates) of nucleotidases detected in cELS using ProteinSimple Wes **(A–J)**. Each antibody was diluted 100-fold and each well contained 3 µl of cELS sample. The antibodies used are described in **Figure 9** and in main text Antibodies. **(K)** Scatter plots of AUC of chemiluminescence (CL) signals normalized per µL loaded cELS sample. Each symbol represents a single loading from 3 cELS samples, loaded in triplicates. Statistical significance is described in main text Results.

significance for the duration of 1 h. No formation of eAMP from eADP was observed in Ca^{2+}-free solutions containing EGTA (**Figure 6F**). The formation of eADO from eADP was decreased at 60 min of reaction in mKBS-A lacking Mg^{2+} and in mKBS-B that lacked Ca^{2+} and contained EGTA (**Figure 6G**).

3.6 Inhibitors of Membrane-Bound Nucleotidases Impede the Hydrolysis of eATP and eADP by Soluble Enzymes Released in the Lamina Propria

3.6.1 Effects of ARL67156

ARL67156 is an ATP analog that was introduced as "an ATPase inhibitor" in the 1990s (Crack et al., 1995). As shown in **Figure 7A**, the degree of eATP decrease in cELS from distended preparations was reduced by ARL67156 (100 μM). The inhibition by ARL67156 was statistically significant at 30–60 min of reaction. At 60 min, eATP was 29.24 ± 6.107% of total purines in controls (n = 9) and 46.87 ± 11.35% in the presence of ARL67156 (n = 5), P = 0.0076. eADP increase was not affected by ARL67156 at all time points of reaction (**Figure 7B**). However, the increase of eAMP was significantly inhibited in the presence of ARL67156 at 10–60 min of enzymatic reaction (**Figure 7C**) and the increase in eADO was almost abolished (**Figure 7D**). When eADP was used as substrate, ARL67156 almost abolished the decrease of eADP and the increase of eAMP and eADO (**Figures 7E–G**).

3.6.2 Effects of POM-1

POM-1 is a polyoxometalate that inhibits ENTPDases (Muller et al., 2006). As shown in **Figure 7**, the hydrolysis of eATP was significantly inhibited by POM-1 (100 μM) since the decrease of eATP at 6–60 min of reaction (**Figure 7A**) and the formation of eADP, eAMP, and eADO (**Figures 7B–D**) were diminished in the presence of POM-1. POM-1 appeared to have a greater effect on the decrease of eATP than ARL67156 (**Figure 7A**); however, the differences between the effects of the two drugs did not reach statistical significance. The increase of eADP was diminished in the presence of POM-1 but not in the presence of ARL-67156 (**Figure 7B**) whereas the formation of eAMP and eADO was decreased by both POM-1 and ARL67156 (**Figures 7C,D**). These data suggest that POM-1 and ARL67156 differ in inhibiting the hydrolysis of eATP.

3.6.3 Effects of PSB06126

The ENTPD3 inhibitor PSB06126 (10 μM), significantly diminished the decrease of eATP from 6 to 60 min of reaction (**Figure 8A**), suggesting that a soluble form of ENTPD3 might be released in the LP. The increase of eADP was diminished in the earlier time points (e.g., 4–10 min) but not in the later time points of reaction (**Figure 8B**). The presence of PSB06126 resulted in less production of eAMP and eADO (**Figures 8C,D**).

3.6.4 Effects of ENPP1-Inhibitor-C

ENPP1 Inhibitor C diminished the decrease of eATP, did not affect the increase of eADP, and significantly reduced the formation of eAMP and eADO (**Figure 8**), suggesting that it likely inhibited the direct hydrolysis of eATP to eAMP and subsequently to eADO.

3.6.5 Effects of L-p-BT

The TNAP inhibitor L-p-BT had no significant effect on the eATP decrease or the eADP, eAMP, and eADO increase (**Figure 8**), suggesting that alkaline phosphatases that are sensitive to this inhibitor do not play a significant role in the degradation of eATP by soluble enzymes in the bladder LP.

3.7 Soluble Enzymes in the Lamina Propria are Similar to Known Membrane-Bound Nucleotidases

Urothelium tissues and cELS collected from distended preparations were investigated by Wes analysis for expression of known membrane-bound nucleotidases that use ATP or ADP as substrates (**Figures 10**, **11**). The antibodies used for identification of ENTPD1, ENTPD2, ENTPD3, ENTPD8, ENPP1, ENPP3, NT5E, TNAP, and NT5C1A were validated in mouse brain homogenates used as positive controls (**Figure 9A**). In addition, each antibody was tested in tissue homogenates in which the indicated nucleotidase has not been detected per The Mouse Gene Expression Database (http://www.informatics.jax.org/expression.shtml) and The Human Protein Atlas (https://www.proteinatlas.org). Thus, tissue homogenates from skeletal muscle, liver, heart, and bronchus as well as from brain of a *Nt5e*$^{-/-}$ mouse were used as negative controls for antibody validation. No signals were detected in the negative control tissue homogenates (**Figure 9B**) using the same antibody dilutions and amounts of negative control tissue homogenates that were used for the corresponding mouse brain homogenate positive controls (**Figure 9A**). These experiments validated that the signals from the urothelium homogenates (**Figure 10**) and cEL samples (**Figure 11**) are due to binding of the antibodies to their respective target antigens, and not from non-specific antibody interactions, or false-positives.

The following enzymes were detected in both urothelium tissue homogenates (**Figure 10**) and cEL samples from distended preparations (**Figure 11**): ENTPD1, ENTPD2, ENTPD3, ENTPD8, ENPP1, ENPP3, NT5E, and TNAP. Note that NT5C1A was not resolved in urothelium, and was not detected in the EL samples, indicating that NT5C1A does not contribute to the pool of released enzymes in the LP. ENTPD1 was the main nucleotidase expressed in urothelium and in cELS ($p < 0.0001$ from all other nucleotidases in each sample kind) whereas ENTPD8 and TNAP were barely detected in both types of samples. Importantly, the relative expression of nucleotidases differed in urothelium and cELS. In the urothelium, ENPP1 was the second highly expressed protein and was significantly higher than ENTPD2 (P = 0.0003), ENTPD3 ($p < 0.0001$), ENPP3 ($p < 0.0001$), NT5E ($p < 0.0001$), ENTPD8 ($p < 0.0001$), and TNAP ($p < 0.0001$),

2way ANOVA with Tuckey multiple comparisons test (**Figure 10**). In the cELS however, ENTPD3 was the second highest protein expressed. The ENPP1 levels were significantly lower than the levels of ENTPD3 ($p < 0.0001$), and did not differ from ENTPD2 ($P = 0.6412$), ENTPD8 ($P = 0.9639$), NT5E ($P = 0.9431$) or TNAP ($P = 0.9657$), 2way ANOVA with Tuckey multiple comparisons test (**Figure 11**). In the urothelium homogenates, the ENPP1 levels were higher than the ENPP3 levels ($p < 0.0001$) (**Figure 10**) whereas in the cELS, the ENPP1 levels were significantly lower than the ENPP3 levels ($P = 0.0006$).

4 DISCUSSION

The present study reports two major findings: 1) distention of the bladder wall during filling is associated with increased metabolism of extracellular purine nucleotides in the LP, and 2) multiple soluble enzymes contribute to mechanosensitive degradation of purines in the LP, in addition to membrane-bound nucleotidases. To the best of our knowledge, mechanosensitive degradation of extracellular mediators has not been reported previously. Such mechanisms in the LP likely contribute to guaranteeing a proper ratio of excitatory-to-inhibitory purine mediators deep in the bladder wall that is necessary to maintain adequate bladder excitability during bladder filling.

During filling, the volume of the urine increases dramatically while the intravesical pressure increases modestly until a point is reached where pressure rises precipitously and voiding occurs. There is no definite explanation of how the urothelium communicates with other cells in the bladder wall to maintain continence or initiate voiding. As discussed in Introduction, based on numerous observations in bladder mucosa sheets, cultured urothelial cells, or in the bladder lumen, a prominent role for urothelial ATP has been proposed in bladder mechanosensation, and mechanotransduction. However, there is still incomplete understanding of the physiological roles of ATP released from the bladder mucosa at low and high intravesical volumes and pressures (Mutafova-Yambolieva and Durnin, 2014; Takezawa et al., 2016b; Dalghi et al., 2020). Studies have suggested that afferent neuron activity and the micturition reflex are attenuated in bladders of mice lacking $P2X_2$, $P2X_3$, and $P2X_{2,3}$ purinergic receptors (Cockayne et al., 2000; Vlaskovska et al., 2001). Recent studies using newer technologies, however, demonstrated unaltered micturition reflex in *P2rx2*$^{-/-}$ and *P2rx3*$^{-/-}$ mice, calling into question the roles of ATP and $P2X_{2/3}$ receptors in the normal micturition reflex (Takezawa et al., 2016a). It is generally assumed that ATP is released from urothelial cells in response to elevated hydrostatic pressure (Ferguson et al., 1997; Dunton et al., 2018). Some reports, however, have argued that stretch and not hydrostatic pressure induces release of ATP from the bladder mucosa (Yu, 2015). Importance of extracellular purinergic signaling in bladder physiology and pathophysiology is widely acknowledged (Merrill et al., 2016; Andersson et al., 2018). Therefore, controversies in the field require further studies to elucidate the role of ATP and other purines in the regulation of bladder excitability during authentic bladder filling.

In the present study, we used a bladder preparation devoid of the detrusor smooth muscle layer to obtain direct access to the LP surface. We demonstrated previously that the volume-pressure relationships of bladder preparations with and without the detrusor layer of muscle were similar (Durnin et al., 2019b), suggesting that the model is suitable for studying mechanisms during authentic bladder filling. We demonstrated that the LP layer of the preparation is preserved when the detrusor layer is carefully removed by cutting (not "peeling") it away from the urothelium (Durnin et al., 2019b). The model was instrumental in confirming that ATP is released in the anti-luminal side of the urothelium at rest and during bladder filling and in suggesting that observations made at the luminal side of bladder mucosa do not reflect faithfully mechanisms in the LP. A surprising finding of the study was that the distribution of adenine purines in the LP at the end of bladder filling was ADO >> AMP > ADP >> ATP so that ATP represented only 5% of the total purines (Durnin et al., 2019b). It is logical to assume that this distribution of purines is primarily determined by sequential hydrolysis of ATP that was released at the LP during bladder filling. Since ATP release on the anti-luminal side of the urothelium is assumed to be caused by mechanical stretch, the goal of the present study was to determine whether the ATP degradation in the LP also changes with distention/stretch of the bladder wall during filling. Thus, we centered the study on metabolism of ATP in the LP of nondistended and distended denuded bladder preparations.

As in previous studies (Todorov et al., 1997; Durnin et al., 2012), we used 1,N^6-etheno-derivatives of ATP, ADP, and AMP as substrates. The enzymatic activities were evaluated by measuring the decrease of substrates and the increase of products in the LP of nondistended and distended preparations. Use of etheno-purines instead of authentic purines as substrates provides a number of advantages: 1) ecto-nucleotidases process 1,N^6-etheno-bridged purine nucleotides similarly to their endogenous counterparts (Jackson et al., 2020b), 2) the sensitivity of detection of etheno-nucleotides and nucleosides is 1,000,000-fold greater than the sensitivity of most detection methods for authentic purine nucleotides (Bobalova et al., 2002); this allows detection of small changes in substrate and product concentrations; 3) unlike authentic AMP and ADO, eAMP, and eADO cannot be diverted to other metabolic pathways *via* deamination because the etheno bridge blocks the N^6 nitrogen in the AMP and ADO molecules; this simplifies to some extent data interpretation; and 4) possible release of endogenous adenine purines remains undetected since the samples that were in contact with tissue do not undergo further etheno-derivatization. To examine the degradation of purine substrates at physiological levels, we chose a concentration (i.e., 2 μM) that is analogous to the concentration of purines previously determined in the same bladder model and with the same detection methodology (Durnin et al., 2019b). Monitoring the enzymatic activities for 1 hour following addition of substrate to the chamber with the bladder preparation seemed to be physiologically relevant as normal mice void on average 3–4 times within a 4-h period (Chen et al., 2017; Marshall et al.,

2020). As anticipated, eATP was degraded to eADP, eAMP, and eADO in contact with the LP of nondistended detrusor-free bladder preparations so that eATP was diminished by 50% 1 h after initiation of reaction. A surprising observation was that eATP was decreased significantly more (by about 80%) in distended preparations for the same time period (i.e., 1 h) after initiation of the enzymatic reaction. This is a particularly intriguing observation, suggesting that during distention of LP caused by bladder filling, the degradation of ATP to ADP, AMP, and ADO is significantly enhanced. Similarly, the degradation of eADP in the LP of distended preparations exceeded the degradation of eADP in nondistended preparations. Interestingly, the degradation of eAMP in the LP was similar in distended and nondistended preparations. These data suggest that nucleotidases with different sensitivities to stretch appear to be present in the LP. The relative extent of substrate catabolism in the course of 1 h was eATP > eADP > eAMP.

We next asked whether eATP hydrolysis occurs in the suburothelium in the presence of detrusor. Microdialysis has been instrumental in examining release of small-molecule substances in the interstitial space of brain, skeletal muscle, liver, kidney, adipose tissue, and skin (Thompson and Shippenberg, 2001; La Favor and Burnett, 2016; Jackson et al., 2020b), but has not been utilized in studies of the bladder wall. In proof-of-principle experiments, we applied eATP *via* a MD probe inserted between the urothelium and the detrusor of *ex vivo* bladder preparations. Despite the extremely limited surface of the microdialysis membrane (~0.6 mm^2), the very low internal volume of the MD probe at the membrane (~0.1 µl), and the short contact of the eATP substrate with LP (~6 s), eATP produced eADP, eAMP, and eADO when perfused through the MD probe. Because the eATP breakdown occurred in such a small fraction of the LP for such a short contact between substrate and enzymes, distention-dependent eATP hydrolysis could not be revealed in these experiments. Importantly, however, this study provided affirmation that eATP can be degraded in the suburothelium and that results obtained in detrusor-free preparations can be extrapolated to the multilayer bladder wall.

Enhanced ATP degradation during filling explains why ATP represents such a small portion of the total purine pool in the LP at the end of bladder filling (Durnin et al., 2019a). However, this observation is at odds with the idea that the concentration of ATP that is released from the urothelium into the LP must reach maximum levels at the end of bladder filling to activate afferent neurons in the LP and trigger the micturition reflex (Burnstock, 2014). Factors other than ATP may be more important for initiation of voiding at the end of bladder filling. Moreover, accumulated ADO in the LP at end of filling might be necessary for optimal bladder excitability and can prevent overactivation of afferent neurons and other neighboring types of cells by ATP, including detrusor smooth muscle cells.

Several mechanisms could underlie increased degradation of purines in preparations that were distended by filling with physiological solution. One possibility is that biaxial stretch of the urothelium during bladder filling is accompanied by increase of surface area, which results in better access of substrate to membrane-bound enzymes. Another possibility is that stretch of cells in the urothelium transduce the mechanical signal into a cascade of biochemical signals resulting in actin cytoskeleton rearrangement, which in turn alters cell shape and plasma membrane assembling (Kessels and Qualmann, 2021). Although future studies are warranted to define such mechanisms, they could not explain straightforwardly the substrate specificity we observed. A third possibility is that increased degradation of purines during stretch is due to additional involvement of soluble enzymes that are released from the anti-luminal surface of the urothelium into the LP. Indeed, we found that eATP and eADP were hydrolyzed to their products when added to solutions that were previously in contact with the LP of denuded bladders. Once again, the degradation of purine substrates in ELS from distended preparations exceeded the degradation of purines in ELS from nondistended preparations. We concluded, therefore, that spontaneous and distention-induced release of nucleotidases occur in the LP. Such soluble nucleotidases, in addition to membrane-bound enzymes, likely control the ultimate availability of bioactive purine mediators in the vicinity of specific purinergic receptors in the LP during bladder filling.

Four major enzyme families are involved in extracellular purine metabolism: 1) the ENTPD family (EC 3.6.1.5), 2) the ENPP family (EC 3.6.1.9; EC 3.1.4.1), 3) Ecto-5-nucleotidase NT5E/CD73 (EC 3.1.3.5), and 4) Alkaline phosphatases (EC 3.1.3.1). (Zimmermann et al., 2012; Yegutkin, 2014). ENTPD1,2,3, and 8 are cell surface-located enzymes that hydrolase preferentially extracellular ATP and ADP whereas ENTPD4–7 are localized in intracellular organelles and have low affinity for ATP (Zimmermann et al., 2012). Of the ENPP family, ENPP1 displays highly efficient ATP hydrolysis to generate AMP and inorganic pyrophosphate PPi. ENPP3 also hydrolases ATP, but to a lesser degree than ENPP1. ENPP4 has been shown to degrade ATP *in vitro*, but the ATP hydrolysis rate by ENPP4 is negligible compared to that of ENPP1 (Borza et al., 2021). Purine nucleotides are not preferred substrates for ENPP2,5,6, and 7 as these enzymes have evolved as phospholipases with phosphodiesterase activities (Borza et al., 2021). Mammalian alkaline phosphatases (ALPLs) are expressed ubiquitously in multiple tissues, display broad substrate specificity and can hydrolyze ATP, ADP, AMP, and PPi among other substrates (Zimmermann, 2006). In fact, ALPLs are the only ecto-nucleotidases that can sequentially dephosphorylate nucleoside triphosphates to the nucleoside. Three isozymes are tissue specific with highly restricted expression to the placenta, germ cells, and intestines, while the fourth isozyme, tissue non-specific alkaline phosphatase (TNAP) is present in numerous tissues, including the kidney, liver, bones, and the central nervous system (Sebastián-Serrano et al., 2014). It is presently unknown whether TNAP plays a role in establishing the ATP/ADO ratio in the bladder wall. NT5E/CD73 is another integral component of the purinergic system. NT5E/CD73 is a ubiquitously expressed glycosylphosphatidylinositol-anchored glycoprotein (GPI-AP) that catalyzes the last step in the extracellular metabolism of ATP

to form ADO. Members of the ENTPD and ENPP families generate AMP from ATP and ADP. Subsequent hydrolysis of AMP to ADO is primarily, but not exclusively, carried out by NT5E/CD73 (Alcedo et al., 2021). In summary, current knowledge about membrane-bound nucleotidases suggests that ENTPD1,2,3, and 8, ENPP1 and 3, NT5E/CD73, and ALPL/TNAP are of most significance to the extracellular hydrolysis of ATP and ADP.

The information about distribution, localization and function of nucleotidases in the non-disease bladder is rather limited. Immunohistochemistry studies of the mouse urinary bladder (Yu et al., 2011; Babou Kammoe et al., 2021) reported that ENTPD1 was expressed primarily on the surface of detrusor smooth muscle cells and in the LP, ENTPD2 was localized between smooth muscle bundles and in the LP, ENTPD3 and 8 were localized in the urothelium and were not resolved in the detrusor layer. NT5E was found localized in detrusor (Yu et al., 2011; Babou Kammoe et al., 2021) and to a lesser degree in the LP (Babou Kammoe et al., 2021). In another immunohistochemistry study, ENTPD3 and ALPL appeared to be localized on basal and intermediate cells of the urothelium but not on umbrella cells (Yu, 2015), suggesting asymmetrical distribution of nucleotidases through layers of the bladder mucosa. The impact of these enzymes on bladder excitability could be profound as they have the potential to inactivate agonists of P2X and P2Y purinergic receptors and to produce ADO as an agonist of the four ADO receptors. In addition, production of the nucleoside ADO secures purine salvage through cellular reuptake of the nucleoside *via* equilibrative nucleoside transporters and re-phosphorylation to AMP inside the cell.

Members of the nucleotidase families demonstrate relative substrate specificity for adenine purines. ENTPD1, 3, and 8 hydrolyze both ATP and ADP; however, the hydrolysis of ATP is more rapid than the hydrolysis of ADP. ENTPD1 hydrolyzes ATP directly to AMP with minimal formation of ADP as an intermediate product (Kukulski et al., 2005; Knowles, 2011). The appearance of ADP could be demonstrated upon hydrolysis of ATP by ENTPD3 and 8 (Kukulski et al., 2005). ENTPD2 hydrolyses primarily ATP to ADP, but it does not hydrolyze ADP causing considerable accumulation of ADP before it is further hydrolyzed to AMP (Zimmermann et al., 2012). ENPP1 preferentially hydrolyses ATP, but it also hydrolyses other nucleotides including ADP (Kumar and Lowery, 2021). As aforementioned, NT5E is the main enzyme that converts AMP into ADO. Importantly, ATP and ADP are competitive inhibitors of mammalian NT5E with Ki values in the low micromolar range (Sträter, 2006). As a result, when cells release ATP or ADP, NT5E is inhibited until ATP and ADP are mostly metabolized to AMP (Zimmermann et al., 2012). This "feed-forward" inhibition could explain the delayed formation of eADO from eATP or eADP in the present study. Likewise, accumulation of ATP and ADP in the presence of ENTPD inhibitors would diminish the ADO production due to inhibited breakdown of AMP by NT5E. Since TNAP can metabolize ATP all the way to ADO, this enzyme may provide an alternative pathway for ADO production, if present.

While membrane-bound forms of nucleotidases have been studied extensively, soluble forms of nucleotidases have received rather little attention. Some amounts of ENTPDs, ENPPs, CD73, and alkaline phosphatase appear to constitutively circulate in human bloodstream and their levels increase in disease states such as inflammation and cancer (Yegutkin et al., 2007; Zimmermann et al., 2012; Borza et al., 2021). Neuronal release of nucleotidases has been suggested as a mechanism for neurotransmitter inactivation (Todorov et al., 1997). In any event, soluble forms considerably broaden the reach of the enzymes by diffusion within a tissue or by their distribution within tissue fluids. To the best of our knowledge, no data are yet available on regulation of bladder excitability by enzymes that are released from the urothelium in the course of bladder filling. One hour after initiation of reaction in large-volume ELS (i.e., 2.5-ml) removed from the tissue bath, eATP was diminished by 20 and 40% in nondistended and distended preparations, respectively, suggesting that eATP-degrading enzymes were released in a stretch dependent manner. Under the same experimental conditions, only 10%–15% of eADP was degraded by released enzymes. The action of released enzymes was significantly underestimated in these studies, because the reactions were carried out in a 500-fold higher volume than the volume of LP which is about 50 μm thick in the mouse bladder (Winder et al., 2014). In 12.5-fold concentrated ELS, eATP was reduced by ~50 and ~80% in nondistended and distended preparations, respectively. The eADP substrate decreased by ~10 and ~30% in cELS from nondistended and distended bladders, respectively. Clearly, distention of the urothelium and suburothelium/LP is associated with greater catabolism of ATP and ADP by soluble nucleotidases that are released in the LP during bladder filling.

All plasma membrane nucleotidases require millimolar concentrations of divalent cations Mg^{2+} and Ca^{2+} for maximal activity (Kukulski et al., 2005; Zimmermann et al., 2012). As part of the general characterization of released enzymes, we evaluated the relative importance of the two cations for the activity of released enzymes. According to MAXCHELATOR [WEBMAXC EXTENDED (ucdavis.edu)] (Bers et al., 2010), 5 mM EGTA chelates ~99.99% of Ca^{2+} and only ~8% of Mg^{2+} in regular KBS (pH 7.4, 37°C) whereas in the absence of Ca^{2+}, ~12% of Mg^{2+} is chelated by 5 mM EGTA. In contrast, 5 mM EDTA chelates ~99.99% of both cations under the same conditions. We took advantage of the different chelating properties of EGTA and EDTA and measured the degradation of eATP and eADP in solutions that contained released enzymes but lacked Ca^{2+} and/or Mg^{2+} with or without addition of EGTA or EDTA. As anticipated, removal of both Ca^{2+} and Mg^{2+} abolished the hydrolysis of eATP and eADP, indicating that Ca^{2+} and Mg^{2+} are crucial for optimal activities of soluble "ATPases" and "ADPases" in the LP. The presence of Ca^{2+} alone or Mg^{2+} alone appeared to be sufficient for the ability of soluble "ATPases" to hydrolyze ATP. Surprisingly, the hydrolysis of eATP was enhanced in the presence of Mg^{2+} and absence of Ca^{2+}. It is possible that Ca^{2+} and Mg^{2+} "compete" for maintaining optimal activity of soluble enzymes so that when Ca^{2+} is removed, Mg^{2+} takes over the maintenance unrestrained. The formation of eADP from eATP followed the relationships described for the eATP decrease: no change in the absence of Mg^{2+} alone, enhanced formation of eADP in the absence of Ca^{2+} plus EGTA, and abolished eADP formation when both Ca^{2+} and

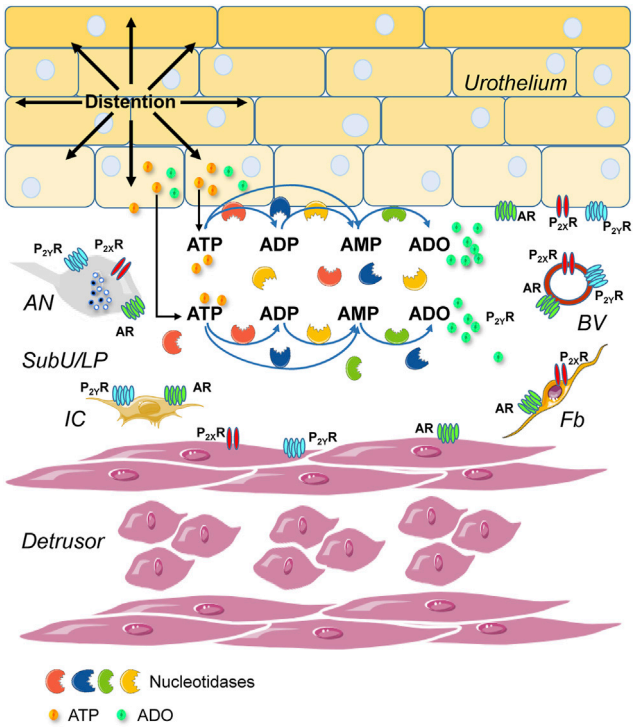

FIGURE 12 | A model depicting mechanisms of purinergic signaling in the lamina propria during bladder filling. Stretch of the bladder wall during filling causes release of ATP from the urothelium into the suburothelium (Birder and Andersson, 2013; Burnstock, 2014; Dalghi et al., 2020). ATP activates P2X (e.g., P2X2/X3) receptors (P2XR) on afferent nerve terminals in urothelium and suburothelium/lamina propria (SubU/LP) and triggers a voiding reflex (Cockayne et al., 2000; Vlaskovska et al., 2001). ATP that is released in the LP is hydrolyzed to ADP, AMP, and adenosine (ADO) by four families of membrane-bound nucleotidases (Zimmermann et al., 2012). Bladder excitability during filling is regulated by excitatory (ATP and ADP) and inhibitory (ADO) purine mediators in the LP that activate specific purinergic receptors. ATP activates ligand-gated P2XR and G protein-coupled P2Y receptors (P2YR), ADP activates P2YR, and ADO activates G-protein coupled adenosine receptors (AR) (Burnstock, 2014). P2XR, P2YR, and AR are ubiquitously expressed in the bladder wall, including in cells in the detrusor, the urothelium, and the LP (Dalghi et al., 2020). Cell types that express purinergic receptors in the LP include afferent neurons (AN), interstitial cells (IC), fibroblasts (Fb), and blood vessels (BV). Nucleotidases have the ability to terminate P2XR or P2YR responses initiated by ATP and to favor the activation of AR or ADP-responding receptors. In addition to the membrane-bound nucleotidases, enzymes that metabolize ATP are released in the LP spontaneously and during distention of the bladder wall during bladder filling. Released enzymes degrade ATP to ADP, AMP, and ADO. The activity of released enzymes is greater in distended LP than in nondistended LP indicating mechanosensitive release of enzymes. Soluble nucleotidases in the LP identify with several membrane-bound nucleotidases and are possibly released in the LP by distention-induced ectodomain shedding (Lichtenthaler et al., 2018). Distention-dependent degradation of ATP by membrane-bound and soluble nucleotidases diminishes the presence of ATP in the LP at the end of bladder filling (Durnin et al., 2019b) to prevent abnormal excitability of the bladder. The proper availability of excitatory and inhibitory purines in the bladder wall is determined by distention-associated purine release and purine metabolism.

Mg^{2+} were absent. Despite increased formation of eADP in the absence of Ca^{2+}, neither the formation of eAMP nor of eADO were significantly enhanced. In fact, the hydrolysis of eADP was modestly inhibited in the absence of Mg^{2+} and significantly inhibited in the absence of Ca^{2+}, suggesting that soluble ADPase(s) requires Ca^{2+} more than Mg^{2+} for its activity. This is in contrast with what we observed with the eATP hydrolysis. Altogether, the present study establishes that Ca^{2+} and Mg^{2+} are essential for the activities of soluble nucleotidases that are released in the LP during bladder filling. However, releasable enzymes that degrade sequentially ATP to ADO appear to depend unequally on extracellular Ca^{2+} and Mg^{2+}: thus, Mg^{2+} might compete with Ca^{2+} for ensuring optimal activity of enzymes that convert ATP to ADP, whereas Ca^{2+} may be more important for the activity of nucleotidases that catabolize ADP to AMP and then to ADO.

We next examined how activities of soluble enzymes in the LP are affected by commonly-used inhibitors of membrane-bound nucleotidases. In cELS collected from nondistended or distended preparations, ARL67156 modestly diminished the decrease of eATP, significantly reduced the increase of eAMP and eADO, but did not affect the intermediate product eADP, suggesting different sensitivity of soluble nucleotidases to ARL67156. A study using recombinant mouse nucleotidases has demonstrated that ARL67156 is a weak competitive inhibitor of ENTPD1, ENTPD3, and ENPP1, and is not an effective inhibitor of ENTPD2 and ENPP3, and inhibits the mouse ENTPD8 (Levesque et al., 2007). POM-1 was proposed as a potent inhibitor of membrane-bound ENTPD1–3 (Muller et al., 2006). In the present study, POM-1 was a more potent inhibitor of the degradation of eATP than ARL67156 and significantly reduced the formation of all three products. The discrepancy in the effects of POM-1 and ARL67156 on eATP hydrolysis was likely due to different efficacy toward the activity of ENTPD2. POM-1 inhibits ENTPD2 (Muller et al., 2006) whereas ARL67156 does not (Levesque et al., 2007). ENTPD2 hydrolyses ATP to ADP with minimal AMP accumulation (Zimmermann et al., 2012). The effects of ARL67156 in the present study suggest that soluble enzymes similar to ENTPD1 and 3, and ENPP1 might be released in the LP whereas the effects of POM-1 suggest that an ENTPD2-like enzyme could also be released in LP during bladder filling. While a number of non-selective ENTPD inhibitors have been developed, potent subtype-specific inhibitors are scarce. PSB06126 is an ENTPD3 inhibitor of the rat isoform of the enzyme and appears to display selectivity over ENTPD1 and 2 (Baqi et al., 2009). It may have similar efficiency profile in the mouse since mouse and rat ENTPD3 share 96% homology (UniProt). In ELS collected from distended preparations, PSB06126 diminished the eATP decrease and the eADP increase and had no effect on eAMP and eADO increase. The ENPP1 Inhibitor C (Kawaguchi et al., 2019) diminished the decrease of eATP but did not affect the formation of eADP since ENPP1 hydrolyses eATP to eAMP directly. Consequently, the formation of eAMP was diminished by ENPP1 inhibitor C. Neither PSB06126 nor ENPP1 Inhibitor C had an effect on the degradation of eATP in nondistended preparations. The TNAP inhibitor L-p-BT (Jackson et al., 2020a) had no effect on eATP decrease or product increase in nondistended or distended preparations. Together, these results suggest that no spontaneous release of ENTPD3, ENPP1, and TNAP occurred in the LP whereas distention of the LP during bladder filling likely

released ENTPD3-and ENPP1-like enzymes, but not TNAP. The relative potency order of nucleotidase inhibitors for distention-released soluble nucleotidases in LP was POM-1 > ARL67156 > PSB06126 = ENPP1 inhibitor C. The pharmacological characterization suggests a release of cocktail of nucleotidases in the LP during bladder filling that likely include ENTPD1–3, ENPP1 and ENPP3, and possibly ENTPD8. However, no indication of the presence of TNAP was obtained with the use of a pharmacological inhibitor.

Poor specificity of enzyme inhibitors poses serious limitations for determining the identity of released enzymes by pharmacological characterization. Therefore, we next sought to determine whether the enzymes suggested by pharmacology studies are indeed present in cELS from distended bladder preparations. Using a highly-sensitive methodology for protein detection was crucial for these experiments given the high dilution of released enzymes in the EL samples. Therefore, we used a capillary western blot method that has the advantage of being a more sensitive and automated approach for protein detection while providing comparable results to traditional western blotting (Chen et al., 2013; Lu et al., 2018). Multiple nucleotidases were found present in urothelium homogenate and in cELS. Of particular interest is the observation that the relative expression of enzymes released in cELS was different from the relative expression of nucleotidases in the mouse urothelium, suggesting that a regulated release of enzymes likely occurs in the LP during bladder filling. Thus, the relative distribution of nucleotidases in urothelium was ENTPD1>>ENPP1>ENTPD2 = ENTPD3 > ENPP3 = NT5E >> ENTPD8 = TNAP and ENTPD1>>ENTPD3>>ENPP3> ENPP1 = ENTPD2 = NT5E >> ENTPD8 = TNAP in cELS. The findings that several enzymes with nucleotidase activities were present in cELS are in accordance with the results from substrate degradation and pharmacological characterization of soluble enzymes in cELS. An intriguing observation was that enzymes that have transmembrane domains in their molecular structure were found released in the solutions bathing the LP. A possible mechanism underlying such release could be through proteolytic removal of membrane protein ectodomains (aka ectodomain shedding) that is a post-translational modification regulating functions of hundreds of membrane proteins (Lichtenthaler et al., 2018). The cleavage reactions are catalyzed by a broad range of proteases, including intramembrane and soluble proteases that can cleave single-pass transmembrane proteins, dual-pass and polytopic membrane proteins or proteins that are attached to the external leaflet of the plasma membrane by a GPI anchor (Lichtenthaler et al., 2018). As discussed, soluble forms of nucleotidases have been reported (Jiang et al., 2014). For example, NT5E and TNAP are GPI-anchored proteins that can be released by endogenous phospholipase C cleavage of GPI, *via* microvesicles or *via* exosomes from cancer cells (Zimmermann et al., 2012). ENPP1 is a single-pass transmembrane enzyme (Borza et al., 2021) whereas ENTPD1,2,3, and 8 have two transmembrane domains close to their N- and C-termini and a large extracellular loop that contains the catalytic domain (Zimmermann et al., 2012). ENTPD1 is preferentially targeted to caveolae, membrane microdomains with specialized structure and function (Kittel et al., 1999; Koziak et al., 2000). There is evidence that catalytically active ENTPD1 can be shed in membrane-bound form from plasma membranes of ENTPD1-expressing cells (Yegutkin et al., 2000; Ceruti et al., 2011) or to be incorporated in membrane particles that are released in the extracellular space (Barat et al., 2007). Shedding of undefined ATP-degrading enzymes has been observed from endothelial cells in response to shear stress and from cultured astrocytes following O_2-glucose deprivation (Yegutkin et al., 2000; Ceruti et al., 2011). Studies have suggested that mechanical stretch could enhance the expression of enzymes involved in steroid biosynthesis (Feng et al., 2019). To the best of our knowledge, however, release of membrane-bound enzymes in response to stretch has not been reported previously. In all membrane-bound nucleotidases, the transmembrane and intracellular domains comprise approximately 10%–13% of the molecule (UniProt), suggesting that no significant differences in the mass of membrane-bound and cleaved enzymes would be detected with western immunoblot methodologies. This might explain the similar masses (molecular weights) of enzymes that are present in urothelial tissue homogenates and in cELS. Studies have suggested that lack of transmembrane domains of nucleotidases may result in reduced catalytic activity (Wang et al., 1998; Grinthal and Guidotti, 2002). Soluble forms of human ENTPDs engineered to comprise of only the extracellular domains demonstrated markedly diminished nucleotide-hydrolyzing capabilities in comparison with native membrane-embedded ENTPDases containing two transmembrane domains (Knowles, 2011). It is currently unknown whether this is true for the enzymes released in the LP during bladder filling. As demonstrated, however, the degradation of eATP by such enzymes was distinct.

There are two important implications of the present study: 1) multiple enzymes that coexist on the cell surface or are released during bladder filling determine the effective concentrations of biologically active mediators in the LP and the degree of activation of purinergic receptors in various types of cells in the bladder wall, and 2) in studies of purinergic signaling, it is important to investigate simultaneously the availability of extracellular ATP and its metabolites.

In summary (**Figure 12**), here we report that several soluble nucleotidases are released in the LP during bladder filling causing enhanced hydrolysis of ATP and ADP at the end of filling. These findings corroborate the hypothesis that distention induced-release of soluble nucleotidases attenuates the excitatory effects of ATP and ADP on cells in the LP and in detrusor and suggest the prospect that inhibition of purine nucleotide degradation could aggravate bladder excitability by accumulation of excitatory urothelial mediators in the bladder wall.

At present, we do not know the mechanisms underlying the distention-induced enzyme release in the LP. The mechanisms of coordination of multiple enzyme activities in regulation of bladder excitability also remain to be unraveled. Future studies aimed at understanding the complexity of purinergic regulation and functions in the bladder will help to guide translational and clinical efforts for bladder motility disorders, inflammation, cancer, and other human diseases.

DATA AVAILABILITY STATEMENT

The raw data supporting the conclusion of this article will be made available by the authors, without undue reservation.

ETHICS STATEMENT

The animal study was reviewed and approved by Institutional Animal Care and Use Committee, IACUC, University of Nevada Reno, Protocol #20-09-1077-1, Approved (Effective Period 10/20/21-10/19/2024).

AUTHOR CONTRIBUTIONS

VM-Y conception and design of research; MAB, AGC, JD, BP, and VM-Y performed research; MAB, JD, AGC, BP, and VM-Y analyzed data; MA, JD, AG, BP, and VM-Y interpreted data; VM-Y and BP prepared figures; VM-Y wrote the manuscript; all authors edited manuscript and approved final version of manuscript.

FUNDING

This research is funded by a R01 grant DK119482 from the National Institute of Diabetes and Digestive and Kidney Diseases awarded to the Principal Investigator VM-Y (corresponding author).

ACKNOWLEDGMENTS

We are thankful for the excellent technical assistance of Benjamin Kwok, Priya Kukadia, James Parke, and Dominika Judenite.

REFERENCES

Abbracchio, M. P., Burnstock, G., Boeynaems, J.-M., Barnard, E. A., Boyer, J. L., Kennedy, C., et al. (2006). International Union of Pharmacology LVIII: Update on the P2Y G Protein-Coupled Nucleotide Receptors: from Molecular Mechanisms and Pathophysiology to Therapy. *Pharmacol. Rev.* 58 (3), 281–341. doi:10.1124/pr.58.3.3

Alcedo, K. P., Bowser, J. L., and Snider, N. T. (2021). The Elegant Complexity of Mammalian Ecto-5'-Nucleotidase (CD73). *Trends Cell Biol.* 31 (10), 829–842. doi:10.1016/j.tcb.2021.05.008

Andersson, K.-E., Fry, C., Panicker, J., and Rademakers, K. (2018). Which Molecular Targets Do We Need to Focus on to Improve Lower Urinary Tract Dysfunction? ICI-RS 2017. *Neurourol. Urodynamics* 37 (S4), S117–S126. doi:10.1002/nau.23516

Babou Kammoe, R. B., Kauffenstein, G., Pelletier, J., Robaye, B., and Sévigny, J. (2021). NTPDase1 Modulates Smooth Muscle Contraction in Mice Bladder by Regulating Nucleotide Receptor Activation Distinctly in Male and Female. *Biomolecules* 11 (2), 147. doi:10.3390/biom11020147

Baqi, Y., Weyler, S., Iqbal, J., Zimmermann, H., and Müller, C. E. (2009). Structure-activity Relationships of Anthraquinone Derivatives Derived from Bromaminic Acid as Inhibitors of Ectonucleoside Triphosphate Diphosphohydrolases (E-NTPDases). *Purinergic Signal.* 5 (1), 91–106. doi:10.1007/s11302-008-9103-5

Barat, C., Martin, G., Beaudoin, A. R., Sévigny, J., and Tremblay, M. J. (2007). The Nucleoside Triphosphate diphosphohydrolase-1/CD39 Is Incorporated into Human Immunodeficiency Type 1 Particles, where it Remains Biologically Active. *J. Mol. Biol.* 371 (1), 269–282. doi:10.1016/j.jmb.2007.05.012

Beckel, J. M., Daugherty, S. L., Tyagi, P., Wolf-Johnston, A. S., Birder, L. A., Mitchell, C. H., et al. (2015). Pannexin 1 Channels Mediate the Release of ATP into the Lumen of the Rat Urinary Bladder. *J. Physiol.* 593 (8), 1857–1871. doi:10.1113/jphysiol.2014.283119

Bers, D. M., Patton, C. W., and Nuccitelli, R. (2010). A Practical Guide to the Preparation of Ca^{2+} Buffers. *Methods Cell Biol.* 99, 1–26. doi:10.1016/b978-0-12-374841-6.00001-3

Bhetwal, B. P., An, C. L., Fisher, S. A., and Perrino, B. A. (2011). Regulation of Basal LC20 Phosphorylation by MYPT1 and CPI-17 in Murine Gastric Antrum, Gastric Fundus, and Proximal Colon Smooth Muscles. *Neurogastroenterol. Motil.* 23 (10), e425–e436. doi:10.1111/j.1365-2982.2011.01769.x

Birder, L., and Andersson, K.-E. (2013). Urothelial Signaling. *Physiol. Rev.* 93 (2), 653–680. doi:10.1152/physrev.00030.2012

Bobalova, J., Bobal, P., and Mutafova-Yambolieva, V. N. (2002). High-Performance Liquid Chromatographic Technique for Detection of a Fluorescent Analogue of ADP-Ribose in Isolated Blood Vessel Preparations. *Anal. Biochem.* 305 (2), 269–276. doi:10.1006/abio.2002.5667

Borza, R., Salgado-Polo, F., Moolenaar, W. H., and Perrakis, A. (2022). Structure and Function of the Ecto-Nucleotide Pyrophosphatase/phosphodiesterase (ENPP) Family: Tidying up Diversity. *J. Biol. Chem.* 298 (2), 101526. doi:10.1016/j.jbc.2021.101526

Burnstock, G. (2014). Purinergic Signalling in the Urinary Tract in Health and Disease. *Purinergic Signal.* 10 (1), 103–155. doi:10.1007/s11302-013-9395-y

Ceruti, S., Colombo, L., Magni, G., Viganò, F., Boccazzi, M., Deli, M. A., et al. (2011). Oxygen-Glucose Deprivation Increases the Enzymatic Activity and the Microvesicle-Mediated Release of Ectonucleotidases in the Cells Composing the Blood-Brain Barrier. *Neurochem. Int.* 59 (2), 259–271. doi:10.1016/j.neuint.2011.05.013

Chen, J.-Q., Heldeman, M. R., Herrmann, M. A., Kedei, N., Woo, W., Blumberg, P. M., et al. (2013). Absolute Quantitation of Endogenous Proteins With Precision And Accuracy Using a Capillary Western System. *Anal. Biochem.* 442 (1), 97–103. doi:10.1-16/j.ab.2013.07.022

Chen, H., Zhang, L., Hill, W. G., and Yu, W. (2017). Evaluating the Voiding Spot Assay in Mice: a Simple Method with Complex Environmental Interactions. *Am. J. Physiology-Renal Physiology* 313 (6), F1274–f1280. doi:10.1152/ajprenal.00318.2017

Cockayne, D. A., Hamilton, S. G., Zhu, Q.-M., Dunn, P. M., Zhong, Y., Novakovic, S., et al. (2000). Urinary Bladder Hyporeflexia and Reduced Pain-Related Behaviour in P2X3-Deficient Mice. *Nature* 407 (6807), 1011–1015. doi:10.1038/35039519

Crack, B. E., Pollard, C. E., Beukers, M. W., Roberts, S. M., Hunt, S. F., Ingall, A. H., et al. (1995). Pharmacological and Biochemical Analysis of FPL 67156, a Novel, Selective Inhibitor of Ecto-ATPase. *Br. J. Pharmacol.* 114 (2), 475–481. doi:10.1111/j.1476-5381.1995.tb13251.x

Dalghi, M. G., Montalbetti, N., Carattino, M. D., and Apodaca, G. (2020). The Urothelium: Life in a Liquid Environment. *Physiol. Rev.* 100 (4), 1621–1705. doi:10.1152/physrev.00041.2019

Dunton, C. L., Purves, J. T., Hughes, F. M., Jr., Jin, H., and Nagatomi, J. (2018). Elevated Hydrostatic Pressure Stimulates ATP Release Which Mediates Activation of the NLRP3 Inflammasome via P2X4 in Rat Urothelial Cells. *Int. Urol. Nephrol.* 50 (9), 1607–1617. doi:10.1007/s11255-018-1948-0

Durnin, L., Corrigan, R. D., Sanders, K. M., and Mutafova-Yambolieva, V. N. (2019a). A Decentralized (*Ex Vivo*) Murine Bladder Model with the Detrusor Muscle Removed for Direct Access to the Suburothelium during Bladder Filling. *J. Vis. Exp.* 153. doi:10.3791/60344

Durnin, L., Kwok, B., Kukadia, P., McAvera, R., Corrigan, R. D., Ward, S. M., et al. (2019b). An *Ex Vivo* Bladder Model with Detrusor Smooth Muscle Removed to Analyse Biologically Active Mediators Released from the Suburothelium. *J. Physiol.* 597 (6), 1467–1485. doi:10.1113/jp276924

Durnin, L., Hayoz, S., Corrigan, R. D., Yanez, A., Koh, S. D., and Mutafova-Yambolieva, V. N. (2016). Urothelial Purine Release during Filling of Murine and Primate Bladders. *Am. J. Physiology-Renal Physiology* 311 (4), F708–F716. doi:10.1152/ajprenal.00387.2016

Durnin, L., Hwang, S. J., Ward, S. M., Sanders, K. M., and Mutafova-Yambolieva, V. N. (2012). Adenosine 5′-Diphosphate-Ribose Is a Neural Regulator in Primate and Murine Large Intestine along with β-NAD^+. *J. Physiol.* 590 (8), 1921–1941. doi:10.1113/jphysiol.2011.222414

Feng, Y., Wu, J., Cheng, Z., Zhang, J., Lu, J., and Shi, R. (2019). Mechanical Stretch Enhances Sex Steroidogenesis in C_2C_{12} Skeletal Muscle Cells. *Steroids* 150, 108434. doi:10.1016/j.steroids.2019.108434

Ferguson, D. R., Kennedy, I., and Burton, T. J. (1997). ATP Is Released from Rabbit Urinary Bladder Epithelial Cells by Hydrostatic Pressure Changes-Aa Possible Sensory Mechanism? *J. Physiol.* 505 (Pt 2) (Pt 2), 503–511. doi:10.1111/j.1469-7793.1997.503bb.x

Fredholm, B. B., Arslan, G., Halldner, L., Kull, B., Schulte, G., and Wasserman, W. (2000). Structure and Function of Adenosine Receptors and Their Genes. *Naunyn Schmiedeb. Arch. Pharmacol.* 362 (4-5), 364–374. doi:10.1007/s002100000313

Grinthal, A., and Guidotti, G. (2002). Transmembrane Domains Confer Different Substrate Specificities and Adenosine Diphosphate Hydrolysis Mechanisms on CD39, CD39L1, and Chimeras. *Biochemistry* 41 (6), 1947–1956. doi:10.1021/bi015563h

Jackson, E. K., Cheng, D., Ritov, V. B., and Mi, Z. (2020a). Alkaline Phosphatase Activity Is a Key Determinant of Vascular Responsiveness to Norepinephrine. *Hypertension* 76 (4), 1308–1318. doi:10.1161/hypertensionaha.120.15822

Jackson, E. K., Gillespie, D. G., Cheng, D., Mi, Z., and Menshikova, E. V. (2020b). Characterization of the N^6-Etheno-Bridge Method to Assess Extracellular Metabolism of Adenine Nucleotides: Detection of a Possible Role for Purine Nucleoside Phosphorylase in Adenosine Metabolism. *Purinergic Signal.* 16 (2), 187–211. doi:10.1007/s11302-020-09699-x

Jiang, Z. G., Wu, Y., Csizmadia, E., Feldbrügge, L., Enjyoji, K., Tigges, J., et al. (2014). Characterization of Circulating Microparticle-Associated CD39 Family Ecto-Nucleotidases in Human Plasma. *Purinergic Signal.* 10 (4), 611–618. doi:10.1007/s11302-014-9423-6

Kawaguchi, M., Han, X., Hisada, T., Nishikawa, S., Kano, K., Ieda, N., et al. (2019). Development of an ENPP1 Fluorescence Probe for Inhibitor Screening, Cellular Imaging, and Prognostic Assessment of Malignant Breast Cancer. *J. Med. Chem.* 62 (20), 9254–9269. doi:10.1021/acs.jmedchem.9b01213

Kessels, M. M., and Qualmann, B. (2021). Interplay between Membrane Curvature and the Actin Cytoskeleton. *Curr. Opin. Cell Biol.* 68, 10–19. doi:10.1016/j.ceb.2020.08.008

Kitta, T., Chancellor, M. B., de Groat, W. C., Kuno, S., Nonomura, K., and Yoshimura, N. (2014). Roles of Adenosine A1 and A2A Receptors in the Control of Micturition in Rats. *Neurourol. Urodynam.* 33 (8), 1259–1265. doi:10.1002/nau.22487

Kittel, A., Kaczmarek, E., Sevigny, J., Lengyel, K., Csizmadia, E., and Robson, S. C. (1999). CD39 as a Caveolar-Associated Ectonucleotidase. *Biochem. Biophysical Res. Commun.* 262 (3), 596–599. doi:10.1006/bbrc.1999.1254

Knowles, A. F. (2011). The GDA1_CD39 Superfamily: NTPDases with Diverse Functions. *Purinergic Signal.* 7 (1), 21–45. doi:10.1007/s11302-010-9214-7

Koziak, K., Kaczmarek, E., Kittel, A., Sévigny, J., Blusztajn, J. K., Schulte am Esch, J., et al. (2000). Palmitoylation Targets CD39/endothelial ATP Diphosphohydrolase to Caveolae. *J. Biol. Chem.* 275 (3), 2057–2062. doi:10.1074/jbc.275.3.2057(

Kukulski, F., Lévesque, S. A., Lavoie, É. G., Lecka, J., Bigonnesse, F., Knowles, A. F., et al. (2005). Comparative Hydrolysis of P2 Receptor Agonists by NTPDases 1, 2, 3 and 8. *Purinergic Signal.* 1 (2), 193–204. doi:10.1007/s11302-005-6217-x

Kumar, M., and Lowery, R. G. (2021). Development of a High-Throughput Assay to Identify Inhibitors of ENPP1. *SLAS Discov.* 26 (5), 740–746. doi:10.1177/2472555220982321

Kumar, V., Chapple, C. R., Surprenant, A. M., and Chess-Williams, R. (2007). Enhanced Adenosine Triphosphate Release from the Urothelium of Patients with Painful Bladder Syndrome: a Possible Pathophysiological Explanation. *J. Urol.* 178 (4 Pt 1), 1533–1536. doi:10.1016/j.juro.2007.05.116

La Favor, J. D., and Burnett, A. L. (2016). A Microdialysis Method to Measure *In Vivo* Hydrogen Peroxide and Superoxide in Various Rodent Tissues. *Methods* 109, 131–140. doi:10.1016/j.ymeth.2016.07.012

Lévesque, S. A., Lavoie, É. G., Lecka, J., Bigonnesse, F., and Sévigny, J. (2007). Specificity of the Ecto-ATPase Inhibitor ARL 67156 on Human and Mouse Ectonucleotidases. *Br. J. Pharmacol.* 152 (1), 141–150. doi:10.1038/sj.bjp.0707361

Levitt, B., Head, R. J., and Westfall, D. P. (1984). High-pressure Liquid Chromatographic-Fluorometric Detection of Adenosine and Adenine Nucleotides: Application to Endogenous Content and Electrically Induced Release of Adenyl Purines in guinea Pig Vas Deferens. *Anal. Biochem.* 137 (1), 93–100. doi:10.1016/0003-2697(84)90352-x

Lewis, S. A., and Lewis, J. R. (2006). Kinetics of Urothelial ATP Release. *Am. J. Physiology-Renal Physiology* 291 (2), F332–F340. doi:10.1152/ajprenal.00340.2005

Li, W., Sasse, K. C., Bayguinov, Y., Ward, S. M., and Perrino, B. A. (2018). Contractile Protein Expression and Phosphorylation and Contractility of Gastric Smooth Muscles from Obese Patients and Patients with Obesity and Diabetes. *J. Diabetes Res.* 2018, 8743874. doi:10.1155/2018/8743874

Lichtenthaler, S. F., Lemberg, M. K., and Fluhrer, R. (2018). Proteolytic Ectodomain Shedding of Membrane Proteins in Mammals-Hardware, Concepts, and Recent Developments. *Embo J.* 37 (15), e99456. doi:10.15252/embj.201899456

Lu, J., Allred, C. C., and Jensen, M. D (2018). Human Adipose Tissue Protein Analyses Using capillary Wetern Blot Technology. *Nutr. Dieabetes.* 8 (1), 26. doi:10.1038/s41387-018-003-4

Marshall, K. L., Saade, D., Ghitani, N., Coombs, A. M., Szczot, M., Keller, J., et al. (2020). PIEZO2 in Sensory Neurons and Urothelial Cells Coordinates Urination. *Nature* 588 (7837), 290–295. doi:10.1038/s41586-020-2830-7

Matsumoto-Miyai, K., Kagase, A., Yamada, E., Yoshizumi, M., Murakami, M., Ohba, T., et al. (2011). Store-operated Ca2+ Entry Suppresses Distention-Induced ATP Release from the Urothelium. *Am. J. Physiology-Renal Physiology* 300 (3), F716–F720. doi:10.1152/ajprenal.00512.2010

McLatchie, L. M., and Fry, C. H. (2015). ATP Release from Freshly Isolated guinea-pig Bladder Urothelial Cells: a Quantification and Study of the Mechanisms Involved. *Bju. Int.* 115 (6), 987–993. doi:10.1111/bju.12954

Merrill, L., Gonzalez, E. J., Girard, B. M., and Vizzard, M. A. (2016). Receptors, Channels, and Signalling in the Urothelial Sensory System in the Bladder. *Nat. Rev. Urol.* 13 (4), 193–204. doi:10.1038/nrurol.2016.13

Müller, C. E., Iqbal, J., Baqi, Y., Zimmermann, H., Röllich, A., and Stephan, H. (2006). Polyoxometalates-a New Class of Potent Ecto-Nucleoside Triphosphate Diphosphohydrolase (NTPDase) Inhibitors. *Bioorg. Med. Chem. Lett.* 16 (23), 5943–5947. doi:10.1016/j.bmcl.2006.09.003

Mutafova-Yambolieva, V. N., and Durnin, L. (2014). The Purinergic Neurotransmitter Revisited: A Single Substance or Multiple Players? *Pharmacol. Ther.* 144 (2), 162–191. doi:10.1016/j.pharmthera.2014.05.012

Radin, J. N., González-Rivera, C., Ivie, S. E., McClain, M. S., and Cover, T. L. (2011). *Helicobacter pylori* VacA Induces Programmed Necrosis in Gastric Epithelial Cells. *Infect. Immun.* 79 (7), 2535–2543. doi:10.1128/iai.01370-10

Sebastián-Serrano, Á., de Diego-García, L., Martínez-Frailes, C., Ávila, J., Zimmermann, H., Millán, J. L., et al. (2014). Tissue-nonspecific Alkaline Phosphatase Regulates Purinergic Transmission in the Central Nervous System during Development and Disease. *Comput. Struct. Biotechnol. J.* 13, 95–100. doi:10.1016/j.csbj.2014.12.004

Silva-Ramos, M., Silva, I., Oliveira, O., Ferreira, S., Reis, M. J., Oliveira, J. C., et al. (2013). Urinary ATP May Be a Dynamic Biomarker of Detrusor Overactivity in Women with Overactive Bladder Syndrome. *Plos. One* 8 (5), e64696. doi:10.1371/journal.pone.0064696

Sträter, N. (2006). Ecto-5'-Nucleotidase: Structure Function Relationships. *Purinergic Signal* 2 (2), 343–350. doi:10.1007/s11302-006-9000-8

Sun, Y., and Chai, T. C. (2006). Augmented Extracellular ATP Signaling in Bladder Urothelial Cells from Patients with Interstitial Cystitis. *Am. J. Physiology-Cell Physiology* 290 (1), C27–C34. doi:10.1152/ajpcell.00552.2004

Takezawa, K., Kondo, M., Kiuchi, H., Ueda, N., Soda, T., Fukuhara, S., et al. (2016a). Authentic Role of ATP Signaling in Micturition Reflex. *Sci. Rep.* 6, 19585. doi:10.1038/srep19585

Takezawa, K., Kondo, M., Nonomura, N., and Shimada, S. (2016b). Urothelial ATP Signaling: what Is its Role in Bladder Sensation? *Neurourol. Urodynam.* 36 (4), 966–972. doi:10.1002/nau.23099

Thompson, A. C., and Shippenberg, T. S. (2001). Microdialysis in Rodents. *Curr. Protoc. Neurosci.* doi:10.1002/0471142301.ns0702s00

Todorov, L. D., Mihaylova-Todorova, S., Westfall, T. D., Sneddon, P., Kennedy, C., Bjur, R. A., et al. (1997). Neuronal Release of Soluble Nucleotidases and Their Role in Neurotransmitter Inactivation. *Nature* 387 (6628), 76–79. doi:10.1038/387076a0

Vlaskovska, M., Kasakov, L., Rong, W., Bodin, P., Bardini, M., Cockayne, D. A., et al. (2001). P2X3Knock-Out Mice Reveal a Major Sensory Role for Urothelially Released ATP. *J. Neurosci.* 21 (15), 5670–5677. doi:10.1523/jneurosci.21-15-05670.2001

Wang, E. C. Y., Lee, J.-M., Ruiz, W. G., Balestreire, E. M., von Bodungen, M., Barrick, S., et al. (2005). ATP and Purinergic Receptor-dependent Membrane Traffic in Bladder Umbrella Cells. *J. Clin. Invest.* 115 (9), 2412–2422. doi:10.1172/jci24086

Wang, T.-F., Ou, Y., and Guidotti, G. (1998). The Transmembrane Domains of Ectoapyrase (CD39) Affect its Enzymatic Activity and Quaternary Structure. *J. Biol. Chem.* 273 (38), 24814–24821. doi:10.1074/jbc.273.38.24814

Winder, M., Tobin, G., Zupančič, D., and Romih, R. (2014). Signalling Molecules in the Urothelium. *Biomed. Res. Int.* 2014, 297295. doi:10.1155/2014/297295

Xie, Y., Han, K. H., Grainger, N., Li, W., Corrigan, R. D., and Perrino, B. A. (2018). A Role for Focal Adhesion Kinase in Facilitating the Contractile Responses of Murine Gastric Fundus Smooth Muscles. *J. Physiol.* 596 (11), 2131–2146. doi:10.1113/jp275406

Yegutkin, G., Bodin, P., and Burnstock, G. (2000). Effect of Shear Stress on the Release of Soluble Ecto-Enzymes ATPase and 5′-nucleotidase along with Endogenous ATP from Vascular Endothelial Cells. *Br. J. Pharmacol.* 129 (5), 921–926. doi:10.1038/sj.bjp.0703136

Yegutkin, G. G., Samburski, S. S., Mortensen, S. P., Jalkanen, S., and González-Alonso, J. (2007). Intravascular ADP and Soluble Nucleotidases Contribute to Acute Prothrombotic State during Vigorous Exercise in Humans. *J. Physiol.* 579 (Pt 2), 553–564. doi:10.1113/jphysiol.2006.119453

Yegutkin, G. G. (2014). Enzymes Involved in Metabolism of Extracellular Nucleotides and Nucleosides: Functional Implications and Measurement of Activities. *Crit. Rev. Biochem. Mol. Biol.* 49 (6), 473–497. doi:10.3109/10409238.2014.953627

Yu, W. (2015). Polarized ATP Distribution in Urothelial Mucosal and Serosal Space Is Differentially Regulated by Stretch and Ectonucleotidases. *Am. J. Physiology-Renal Physiology* 309 (10), F864–F872. doi:10.1152/ajprenal.00175.2015

Yu, W., Robson, S. C., and Hill, W. G. (2011). Expression and Distribution of Ectonucleotidases in Mouse Urinary Bladder. *Plos. One* 6 (4), e18704. doi:10.1371/journal.pone.0018704

Yu, W., Sun, X., Robson, S. C., and Hill, W. G. (2014). ADP-induced Bladder Contractility Is Mediated by P2Y 12 Receptor and Temporally Regulated by Ectonucleotidases and Adenosine Signaling. *FASEB J.* 28 (12), 5288–5298. doi:10.1096/fj.14-255885

Zimmermann, H. (2006). Ectonucleotidases in the Nervous System. *Novartis. Found. Symp.* 276, 113–128.

Zimmermann, H. (2021). History of Ectonucleotidases and Their Role in Purinergic Signaling. *Biochem. Pharmacol.* 187, 114322. doi:10.1016/j.bcp.2020.114322

Zimmermann, H., Zebisch, M., and Sträter, N. (2012). Cellular Function and Molecular Structure of Ecto-Nucleotidases. *Purinergic Signal.* 8 (3), 437–502. doi:10.1007/s11302-012-9309-4

Conflict of Interest: The authors declare that the research was conducted in the absence of any commercial or financial relationships that could be construed as a potential conflict of interest.

Publisher's Note: All claims expressed in this article are solely those of the authors and do not necessarily represent those of their affiliated organizations, or those of the publisher, the editors and the reviewers. Any product that may be evaluated in this article, or claim that may be made by its manufacturer, is not guaranteed or endorsed by the publisher.

frontiers | Frontiers in Genetics

ORIGINAL RESEARCH
published: 23 June 2022
doi: 10.3389/fgene.2022.896125

Expanding the *HPSE2* Genotypic Spectrum in Urofacial Syndrome, A Disease Featuring a Peripheral Neuropathy of the Urinary Bladder

Glenda M. Beaman[1,2†], Filipa M. Lopes[3†], Aybike Hofmann[4], Wolfgang Roesch[4], Martin Promm[4], Emilia K. Bijlsma[5], Chirag Patel[6], Aykut Akinci[7], Berk Burgu[7], Jeroen Knijnenburg[5], Gladys Ho[8,9], Christina Aufschlaeger[4], Sylvia Dathe[4,10], Marie Antoinette Voelckel[11], Monika Cohen[12], Wyatt W. Yue[13], Helen M. Stuart[1,2], Edward A. Mckenzie[14], Mark Elvin[15], Neil A. Roberts[3], Adrian S. Woolf[3 16†] and William G. Newman[1,2*†]*

[1]Manchester Centre for Genomic Medicine, Manchester University NHS Foundation Trust, Manchester, United Kingdom, [2]Division of Evolution, Infection, and Genomics, Faculty of Biology, Medicine, and Human Sciences, University of Manchester, Manchester, United Kingdom, [3]Division of Cell Matrix Biology and Regenerative Medicine, School of Biological Sciences, Faculty of Biology Medicine and Health, University of Manchester, Manchester, United Kingdom, [4]Department of Pediatric Urology, KUNO Clinic St. Hedwig Clinic, University Medical Center Regensburg, Regensburg, Germany, [5]Department of Clinical Genetics, Leiden University Medical Centre, Leiden, Netherlands, [6]Genetic Health Queensland, Royal Brisbane and Women's Hospital, Herston, QLD, Australia, [7]Department of Pediatric Urology, Ankara University School of Medicine, Cebeci Children's Hospital, Ankara, Turkey, [8]Sydney Genome Diagnostics, Children's Hospital at Westmead, Westmead, NSW, Australia, [9]Disciplines of Child and Adolescent Health and Genomic Medicine, University of Sydney, Sydney, NSW, Australia, [10]Städtisches Klinikum Dessau, Dessau-Roslau, Germany, [11]Department of Medical Genetics, Hospital La Timone, Marseille, France, [12]Center for Human Genetics and Laboratory Diagnostics (AHC) Medical Labs Martinsried, Martinsried, Germany, [13]Biosciences Institute, Medical School, Newcastle University, Newcastle, United Kingdom, [14]Protein Expression Facility, Manchester Institute of Biotechnology, University of Manchester, Manchester, United Kingdom, [15]Peak Proteins Ltd., Macclesfield, United Kingdom, [16]Royal Manchester Children's Hospital, Manchester University NHS Foundation Trust, Manchester Academic Health Science Centre, Manchester, United Kingdom

Urofacial (also called Ochoa) syndrome (UFS) is an autosomal recessive congenital disorder of the urinary bladder featuring voiding dysfunction and a grimace upon smiling. Biallelic variants in *HPSE2*, coding for the secreted protein heparanase-2, are described in around half of families genetically studied. *Hpse2* mutant mice have aberrant bladder nerves. We sought to expand the genotypic spectrum of UFS and make insights into its pathobiology. Sanger sequencing, next generation sequencing and microarray analysis were performed in four previously unreported families with urinary tract disease and grimacing. In one, the proband had kidney failure and was homozygous for the previously described pathogenic variant c.429T>A, p.(Tyr143*). Three other families each carried a different novel *HPSE2* variant. One had homozygous triplication of exons 8 and 9; another had homozygous deletion of exon 4; and another carried a novel c.419C>G variant encoding the missense p.Pro140Arg in *trans* with c.1099-1G>A, a previously reported pathogenic splice variant. Expressing the missense heparanase-2 variant *in vitro* showed that it was secreted as normal, suggesting that 140Arg has aberrant functionality after secretion. Bladder autonomic neurons emanate from pelvic ganglia where resident neural cell bodies derive from migrating neural crest cells. We demonstrated that, in normal human embryos, neuronal precursors near the developing hindgut and lower urinary tract

OPEN ACCESS

Edited by:
Tommaso Pippucci, Policlinico Sant'Orsola-Malpighi, Italy

Reviewed by:
Warren G. Hill, Beth Israel Deaconess Medical Center and Harvard Medical School, United States
Xiaoli Chen, Capital Institute of Pediatrics, China

***Correspondence:**
Adrian S. Woolf
adrian.woolf@manchester.ac.uk
William G. Newman
william.newman@manchester.ac.uk

†These authors have contributed equally to this work

Specialty section:
This article was submitted to Genetics of Common and Rare Diseases, a section of the journal Frontiers in Genetics

Received: *15 March 2022*
Accepted: *23 May 2022*
Published: *23 June 2022*

Citation:
Beaman GM, Lopes FM, Hofmann A, Roesch W, Promm M, Bijlsma EK, Patel C, Akinci A, Burgu B, Knijnenburg J, Ho G, Aufschlaeger C, Dathe S, Voelckel MA, Cohen M, Yue WW, Stuart HM, Mckenzie EA, Elvin M, Roberts NA, Woolf AS and Newman WG (2022) Expanding the HPSE2 Genotypic Spectrum in Urofacial Syndrome, A Disease Featuring a Peripheral Neuropathy of the Urinary Bladder. Front. Genet. 13:896125. doi: 10.3389/fgene.2022.896125

were positive for both heparanase-2 and leucine rich repeats and immunoglobulin like domains 2 (LRIG2). Indeed, biallelic variants of *LRIG2* have been implicated in rare UFS families. The study expands the genotypic spectrum in *HPSE2* in UFS and supports a developmental neuronal pathobiology.

Keywords: HPSE2, urofacial, heparanase-2, LRIG2, missense, Ochoa syndrome, triplication, rare disease

INTRODUCTION

Urofacial (Ochoa) syndrome (UFS) is rare autosomal recessive disease featuring urinary voiding dysfunction and a grimace upon smiling (Elejalde, 1979; Ochoa 2004; Newman and Woolf, 2018; Osorio et al., 2021). The urinary tract phenotype is characterized by bladder dyssynergia, with the detrusor contracting against and incompletely dilated outflow tract. This is manifest by dribbling incontinence of urine, and the residual urine is prone to bacterial infection. Moreover, high intravesical pressures lead to vesicoureteric reflux (VUR) which, if accompanied by urosepsis, can cause kidney infections, scarring and end-stage kidney failure. The characteristic grimace when smiling or laughing results from an abnormal contraction of the corners of the mouth and eyes (Ochoa 2004; Aydogdu et al., 2010).

Biallelic variants in *HPSE2*, coding for the secreted protein heparanase-2 (McKenzie et al., 2000; McKenzie 2020), was the first gene implicated in UFS (UFS1; Mendelian Inheritance in Man #236730). Indeed, *HPSE2* variants have been described in around half of the families with the syndrome who have been genetically investigated (Newman and Woolf, 2018). There is variability in phenotypic expression, even in a single family, and a small proportion of affected individuals may manifest only the grimace or urinary voiding dysfunction (Newman and Woolf, 2018). Previous reports of pathogenic variants in *HPSE2* feature stop-gain variants, splice variants and deletions (Daly et al., 2010; Pang et al., 2010; Al Badr et al., 2011; Stuart et al., 2015; Bulum et al., 2015; Vivante et al., 2017; van der Ven et al., 2018; Cesur Baltacı et al., 2021), all consistent with a loss of function mechanism. There exists only a single report of a homozygous missense, p.(Asn543Ile), in *HPSE2* associated with UFS (Mahmood et al., 2012).

In mice, heparanase-2 has been immunodetected in pelvic ganglia (Stuart et al., 2015), structures that send postganglionic autonomic neurons to the bladder (Keast et al., 2015). *Hpse2* mutant mice have dysfunctional bladders (Guo et al., 2015; Stuart et al., 2015) with impaired dilatation of the bladder outflow tract (Manak et al., 2020) and abnormal patterns of bladder nerves (Roberts et al., 2019). Moreover, experimental knockdown of *hpse2* in *Xenopus* leads to dysmorphic peripheral nerves (Robert et al., 2014). The specific biological role, or roles, of heparanase-2 are less clear but the protein has the abilities to bind heparin and heparin sulphate, and to inhibit the enzymatic (e.g., heparan sulfate degrading) activity of classical heparanase (Levy-Adam et al., 2010), here called heparanase-1, by outcompeting binding to its heparan sulfate substrate. Heparanase-2 also modulates both the migration of human tumour cells *in vitro* and experimental tumour growth *in vivo* (Gross-Cohen et al., 2021a; Gross-Cohen et al., 2021b).

Rarer individuals with classical features of UFS have biallelic variants in *LRIG2* (UFS2; Mendelian Inheritance in Man #615112), encoding a plasma membrane associated protein called leucine rich repeats and immunoglobulin like domains 2 (Stuart et al., 2013; Fadda et al., 2016; Sinha et al., 2018). Biallelic missense variants in *LRIG2* have also been reported in rare individuals with bladder dysfunction and renal failure, but who lack the facial phenotype (Roberts et al., 2019). Like heparanase-2, LRIG2 is detected in mouse pelvic ganglia (Stuart et al., 2015), and homozygous *Lrig2* mutant mice have bladder dysfunction and abnormally patterned bladder nerves (Roberts et al., 2019).

In this study, we sought to expand the *HPSE2* genotypic spectrum in families with UFS and make further insights into its pathobiology by seeking heparanase-2 and LRIG2 proteins in peripheral nerve precursors in human embryos.

PATIENTS AND METHODS

Genetic analyses of *HPSE2* and *LRIG2*

All individuals reported in this study provided consent to participate in a study to define the genetic cause of their family diagnosis. Institutional ethical approval for the study was granted (United Kingdom; University of Manchester [06138] and National Research Ethics Service Northwest, Greater Manchester Central ethics committee [06/Q1406/52 and 11/NW/0021]). Where a clinical diagnosis of UFS was made prior to genetic testing a targeted approach of sequencing *HPSE2* and *LRIG2* was employed. Where there was clinical uncertainty, but UFS lay within the differential diagnosis a broader candidate gene or unbiased exome approach was employed. In Families 1 and 4, Sanger sequencing was undertaken for all coding exons of *HPSE2* and *LRIG2*. Primers for amplification of exons and exon-intron boundaries of *HPSE2* and *LRIG2* were designed with Primer3Plus. For *HPSE2* NM_021828.4 for exons 1 to 12 and NM_001166246.1 for transcript variant 4 alternative exon 12 (exon12b) was used (details available on request). For *LRIG2* NM_014813 for exons 1–18 was sequenced (details available on request). Sanger sequencing was performed using the BigDye Terminator v3.1 kit (Life Technologies, CA, United States) according to manufacturer's instructions and resolved on an ABI3730 sequencer (Life Technologies, CA, United States). Genotyping for *HPSE2* and *LRIG2* variants was undertaken by sequencing the relevant amplicons in other family members. In Family 2, genetic testing was performed by a TruSight One capture kit (Illumina) using Nextera rapid capture for 4813 genes that were considered clinically relevant

at the time of the design. This was sequenced on a NextSeq550 (Illumina) with 2 × 150 bp paired-end reads. The alignment to GRCh37 was performed on NextGene (SoftGenetics, v2.4.1) with the in-built copy number variation (CNV) tool for CNV detection. Bioinformatic analysis of 57 genes (**Supplementary Data**) associated with urinary tract malformations was performed. In Family 2, confirmation of the CNV detected and cascade testing of family members were undertaken on an Agilent SurePrint G3 Human whole genome microarray. In Family 3, a trio analysis with a CytoScan HD single nucleotide polymorphism array was undertaken (ThermoFisher Scientific). Data were processed and analysed using NxClinical v5.1 software (BioDiscovery, CA, United States). Results were confirmed visually in whole exome sequencing data. In short, capture was performed using the SureSelect Human All Exon V7 capture kit (Agilent) according to manufacturer's instructions and subsequent sequencing was performed on a NovaSeq 6000 sequencing system (Illumina). Mapping was performed using an in-house GATK-based pipeline and resulting data was visualized using the Integrative Genomics Viewer (IGV, Broad Institute, CA, United States) (Robinson et al., 2017).

Transfection of HPSE2 in Mammalian Cells

FreestyleTM HEK293-F cells (Thermo Scientific) were transiently transfected in FreestyleTM 293 expression medium (Thermo Scientific) in duplicate with either wild-type pcDNA3: HPSE2c myc, or the myc-tagged p.Asn543Ile (Mahmood et al., 2012) or p.Pro140Arg (current paper) variant constructs. Three days after transfection at 37°C shaking at 130 rpm, the cultures were split and heparin (10 μg/ml) was added to one set and left to grow for a further 24 h with shaking at 37°C. Heparin is known to bind wild type heparanase-2 and in cultured cells adding heparin to the media will sequester heparanase-2 protein that was associated with the cell surface (Levy-Adam et al., 2010; McKenzie, 2020). The conditioned media was clarified and concentrated 10-fold using a vivaspin 5 KDa concentrator. Ten μg of cell lysate protein per lane was used for western blotting. β-actin was used as a cellular loading control. For the supernatant lane loadings equal amounts of cells were quantified using a haemocytometer and the clarified media was collected next day for blotting. All samples were concentrated to the same volume to standardise before SDS analysis and blotting. RIPA lysis buffer was added to the cell pellets on ice and left for 30 min. The lysates were sonicated (30% setting for 30 s on ice) and then centrifuged at 15,000 g for 30 min at 4°C. Samples were removed and mixed with 2 x SDS Laemmlli buffer containing 2-mercaptoethanol and heated for ^{95o}C for 5 min. Samples were resolved on a 4–20% SDS PAGE gel and blotted onto polyvinylidene fluoride membranes. Membranes were blocked in PBS-T, 5% skimmed milk for 1 h and then incubated overnight with anti-myc antibody (Sigma) at 4oC. Next day, membranes were washed with PBS-T, milk and incubated with secondary mouse anti-myc antibody for 1 h in PBS-T milk. Blots were finally washed in PBS-T and incubated with ECL reagents (GE). Chemiluminescence was detected using the Syngene western blot system.

Immunohistochemistry

Human embryonic tissues, collected after maternal consent and with ethical approval (REC18/NE/0290), were sourced from the Medical Research Council and WellcomeTrust Human Developmental Biology Resource (https://www.hdbr.org/). Seven week embryonic tissues were fixed, paraffin embedded, and sectioned as described (Lopes et al., 2019) and serial sections were immunostained with one of the following primary antibodies: rabbit anti-heparanase-2 (1:200; custom made and raised against an epitope starting at amino acid 82) (Roberts et al., 2014); rabbit anti-LRIG2 (1:200; AP13821b; Abgent); or chicken anti-β3-tubulin (1:400; AB9354; Millipore). The primary antibodies were detected with secondary antibody and signals generated with a peroxidase-based system, as described (Lopes et al., 2019).

RESULTS

Family 1

The proband (II:1) is a 20 year old male from a consanguineous Turkish family (**Figure 1**). His clinical course featured recurrent urinary tract infections (UTIs), and VUR was diagnosed when he was 7 years old. He was initially treated with intermittent bladder catheterization and anticholinergic medication. His small capacity bladder was surgically augmented when he was 12 years old. Subsequently, he reached end-stage renal failure and received a kidney transplant at the age 17 years. UTIs persisted and a video-urodynamic study demonstrated VUR into both his native kidneys and into the transplanted kidney. He has a striking grimace upon attempting to smile (**Supplementary Video S1**). The proband's parents are clinically unaffected. Sequencing of *LRIG2* revealed no significant variants. Sequencing of *HPSE2* in the proband revealed a homozygous pathogenic variant, as defined under ACMG guidelines (PVS1, PM2_Mod, PS4_Supp) (Richards et al., 2015) c.429T>A, p.(Tyr143*), which has previously been reported in a family affected by UFS (Stuart et al., 2015). Segregation analysis revealed that his parents, who were each clinically unaffected, were each heterozygous for the variant, as were two of the proband's clinically unaffected brothers (II:2 and II:3) where DNA samples were available. A sample from the other unaffected brother (II:4) was not available.

Family 2

The proband (II:2), is the middle of three sisters born to a non-consanguineous couple (**Figure 2**) from the Torres Strait Islands, Australia. The pregnancy leading to her birth, and the birth itself, were uneventful. She has a grimace typical of UFS. She presented aged 3 years with recurrent UTIs. Investigations revealed that she had a thickened bladder wall, VUR and hydronephrosis. She had a bladder stoma fashioned at that point. She had an ileocystoplasty bladder augmentation in her early teenage years and she currently self-catheterises. Investigations in her early

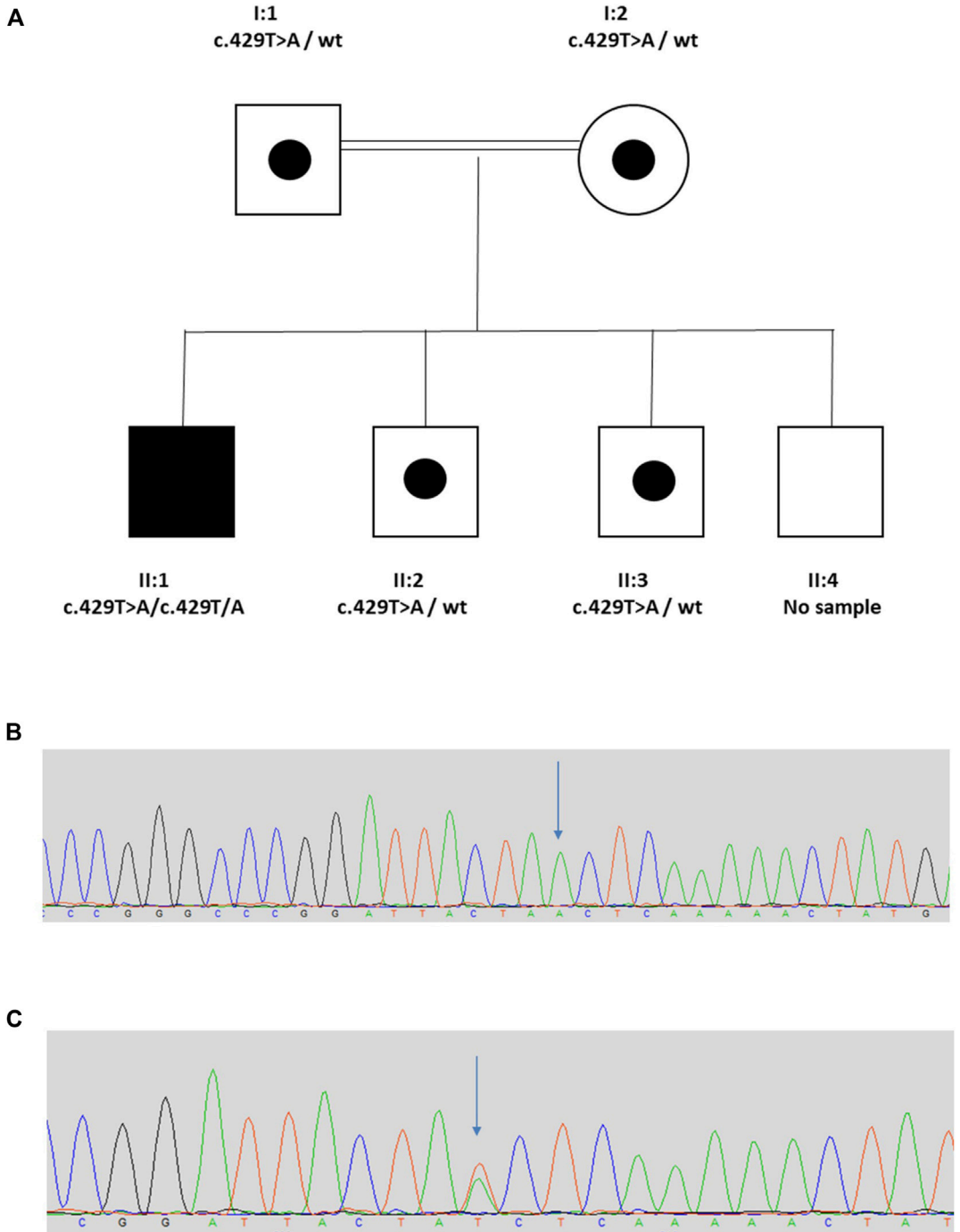

FIGURE 1 | Family 1. **(A)**. Pedigree of Family 1 with individual affected with UFS (II:1) shaded. Dots represent clinically unaffected individuals confirmed to carry a *HPSE2* heterozygous variant. **(B,C)**, Genomic sequence chromatograms, showing variant c.429T>A indicated by an arrow **(B)** homozygous variant for affected, **(C)** heterozygous variant for carriers. Please see Supplementary Video 1 for the grimace upon smiling.

teenage years revealed persistent thickening of the bladder wall, with bladder diverticulae and a large residual volume after micturition, together with VUR, bilateral hydronephrosis and kidney cortical scarring. Her blood creatinine was elevated at 106 μmol/L (upper normal for age 82 μmol/L). II:3 is her younger sister who presented with a UTI aged 4 years. Investigations revealed bilateral VUR with a thickened neurogenic bladder. She currently self-catheterises. Like II:2, II:3 has a grimace typical of UFS, and she also had a bladder that failed to void completely, with a residual of 117 ml, with a thickened wall and

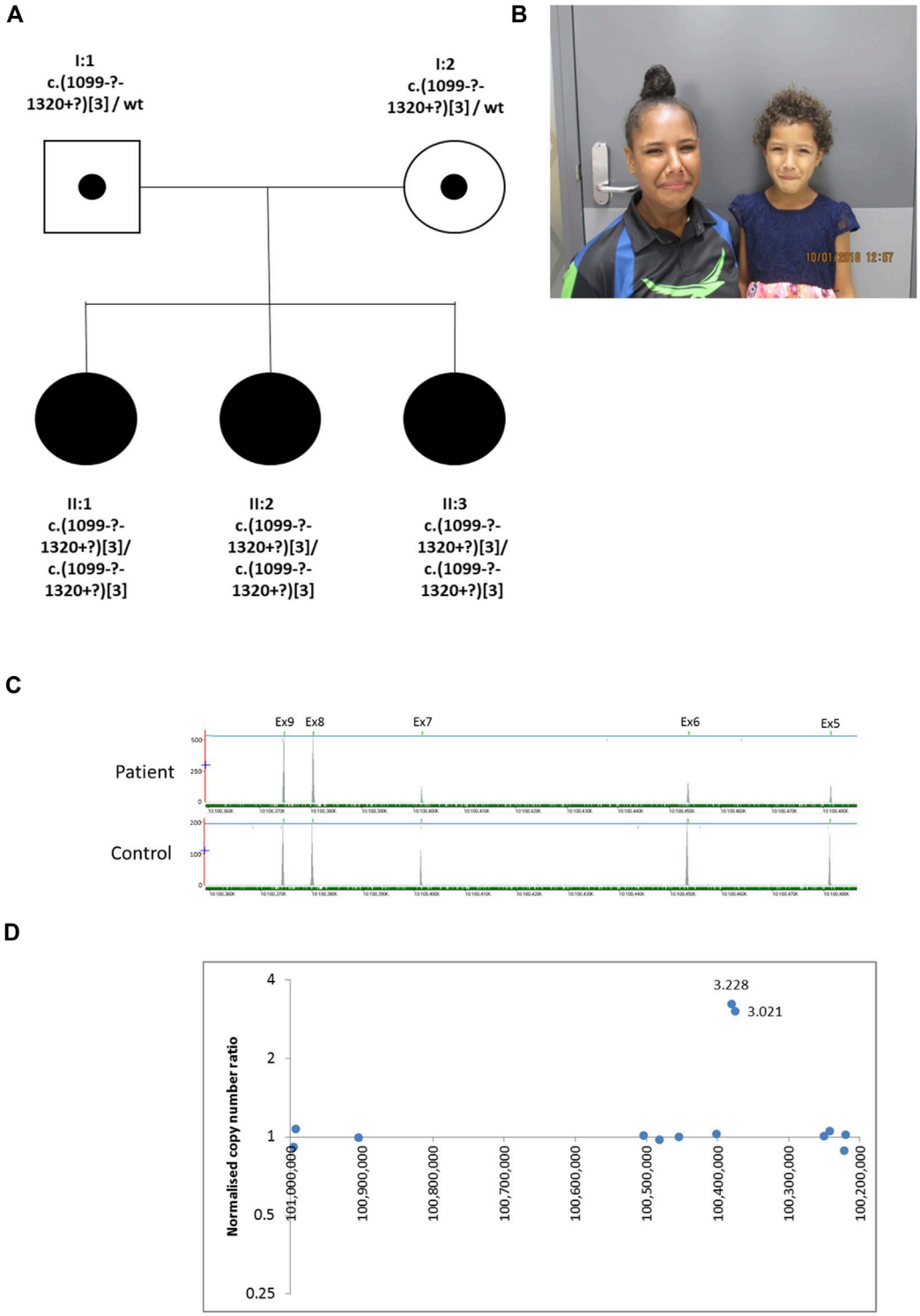

FIGURE 2 | Family 2. **(A)**. Pedigree of the Family 2 with three individuals affected with UFS (shaded). Dots represent clinically unaffected individuals confirmed to carry a *HPSE2* heterozygous variant **(B)**. Grimace when smiling characteristic of UFS in individuals II:2 and II:3. **(C)**. Y-axis indicates raw depth of coverage after alignment from NGS gene panel; X-axis chromosomal coordinates in chr10 (Note that *HPSE2* is on the minus strand). The blue line indicates the gene *HPSE2* and the green dashes the exons within *HPSE2* Exon numbering according to NM_021828.4. **(D)** Copy number analysis in *HPSE2*: Normalised copy number ratio of patient against sex-matched controls. Data points for captured regions within *HPSE2*. Y-axis shows relative copy number against control samples, where 1 indicates having normal diploidy; X-axis chromosomal coordinates on chromosome 10 in reverse orientation. Two consecutive exons in *HPSE2* showed high normalised copy number ratio indicative of homozygous triplication (total of six copies).

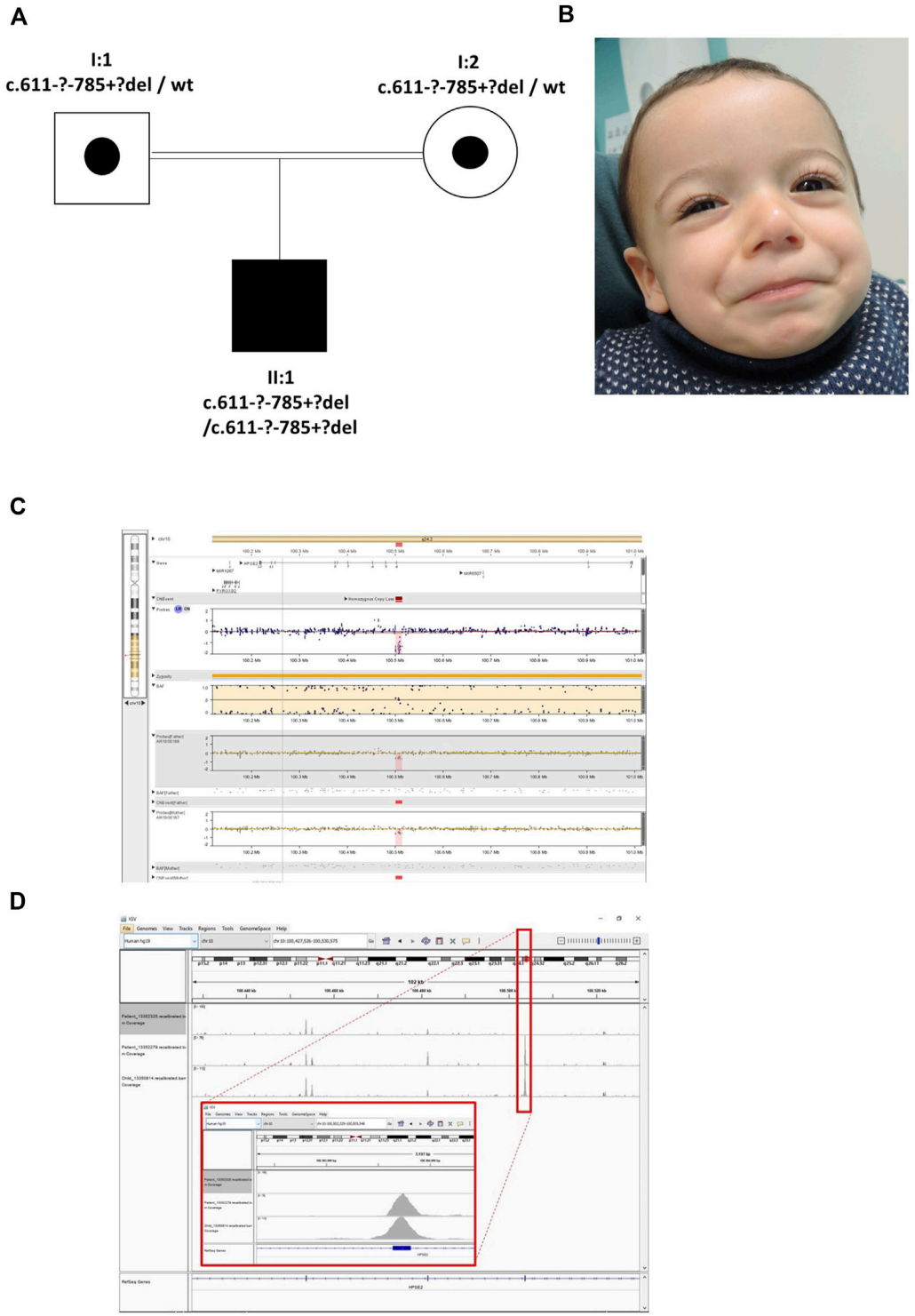

FIGURE 3 | Family 3. **(A)**. Pedigree of the Family 3 with individual affected with UFS (shaded). Dots represent clinically unaffected individuals proven to carry a *HPSE2* heterozygous variant. **(B)**. Facial appearance of child demonstrating downturned corners of the mouth when smiling. **(C)**. The SNP array shows the proband (top track) with the father and mother below, both with a heterozygous deletion. The BAF (B allele frequency) panel of the picture shows a part of the region of homozygosity (marked yellow) and in the probes track the homozygous deletion depicted in pink/red. **(D)**. The IGV image shows the coverage of the WES zoomed to encompass *HPSE2* exon 4. The top track is the proband with the homozygous deletion (no coverage of exon 4). The two tracks below are two control individuals in the same WES capture/sequence run demonstrating exon coverage.

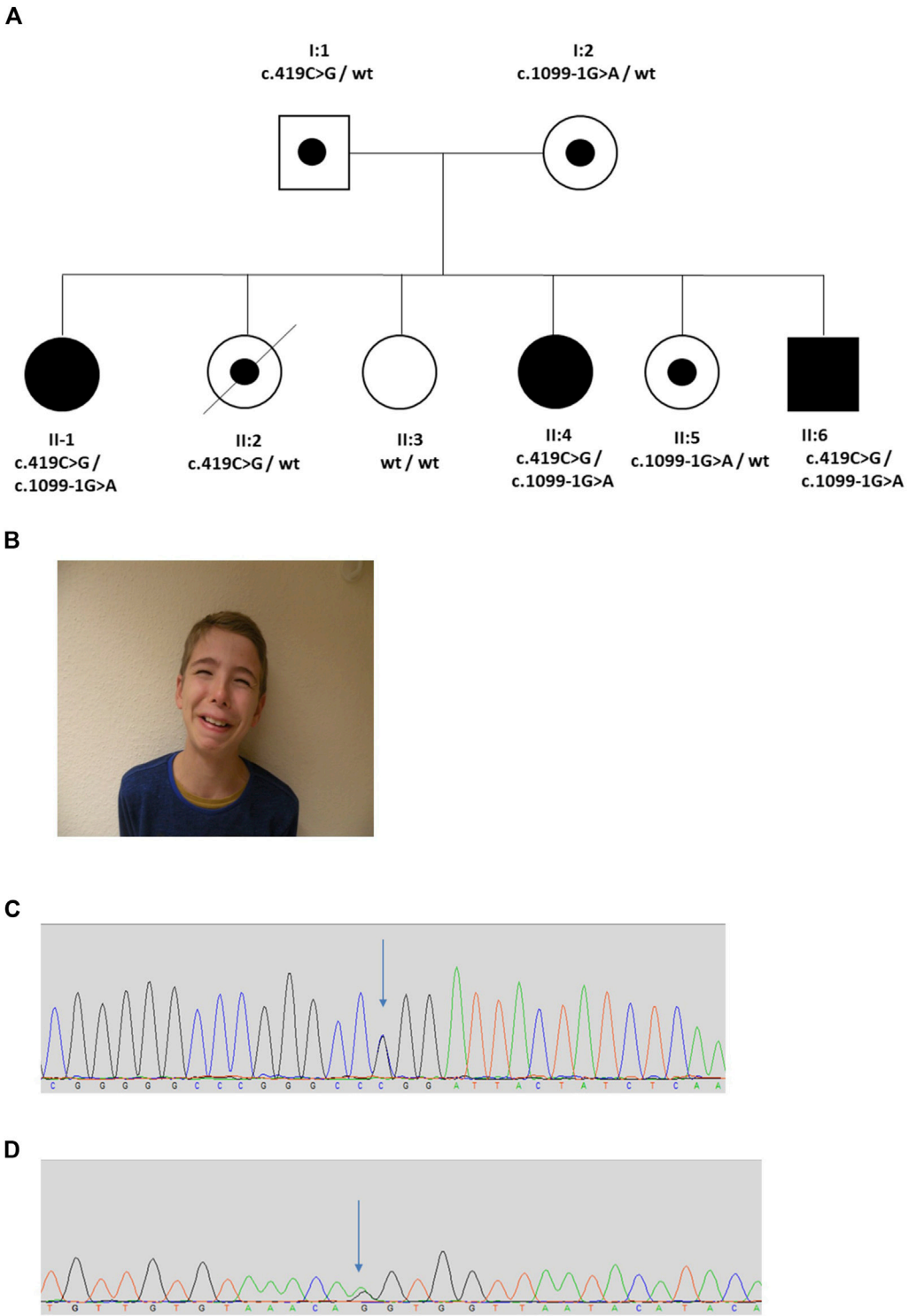

FIGURE 4 | Family 4. **(A)**. Pedigree of the Family 4 with three individuals affected with UFS (shaded). Dots represent clinically unaffected individuals confirmed to carry a *HPSE2* heterozygous variant. **(B)**. Grimace when smiling characteristic of UFS in individual II:6 in the family. **(C,D)**. Genomic sequence chromatograms showing the *HPSE2* heterozygous variants indicated by an arrow **(C)** c.419C>G, and **(D)** c.1099-1G>A.

bilateral VUR. II:3's blood creatinine was elevated at 63 μmol/L (upper normal for age 58 μmol/L). The eldest sister, II:1, had had several UTIs as a child but did not report other urinary symptoms. Ultrasonography revealed a normal bladder capacity (205 ml) and a minimal residual volume (2 ml) after micturition, and the upper urinary tract also appeared normal. She did not have an overt grimace on attempting to smile. In the proband in Family 2 next generation sequencing of a panel of genes associated with urinary tract malformations identified a potential homozygous triplication of exons 8 and 9 in *HPSE2*, p.(Val367_Pro [3]). This variant is defined as variant of uncertain significance (4F, 5D) using the ACMG and ClinGen guidelines (Rooney Riggs et al., 2020). This was confirmed by a high resolution microarray (arr [GRCh37] 10q24.2 (100365741_100390995)x6. Segregation analysis by microarray revealed that the two sisters were also homozygous for the triplication and the parents were heterozygous. Sequencing of *LRIG2* revealed no significant variants in the proband.

Family 3

The proband was the son of consanguineous first cousin Turkish parents (**Figure 3**) who had been referred with a tentative diagnosis of facial nerve paresis. Otherwise, he was fit and well with no developmental problems. He was toilet trained at 3 years of age, with only occasional episodes of enuresis. There was no history of UTIs and a bladder ultrasound at 3 years of age was normal, with no residual urine volume after micturition. Later in childhood, however, there was a history of mild dribbling urinary incontinence during the day, and there was a significant volume (70–158 ml) of urine after micturition. He defecates small amounts, four to five times a day. SNP microarray of the proband revealed a potential homozygous deletion of exon 4 in *HPSE2*, arr [GRCh37] 10q24.2 (100501035_100514963)x0. with a minimal size of 13.9 kb. Subsequent exome sequencing confirmed this finding. His parents had no urinary tract symptoms or facial signs, and they were both heterozygous for the deletion. The deletion of exon 4 is in frame, leading to the predicted loss of 58 amino acids and formation of a truncated protein p.(Ala_Asn261del). This variant is defined as a variant of uncertain significance (2E, 5H) using the ACMG and ClinGen guidelines (Rooney Riggs et al., 2020). Upon further assessment, the proband's abnormal smile, with downturned corners of the mouth upon smiling, was considered consistent with UFS. Sequencing of *LRIG2* revealed no significant variants in the proband.

Family 4

The proband (II:1) was female and the first child of healthy non-consanguineous German parents (**Figure 4**). She presented in early childhood with recurrent UTIs associated with poor bladder emptying and she was initially treated with intermittent bladder catheterization and anticholinergics. Magnetic resonance imaging revealed normal spinal anatomy. She underwent a vesicostomy aged 4 years and assessment in her seventh year led to a diagnosis of neurogenic bladder with detrusor sphincter dyssynergia. Her course was complicated by VUR and damage to her left kidney so that, as assessed by isotope scanning when 12 years old, it contributed only 22% of total kidney function. The next two siblings (II-2 and II-3) were also female. They had no urinary symptoms, but II-2 died at 18 years from epilepsy. The next sibling (II:4), another girl, presented *in utero* with a thickened bladder wall reported on an anomaly screening ultrasound scan. After birth, a micturating cystourethrogram (MCU) was abnormal, consistent with a neurogenic bladder. When assessed aged 17 years, urodynamics revealed a low compliance bladder with high intravesical pressures of 70 cm H_2O after filling, rising to 180 cm H_2O during micturition, the latter over three times the upper limit of normal (Lemack et al., 2002). MCU revealed incomplete bladder emptying with 130 ml residual urine. Ultrasonography revealed bilateral hydronephrosis and her overall renal function was impaired with a blood creatinine of 114.4 μmol/L (upper normal 105.6 μmol/L). The fifth sibling (II:5) was a healthy female. The sixth and final sibling (II:6) was a boy. He was investigated for nocturnal enuresis aged 10 years when urodynamics revealed a low compliance and low-capacity bladder with staccato micturition. Ultrasonography showed normal kidneys and blood tests showed normal renal function. He commenced intermittent self-catheterization and anticholinergic therapy. A grimace when smiling was noted and the diagnosis of UFS was considered; in further inspection the two other siblings with urinary tract disease were also noted to have a grimace. Sequencing of *LRIG2* revealed no significant variants. Sanger sequencing of *HPSE2* identified two variants, c.419C>G, p.Pro140Arg and c.1099-1G>A in the three affected children (II:1, II:4, and II:6). Two sisters unaffected by urinary disease (II:2 and II:5) were carriers for a single variant, and the third clinically unaffected sister (II:3) was wild type. The parents were heterozygous carriers, confirming that the variants were on separate alleles, consistent with autosomal recessive inheritance. The c.1099-1G>A variant has previously been reported in a patient with UFS (Stuart et al., 2015) and is predicted to result in the loss of a splice acceptor within exon 8, so introducing a premature stop codon. This variant was classified as pathogenic (PVS1, PM2_Mod, PS4_Supp, PP1_Supp, PM3_Mod) by ACMG guidelines (Richards et al., 2015; Ellard et al., 2020). Before this report, however, the c.419C>G variant has not been associated with UFS. This variant occurs at a minor allele frequency of 0.00001 (i.e., 2 in 152,996 alleles in the gnomAD database) (Karczewski et al., 2020). The c.419C>G variant is a missense change, predicted to result in the substitution of a proline for an arginine residue, p.Pro140Arg. This proline residue is conserved in heparanase-2 between humans to zebrafish. *In silico* tools of pathogenicity gave conflicting predictions: the variant was disease-causing as assessed with Mutation Taster (http://www.mutationtaster.org/); benign on Polyphen-2 (http://genetics.bwh.harvard.edu/pph2/); but tolerated using the Sorting Intolerant From Tolerant (SIFT) tool (http://sift.bii.a-star.edu.sg/); and with a Combined Annotation Dependent Depletion (CADD) score of 22.4 (a score of >20 predicts that this variant in the top 1% of most likely deleterious variants) (Rentzsch et al., 2019). This variant is classified as a VUS (PM2_Mod, PP3, PM3_Mod, PP1_Supp) according to ACMG guidelines (Richards et al., 2015; Ellard et al., 2020).

Protein Modelling and *in vitro* Expression of Heparanase-2 Missense Variants

In order to learn more about missense variant discovered in Family 4, we undertook further analyses. First, we expressed the p.Pro140Arg variant in cultured cells, and compared it with the p.(Asn543Ile) variant previously reported in a family with UFS (Mahmood et al., 2012). Each protein was expressed as a myc-tagged protein in HEK293 cells (**Figure 5**). Each variant protein was detected in cell lysates, as for cells transfected with a wild-type *HPSE2* construct, also myc-tagged. As expected for a secreted protein, wild-type heparanase-2 was also detected in the conditioned media. In this context, however, there was a contrast between the two missense proteins, with only p.Pro140Arg being detected in the media. In parallel experiments, heparin, a molecule that binds wild-type heparanase-2 (McKenzie, 2020), was added to the media. Again, the myc-tagged p.Asn543Ile variant was not detected in the supernatant. In blots of both the wild-type and the p.Pro140Arg variant, the addition of heparin to the media appeared to increase the intensities of the detected protein bands in the supernatant compared with the intensities of the bands that were cell associated.

Second, we undertook protein modelling. No heparanase-2 structural information exists. The closest structural homologue is human heparanase-1 (encoded by *HPSE*) with approximately 50% sequence identity at the protein level (Wu et al., 2015). The heparanase-1 precursor is arranged into signal peptide-small subunit-proteolytic linker-large subunit. In the mature protein, the linker is cleaved off to form a 'heterodimer' of small and large subunits. The residue Asn543 in heparanase-2 (Mahmood et al., 2012) corresponds to Asn496 in heparanase-1 (using precursor numbering). This Asn position is strictly invariant in the heparanase-1/heparanase-2 orthologues and is located in the large subunit as part of the beta-sandwich domain. Asn496 in heparanase-1 forms main-chain hydrogen bonds with a nearby beta-strand to maintain the sandwich domain. These hydrogen bonds are likely conserved in heparanase-2, as suggested by the Alphafold predicted model (Tunyasuvunakool et al., 2021) and the p.Asn543Ile substitution in heparanase-2 is predicted to interfere with these hydrogen bonds. The effect of altering the residue Pro140 in heparanase-2 is more complex to rationalise (**Supplementary Figure S1**). Pro140 (underlined and cyan shaded in **Supplementary Figure S1**) and the surrounding residues are not well conserved with heparanase-1 in terms of sequence and structure. The equivalent region in the latter is part of the proteolytic linker (red letters) that gets cleaved off during activation to form the mature protein. It is therefore difficult to predict a possible effect of this variant in the absence of the heparanase-2 structure.

Immunolocalisation of Heparanase-2 and LRIG2 in Normal Human Embryos

We studied histology sections of two human embryos, each of 7 weeks gestation. At this stage, the hindgut has separated from the urogenital sinus, the latter being the precursor of the urinary bladder (Jenkins et al., 2007). The immunostaining patterns were similar in each embryo. Heparanase-2 was immunodetected in loosely aggregated collections of cells flanking the hindgut (**Figure 6**), and also in the in the primitive urethra and in the genital tubercule. In transverse sections more cranial to these, heparanase-2 was detected in

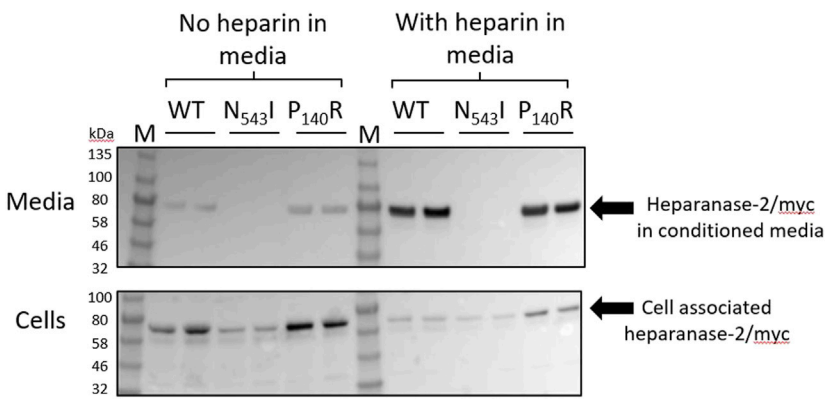

FIGURE 5 | Expression of wild type and missense variant proteins in HEK293 cells. Non quantitative western blot analyses using anti-myc antibody. HEK293 cells were transfected with pCDNA3:HPSE2cmyc wild-type (*WT*) or the myc-tagged the p.Asn543Ile variant (abbreviated to *N543I* in the annotated image) or the p.Pro140Arg variant (abbreviated to P140R in the annotated image) variant. Samples, with two replicates shown for each condition, were studied at both 3 days after transfection (*No heparin in media*) and also 24 h later after the addition of heparin to the media (*With heparin in media*). The upper blot is of the conditioned media (*Heparanase-2/myc in condition media*), while the lower blot is from cell lysates (*Cell associated heparanse-2/myc*). Note that all three proteins were detected in cells, and that the wild-type and the p.Pro140Arg variant were detected in the conditioned media. The lack of the p.Asn543Ile variant in conditioned media was documented both before and after adding heparin to the media; this molecule is known to bind native heparanase-2 (McKenzie, 2020). In blots of both the wild-type and the p.Pro140Arg variant, the addition of heparin to the media appeared to increase the intensities of the detected protein bands in the supernatant compared with the intensities of the bands that were cell-associated.

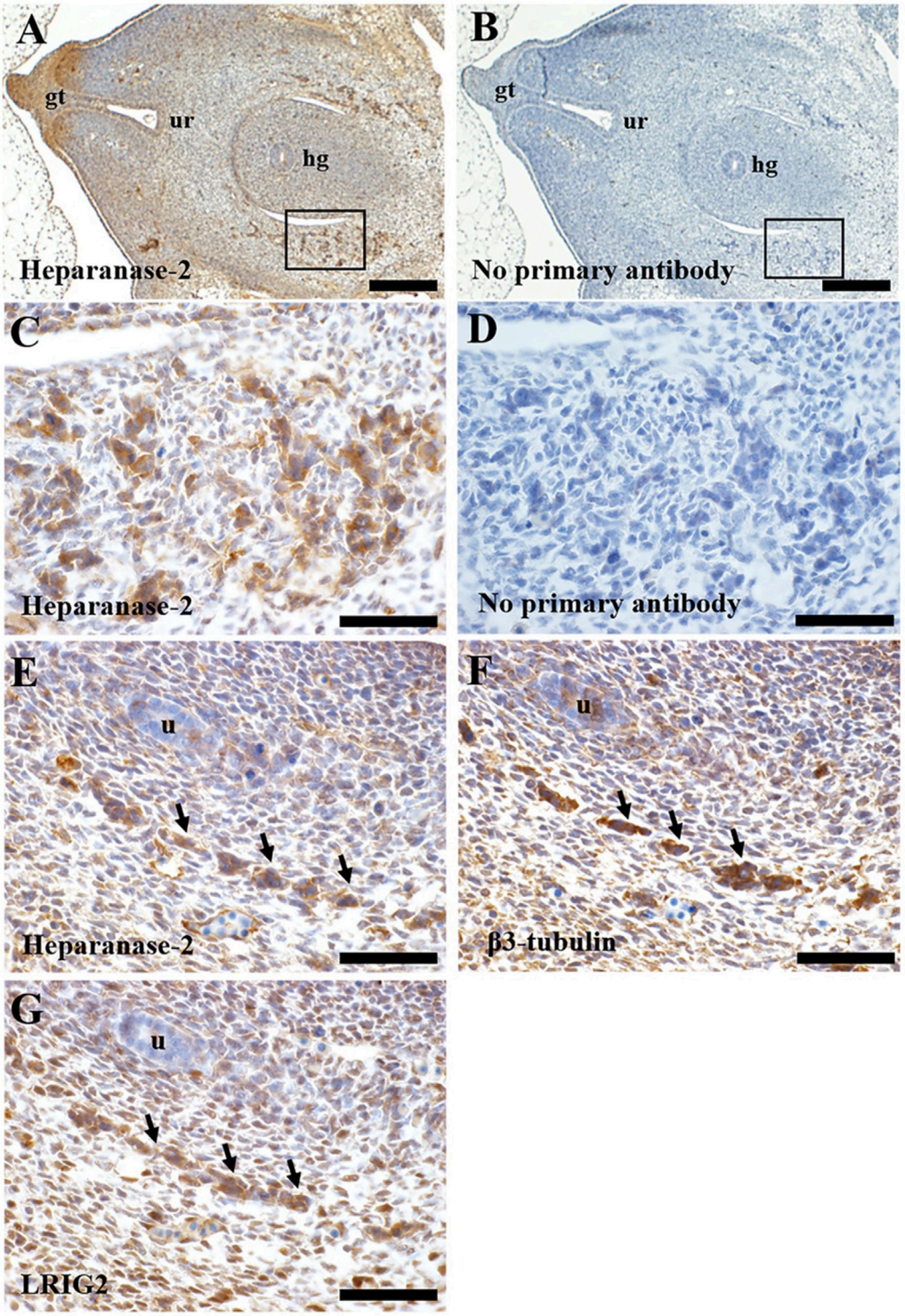

FIGURE 6 | Immunohistochemistry of human embryos. Transverse sections through a seven-week human embryo at the level of the hindgut. All sections were counterstained with haematoxylin (blue nuclei). In all sections, ventral (the front of the embryo) is to the left, and dorsal is to the right. A and B are low power views, while the other frames are high power views. **(A)**. Immunostaining for heparanase-2 (brown signal). Note positive staining in collections of cells (one area is boxed) flanking the hindgut (hg). Positive immunostaining is also evident in the genital tubercle (gt) and the forming urethra (ur). **(B)**. Adjacent section with primary antibody omitted; no brown signal is detected. **(C)**. High power approximating to the boxed area in **(A)**. Note collections of cells that immunostain for heparanase-2. **(D)**. Adjacent section to that depicted in **(C)** but with primary antibody omitted. **(E–G)**. These are serial sections flanking the hindgut taken from the same embryo but more cranial to the area viewed in **(C)**. Note the cord of cells (arrowed) that are positive for each of these three proteins: heparanase-2 **(E)**; β3-tubulin **(F)**, a protein enriched in neurons; and LRIG2 **(G)**. The embryonic ureter (u) is seen in the same three sections. Scale bar is 200 μm in A and B, and 20 μm in **(C–G)**.

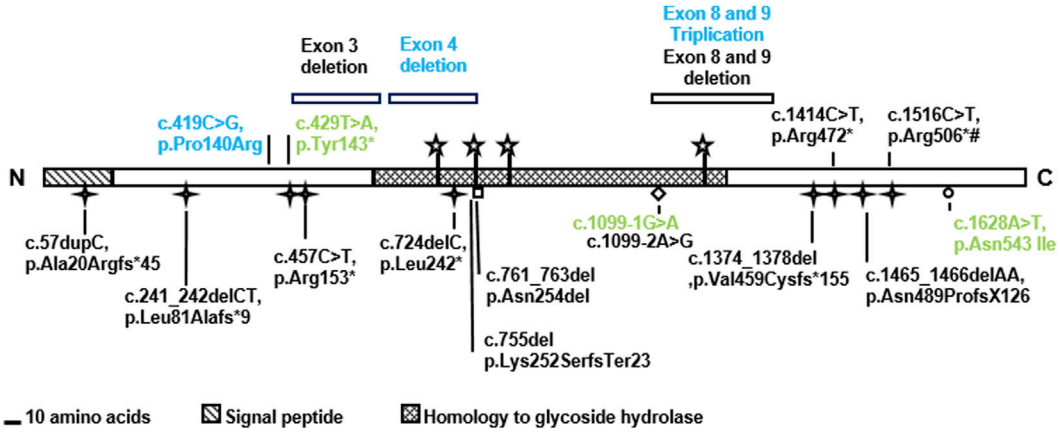

FIGURE 7 | Summary of *HPSE2* variants associated with UFS. The novel variants found in the three families in the current report are shown in blue. The variants in green have been reported in previous studies. Two of them were identified in the affected individuals in this study and the missense variant p.Asn542Ile was considered for its functional consequence. Yet other variants, shown in black, have been reported in previous publications that investigated UFS.

TABLE 1 | Summary of HPSE2 variants associated with UFS. The table contains both results from historical reports as well as the current report.

***HPSE2* mutation**	**Predicted protein change**	**Reference**
c.57dupC	p.(Ala20Argfs*45)	Daly et al. (2010)
c.241-242delCT	p.(Leu81Alafs*9)	Pang et al. (2010)
c.419C>G	p.Pro140Arg	Current report
c.429T>A	p.(Tyr143*)	Stuart et al. (2015) and current report
c.457C>T	p.(Arg153*)	Daly et al. (2010) Bulum et al. (2015) Vivante et al. (2017)
c.724delC	p.(Leu242*)	Stuart et al. (2015)
c.755del	p.(Lys252SerfsTer23)	Cesur Baltacı et al. (2021)
c.761-763del	p.(Asn254del)	Stuart et al. (2015)
c.1099-1G>A	p.(Val367Glyfs*2) or p.(Val367Lysfs*6)	Stuart et al., 2015., and current report
c.1099-2A>G	p.(Val367Glyfs*2) or p.(Val367Lysfs*6)	van der Ven et al. (2018)
c.1374-1378del	p.(Val459Cysfs*155)	Al Badr et al. (2011)
c.1414C>T	p.(Arg472*)	Daly et al. (2010)
c.1465-1466delAA	p.(Asn489Profs*126)	Daly et al. (2010)
c.1516C>T	p.(Arg506*)	Pang et al. (2010)
c.1628A>T	p.Asn543Ile	Mahmood et al. (2012)
Exon 3 deletion c.449-?-610+?del	p.(Asp150-Thr203del)	Daly et al. (2010)
Exon 4 deletion c.611-?-785+?del	p.(Ala204-Asn261del)	Current report
Exon 8-9 deletion/insertion c.1099–4166-1320 + 840delins23	p.(Val367-Pro440del)	Daly et al. (2010)
Exon 8–9 triplication c.(1099-?-1320+?)[3]	p.(Val367-Pro440 [3])	Current report

cords on cells flanking the hindgut and near the embryonic ureter. Serial sections revealed that these structures immunostained for the neural marker β3-tubulin as well as for LRIG2. The latter protein was also detected in other cells in this region, including loosely packed stromal-like cells.

DISCUSSION

Our study expands the genotypic spectrum in *HPSE2* in UFS and supports a developmental neuronal pathobiology. In a broader context, *HPSE2*-related disease can be placed among other early onset lower urinary tract dysfunctional diseases associated with variants in genes that code for other molecules involved in neural and smooth muscle maturation (Beaman et al., 2019; Houweling et al., 2019; Mann et al., 2019; Woolf et al., 2019).

We studied four previously unreported families with UFS carrying *HPSE2* variants. In one family, the proband had end stage kidney failure and was homozygous for the previously described pathogenic variant c.429T>A, p.(Tyr143*). The three other families each carried a different novel *HPSE2* variant. One had homozygous triplication of exons 8 and 9; another had a

homozygous deletion of exon 4; and one carried a novel c.419C>G variant encoding the missense p.Pro140Arg in *trans* with c.1099-1G>A, a previously reported pathogenic splice variant. Expressing the missense heparanase-2 variant *in vitro* showed that it was secreted as normal, suggesting that 140Arg has aberrant functionality after secretion. The c.419C>G missense variant is only the second reported case in which a variant of a missense variant in *HPSE2* associated with UFS (Mahmood et al., 2012) and no previous cases of *HPSE2* exon triplication have been associated with UFS. The study therefore expands the *HPSE2* genotypic spectrum associated with UFS (**Figure 7** and **Table 1**).

It is likely that UFS is under-reported with few individuals with urinary bladder voiding under-going genetic studies and the association between a facial grimace and bladder dysfunction not being considered (Newman and Woolf 2018). It is still surprising, however, how few missense variants in this gene have been associated with disease. Furthermore, there are many genetic mechanisms by which loss of function can arise and these new findings of copy number variation demonstrate the importance of incorporating comprehensive analysis methods in diagnostic testing when UFS is suspected. Deletion of exon 3 and a complex deletion of exons 8 and 9 in *HPSE2* have previously been reported (Daly et al., 2010; Stuart et al., 2015).

Exon (Lücking et al., 2001) or whole gene (Singleton et al., 2003) triplication is very rarely reported as a mutational mechanism in Mendelian disorders and has not previously been reported for *HPSE2*. It is interesting to note that an insertion-deletion of exons 8 and 9 in *HPSE2* has been reported associated with UFS (Daly et al., 2010). We did not define the breakpoints or exact rearrangement of the triplication and it is not possible to know if it is in frame or not and how it would impact on protein coding. If in frame, the translation would result in a significant structural change to the protein and alter its stability, whereas an out of frame change would be predicted to result in nonsense-mediated decay. Each would be consistent with the loss of function of mechanism associated with other *HPSE2* variants in UFS (Newman and Woolf 2018).

Four potential isoforms of heparanase-2 have been envisaged as a consequence of differential splicing of exons 3 and 4 (McKenzie et al., 2000; McKenzie 2020). Previously, we identified a whole exon deletion of exon 3 in a family with UFS (Daly et al., 2010). Our finding in the current report of a child with UFS with a homozygous exon 4 deletion suggests that the isoforms containing both exons 3 and 4 are critical for heparanase-2 function.

In the current study, we demonstrate that the previously reported p.Asn543Ile amino acid substitution in heparanase-2 in a family with UFS (Mahmood et al., 2012) generates a protein that apparently fails to be secreted. Hence this missense variant likely acts through a loss of function mechanism, providing experimental evidence that this a potential mechanism for other putative loss of function variants (Newman and Woolf 2018). In contrast with the p.Asn543Ile variant, the p.Pro140Arg variant reported here encodes a secreted protein. The functional effect of this variant is still to be elucidated but may result, for example, in altered interaction with heparanase-1 (Levy-Adam et al., 2010) together with, for example, disruption in potential downstream intracellular signalling (Roberts et al., 2014; Roberts et al., 2016). The variable clinical presentations in the affected individuals in Family 4 (e.g. the milder urinary tract phenotype in II:6), suggests that additional factors beyond the *HPSE2* genotype contribute to the phenotype. These co-factors include the severity, frequency and type of UTIs and modifier genotypes.

Although there are a limited number of reports of individuals with variants in *HPSE2* and *LRIG2* to draw definitive phenotype-genotype correlations it is of interest to explore if there are differences. The similarity of clinical phenotype between cases with biallelic loss of function and missense variants in *HPSE2* suggests that these missense variants result in a loss of function (Daly et al., 2010; Pang et al., 2010; Mahmood et al., 2012; Stuart et al., 2015). This contrasts with the spectrum of disease associated with *LRIG2* variants where biallelic loss of function variants result in classical UFS whereas biallelic missense variants cause severe bladder voiding dysfunction with no facial phenotype (Stuart et al., 2013; Roberts et al., 2019). This suggests that hypomorphic missense variants of *LRIG2*, resulting in reduced function or expression, have a clinical phenotype whereas there is no evidence to date that hypomorphic *HPSE2* variants result in disease. It is possible that such hypomorphic variants in *HPSE2*, if they exist, result in a different clinical phenotype.

Finally, our new observations of heparanase-2 localisation in early human embryogenesis is broadly consistent with the hypothesis that the bladder manifestations of UFS are the result of, at least in part, a peripheral neuropathy affecting the lower urinary tract (Roberts et al., 2016; Roberts and Woolf 2020). We detected both heparanase-2 and LRIG2 in neural-like cells with a migratory phenotype and these are postulated to be pelvic ganglia precursors (Keast et al., 2015). The current results complement an existing human report that, later in the first trimester, both proteins are present in nerves located between detrusor muscle bundles (Stuart et al., 2013). While the pattern of bladder nerves not been studied in native tissues of individual with UFS, it is notable that mice carrying mutations of either *Hpse2* or *Lrig2* each have bladder bodies and outflow tracts containing abnormally patterned neurons (Roberts et al., 2019). It can be postulated that heparanase-2 is required for the normal differentiation and functionality of human bladder nerves. In this context, an interaction with heparanase-1 is possible because this protein is also detected in pelvic ganglia (Stuart et al., 2015) and, at least in rat phaeochromocytoma cells, heparanase-1 modulates neuritogenesis (Cui et al., 2011). Of note, cell biology experiments implicate LRIG2 in axon guidance (van Erp et al., 2015) and in controlling cell turnover in neural tumour cells (Xiao et al., 2018). Further experiments are now required to determine the possible effects of LRIG2 on bladder nerve precursor cells.

DATA AVAILABILITY STATEMENT

The original contributions presented in the study are included in the article/**Supplementary Material**, further inquiries can be directed to the corresponding authors. The data presented in the study are deposited in the CLINVAR repository, accession numbers SCV002525226-SCV002525230.

ETHICS STATEMENT

The studies involving human participants were reviewed and approved by Institutional ethical for the study was granted (United Kingdom; University of Manchester [06138] and Nation-al Research Ethics Service North West, Greater Manchester Central ethics committee [06/Q1406/52 and 11/NW/0021]). Written informed consent to participate in this study was provided by the participants' legal guardian/next of kin. Written informed consent was obtained from the individual(s), and minor(s)' legal guardian/next of kin, for the publication of any potentially identifiable images or data included in this article.

AUTHOR CONTRIBUTIONS

WN, GB, and AW conceived the study and drafted the paper. EM and ME undertook biochemical studies. FL, AW, and NR undertook immunohistochemistry studies. WY undertook protein modelling. AH, WR, MP, EB, CP, AA, BB, JK, GH, CA, SD, MV, MC, HS, WN, and GB provided clinical details, patient samples and/or undertook genetic analyses. All authors approved the final manuscript.

FUNDING

Funding grant support from: Medical Research Council (project grant MR/L002744/1 to AW and WN, and project grant MR/T016809/1 to AW, NR, and FL); Kidney Research United Kingdom (project grant Paed_RP_002_20190925 to WN, GB, and AW; and Paed_RP_005_20190925 to NR and AW); ; Newlife Foundation (project grants 15-15/03 and 15-16/06 to WN and AW); the NIHR Academic Lecturer scheme (HMS); and the Manchester NIHR BRC (IS-BRC-1215-20007 to WN); Kidneys for Life (start-up grant 2018 to NR); and the KUNO Foundation Regensburg.

ACKNOWLEDGMENTS

We thank the patients and their family members for supporting the study. We would also like to thank James O'Sullivan for his support with ACMG variant classification.

SUPPLEMENTARY MATERIAL

The Supplementary Material for this article can be found online at: https://www.frontiersin.org/articles/10.3389/fgene.2022.896125/full#supplementary-material

REFERENCES

Al Badr, W., Al Bader, S., Otto, E., Hildebrandt, F., Ackley, T., Peng, W., et al. (2011). Exome Capture and Massively Parallel Sequencing Identifies a Novel HPSE2 Mutation in a Saudi Arabian Child with Ochoa (Urofacial) Syndrome. *J. Pediatr. Urology* 7, 569–573. doi:10.1016/j.jpurol.2011.02.034

Aydogdu, O., Burgu, B., Demirel, F., Soygur, T., Ozcakar, Z. B., Yalcınkaya, F., et al. (2010). Ochoa Syndrome: a Spectrum of Urofacial Syndrome. *Eur. J. Pediatr.* 169, 431–435. doi:10.1007/s00431-009-1042-9

Beaman, G. M., Galatà, G., Teik, K. W., Urquhart, J. E., Aishah, A., O'Sullivan, J., et al. (2019). A Homozygous Missense Variant in CHRM3 Associated with Familial Urinary Bladder Disease. *Clin. Genet.* 96, 515–520. doi:10.1111/cge.13631

Bulum, B., Özçakar, Z. B., Duman, D., Cengiz, F. B., Kavaz, A., Burgu, B., et al. (2015). HPSE2 Mutations in Urofacial Syndrome, Non-neurogenic Neurogenic Bladder and Lower Urinary Tract Dysfunction. *Nephron* 130, 54–58. doi:10.1159/000381465

Cesur Baltacı, H. N., Taşdelen, E., Topçu, V., Eminoğlu, F. T., and Karabulut, H. G. (2021). Dual Diagnosis of Ochoa Syndrome and Niemann-Pick Disease Type B in a Consanguineous Family. *J. Pediatr. Endocrinol. Metab.* 34, 653–657. doi:10.1515/jpem-2020-0367

Cui, H., Shao, C., Liu, Q., Yu, W., Fang, J., Yu, W., et al. (2011). Heparanase Enhances Nerve-Growth-Factor-Induced PC12 Cell Neuritogenesis via the P38 MAPK Pathway. *Biochem. J.* 440, 273–282. doi:10.1042/bj20110167

Daly, S. B., Urquhart, J. E., Hilton, E., McKenzie, E. A., Kammerer, R. A., Lewis, M., et al. (2010). Mutations in HPSE2 Cause Urofacial Syndrome. *Am. J. Hum. Genet.* 86, 963–969. doi:10.1016/j.ajhg.2010.05.006

Elejalde, B. R., and Gorlin, R. J. (1979). Genetic and Diagnostic Considerations in Three Families with Abnormalities of Facial Expression and Congenital Urinary Obstruction: "The Ochoa Syndrome". *Am. J. Med. Genet.* 3, 97–108. doi:10.1002/ajmg.1320030114

Ellard, S., Baple, E. L., Callaway, A., Berry, I., Forrester, N., Turnbull, C., et al. (2020). *ACGS Best Practice Guidelines for Variant Classification in Rare Disease 2020 v4.01*. Available at: https://www.acgs.uk.com/quality/best-practice-guidelines/ (accessed April 25, 2022).

Fadda, A., Butt, F., Tomei, S., Deola, S., Lo, B., Robay, A., et al. (2016). Two Hits in One: Whole Genome Sequencing Unveils LIG4 Syndrome and Urofacial Syndrome in a Case Report of a Child with Complex Phenotype. *BMC Med. Genet.* 17, 84. doi:10.1186/s12881-016-0346-7

Gross-Cohen, M., Feld, S., Arvatz, G., Ilan, N., and Vlodavsky, I. (2021a). Elucidating the Consequences of Heparan Sulfate Binding by Heparanase 2. *Front. Oncol.* 10 (10), 627463. doi:10.3389/fonc.2020.627463

Gross-Cohen, M., Yanku, Y., Kessler, O., Barash, U., Boyango, I., Cid-Arregui, A., et al. (2021b). Heparanase 2 (Hpa2) Attenuates Tumor Growth by Inducing Sox2 Expression. *Matrix Biol.* 99, 58–71. doi:10.1016/j.matbio.2021.05.001

Guo, C., Kaneko, S., Sun, Y., Huang, Y., Vlodavsky, I., Li, X., et al. (2015). A Mouse Model of Urofacial Syndrome with Dysfunctional Urination. *Hum. Mol. Genet.* 24, 1991–1999. doi:10.1093/hmg/ddu613

Houweling, A. C., Beaman, G. M., Postma, A. V., Gainous, T. B., Lichtenbelt, K. D., Brancati, F., et al. (2019). Loss-of-function Variants in Myocardin Cause Congenital Megabladder in Humans and Mice. *J. Clin. Invest* 129, 5374–5380. doi:10.1172/jci128545

Jenkins, D., Winyard, P. J. D., and Woolf, A. S. (2007). Immunohistochemical Analysis of Sonic Hedgehog Signalling in Normal Human Urinary Tract Development. *J. Anat.* 211, 620–629. doi:10.1111/j.1469-7580.2007.00808.x

Karczewski, K. J., Francioli, L. C., Tiao, G., Cummings, B. B., Alföldi, J., Wang, Q., et al. (2020). The Mutational Constraint Spectrum Quantified from Variation in 141,456 Humans. *Nature* 581, 434–443. doi:10.1038/s41586-020-2308-7

Keast, J. R., Smith-Anttila, C. J. A., and Osborne, P. B. (2015). Developing a Functional Urinary Bladder: a Neuronal Context. *Front. Cell Dev. Biol.* 3, 53. doi:10.3389/fcell.2015.00053

Lemack, G. E., Baseman, A. G., and Zimmern, P. E. (2002). Voiding Dynamics in Women: a Comparison of Pressure-Flow Studies between Asymptomatic and Incontinent Women. *Urology* 59, 42–46. doi:10.1016/s0090-4295(01)01462-5

Levy-Adam, F., Feld, S., Cohen-Kaplan, V., Shteingauz, A., Gross, M., Arvatz, G., et al. (2010). Heparanase 2 Interacts with Heparan Sulfate with High Affinity and Inhibits Heparanase Activity. *J. Biol. Chem.* 285, 28010–28019. doi:10.1074/jbc.m110.116384

Lopes, F. M., Roberts, N. A., Zeef, L. A., Gardiner, N. J., and Woolf, A. S. (2019). Overactivity or Blockade of Transforming Growth Factor-β Each Generate a Specific Ureter Malformation. *J. Pathol.* 249, 472–484. doi:10.1002/path.5335

Lücking, C. B., Bonifati, V., Periquet, M., Vanacore, N., Brice, A., and Meco, G. (2001). Pseudo-dominant Inheritance and Exon 2 Triplication in a Family with Parkin Gene Mutations. *Neurology* 57, 924–927. doi:10.1212/wnl.57.5.924

Mahmood, S., Beetz, C., Tahir, M., Imran, M., Mumtaz, R., Bassmann, I., et al. (2012). First HPSE2 Missense Mutation in Urofacial Syndrome. *Clin. Genet.* 81, 88–92. doi:10.1111/j.1399-0004.2011.01649.x

Manak, I., Gurney, A. M., McCloskey, K. D., Woolf, A. S., and Roberts, N. A. (2020). Dysfunctional Bladder Neurophysiology in Urofacial Syndrome Hpse2 Mutant Mice. *Neurourol. Urodynamics* 39, 1930–1938. doi:10.1002/nau.24450

Mann, N., Kause, F., Henze, E. K., Gharpure, A., Shril, S., Connaughton, D. M., et al. (2019). CAKUT and Autonomic Dysfunction Caused by Acetylcholine Receptor Mutations. *Am. J. Hum. Genet.* 105, 1286–1293. doi:10.1016/j.ajhg.2019.10.004

McKenzie, E. (2020). Hpa2 Gene Cloning. *Adv. Exp. Med. Biol.* 1221, 787–805. doi:10.1007/978-3-030-34521-1_34

McKenzie, E., Tyson, K., Stamps, A., Smith, P., Turner, P., Barry, R., et al. (2000). Cloning and Expression Profiling of Hpa2, a Novel Mammalian Heparanase Family Member. *Biochem. Biophysical Res. Commun.* 276, 1170–1177. doi:10.1006/bbrc.2000.3586

Newman, W. G., and Woolf, A. S. (2013). "Urofacial Syndrome," in *GeneReviews® [Internet]*. Editors MP Adam, H. H. Ardinger, R. A. Pagon, S. E. Wallace, L. J. H. Bean, K. W. Gripp, et al. (Seattle (WA): University of Washington, Seattle), 1993–2022.

Ochoa, B. (2004). Can a Congenital Dysfunctional Bladder Be Diagnosed from a Smile? the Ochoa Syndrome Updated. *Pediatr. Nephrol.* 19, 6–12. doi:10.1007/s00467-003-1291-1

Osorio, S., Rivillas, N. D., and Martinez, J. A. (2021). Urofacial (Ochoa) Syndrome: A Literature Review. *J. Pediatr. Urology* 17, 246–254. doi:10.1016/j.jpurol.2021.01.017

Pang, J., Zhang, S., Yang, P., Hawkins-Lee, B., Zhong, J., Zhang, Y., et al. (2010). Loss-of-function Mutations in HPSE2 Cause the Autosomal Recessive Urofacial Syndrome. *Am. J. Hum. Genet.* 86, 957–962. doi:10.1016/j.ajhg.2010.04.016

Rentzsch, P., Witten, D., Cooper, G. M., Shendure, J., and Kircher, M. (2019). CADD: Predicting the Deleteriousness of Variants throughout the Human Genome. *Nucleic Acids Res.* 47, D886–D894. doi:10.1093/nar/gky1016

Richards, S., Aziz, N., Bale, S., Bick, D., Das, S., Gastier-Foster, J., et al. (2015). Standards and Guidelines for the Interpretation of Sequence Variants: a Joint Consensus Recommendation of the American College of Medical Genetics and Genomics and the Association for Molecular Pathology. *Genet. Med.* 17, 405–424. doi:10.1038/gim.2015.30

Riggs, E. R., Andersen, E. F., Cherry, A. M., Kantarci, S., Kearney, H., Patel, A., et al. (2020). Technical Standards for the Interpretation and Reporting of Constitutional Copy-Number Variants: a Joint Consensus Recommendation of the American College of Medical Genetics and Genomics (ACMG) and the Clinical Genome Resource (ClinGen). *Genet. Med.* 22, 245–257. doi:10.1038/s41436-019-0686-8

Roberts, N. A., Hilton, E. N., Lopes, F. M., Singh, S., Randles, M. J., Gardiner, N. J., et al. (2019). Lrig2 and Hpse2, Mutated in Urofacial Syndrome, Pattern Nerves in the Urinary Bladder. *Kidney Int.* 95, 1138–1152. doi:10.1016/j.kint.2018.11.040

Roberts, N. A., Hilton, E. N., and Woolf, A. S. (2016). From Gene Discovery to New Biological Mechanisms: Heparanases and Congenital Urinary Bladder Disease. *Nephrol. Dial. Transpl.* 31, 534–540. doi:10.1093/ndt/gfv309

Roberts, N. A., and Woolf, A. S. (2020). Heparanase 2 and Urofacial Syndrome, a Genetic Neuropathy. *Adv. Exp. Med. Biol.* 1221, 807–819. doi:10.1007/978-3-030-34521-1_35

Roberts, N. A., Woolf, A. S., Stuart, H. M., Thuret, R., McKenzie, E. A., Newman, W. G., et al. (2014). Heparanase 2, Mutated in Urofacial Syndrome, Mediates Peripheral Neural Development in Xenopus. *Hum. Mol. Genet.* 23, 4302–4314. doi:10.1093/hmg/ddu147

Robinson, J. T., Thorvaldsdóttir, H., Wenger, A. M., Zehir, A., and Mesirov, J. P. (2017). Variant Review with the Integrative Genomics Viewer. *Cancer Res.* 77, e31–e34. doi:10.1158/0008-5472.can-17-0337

Singleton, A. B., Farrer, M., Johnson, J., Singleton, A., Hague, S., Kachergus, J., et al. (2003). α-Synuclein Locus Triplication Causes Parkinson's Disease. *Science* 302, 841. doi:10.1126/science.1090278

Sinha, R., Banerji, N., and Saha, S. (2018). Recurrent UTI - Make the Child Smile! *Indian Pediatr.* 55, 169. doi:10.1007/s13312-018-1254-z

Stuart, H. M., Roberts, N. A., Burgu, B., Daly, S. B., Urquhart, J. E., Bhaskar, S., et al. (2013). LRIG2 Mutations Cause Urofacial Syndrome. *Am. J. Hum. Genet.* 92, 259–264. doi:10.1016/j.ajhg.2012.12.002

Stuart, H. M., Roberts, N. A., Hilton, E. N., McKenzie, E. A., Daly, S. B., Hadfield, K. D., et al. (2015). Urinary Tract Effects ofHPSE2Mutations. *J. Am. Soc. Nephrol.* 26, 797–804. doi:10.1681/asn.2013090961

Tunyasuvunakool, K., Adler, J., Wu, Z., Green, T., Zielinski, M., Žídek, A., et al. (2021). Highly Accurate Protein Structure Prediction for the Human Proteome. *Nature* 596, 590–596. doi:10.1038/s41586-021-03828-1

van der Ven, A. T., Connaughton, D. M., Ityel, H., Mann, N., Nakayama, M., Chen, J., et al. (2018). Whole-Exome Sequencing Identifies Causative Mutations in Families with Congenital Anomalies of the Kidney and Urinary Tract. *J. Am. Soc. Nephrol.* 29, 2348–2361. doi:10.1681/asn.2017121265

van Erp, S., van den Heuvel, D. M. A., Fujita, Y., Robinson, R. A., Hellemons, A. J. C. G. M., Adolfs, Y., et al. (2015). Lrig2 Negatively Regulates Ectodomain Shedding of Axon Guidance Receptors by ADAM Proteases. *Dev. Cell* 35, 537–552. doi:10.1016/j.devcel.2015.11.008

Vivante, A., Hwang, D.-Y., Kohl, S., Chen, J., Shril, S., Schulz, J., et al. (2017). Exome Sequencing Discerns Syndromes in Patients from Consanguineous Families with Congenital Anomalies of the Kidneys and Urinary Tract. *J. Am. Soc. Nephrol.* 28, 69–75. doi:10.1681/asn.2015080962

Woolf, A. S., Lopes, F. M., Ranjzad, P., and Roberts, N. A. (2019). Congenital Disorders of the Human Urinary Tract: Recent Insights from Genetic and Molecular Studies. *Front. Pediatr.* 7, 136. doi:10.3389/fped.2019.00136

Wu, L., Viola, C. M., Brzozowski, A. M., and Davies, G. J. (2015). Structural Characterization of Human Heparanase Reveals Insights into Substrate Recognition. *Nat. Struct. Mol. Biol.* 22, 1016–1022. doi:10.1038/nsmb.3136

Xiao, Q., Dong, M., Cheng, F., Mao, F., Zong, W., Wu, K., et al. (2018). LRIG2 Promotes the Proliferation and Cell Cycle Progression of Glioblastoma Cells *In Vitro* and *In Vivo* through Enhancing PDGFRβ Signaling. *Int. J. Oncol.* 53, 1069–1082. doi:10.3892/ijo.2018.4482

Conflict of Interest: Author ME was employed by the company Peak Proteins Ltd.

The remaining authors declare that the research was conducted in the absence of any commercial or financial relationships that could be construed as a potential conflict of interest.

Publisher's Note: All claims expressed in this article are solely those of the authors and do not necessarily represent those of their affiliated organizations, or those of the publisher, the editors and the reviewers. Any product that may be evaluated in this article, or claim that may be made by its manufacturer, is not guaranteed or endorsed by the publisher.

frontiers | Frontiers in Physiology

ORIGINAL RESEARCH
published: 01 July 2022
doi: 10.3389/fphys.2022.890102

Myosin 5a in the Urinary Bladder: Localization, Splice Variant Expression, and Functional Role in Neurotransmission

Josephine A. Carew[1,2,3*†], *Vivian Cristofaro*[1,2,3†], *Suhas P. Dasari*[1], *Sean Carey*[1], *Raj K. Goyal*[1,3] *and Maryrose P. Sullivan*[1,2,3]

[1]Urology Research, VA Boston Healthcare System, Boston, MA, United States, [2]Harvard Medical School, Boston, MA, United States, [3]Brigham and Women's Hospital, Boston, MA, United States

Dysregulation of neurotransmission is a feature of several prevalent lower urinary tract conditions, but the mechanisms regulating neurotransmitter release in the bladder are not completely understood. The unconventional motor protein, Myosin 5a, transports neurotransmitter-containing synaptic vesicles along actin fibers towards the varicosity membrane, tethering them at the active zone prior to reception of a nerve impulse. Our previous studies indicated that Myosin 5a is expressed and functionally relevant in the peripheral nerves of visceral organs such as the stomach and the *corpora cavernosa*. However, its potential role in bladder neurotransmission has not previously been investigated. The expression of *Myosin 5a* was examined by quantitative PCR and restriction analyses in bladders from DBA (dilute-brown-nonagouti) mice which express a Myosin 5a splicing defect and in control mice expressing the wild-type *Myosin 5a* allele. Functional differences in contractile responses to intramural nerve stimulation were examined by *ex vivo* isometric tension analysis. Data demonstrated Myosin 5a localized in cholinergic nerve fibers in the bladder and identified several Myosin 5a splice variants in the detrusor. Full-length Myosin 5a transcripts were less abundant and the expression of splice variants was altered in DBA bladders compared to control bladders. Moreover, attenuation of neurally-mediated contractile responses in DBA bladders compared to control bladders indicates that Myosin 5a facilitates excitatory neurotransmission in the bladder. Therefore, the array of Myosin 5a splice variants expressed, and the abundance of each, may be critical parameters for efficient synaptic vesicle transport and neurotransmission in the urinary bladder.

Keywords: bladder smooth muscle, protein splice variants, neurotransmission, myosin motor, peripheral nerve, Myosin 5a

OPEN ACCESS

Edited by:
Russ Chess-Williams, Bond University, Australia

Reviewed by:
Maria Jolanta Redowicz, Nencki Institute of Experimental Biology (PAS), Poland
Nicolas Montalbetti, University of Pittsburgh, United States
Luke Grundy, Flinders University, Australia

***Correspondence:**
Josephine A. Carew
josephine_carew@hms.harvard.edu

†*These authors contributed equally to this work*

Specialty section:
This article was submitted to Integrative Physiology, a section of the journal Frontiers in Physiology

Received: *05 March 2022*
Accepted: *08 June 2022*
Published: *01 July 2022*

Citation:
Carew JA, Cristofaro V, Dasari SP, Carey S, Goyal RK and Sullivan MP (2022) Myosin 5a in the Urinary Bladder: Localization, Splice Variant Expression, and Functional Role in Neurotransmission. Front. Physiol. 13:890102. doi: 10.3389/fphys.2022.890102

INTRODUCTION

The process of micturition provides periodic emptying of the bladder by simultaneous relaxation of the urethral sphincter and strong contraction of the detrusor. The latter is largely a consequence of local release of excitatory neurotransmitters from nerves permeating the detrusor. Within the bladder wall, intramuscular nerve bundles branch repeatedly into single fibers consisting of varicosities and intervaricose segments (Gabella, 1995). From varicosities formed along the

axons, excitatory neurotransmission in the non-primate detrusor is accomplished primarily by exocytosis of the contents of acetylcholine- and ATP-containing synaptic vesicles. These neurotransmitters respectively activate muscarinic and purinergic receptors on bladder smooth muscle cells, inducing contraction. The complex process whereby neurotransmitter-containing vesicles are transported to the active zone in the varicosity membrane of bladder nerves has received little attention to date, although dysregulation of neuromuscular transmission may underpin a number of prevalent disorders of bladder function, including neurogenic, diabetic and obstructive urinary bladder dysfunction. In axons of the central nervous system, where neurotransmission processes have been extensively studied, the directed motion of synaptic vesicles along subcortical actin fibers is facilitated by the motor protein, Myosin 5a (Myo5a). The present study investigated the role of this motor protein in the regulation of excitatory neurotransmission in the bladder.

Myo5a is a processive motor that enables the short-range intracellular transport of molecular cargo along actin filaments. Expressed by many cell types specialized for secretion, Myo5a is a dimer composed of two heavy chains, each consisting of distinct domains that coordinate to carry out its functional roles. The N-terminus contains actin-binding and ATP-hydrolyzing motor regions, followed by a neck (or IQ domain) segment with six binding sites for Myo5a light chains, which include the calcium-sensing protein, calmodulin. The central portion contains the alpha-helical dimerization interface, consisting of three coiled-coil regions. This segment of heavy chain partially overlaps with a region of alternative exons (termed consecutively A, B, C, D, E, and F) which may occur in different spliced arrangements (Seperack et al., 1995; Lambert et al., 1998; Au and Huang, 2002; Wagner et al., 2006). Immediately following the alternate exon region is the C-terminal globular tail domain (GTD), which facilitates direct interactions with cargos to be transported.

The effects of *Myosin 5a* (*Myo5a*) genetic defects are often identified by pigmentation abnormalities, because Myo5a is required for melanosome transport in melanocytes. However, the more devastating consequences of Myo5a deletion or mutation are neurological. Homozygosity for the *Myo5a* null allele is a fatal trait associated with opisthotonus and convulsions leading to death in early infancy, as has been shown in the equine lavender foal, the dilute-opisthotonus and BD-IV rats, and the dilute-lethal mouse (Mercer et al., 1991; Futaki et al., 2000; Brooks et al., 2010; Landrock et al., 2018). In humans, *MYO5a* mutations cause the autosomal recessive disorder, Griscelli syndrome type I, in which hypopigmentation is coupled with cognitive impairment, delayed motor development, and hypotonia (Griscelli et al., 1978; Pastural et al., 1997). Interestingly, a variant of this syndrome was described with abnormal pigmentation as the only sign; the causal mutation was deletion of the segment encoding alternative exon F (Menasche et al., 2003; Yilmaz et al., 2014). Two *Myo5a* mutations that also cause exon F skipping have been characterized among non-lethal strains of dilute mice (Huang et al., 1998). Myo5a lacking exon F cannot bind well to and efficiently transport melanosomes, accounting for abnormal coloration in the absence of severe neurological defects in the affected Griscelli syndrome patients and the two dilute mouse strains. As the latter examples illustrate, not all *Myo5*a defects carry grievous neurological consequences. The homozygous dilute/brown/non-agouti (or DBA) mouse also has a non-lethal defect in *Myo5a* expression, which includes reduced pigmentation but not severe neurologic abnormalities.

The defect in DBA animals results from integration of the ectopic murine leukemia virus, Emv-3, within the intronic region of *Myo5a* between exons C and D, which disrupts normal mRNA splicing. While a fraction of transcripts produced in DBA mice carry exon C aberrantly spliced to the murine leukemia virus sequence and then prematurely truncated, such read-through transcripts are found more frequently in skin where exon C is often spliced to exon D, than in brain where exon C is predominantly spliced to exon E (Seperack et al., 1995). In the brains of DBA mice, the correct neuronal splice variant (ABCE) is expressed almost exclusively, and to an extent that is clearly sufficient to support normal neurological development and brain function.

In contrast to its expression in skin and brain, *Myo5a* expression in the peripheral nervous system has received less study. However, Myo5a has been identified in enteric nerves (Drengk et al., 2000) as well as the peritracheal and peribronchial plexuses (Buttow et al., 2006). Our previous work demonstrated that Myo5a is a constituent of peripheral nerves in the gastric *fundus* and *corpus cavernosum* (Chaudhury et al., 2011, 2012; Chaudhury et al., 2014). With respect to the bladder, Myo5a has been seen in the umbrella cells of the uroepithelium (Khandelwal et al., 2013) as well as in bladder tissue at both mRNA and protein levels, where its expression has been shown to increase then decline in the detrusor during the course of streptozotocin-induced diabetes (Yang et al., 2019). However, no study has examined the particular Myo5a splice variants expressed in bladder or the functional contribution of this motor protein to bladder neurotransmission. We recently demonstrated that multiple Myo5a splice variants exist in nerves of the myenteric plexus, embedded between the gastric longitudinal and circular muscle layers, as well as in their axons which course throughout the smooth muscle (Carew et al., 2021). The repertoire of Myo5a splice variants and their relative amounts in bladder nerves are likely to be adapted to the particular demands for molecular cargo transport that are relevant to neurotransmission in this organ. Therefore, in the present work we first analyzed expression of Myo5a splice variants, and then exploited the Myo5a deficiency of the DBA mouse to correlate the molecular characteristics of bladder Myo5a with the extent of excitatory neurotransmitter release from bladder varicosities, as reflected by detrusor contractile patterns.

MATERIALS AND METHODS

Animals

All animal procedures were approved by the Institutional Animal Care and Use Committee of the VA Boston Healthcare System.

Age-matched male C57/BL6 (RRID:IMSR_JAX:000664) and DBA/2J (RRID:IMSR_JAX:000671) mice were obtained from Jackson Labs (Bar Harbor, ME, United States). Following euthanasia by CO_2 asphyxiation, urinary bladders intended for *ex vivo* functional studies were quickly removed and placed in cold Kreb's solution (NaCl 120mM; KCl 5.9mM; $NaHCO_3$ 25mM; $Na_2H_3PO_4$ 1.2mM; $MgCl_2 \bullet 6H_2O$ 1.2mM; $CaCl_2$ 2.5mM; dextrose 11.5 mM). The base of the bladder was removed and the mucosa was separated from the detrusor by sharp and blunt dissection under a stereomicroscope. Samples of the detrusor (*muscularis propria*) intended for mRNA analyses were stabilized by immediate immersion in RNA-later solution (Sigma-Aldrich, St Louis, MO, United States), while those intended for protein analyses were snap-frozen and stored at −80°C until extraction. In addition, the cortical region of the brain, a portion of skin, and the bladder mucosa were obtained from each animal, stabilized in RNA-later or snap-frozen, then analyzed in some aspects of this study. Bladder tissue with intact mucosa to be used for histology was fixed in Bouin's solution (7 h, room temperature) and embedded in paraffin. Tissue intended for confocal microscopy was embedded in OCT compound and immediately snap frozen.

Histology

Full thickness bladder tissue sections from WT ($N = 3$) and DBA ($N = 3$) mice were cut on a microtome and processed with hematoxylin and eosin (H&E) or Masson's Trichrome (MT) stains according to standard procedures, which were performed at the Rodent Histopathology (DF/HCC) Core, Harvard Medical School. In tissue sections stained with MT, images were acquired from at least 6 regions of separate sections from each bladder from each strain and the areas of collagen and smooth muscle were determined by ImageJ software. The ratio of collagen to smooth muscle was compared between WT and DBA bladders.

Antibodies

Antibody to Myo5a was obtained from Sigma-Aldrich (St Louis, MO, United States; M4812-LF18, RRID:AB_260545, referred to as LF18). LF18 does not recognize a Myo5a target in the S91 cell line, which was derived from melanocytes of a Myo5a-null mouse (Seperack et al., 1995), although it does recognize a target protein present in normal melanocytes and in HeLa cells, which is diminished in the presence of Myo5a-targeting siRNAs (Lindsay and McCaffrey, 2011). Antibodies to the internal control protein, β-actin (sc-47778, RRID:AB_2714189), to the muscarinic M_3 and M_1 receptors (M_3R, sc-9108, RRID: AB_2291779; M_1R, sc-365966, RRID:AB_10847359), to vesicular acetylcholine transporter (VAChT, sc-7716; RRID: AB_2188145), to the urothelial marker Uroplakin-3 (UPIIIa, sc-166808, RRID:AB_2241422), and to the smooth muscle marker myosin heavy chain (Myh11, sc-98705, RRID: AB_2282267) were obtained from Santa Cruz Biotechnology, Santa Cruz CA, United States). Antibodies to the neural markers synaptophysin (ab72242, RRID:AB_1271107) and peripherin were from Abcam (Cambridge, MA, United States) and Chemicon International (AB1530, RRID: AB_90725). The $P2X_1$ purinergic receptor ($P2X_1$R) antibody (APR-001, RRID: AB_2040052) was from Alomone Labs (Jerusalem, Israel). Horseradish peroxidase (HRP)-conjugated secondary antibodies for Western blotting were obtained from Santa Cruz (sc-2357, RRID:AB_2687626; sc-2357,RRID:AB_628497; sc-2354, RRID:AB_628490), while AlexaFluor-conjugated secondary antibodies for confocal microscopy were from Thermo-Fisher Scientific (Waltham, MA, United States: A11011, RRID:AB_143157; A21202, RRID:AB_141607; A21467, RRID:AB_10055703).

Laser Scanning Confocal Microscopy

Full thickness WT bladder sections were cut on a cryostat (10–12 µm) and fixed with cold acetone for 10 min. After rinsing in phosphate buffered saline (PBS), sections were blocked with 5% donkey serum and 0.05% triton X-100 in PBS for an hour, then incubated overnight with rabbit primary antibody against Myo5a (1:500 dilution.) After extensive washing in PBS, sections were incubated with fluorescent secondary antibody diluted in PBS for 2 h at room temperature. Sections were double labeled with either mouse anti-synaptophysin (1:10) or goat anti-VAChT antibody (1:200) followed by anti-mouse or anti-goat AlexaFluor 488 (1:2000), respectively. Secondary antibodies were affinity-purified to reduce cross reactivity with endogenous or off-target species of immunoglobulins. On other tissue sections, Alexa Fluor 488 conjugated-UPIIIa (1:250) was used to mark the urothelial layer. Control slides in which the primary antibodies were omitted from preparations were processed in parallel. Sections were mounted using Fluoromount-G (Southern Biotech, Birmingham, AL, United States) and examined by confocal microscopy (Zeiss, LSM 710). For image acquisition of double-labelled tissue, slides were scanned separately at each excitation wavelength to minimize emission crosstalk.

RNA Extraction and Analyses

Total RNA purification was carried out using the Qiagen RNeasy Plus Mini kit according to the manufacturer's directions. Tissues were disrupted in buffer RLT plus ß-mercaptoethanol using the Tissue Lyser II mill-bead apparatus (Qiagen, Gaithersburg, MD, United States) by two cycles of 2 minutes each at 30 Hz with a 5 mm stainless steel bead. RNA concentration and purity were determined by ultraviolet spectrophotometry.

To prepare total RNA for reverse-transcriptase realtime PCR (RT-PCR), 100 ng aliquots were converted to cDNA using the High-capacity RNA to cDNA kit and random octamer primers. The cDNA was then tested with universal PCR mastermix and TaqMan primer/probe sets Mm00487823_m1, Mm01146036_m1, Mm01170524_m1 and Mm01146042_m1 which detect, respectively, the N-terminal motor domain, exon B, exon F, and the C-terminal globular tail domain of murine Myo5a. All reagents were from Thermo-Fisher Scientific (Waltham, MA, United States). RT-PCR was performed on an Applied Biosystems QuantStudio 6 Flex under a standard protocol of 40 amplification cycles of 15 s at 94°C and 60 s at 60°C. Each cDNA sample was assayed in triplicate for the primer/probe sets, and normalized using an internal control reaction

TABLE 1 | Primers used for Myo5a PCR.

Primer pair	Forward (5′-3′)	Reverse (5′-3′)
1	GCAGAAACTGAAGACATTGCAC	TCAGATTGACAGCCACACCA
2	ACTAGAGTATGAGTCTCTCAAGCG	TCAGATTGACAGCCACACCA
3	ACTAGAGTATGAGTCTCTCAAGCG	TCAGCCGGGTGATCTCATGCTGCAGG
4	ACTAGAGTATGAGTCTCTCAAGCG	TGATACTTCTTAGGGTCATCGC

measuring 18S RNA. No-template controls were performed for each assay, and the results were analyzed by the ΔΔCt method for comparative gene expression.

For standard PCR, cDNA was prepared from 100 ng total RNA using an oligo-dT primer and the Superscript IV (VILO) kit (Thermo-Fisher Scientific). cDNA aliquots were used as templates for PCR using a forward primer within Myo5a exon A and reverse primer within the GTD. Products from this initial PCR with primer pair 1 (see **Table 1** for sequences) were purified with the Qia-quick PCR-purification kit (Qiagen), then used as templates for nested PCR with internal primers (pairs 2, 3 and 4. **Table 1**). Twenty-five cycles of PCR under standard conditions were performed in an Eppendorf thermal cycler (Hauppauge, NY, United States) using the Taq PCR mastermix (Qiagen). PCR products were assessed in comparison to mass standards before and/or after digestion with restriction enzymes (Sty I or Ban II, New England Biolabs, Ipswich, MA, United States), by electrophoresis in Tris/acetate/EDTA buffer, on 2% MetaPhor agarose gels (Lonza, Rockland, ME United States) containing fluorescent Sybr-green dye. Gels were imaged using an Amersham Imager 600 (General Electric, Pittsburgh, PA, United States). The fluorescence intensity of each band was measured and corrected for fragment size, then the percent of fluorescent signal present in each band was calculated for each lane, and the averages for WT and DBA detrusors were determined.

Protein Extraction and Western Blotting

Tissues were homogenized in RIPA buffer (Santa Cruz Biotechnology) supplemented with protease- and phosphatase-inhibitor cocktails (Sigma Aldrich), using the Tissue Lyser II apparatus by two cycles of 3 minutes each at 30 Hz with a stainless-steel bead. Following centrifugation to remove insoluble materials, total protein concentration was determined with the bicinchoninic acid protein assay (Sigma Aldrich) by measuring the absorbance at 280 nm with a biophotometer (Eppendorf). Samples of equivalent protein concentration were directly compared by electrophoresis, which was performed on Nu-PAGE (either 3–8% Tris-acetate or 4–12% Bis-Tris gels) followed by transfer to nitrocellulose membranes using the iBlot II semi-dry apparatus (Thermo-Fisher Scientific). To prevent non-specific antibody binding, blots were blocked in Tris-buffered saline plus 0.05% Tween-20 with 5% dry milk. Membranes were incubated overnight at 4°C with primary antibodies, then after extensive washing were incubated for 1 h at room temperature with HRP-conjugated secondary antibodies. After further washing, protein bands were developed on the membranes with Western-Lightening ECL reagents (Perkin-Elmer, Waltham, MA), and visualized using the Amersham Imager 600.

Functional Analyses

After the bladder base and mucosa were removed, bladder smooth muscle tissue from each WT and DBA mouse was cut into longitudinal strips and mounted for isometric tension analysis, as described previously (Cristofaro et al., 2012). Briefly, each strip was connected to a force transducer (Grass Instruments, Middleton, WI, United States) on one end and to a fixed hook on the other end. Tissue was mounted between platinum electrodes in organ baths containing Krebs's solution maintained at 37°C and bubbled with a mixture of 95% O_2 and 5% CO_2. Bladder tissue was stretched to passive tension of 0.5 g and equilibrated for at least an hour. Data was acquired at 40 Hz by DataQ data acquisition system driven by WinDaq software.

Neurally-mediated contractions were induced by electrical field stimulation (EFS) over a range of frequencies (1–64 Hz, 40 V, 0.5 ms pulse width, 10 s duration). Features of the resulting contractions were defined by the following parameters: maximum amplitude, area under the curve (AUC), slope (the first derivative of the rising phase, dF/dT), time to peak (interval between start of contraction and peak force), as well as tau (time constant of a decaying exponential fit to the descending phase of the contraction below 50% of the peak). EFS-induced contractions were repeated after cholinergic or purinergic inhibition. The cholinergic component of the contraction was inhibited with the muscarinic receptor antagonist atropine (1 μM) by pre-incubating the tissue for 30 min. To inhibit the purinergic component of the contraction, tissue was pre-incubated for 30 min with the selective purinergic receptor antagonists, NF449 (50 μM) and 5-BDBD (50 μM). The contractile responses to KCl (120 mM), α-β-methyl-ATP (10 μM) and carbachol (CCh, 10 μM), were also measured in each bladder strip. In some experiments, contractile responses to CCh were repeated in the presence of muscarinic M_1 receptor antagonist, pirenzepine (0.1 μM). At the end of each experiment, the weight and length of each tissue strip was measured after blotting excess liquid on filter paper. Active stress was calculated as the measured force/cross-sectional area. NF449, 5-BDBD, CCh, α-β-methyl-ATP, atropine and pirenzepine were purchased from Sigma and Tocris (Minneapolis, MN, United States).

Data Analysis

Differences between WT and DBA in band intensity on western blots, fold change in gene expression, or contractile responses were determined by Student's *t*-test after testing for normality

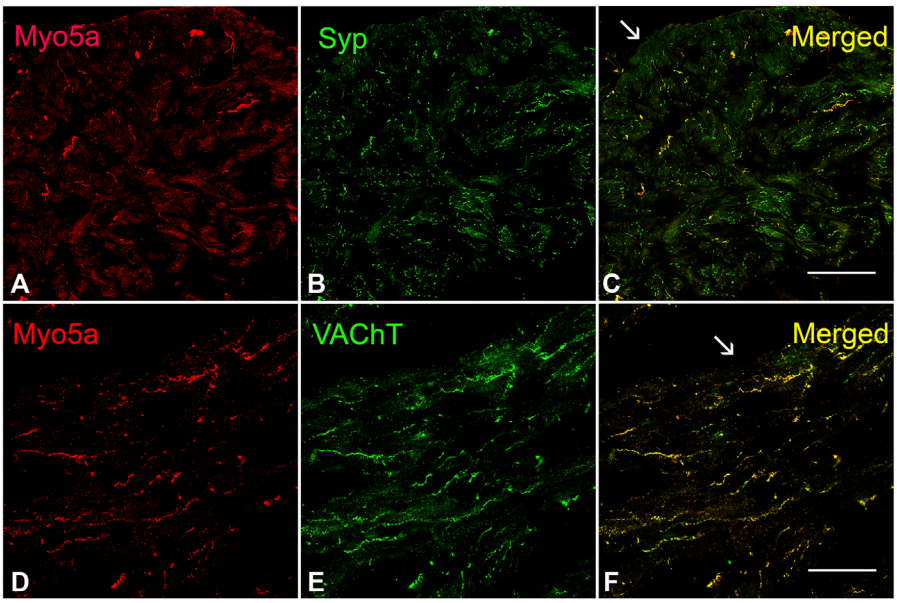

FIGURE 1 | Expression of Myo5a in bladder tissue. **(A–C)** Laser scanning confocal microscopy of sections from WT detrusor detected Myo5a immunoreactivity (red staining) on nerve fibers that were immunoreactive for the pan-neuronal marker synaptophysin (Syp, green staining). The merged image on the right shows co-localization of these markers in yellow. **(D–F)** Immunoreactivity for Myo5a (red staining) and vesicular acetylcholine transporter (VAChT, green staining) in WT bladder *muscularis*. Co-localization of these two proteins in the merged panel (yellow) indicates expression of Myo5a in cholinergic fibers of the urinary bladder. Arrows indicate serosa. (Scale bar = 50 μm; Mag ×40).

and equal variance. If these assumptions were not met, a Mann-Whiney *U* test or a Welch's *t*-test, respectively was used. Differences in EFS responses between groups before and after antagonists were analyzed by a repeated measures two-way ANOVA followed by Holm-Sidak test for multiple comparison. Data are presented as mean ± SEM, and $p < 0.05$ were considered significant.

RESULTS

The animal strains used for these studies, C57/BL6 (homozygous, expressing the wild-type *Myo5a* allele, and referred to as WT) and DBA/2J (homozygous, expressing a mutated *Myo5a* allele, and referred to as DBA) were closely matched in general characteristics. The mean age of WT animals was 20.2 ± 1.7 weeks old, which was not significantly different from that of DBA animals (21.8 ± 1.7 weeks old). In addition, the average body weight (30.38 ± 1.03 g) and bladder weight (0.0280 ± 0.009 g) of WT animals were not different from the average body weight (30.03 ± 0.88 g) and bladder weight (0.0296 ± 0.002 g) of DBA animals.

Myo5a is Expressed in the Bladder and Localized on Intramural Nerve Fibers

The presence of Myo5a protein in the WT bladder, examined by confocal microscopy, was indicated by abundant immunoreactivity for Myo5a distributed throughout the bladder wall. As demonstrated by the co-localization of Myo5a staining with immunoreactivity for the varicosity marker, synaptophysin (Syp), as well as with the specific cholinergic varicosity marker, vesicular acetylcholine transporter (VAChT), Myo5a expressed in the detrusor layer was predominantly localized in cholinergic nerve fibers (**Figure 1**). No immunofluorescence was detected in negative controls (**Supplementary Figure S1**). Positive immunoreactivity for Myo5a was also detected within the urothelial and sub-urothelial layers (**Supplementary Figure S2**).

To address whether the *Myo5a* gene was expressed to the same extent in DBA as in WT bladders, the relative levels of Myo5a mRNA and protein were determined in those tissues by RT-PCR and immunoblotting, respectively. The relative regions of the Myo5a transcript sequence identified by two Taq-Man assays are widely separated and common to all potential full-length splice variants, as shown in **Figure 2**. The pan-Myo5a N-terminal assay spans the border between exons 8-9 within the region encoding the motor domain, while the pan-Myo5a GTD assay spans the border between exons 33–34 within the GTD. As shown in **Figure 3A**, *Myo5a* expression measured with the N-terminal assay was significantly higher in DBA detrusor compared to WT detrusor. Inversely, the level of expression measured with the GTD assay was significantly lower in DBA bladder than in WT bladder. However, *Myo5a* expression in WT versus DBA brains measured with the N-terminal assay was not different. Taken together, these data suggested reduced full-length Myo5a transcripts, despite increased transcriptional initiation in DBA detrusor compared to WT detrusor.

Anticipating that expression of Myo5a protein would be similarly decreased in DBA compared to WT detrusors,

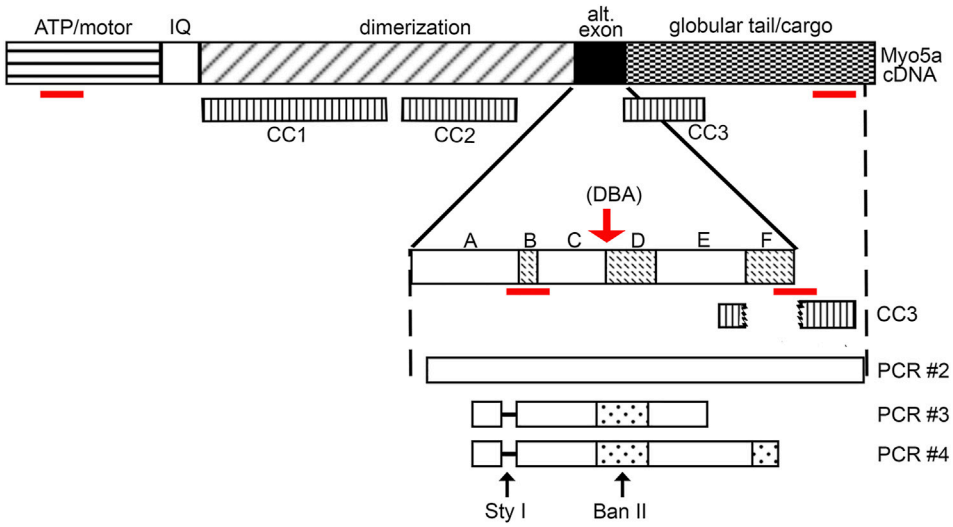

FIGURE 2 | Myo5a schematic. Schematic of Myo5a mRNA/cDNA, depicting regions encoding the major structural domains of the Myo5a protein monomer: the ATP hydrolyzing/actin binding motor domain, the light-chain binding IQ domain, the central dimerization domain, the alternative exon domain, and the globular tail/cargo binding domain. Three coiled-coil regions (CC1, CC2, and CC3) have been described and are shown in the second line; CC1 and CC2 are within the dimerization domain, while CC3 is intact only in variants that do not contain exon F (such as the predominant brain form of Myo5a, ABCE), since it includes part of exon E sequence and part of globular tail domain sequence. CC3 is bisected by exon F, if present. Alternative exons are shown in the expansion; sequence encoding the constitutive exons A, C and E and the optional exons B, D and F are indicated by solid and speckled patterns, respectively. The red arrow indicates the position of the molecular defect in the *Myo5a* gene in the DBA mouse, which impairs mRNA splicing. Below, the products of detrusor nested PCR reactions are shown, as are the locations of restriction enzyme cleavage sites. The absence of exon B (and its diagnostic Sty I restriction site) in detrusor nested PCR products is indicated by the dashed line. The red lines indicate the positions of the RT-PCR assays employed.

immunoblotting was performed with the same antibody used for Myo5a detection in **Figure 1**. The epitope for antibody LF-18 is residues 1782–1799 within the GTD, which is present in all Myo5a splice variants. In tissue lysates from both WT and DBA detrusor, a protein band of electrophoretic mobility consistent with the predicted Myo5a molecular weight (~200 kDa) was detected. Because alternative exons B, D, and F are small (3, 27, and 25 amino acids respectively, compared to 1850 amino acids for Myo5a without these exons), it was expected that different variant proteins would be difficult to resolve from one another by gel electrophoresis. However, and in contrast to the Myo5a mRNA expression findings, Myo5a protein band intensities were not different between WT and DBA detrusors (**Figure 3B**). The reason for this result is not known, but was somewhat surprising, since the RT-PCR results of **Figure 3A** had implied that, in DBA detrusor, a significant fraction of Myo5a transcripts likely contained exon C incorrectly spliced to the ectopic Emv-3 sequence rather than to exon D or exon E, producing incomplete transcripts which could not be translated into a functional protein.

Expresssion of Myo5a Exons D and F in Bladder Varies by Genotype

Intriguingly, the discrepancy between WT and DBA detrusors, but not brains, with regard to total Myo5a measured by the N-terminal pan-Myo5a assay, also implied that non-brain Myo5a splice variants were expressed among the full-length Myo5a transcripts of bladder nerves. To examine detrusor Myo5a for the presence of alternative exons B, D and F, additional RT-PCR, as well as standard PCR experiments (schematized in **Figure 2**), were carried out.

The relative expression of Myo5a mRNA in WT versus DBA detrusor was compared using TaqMan assays targeted within the alternative exon region of the Myo5a transcript. One assay employed spans exon B while the second is directed against the exon F/GTD junction. Because these assays positively identify the hallmark exons of "brain" (exon B) and "skin" (exon F) among Myo5a transcripts, samples from skin and brain were concurrently assessed as controls for detrusor. (Data obtained in parallel for bladder mucosa are presented in **Supplementary Figure S2**)

The results, shown in **Figure 4**, corroborate several key conclusions that have previously been established. Brain Myo5a mRNA overwhelmingly included exon B, and exon B expression was comparable in the brains of WT and DBA animals. Also, exon B was undetectable in skin, while exon F-containing variants were abundant in WT skin, but significantly reduced in DBA skin. However, the data also illustrated several unexpected features of Myo5a expression in the detrusor. First, exon B was not detected in bladder of either WT or DBA animals (**Figure 4A**). In contrast, exon F expression was seen in all WT tissues examined, including the brain (albeit at low levels). Furthermore, in comparison to the corresponding WT tissue, DBA detrusor evinced significantly reduced exon F expression (**Figure 4B**).

The hypothesis that DBA bladder was deficient in the larger Myo5a splice variants was also investigated by standard PCR and

restriction enzyme analysis, a method which confers two advantages. First, it allows direct demonstration of the presence/absence of exon D (for which no RT-PCR reagents are available) and second, it permits amplification of fragments large enough to encompass multiple alternative exons, so that their linear arrangements can be discerned. Inspection of the sequence of murine Myo5a indicated that there are, within the common exons (A, C and E), a single consensus sequence apiece for restriction enzymes Sty I and Ban II (**Figure 2**). The nucleotide sequences encoding the alternative exons revealed that exon B introduces a second consensus Sty I site, while exon D introduces a second Ban II site. The susceptibility of PCR products to digestion and the relative sizes of the fragments generated with these enzymes (see **Table 2**) thus indicate compositions and linear arrangements of alternative exons in Myo5a bladder transcripts.

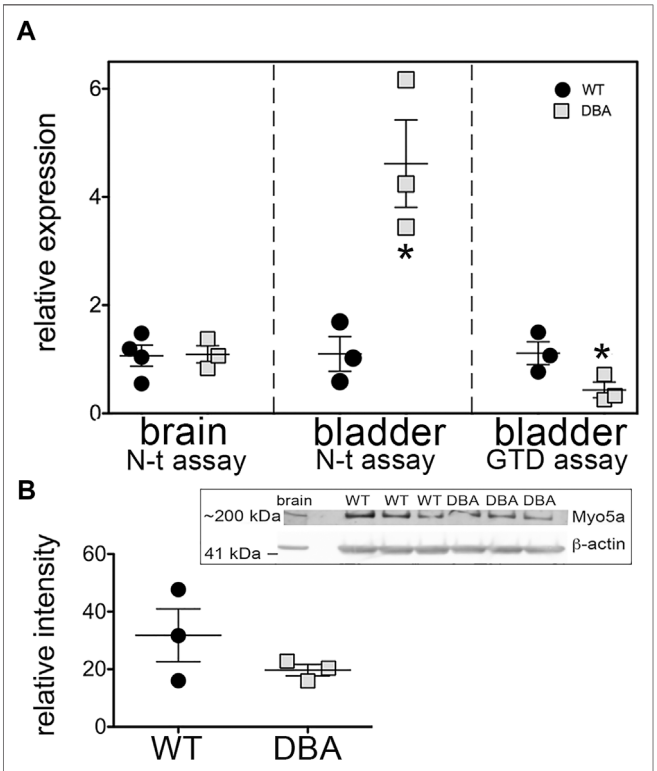

FIGURE 3 | Overall Myo5a expression in bladder. **(A)** cDNA from brains and detrusors of WT (black circles, $N = 3$) and DBA animals (gray squares, $N = 3$) was assayed in triplicate for the two different pan-Myo5a RT-PCR primer/probe sets indicated, and for 18S rRNA as internal control. Expression was determined by the ΔΔCt method and graphed relative to WT within each organ. Comparison of WT vs. DBA brain was not significant ($p = 0.67$), but of WT vs. DBA detrusor was significantly higher for the N-terminal (N-t) assay and lower for the globular tail domain (GTD) assay (*$p < 0.05$). **(B)** Representative immunoblot (inset box) and quantitative graph showing the expression of Myo5a protein in lysates from WT (black circles, $N = 3$) and DBA detrusors (gray circles, $N = 3$). 30 µg aliquots of detrusor extracts were immunoblotted with Myo5a antibody (LF-18). Brain extract was loaded in lane 1 as a positive control. When intensities of the ~200 kDa Myo5a band were corrected for intensities of the 42 kDa ß-actin loading control, WT and DBA Myo5a protein levels were not significantly different ($p = 0.4$).

Primer pair 2 is predicted to generate nested PCR fragments spanning the entire alternate exon region, and ranging in size between 824 base pairs (bp) (for ACE, the smallest possible product) and 989 bp (for ABCDEF, the largest possible product). **Figure 5A** depicts the nested PCR products obtained from brain and detrusor cDNAs of a WT and of a DBA animal using this primer pair, as well as their restriction digestion patterns. The masses of the predominant WT and DBA brain products were identical. Since exon B is only 9 bp long, its presence cannot be inferred from uncut fragment mass alone. However, the brain product was cleaved by Sty I into fragment sizes indicative of exon B inclusion. When brain PCR products were digested with Ban II, no digestion product suggesting the

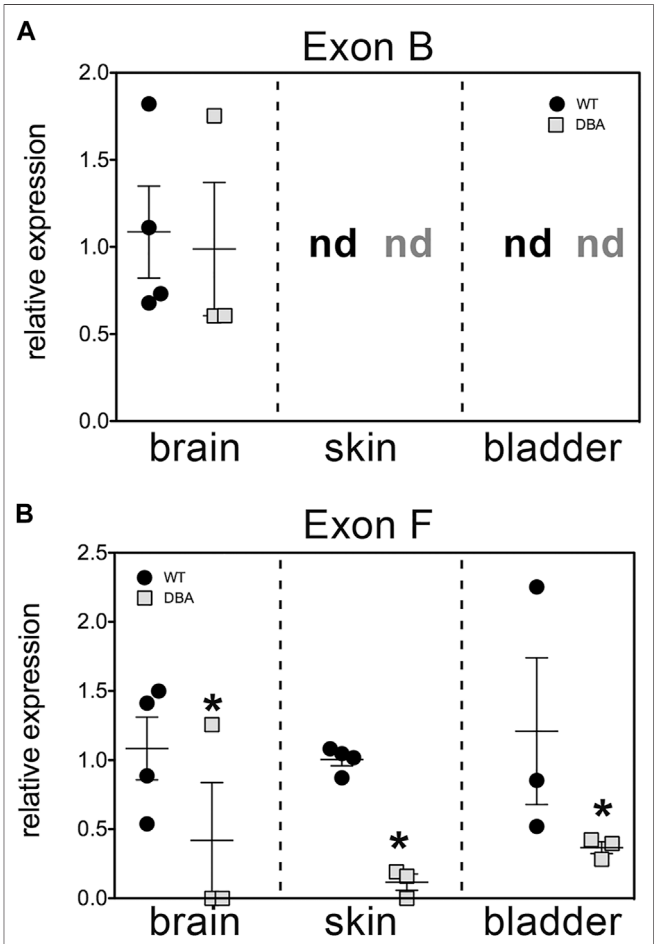

FIGURE 4 | Relative expression of variant exons in WT and DBA tissues. cDNAs made from total RNA of brain, skin and detrusor of WT animals (black circles, $N = 4$) and DBA animals (gray squares, $N = 3$) were assayed in triplicate for Myo5a exon B or for exon F with their specific TaqMan assays, and for 18S rRNA as an internal control. Expression was determined by the ΔΔCt method and graphed relative to WT within each tissue. Horizontal line indicates average relative expression ±SEM. **(A)** Expression of exon B in brain was not different in DBA compared to WT ($p = 0.67$). In detrusor and skin, exon B was not detected (nd) and therefore differences between strains could not be determined. **(B)** Expression of exon F was lower in DBA brain, skin and detrusor (*$p < 0.05$) than in corresponding WT tissues.

TABLE 2 | Nested PCR products and digestion fragments.

Primer Pair	Exons	Uncut (bp)	Sty I (bp) exon B	Ban II (bp) exon F
2	+B + D + F	989	**246**, 649, 94	177, **228, 584**
	+B + D – F	914	**246**, 674, 94	177, **228, 509**
	+B – D + F	908	**246**, 568, 94	177, **656**
	+B – D – F	833	**246**, 493, 94	177, **731**
	–B + D + F	980	**886**, 94	177, **219, 584**
	–B + D – F	905	**811**,94	177, **219, 509**
	–B – D + F	899	**805**, 94	177, **722**
	–B – D – F	824	**730**, 94	177, **647**
3	–B + D	421	421	**200/221**
	–B – D	340	340	340
4	–B + D + F	475	475	**200/275**
	–B – D + F	394	394	394

PCR products generated using primer pairs 2—4 for the potential alternative exon sequence arrangements shown in the second column are given in base pairs (bp). Digestion of these products with restriction enzyme Sty I or Ban II, is predicted to generate fragments of the sizes shown. Digestion fragments which are common to digestion of all potential sequences are depicted in regular type; those which confirm the presence or absence of exon B or exon D in each context are shown in bold type. For PCR with primers pairs 3 and 4, sequences with exon B were not considered, since it is not detectable in detrusor.

presence of exon D or exon F was recovered, confirming their assignment as the expected arrangement, ABCE.

The same nested PCR performed on the WT and DBA detrusors presented a more complex pattern, with each genotype having at least two products giving rise to a mixture of digestion fragments. Confirming the RT-PCR results, Sty I digestion did not generate the 246 bp fragment diagnostic for exon B, which had been obvious in the digested brain PCR samples. In contrast, Ban II digestions were distinct according to strain. In the Ban II digest from WT detrusor, fragments suggesting arrangements ACDEF and ACDE among the initial products were evident. An approximately 250 bp fragment was identified, independently confirming inclusion of exon D in some WT detrusor products. However, the latter fragment was not visible in the Ban II digest of DBA detrusor products, where instead there was a prominent digestion fragment of approximately 750 base pairs, suggesting the presence of ACEF in the initial mixture (**Figure 5A**).

Exclusion of exon B from detrusor Myo5a, coupled with inclusion of exons D and F, suggested that the splice variants of bladder nerve Myo5a more closely resembled the pattern of skin than of brain. To explore this possibility, skin and brain from a second WT and DBA animal pair were used for nested PCR with primer pair 2, digested with Ban II, and compared to detrusor products by agarose gel electrophoresis (**Figure 5B**). Again, the brain digestion patterns indicated a single predominant product, consistent with arrangement ABCE. The WT detrusor digestion pattern indicated ample amounts of arrangements ACDE and ACDEF, while the DBA detrusor pattern indicated predominantly ACE with minor contributions from ACEF and ACDE. The WT skin pattern suggested that there was a predominant splice variant in this particular sample, and Ban II digestion identified it as ACDE, although fragments indicative of ACDEF and ACEF were also detected. Products from the DBA skin sample were digested by Ban II into fragments indicating that ACE was the most abundant variant amplified, with lesser amounts of ACEF, ACDE and ACDEF. Thus, Ban II digestion confirmed that Myo5a of WT skin included exons D and F, while DBA skin was deficient.

To more rigorously interrogate multiple detrusor cDNA samples for inclusion of exon D, nested PCR was also done with primer pair 3 (**Figure 6A**), in which the forward primer is situated near the 3' side of exon A and the reverse primer within exon E. Given the location of the primers, only two fragments were possible, differing in mass by the 81 bp encoding exon D. The amount of each fragment was quantitated as a fluorescent signal, corrected for fragment size, and compared to the other independent samples across the gel. Both the minus-exon D and plus-exon D products were observed in WT detrusor samples, but the plus-exon D product was significantly greater in WT compared to DBA detrusor (**Figure 6B**). Consequently, the minus-exon D product predominated in DBA detrusor samples.

The presence of exon D in PCR products that also included exon F was examined by nested PCR with primer pair 4, in which the forward primer sequence was again located within exon A but the reverse primer sequence was entirely within exon F (**Figure 6C**). In this reaction also, only two PCR products were possible, differing in undigested mass depending on the inclusion of exon D, which introduces a cleavage site for restriction enzyme Ban II. Cleavage of the larger, exon D-containing product generated a pair of smaller bands. The results indicated that in both WT and DBA detrusors, exon F was found predominantly in a linear arrangement with exon D. However, the proportion of the PCR product including both exons D and F was greater in WT detrusor (~86%) than in DBA detrusor (~62%), and this difference was significant (**Figure 6D**).

Intrinsic Contractile Properties are Comparable in WT and DBA Detrusors

The histological features observed by H&E staining of bladder sections were comparable between WT and DBA mice. Tissue architecture, consisting of a distinct luminal epithelium, a collagen-rich lamina propria, and an outer layer of smooth

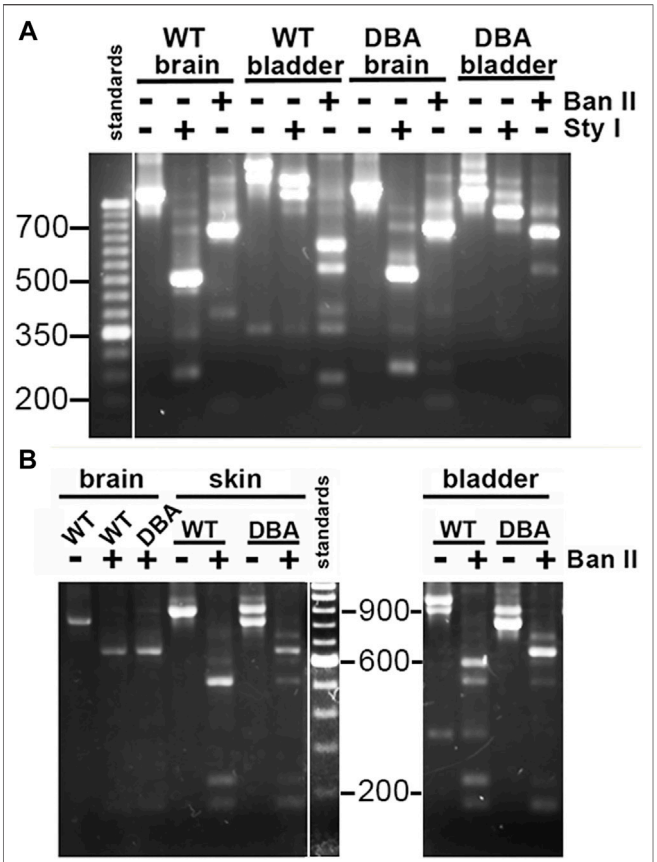

FIGURE 5 | Myo5a splice variants in tissues of WT and DBA mice. **(A)** Illustration of differential Myo5a variant expression pattern in detrusor and brain from WT and DBA mice. Nested PCR fragments of brain and detrusor cDNAs from a WT and a DBA mouse pair were prepared with primer pair 2, then compared by agarose gel electrophoresis either undigested or digested with Sty I or Ban II, as shown above the lanes. A 50 base pair (bp) ladder with weighted 350 bp standard is at left. Contrast was adjusted separately for the standard lane, to bring out the positions of the smaller standards. **(B)** Nested PCR fragments prepared from brain, skin, and detrusor of a WT and DBA mouse with primer pair 2, were compared before and after digestion with Ban II. A100 bp ladder with weighted 600 bp standard is shown and contrast was adjusted separately. All lanes were from a single gel; those for detrusor PCRs and digests were moved to the right, so that sizes of the standard fragments could be added.

muscle bundles appeared to be normal in DBA bladders (**Figure 7A**). Additionally, the ratio of collagen to smooth muscle area, determined by quantification of MT images, was not different between strains (**Figures 7B,C**). The expression of the smooth muscle marker, myosin heavy chain (Myh11), was not different between WT and DBA detrusors (**Figures 7D,E**). These findings confirm the absence of morphological abnormalities in DBA bladder such as fibrosis, hypertrophy, or contractile protein deficits that could negatively alter smooth muscle responses. The functional integrity of the intrinsic contractile machinery of DBA bladder smooth muscle was established by measuring isometric tension in response to a high potassium Kreb's solution (HPK, 120 mM KCl). The amplitudes of contractions induced by HPK were not different between WT and DBA mice (**Figure 7F**).

Contractile Responses to Nerve Stimulation are Impaired in DBA Mice

Functional studies were performed to determine whether differences in Myo5a variant expression were associated with differences in neuromuscular transmission between WT and DBA detrusors. To determine whether the extent of detrusor innervation was comparable between strains, the expression of the nerve marker, peripherin (an intermediate neurofilament protein), was determined by Western blot. No difference in immunoreactivity for peripherin was detected in WT and DBA detrusor lysates (**Figure 8A**). Frequency-dependent force generation in response to EFS-induced nerve stimulation was detected in both WT and DBA detrusors (**Figure 8B**). However, the contractile responses to EFS in DBA detrusors were significantly lower in amplitude at all stimulation frequencies, and in AUC at frequencies of stimulation below 64Hz, compared to WT detrusors (**Figures 8C,D**). In addition, compared to WT, the frequency response curves in DBA detrusors were characterized by reduced rate of rise, longer time to peak (significant at 8–32 Hz), as well as slower rate of decay (significant at 16–64 Hz), (**Figures 8E–G**).

After inhibition of the purinergic component of the neurogenic contractions, the amplitude of EFS responses was significantly decreased in both WT and DBA detrusors compared to baseline responses (**Figures 9A,B**). The effect of purinergic inhibition was frequency dependent in DBA detrusor tissue, but not in WT tissue. In DBA detrusors, the extent of inhibition was significantly less than that seen in WT detrusors at frequencies greater than 8 Hz (**Figure 9C**).

Inhibition of the cholinergic component decreased the amplitude of EFS responses in both WT and DBA bladder tissues compared to their respective baseline responses (**Figures 9D,E**). The effect of atropine generally increased with higher frequencies in both groups. At frequencies below 16 Hz in DBA tissue, the cholinergic component was significantly lower than that of WT tissue (**Figure 9F**).

To assess the capacity of WT and DBA detrusor smooth muscle to respond to purinergic stimulation, the amplitude of contractions induced by exogenous administration of the $P2X_1R$ agonist, αβ-meATP, was measured. No significant difference in the responses of WT and DBA bladders was observed (**Figure 10A**); furthermore, expression of the predominant purinergic receptor, $P2X_1R$, was comparable in WT and DBA detrusor lysates (**Figures 10B,C**). These data indicate that smooth muscle contractions mediated by post-junctional purinergic activation are normal in DBA detrusor.

While contractions induced in response to administration of the cholinergic agonist CCh were significantly lower in DBA detrusors than WT detrusors (**Figure 11A**), expression of the M_3R was not different (**Figures 11B,C**). To resolve these divergent findings, responses to CCh were repeated in the presence of pirenzepine, a selective inhibitor of the muscarinic M_1R. This receptor is expressed in bladder nerve fibers where it facilitates pre-junctional release of acetylcholine (Somogyi et al., 1994; Chess-Williams, 2002). In WT detrusors, the amplitude of the CCh response decreased significantly

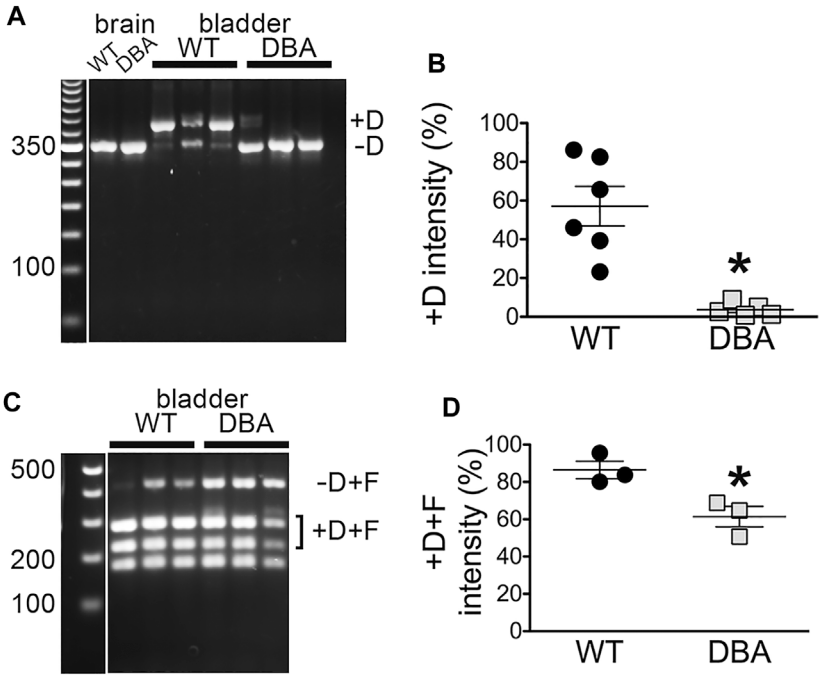

FIGURE 6 | Myo5a exons D and F in bladders from WT and DBA mice. **(A)** Nested PCR fragments from detrusors of WT ($N = 6$) and DBA ($N = 5$) animals were prepared with primer pair 3 and electrophoresed. A representative agarose gel with bands corresponding to fragments with and without exon D from three WT and three DBA detrusors is shown, with individual WT and DBA brain samples as controls. Exposure of the 50 bp standard lane, with weighted 350 bp band, was adjusted separately. **(B)** The intensity of +D bands is graphed as a proportion of total intensity in each lane (sum of +D and –D) and plotted for WT (black circles), and DBA (gray squares). Horizontal line indicates average intensity in % ± SEM for the +D band in all replicates. The comparison between WT and DBA detrusor was significant (*$p = 0.015$). **(C)** Nested PCR fragments from detrusor of three WT and three DBA animals were prepared with primer pair 4, digested with Ban II to cleave the +D band, and electrophoresed. The relative positions of detrusor exon F-containing digestion fragments including or lacking exon D are indicated, and a flanking lane with 100 bp standards is marked. Contrast for the standard lane was adjusted separately. **(D)** Data are graphically represented; the horizontal line indicates average intensities in % ± SEM for PCR product containing exon D (black circles, WT; gray squares, DBA) are graphed. Coincidence of exons D and F in the same cDNA fragment was significantly reduced in DBA detrusor ($p = 0.03$).

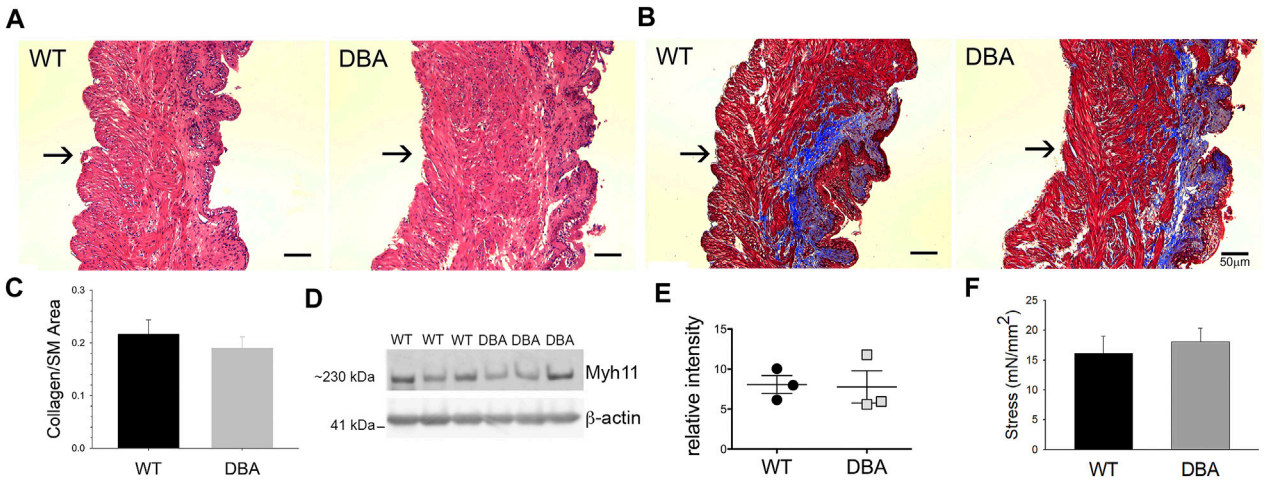

FIGURE 7 | Morphologic, functional and molecular evaluation of bladder smooth muscle contractile apparatus. Histomorphometric evaluation of bladder tissue sections stained with H&E **(A)** and MT **(B)** from WT ($N = 3$) and DBA ($N = 3$) mice (Mag X10, scale bar 50 µm, arrows indicate serosa). **(C)** Quantification of the collagen/smooth muscle (SM) ratio was comparable between WT (black bar) and DBA (gray bar) bladders. **(D)** Representative Western blot and **(E)** quantitative graph of intensity of myosin heavy chain (Myh11) immunoreactivity detected in protein lysates from mucosa-denuded WT and DBA bladders. Band intensities in WT (black circles, $N = 3$) were not different from DBA (gray squares, $N = 3$) when normalized by ß-actin, which was used as the loading control. **(F)** Contractile responses induced by direct smooth muscle depolarization achieved by KCl 120 mM in WT ($N = 11$, black bar) and DBA ($N = 13$, gray bar) bladders were not different.

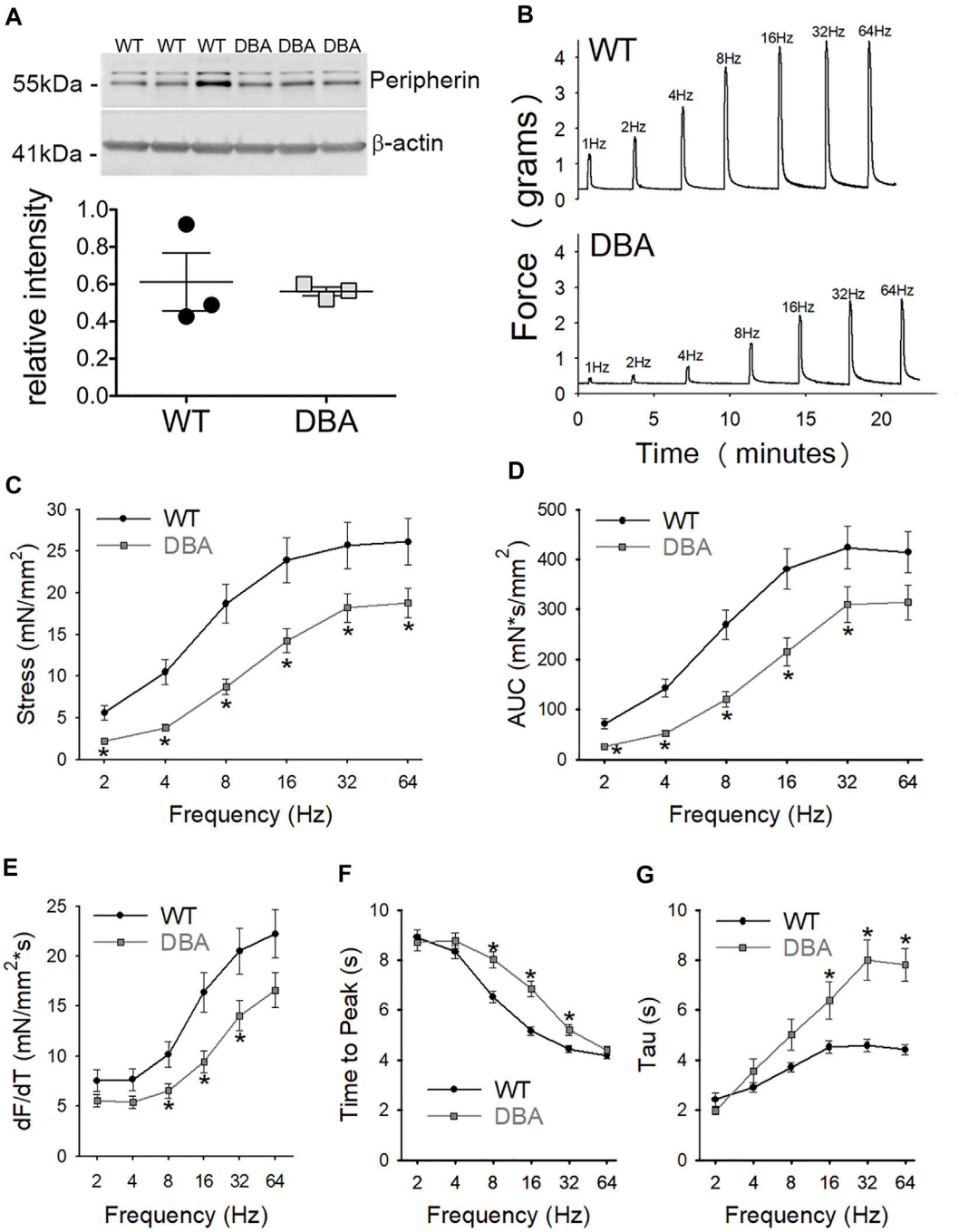

FIGURE 8 | Contractile responses to EFS in WT and DBA bladders. **(A)** Representative membrane and quantitative graph showing the expression of neuronal marker peripherin in WT (*N* = 3, black circles) and DBA (*N* = 3, gray squares) detrusor lysates. The intensity of both immunoreactive bands, corresponding to the ~56 and ~58 kDa peripherin isoforms (Landon et al., 2000) were normalized by internal control β-actin. No differences in peripherin expression were detected between WT and DBA detrusors. **(B)** Representative tracing showing the contractile responses to EFS at frequencies between 2 and 64 Hz in WT (top trace) vs. DBA (bottom trace) detrusors. **(C)** The amplitude and **(D)** the area under the curve (AUC) of EFS-induced contractions of WT (black circles) and DBA (gray squares) detrusor tissue are plotted. Contractile responses of DBA detrusor were significantly lower than that of WT detrusor over a range of frequencies, as indicated by the asterisks. **(E)** The peak rate of rise of the ascending phase of the contraction, **(F)** the time to peak, as well as **(G)** the rate of decay (Tau) of the descending phase of the neurogenic contractions are graphed for WT (black circles) and DBA (gray squares) detrusors. Especially at middle to higher frequencies of stimulation, contractions in DBA mice were significantly decreased in slope with delayed time to peak and prolonged recovery time, compared to those measured in WT (*N* = 11 WT, *N* = 13 DBA; $^*p < 0.05$).

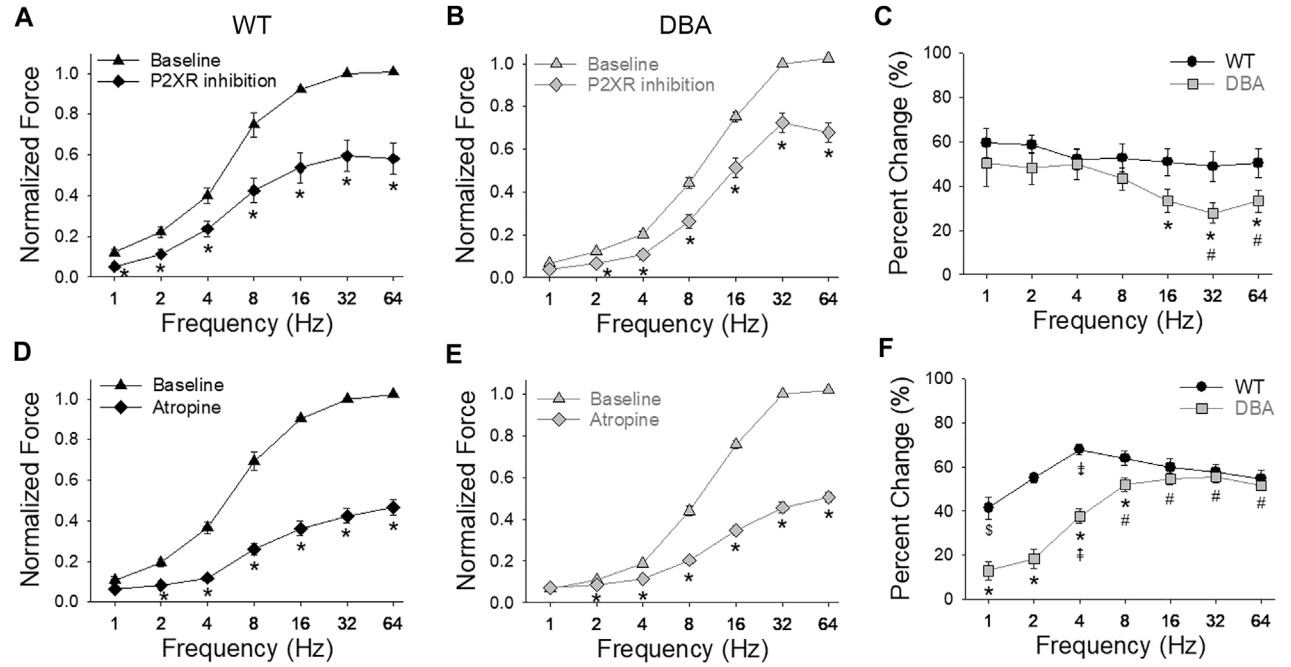

FIGURE 9 | Purinergic and cholinergic inhibition of neurally evoked contractile responses. Effect of post-junctional inhibition on the frequency-response curves in WT [**(A,D)**, black symbols] and DBA [**(B,E)**, gray symbols] detrusors. Contractile responses to EFS in the absence (triangles) versus the presence (diamonds) of P2XR antagonists (NF449 and 5BDBD) in detrusors from **(A)** WT and **(B)** DBA mice. Following purinergic inhibition, responses to EFS of both WT and DBA detrusors were significantly reduced at all frequencies as indicated by asterisks. Data are normalized by the baseline response (without inhibitors) at 32 Hz. **(C)** Compared to WT (black circles), the reduction in force relative to the baseline response due to purinergic inhibition (change from baseline) was significantly lower in DBA detrusors (gray squares) at frequencies of stimulation above 8 Hz (*significantly lower than WT at this frequency; # significantly lower than 2 and 4 Hz within DBA). Comparison of the effect of muscarinic receptor antagonist atropine on nerve-mediated contractile responses in **(D)** WT and **(E)** DBA detrusors. Normalized force is graphed versus stimulation frequency, in the absence (triangles) and presence (diamonds) of atropine. Data are normalized by baseline responses at 32 Hz. Atropine significantly reduced the responses of both WT and DBA detrusor to EFS at frequencies greater than 1 Hz (*). **(F)** The inhibitory effect of atropine on nerve mediated responses relative to baseline conditions was significantly less in DBA (gray squares) at stimulations from 1 to 8 Hz compared to the effect in WT (black circles). (* significantly lower than WT at this frequency; # significantly higher than 1–4 Hz within DBA; ‡ significantly higher than 1 and 2 Hz within DBA; ‡ significantly different than 1, 2, 32 and 64 Hz within WT; $ significantly lower than 8–32 Hz within WT (N = 11 WT, N = 13 DBA, symbols indicate $p < 0.05$)).

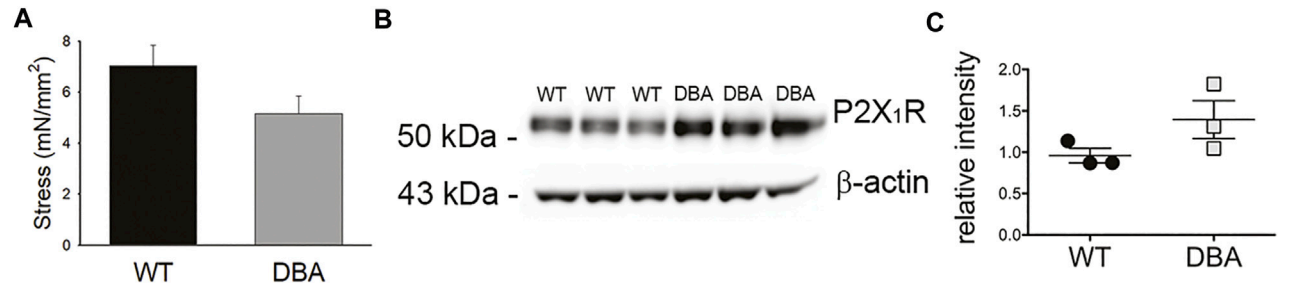

FIGURE 10 | Purinergic responses of WT and DBA bladders. **(A)** Comparison of the contractile response of WT (black bar) and DBA (gray bar) bladder smooth muscle to the purinergic receptor agonist, αβmeATP (10 μM). Contractions of WT and DBA bladders were not significantly different under this condition ($N = 11$ WT, $N = 13$ DBA; $p = 0.21$). **(B)** Western blot comparing expression of the $P2X_1$ purinergic receptor in WT and DBA extracts from bladder tissue devoid of mucosa. β-actin, shown in bottom panel, served as loading control. Molecular weights of mass standards (in kDa) are indicated at tick marks. **(C)** Quantitative data for WT (black circles) and DBA (gray squares) are graphed at right. The intensity of $P2X_1$ receptor immunoreactivity, normalized by intensity of β-actin, was not different between groups ($N = 3$, $p = 0.2$).

in the presence of pirenzepine to 70 ± 0.24% of the CCh response generated under baseline conditions ($p = 0.033$). In contrast, pirenzepine did not significantly alter the amplitude of CCh-induced contractile responses in DBA detrusors (90 ± 0.22% of the baseline response). Therefore, in the presence of pirenzepine, the CCh response in WT tissue was not different from DBA detrusors

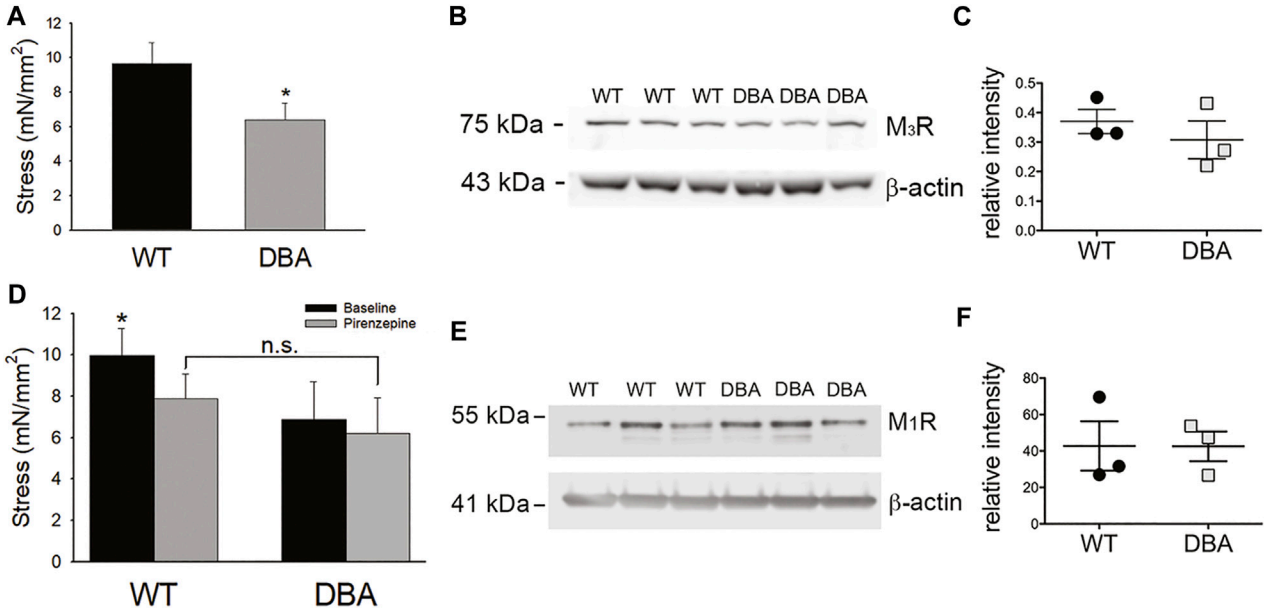

FIGURE 11 | Cholinergic responses of WT and DBA bladders. **(A)** Contractile responses of DBA (gray bar) bladder smooth muscle to the muscarinic receptor agonist CCh, was significantly lower than WT (black bar) responses ($N = 11$ WT, $N = 13$ DBA, $^*p = 0.041$). **(B)** Western blot comparing expression of M_3R in WT and DBA bladder smooth muscle extracts, relative to β-actin loading control. The molecular weight in kDa of mass standards are shown by the tick marks. **(C)** Quantitative data indicate that muscarinic M_3R expression in WT (black circles) and DBA (gray squares) detrusors was not significantly different ($N = 3$, $p = 0.8$). **(D)** Contractile responses induced by CCh in WT and DBA detrusors were generated before (black bars) and after (gray bars) inhibition of the M_1R inhibitor with pirenzepine. In WT detrusors, CCh-evoked contractions were significantly inhibited by pirenzepine ($N = 7$; $^*p = 0.008$), while contractions in DBA detrusors were not affected ($N = 5$, $p = 0.31$). In the presence of pirenzepine, the contractile response to CCh in WT was not different from DBA ($p = 0.25$). **(E)** Western blot comparing the expression of the facilitatory muscarinic receptor, M_1R, in three WT and three DBA bladder muscularis extracts. Molecular weight in kDa of mass standards is indicated at tick marks. **(F)** The intensity of M_1R immunoreactivity, normalized to the β-actin loading control, was not significantly different in WT (black circles) and DBA (gray squares) bladders ($N = 3$, $p = 0.7$).

(**Figure 11D**). Moreover, the expression of the M_1 receptor was comparable in WT and DBA detrusors (**Figures 11E,F**).

DISCUSSION

The motor protein Myo5a has been shown to facilitate directed vesicle motion along actin fibers; however, its role in bladder neurotransmission has not been previously explored. The data presented in this study establish that Myo5a is expressed by and localized in peripheral nerves of the urinary bladder. Notably, the well-characterized brain variant of Myo5a (which is abundant in neurons of the central nervous system) was not detected in detrusors of either DBA or WT animals, which are homozygous for, respectively, mutated and wild-type *Myo5a* alleles. The expressed Myo5a detrusor variants also differed by genotype. Moreover, compared to detrusors from WT mice, neurogenic contractions were attenuated in DBA detrusors. Together, these results indicated that Myo5a-dependent processes are crucial for efficient excitatory neurotransmission in the bladder, and demonstrated that molecular changes in Myo5a structure can be reflected in functional deficits in neurotransmission in this organ.

The seminal studies of Myo5a in the DBA mouse were largely confined to analysis of the mRNAs transcribed, and demonstrated that incorrectly spliced transcripts including Emv3 viral sequence could be identified in both brain and skin, but were more prevalent in skin. It was inferred that sufficient Myo5a brain variant protein was expressed in neurons to support normal development and neurological function in these mice, but that insufficient Myo5a skin variant proteins were expressed in melanocytes to support typical pigmentation (Seperack et al., 1995). This is consistent with our findings showing that the expression of the Myo5a brain variant incorporating exon B was not different between WT and DBA brains. Indeed, it has long been believed that dilute/gray fur color is the only phenotype of DBA mice resulting from their particular genetic alteration in the *Myo5a* gene. Compared with the more severe, and often lethal, phenotypes described in other *Myo5a* mutant strains, DBA mice do not display overt neurological dysfunction. However, we found reduced *Myo5a* expression in the detrusor of these mice, pointing to a previously unexplored autonomic peripheral neuropathy. Interestingly, elevated transcriptional initiation was also suggested in DBA compared to WT detrusor using the pan-Myo N-t realtime PCR assay, which targeted an exon boundary upstream of the alternative exon region. In contrast, the pan-Myo GTD assay, which targeted an exon boundary downstream of that region indicated reduced production of full-length Myo5a transcripts. This discrepancy implied that, despite a higher initiation of

Myo5a transcription in DBA detrusor, fewer authentic processed transcripts were produced than in WT detrusor, presumably due to the misincorporation of viral sequence and premature termination of chimeric transcripts.

Our previous work challenges the viewpoint that Myo5a-dependent neurotransmitter transport is largely spared in the DBA mice. Our group previously provided evidence of subtle functional defects in peripheral innervation in DBA animals affecting the gastric fundus and the corpora cavernosa of the penis, organs in which nitric oxide and ATP are inhibitory neurotransmitters. We demonstrated impaired relaxation responses in DBA, attributing them to a reduced ability of Myo5a to effect transport of neuronal nitric oxide synthase (the enzyme that is activated and produces nitric oxide at the varicosity membrane), and of synaptic vesicles carrying ATP (Chaudhury et al., 2011, 2012; Chaudhury et al., 2014). Those data indicated a role for Myo5a in non-vesicular as well as vesicular transport of inhibitory neurotransmitters along peripheral nerve endings. The data presented here extend our observations to transport of excitatory neurotransmitters in efferent nerves of the urinary bladder, and additionally suggest that the exon D/F splice variants of Myo5a are involved in this process.

In rodent urinary bladder, the neurotransmitters acetylcholine and ATP are primarily responsible for parasympathetic contractions through activation of muscarinic M_3 receptors and purinergic $P2X_1$ receptors, respectively. Profound deficits in neurally-mediated responses were detected in DBA mice in this study, even though age, body or bladder weights, bladder tissue morphology, receptor-independent detrusor contractions, and the integrity of innervation were not different from those of WT mice. Given the comparable expression and function of purinergic receptors in DBA and WT bladder smooth muscle, the reduction in neurally-mediated contractile responses observed in DBA mice is consistent with a pre-junctional defect in release of ATP, rather than an altered smooth muscle response to direct purinergic receptor activation. Similarly, no differences between DBA and WT were detected in muscarinic receptor expression or in the contractile response to concurrent smooth muscle muscarinic receptor activation and presynaptic M_1R inhibition. The lack of effect of pirenzepine in DBA detrusors likely reflects reduced acetylcholine release that is insufficient to provoke appreciable presynaptic facilitation. Together, these data provide evidence of reduced neurotransmission in DBA detrusors despite normal operation of smooth muscle contractile machinery.

Several aspects of neurotransmission were found to be defective in DBA detrusors. Both amplitude and AUC of nerve-mediated contractions were significantly lower in DBA compared to WT, and the temporal course of EFS-induced contractions was also remarkably different. With unaltered post-junctional contractility, the slower rate of the rising phase of contractions along with the longer time to peak and decay time constant of DBA contractions likely reflect a reduced amount and dampened kinetics of neurotransmitter release. Furthermore, the extent to which the purinergic and cholinergic components of neurogenic contractions were reduced in DBA detrusors displayed a complementary pattern that depended on the stimulation frequency. In particular, the effect of purinergic inhibition was similar in DBA and WT detrusors at lower frequencies, but became significantly reduced at higher frequencies (16–64 Hz). In contrast, cholinergic inhibition was less efficient in DBA than WT at frequencies up to 8 Hz, but similar to WT at higher frequencies of stimulation. These data are fully consistent with the diminished amplitude of EFS-induced contractions over the entire range of frequencies observed in DBA in the absence of receptor antagonists and suggest a frequency-dependent susceptibility of neurotransmitters to altered Myo5a splice variants in these mice.

The specific contribution of individual Myo5a splice variants to bladder neurotransmission have not been addressed in this initial study. However, one important implication of the data we present here is that variants with exons D/F but which lack exon B, are required for the Myo5a-dependent transport of ATP- and acetylcholine-containing synaptic vesicles in bladder motor nerve varicosities. To our knowledge, this is the first indication of a role for these Myo5a variants in excitatory neurotransmission.

Identification of the splice variants comprising the population of Myo5a proteins in the detrusor may be relevant for predicting their interacting Rabs (the membrane-bound GTPases which regulate all aspects of vesicle trafficking) and ultimately their neurotransmitter-containing cargo. For example, exon D has been shown to mediate interactions between Myo5a and Rabs 8a and 10 (Roland et al., 2009; Lindsay et al., 2013), which in adipocytes facilitate Myo5a-dependent translocation of Glut4-containing vesicles to the plasma membrane (Chen et al., 2012; Sun et al., 2014). Moreover, exon F is required for the Myo5a-dependent transport of melanosomes, forming a tripartite complex with melanophilin and the melanosome membrane binding protein, Rab27a (Lambert et al., 1998; Au and Huang, 2002; Fukuda et al., 2002; Wu et al., 2002). Additional roles for exon F are emerging from studies conducted in other cell types, perhaps reflecting the structural influence that exon F exerts on Myo5a conformation (**Figure 2**; Seperack et al., 1995; Au and Huang, 2002) which could markedly affect GTD-cargo interactions. Effector proteins such as MyRIP (myosin and Rab27a interacting protein) and rabphilin bind to Rab27a and Myo5a in endocrine cells (Desnos et al., 2003; Brozzi et al., 2012). In endothelial cells, multimers of the hemostatic protein, von Willebrand factor, are secreted from specialized granules (Weible-Palade bodies) in a process involving Rab27a, MyRIP, and the Myo5a variants ABCEF and ABCDEF (Rojo Pulido et al., 2011). In the urothelium, Myo5a complexes with Rab27b to tether uroplakin-positive fusiform vesicles to cortical actin filaments in umbrella cells (Wankel et al., 2016). Also, several Rabs (3a, 10, 11, 14, and 27b) which bind to Myo5a either directly or through an accessory protein, associate with synaptic vesicles in neurons (Pavlos et al., 2010; Lindsay et al., 2013). Our future work will examine the interactions of bladder Myo5a variants with these vesicle constituents to discern their mechanisms of action in neurotransmitter secretion.

CONCLUSION

Myo5a is involved in multiple and sequential effector interactions during the transport, tethering and release of neurotransmitter-

containing vesicles at nerve varicosities. In murine bladder nerves, the shorter Myo5a variant characteristic of brain neurons (ABCE), was not detected while longer variants typical of skin (ACDE, ACEF, ACDEF) predominated. Reduced total Myo5a expression, as well as limited production of these longer splice variants, are factors implicated in deficiencies of neurogenic smooth muscle contraction in DBA bladder described here. This first study of Myo5a splice variants in peripheral motor nerves in the bladder may have broader implications for Myo5a-dependent neurotransmission in other visceral organs, with the array of splice variants expressed, as well as the ratios among them, reflective of the particular functional requirements of each organ and cell type.

DATA AVAILABILITY STATEMENT

The original contributions presented in the study are included in the article/**Supplementary Material**. Further inquiries can be directed to the corresponding author.

ETHICS STATEMENT

The animal study was reviewed and approved by the Institutional Animal Care and Use Committee of the VA Boston Healthcare System.

AUTHOR CONTRIBUTIONS

JC, VC, RG, and MS conceived the study; JC, VC, and MS designed experiments; JC, VC, SD, SC, and MS performed experiments and analyzed data; JC, VC, and MS wrote the manuscript. JC and VC contributed equally to this work and share first authorship.

FUNDING

This work was supported by VA Merit Review awards to MS (BX001790, BX003680) and RG (BX002806) from the United States Department of Veteran's Affairs Medical Research Service, Washington D. C, United States of America.

SUPPLEMENTARY MATERIAL

The Supplementary Material for this article can be found online at: https://www.frontiersin.org/articles/10.3389/fphys.2022.890102/full#supplementary-material

Supplementary Figure S1 | Negative control for immunofluorescence microscopy. Confocal microscopy image of mouse bladder tissue sections (12 µm) in which the primary antibody was omitted (left image) showed no green fluorescent signal compared to tissue incubated for the same amount of time with mouse anti-Synaptophysin antibody (Abcam SY38, 1:10; right image). Alexa Fluor 488 donkey anti-mouse IgG (H + L) highly cross-adsorbed secondary antibody (A-21202, RRID AB_141607; Thermo-Fisher) was applied on both preparations at dilution of 1:2000. The superimposed differential interference contrast image (DIC) delineates tissue morphology (Magnification ×40, scale bar 50 µm).

Supplementary Figure S2 | Myo5a localization and variant expression in bladder mucosa. **(A)** Image from confocal microscopy of bladder sections stained with Myo5a antibody (red staining) and counterstained with urothelial marker uroplakin-3 (UPIII, green staining). Differential interference contrast (DIC) image was superimposed to visualize tissue anatomy. Myo5a showed abundant immunoreactivity in nerves fibers running within the muscle bundles as well as in the *lamina propria*. Less intense staining for Myo5a was detected in the urothelial layers as shown by the merged image (Scale bar = 200 µm; Mag ×20). **(B)** cDNAs from bladder mucosa total RNA of WT (black circles, $N = 4$) and DBA animals (gray squares, $N = 3$) were assayed by RT-PCR in triplicate for Myo5a exon B or exon F, as indicated, with their specific TaqMan assays, and for 18S rRNA as an internal control. Expression was determined by the ΔΔCt method and the average % intensity, shown by the horizontal line, ± SEM was graphed relative to WT. Expression of exon B was not detected (nd) in either WT or DBA mucosa; exon F was detected but expression did not differ by genotype ($p = 0.52$). **(C)** cDNAs from mucosae of WT ($N = 3$) and DBA ($N = 3$) animals were used for nested PCR with primer pair 3 which spans alternative exon D sequence. Products were digested with Ban II to indicate the presence of exon D, and electrophoresed on a 2% MetaPhor agarose gel with a 50 bp mass standard ladder to assess fragment sizes. The mobility of bands without (-D) and with (+D) exon D are shown at the right. **(D)** The intensity of each band as a percentage of the total intensity in each lane was determined, and the average % intensity ± SEM of +D products, shown by the horizontal lines is graphed for all replicates of each genotype. There was more exon D-containing PCR product seen in WT mucosa (black circles) compared to DBA mucosa (gray squares) ($^*p < 0.05$). **(E)** Nested PCR was also performed with primer pair 4, in which the reverse primer is within exon F. Products were digested with Ban II and electrophoresed with a 100 bp mass standard ladder, to indicate the proportion of exon F-containing transcripts that also contain exon D. The second and third lanes of this gel contain an undigested aliquot of WT and DBA mucosa from these PCR reactions, respectively. The mobility of bands without (–D +F) and with (+D+F) exon D are indicated at the right. The intensity of each band as a percentage of the total intensity in each lane was determined, and the average +D+F band intensity ± SE is graphed for all replicates of each genotype in panel **(F)**. Black circles represent WT mucosa, gray squares, DBA mucosa. There was more exon D-containing PCR product seen in WT mucosa compared to DBA mucosa ($^*p < 0.05$).

REFERENCES

Au, J. S.-Y., and Huang, J.-D. (2002). A Tissue-specific Exon of Myosin Va Is Responsible for Selective Cargo Binding in Melanocytes. *Cell Motil. Cytoskelet.* 53 (2), 89–102. doi:10.1002/cm.10061

Brooks, S. A., Gabreski, N., Miller, D., Brisbin, A., Brown, H. E., Streeter, C., et al. (2010). Whole-genome SNP Association in the Horse: Identification of a Deletion in Myosin Va Responsible for Lavender Foal Syndrome. *PLoS Genet.* 6 (4), e1000909. doi:10.1371/journal.pgen.1000909

Brozzi, F., Diraison, F., Lajus, S., Rajatileka, S., Philips, T., Regazzi, R., et al. (2012). Molecular Mechanism of Myosin Va Recruitment to Dense Core Secretory Granules. *Traffic* 13 (1), 54–69. doi:10.1111/j.1600-0854.2011.01301.x

Buttow, N. C., Espreafico, E. M., de Souza, R. R., and Romano, E. B. (2006). Immunolocalization of Myosin-V in the Peribronchial, Intrapulmonary Peritracheal Plexuses of the Wistar Rat. *J. Neurosci. Methods* 152 (1-2), 274–277. doi:10.1016/j.jneumeth.2005.09.012

Carew, J. A., Cristofaro, V., Siegelman, N. A., Goyal, R. K., and Sullivan, M. P. (2021). Expression of Myosin 5a Splice Variants in Murine Stomach. *Neurogastroenterol. Motil.* 33 (10), e14162. doi:10.1111/nmo.14162

Chaudhury, A., Cristofaro, V., Carew, J. A., Goyal, R. K., and Sullivan, M. P. (2014). Myosin Va Plays a Role in Nitrergic Smooth Muscle Relaxation in Gastric Fundus and Corpora Cavernosa of Penis. *PLoS One* 9 (2), e86778. doi:10.1371/journal.pone.0086778

Chaudhury, A., He, X.-D., and Goyal, R. K. (2011). Myosin Va Plays a Key Role in Nitrergic Neurotransmission by Transporting nNOSα to Enteric Varicosity Membrane. *Am. J. Physiology-Gastrointestinal Liver Physiology* 301 (3), G498–G507. doi:10.1152/ajpgi.00164.2011

Chaudhury, A., He, X.-D., and Goyal, R. K. (2012). Role of Myosin Va in Purinergic Vesicular Neurotransmission in the Gut. *Am. J. Physiology-Gastrointestinal Liver Physiology* 302 (6), G598–G607. doi:10.1152/ajpgi.00330.2011

Chen, Y., Wang, Y., Zhang, J., Deng, Y., Jiang, L., Song, E., et al. (2012). Rab10 and Myosin-Va Mediate Insulin-Stimulated GLUT4 Storage Vesicle Translocation in Adipocytes. *J. Cell Biol.* 198, 545–560. doi:10.1083/jcb.201111091

Chess-Williams, R. (2002). Muscarinic Receptors of the Urinary Bladder: Detrusor, Urothelial and Prejunctional. *Aut. Auta Pharm* 22 (3), 133–145. doi:10.1046/j.1474-8673.2002.00258.x

Cristofaro, V., Yalla, S. V., and Sullivan, M. P. (2012). Altered Caveolar Mediated Purinergic Signaling in Spontaneously Hypertensive Rats with Detrusor Overactivity. *J. Urology* 188 (3), 1017–1026. doi:10.1016/j.juro.2012.04.100

Desnos, C., Schonn, J.-S., Huet, S., Tran, V. S., El-Amraoui, A., Raposo, G., et al. (2003). Rab27A and its Effector MyRIP Link Secretory Granules to F-Actin and Control Their Motion towards Release Sites. *J. Cell Biol.* 163 (3), 559–570. doi:10.1083/jcb.200302157

Drengk, A. C., Kajiwara, J. K., Garcia, S. B., Carmo, V. S., Larson, R. E., Zucoloto, S., et al. (2000). Immunolocalisation of Myosin-V in the Enteric Nervous System of the Rat. *J. Auton. Nerv. Syst.* 78 (2-3), 109–112. doi:10.1016/s0165-1838(99)00073-9

Fukuda, M., Kuroda, T. S., and Mikoshiba, K. (2002). Slac2-a/Melanophilin, the Missing Link between Rab27 and Myosin Va. *J. Biol. Chem.* 277 (14), 12432–12436. doi:10.1074/jbc.C200005200

Futaki, S., Takagishi, Y., Hayashi, Y., Ohmori, S., Kanou, Y., Inouye, M., et al. (2000). Identification of a Novel Myosin-Va Mutation in an Ataxic Mutant Rat, Dilute-Opisthotonus. *Mamm. Genome* 11 (8), 649–655. doi:10.1007/s003350010121

Gabella, G. (1995). The Structural Relations between Nerve Fibres and Muscle Cells in the Urinary Bladder of the Rat. *J. Neurocytol.* 24 (3), 159–187. doi:10.1007/bf01181533

Griscelli, C., Durandy, A., Guy-Grand, D., Daguillard, F., Herzog, C., and Prunieras, M. (1978). A Syndrome Associating Partial Albinism and Immunodeficiency. *Am. J. Med.* 65 (4), 691–702. doi:10.1016/0002-9343(78)90858-6

Huang, J.-D., Mermall, V., Strobel, M. C., Russell, L. B., Mooseker, M. S., Copeland, N. G., et al. (1998). Molecular Genetic Dissection of Mouse Unconventional Myosin-VA: Tail Region Mutations. *Genetics* 148, 1963–1972. doi:10.1093/genetics/148.4.1963

Khandelwal, P., Prakasam, H. S., Clayton, D. R., Ruiz, W. G., Gallo, L. I., van Roekel, D., et al. (2013). A Rab11a-Rab8a-Myo5B Network Promotes Stretch-Regulated Exocytosis in Bladder Umbrella Cells. *MBoC* 24 (7), 1007–1019. doi:10.1091/mbc.E12-08-0568

Lambert, J., Naeyaert, J. M., Callens, T., De Paepe, A., and Messiaen, L. (1998). Human Myosin V Gene Produces Different Transcripts in a Cell Type-specific Manner. *Biochem. Biophysical Res. Commun.* 252 (2), 329–333. doi:10.1006/bbrc.1998.9644

Landon, F., Wolff, A., and Néchaud, B. (20002000). Mouse Peripherin Isoforms. *Biol. Cell* 92 (6), 397–407. doi:10.1016/s0248-4900(00)01099-6

Landrock, K. K., Sullivan, P., Martini-Stoica, H., Goldstein, D. S., Graham, B. H., Yamamoto, S., et al. (2018). Pleiotropic Neuropathological and Biochemical Alterations Associated with Myo5a Mutation in a Rat Model. *Brain Res.* 1679, 155–170. doi:10.1016/j.brainres.2017.11.029

Lindsay, A. J., Jollivet, F., Horgan, C. P., Khan, A. R., Raposo, G., McCaffrey, M. W., et al. (2013). Identification and Characterization of Multiple Novel Rab-Myosin Va Interactions. *MBoC* 24 (21), 3420–3434. doi:10.1091/mbc.E13-05-0236

Lindsay, A. J., and McCaffrey, M. W. (2011). Myosin Va Is Required for P Body but Not Stress Granule Formation. *J. Biol. Chem.* 286, 11519–11528. doi:10.1074/jbc.M110.1828010.1074/jbc.m110.182808

Ménasché, G., Ho, C. H., Sanal, O., Feldmann, J., Tezcan, I., Ersoy, F., et al. (2003). Griscelli Syndrome Restricted to Hypopigmentation Results from a Melanophilin Defect (GS3) or a MYO5A F-Exon Deletion (GS1). *J. Clin. Invest.* 112 (3), 450–456. doi:10.1172/JCI1826410.1172/jci200318264

Mercer, J. A., Seperack, P. K., Strobel, M. C., Copeland, N. G., and Jenkins, N. A. (1991). Novel Myosin Heavy Chain Encoded by Murine Dilute Coat Colour Locus. *Nature* 349 (6311), 709–713. doi:10.1038/349709a0

Pastural, E., Barrat, F. J., Dufourcq-Lagelouse, R., Certain, S., Sanal, O., Jabado, N., et al. (1997). Griscelli Disease Maps to Chromosome 15q21 and Is Associated with Mutations in the Myosin-Va Gene. *Nat. Genet.* 16 (3), 289–292. doi:10.1038/ng0797-289

Pavlos, N. J., Gronborg, M., Riedel, D., Chua, J. J. E., Boyken, J., Kloepper, T. H., et al. (2010). Quantitative Analysis of Synaptic Vesicle Rabs Uncovers Distinct yet Overlapping Roles for Rab3a and Rab27b in Ca2+-Triggered Exocytosis. *J. Neurosci.* 30, 13441–13453. doi:10.1523/jneurosci.0907-10.2010

Rojo Pulido, I., Nightingale, T. D., Darchen, F., Seabra, M. C., Cutler, D. F., and Gerke, V. (2011). Myosin Va Acts in Concert with Rab27a and MyRIP to Regulate Acute Von-Willebrand Factor Release from Endothelial Cells. *Traffic* 12, 1371–1382. doi:10.1111/j.1600-0854.2011.01248.x

Roland, J. T., Lapierre, L. A., and Goldenring, J. R. (2009). Alternative Splicing in Class V Myosins Determines Association with Rab10. *J. Biol. Chem.* 284 (2), 1213–1223. doi:10.1074/jbc.M805957200

Seperack, P. K., Mercer, J. A., Strobel, M. C., Copeland, N. G., and Jenkins, N. A. (1995). Retroviral Sequences Located within an Intron of the Dilute Gene Alter Dilute Expression in a Tissue-specific Manner. *EMBO J.* 14 (10), 2326–2332. doi:10.1002/j.1460-2075.1995.tb07227.x

Somogyi, G. T., Tanowitz, M., and de Groat, W. C. (1994). M1 Muscarinic Receptor-Mediated Facilitation of Acetylcholine Release in the Rat Urinary Bladder. *J. Physiol.* 480 (Pt 1), 81–89. doi:10.1113/jphysiol.1994.sp020342

Sun, Y., Chiu, T. T., Foley, K. P., Bilan, P. J., and Klip, A. (2014). Myosin Va Mediates Rab8A-Regulated GLUT4 Vesicle Exocytosis in Insulin-Stimulated Muscle Cells. *MBoC* 25 (7), 1159–1170. doi:10.1091/mbc.E13-08-0493

Wagner, W., Fodor, E., Ginsburg, A., and Hammer, J. A., 3rd (2006). The Binding of DYNLL2 to Myosin Va Requires Alternatively Spliced Exon B and Stabilizes a Portion of the Myosin's Coiled-Coil Domain. *Biochemistry* 45 (38), 11564–11577. doi:10.1021/bi061142u

Wankel, B., Ouyang, J., Guo, X., Hadjiolova, K., Miller, J., Liao, Y., et al. (2016). Sequential and Compartmentalized Action of Rabs, SNAREs, and MAL in the Apical Delivery of Fusiform Vesicles in Urothelial Umbrella Cells. *MBoC* 27, 1621–1634. doi:10.1091/mbc.E15-04-0230

Wu, X., Wang, F., Rao, K., Sellers, J. R., and Hammer, J. A., 3rd (2002). Rab27a Is an Essential Component of Melanosome Receptor for Myosin Va. *MBoC* 13 (5), 1735–1749. doi:10.1091/mbc.01-12-0595

Yang, X. f., Wang, J., Rui-Wang, W., Xu, Y. f., Chen, F. j., Tang, L. y., et al. (2019). Time-dependent Functional, Morphological, and Molecular Changes in Diabetic Bladder Dysfunction in Streptozotocin-induced Diabetic Mice. *Neurourol. Urodynamics* 38 (5), 1266–1277. doi:10.1002/nau.24008

Yılmaz, M., Çağdaş, D., Grandin, V., Altıntaş, D. U., Tezcan, İ., de Saint Basile, G., et al. (2014). Griscelli Syndrome Type 3-like Phenotype with MYO-5A Exon-F Deletion. *Pediatr. Allergy Immunol.* 25 (8), 817–819. doi:10.1111/pai.12285

Conflict of Interest: The authors declare that the research was conducted in the absence of any commercial or financial relationships that could be construed as a potential conflict of interest.

frontiers | Frontiers in Physiology

REVIEW
published: 04 July 2022
doi: 10.3389/fphys.2022.886782

Urinary Tract Infection in Overactive Bladder: An Update on Pathophysiological Mechanisms

Kylie J. Mansfield[1], *Zhuoran Chen*[2], *Kate H. Moore*[2] *and Luke Grundy*[3,4]*

[1]Illawarra Health and Medical Research Institute and School of Medicine, University of Wollongong, Wollongong, NSW, Australia, [2]Department of Urogynaecology, St George Hospital, University of New South Wales, Kogarah, NSW, Australia, [3]Visceral Pain Research Group, College of Medicine and Public Health, Flinders Health and Medical Research Institute (FHMRI), Flinders University, Bedford Park, SA, Australia, [4]Hopwood Centre for Neurobiology, Lifelong Health Theme, South Australian Health and Medical Research Institute (SAHMRI), Adelaide, SA, Australia

Overactive bladder (OAB) is a clinical syndrome defined by urinary urgency, increased daytime urinary frequency and/or nocturia, with or without urinary incontinence, that affects approximately 11% of the western population. OAB is accepted as an idiopathic disorder, and is charactersied clinically in the absence of other organic diseases, including urinary tract infection. Despite this, a growing body of research provides evidence that a significant proportion of OAB patients have active bladder infection. This review discusses the key findings of recent laboratory and clinical studies, providing insight into the relationship between urinary tract infection, bladder inflammation, and the pathophysiology of OAB. We summarise an array of clinical studies that find OAB patients are significantly more likely than control patients to have pathogenic bacteria in their urine and increased bladder inflammation. This review reveals the complex nature of OAB, and highlights key laboratory studies that have begun to unravel how urinary tract infection and bladder inflammation can induce urinary urgency and urinary frequency. The evidence presented in this review supports the concept that urinary tract infection may be an underappreciated contributor to the pathophysiology of some OAB patients.

Keywords: bladder, overactive bladder, urinary tract infection, bacterial cystitis, inflammation, hypersensitivity

OPEN ACCESS

Edited by:
Russ Chess-Williams, Bond University, Australia

Reviewed by:
Dale Edmond Bjorling, University of Wisconsin-Madison, United States
Betty Exintaris, Monash University, Parkville campus, Australia

***Correspondence:**
Luke Grundy
luke.grundy@flinders.edu.au

Specialty section:
This article was submitted to Integrative Physiology, a section of the journal Frontiers in Physiology

Received: *28 February 2022*
Accepted: *23 May 2022*
Published: *04 July 2022*

Citation:
Mansfield KJ, Chen Z, Moore KH and Grundy L (2022) Urinary Tract Infection in Overactive Bladder: An Update on Pathophysiological Mechanisms. Front. Physiol. 13:886782. doi: 10.3389/fphys.2022.886782

INTRODUCTION

Overactive bladder (OAB) is a clinical syndrome defined by urinary urgency, increased daytime urinary frequency and/or nocturia, with or without urinary incontinence (Wein and Rovner, 2002). OAB by definition is idiopathic, "a disease of unknown cause" which is only diagnosed in the absence of other organic disease, such as cancer, neurological or structural abnormalities, or urinary tract infection. Based on these criteria, OAB effects approximately 11% of the western population, significantly reducing quality of life (Wein and Rovner, 2002; Coyne et al., 2011; Eapen and Radomski, 2016; Kinsey et al., 2016).

Despite the accepted idiopathic nature of OAB, several studies in the last decade have provided a new aetiological paradigm; low levels of pathogenic bacteriuria (bacteria in urine) and inflammation are found in substantial proportions of OAB patients (Moore et al., 2000; Walsh et al., 2011; Walsh et al., 2011; Walsh and Moore, 2011; Digesu et al., 2013; Khasriya et al., 2013; Moore et al., 2013; Moore and Malykhina, 2014; Reynolds et al., 2016; Chen et al., 2018) and in a significant portion of women with newly diagnosed OAB (Ognenovska et al., 2021). These discoveries have highlighted key

questions: Is the pathophysiology of OAB more complicated and multifaceted than has traditionally been proposed? And what is the mechanism whereby chronic low grade bacterial cystitis could promote sensory dysfunction and incontinence?

This review summarises the key findings of recent laboratory and clinical studies which provide further insight into the relationship between chronic bacteriuria and associated inflammatory mediators in OAB patients.

CLINICAL SIGNIFICANCE OF OVERACTIVE BLADDER

Approximately 11% of women from western countries are diagnosed with OAB based on the clinical symptoms of urinary urgency, urinary frequency, nocturia, and in some cases, urge incontinence (Eapen and Radomski, 2016). In patients over 40 years of age, the prevalence in European countries is 17% (Milsom et al., 2001). These symptoms severely affect quality of life, contributing to significant psycho-social comorbidities including increased incidence and severity of depression, anxiety, and social isolation, which contribute to declining mental and physical health (Coyne et al., 2011; Kinsey et al., 2016). OAB patients also incur significant personal and societal health care costs associated with repeated primary health care visits and reduced professional opportunities (Coyne et al., 2011; Kinsey et al., 2016; Reynolds et al., 2016). The direct and indirect health care costs associated with OAB have been calculated as over $100 Billion per annum in the United States alone (Ganz et al., 2010; Pierce et al., 2015; Reynolds et al., 2016).

DIAGNOSIS, TREATMENT, AND PATHOPHYSIOLOGY OF OVERACTIVE BLADDER

In the typical clinical care pathway, patients presenting with symptoms of urinary urgency, urinary frequency and nocturia often undergo a diagnostic test involving filling the bladder with saline and observing the presence of spasms of the detrusor muscle (*via* intravesical manometry line), which is termed Detrusor Overactivity. In the absence of organic disease, the condition is termed "Idiopathic," which is predominant in women but quite uncommon in men. Therefore, while the pathophysiological consequence of the disease is defined by the cystometry testing (i.e. detrusor overactivity), the aetiology underlying this condition remains unknown.

As the chief symptoms of OAB are related to sensory dysfunction, it is logical that the mechanisms underlying OAB are likely related to changes in neuronal excitability and/or exaggerated neuronal firing during bladder filling. This hypothesis is well supported by investigations conducted using animal models of bladder dysfunction (Yoshimura et al., 2014; Grundy et al., 2019). Despite this, OAB patients are initially treated with anticholinergic medications which reduce detrusor muscle contractions and improve bladder capacity, thus lessening their incontinence/frequency/urgency of micturition (Moore and Malykhina, 2014). Unsurprisingly, with little fundamental basis in pathophysiology, these treatments have only limited benefits over placebo and poor continuation rates (Wagg et al., 2012; Kim and Lee, 2016; Yeowell et al., 2018). Our longitudinal study revealed that after 8 years, only 20% of patients treated with antimuscarinic agents have long-lasting improvement (Morris et al., 2008). Unfortunately, about 30%–40% of patients do not respond to these medicines at all. Such non-responsive patients are then denoted as having "Refractory OAB" (Moore and Malykhina, 2014). For these refractory patients, the absence of a defined pathology guarantees patients undergo a diagnostic odyssey, incorporating multiple invasive and non-invasive tests, and numerous prescriptions in an effort to exclude various pathophysiology (Gormley et al., 2015). Such "Refractory" patients may suffer lifelong debilitating symptoms, placing a significant burden on both the patient and the health system.

The large proportion of patients refractory to pharmacotherapy also supports an alternative pathophysiology to detrusor overactivity seen in OAB. Indeed, the relative success of neurotoxins that inhibit sensory nerve activity, such as resiniferatoxin and BOTOX (Guo et al., 2013; Hsieh et al., 2016; Cui et al., 2021), in relieving OAB symptoms refractory to pharmacotherapy suggests increased sensory outflow is responsible for the symptoms of urgency and urinary frequency. However, BOTOX treatment is invasive, has been associated with frequent side effects, and requires repeated doses at approximately 6 months intervals (Schurch et al., 2005; Apostolidis et al., 2009; Chen and Kuo, 2020) indicating the treatment is masking, rather than treating the underlying cause of bladder sensory neuron hypersensitivity.

The initiating or contributing factors in the development of neuronal hypersensitivity in OAB remain to be determined. Numerous aetiologies have been proposed, including altered bladder permeability, inflammation, cross-organ sensitisation, and dysregulation of spinal and/or cortical networks (de Groat et al., 2015; Grundy et al., 2018a). Amongst these potential mechanisms, there is mounting evidence that chronic bacterial infection of the bladder may contribute to the exacerbation of OAB symptoms in susceptible populations *via* direct or indirect sensitisation of sensory neurons (Moore et al., 2000; Walsh C et al., 2011; Brierley et al., 2020).

URINARY TRACT INFECTIONS

Prevalence and Diagnosis

A urinary tract infection (UTI) is an infection in any part of the upper or lower urinary tract, including kidneys (e.g., pyelonephritis), ureters, bladder, and urethra (Smelov et al., 2016). UTI's are amongst the most common bacterial infections in the world, affecting more than 150 million people annually worldwide (Smelov et al., 2016; Tandogdu and Wagenlehner, 2016). Despite this prevalence, the vast majority of these infections are caused by a limited number of bacterial species, with *Escherichia coli (E. coli)* that exhibit evolutionary specialisations (Uropathogenic *E. coli,* UPEC) being the

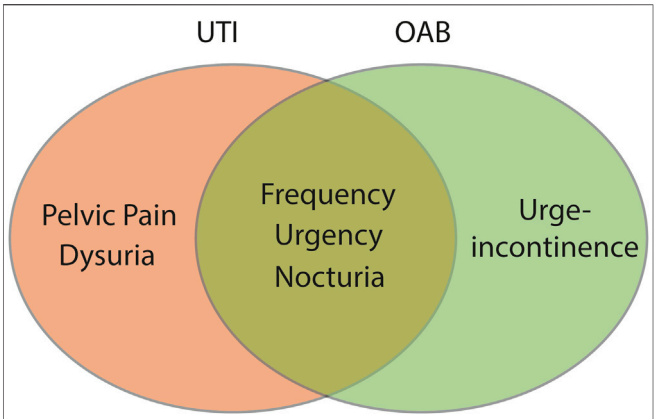

FIGURE 1 | The primary symptoms of OAB and UTI overlap. Urinary frequency, urinary urgency, and nocturia are key symptoms associated with both OAB and acute UTI. Clinically, OAB is differentiated from acute UTI by the absence of bacteriuria and/or a negative dip-stick test.

stereotypical species (Smelov et al., 2016). UTI's occur most frequently in the lower urinary tract and typically present with some or all of the following symptoms: dysuria (painful urination), urgency, frequency, and pelvic pain (Chu and Lowder, 2018). These symptoms overlap significantly with those observed in OAB, making exclusion of a UTI a key component in OAB diagnosis (**Figure 1**).

UTI's are typically diagnosed in general practice using a urine dipstick as an indirect measure to identify white blood cells (pyuria), production of nitrates in the urine typical of bacteriuria, and the presence of microscopic haematuria as evidence of severe inflammation. If the dipstick test is positive (or symptoms are clearly suggestive) then a fresh unspun midstream (MSU) sample is sent for microscopy to identify 10 or more white blood cells (wbc)/μl (pyuria). The urine is then cultured, and "classical" UTI is diagnosed as greater than 10^5 CFU of bacteria/ml (Smelov et al., 2016; Tandogdu and Wagenlehner, 2016; Chu and Lowder, 2018). The relative sensitivity and accuracy of these tests is thus a key factor in determining what is a genuine UTI, and determining diagnosis and subsequent treatment.

Ever since the 1950s, when pyelonephritis was a frequent cause of mortality, the threshold of 10^5 CFU/ml from MSU samples was widely accepted as a cut off to diagnose "Classical UTI" (Chu and Lowder, 2018). However, whilst a cut-off of 10^5 CFU/ml from MSU will accurately confirm bladder infection, several studies have identified limitations of this stringent criterion as regards bacterial cystitis, i.e., significant lack of sensitivity. Around 50% of patients who present with symptoms of acute UTI that respond positively to antibiotic treatment are mis-diagnosed as "normal" using the 10^5 CFU/ml cut-off (Stamm et al., 1982; Stark and Maki, 1984). A fine balance must be made, however, as having the criteria too low risks false positives, incorrect diagnosis, and the unnecessary prescription of antibiotics. A criterion of $\geq 10^2$ or 10^3 CFU/ml from MSU have been identified as the threshold that resulted in optimal sensitivity and specificity, accurately detecting the majority of genuine infections with low false-positive rates (Stamm et al., 1982; Kunin et al., 1993; Price et al., 2016).

Using this lower criterium of $\geq 10^{2-3}$ CFU/ml from MSU, however, revealed that a proportion of patients diagnosed with OAB may have low-level bacterial infection that was previously missed by routine "classical" testing methods (Walsh et al., 2011; Walsh et al., 2011; Walsh and Moore, 2011; Moore and Malykhina, 2014). This has profound implications for effective clinical treatment.

THE EMERGING ROLE OF URINARY TRACT INFECTION IN OVERACTIVE BLADDER

Bacteriuria in Overactive Bladder

Even when using a conventional 10^5 CFU/ml MSU culture, 6%–17% of women diagnosed with OAB have been found to have a UTI, compared to just 0.5%–2% of women from control groups (Moore et al., 2000; Khasriya et al., 2013; Gill et al., 2021). Similar results have been obtained from MSU samples taken specifically during symptom flares of refractory OAB patients, with 17% of patients versus 2% of the control group showing positive cultures at 10^5 CFU/ml (Walsh et al., 2011). Interestingly, when both standard (10^5 CFU/ml) and low-count criteria (10^{2-3} CFU/ml) are used in samples from the same patient cohort, the proportion of those positive for bacteriuria increases (from 17% to 39%), compared to those of a control group (from 2% to 6%) (Walsh et al., 2011) showing that low-count MSU culture may reveal genuine infections in OAB patients that would otherwise be overlooked. Enhanced culture techniques have also revealed higher rates of infection that were previously missed by routine culture, identifying 23% of patients with OAB as positive for UTI, vs. 10% of controls, in a prospective blinded case control study (Khan et al., 2021).

Analysis of catheter (CSU), rather than mid-stream specimens of urine revealed similar results, with the proportion of OAB patients with positive cultures rising from 15% at 10^5 CFU/ml to 21% at 10^2 CFU/ml (Khasriya et al., 2010). Two additional studies support the concept that OAB patients have low-count bacteriuria but did not compare directly to an appropriate control group, including a follow up study that investigated catheter rather than MSU specimens from patients with refractory OAB (Walsh et al., 2013). Despite the lack of controls, these studies report similar proportions (27%–29%) of OAB patients with bacteriuria when using the low-count threshold (Hessdoerfer et al., 2011; Walsh et al., 2013).

Intracellular Bacterial Colonies in Overactive Bladder

Whilst low-count bacteriuria can be quite easily identified by reducing the CFU threshold upon culture, a growing number of studies have shown that uropathogenic *E. coli* invade urothelial cells and form intracellular bacterial communities (IBC's). A variety of studies have since identified large

TABLE 1 | A summary of the literature reports of changes in the levels of urinary cytokines in adult patients with UTI or OAB.

Cytokine	UTI	OAB
A. Pro-inflammatory cytokines		
IL1ß	0.005 Davidoff et al. (1997); 0.001 Sundac et al. (2016)	0.023 Chen et al. (2019)
IL2		0.04 Chen et al. (2019)
IL6	0.01 Davidoff et al. (1997); ↓0.01 Tyagi et al. (2010); 0.001 Sundac et al. (2016)	↓0.01 Tyagi et al. (2010); 0.05 Gill et al. (2021)
IL7	0.001 Sundac et al. (2016)	0.07 Chen et al. (2019)
IL9	0.0001 Sundac et al. (2016)	
IL12p_{70}	0.0001 Sundac et al. (2016)	↓0.02 Pillalamarri et al. (2018); 0.0002 Chen et al. (2019)
IL17	↓0.014 Tyagi et al. (2010); 0.01 Sundac et al. (2016)	
TNF-α	0.05 Cheng et al. (2016); 0.017 Tyagi et al. (2010); 0.001 Sundac et al. (2016)	0.017 Tyagi et al. (2010) 0.027 Ma et al. (2016), 0.04 Chen et al. (2019)
IFN-γ	0.001 Sundac et al. (2016)	
B. Chemokines		
IL8	0.018 Tyagi et al. (2010) 0.05 Hannan et al. (2014) 0.01 Tyagi et al. (2016); 0.001 Sundac et al. (2016)	↓0.01 Tyagi et al. (2016); 0.006 Chen et al. (2019)
	0.01 Tyagi et al. (2016), 0.001 Sundac et al. (2016)	↓0.01 Tyagi et al. (2016); 0.001 Chen et al. (2019)
CXCL 10		
MCP-1	0.05 Sundac et al. (2016)	0.05 Tyagi et al. (2010); 0.05 Gill et al. (2018); 0.001 Farhan et al. (2019); 0.0001 Ghoniem et al. (2020), 0.04 Chen et al. (2019)
MIP-1α	0.0001 Sundac et al. (2016)	0.05 Tyagi et al. (2010), 0.035 Ma et al. (2016)
MIP-1ß	0.0001 Sundac et al. (2016)	
	0.05 Tyagi et al. (2010); 0.05 Sundac et al. (2016)	0.034 Chen et al. (2019)
RANTES		
Eotaxin	0.01 Sundac et al. (2016)	
C. Anti-inflammatory cytokines		
IL1ra	↓0.05 Tyagi et al. (2016); 0.01 Sundac et al. (2016)	↓0.05 Tyagi et al. (2016)
IL4	0.001 Sundac et al. (2016)	↓0.014 Ma et al. (2016)
IL5		↓0.05 Tyagi et al. (2010)
IL10	0.001 Sundac et al. (2016)	0.05 Tyagi et al. (2010); ↓0.02 Pillalamarri et al. (2018)
IL13		↓0.02 Pillalamarri et al. (2018)

Unless otherwise indicated increased concentrations of cytokines are seen in UTI or OAB patients. ↓ indicates decreased cytokine concentration. p-values are reported in the literature vs. appropriate control patient cohorts.

numbers of bacteria undetected in routine MSU or CSU specimens within cultures from bladder biopsies or shed urothelial cells from OAB patients examined by immunohistochemistry or confocal microscopy of centrifuged/cytospin specimens (Rosen et al., 2007; Vijaya et al., 2013a; Khasriya et al., 2013; Cheng et al., 2016; Gill et al., 2018). However, intracellular bacteria have also routinely been found in large numbers of asymptomatic, or control patients (Khasriya et al., 2013; Cheng et al., 2016), suggesting that the presence of IBC's alone is not enough to accurately differentiate OAB and control patients. As such, it may not be the simple identification of IBC's in urine, but a more nuanced diagnostic marker that reveals an accurate distinction between genuine and asymptomatic infection. Our own detailed analysis of exfoliated urothelial cell samples obtained from the urine of patients with OAB or controls revealed filamentous bacteria were significantly more common in patients with OAB (Cheng et al., 2016). Filamentous bacteria are associated with intracellular bacterial growth and bacteria fluxing out of the urothelial cells to recolonise the bladder (Justice et al., 2006). In this context, *E. coli*, the species of bacteria most commonly implicated in UTIs, was found more closely associated with urothelial cells from sediment cultures (*via* confocal microscopy) only in OAB patient samples (Khasriya et al., 2013). Similarly, our further study of urothelial cells obtained from OAB patients demonstrated that high- but not low-density intracellular bacteria correlate with OAB symptom severity, measured by leakage on pad test, leaks per day, and voids per day (Ognenovska et al., 2021).

The contribution of IBC's to UTI pathophysiology is an emerging field of research. These initial reports suggest that IBC's within the urothelium may also be an underappreciated component in the symptomology of OAB. Importantly, these bacteria are unlikely to be picked up by increasing the sensitivity of MSU or CSU culture, raising further questions as to the interpretation of urine culture as the gold standard for ruling out genuine UTI's. The identification and classification of IBC's is currently impractical for routine clinical practice. However, if the relevance of IBC's in OAB is confirmed by additional high-quality studies, further urine analysis may be a useful tool in elucidating the pathophysiology underlying the

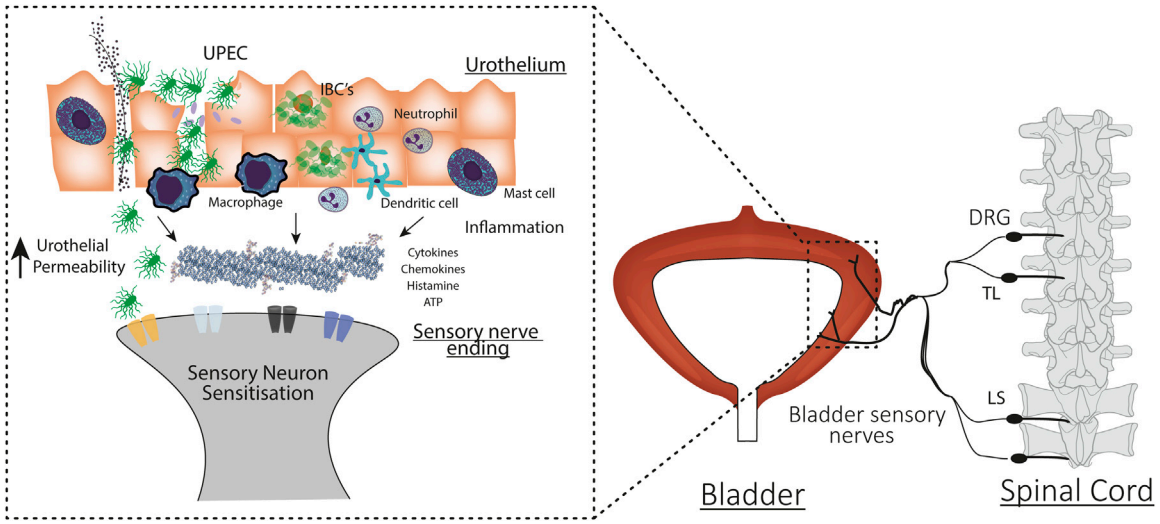

FIGURE 2 | Mechanisms underlying urinary tract infection induced bladder hypersensitivity. Uropathogenic *E. coli* (UPEC) invade urothelial cells during bladder colonisation. UPEC infection evokes an inflammatory response and the recruitment and activation of immune cells. UPEC also form intracellular bacterial colonies (IBCs) to evade the immune system and prolong urothelial colonisation. UPEC infection induces urothelial sloughing and apoptosis, increasing bladder permeability and allowing the toxic contents of the urine and bacteria to access the underlying interstitium. In response to damage, immune cells and the urothelium also release cytokines, chemokines, and neurotransmitters that can bind to receptors and ion channels on the peripheral ends of bladder-innervating sensory neurons. Immune and urothelial cell secretions, bacteria, and urine combine to sensitise the peripheral ends of bladder neurons. Sensitised neurons respond to bladder distension with higher intensity firing. This exaggerated signal travels to the spinal cord and activates second order neurons that travel to the brainstem and brain to induce exaggerated bladder sensation.

symptoms for OAB patients refractory to traditional treatments.

INFECTION INDUCED INFLAMMATION IN PATIENTS WITH OVERACTIVE BLADDER

Clinical Analysis

The relative abundance of low-count bacteriuria and IBCs in urothelial cells isolated from both OAB patients and asymptomatic controls points to the necessity for a distinction between bacterial colonisation, and infection (which is associated with inflammation and host-defence) when determining clinical intervention strategies. One of the challenges we face is that the immune response drives bacteria to localise intracellularly to form IBC's, where they can evade our traditional host-defence mechanisms. Furthermore, providing distinction between bacterial colonisation and infection will likely have greater relevance going forwards, with the identification of a bladder microbiome consisting of a diverse microbiological flora in the healthy bladder (Neugent et al., 2020).

Pyuria is the clinical standard for identifying localised bladder inflammation in the context of UTI, defined as the presence of 10 or more white blood cells (WBC)/mm^3 in fresh uncentrifuged urine (Chu and Lowder, 2018). However, pyuria is more commonly determined indirectly *via* the dip-stick test, by detecting leukocyte esterase. As would be expected, the prevalence of pyuria rises with the level of bacteriuria in uncomplicated cystitis and thus, if OAB patients with bacteriuria have genuine bacterial infections, pyuria, and changes in markers of inflammation should be apparent. Indeed, positive routine culture has been shown to be predictive of pyuria in a cohort of OAB patients (Khasriya et al., 2013). OAB patients are significantly more likely than control cohorts to demonstrate a positive dipstick test for leukocytes (39% vs. 9%) (Gill et al., 2021), and 30%–40% of OAB patients have been shown to have pyuria following microscopic analysis of urine (Khasriya et al., 2013; Contreras-Sanz et al., 2016). OAB patients also showed consistently higher microscopic pyuria counts on fresh urine microscopy compared to asymptomatic controls (Gill et al., 2018). Interestingly, pyuria identified by microscopic analysis of urine was recently shown by a group in the United Kingdom to be the most important correlate of symptom severity in OAB, with urgency correlating highly with both pyuria and epithelial cell shedding (Gill et al., 2018), a secondary, and potentially key additional indicator of active infection or inflammation (Mulvey et al., 2001; Klumpp et al., 2006).

Cytokine Analysis

In addition to immune cells, the inflammatory response to bacteriuria is also mediated by cytokines. Cytokines are essential regulators of both the innate immune response to infection and the inflammatory response to injury, with the concentration of urinary cytokines correlating with symptomatic UTI (Rodhe et al., 2009; Armbruster et al., 2018). Bacteria induced inflammation of the bladder stimulates the release of a large variety of both pro- and anti-inflammatory cytokines and chemokines (**Table 1**). Some cytokines have been consistently reported to increase during UTI, including IL-1β

(Davidoff et al., 1997; Sundac et al., 2016), IL-6 (Davidoff et al., 1997; Tyagi et al., 2010; Sundac et al., 2016), TNFα (Davidoff et al., 1997; Tyagi et al., 2010; Sundac et al., 2016), IL-8 (Tyagi et al., 2010; Hannan et al., 2014; Sundac et al., 2016; Tyagi et al., 2016), and CXCL-10 (Sundac et al., 2016; Tyagi et al., 2016). Similar elevations in the levels of pro-inflammatory cytokines and chemokines have also been reported in murine models of uropathogenic *E. coli* induced UTI (Engel et al., 2006; Hannan et al., 2010; Duell et al., 2012; Tan et al., 2012). This further supports the crucial role of the innate immune system in the bladder response to the presence of bacteria during an acute UTI.

As a result, numerous studies have investigated urinary cytokines as biomarkers for infection-induced inflammation in OAB patients. In support of the concept that a subpopulation of OAB patients symptoms are driven by an infectious/inflammatory state, a number of studies have shown altered cytokine and chemokine profiles in the urine of patients with OAB (**Table 1**) (Tyagi et al., 2010; Ghoniem et al., 2011; Tyagi et al., 2014; Ma et al., 2016; Tyagi et al., 2016; Alkis et al., 2017; Pillalamarri et al., 2018). This can manifest as changes in either pro- or anti-inflammatory cytokines, or both. Furthermore, a number of studies have reported that changes in urine cytokine concentration correlates with OAB symptom severity (Smelov et al., 2016; Pillalamarri et al., 2018; Gill et al., 2021), as well as bacterial growth and pyuria count (Gill et al., 2021). In general, however, a large amount of inter-study variability exists in the specific cytokines measured, and the relative changes in urine cytokine concentrations in these OAB patient cohorts. This variability is further compounded by the relatively small number of patients included in these studies. Despite these issues, there is a growing consistency in the evidence for elevations in pro-inflammatory cytokines TNF-α (Tyagi et al., 2010; Ma et al., 2016; Chen et al., 2019), MCP-1 (Tyagi et al., 2010; Chen et al., 2019; Farhan et al., 2019; Ghoniem et al., 2020) and MIP-1 (Tyagi et al., 2010; Ma et al., 2016) as well as reductions in anti-inflammatory cytokines IL-10, IL-1 receptor antagonist, and IL-4 (Ma et al., 2016; Tyagi et al., 2016; Pillalamarri et al., 2018) in OAB patients. A shift in the balance of these cytokines to a more pro-inflammatory state, and a lack of anti-inflammatory cytokines in women with OAB, may allow an inflammatory response to proliferate, thus contributing to the pathogenesis of the disease (Pillalamarri et al., 2018). A thorough, large scale trial, including well characterised patient cohorts is required to determine the true incidence and relative changes in urinary cytokines in OAB patients.

Considerable evidence is emerging from experiments in rodents indicating that hyperexcitability of bladder-innervating sensory neurons is triggered by bladder inflammation and may play a critical role in the pathogenesis of OAB (Grundy et al., 2018a; Geppetti et al., 2008). As described in **Figure 2**, the myriad molecular products of inflammation are able to act as potent neuromodulators, increasing the excitability of sensory neurons to physiological stimuli in a wide variety of organs (Pinho-Ribeiro et al., 2017). Evidence for inflammatory mediators increasing the excitability of bladder innervating sensory neurons, and the importance of inflammation in translating urinary tract infection into the symptoms of urgency and frequency experienced in patients with OAB, will be discussed in detail below.

TRANSLATION OF INFECTION AND INFLAMMATION INTO OVERACTIVE BLADDER SYMPTOMS

Bladder Sensation

Bladder sensation is initiated *via* the activation of primary sensory neurons embedded throughout the bladder wall, innervating both the detrusor smooth muscle and urothelium (Spencer et al., 2018). Sensory signals are generated by the activation of mechanosensory ion channels on bladder-innervating neurons during bladder stretch. This sensory information is relayed *via* synapses within the spinal cord dorsal horn to the brainstem or thalamus (Fowler et al., 2008). The intensity of this sensory signal is proportional to the degree of bladder stretch, leading to the progression of bladder sensations from fulness, to urge, discomfort and finally pain (Fowler et al., 2008; Grundy et al., 2018b). An increase in the intensity of this sensory afferent signal thus leads to exaggerated sensation at lower bladder volumes.

Mechanisms of Infection/Inflammation Induced Hypersensitivity

The penetration of bladder-innervating sensory neurons into the sub-urothelium and urothelium provides the underlying physiological architecture to allow urinary tract infection and inflammation to induce the symptoms of OAB (Spencer et al., 2018). A number of mouse studies have shown that various inflammatory conditions and inflammatory mediators increase the excitability of bladder innervating sensory neurons (de Groat and Yoshimura, 2009; Grundy et al., 2020a). Furthermore, and as described above, it is well established that acute urinary tract infection evokes a potent inflammatory response in mice, consisting of a significant increase in cytokines and other secreted factors (Abraham and Miao, 2015; Brierley et al., 2020).

In order to test the hypothesis that UTI induced inflammation causes exaggerated bladder sensory signalling, our recent study investigated how inflammatory mediators released during acute UTI in mice altered bladder sensory nerve activity to distension utilising an established *ex-vivo* bladder afferent recording model (Grundy et al., 2018b; Grundy et al., 2020a; Grundy et al., 2020b; Brierley et al., 2020). Pooled inflammatory supernatants containing an array of cytokines were isolated from mice 8 h after infection with uropathogenic *E. coli*. This inflammatory supernatant was then instilled into the bladder lumen of non-infected mice, and both intra-bladder pressure and sensory nerve activity during graded bladder distension were recorded. Through these experiments we were able to show that the inflammatory environment that is generated during UTI is able to sensitise bladder sensory neurons to distension,

exaggerating the mechanosensitive response to bladder filling and reducing the activation threshold pressure (Brierley et al., 2020). As such, neurons that usually only respond to noxious levels of bladder distension (high-threshold afferents), now exhibited robust responses to physiological levels of distension in the presence of the UTI supernatant. In addition, previously mechanically insensitive "silent" afferents became mechanosensitive in the presence of inflammatory supernatants, further increasing the overall sensory output from the bladder. These experiments in rodents provide key mechanistic insights into the molecular interactions that may mediate the development of infection induced bladder hypersensitivity in patients. The real life significance of these molecular interactions is that hyperexcitability of bladder sensory pathways translates to lower perception thresholds, which may generate the primary symptoms of OAB seen in patients, including urgency, frequency, and nocturia (Parsons and Drake, 2011; Yoshimura et al., 2014; Grundy et al., 2020a; Grundy et al., 2020b; Brierley et al., 2020).

It is also possible that bacteria are able to directly and indirectly sensitise bladder-innervating sensory neurons. Bacteria can activate sensory neurons that modulate pain in the skin (Chiu et al., 2013). Furthermore, the toxins and metabolites released during bacterial growth and invasion are able to sensitise neurons, as well as in-directly activate neurons and evoke pain (Chiu et al., 2013; Yang and Chiu, 2017; Blake et al., 2018; Uhlig et al., 2020). This has recently been explored *in vitro* using the cell bodies of bladder-innervating sensory neurons isolated from the dorsal root ganglia (DRG) of mice (Montalbetti et al., 2022). In these experiments, both LPS and the virulence factors produced by UPEC during growth were able to sensitise subsets of bladder-innervating sensory neurons to enhance their excitability, representing an additional mechanism whereby infection may be able to evoke hypersensitive bladder symptoms.

Indirect Mechanisms

As well as directly activating bladder afferent nerves, bladder infection also promotes urothelial shedding, a host-defence mechanism that rapidly removes infected urothelial cells from the bladder wall (Rosen et al., 2007; Smith et al., 2008; Thumbikat et al., 2009; Wood et al., 2012). Whilst effective in preventing bacteria establishing a foothold within the urothelium, this mechanism transiently increases bladder permeability until the infection is cleared and injury-induced proliferation of urothelial cells restores urothelial barrier integrity (Mysorekar et al., 2009; Shin et al., 2011). Increased urothelial permeability provides an opportunity for the toxic contents of the urine, that are usually sequestered in the bladder lumen, to access underlying sensory nerves. In our model of experimentally induced bladder permeability in mice we have been able to show increased urothelial permeability induces excitability of mechanosensitive bladder afferents (Grundy et al., 2020b), suggesting that increased bladder permeability alone may give rise to bladder sensory symptoms associated with neuronal hyperexcitability.

EVIDENCE AND IMPLICATIONS FOR CLINICAL PRACTICE

The information presented in this review poses a number of questions relating to the treatment and diagnosis of OAB. Chief amongst these include the potential use of antibiotics and anti-inflammatory drugs in the treatment of subsets of OAB patients. And could the presence of specific inflammatory mediators or intracellular bacterial colonies in the urine be exploited as a novel diagnostic biomarker for identifying these otherwise overlooked patients?

Does Antibiotic Treatment of Urinary Tract Infections Relieve Overactive Bladder Symptoms?

There have been two prospective trials of rotating antibiotics for patients with OAB (Khasriya et al., 2011; Vijaya et al., 2013b). The first study demonstrated improvements in urinary leakage and urgency in women treated with prolonged courses of antibiotics in addition to standard anticholinergic therapy (Khasriya et al., 2011). This was followed by a second study confirming similar results in a more refractory OAB group (Vijaya et al., 2013b).

As a result of the promising outcome from the two prospective studies we conducted a placebo controlled randomised trial involving 6 weeks of antibiotics in addition to standard anticholinergic therapy in patients with refractory detrusor overactivity (Chen et al., 2021a). Microbiological data was collected throughout the trial with 10 samples per patient collected over 6 months. This phase IIb trial revealed that antibiotic therapy reduced UTI rates, and corresponded with a clinically significant reduction in urinary incontinence on 24 h pad test (pad weight reduced by 75 g, $p < 0.008$) at 6 months. Improvements were also seen in measures of OAB symptoms such as leaks per day (1 less leak by 6 weeks and 2 less leaks per day by 6 months). In addition, patients who received antibiotics reported improvements on quality of life measures such as ICIQ, and OAB-q. Importantly, this improvement was sustained throughout the next 6 months [significant lower ICIQ score (Mean −5.57)], despite only 6 weeks of antibiotic therapy. Because of the robust collection and analysis of the relevant outcome measures, this study was able to provide objective evidence (i.e., reduced amount of leakage experienced in 24 h) of the biological effect of antibiotics in patients with OAB who were refractory to standard treatments. Based on these findings we concluded that lower rates of UTI experienced by OAB patients treated with antibiotics, and thus lower inflammation, may account for the increased response to anticholinergics in the subsequent months.

In addition to the findings described above, the longitudinal nature of the trial also revealed UTI requiring antibiotic treatment in over 40% of the OAB women who were in the placebo arm. In addition, post antibiotic therapy, breakthrough infections were identified in almost 20% of the women in the antibiotic group. The high rates of symptomatic UTI in the refractory OAB cohort emphasises the importance of UTI to the aetiology of this condition, and supports the proposed

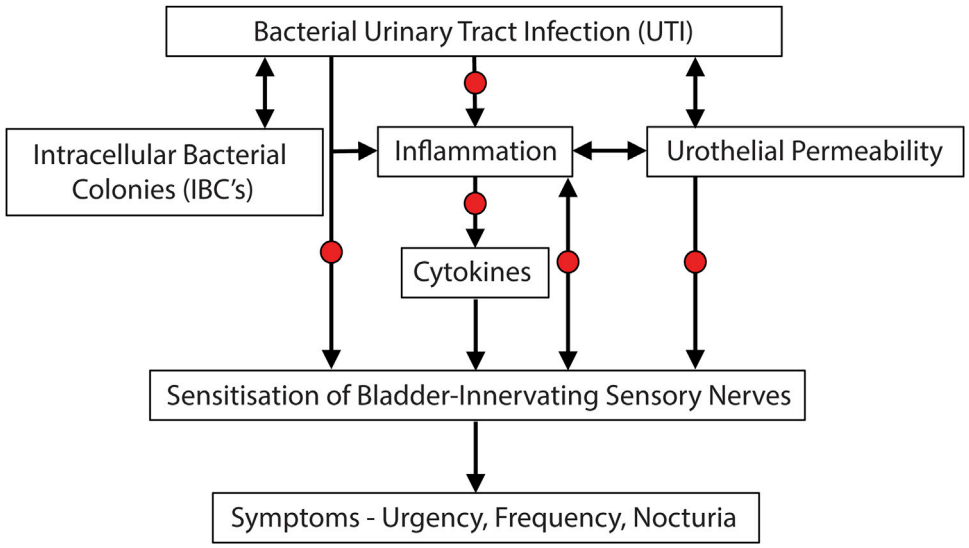

FIGURE 3 | Potential etiological cascade and pathogenesis underlying UTI induced symptoms of bladder hypersensitivity. Evidence is accumulating that subsets of OAB patients may in fact have an underlying bacterial infection, leading to inflammation and the sensitisation of bladder-innervating sensory nerves. Arrows represent causative links. Red dots represent potential opportunities for treatment of UTI induced OAB symptoms.

paradigm of an infectious subgroup of OAB patients. The trial was halted after interim analysis, due to recruitment issues and ethical concerns raised by the high rates of UTI in these patients.

Does Antibiotic Treatment of Urinary Tract Infections Reduce Inflammation and Intracellular Bacterial Colonies?

Using samples collected as part of the phase IIb trial described above, we were able to investigate the mechanisms behind the improvement in outcomes in the OAB patients. Our follow-up analysis of the trial cohort revealed that cytokines associated with activation of the innate immune system are reduced by antibiotic therapy in women with OAB (Chen et al., 2021b). In particular, antibiotic treatment was associated with significant reductions of pro-inflammatory cytokines IL-1α, IL-1Ra, IL-6, IL-8, and CXCL-10 and the anti-inflammatory cytokine IL-10, which are all cytokines typically present in UTIs (Sundac et al., 2016). The lower concentrations of the pro-inflammatory cytokines, especially CXCL-10, were associated with lower OAB symptom score, suggesting decreasing the inflammatory response leads to less urgency experienced by OAB patients treated with antibiotics. Other studies also support the hypothesis that changes in cytokine concentrations correlates with symptom severity. For example, Pillalamarri et al. (2018) reported that the pro-inflammatory cytokine IL-1β expression was significantly associated with worsening OAB symptoms (Pillalamarri et al., 2018). A recent longitudinal study showed the anti-inflammatory cytokine IL-6 was found to be significantly higher in OAB patients when compared with controls, which also correlated with both bacterial growth and pyuria count over a 12 month period (Smelov et al., 2016). Another longitudinal study (conducted over 12–14 weeks) reported that at the initial visit MCP-1 levels correlated with symptom severity and that MCP-1 levels decreased in women who responded to treatment (Ghoniem et al., 2020).

As well as affecting release of proinflammatory cytokines, antibiotic treatment was also found to significantly reduced high-density IBC's in exfoliated urothelial cells from OAB patients (Ognenovska et al., 2021). The decrease in high-density IBC's significantly correlated with improved symptom scores (reduction in urinary incontinence, decreased leaks per day and decreased voids per day) (Ognenovska et al., 2021). Antibiotic therapy also significantly reduced the likelihood of identifying bacterial filaments in samples from women with OAB (Ognenovska et al., 2021). As mentioned previously, bacterial filaments are associated with intracellular growth of UPEC (Justice et al., 2006). In addition, antibiotic therapy increased the proportion of urothelial cells that were free of bacteria.

Thus, while antibiotic therapy appears to be effective in relieving OAB symptoms, issues surrounding microbial resistance and breakthrough infection suggest that alternative treatments for UTI are warranted. Recently, anti-inflammatory agents such as ibuprofen and indomethacin have been shown to improve symptoms of acute UTI in patients without OAB (Gágyor et al., 2015; Kronenberg et al., 2017). Randomised trials have also shown that ibuprofen given to woman with suspected UTI can reduce dysuria and need for subsequent antibiotics (Moore et al., 2019). Interestingly, two small studies in the 1980s demonstrated that indomethacin significantly improved urge incontinence symptoms in women with OAB (Cardozo and Stanton, 1980; Delaere et al., 1981). However, due to limited understanding of the role of urinary tract infections in

OAB at the time, no further studies using these therapies were undertaken.

The studies outlined above have determined that antibiotic therapy leads to improvement in OAB symptoms in women who are refractory to other standard treatments. This improvement in symptoms is associated with a decrease in the urine concentration of pro-inflammatory cytokines and a decrease in the presence of bacteria associated with the urothelium. Combined these studies provide evidence for an inflammatory/infectious aetiology of OAB in women who are refractory to standard therapy. We therefore hypothesise that in women who are refractory to standard therapy, UTI leads to intracellular colonisation of urothelial cells, triggering an inflammatory response (with release of cytokines) and an increase in urothelial permeability. This then sensitises bladder sensory nerves so that they respond more easily to mechanical stretch of the bladder wall. This sensitisation then triggers the symptoms associated with OAB including urgency, frequency and nocturia (**Figure 3**).

CONCLUSION

There is accumulating evidence that we need to revisit the OAB phenotype given the association of the condition with bacterial colonisation of the urothelium. Multiple studies now implicate genuine UTI in the pathogenesis of OAB for a sub-group of patients who are refractory to standard therapy. The detection of bacterial invasion of urothelial cells, and subsequent inflammation, are shown to be key elements in prompting sensitisation of bladder-innervating sensory nerves to bladder distension, which would then evoke the symptoms of urgency, frequency, and nocturia. Small scale trials have shown antibiotics may be a useful tool to treat these patients, however, due to the growing risk of antibiotic resistance, prescription of antibiotics to large cohorts of patients is not desirable. As such, there is a need for alternative therapies to treat the infection and pro-inflammatory state that may include anti-inflammatory agents, or other treatments targeting the microbiome and urothelial environment. In addition, the methods used to diagnose UTI need to be improved. The current threshold values used to diagnose UTI are misleading and the culture techniques used often fail to detect the presence of bacteria. Improvements in our approaches for identifying the presence of bacteria in urine would greatly enhance our capacity to accurately diagnose UTI.

AUTHOR CONTRIBUTIONS

All authors contributed to the conceptualisation and completion of this manuscript. LG drafted the manuscript with significant contributions from KJM, ZC, and KHM.

FUNDING

Work was supported by a research grant awarded to LG by the Flinders Foundation, a research grant awarded to ZC by the Urogynaecological Society of Australasia and a research grant awarded to KHM through the BUPA Health Foundation (grant reference: RG140045).

ACKNOWLEDGMENTS

This work was originally collated for an International Continence Society (ICS) workshop at the 2021 annual scientific meeting and presented by KJM, ZC, KHM, and LG. We would like to thank the ICS for the opportunity to present this work.

REFERENCES

Abraham, S. N., and Miao, Y. (2015). The Nature of Immune Responses to Urinary Tract Infections. *Nat. Rev. Immunol.* 15 (10), 655–663. doi:10.1038/nri3887

Alkis, O., Zumrutbas, A. E., Toktas, C., Aybek, H., and Aybek, Z. (2017). The Use of Biomarkers in the Diagnosis and Treatment of Overactive Bladder: Can We Predict the Patients Who Will Be Resistant to Treatment? *Neurourol. Urodynam.* 36 (2), 390–393. doi:10.1002/nau.22939

Apostolidis, A., Dasgupta, P., Denys, P., Elneil, S., Fowler, C. J., Giannantoni, A., et al. (2009). Recommendations on the Use of Botulinum Toxin in the Treatment of Lower Urinary Tract Disorders and Pelvic Floor Dysfunctions: a European Consensus Report. *Eur. Urol.* 55 (1), 100–120. doi:10.1016/j.eururo.2008.09.009

Armbruster, C. E., Smith, S. N., Mody, L., and Mobley, H. L. T. (2018). Urine Cytokine and Chemokine Levels Predict Urinary Tract Infection Severity Independent of Uropathogen, Urine Bacterial Burden, Host Genetics, and Host Age. *Infect. Immun.* 86 (9), e00327. doi:10.1128/IAI.00327-18

Blake, K. J., Baral, P., Voisin, T., Lubkin, A., Pinho-Ribeiro, F. A., Adams, K. L., et al. (2018). *Staphylococcus aureus* Produces Pain through Pore-Forming Toxins and Neuronal TRPV1 that Is Silenced by QX-314. *Nat. Commun.* 9 (1), 37. doi:10.1038/s41467-017-02448-6

Brierley, S. M., Goh, K. G. K., Sullivan, M. J., Moore, K. H., Ulett, G. C., and Grundy, L. (2020). Innate Immune Response to Bacterial Urinary Tract Infection Sensitises High-Threshold Bladder Afferents and Recruits Silent Nociceptors. *Pain* 161 (1), 202–210. doi:10.1097/j.pain.0000000000001692

Cardozo, L. D., and Stanton, S. L. (1980). A Comparison between Bromocriptine and Indomethacin in the Treatment of Detrusor Instability. *J. Urology* 123 (3), 399–401. doi:10.1016/s0022-5347(17)55955-8

Chen, J. L., and Kuo, H. C. (2020). Clinical Application of Intravesical Botulinum Toxin Type A for Overactive Bladder and Interstitial Cystitis. *Investig. Clin. Urol.* 61 (Suppl. 1), S33–S42. doi:10.4111/icu.2020.61.S1.S33

Chen, Z., Ognenovska, S., Mansfield, K. J., Dally, E., Sluyter, R., Moore, K. H., et al. (2019). *Are Urinary Cytokines Signalling Altered in Refractory Detrusor Overactivity Women with Urinary Tract Infections?*, International Continence Society meeting Gothenburg, Sweden, 3-6 September 2019, Abstract 568

Chen, Z., Moore, K. H., Mansfield, K. J., Ognenovska, S., Allen, W., Parkin, K., et al. (2021). Effect of Antibiotics on Urine Leakage in Women with Refractory Detrusor Overactivity: A Phase IIb Randomized Trial. *Neurourol. Urodynamics* 40 (1), 158–167. doi:10.1002/nau.24525

Chen, Z., Ognenovska, S., Sluyter, R., Moore, K. H., and Mansfield, K. J. (2021). Urinary Cytokines in Women with Refractory Detrusor Overactivity: A Longitudinal Study of Rotating Antibiotic versus Placebo Treatment. *PLoS One* 16 (3), e0247861. doi:10.1371/journal.pone.0247861

Chen, Z., Phan, M.-D., Bates, L. J., Peters, K. M., Mukerjee, C., Moore, K. H., et al. (2018). The Urinary Microbiome in Patients with Refractory Urge Incontinence

and Recurrent Urinary Tract Infection. *Int. Urogynecol J.* 29 (12), 1775–1782. doi:10.1007/s00192-018-3679-2

Cheng, Y., Chen, Z., Gawthorne, J. A., Mukerjee, C., Varettas, K., Mansfield, K. J., et al. (2016). Detection of Intracellular Bacteria in Exfoliated Urothelial Cells from Women with Urge Incontinence. *Pathog. Dis.* 74 (7), ftw067. doi:10.1093/femspd/ftw067

Chiu, I. M., Heesters, B. A., Ghasemlou, N., Von Hehn, C. A., Zhao, F., Tran, J., et al. (2013). Bacteria Activate Sensory Neurons that Modulate Pain and Inflammation. *Nature* 501 (7465), 52–57. doi:10.1038/nature12479

Chu, C. M., and Lowder, J. L. (2018). Diagnosis and Treatment of Urinary Tract Infections across Age Groups. *Am. J. Obstetrics Gynecol.* 219 (1), 40–51. doi:10.1016/j.ajog.2017.12.231

Contreras-Sanz, A., Krska, L., Balachandran, A. A., Curtiss, N. L., Khasriya, R., Kelley, S., et al. (2016). Altered Urothelial ATP Signaling in a Major Subset of Human Overactive Bladder Patients with Pyuria. *Am. J. Physiology-Renal Physiology* 311 (4), F805–F816. doi:10.1152/ajprenal.00339.2015

Coyne, K. S., Sexton, C. C., Kopp, Z. S., Ebel-Bitoun, C., Milsom, I., and Chapple, C. (2011). The Impact of Overactive Bladder on Mental Health, Work Productivity and Health-Related Quality of Life in the UK and Sweden: Results from EpiLUTS. *BJU Int.* 108 (9), 1459–1471. doi:10.1111/j.1464-410x.2010.10013.x

Cui, Y., Cai, T., Dong, T., Zhang, X., Zhou, Z., Lu, Y., et al. (2021). Trigonal-Sparing vs. Trigonal-Involved OnabotulinumtoxinA Injection for the Treatment of Overactive Bladder: A Systematic Review and Meta-Analysis. *Front. Neurol.* 12, 651635. doi:10.3389/fneur.2021.651635

Davidoff, R., Yamaguchi, R., Leach, G. E., Park, E., and Lad, P. M. (1997). Multiple Urinary Cytokine Levels of Bacterial Cystitis. *J. Urology* 157 (5), 1980–1985. doi:10.1097/00005392-199705000-00125

de Groat, W. C., Griffiths, D., and Yoshimura, N. (2015). Neural Control of the Lower Urinary Tract. *Compr. Physiol.* 5 (1), 327–396. doi:10.1002/cphy.c130056

de Groat, W. C., and Yoshimura, N. (2009). Afferent Nerve Regulation of Bladder Function in Health and Disease. *Handb. Exp. Pharmacol.* (194), 91–138. doi:10.1007/978-3-540-79090-7_4

Delaere, K. P. J., Debruyne, F. M. J., and Moonen, W. A. (1981). The Use of Indomethacin in the Treatment of Idiopathic Bladder Instability. *Urol. Int.* 36 (2), 124–127. doi:10.1159/000280402

Digesu, G. A., Sadenghi, P., Sharma, S., Puccini, F., Tubaro, A., Fernando, R., et al. (2013). The Importance of Cystoscopy and Bladder Biopsy in Women with Refractory Overactive Bladder: the Urogynaecologist's Point of View? *Eur. J. Obstetrics Gynecol. Reproductive Biol.* 169 (2), 408–411. doi:10.1016/j.ejogrb.2013.05.027

Duell, B. L., Carey, A. J., Tan, C. K., Cui, X., Webb, R. I., Totsika, M., et al. (2012). Innate Transcriptional Networks Activated in Bladder in Response to Uropathogenic *Escherichia coli* Drive Diverse Biological Pathways and Rapid Synthesis of IL-10 for Defense against Bacterial Urinary Tract Infection. *J. Immunol.* 188 (2), 781–792. doi:10.4049/jimmunol.1101231

Eapen, R., and Radomski, S. (2016). Review of the Epidemiology of Overactive Bladder. *Res. Rep. Urol.* 8, 71–76. doi:10.2147/rru.s102441

Engel, D., Dobrindt, U., Tittel, A., Peters, P., Maurer, J., Gütgemann, I., et al. (2006). Tumor Necrosis Factor Alpha- and Inducible Nitric Oxide Synthase-Producing Dendritic Cells Are Rapidly Recruited to the Bladder in Urinary Tract Infection but Are Dispensable for Bacterial Clearance. *Infect. Immun.* 74 (11), 6100–6107. doi:10.1128/iai.00881-06

Farhan, B., Chang, H., Ahmed, A., Zaldivair, F., and Ghoniem, G. (2019). Characterisation of Urinary Monocyte Chemoattractant Protein 1: Potential Biomarker for Patients with Overactive Bladder. *Arab J. Urology* 17 (1), 58–60. doi:10.1080/2090598x.2019.1589932

Fowler, C. J., Griffiths, D., and de Groat, W. C. (2008). The Neural Control of Micturition. *Nat. Rev. Neurosci.* 9 (6), 453–466. doi:10.1038/nrn2401

Gágyor, I., Jutta, B., Michael, M. K., Guido, S., Karl, W., Eva, H-P., et al. (2015). Ibuprofen versus Fosfomycin for Uncomplicated Urinary Tract Infection in Women: Randomised Controlled Trial. *BMJ* 351, h6544. doi:10.1136/bmj.h6544

Ganz, M. L., Smalarz, A. M., Krupski, T. L., Anger, J. T., Hu, J. C., Wittrup-Jensen, K. U., et al. (2010). Economic Costs of Overactive Bladder in the United States. *Urology* 75 (3), 526e1–53218. doi:10.1016/j.urology.2009.06.096

Geppetti, P., Nassini, R., Materazzi, S., and Benemei, S. (2008). The Concept of Neurogenic Inflammation. *BJU Int.* 101 (Suppl. 3), 2–6. doi:10.1111/j.1464-410X.2008.07493.x

Ghoniem, G., Farhan, B., Csuka, D., and Zaldivar, F. (2020). Potential Role of Monocyte Chemoattractant Protein-1 in Monitoring Disease Progression and Response to Treatment in Overactive Bladder Patients. *Int. Neurourol. J.* 24 (4), 341–348. doi:10.5213/inj.2040366.183

Ghoniem, G., Faruqui, N., Elmissiry, M., Mahdy, A., Abdelwahab, H., Oommen, M., et al. (2011). Differential Profile Analysis of Urinary Cytokines in Patients with Overactive Bladder. *Int. Urogynecol J.* 22 (8), 953–961. doi:10.1007/s00192-011-1401-8

Gill, K., Horsley, H., Swamy, S., Khasriya, R., and Malone-Lee, J. (2021). A Prospective Observational Study of Urinary Cytokines and Inflammatory Response in Patients with Overactive Bladder Syndrome. *BMC Urol.* 21 (1), 39. doi:10.1186/s12894-021-00809-4

Gill, K., Kang, R., Sathiananthamoorthy, S., Khasriya, R., and Malone-Lee, J. (2018). A Blinded Observational Cohort Study of the Microbiological Ecology Associated with Pyuria and Overactive Bladder Symptoms. *Int. Urogynecol J.* 29 (10), 1493–1500. doi:10.1007/s00192-018-3558-x

Gormley, E. A., Lightner, D. J., Faraday, M., and Vasavada, S. P. (2015). Diagnosis and Treatment of Overactive Bladder (Non-neurogenic) in Adults: AUA/SUFU Guideline Amendment. *J. Urology* 193 (5), 1572–1580. doi:10.1016/j.juro.2015.01.087

Grundy, L., Andrea, M. H., Ashlee, C., Joel, C., Vasiliki, S., Vladimir, P. Z., et al. (2018). Translating Peripheral Bladder Afferent Mechanosensitivity to Neuronal Activation within the Lumbosacral Spinal Cord of Mice. *Pain* 160 (4), 793–804. doi:10.1097/j.pain.0000000000001453

Grundy, L., Caldwell, A., and Brierley, S. M. (2018). Mechanisms Underlying Overactive Bladder and Interstitial Cystitis/Painful Bladder Syndrome. *Front. Neurosci.* 12, 931. doi:10.3389/fnins.2018.00931

Grundy, L., Caldwell, A., Garcia Caraballo, S., Erickson, A., Schober, G., Castro, J., et al. (2020). Histamine Induces Peripheral and Central Hypersensitivity to Bladder Distension *via* the Histamine H1 Receptor and TRPV1. *Am. J. Physiology-Renal Physiology* 318 (2), F298–f314. doi:10.1152/ajprenal.00435.2019

Grundy, L., Caldwell, A., Lumsden, A., Mohammadi, E., Hannig, G., Greenwood Van-Meervald, B., et al. (2020). Experimentally Induced Bladder Permeability Evokes Bladder Afferent Hypersensitivity in the Absence of Inflammation. *Front. Neurosci.* 14, 590871. doi:10.3389/fnins.2020.590871

Grundy, L., Erickson, A., and Brierley, S. M. (2019). Visceral Pain. *Annu. Rev. Physiol.* 81, 261–284. doi:10.1146/annurev-physiol-020518-114525

Guo, C., Yang, B., Gu, W., Peng, B., Xia, S., Yang, F., et al. (2013). Intravesical Resiniferatoxin for the Treatment of Storage Lower Urinary Tract Symptoms in Patients with Either Interstitial Cystitis or Detrusor Overactivity: A Meta-Analysis. *PLOS ONE* 8 (12), e82591. doi:10.1371/journal.pone.0082591

Hannan, T. J., Mysorekar, I. U., Hung, C. S., Isaacson-Schmid, M. L., and Hultgren, S. J. (2010). Early Severe Inflammatory Responses to Uropathogenic *E. coli* Predispose to Chronic and Recurrent Urinary Tract Infection. *PLoS Pathog.* 6 (8), e1001042. doi:10.1371/journal.ppat.1001042

Hannan, T. J., Roberts, P. L., Riehl, T. E., van der Post, S., Binkley, J. M., Schwartz, D. J., et al. (2014). Inhibition of Cyclooxygenase-2 Prevents Chronic and Recurrent Cystitis. *EBioMedicine* 1 (1), 46–57. doi:10.1016/j.ebiom.2014.10.011

Hessdoerfer, E., Jundt, K., and Peschers, U. (2011). Is a Dipstick Test Sufficient to Exclude Urinary Tract Infection in Women with Overactive Bladder? *Int. Urogynecol J.* 22 (2), 229–232. doi:10.1007/s00192-010-1263-5

Hsieh, P.-F., Chiu, H.-C., Chen, K.-C., Chang, C.-H., and Chou, E. (2016). Botulinum Toxin A for the Treatment of Overactive Bladder. *Toxins* 8 (3), 59. doi:10.3390/toxins8030059

Justice, S. S., Hunstad, D. A., Seed, P. C., and Hultgren, S. J. (2006). Filamentation by *Escherichia coli* Subverts Innate Defenses during Urinary Tract Infection. *Proc. Natl. Acad. Sci. U.S.A.* 103 (52), 19884–19889. doi:10.1073/pnas.0606329104

Khan, Z., Healey, G. D., Paravati, R., Berry, N., Rees, E., Margarit, L., et al. (2021). Chronic Urinary Infection in Overactive Bladder Syndrome: A Prospective, Blinded Case Control Study. *Front. Cell. Infect. Microbiol.* 11, 752275. doi:10.3389/fcimb.2021.752275

Khasriya, R. K., Brackenridge, A., Horsley, L., Sathiananthamoorthy, H., and Malone-Lee, S. J. (2011). The Antibiotic Treatment of OAB Cohort. 36th

Annual IUGA Meeting, Lisbon, Portugal, 28 June – 2 July 2011. *Int. Urogynecology J.* 22 (1), 1–195.

Khasriya, R., Khan, S., Lunawat, R., Bishara, S., Bignal, J., Malone-Lee, M., et al. (2010). The Inadequacy of Urinary Dipstick and Microscopy as Surrogate Markers of Urinary Tract Infection in Urological Outpatients with Lower Urinary Tract Symptoms without Acute Frequency and Dysuria. *J. Urology* 183 (5), 1843–1847. doi:10.1016/j.juro.2010.01.008

Khasriya, R., Sathiananthamoorthy, S., Ismail, S., Kelsey, M., Wilson, M., Rohn, J. L., et al. (2013). Spectrum of Bacterial Colonization Associated with Urothelial Cells from Patients with Chronic Lower Urinary Tract Symptoms. *J. Clin. Microbiol.* 51 (7), 2054–2062. doi:10.1128/jcm.03314-12

Kim, T. H., and Lee, K.-S. (2016). Persistence and Compliance with Medication Management in the Treatment of Overactive Bladder. *Investig. Clin. Urol.* 57 (2), 84–93. doi:10.4111/icu.2016.57.2.84

Kinsey, D., Pretorius, S., Glover, L., and Alexander, T. (2016). The Psychological Impact of Overactive Bladder: A Systematic Review. *J. Health Psychol.* 21 (1), 69–81. doi:10.1177/1359105314522084

Klumpp, D. J., Rycyk, M. T., Chen, M. C., Thumbikat, P., Sengupta, S., and Schaeffer, A. J. (2006). Uropathogenic *Escherichia coli* Induces Extrinsic and Intrinsic Cascades to Initiate Urothelial Apoptosis. *Infect. Immun.* 74 (9), 5106–5113. doi:10.1128/iai.00376-06

Kronenberg, A., Bütikofer, L., Odutayo, A., Mühlemann, K., da Costa, B. R., Battaglia, M., et al. (2017). Symptomatic Treatment of Uncomplicated Lower Urinary Tract Infections in the Ambulatory Setting: Randomised, Double Blind Trial. *Bmj* 359, j4784. doi:10.1136/bmj.j4784

Kunin, C. M., White, L. V., and Hua, T. H. (1993). A Reassessment of the Importance of Low-Count Bacteriuria in Young Women with Acute Urinary Symptoms. *Ann. Intern Med.* 119 (6), 454–460. doi:10.7326/0003-4819-119-6-199309150-00002

Ma, E., Vetter, J., Bliss, L., Lai, H. H., Mysorekar, I. U., and Jain, S. (2016). A Multiplexed Analysis Approach Identifies New Association of Inflammatory Proteins in Patients with Overactive Bladder. *Am. J. Physiology-Renal Physiology* 311 (1), F28–F34. doi:10.1152/ajprenal.00580.2015

Milsom, I., Abrams, P., Cardozo, L., Roberts, R. G., Thüroff, J., and Wein, A. J. (2001). How Widespread Are the Symptoms of an Overactive Bladder and How Are They Managed? A Population-Based Prevalence Study. *BJU Int.* 87 (9), 760–766. doi:10.1046/j.1464-410x.2001.02228.x

Montalbetti, N., Dalghi, M. G., Bastacky, S. I., Clayton, D. R., Ruiz, W. G., Apodaca, G., et al. (2022). Bladder Infection with Uropathogenic *Escherichia coli* Increases the Excitability of Afferent Neurons. *Am. J. Physiology-Renal Physiology* 322 (1), F1–F13. doi:10.1152/ajprenal.00167.2021

Moore, K. H., Simons, A., Mukerjee, C., and Lynch, W. (2000). The Relative Incidence of Detrusor Instability and Bacterial Cystitis Detected on the Urodynamic-Test Day. *BJU Int.* 85 (7), 786–792. doi:10.1046/j.1464-410x.2000.00619.x

Moore, K. H., Allen, W., Woodman, J., Bushati, A., and Burcher, E. (2013). Response to Resiniferatoxin in Women with Refractory Detrusor Overactivity: Role of Bacterial Cystitiss. *Aust. N. Z. Cont. J.* 19 (3), 66–73. doi:10.3316/informit.603263633470359

Moore, K. H., and Malykhina, A. P. (2014). What Is the Role of Covert Infection in Detrusor Overactivity, and Other LUTD? ICI-RS 2013. *Neurourol. Urodynam.* 33 (5), 606–610. doi:10.1002/nau.22589

Moore, M., Trill, J., Simpson, C., Webley, F., Radford, M., Stanton, L., et al. (2019). Uva-ursi Extract and Ibuprofen as Alternative Treatments for Uncomplicated Urinary Tract Infection in Women (ATAFUTI): a Factorial Randomized Trial. *Clin. Microbiol. Infect.* 25 (8), 973–980. doi:10.1016/j.cmi.2019.01.011

Morris, A. R., Westbrook, J. I., and Moore, K. H. (2008). A Longitudinal Study over 5 to 10 Years of Clinical Outcomes in Women with Idiopathic Detrusor Overactivity. *Bjog* 115 (2), 239–246. doi:10.1111/j.1471-0528.2007.01527.x

Mulvey, M. A., Schilling, J. D., and Hultgren, S. J. (2001). Establishment of a Persistent *Escherichia coli* Reservoir during the Acute Phase of a Bladder Infection. *Infect. Immun.* 69 (7), 4572–4579. doi:10.1128/iai.69.7.4572-4579.2001

Mysorekar, I. U., Isaacson-Schmid, M., Walker, J. N., Mills, J. C., and Hultgren, S. J. (2009). Bone Morphogenetic Protein 4 Signaling Regulates Epithelial Renewal in the Urinary Tract in Response to Uropathogenic Infection. *Cell host microbe* 5 (5), 463–475. doi:10.1016/j.chom.2009.04.005

Neugent, M. L., Hulyalkar, N. V., Nguyen, V. H., Zimmern, P. E., and De Nisco, N. J. (2020). Advances in Understanding the Human Urinary Microbiome and its Potential Role in Urinary Tract Infection. *mBio* 11 (2), e00218. doi:10.1128/mBio.00218-20

Ognenovska, S., Chen, Z., Mukerjee, C., Moore, K. H., and Mansfield, K. J. (2021). Bacterial Colonization of Bladder Urothelial Cells in Women with Refractory Detrusor Overactivity: the Effects of Antibiotic Therapy. *Pathog. Dis.* 79 (6), ftab031. doi:10.1093/femspd/ftab031

Parsons, B. A., and Drake, M. J. (2011). Animal Models in Overactive Bladder Research. *Handb. Exp. Pharmacol.* (202), 15–43. doi:10.1007/978-3-642-16499-6_2

Pierce, A. N., and Christianson, J. A. (2015). "Stress and Chronic Pelvic Pain. *Prog. Mol. Biol. Transl. Sci.* 131, 509–535. doi:10.1016/bs.pmbts.2014.11.009

Pillalamarri, N., Shalom, D. F., Pilkinton, M. L., Winkler, H. A., Chatterjee, P. K., Solanki, M., et al. (2018). Inflammatory Urinary Cytokine Expression and Quality of Life in Patients with Overactive Bladder. *Female Pelvic Med. Reconstr. Surg.* 24 (6), 449–453. doi:10.1097/spv.0000000000000492

Pinho-Ribeiro, F. A., Verri, W. A., Jr., and Chiu, I. M. (2017). Nociceptor Sensory Neuron-Immune Interactions in Pain and Inflammation. *Trends Immunol.* 38 (1), 5–19. doi:10.1016/j.it.2016.10.001

Price, T. K., Dune, T., Hilt, E. E., Thomas-White, K. J., Kliethermes, S., Brincat, C., et al. (2016). The Clinical Urine Culture: Enhanced Techniques Improve Detection of Clinically Relevant Microorganisms. *J. Clin. Microbiol.* 54 (5), 1216–1222. doi:10.1128/jcm.00044-16

Reynolds, W. S., Fowke, J., and Dmochowski, R. (2016). The Burden of Overactive Bladder on US Public Health. *Curr. Bladder Dysfunct. Rep.* 11 (1), 8–13. doi:10.1007/s11884-016-0344-9

Rodhe, N., Löfgren, S., Strindhall, J., Matussek, A., and Mölstad, S. (2009). Cytokines in Urine in Elderly Subjects with Acute Cystitis and Asymptomatic Bacteriuria. *Scand. J. Prim. Health Care* 27 (2), 74–79. doi:10.1080/02813430902757634

Rosen, D. A., Hooton, T. M., Stamm, W. E., Humphrey, P. A., and Hultgren, S. J. (2007). Detection of Intracellular Bacterial Communities in Human Urinary Tract Infection. *PLoS Med.* 4 (12), e329. doi:10.1371/journal.pmed.0040329

Schurch, B., de Sèze, M., Denys, P., Chartier-kastler, E., Haab, F., Everaert, K., et al. (2005). Botulinum Toxin Type a Is a Safe and Effective Treatment for Neurogenic Urinary Incontinence: Results of a Single Treatment, Randomized, Placebo Controlled 6-month Study. *J. Urology* 174 (1), 196–200. doi:10.1097/01.ju.0000162035.73977.1c

Shin, K., Lee, J., Guo, N., Kim, J., Lim, A., Qu, L., et al. (2011). Hedgehog/Wnt Feedback Supports Regenerative Proliferation of Epithelial Stem Cells in Bladder. *Nature* 472 (7341), 110–114. doi:10.1038/nature09851

Smelov, V., Naber, K., and Bjerklund Johansen, T. E. (2016). Improved Classification of Urinary Tract Infection: Future Considerations. *Eur. Urol. Suppl.* 15 (4), 71–80. doi:10.1016/j.eursup.2016.04.002

Smith, Y. C., Rasmussen, S. B., Grande, K. K., Conran, R. M., and O'Brien, A. D. (2008). Hemolysin of Uropathogenic *Escherichia coli* Evokes Extensive Shedding of the Uroepithelium and Hemorrhage in Bladder Tissue within the First 24 hours after Intraurethral Inoculation of Mice. *Infect. Immun.* 76 (7), 2978–2990. doi:10.1128/iai.00075-08

Spencer, N. J., Greenheigh, S., Kyloh, M., Hibberd, T. J., Sharma, H., Grundy, L., et al. (2018). Identifying Unique Subtypes of Spinal Afferent Nerve Endings within the Urinary Bladder of Mice. *J. Comp. Neurol.* 526 (4), 707–720. doi:10.1002/cne.24362

Stamm, W. E., Counts, G. W., Running, K. R., Fihn, S., Turck, M., and Holmes, K. K. (1982). Diagnosis of Coliform Infection in Acutely Dysuric Women. *N. Engl. J. Med.* 307 (8), 463–468. doi:10.1056/nejm198208193070802

Stark, R. P., and Maki, D. G. (1984). Bacteriuria in the Catheterized Patient. What Quantitative Level of Bacteriuria Is Relevant? *N. Engl. J. Med.* 311 (9), 560–564. doi:10.1056/nejm198408303110903

Sundac, L., Dando, S. J., Sullivan, M. J., Derrington, P., Gerrard, J., and Ulett, G. C. (2016). Protein-based Profiling of the Immune Response to Uropathogenic *Escherichia coli* in Adult Patients Immediately Following Hospital Admission for Acute Cystitis. *Pathog. Dis.* 74 (6), ftw062. doi:10.1093/femspd/ftw062

Tan, C. K., Carey, A. J., Cui, X., Webb, R. I., Ipe, D., Crowley, M., et al. (2012). Genome-wide Mapping of Cystitis Due to Streptococcus Agalactiae and *Escherichia coli* in Mice Identifies a Unique Bladder Transcriptome that

Signifies Pathogen-specific Antimicrobial Defense against Urinary Tract Infection. *Infect. Immun.* 80 (9), 3145–3160. doi:10.1128/iai.00023-12

Tandogdu, Z., and Wagenlehner, F. M. E. (2016). Global Epidemiology of Urinary Tract Infections. *Curr. Opin. Infect. Dis.* 29 (1), 73–79. doi:10.1097/qco.0000000000000228

Thumbikat, P., Berry, R. E., Zhou, G., Billips, B. K., Yaggie, R. E., Zaichuk, T., et al. (2009). Bacteria-induced Uroplakin Signaling Mediates Bladder Response to Infection. *PLoS Pathog.* 5 (5), e1000415. doi:10.1371/journal.ppat.1000415

Tyagi, P., Barclay, D., Zamora, R., Yoshimura, N., Peters, K., Vodovotz, Y., et al. (2010). Urine Cytokines Suggest an Inflammatory Response in the Overactive Bladder: a Pilot Study. *Int. Urol. Nephrol.* 42 (3), 629–635. doi:10.1007/s11255-009-9647-5

Tyagi, P., Tyagi, V., Qu, X., Chuang, Y. C., Kuo, H.-C., and Chancellor, M. (2016). Elevated CXC Chemokines in Urine Noninvasively Discriminate OAB from UTI. *Am. J. Physiology-Renal Physiology* 311 (3), F548–F554. doi:10.1152/ajprenal.00213.2016

Tyagi, P., Tyagi, V., Qu, X., Lin, H.-T., Kuo, H.-C., Chuang, Y.-C., et al. (2014). Association of Inflammaging (Inflammation + Aging) with Higher Prevalence of OAB in Elderly Population. *Int. Urol. Nephrol.* 46 (5), 871–877. doi:10.1007/s11255-013-0621-x

Uhlig, F., Grundy, L., Garcia-Caraballo, S., Brierley, S. M., Foster, S. J., and Grundy, D. (2020). Identification of a Quorum Sensing-dependent Communication Pathway Mediating Bacteria-Gut-Brain Cross Talk. *iScience* 23 (11), 101695. doi:10.1016/j.isci.2020.101695

Vijaya, G., Puccini, F., Dutta, S., Singh, A., Bray, R., Digesu, A., et al. (2013). 38th Annual IUGA Meeting, Dublin, Ireland, 28 May – 1 June 2013: Oral Presentations. *Int. Urogynecology J.* 24 (1), 79.

Vijaya, G., Cartwright, R., Derpapas, A., Gallo, P., Fernando, R., and Khullar, V. (2013). Changes in Nerve Growth Factor Level and Symptom Severity Following Antibiotic Treatment for Refractory Overactive Bladder. *Int. Urogynecol J.* 24 (9), 1523–1528. doi:10.1007/s00192-012-2038-y

Wagg, A., Compion, G., Fahey, A., and Siddiqui, E. (2012). Persistence with Prescribed Antimuscarinic Therapy for Overactive Bladder: a UK Experience. *BJU Int.* 110 (11), 1767–1774. doi:10.1111/j.1464-410x.2012.11023.x

Walsh, C. A., Cheng, Y., Mansfield, K. J., Parkin, K., Mukerjee, C., and Moore, K. H. (2013). Decreased Intravesical Adenosine Triphosphate in Patients with Refractory Detrusor Overactivity and Bacteriuria. *J. Urology* 189 (4), 1383–1387. doi:10.1016/j.juro.2012.10.003

Walsh, C. A., and Moore, K. H. (2011). Overactive Bladder in Women: Does Low-Count Bacteriuria Matter? A Review. *Neurourol. Urodyn.* 30 (1), 32–37. doi:10.1002/nau.20927

Walsh, C. A., Siddins, A., Parkin, K., Mukerjee, C., and Moore, K. H. (2011). Prevalence of "Low-Count" Bacteriuria in Female Urinary Incontinence versus Continent Female Controls: a Cross-Sectional Study. *Int. Urogynecol J.* 22 (10), 1267–1272. doi:10.1007/s00192-011-1506-0

Walsh, C. A., Allen, W., Parkin, K., Mukerjee, C., Moore, C. H., et al. (2011). Low-count Bacteriuria in Refractory Idiopathic Detrusor Overactivity versus Controls. *Urogynaecol. Int. J.* 25 (1). doi:10.4081/uij.2011.e4

Wein, A. J., and Rovner, E. S. (2002). Definition and Epidemiology of Overactive Bladder. *Urology* 60 (5 Suppl. 1), 7–12. discussion 12. doi:10.1016/s0090-4295(02)01784-3

Wood, M. W., Breitschwerdt, E. B., Nordone, S. K., Linder, K. E., and Gookin, J. L. (2012). Uropathogenic *E. coli* Promote a Paracellular Urothelial Barrier Defect Characterized by Altered Tight Junction Integrity, Epithelial Cell Sloughing and Cytokine Release. *J. Comp. pathology* 147 (1), 11–19. doi:10.1016/j.jcpa.2011.09.005

Yang, N. J., and Chiu, I. M. (2017). Bacterial Signaling to the Nervous System through Toxins and Metabolites. *J. Mol. Biol.* 429 (5), 587–605. doi:10.1016/j.jmb.2016.12.023

Yeowell, G., Smith, P., Nazir, J., Hakimi, Z., Siddiqui, E., and Fatoye, F. (2018). Real-world Persistence and Adherence to Oral Antimuscarinics and Mirabegron in Patients with Overactive Bladder (OAB): a Systematic Literature Review. *BMJ Open* 8 (11), e021889. doi:10.1136/bmjopen-2018-021889

Yoshimura, N., Ogawa, T., Miyazato, M., Kitta, T., Furuta, A., Chancellor, M. B., et al. (2014). Neural Mechanisms Underlying Lower Urinary Tract Dysfunction. *Korean J. Urol.* 55 (2), 81–90. doi:10.4111/kju.2014.55.2.81

Conflict of Interest: The authors declare that the research was conducted in the absence of any commercial or financial relationships that could be construed as a potential conflict of interest.

frontiers | Frontiers in Physiology

ORIGINAL RESEARCH
published: 19 July 2022
doi: 10.3389/fphys.2022.920636

Unveiling the Angiotensin-(1–7) Actions on the Urinary Bladder in Female Rats

*Gustavo B. Lamy[1], Eduardo M. Cafarchio[1], Bárbara do Vale[1], Bruno B. Antonio[1], Daniel P. Venancio[1], Janaina S. de Souza[2], Rui M. Maciel[3], Gisele Giannocco[2,3], Artur F. Silva Neto[4], Lila M. Oyama[4], Patrik Aronsson[5] and Monica A. Sato[1]**

[1]Department Morphology and Physiology, Centro Universitario FMABC, Santo Andre, Brazil, [2]Department Biological Sciences, Federal University of Sao Paulo, Diadema, Brazil, [3]Department Medicine, Federal University of Sao Paulo, Sao Paulo, Brazil, [4]Department Physiology, Federal University of Sao Paulo, Sao Paulo, Brazil, [5]Department Pharmacology, Institute of Neuroscience and Physiology, Sahlgrenska Academy, University of Gothenburg, Gothenburg, Sweden

Angiotensin-(1–7) is a peptide produced by different pathways, and regardless of the route, the angiotensin-converting enzyme 2 (ACE-2) is involved in one of the steps of its synthesis. Angiotensin-(1–7) binds to Mas receptors localized in different cells throughout the body. Whether angiotensin-(1–7) exerts any action in the urinary bladder (UB) is still unknown. We investigated the effects of intravenous and topical (*in situ*) administration of angiotensin-(1–7) on intravesical pressure (IP) and cardiovascular variables. In addition, the Mas receptors and ACE-2 gene and protein expression were analyzed in the UB. Adult female Wistar rats were anesthetized with 2% isoflurane in 100% O_2 and submitted to the catheterization of the femoral artery and vein for mean arterial pressure (MAP) and heart rate (HR) recordings, and infusion of drugs, respectively. The renal blood flow was acquired using a Doppler flow probe placed around the left renal artery and the renal conductance (RC) was calculated as a ratio of Doppler shift (kHz) and MAP. The cannulation of the UB was performed for IP recording. We observed that angiotensin-(1–7) either administered intravenously [115.8 ± 28.6% angiotensin-(1–7) vs. −2.9 ± 1.3% saline] or topically [147.4 ± 18.9% angiotensin-(1–7) vs. 3.2 ± 2.8% saline] onto the UB evoked a significant ($p < 0.05$) increase in IP compared to saline and yielded no changes in MAP, HR, and RC. The marked response of angiotensin-(1–7) on the UB was also investigated using quantitative real-time polymerase chain reaction and western blotting assay, which demonstrated the mRNA and protein expression of Mas receptors in the bladder, respectively. ACE-2 mRNA and protein expression was also observed in the bladder. Therefore, the findings demonstrate that angiotensin-(1–7) acts in the UB to increase the IP and suggest that this peptide can be also locally synthesized in the UB.

Keywords: intravesical pressure, ACE-2, Mas receptors, micturition, urinary bladder

OPEN ACCESS

Edited by:
Christian Moro,
Bond University, Australia

Reviewed by:
Iris Lim,
Bond University, Australia
Dominga Lapi,
University of Naples Federico II, Italy
Petya Hadzhibozheva,
Trakia University, Bulgaria

****Correspondence:***
Monica A. Sato
monica.akemi.sato@gmail.com

Specialty section:
This article was submitted to Integrative Physiology, a section of the journal Frontiers in Physiology

Received: *14 April 2022*
Accepted: *13 June 2022*
Published: *19 July 2022*

Citation:
Lamy GB, Cafarchio EM, do Vale B, Antonio BB, Venancio DP, de Souza JS, Maciel RM, Giannocco G, Silva Neto AF, Oyama LM, Aronsson P and Sato MA (2022) Unveiling the Angiotensin-(1–7) Actions on the Urinary Bladder in Female Rats. Front. Physiol. 13:920636. doi: 10.3389/fphys.2022.920636

INTRODUCTION

Urinary bladder (UB) disorders affect the daily life of several patients worldwide due to mental and social discomfort (Kajiwara et al., 2004; Sureshkumar et al., 2009). It has been reported that UB symptoms show a higher prevalence in women (Aoki et al., 2017).

The storage and subsequent expulsion of urine from the bladder are mediated through both central and peripheral mechanisms that remain to be fully elucidated. Reflexes important for these

functions are subject to direct cortical modulation, involving both facilitatory and inhibitory mechanisms. The Pontine Urine Storage Center, situated in the relative vicinity of the Pontine Micturition Center (PMC), which in turn initiates micturition (de Groat, 1998), regulates the storage of urine.

Neurons at several levels in the lumbosacral spinal cord and brain (raphe nucleus, reticular formation, locus coeruleus, red nucleus, PMC, hypothalamus, and cortex) have been shown to be connected to the UB, as demonstrated by retrograde labeling with pseudorabies virus (Nadelhaft et al., 1992).

Previous reports have shown that angiotensin II causes UB smooth muscle contraction in several species, including rabbits, monkeys, dogs, and humans (Falconieri-Erspamer et al., 1973; Lam et al., 2000). In the UB of adult humans, the action of angiotensin II is dependent on functional AT1 rather than on AT2 receptors (Andersson et al., 1992; Saito et al., 1993; Lam et al., 2000). Tanabe et al. (1993) have further demonstrated that AT1 receptors mediate contractions to angiotensin II in the rat bladder smooth muscle also *in vitro*. The UB dysfunction, which occurs after bladder outlet obstruction, has been attributed at least in part to angiotensin II acting on the AT1 receptor subtype (Yamada et al., 2009).

Angiotensin-(1–7) [Ang-(1–7)], an agonist on the Mas receptor, is synthesized in several pathways, for instance by cleavage of angiotensin I to angiotensin-(1–9) by ACE-2, and subsequent break-down by ACE and neutral endopeptidase 24.11 (NEP) (Chappell et al., 2000; Rice et al., 2004). In other words, angiotensin II cleavage into Ang-(1–7) by ACE-2 constitutes a physiologically important route (Vickers et al., 2002). Evidence in human ACE2 has demonstrated that its catalytic efficiency is 400-fold higher with angiotensin II as a substrate than with angiotensin I (Vickers et al., 2002; Rice et al., 2004). Likewise, this system (ACE-2/Ang-(1–7)/Mas receptor) is important in balancing detrimental actions of the ACE/Angiotensin II/AT-1 receptor axis, such as hypertension, atherosclerosis, and cardiac hypertrophy and fibrosis (Ferreira and Santos, 2005; Santos et al., 2018), albeit this mechanism alone does not explain all effects observed (Santos et al., 2000). Previous studies in Mas-knockout mice have demonstrated cardiovascular changes, ranging from induced hypertension and structural alterations in blood vessels to metabolic problems (Santos et al., 2006) (Xu et al., 2008), (de Moura et al., 2010) (Xu et al., 2008) (Santos et al., 2006).

Lamy et al. (2021) have demonstrated that Ang-(1–7) synthesized locally in the lateral preoptic area activates Mas receptors, which increases the IP without changes in renal conductance (RC) and cardiovascular variables. Despite Ang-(1–7) being found both peripherally and centrally (Santos and Campagnole-Santos, 1994), the role of Ang-(1–7) in the peripheral mechanisms involved in UB control is, to the best of our knowledge, largely unknown.

It is unclear whether peripheral Ang-(1–7) can act on the UB and, if so, would have any influence on UB dysfunctions or not. Furthermore, the presence of Mas receptors in the bladder or the existence of local synthesis of Ang-(1–7) mediated by ACE-2 in the UB is unknown. Thus, the present study focused on characterizing the effects of intravenous infusion and topical (*in situ*) administration of Ang-(1–7) on the UB and its impact on cardiovascular parameters. In addition, Mas receptor and ACE-2 gene and protein expression in the UB was investigated.

MATERIALS AND METHODS

Animals

Female Wistar rats (~230–250 g, 14–16 weeks old) supplied by the Animal Facility of the Faculdade de Medicina do ABC/Centro Universitario FMABC were used. The animals were housed in plastic cages in groups of four rats each and had free access to standard chow pellets (Nuvilab®) and tap water *ad libitum*. The animals were in an air-conditioned room with a temperature between 20°C and 24°C and a 12:12-h light–dark cycle. The humidity in the animal room was controlled and maintained at ~70%. All procedures of this study were carried out in accordance with the National Institutes of Health Guide for the Care and Use of Laboratory Animals. This study was approved by the Animal Ethics Committee of the Faculdade de Medicina do ABC/Centro Universitario ABC (protocol number 13/2017).

Cannulation of the Urinary Bladder

A small incision was carried out in the apex of the UB wall for insertion of a polyethylene tubing (PE-50 connected to PE-10, Clay Adams, NJ, United States) filled with saline as previously described by Cafarchio et al. (2016, 2018, and 2020), Magaldi et al. (2020), and Lamy et al. (2021). Tissue glue was used to keep the catheter fixed on the bladder wall for intravesical pressure (IP) recordings in a data acquisition system (PowerLab 16 SP, AD Instruments, Castle Hill, AU). The urethra outlet was not ligated to allow the bladder voiding if necessary. The baseline IP value was set at ~6–8 mmHg, and the adjustment of the baseline IP was done by infusion of saline or urine withdrawal through the catheter inserted into the bladder. Percent changes in IP (%ΔIP) were calculated as [(peak IP response—baseline IP)/baseline IP] × 100.

Cannulation of the Femoral Artery and Vein

The catheterization of the femoral artery and vein was performed through the insertion of a polyethylene tubing (PE-50 connected to PE-10, Clay Adams, NJ, United States) to measure pulsatile arterial pressure (PAP), mean arterial pressure (MAP), and heart rate (HR) in the data acquisition system (PowerLab 16 SP, AD Instruments, Castle Hill, AU) and injections of drugs, respectively.

Measurement of Regional Blood Flow

Rats underwent a midline laparotomy for placement of a miniaturized pulsed Doppler flow probe (0.8 mm in diameter, Iowa Doppler Products, Iowa City, IA, United States) around the left renal artery for indirect measurement of the blood flow. The probe was connected to a Doppler flowmeter (Department of Bioengineering, The University of Iowa, Iowa City, IA, United States), and the amplified signal was digitalized in a

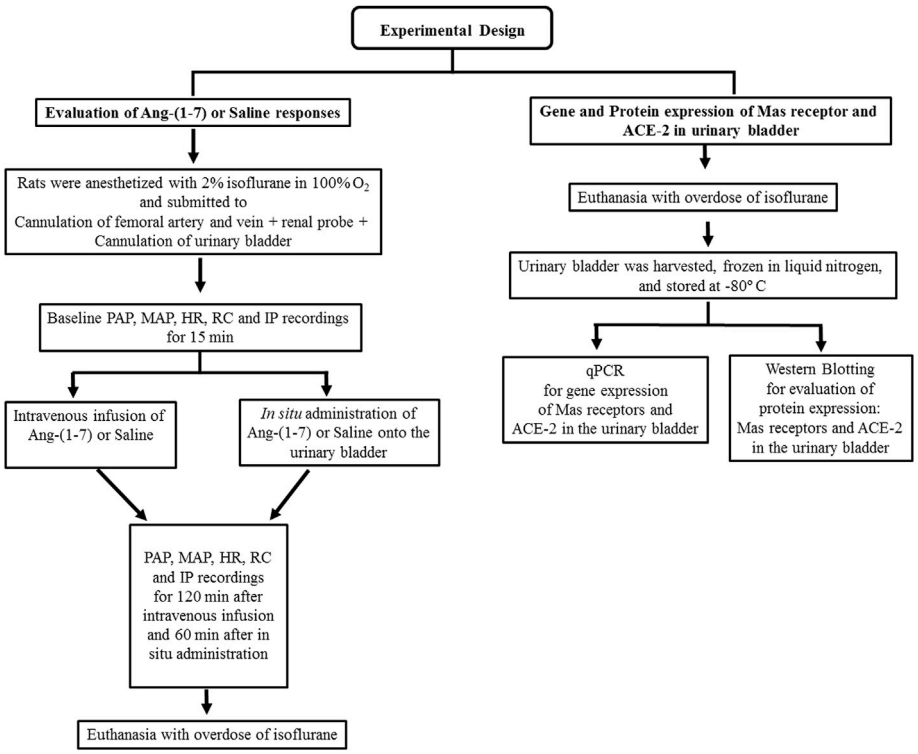

FIGURE 1 | Flowchart showing the experimental design of the study.

data acquisition system (PowerLab 16 SP, AD Instruments, Castle Hill, AU). Details about the readability of this method for estimation of the blood velocity and regarding the Doppler technique have been previously described by Haywood et al. (1981). Relative renal vascular conductance was calculated as the ratio of Doppler shift (kHz) and MAP (mmHg). Results were presented as percent change from the baseline [(final conductance − initial conductance)/initial conductance × 100].

Topical (*in situ*) Drug Administration

The topical administration of Ang-(1–7) was always performed at a dose of 100 ng/ml in a volume of 0.1 ml directly onto the surface of the UB.

Intravenous Drug Administration

Ang-(1–7) was administered intravenously at a dose of 0.24 μg/kg/min using an infusion pump (Insight Ltda, Ribeirão Preto, SP). The solution of Ang-(1–7) was prepared at a concentration of 0.24 μg/ml.

Experimental Protocols

Evaluation of Intravenous Administration of Angiotensin-(1–7) on Intravesical Pressure and Cardiovascular Variables in Female Wistar Rats (*N* = 6)

Rats anesthetized with isoflurane 2% in 100% O_2 were submitted to cannulation of the femoral artery and vein. A laparotomy was performed for placement of a miniaturized Doppler flowmeter probe around the left renal artery to measure the renal blood flow. The UB was also cannulated with a polyethylene tubing for IP recording. After baseline measurement of IP, arterial pressure, HR, and renal blood flow for 15 min, an infusion of Ang-(1–7) 0.24 μg/kg/min or saline (vehicle) was performed intravenously and the variables were measured for another 120 min (**Figure 1**). We have chosen the dose of Ang-(1–7) 0.24 μg/kg i.v. because it is equivalent to the lowest dose used by Durik et al. (2012) with stabilized Ang-(1–7) analog molecule that did not cause changes in cardiac parameters.

Evaluation of Topic (*in situ*) Administration of Angiotensin-(1–7) on Intravesical Pressure and Cardiovascular Variables in Female Wistar Rats (N = 6)

The animals were anesthetized with isoflurane 2% in O_2 100% and submitted to the same surgical procedures described in section 7.1. After baseline IP, arterial pressure, HR, and renal blood flow recordings for 15 min, topical (*in situ*) administration of Ang-(1–7) was done at a dose of 100 ng/ml in a volume of 0.1 ml or saline (0.1 ml). The topical administration was performed by dropping Ang-(1–7) or saline onto the surface of the UB, and the variables were measured for another 60 min (**Figure 1**).

This protocol was carried out to verify if Ang-(1–7) would elicit direct effects on the detrusor muscle of Wistar rats.

Gene Expression of Mas Receptors and ACE-2 in the Urinary Bladder (*n* = 6)

As shown in **Figure 1**, animals used in this protocol were not previously instrumented for IP and cardiovascular recordings. Rats

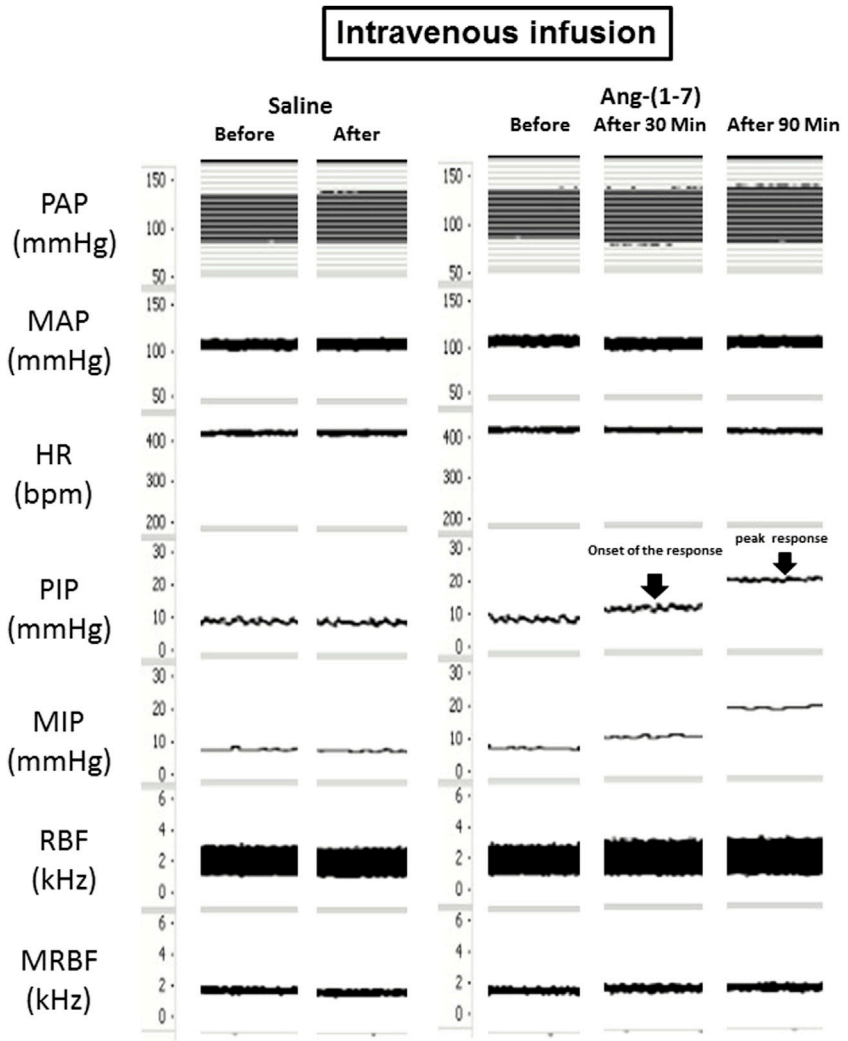

FIGURE 2 | Tracings showing the baseline pulsatile arterial pressure (PAP, mmHg), mean arterial pressure (MAP, mmHg), heart rate (HR, bpm), pulsatile intravesical pressure (PIP, mmHg), mean intravesical pressure (MIP, mmHg), renal blood flow (RBF, kHz) and mean renal blood flow (MRBF, kHz) and the responses induced by intravenous administration of angiotensin-(1–7) (0.24 μg/kg) or saline.

were deeply anesthetized with isoflurane 4% in 100 O_2 and submitted to a laparotomy for UB withdrawal. The bladder was immediately frozen in liquid nitrogen and stored at −80°C in an ultrafreezer until the day of total RNA extraction with the TRizol® reagent. The procedures for Mas receptors, ACE-2, and cyclophilin A gene expression were carried out through quantitative real-time polymerase chain reaction (qPCR) as follows.

Isolation of total mRNA from frozen UB samples was made with TRIzol Reagent® (Thermo Fisher Scientific) as suggested by the manufacturer's protocol. mRNA integrity was analyzed via agarose gel electrophoresis, and mRNA purity reached the following criteria: A260/280 ≥ 1.8. The extracted total mRNA concentration was measured using a NanoDrop™ (One-One c) spectrophotometer (Thermo Fisher Scientific). We used 1 μg of total mRNA for the reverse transcription reaction. Complementary DNA (cDNA) synthesis was obtained using the ImProm-II™ Reverse Transcription System (Promega, Madison, WC, United States), following the manufacturer's protocol. qPCR was performed using 2 μl of cDNA and the Eva Green™ qPCR Mix Plus (Solis BioDyne, Tartu, Estonia) in the ABI Prism 7500 Sequence Detection System (Applied Biosystems, Foster City, CA) to amplify specific primers sequences for the Mas receptors, ACE-2, and cyclophilin A. The forward and reverse primers sequences (Thermo Fisher Scientific) for rats are shown below:

Mas receptor:
(forward) 5′- CCTGCATACTGGGAAGACCA-3′
(reverse) 5′- TCCCTTCCTGTTTCTCATGG-3′
ACE-2:
(forward) 5′- TTGAACCAGGATTGGACGAAA-3′
(reverse) 5′- GCCCAGAGCCTACGATTGTAGT-3′
Cyclophilin A:
(forward) - 5′-CCCACCGTGTTCTTCGACAT-3′
(reverse) - 5′-CTGTCTTTGGAACTTTGTCTGCAA-3′

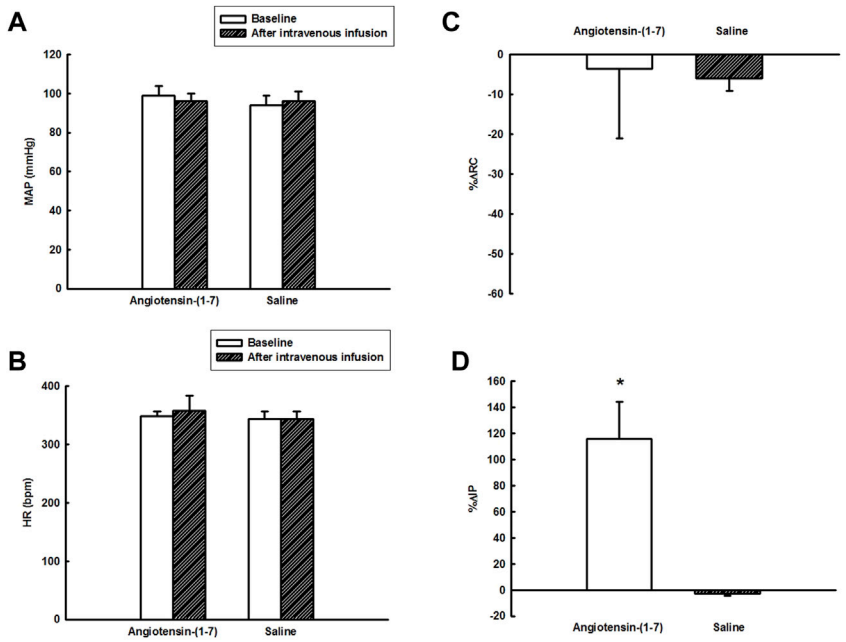

FIGURE 3 | (A) Mean arterial pressure (mmHg) and **(B)** heart rate (bpm) at baseline and after intravenous administration of angiotensin-(1–7) (0.24 μg/kg) or saline, **(C)** percent change in renal conductance (%ΔRC), and **(D)** percent change in intravesical pressure (%ΔIP) evoked by intravenous administration of angiotensin-(1–7) (0.24 μg/kg) or saline (n = 6). *p < 0.05 vs. saline (Student´s t-test).

The internal control (housekeeping gene) used in this protocol was cyclophilin A. The procedure followed an initial step of 10 min at 95°C, followed by 45 cycles of 20 s each at 95°C, 20 s at 58°C, and 20 s at 72°C. Gene expression was determined using threshold cycle (CT) (arbitrary units, A.U.), and all values were expressed using cyclophilin A as an internal control.

Protein Expression of theas Receptor and ACE-2 in the Urinary Bladder (n = 6)

As described in **Figure 1**, we used different groups of rats for protein and gene expression. Animals were deeply anesthetized with isoflurane 4% in 100% O_2. A laparotomy was carried out, and the UB was harvested and immediately frozen in liquid nitrogen. Bladder samples were stored at −80°C in an ultrafreezer for later determination of Mas receptor and ACE-2 protein expression in the UB via western blotting. The rats used in this protocol were not previously submitted to any surgery or IP and cardiovascular recordings. The procedures for the western blotting assay followed the steps described below.

The lysate of UB samples was obtained using radioimmunoprecipitation assay lysis and extraction buffer, added with a mixture of protease and phosphatase inhibitors (Thermo Fisher Scientific). The samples were homogenized in lysis buffer, incubated on ice for 10 min, and centrifuged at 7000 g for 5 min at 4°C. The supernatant containing the soluble proteins was stored at −80°C. The protein concentration was determined using NanoDrop™ (One-One c) spectrophotometer (Thermo Fisher Scientific). The total proteins were separated on a 10% sodium dodecyl sulfate–acrylamide gel and transferred to the nitrocellulose membrane (Bio-rad) by electrophoresis using the Trans-blot Turbo Transfer device (Bio-rad). Ponceau solution was used to stain the membrane to check successful transfer. The membrane was photographed in the Chemidoc device (Bio-rad) for the determination of total protein by densitometry using the Image Lab™ software (Bio-rad). Afterward, the membrane was washed with milli-Q water at least three times. The membrane was incubated for 1 h with 5% nonfat milk in Tris-buffered saline- 0.1% Tween 20 (TBS-T). Then, the solution was discarded and the membrane was incubated at 4°C, overnight, with a polyclonal primary antibody specific for the Mas receptor (rabbit anti-Mas, Novus Biologicals, catalog # NBP1-78444) and for ACE-2 (rabbit anti-ACE-2, Cloud-Clone Corp., catalog # PAB886Ra01) diluted to a concentration of 1: 250 in TBS-T. The blots were washed with TBS-T and afterward, incubated with goat–anti-rabbit secondary antibody (Alexa Fluor 488, Thermo Fischer Scientific) in a 1:10,000 dilution for 1 h, which causes a chemiluminescent reaction. The membrane was filmed in the Chemidoc device (Bio-rad). The Image Lab software ™ (Bio-rad) was used to quantify the densitometry of the blot containing the corresponding protein of interest. The optical density (OD) of Mas receptors and ACE-2 was normalized by the expression of total protein, as described in a previous study by Lamy et al. (2021).

Statistics

The Kolmogorov–Smirnov test was carried out to evaluate the normality of data distribution. Results were expressed as mean ± S.E.M as they showed a normal distribution. Unpaired Student's t-test was used for comparison between the %ΔIP or %ΔRC responses evoked by Ang-(1–7) versus saline administered

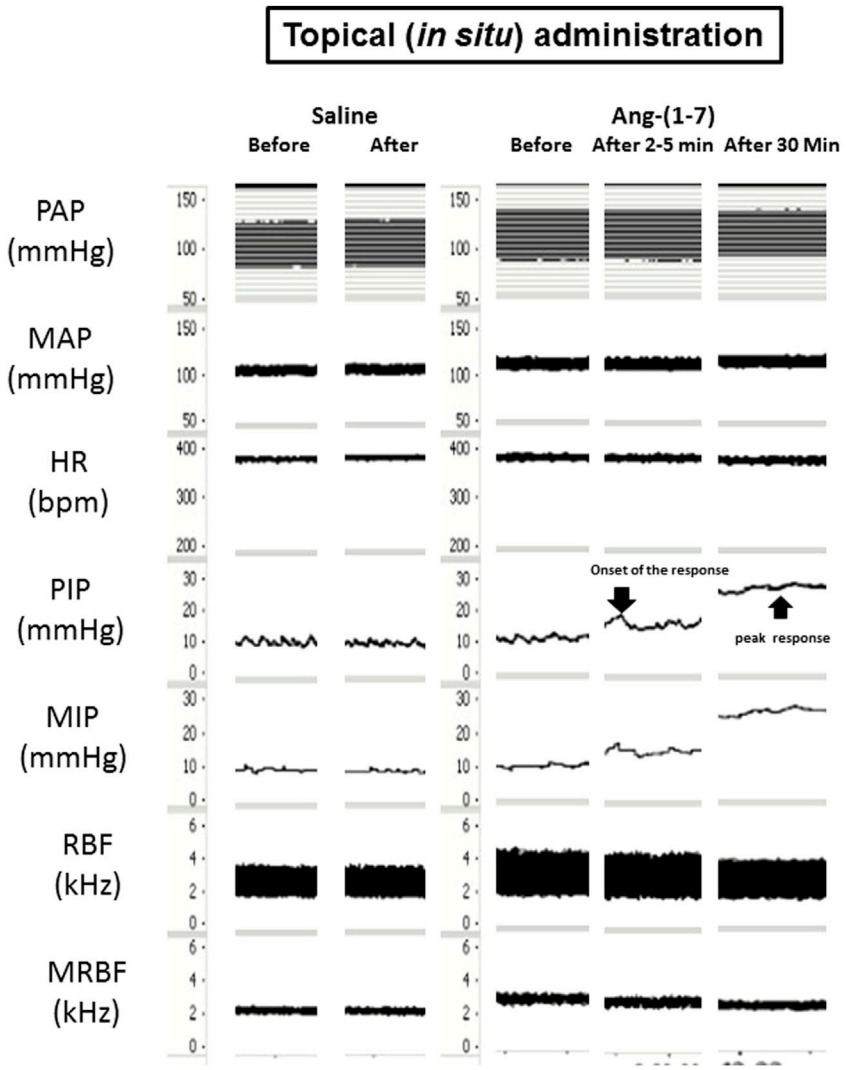

FIGURE 4 | Tracings showing the baseline pulsatile arterial pressure (PAP, mmHg), mean arterial pressure (MAP, mmHg), heart rate (HR, bpm), pulsatile intravesical pressure (PIP, mmHg), mean intravesical pressure (MIP, mmHg), renal blood flow (RBF, kHz) and mean renal blood flow (MRBF, kHz) and the responses yielded by *in situ* administration of angiotensin-(1–7) (100 ng/ml, 0.1 ml per rat) or saline (0.1 ml) onto the urinary bladder.

intravenously or *in situ* onto the UB. Comparisons of MAP and HR before and after i.v. or *in situ* Ang-(1–7) or saline were analyzed using paired Student´s t-test. The statistical software package Sigma Stat 3.5 was used for all the analyses, and the data were considered significant at $p < 0.05$.

RESULTS

Responses in Intravesical Pressure and Cardiovascular Parameters Evoked by Intravenous Administration of Angiotensin-(1–7) in Wistar Rats (n = 6).

Before infusions of saline or Ang-(1–7) intravenously, the baseline MAP was 94 ± 5 mmHg (before saline) and 99 ± 5 mmHg [before Ang-(1–7)], the HR was 344 ± 13 bpm (before saline) and 348 ± 9 bpm [before Ang-(1–7)], and the IP was 8.38 ± 0.64 mmHg (before saline) and 7.72 ± 0.81 mmHg [before Ang-(1–7)] (n = 6) (**Figures 2**, **3A**,**B**).

The intravenous administration of Ang-(1–7) significantly increased IP (115.8 ± 28.6%, $p < 0.05$) compared to saline (−2.9 ± 1.3%). The onset of IP increase induced by Ang-(1–7) administered intravenously had a latency of ~30 min and the peak response was achieved at ~90 min after the injection (**Figures 2**, **3D**). After 120 min, the IP values recovered to the baseline values.

However, no significant changes were observed in MAP [2 ± 1 mmHg after saline vs. −3 ± 3 mmHg after Ang-(1–7)], HR [1 ± 2 bpm after saline vs. 10 ± 18 bpm after Ang-(1–7)], and RC [6.0 ± 3.2% after saline vs. −3.6 ± 17.4% after Ang-(1–7)] after intravenous infusion of saline or Ang-(1–7) (**Figures 2**, **3A**–**C**).

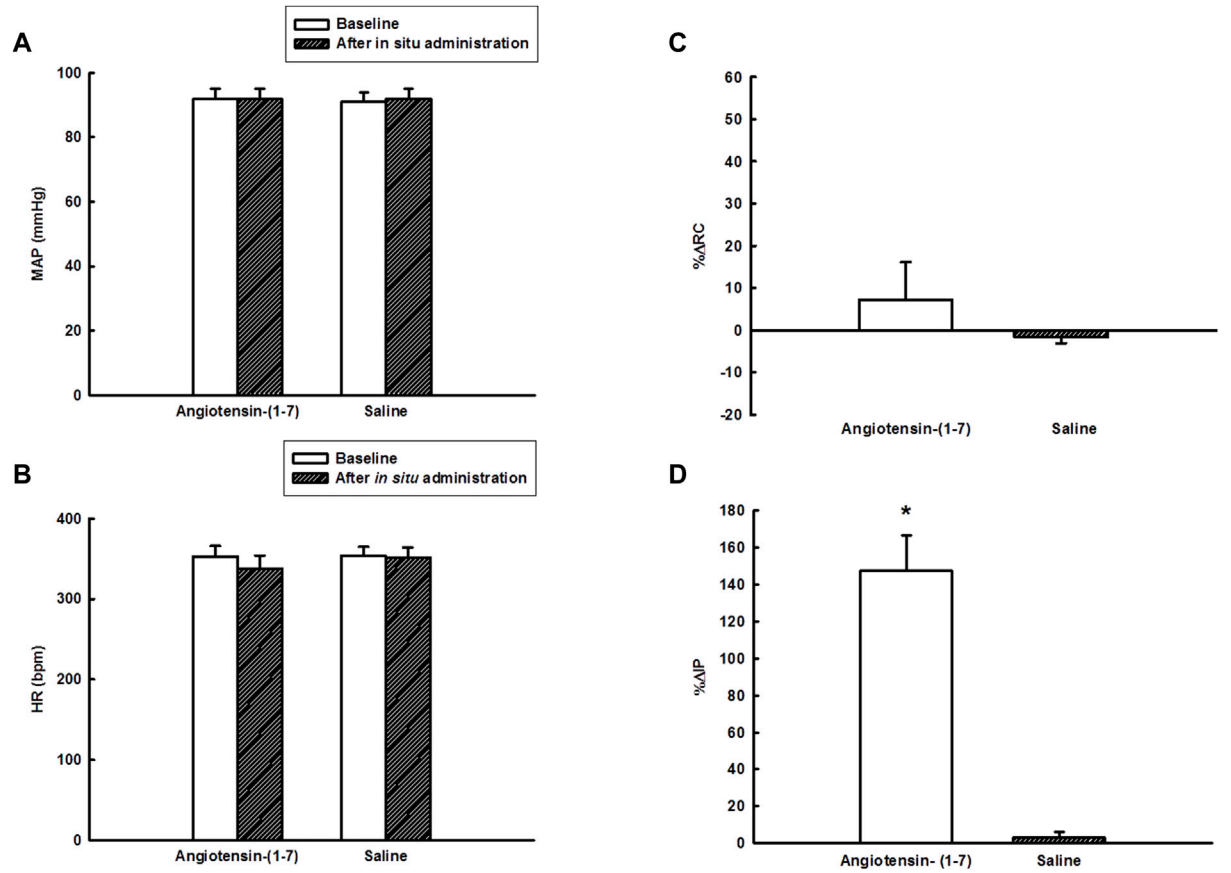

FIGURE 5 | (A) Mean arterial pressure (mmHg) and **(B)** heart rate (bpm) at baseline and after *in situ* administration of angiotensin-(1–7) (100 ng/ml, 0.1 ml per rat) or saline (0.1 ml), **(C)** percent change in renal conductance (%ΔRC), and **(D)** percent change in intravesical pressure (%ΔIP) elicited by *in situ* administration of angiotensin-(1–7) (100 ng/ml, 0.1 ml per rat) or saline (0.1 ml) on the urinary bladder (n = 6). *p < 0.05 vs. saline (Student´s t-test).

Responses in Intravesical Pressure and Cardiovascular Parameters Elicited by Topic (*in situ*) Administration of Angiotensin-(1–7) Onto the Urinary Bladder in Wistar Rats (N = 6).

Before application of saline or Ang-(1–7) *in situ* on the UB, the baseline MAP was 91 ± 3 mmHg (before saline) and 92 ± 3 mmHg [before Ang-(1–7)], the HR was 354 ± 11 bpm (before saline) and 353 ± 13 bpm [before Ang-(1–7)], and the IP was 5.98 ± 0.65 mmHg (before saline) and 6.85 ± 0.64 mmHg [before Ang-(1–7)] (n = 6) (**Figures 4**, **5A**,**B**).

The topic (*in situ*) administration of Ang-(1–7) onto the UB significantly increased the IP (147.4 ± 18.9%, $p < 0.05$) compared to saline (3.2 ± 2.8%). The onset of IP increase evoked by Ang-(1–7) administered *in situ* onto the UB had a latency of ~2–5 min and the peak response was observed at ~30 min after the administration (**Figures 4**, **5D**). After 60 min, the IP values drop back to baseline values.

Nevertheless, the topic (*in situ*) administration of Ang-(1–7) on the UB elicited no change in MAP (0.3 ± 1 mmHg vs. 0.5 ± 0.6 mmHg, saline), HR (−15 ± 4 bpm vs. −2 ± 1 bpm, saline) and RC (7.2 ± 8.9% vs. −1.6 ± 1.5%, saline) compared to saline administration (**Figure 4**, **5A**–**C**).

Determination of Mas Receptors and ACE-2 Gene Expression in the Urinary Bladder (N = 6)

We observed that the Mas receptors (CT = 28.56 ± 0.124 arbitrary units, A.U.) and ACE-2 gene (CT = 28.54 ± 2.05 A.U.), as well as the housekeeping gene cyclophilin A (18.89 ± 0.81 A.U.), were expressed, and thereby, these genes are present in the UB samples (N = 6) (**Figure 6A**).

Determination of Protein Expression of Mas Receptors and ACE-2 in the Urinary Bladder (N = 6)

We found by western blotting assay that Mas receptors (0.54 ± 0.07 O.D.) and ACE-2 (0.57 ± 0.08 O.D.) proteins are expressed in the UB samples (N = 6) (**Figures 6B,C**).

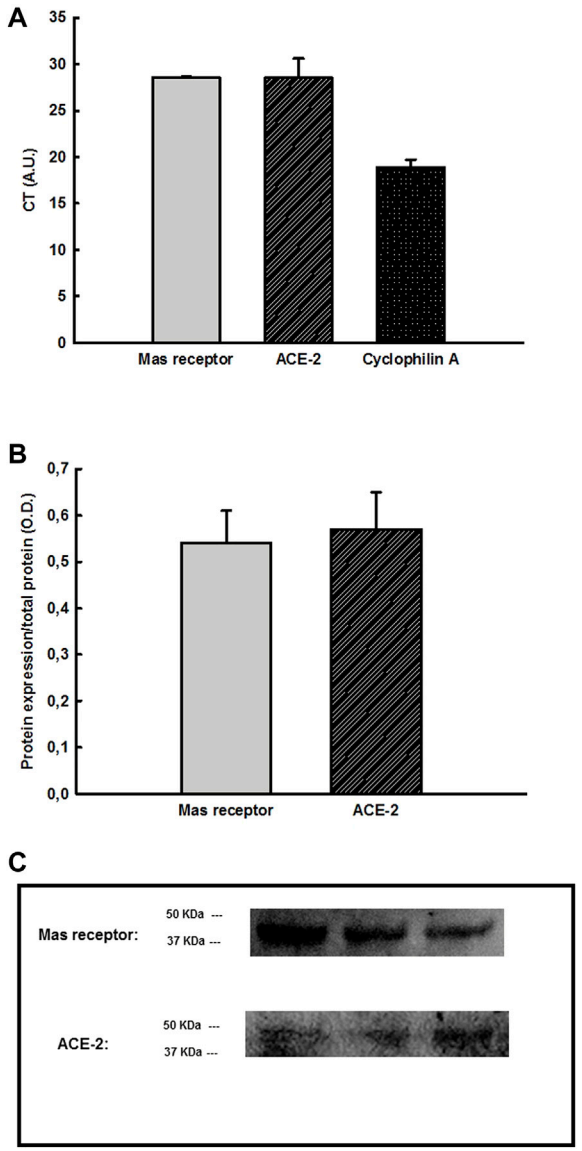

FIGURE 6 | (A) CT values obtained by qPCR showing the Mas receptors, ACE-2, and cyclophilin A (housekeeping gene) gene expression in the urinary bladder (UB) (n = 6), **(B)** Mas receptors and ACE-2 protein expression normalized by total protein in the UB by western blotting assay (n = 6), **(C)** Blots labeled for Mas receptors and ACE-2 in the UB samples by western blotting. Abbreviation: OD, Optical density.

DISCUSSION

Our data demonstrated that intravenous infusions of Ang-(1–7) elicited a marked increase in IP compared to saline. Nevertheless, the RC, arterial pressure, and HR were not affected by i.v. Ang-(1–7) in the dose used in this study. Those findings indicate that the increase in IP is not likely dependent on higher urinary volume caused by an increase in the glomerular filtration rate. The topical (*in situ*) administration of Ang-(1–7) also yielded an increase in IP and elicited no changes in cardiovascular parameters in the rats, showing similar effects compared to intravenously infused Ang-(1–7). It is noteworthy that the latency for the increase in intravesical evoked by *in situ* application of Ang-(1–7) on the UB was shorter (5 min) compared to the response elicited by intravenous administration (30 min). We also demonstrated the presence of Mas receptors in the UB either by gene or protein expression, which suggests that Ang-(1–7) is likely binding to these receptors for increasing the IP. Furthermore, we showed the existence of gene and protein expression of ACE-2 in the UB samples, which is suggestive that Ang-(1–7) can be locally produced in the UB cells.

The regulation of UB function is dependent on the autonomic and somatic nervous systems. Cholinergic (via muscarinic receptors) and adrenergic (via α and β receptors) transmissions, as well as noncholinergic/nonadrenergic mechanisms (NCNA), exert an important function in the storage of urine and voiding (Juszczak and Maciukiewicz, 2017). Several neurotransmitters of the NCNA branch of the autonomic nervous system, for instance, ATP, substance P, and neuropeptide Y, can play stimulatory or inhibitory neuromodulation of cholinergic, adrenergic, or purinergic transmission in the lower urinary tract (Hoyle, 1994; Juszczak and Maciukiewicz, 2017). *In vitro* studies performed by Tanabe et al. (1993) demonstrated that the AT1 receptors, instead of AT2 receptors, mediate the contractions elicited by angiotensin II in the smooth muscle of rat UB strips. The function of the renin–angiotensin–aldosterone system on the lower urinary tract is not fully understood, and our study is the first to show the effects of intravenous Ang-(1–7) or *in situ* Ang-(1–7) onto the UB on the IP, as well the existence of Mas receptors and ACE-2 in the bladder by gene and protein expression.

Although Ang-(1–7) promoted increases in IP after *in situ* administration onto the UB, it is not possible to infer physiologically whether the plasma Ang-(1–7) or this peptide locally synthesized in the cells of the UB yields the increases in IP. We have shown the existence of gene and protein expression of ACE-2, which is the enzyme responsible for the synthesis of Ang-(1–7) breaking the angiotensin I (Chappell et al., 2000; Rice et al., 2004) or alternatively from the cleavage of angiotensin II (Vickers et al., 2002). This allows us to hypothesize that Ang-(1–7) is locally produced in the cells of the UB and possibly exerts a paracrine or autocrine action and thereby could increase the IP.

Previous studies have demonstrated that intrarenal infusion of Ang-(1–7) at a rate of 0.1 and 1 nmol.min^{-1}.kg^{-1} had minimal effects on renal blood flow and arterial pressure but raised the urinary excretion of sodium and water in comparison to the control (saline-infused) group (Handa et al., 1996). This effect was attributed to a possible action of Ang-(1–7) in the proximal tubule cells, where Ang-(1–7) could inhibit an ouabain-sensitive Na^+-K^+-ATPase. This inhibitory action of Ang-(1–7) was attributed mainly to a non-AT1, non-AT2 angiotensin receptor, and in minor proportion to AT-1 receptors (Handa et al., 1996). Nevertheless, the study of Handa et al. (1996) has not investigated whether the Mas receptor could be involved or not in the response evoked by Ang-(1–7). Despite we have demonstrated that Ang-(1–7) administered either

intravenously or *in situ* has not affected the renal blood flow, we have not evaluated the urine volume compared to saline administration (control group), which is a limitation of this study. Considering that the topical (*in situ*) administration of Ang-(1–7) onto the UB elicited an increase in IP with a latency of 2–5 min, we do not believe that this response would be dependent on an increase in the urinary volume. By contrast, we cannot assure that the marked increase in IP yielded by intravenous infusion of Ang-(1–7) could cause an increase in UB dependent on an intrarenal action due to the long latency for the onset of the response of roughly 30 min.

On the other hand, another hypothesis is that Ang-(1–7) infused intravenously could also act centrally in the lateral preoptic area and bind to the Mas receptors of this area. Previous report has shown that Ang-(1–7) injected into the lateral preoptic area increases IP with a latency for the response of approximately 10 min and achieves a peak response approximately 25 min after injection without inducing any changes in RC and arterial pressure (Lamy et al., 2021). Hence, the response observed with Ang-(1–7) infused intravenously in the current study could be dependent on direct action on the UB and/or be due to an action at the intrarenal level and/or through activation of Mas receptors in the lateral preoptic area.

In the present study, we could not test if the Ang-(1–7) administered intravenously was binding to Mas receptors in the UB by pharmacological blockade of these receptors. Preliminary findings in our laboratory (data not shown) indicated that the intravenous administration of A-779, a Mas receptors antagonist, even in the highest dose, causes the blockade of these receptors for less than 30 min. Even with an experimental protocol in which the administration of A-779 was followed by immediate administration of Ang-(1–7) intravenously, we would not be able to see if the IP response evoked by Ang-(1–7) could be attenuated as the blockade of Mas receptors had already quited. Thereafter, performing this experimental protocol has become unfeasible, which is a limitation of this study.

Micturition and urine storage depend on the coordination between the bladder and the urethra (de Groat, 1998; Andersson and Hedlund, 2002). An increasing number of people worldwide suffer from UB dysfunctions (Bettez et al., 2012; Dorsher and McIntosh, 2012; Ruffion et al., 2013). Nevertheless, the pharmacological approaches and therapies currently applied still cause many side effects. As we have shown that Ang-(1–7) acts in the UB increasing the IP, the Mas receptors and ACE-2 in the bladder could be considered to be novel possible targets for drug development and possible therapy in patients who suffer from urinary disorders.

In conclusion, our findings suggest that intravenous Ang-(1–7) can act in the UB, leading to an increase in the IP. This effect is similar to that observed by *in situ* administration onto the UB but with different latencies for the onset of the responses. In addition, the existence of ACE-2 in the UB suggests that Ang-(1–7) can be locally produced and is likely able to exert a paracrine or autocrine action in the UB binding to Mas receptors present in this organ.

DATA AVAILABILITY STATEMENT

The original contributions presented in the study are included in the article/supplementary material, further inquiries can be directed to the corresponding author.

ETHICS STATEMENT

The animal study was reviewed and approved by the Animal Ethics Committee of the Faculdade de Medicina do ABC/Centro Universitario ABC (protocol number 13/2017).

AUTHOR CONTRIBUTIONS

GL have performed the functional experiments. JS, RM, and GG were responsible for the qPCR experiments. GL, BV, BA, DV, AN, LO, and MS have carried out the western blotting assays. GL, EC, BA, DV, and PA have worked on data analysis and discussion. MS has designed the experiments, performed the statistical analysis, obtained the research grant, and has written the manuscript with GL and PA. All the authors equally contributed to this study.

FUNDING

We gratefully thank Sao Paulo Research Foundation (FAPESP, grant # 2018/00191–4) for the financial support to our research project and scholarship to GL (grant#2017/07161–0).

ACKNOWLEDGMENTS

We would like to thank Nuha A. Dsouki for the technical assistance in the lab at Faculdade de Medicina do ABC/Centro Universitario FMABC. We also appreciate the support of Federal University of Sao Paulo for providing the conditions for the development of this study.

REFERENCES

Andersson, K.-E., Hedlund, H., and Stahl, M. (1992). Contractions Induced by Angiotensin I, Angiotensin II and Bradykinin in Isolated Smooth Muscle from the Human Detrusor. *Acta Physiol. Scand.* 145, 253–259. doi:10.1111/j.1748-1716.1992.tb09362.x

Andersson, K. E., and Hedlund, P. (2002). Pharmacologic Perspective on the Physiology of the Lower Urinary Tract. *Urology* 60 (5 Suppl. 1), 13–20. doi:10.1016/s0090-4295(02)01786-7

Aoki, Y., Brown, H. W., Brubaker, L., Cornu, J. N., Daly, J. O., and Cartwright, R. (2017). Urinary Incontinence in Women. *Nat. Rev. Dis. Prim.* 3, 17042. doi:10.1038/nrdp.2017.42

Bettez, M., Tu, L. M., Carlson, K., Corcos, J., Gajewski, J., Jolivet, M., et al. (2012). 2012 Update: Guidelines for Adult Urinary Incontinence Collaborative

Consensus Document for the Canadian Urological Association. *Cuaj* 6 (5), 354–363. doi:10.5489/cuaj.12248

Cafarchio, E. M., Auresco, L. C., da Silva, L. A., Rodart, I. F., do Vale, B., de Souza., J. S., et al. (2018). Unravelling the Intravenous and *In Situ* Vasopressin Effects on the Urinary Bladder in Anesthetized Female Rats: More Than One Vasopressin Receptor Subtype Involved? *Eur. J. Pharmacol.* 834, 109–117. doi:10.1016/j.ejphar.2018.07.024

Cafarchio, E. M., da Silva, L. A., Auresco, L. C., Ogihara, C. A., Almeida, R. L., Giannocco, G., et al. (2016). Cholinergic Activation of Neurons in the Medulla Oblongata Changes Urinary Bladder Activity by Plasma Vasopressin Release in Female Rats. *Eur. J. Pharmacol.* 776, 116–123. doi:10.1016/j.ejphar.2016.02.043

Cafarchio, E. M., da Silva, L. A., Auresco, L. C., Rodart, I. F., de Souza, J. S., Antonio, B. B., et al. (2020). Oxytocin Reduces Intravesical Pressure in Anesthetized Female Rats: Action on Oxytocin Receptors of the Urinary Bladder. *Front. Physiol.* 11, 382. doi:10.3389/fphys.2020.00382

Chappell, M. C., Gomez, M. N., Pirro, N. T., and Ferrario, C. M. (2000). Release of Angiotensin-(1-7) from the Rat Hindlimb. *Hypertension* 35, 348–352. doi:10.1161/01.hyp.35.1.348

de Groat, W. C. (1998). Anatomy of the Central Neural Pathways Controlling the Lower Urinary Tract. *Eur. Urol.* 34 Suppl 1 (Suppl. 1), 2–5. doi:10.1159/000052265

de Moura, M. M., dos Santos, R. A. S., Campagnole-Santos, M. J., Todiras, M., Bader, M., Alenina, N., et al. (2010). Altered Cardiovascular Reflexes Responses in Conscious Angiotensin-(1-7) Receptor Mas-Knockout Mice. *Peptides* 31 (10), 1934–1939. doi:10.1016/j.peptides.2010.06.030

Dorsher, P. T., and McIntosh, P. M. (2012). Neurogenic Bladder. *Adv. Urology* 2012, 1–16. doi:10.1155/2012/816274

Durik, M., van Veghel, R., Kuipers, A., Rink, R., Haas Jimoh Akanbi, M., Moll, G., et al. (2012). The Effect of the Thioether-Bridged, Stabilized Angiotensin-(1-7) Analogue Cyclic Ang-(1-7) on Cardiac Remodeling and Endothelial Function in Rats with Myocardial Infarction. *Int. J. Hypertens.* 2012, 1–8. doi:10.1155/2012/536426

Erspamer, G. F., Negri, L., and Piccinelli, D. (1973). The Use of Preparations of Urinary Bladder Smooth Muscle for Bioassay of and Discrimination between Polypeptides. *Schmiedeb. Arch. Pharmacol.* 279, 61–74. doi:10.1007/bf00502068

Ferreira, A. J., and Santos, R. A. S. (2005). Cardiovascular Actions of Angiotensin-(1-7). *Braz. J. Med. Biol. Res.* 38, 499–507. doi:10.1590/s0100-879x2005000400003

Handa, R. K., Ferrario, C. M., and Strandhoy, J. W. (1996). Renal Actions of Angiotensin-(1-7): *In Vivo* and *In Vitro* Studies. *Am. J. Physiology-Renal Physiology* 270, F141–F147. doi:10.1152/ajprenal.1996.270.1.f141

Haywood, J. R., Shaffer, R. A., Fastenow, C., Fink, G. D., and Brody, M. J. (1981). Regional Blood Flow Measurement with Pulsed Doppler Flowmeter in Conscious Rat. *Am. J. Physiology-Heart Circulatory Physiology* 241, H273–H278. doi:10.1152/ajpheart.1981.241.2.h273

Hoyle, C. H. (1994). Non-adrenergic, Non-cholinergic Control of the Urinary Bladder. *World J. Urol.* 12, 233–244. doi:10.1007/BF00191202

Juszczak, K., and Maciukiewicz, P. (2017). The Angiotensin II Receptors Type 1 Blockage Affects the Urinary Bladder Activity in Hyperosmolar-Induced Detrusor Overactivity in Rats: Preliminary Results. *Adv. Clin. Exp. Med.* 26 (7), 1047–1051. doi:10.17219/acem/64939

Kajiwara, M., Inoue, K., Usui, A., Kurihara, M., and Usui, T. (2004). The Micturition Habits and Prevalence of Daytime Urinary Incontinence in Japanese Primary School childrenThe Micturition Habits and Prevalence of Daytime Urinary Incontinence in Japanese Primary School Children. *J. Urology* 171 (1), 403–407. doi:10.1097/01.ju.0000101907.87169.06

Lam, D. S. H., Dias, L. S., Moore, K. H., and Burcher, E. (2000). Angiotensin II in Child Urinary Bladder: Functional and Autoradiographic Studies. *B.J.U. Int.* 86, 494–501. doi:10.1046/j.1464-410x.2000.00771.x

Lamy, G. B., Cafarchio, E. M., do Vale, B., Antonio, B. B., Venancio, D. P., de Souza, J. S., et al. (2021). Lateral Preoptic Area Neurons Activated by Angiotensin-(1-7) Increase Intravesical Pressure: A Novel Feature in Central Micturition Control. *Front. Physiol.* 12, 682711. doi:10.3389/fphys.2021.682711

Magaldi, F. M., Moreno, M., Magaldi, C. M., Cafarchio, E. M., Aronsson, P., Sato, M. A., et al. (2020). Resistance Exercise Evokes Changes on Urinary Bladder Function and Morphology in Hypoestrogen Rats. *Front. Physiol.* 10, 1605. doi:10.3389/fphys.2019.01605

Nadelhaft, I., Vera, P. L., Card, J. P., and Miselis, R. R. (1992). Central Nervous System Neurons Labelled Following the Injection of Pseudorabies Virus into the Rat Urinary Bladder. *Neurosci. Lett.* 143 (1-2), 271–274. doi:10.1016/0304-3940(92)90281-b

Rice, G. I., Thomas, D. A., Grant, P. J., Turner, A. J., and Hooper, N. M. (2004). Evaluation of Angiotensin-Converting Enzyme (ACE), its Homologue ACE2 and Neprilysin in Angiotensin Peptide Metabolism. *Biochem. J.* 383, 45–51. doi:10.1042/bj20040634

Ruffion, A., Castro-Diaz, D., Patel, H., Khalaf, K., Onyenwenyi, A., Globe, D., et al. (2013). Systematic Review of the Epidemiology of Urinary Incontinence and Detrusor Overactivity Among Patients with Neurogenic Overactive Bladder. *Neuroepidemiology* 41, 146–155. doi:10.1159/000353274

Saito, M., Kondo, A., Kato, T., and Miyare, K. (1993). Response of the Human Urinary Bladder to Angiotensins: A Comparison between Neurogenic and Control Bladders. *J. Urology* 149, 408–411. doi:10.1016/s0022-5347(17)36105-0

Santos, R. A., and Campagnole-Santos, M. J. (1994). Central and Peripheral Actions of Angiotensin-(1-7). *Braz J. Med. Biol. Res.* 27 (4), 1033–1047.

Santos, R. A. S., Campagnole-Santos, M. J., and Andrade, S. P. (2000). Angiotensin-(1-7): an Update. *Regul. Pept.* 91, 45–62. doi:10.1016/s0167-0115(00)00138-5

Santos, R. A. S., Castro, C. H., Gava, E., Pinheiro, S. V. B., Almeida, A. P., de Paula, R. D., et al. (2006). Impairment of *In Vitro* and *In Vivo* Heart Function in Angiotensin-(1-7) Receptor Mas Knockout Mice. *Hypertension* 47, 996–1002. doi:10.1161/01.hyp.0000215289.51180.5c

Santos, R. A. S., Sampaio, W. O., Alzamora, A. C., Motta-Santos, D., Alenina, N., Bader, M., et al. (2018). The ACE2/Angiotensin-(1-7)/MAS Axis of the Renin-Angiotensin System: Focus on Angiotensin-(1-7). *Physiol. Rev.* 98 (1), 505–553. doi:10.1152/physrev.00023.2016

Sureshkumar, P., Jones, M., Cumming, R., and Craig, J. (2009). A Population Based Study of 2,856 School-Age Children with Urinary Incontinence. *J. Urology* 181 (2), 808–816. doi:10.1016/j.juro.2008.10.044

Tanabe, N., Ueno, A., and Tsujimoto, G. (1993). Angiontensin II Receptors in the Rat Urinary Bladder Smooth Muscle: Type 1 Subtype Receptors Mediate Contractile Responses. *J. Urology* 150, 1056–1059. doi:10.1016/s0022-5347(17)35685-9

Vickers, C., Hales, P., Kaushik, V., Dick, L., Gavin, J., Tang, J., et al. (2002). Hydrolysis of Biological Peptides by Human Angiotensin-Converting Enzyme-Related Carboxypeptidase. *J. Biol. Chem.* 277, 14838–14843. doi:10.1074/jbc.m200581200

Xu, P., Costa-Goncalves, A. C., Todiras, M., Rabelo, L. A., Sampaio, W. O., Moura, M. M., et al. (2008). Endothelial Dysfunction and Elevated Blood Pressure in MAS Gene-Deleted Mice. *Hypertension* 51, 574–580. doi:10.1161/hypertensionaha.107.102764

Yamada, S., Takeuchi, C., Oyunzul, L., and Ito, Y. (2009). Bladder Angiotensin-II Receptors: Characterization and Alteration in Bladder Outlet Obstruction. *Eur. Urol.* 55, 482–490. doi:10.1016/j.eururo.2008.03.015

Conflict of Interest: The authors declare that the research was conducted in the absence of any commercial or financial relationships that could be construed as a potential conflict of interest.

Publisher's Note: All claims expressed in this article are solely those of the authors and do not necessarily represent those of their affiliated organizations or those of the publisher, the editors, and the reviewers. Any product that may be evaluated in this article or claim that may be made by its manufacturer is not guaranteed or endorsed by the publisher.

frontiers | Frontiers in Physiology

TYPE Original Research
PUBLISHED 08 August 2022
DOI 10.3389/fphys.2022.923555

OPEN ACCESS

EDITED BY
Monica Akemi Sato,
Faculdade de Medicina do ABC, Brazil

REVIEWED BY
Yagna Jarajapu,
North Dakota State University, United States
Humberto Dellê,
Universidade Nove de Julho, Brazil

*CORRESPONDENCE
Martin C. Michelm,
marmiche@uni-mainz.de

†PRESENT ADDRESS
Ralf Elvert,
Evotec International GmbH, Göttingen, Germany

SPECIALTY SECTION
This article was submitted to Integrative Physiology, a section of the journal Frontiers in Physiology

RECEIVED 19 April 2022
ACCEPTED 07 July 2022
PUBLISHED 08 August 2022

CITATION
Yesilyurt ZE, Matthes J, Hintermann E, Castañeda TR, Elvert R, Beltran-Ornelas JH, Silva-Velasco DL, Xia N, Kannt A, Christen U, Centurión D, Li H, Pautz A, Arioglu-Inan E and Michel MC (2022), Analysis of 16 studies in nine rodent models does not support the hypothesis that diabetic polyuria is a main reason of urinary bladder enlargement. *Front. Physiol.* 13:923555. doi: 10.3389/fphys.2022.923555

Analysis of 16 studies in nine rodent models does not support the hypothesis that diabetic polyuria is a main reason of urinary bladder enlargement

Zeynep E. Yesilyurt[1], Jan Matthes[2], Edith Hintermann[3], Tamara R. Castañeda[4], Ralf Elvert[4†], Jesus H. Beltran-Ornelas[5], Diana L. Silva-Velasco[5], Ning Xia[6], Aimo Kannt[4,7], Urs Christen[3], David Centurión[5], Huige Li[6], Andrea Pautz[6], Ebru Arioglu-Inan[1] and Martin C. Michel[6]*

[1]Department of Pharmacology, School of Pharmacy, Ankara University, Ankara, Turkey, [2]Department of Pharmacology, University of Cologne, Cologne, Germany, [3]Pharmazentrum, Goethe University, Frankfurt, Germany, [4]Sanofi Research and Development, Frankfurt, Germany, [5]Department of Pharmacobiology, Cinvestav IPN, Mexico City, Mexico, [6]Department of Pharmacology, Johannes Gutenberg University, Mainz, Germany, [7]Fraunhofer Institute for Translational Medicine and Pharmacology ITMP, Frankfurt, Germany

The urinary bladder is markedly enlarged in the type 1 diabetes mellitus model of streptozotocin-injected rats, which may contribute to the frequent diabetic uropathy. Much less data exists for models of type 2 diabetes. Diabetic polyuria has been proposed as the pathophysiological mechanism behind bladder enlargement. Therefore, we explored such a relationship across nine distinct rodent models of diabetes including seven models of type 2 diabetes/obesity by collecting data on bladder weight and blood glucose from 16 studies with 2–8 arms each; some studies included arms with various diets and/or pharmacological treatments. Data were analysed for bladder enlargement and for correlations between bladder weight on the one and glucose levels on the other hand. Our data confirm major bladder enlargement in streptozotocin rats and minor if any enlargement in fructose-fed rats, db/db mice and mice on a high-fat diet; enlargement was present in some of five not reported previously models. Bladder weight was correlated with blood glucose as a proxy for diabetic polyuria within some but not other models, but correlations were moderate to weak except for RIP-LCMV mice (r^2 of pooled data from all studies 0.0621). Insulin levels also failed to correlate to a meaningful extent. Various diets and medications (elafibranor, empagliflozin, linagliptin, semaglutide) had heterogeneous effects on bladder weight that often did not match their effects on glucose levels. We conclude that the presence and extent of bladder enlargement vary markedly across diabetes models, particularly type 2 diabetes models; our data do not support the idea that bladder enlargement is primarily driven by glucose levels/glucosuria.

KEYWORDS
animal model, bladder, diabetes, diet, glucosuria, hypertrophy, insulin, treatment

1 Introduction

Diabetes mellitus causes major morbidity and mortality related to cardiovascular, renal and ocular function (Mensah et al., 2017). Lower urinary tract dysfunction (LUTD) in general and that of the urinary bladder in particular are at least as common, occurring in 80% and 50% of diabetic patients, respectively (Daneshgari and Moore, 2006). While LUTD does not lead to major morbidity or mortality, it reduces the quality of life of the afflicted patients (Irwin et al., 2008; Benner et al., 2009) and their partners (Mitroupoulos et al., 2002) by impairing social interactions during the day and sleep during the night; LUTD is also associated with emergency room visits, hospitalizations and loss of work productivity (Kannan et al., 2009).

The pathophysiology of LUTD in diabetes is poorly understood and dedicated therapeutic strategies other than normalizing glucose levels are lacking. An enlargement of the urinary bladder appears to be part of LUTD in diabetes and is consistently found in the streptozotocin (STZ)-induced rat model of type 1 diabetes, by average resulting in a doubling of bladder weight (BW) (Arioglu Inan et al., 2018). While studied much less frequently, a comparable enlargement of the urinary bladder appears to exist in the other type 1 diabetes models that have been tested (Ellenbroek et al., 2018). Much fewer studies have explored bladder enlargement in animal models of type 2 diabetes and have yielded inconsistent results (Ellenbroek et al., 2018). Thus, it remains unclear whether bladder enlargement occurs in diabetes in general, is restricted to type 1 diabetes models or occurs in some but not all type 2 diabetes models. Treatment with insulin prevents and reverses bladder enlargement in STZ-injected rats (Arioglu Inan et al., 2018). However, no treatment studies have reported effects on BW in animal models of type 2 diabetes or with treatments other than insulin in those of type 1 diabetes.

The mechanisms underlying diabetes-associated bladder enlargement are largely unknown. A prevailing theory is that increased glucose levels act as an osmotic diuretic when exceeding the renal reabsorption threshold of 9–10 mM and that the bladder enlarges as a response to increased urine flow (diabetic polyuria). This theory is largely based on studies in rats in which treatment with the osmotic diuretic sucrose yielded similar degrees of diuresis and of bladder enlargement as compared to STZ injection (Kudlacz et al., 1988; Eika et al., 1994; Fukumoto et al., 1994; Tammela et al., 1994; Tammela et al., 1995; Liu and Daneshgari, 2005; Xiao et al., 2013). It implies that bladder enlargement should be correlated to blood glucose levels if these exceed the renal reabsorption threshold. However, this mechanism has been questioned (Ellenbroek et al., 2018; Yesilyurt et al., 2019).

Therefore, we have explored the presence and extent of bladder enlargement across a wide range of rodent models of diabetes, particularly of type 2 diabetes and including various diets and pharmacological treatments other than insulin and its correlation with blood glucose and, as a *post hoc* analysis, serum insulin. For this purpose, we have collected data on glucose (in some cases also insulin), BW and body weight from various studies primarily designed to address questions unrelated to the urinary bladder. This has allowed us to collect data from 16 studies with 2–8 arms each representing nine distinct rat and mouse models and a total of 513 animals without sacrificing a single animal for the purpose of our study. Taken together we present what may be the most comprehensive inter-model comparison ever reported for any parameter in diabetes.

2 Materials and methods

2.1 Animal models

To collect information from a wide range of rodent models of diabetes in the spirit of the 3R principles (Kilkenny et al., 2010), the present study is based on data from ongoing studies designed for other purposes; primary outcomes of these studies will be reported elsewhere by the respective investigators. Details of each model according to the ARRIVE guidelines (Percie du Sert et al., 2020) are provided in the Supplementary Material. Each of the underlying studies had been approved by the applicable independent committee or government agency for use and protection of experimental animals, and all studies were in line with the NIH guidelines for care and use of experimental animals (for details see Supplementary Material). In each study, blood glucose concentration, body weight and BW were determined at study end in each animal and bladder/body weight ratio (BBW) was calculated. Plasma insulin levels were available from six studies. No treatments other than those being stated explicitly were applied.

2.2 Data analysis

The following pre-specified analyses were done for each study: The primary outcome parameter within each study was BW, analysed as difference between the main hyperglycaemic/diabetic and its control group with its 95% CI as derived from an unpaired, two-tailed *t*-test assuming comparable variability in both groups. The key secondary outcome parameter within each study was the correlation between blood glucose and BW based on individual animal data of all groups with strengths of correlation assessed as the square of the Pearson correlation coefficient (r^2) with its associated descriptive *p*-value. Other secondary outcome parameters were within-study group differences and correlations based on BBW. To explore correlations across groups, BW and BBW data from all animals other than those in the primary control group were

TABLE 1 Blood glucose, insulin (selected studies only), body weight, bladder weight, and bladder/body weight across animal models.

	n	Blood glucose, mM	Insulin, ng/l	Body weight, g	Bladder weight, mg	Bladder/body weight, mg/g
Type 1 diabetes models						
STZ-injected rats (Mexico City)						
Control	11	5.48 ± 0.48	—	426.3 ± 46.0	134.2 ± 32.1	0.314 ± 0.066
STZ	10	28.01 ± 3.98	—	244.4 ± 36.1	171.0 ± 28.5	0.710 ± 0.161
STZ-injected rats (Ankara)						
Control	11	5.56 ± 0.25	—	511.5 ± 80.5	122.8 ± 12.0	0.245 ± 0.042
Empagliflozin	14	5.15 ± 0.25	—	526.3 ± 73.2	177.3 ± 28.6	0.346 ± 0.090
Linagliptin	12-13	5.57 ± 0.38	—	532.5 ± 86.2	158.7 ± 53.5	0.307 ± 0.103
STZ	13-14	31.31 ± 3.91	—	327.0 ± 78.6	291.7 ± 41.9	0.900 ± 0.267
STZ + empagliflozin	15	19.38 ± 7.80	—	334.8 ± 76.2	368.9 ± 160.9	1.215 ± 0.745
STZ + linagliptin	14	31.95 ± 2.27	—	336.6 ± 60.4	373.3 ± 157.3	1.210 ± 0.822
RIP-LCMV mice (Frankfurt)						
Control	15	8.31 ± 1.09	—	27.51 ± 5.96	24.27 ± 5.02	0.891 ± 0.115
RIP-LCMV-GP	12	28.34 ± 8.49	—	24.04 ± 3.72	43.00 ± 14.21	1.830 ± 0.696
Type 2 diabetes models						
ZSF1 rats (20-weeks, Hoechst)						
Lean control	6	4.54 ± 0.86	<0.512	461.7 ± 32.3	95.0 ± 16.4	0.207 ± 0.039
Obese	6	12.97 ± 2.68	4.858 ± 1.957	603.0 ± 14.2	193.3 ± 29.4	0.321 ± 0.052
Obese canoletta	6	8.59 ± 0.75	9.118 ± 2.883	804.3 ± 31.8	136.7 ± 13.7	0.170 ± 0.021
Obese 0% choline/0.2% methionine	6	13.87 ± 4.47	5.313 ± 1.571	819.3 ± 31.7	268.3 ± 66.8	0.328 ± 0.080
Obese AMLN	6	8.58 ± 1.62	8.100 ± 3.405	798.2 ± 26.8	163.3 ± 60.2	0.206 ± 0.077
ZSF1 rats (28-weeks, Hoechst)						
Lean control	6	5.35 ± 0.35	0.676 ± 0.271	535.5 ± 33.0	113.3 ± 10.3	0.213 ± 0.024
Obese	6	16.63 ± 1.26	3.517 ± 0.766	679.9 ± 37.9	231.7 ± 39.7	0.340 ± 0.046
Obese canoletta	6	9.31 ± 1.52	8.160 ± 3.573	1,082 ± 58.5	156.7 ± 10.3	0.145 ± 0.00/
Obese 0% choline/0.2% methionine	5	14.94 ± 2.68	5.542 ± 1.744	795.7 ± 26.5	378.0 ± 151.7	0.474 ± 0.186
Obese AMLN-vehicle	5	10.82 ± 1.03	7.678 ± 1.673	1,029 ± 31.8	156.0 ± 37.8	0.152 ± 0.041
Obese AMLN- elafibranor (30 mg/kg)	5	9.40 ± 1.09	4.260 ± 1.187	873.6 ± 44.9	132.0 ± 8.4	0.152 ± 0.016
Obese AMLN-oil	6	12.00 ± 0.99	7.857 ± 0.551	1,072 ± 73.1	165.0 ± 27.4	0.155 ± 0.030
Obese AMLN- CCl_4 (0.2 mg/kg)	6	11.00 ± 1.45	7.940 ± 1.640	1,065 ± 76.3	155.0 ± 33.9	0.146 ± 0.034
Fructose-fed rats I (Mexico City)						
Control	6	4.67 ± 0.52	3.302 ± 1.347	546.0 ± 30.9	130.5 ± 10.7	0.240 ± 0.030
Fructose-fed	6	4.88 ± 0.56	7.902 ± 0.292	564.7 ± 48.3	209.5 ± 22.4	0.374 ± 0.052
Fructose-fed rats II (Mexico City)						
Control	6	4.67 ± 0.52	—	468.3 ± 42.2	146.5 ± 10.3	0.315 ± 0.034
Fructose-fed	6	4.95 ± 0.76	5.938 ± 2.572	535.7 ± 48.2	136.1 ± 29.5	0.254 ± 0.048
Fructose-fed rats III (Mexico City)						
Control	8	5.20 ± 0.54	4.172 ± 2.538	518.8 ± 56.2	159.0 ± 21.6	0.307 ± 0.037
Fructose-fed	8	6.15 ± 0.92	9.831 ± 2.548	623.3 ± 46.9	158.1 ± 21.0	0.254 ± 0.032
Rats with neonatal STZ injection (Mexico City)						
Control	8	3.80 ± 0.84	—	464.8 ± 41.2	147.8 ± 29.3	0.318 ± 0.059
Neonatal STZ	8	9.06 ± 7.03	—	420.8 ± 58.0	184.6 ± 39.3	0.453 ± 0.149
IRS2 knock-out mice (Cologne)						
C57BL/6J	12	8.98 ± 1.59	—	31.52 ± 5.70	30.28 ± 6.11	0.982 ± 0.217

(Continued on following page)

TABLE 1 (*Continued*) Blood glucose, insulin (selected studies only), body weight, bladder weight, and bladder/body weight across animal models.

	n	Blood glucose, mM	Insulin, ng/l	Body weight, g	Bladder weight, mg	Bladder/body weight, mg/g
IRS2 knock-out	12	16.02 ± 9.27	—	31.73 ± 5.27	25.96 ± 7.30	0.824 ± 0.230
ob/ob mice (Cologne)						
C57BL/6J	9	9.40 ± 2.24	—	30.19 ± 5.32	25.89 ± 5.64	0.865 ± 0.175
ob/ob	14	9.19 ± 2.91	—	64.70 ± 6.09	36.59 ± 13.05	0.565 ± 0.195
ob/ob and db/db mice (Hoechst)						
C57BL/6J	31	7.89 ± 1.25	—	23.57 ± 3.61	23.52 ± 4.50	1.000 ± 0.135
ob/ob	31	14.88 ± 8.05	—	46.56 ± 16.16	28.80 ± 10.40	0.557 ± 0.222
db/db	32	26.03 ± 4.33	—	49.03 ± 2.78	25.94 ± 4.31	0.530 ± 0.090
HFD mice (Hoechst)						
C57BL/6N	32	7.64 ± 0.95	—	23.97 ± 2.81	28.25 ± 5.93	1.177 ± 0.201
C57BL/6N HFD	32	9.36 ± 1.15	—	47.08 ± 4.12	31.10 ± 9.81	0.660 ± 0.202
HFD mice + semaglutide (Hoechst)						
C67BL/6N	8	9.35 ± 0.62	643.8 ± 151.7	34.76 ± 0.71	66.91 ± 31.93	1.930 ± 0.923
C67BL/6N HFD	8	9.23 ± 0.54	1,021 ± 263.2	43.72 ± 2.66	44.25 ± 12.44	1.025 ± 0.345
HFD + semaglutide	7	7.92 ± 0.62	682.9 ± 228.4	36.26 ± 2.04	37.56 ± 7.43	1.045 ± 0.253
HFD mice (Mainz)						
C57BL/6J	12	5.96 ± 0.72	284.8 ± 205.5	34.07 ± 2.65	33.33 ± 5.33	0.980 ± 0.149
C57BL/6J HFD	12	9.68 ± 1.82	4,431 ± 819	49.25 ± 2.31	35.17 ± 6.93	0.713 ± 0.125

Data are shown as means ± SD of the indicated number of animals. Insulin concentrations were below detection limit (0.000512 ng/ml) in lean ZSF1 rats in all animals in the 20- and 4/6 in the 28-weeks study; for calculation purposes they were set to 0.000512 ng/ml. Data from each individual animal of each study are shown in the Supplementary Material.

expressed as % of the mean of the corresponding control group. This was followed by correlation analysis of the pooled data based on individual animal data across all models for comparison of BW and BBW vs. glucose. Similar correlations with insulin were done as *post-hoc* analyses.

In line with recent guidelines and recommendations (Michel et al., 2020; Vollert et al., 2020), we consider all analyses reported here as exploratory. Therefore, no hypothesis-testing statistical analysis was applied and reported *p*-values should be considered descriptive and not hypothesis-testing. We rather focus on reporting of effect sizes with their 95% confidence intervals (CI). All calculations were performed using Prism (v9.03; GraphPad, Los Angeles, CA, United States). Additional information on data quality measures is provided in the Supplementary Material.

3 Results

3.1 Model characterization

3.1.1 Glycaemic state

Based on an operational definition of normoglycaemia (<8 mM), hyperglycaemia (8–16 mM), and overt diabetes (>16 mM), some control groups were mildly hyperglycaemic (RIP-LCMV mice, one study each in C57BL/6J and in C57BL/6N mice). Similarly, the disease groups did not exhibit overt diabetes in all studies (20-weeks old ZSF1 rats, rats with neonatal STZ injection, fructose-fed rats, ob/ob mice and mice on a high-fat diet (HFD), and some diets and treatments (empagliflozin and semaglutide) lowered glucose in diabetic animals without restoring normoglycemia (Table 1).

In all six studies with available insulin data, hyperinsulinemia relative to the respective control was observed (Table 1). Among treatments, canoletta and AMLN diets further increased insulin concentration in both ZSF1 rat studies, whereas 0% choline/0.2% methionine and elafibranor had no major effect; semaglutide lowered insulin concentration in HFD mice (Table 1).

3.1.2 Body weight

Body weight was markedly reduced in STZ rats (>40%) and by <15% in RIP-LCMV mice (Table 1). Among type 2 diabetes/obesity models, body weight was markedly increased in ZSF1 rats of either age, in both studies with ob/ob mice, in db/db mice, and in HFD mice (Table 1). Fructose-feeding markedly increased body weight in two studies, but much less so in a third one (Table 1). Rats with neonatal STZ injection and IRS2 knock-out mice did not exhibit major alterations of body weight (Table 1). Empagliflozin and linagliptin had no major effects on body weight, whereas semaglutide normalized body weight and elafibranor reduced it by almost 40% relative to its control (AMLN vehicle; Table 1).

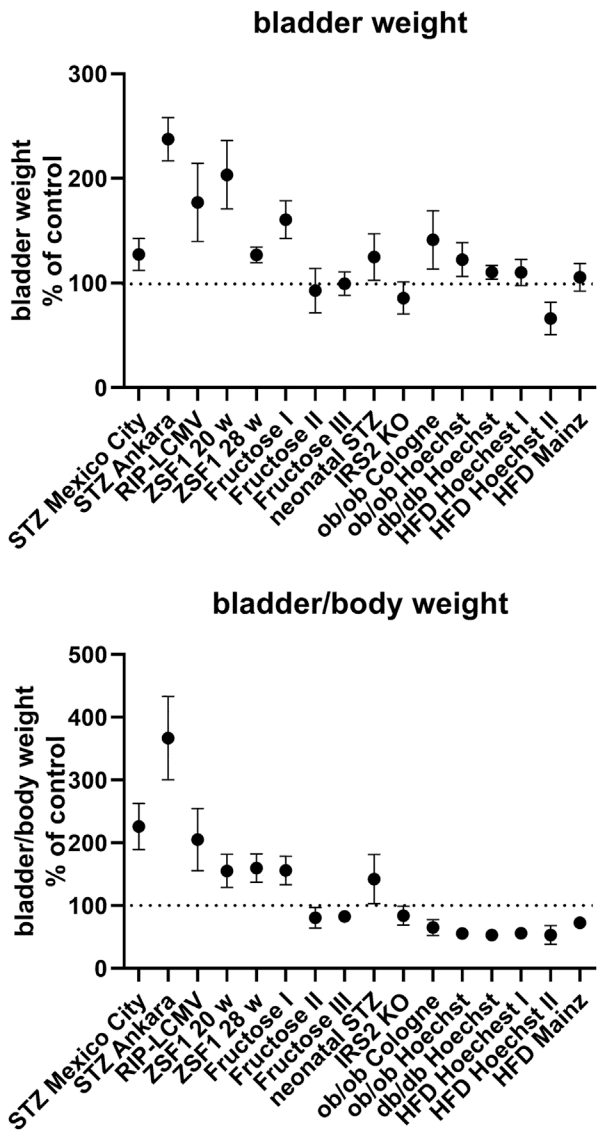

FIGURE 1
Bladder and bladder/body weight differences across studies. Data are shown as effect sizes comparing the primary hyperglycaemic/diabetic vs. the control group expressed as mean difference with its 95% confidence interval. Note that the same control group was used in the calculation of the ob/ob and db/db Hoechst groups.

TABLE 2 Correlation between blood glucose and bladder and bladder/body weight across animal models.

n total	Bladder weight		Bladder/body weight	
	r^2	*p*	r^2	*p*
Type 1 diabetes models				
STZ-injected rats (Mexico City)				
21	0.2346	0.0261	0.6368	<0.0001
STZ-injected rats (Ankara)				
79	0.3795	<0.0001	0.3220	<0.0001
RIP-LCMV mice (Frankfurt)				
27	0.7226	<0.0001	0.7322	<0.0001
Type 2 diabetes models				
ZSF1 rats (20-weeks, Hoechst)				
30	0.3632	0.0004	0.2428	0.0057
ZSF1 rats (28-weeks, Hoechst)				
45	0.4127	<0.0001	0.3168	<0.0001
Fructose-fed rats I (Mexico City)				
12	0.0109	0.7465	0.0044	0.8384
Fructose-fed rats II (Mexico City)				
12	0.1979[a]	0.1473	0.2545[a]	0.0944
Fructose-fed rats III (Mexico City)				
14	0.0488	0.4481	0.0465[a]	0.4590
Rats with neonatal STZ injection (Mexico City)				
16	0.3302	0.0199	0.6262	0.0003
IRS2 knock-out mice (Cologne)				
24	0.1256	0.0893	0.1009	0.1305
ob/ob mice (Cologne)				
23	0.0053	0.7410	0.0001	0.9593
ob/ob mice (Hoechst)				
62	0.0339	0.1519	0.0761[a]	0.0300
db/db mice (Hoechst)				
63	0.1203	0.0054	0.6743[a]	<0.0001
HFD mice (Hoechst)				
64	0.0054	0.5655	0.0383	0.1214
HFD mice + semaglutide (Hoechst)				
23	0.0787	0.1947	0.0522	0.2945
HFD mice (Mainz)				
24	0.0231	0.4783	0.3614[a]	0.0019

Animals from diabetic and non-diabetic group were pooled for each correlation analysis. Shown are total number of animals per model, squared correlation coefficient (r^2) and descriptive *p*-value.
[a]negative slope (inverse correlation).
A graphical representation of representative groups is shown in Figure 2, all other groups in the Supplementary Material.

3.1.3 Bladder enlargement

BW was increased in all type 1 diabetes models and in some type 2 diabetes/obesity models (both studies with ZSF1 rats, one of the three studies with fructose-fed rats, study with rats with neonatal STZ injection, both studies with ob/ob mice and in db/db mice; Table 1; Figure 1). In contrast, no bladder enlargement was observed in the other type 2 diabetes models (two out of three studies with fructose-fed rats, IRS2 knock-out mice, all three studies with HFD in mice). As body weight exhibited major changes in some of the models, a different picture was obtained for bladder/body weight (BBW; Table 1; Figure 1).

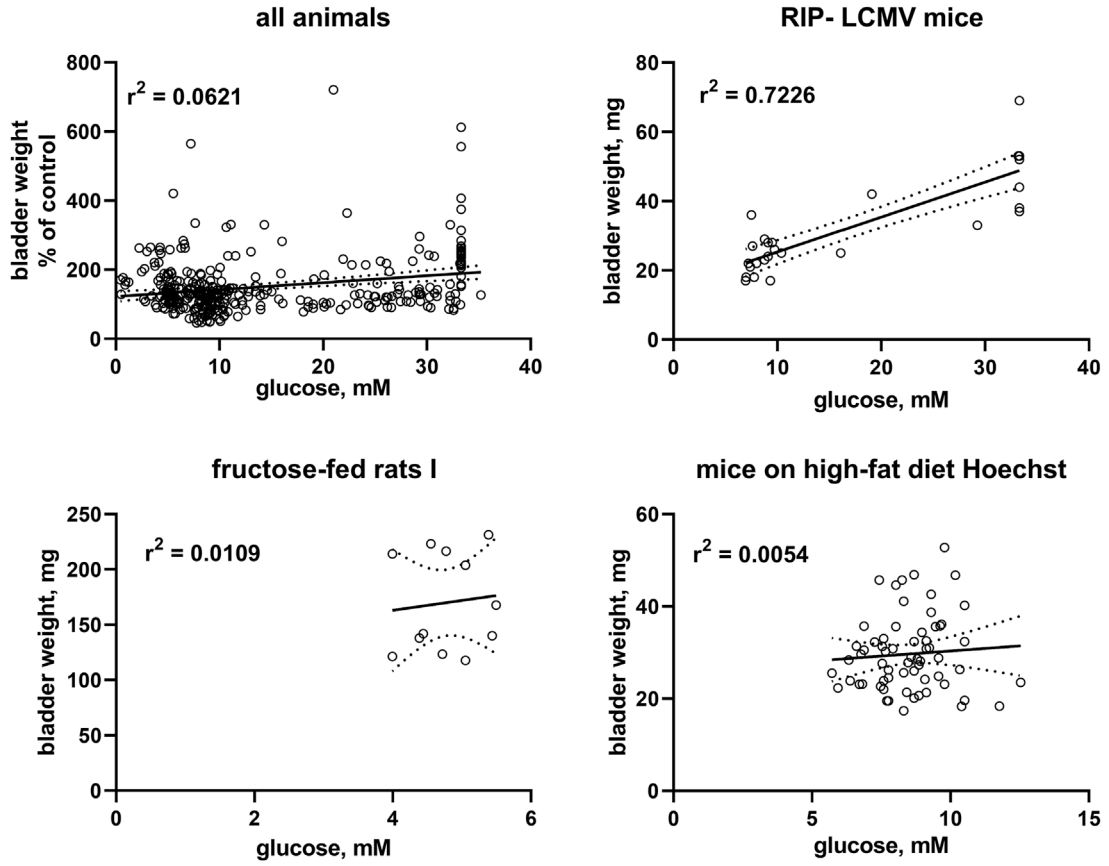

FIGURE 2
Correlation of bladder and bladder/body weight with glucose levels. To enable pooling of data from all studies, those for the upper left panel shows bladder weight only from the non-control groups expressed as % of mean values in the control group within a study. The other three panels show correlations within three representative studies; data from the remaining studies are shown in the Supplementary Material. A quantitative description of the correlations is shown in Table 2. Mean values of bladder weight and glucose level in each study are shown in Table 1.

While HFD did not affect BW in mice (see above), addition of canoletta reduced BW in obese ZSF1 rats assessed at an age of 20 weeks [mean difference −56.7 mg (−86.2; −27.1)], a diet containing 0% choline/0.2% methionine increased BW [mean difference 75.0 mg (CI 8.6; 141.4)], and the AMLN diet had no detectable effect [mean difference −30 mg (CI −91.0; 31.0); Table 1]; however, all three estimates had wide CI making interpretation difficult. Similar effects of the three diets were seen at an age of 28 weeks.

Among pharmacological treatments, empagliflozin and linagliptin led to numerically large increases of BW in STZ rats, but these could not easily be interpreted due to large CI [mean difference 77.2 mg (CI −17.4; 171.8) and 81.6 mg (CI −11.3; 174.5), respectively; Table 1]. Elafibranor induced a moderate reduction in BW as compared to obese ZSF1 rats on AMLN diet [mean difference −33 mg (CI −62.0; −4.0)]. Semaglutide had no clear effect on BW [mean difference −6.7 mg (CI −18.4; 5.0)].

3.2 Correlation analysis between blood glucose and bladder weight

Among models with blood glucose levels greater than the renal reabsorption threshold (>10 mM), IRS2 knock-out mice lacked and db/db exhibited only a minor increase in BW (Table 1; Figure 1). In contrast, bladder enlargement was observed in one study with a glucose level below the threshold (<9 mM; fructose-fed rat I), whereas studies with glucose levels approximately in the range of the threshold (9–10 mM) exhibited bladder enlargement in two but not in three other studies (Table 1; Figure 1).

Correlation analysis was performed within each model based on individual animal data (Table 2; Figure 2). Strength of correlation between glucose level and BW (expressed as r^2) varied markedly between models and ranged from 0.7226 in RIP-LCMV mice to 0.005 in one of the HFD mice studies. Except for the two ZSF1 rat studies, all groups had r^2 values of <0.2, indicating that inter-animal variability of glucose levels, serving as a proxy of diabetic polyuria, statistically accounted for less

TABLE 3 Correlation between plasma insulin and bladder and bladder/body weight across animal models of type 2 diabetes.

n total	Bladder weight		Bladder/body weight	
	r^2	*p*	r^2	*p*
ZSF1 rats (20-weeks, Hoechst)				
30	0.0209	0.4461	0.0335[a]	0.3329
ZSF1 rats (28-weeks, Hoechst)				
45	0.0058[a]	0.6192	0.0557[a]	0.1186
Fructose-fed rats I (Mexico City)				
12	0.5127	0.0088	0.4773	0.0129
Fructose-fed rats III (Mexico City)				
14	0.0080	0.7605	0.1626[a]	0.1529
HFD mice + semaglutide (Hoechst)				
23	0.0529[a]	0.2912	0.1046[a]	0.1322
HFD mice (Mainz)				
18	0.1319	0.2459	0.3389[a]	0.0470

Animals from diabetic and non-diabetic group were pooled for each correlation analysis. Shown are total number of animals per model, squared correlation coefficient (r^2) and descriptive *p*-value.
[a]negative slope (inverse correlation).
A graphical representation of representative groups is shown in Figure 3, all other groups in the Supplementary Material.

than 20% of variability in BW. Comparable strength of correlation was found when glucose levels were compared to BBW; however, as a notable exception an r^2 of 0.674 was found for db/db mice, a model in which BW was not markedly changed but body weight about doubled (Table 2). When data from the hyperglycaemic/diabetic animals of all studies were pooled, r^2 was 0.0621 (Figure 2), indicating that glucose did not explain bladder weight variability in an inter-model analysis.

3.3 Correlation between serum insulin and bladder weight

In *post-hoc* correlation analyses between insulin levels and BW within each of the six studies with available insulin data (Table 3) and in a pooled analysis of all studies (Figure 3), a strong correlation was observed in one study with fructose-fed rats ($r^2 = 0.5127$), this was neither confirmed in another study in this model nor in both studies with ZSF1 rats or in two studies with HFD; of note, a numerically inverse correlation was observed in one study with HFD mice (see Supplementary Material). In a pooled analysis of data from all animals in the hyperglycaemic/diabetic groups, a week inverse correlation was observed (Figure 3, $r^2 = 0.0718$, descriptive *p*-value 0.0077). Plasma insulin levels also positively correlated with BBW in the first fructose-feeding study but, if anything, inversely in the other five studies with available insulin data (Table 3).

4 Discussion

We have used data from 16 studies representing nine distinct rodent models of diabetes and 513 animals to address three specific questions:

- How widespread is urinary bladder enlargement in rodent models of experimental diabetes, particularly type 2 diabetes?
- How do diets and treatments other than insulin affect bladder enlargement?
- Is diabetic polyuria the key driver of diabetes-associated bladder enlargement across animal models?

4.1 Critique of methods

It is a unique feature of the present study that it is fully based on data from experiments designed and conducted for other purposes. This is a limitation and a strength. The limitation results from the fact that the original studies were neither designed nor powered to explore bladder enlargement and its causes; moreover, the 16 studies were heterogeneous in species (rat and mouse), type 1 vs. type 2 diabetes, specific aspects of models including hereditary vs. acquired disease, duration of observation, and possible centre differences between contributing laboratories. To accommodate this limitation, we have expressed data in the hyperglycaemic/diabetic groups as % of the mean value in the corresponding euglycemic group for all inter-study analyses.

The 16 studies also varied in time from onset of diabetes to tissue harvesting, which raises the question whether that time period had been sufficient to induce the bladder weight phenotype. While none of the 16 studies had been designed to assess the bladder weight phenotype, we feel comfortable that time between onset and harvesting was sufficient to increase bladder weight if it occurs in a given model for two reasons. Firstly, each study had been designed and conducted to measure a specific phenotype; this target phenotype (distinct for each study) was reached in all studies. Second, we have previously analysed 83 groups of STZ vs. control rats (Arioglu Inan et al., 2018). Pooled analysis of extent of bladder enlargement vs. time suggested that bladder enlargement was largely complete after about 1 week after STZ injection. This was corroborated by looking at the time courses of the 10 studies that had tested three or more time points.

These limitations are outweighed by using an unprecedented number of models and studies. Given that each animal model of diabetes has limitations (Islam, 2013; Lenzen, 2017), use of such variety of models should help to obtain data applicable to the heterogeneous population of diabetic patients (Ahlqvist et al., 2020). Moreover, using data from studies designed for other purposes fulfils the ethical mandate of the 3R principles to reduce the use of experimental animals wherever possible (Kilkenny et al., 2010). Generating a comparable number of models and

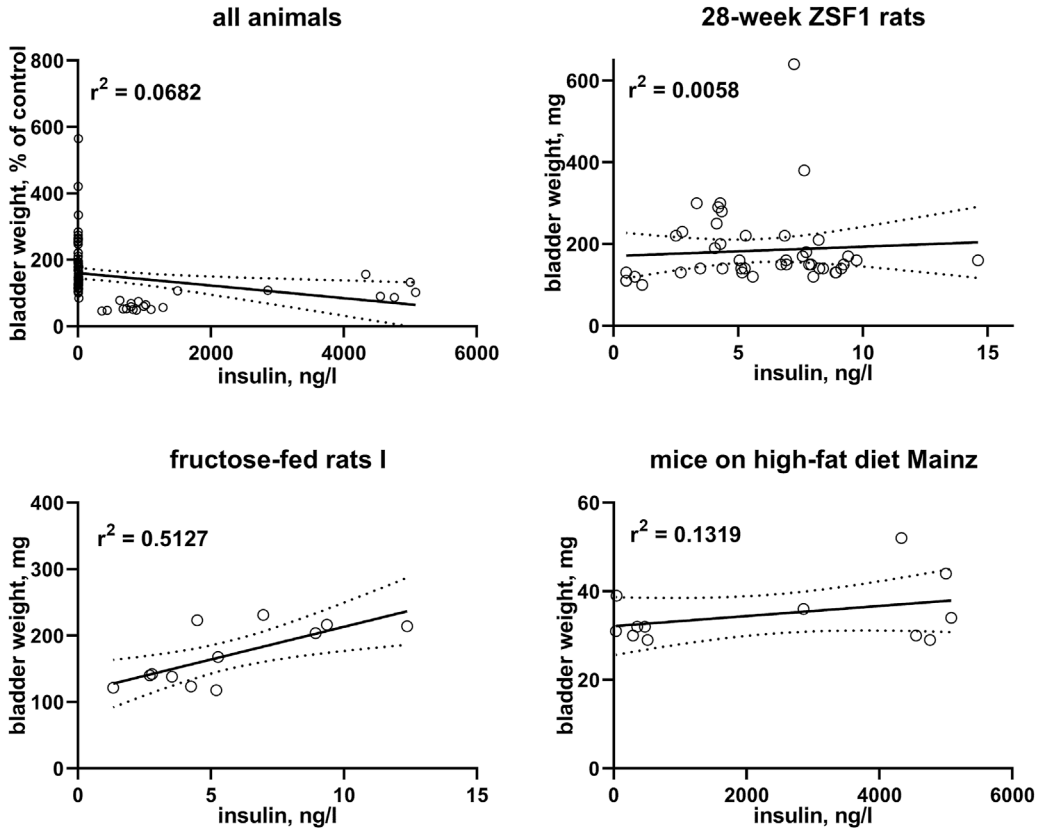

FIGURE 3
Correlation of bladder weight with insulin levels. To enable pooling of data from all studies, those for the upper left panel shows bladder weight only from the non-control groups expressed as % of mean values in the control group within a study. The other three panels show correlations within three representative studies; data from the remaining studies are shown in the Supplementary Material. A quantitative description of the correlations is shown in Table 3. Mean values of bladder weight and insulin level in each study are shown in Table 1.

studies for the primary purpose of the present analyses would have been too resource-intensive to be justifiable and perhaps even unethical. Thus, the present analyses probably represent the largest collection of models and studies ever analysed for any outcome parameter within a single project in diabetes research.

4.2 Bladder enlargement across models

More than 70 previous studies have demonstrated a consistent enlargement of the urinary bladder in rats injected with STZ (mean BW 178% of control; range 99%–440%) (Arioglu Inan et al., 2018). A similar degree of enlargement was observed in a small number of studies with STZ-injected mice and rabbits, while other type 1 diabetes models including alloxan-injected rats and rabbits, BB/Wor rats and Akita mice exhibited a less pronounced increase in BW (Ellenbroek et al., 2018). Our studies with STZ-injected rats [two reported here, a third reported elsewhere (Yesilyurt et al., 2021)] confirm these findings. Moreover, we extend this to another model of type 1 diabetes, RIP-LCMV mice, for which no BW data have been reported in the past.

Previous data in animal models of type 2 diabetes/obesity was limited to five models: fructose-fed rats, HFD mice, Goto-Kakizaki rats, Zucker diabetic fatty rats, and db/db mice (Ellenbroek et al., 2018). Across those models, bladder enlargement was small (about 150% of control) in fructose-fed rats and db/db mice, largely absent in HFD mice and in Goto-Kakizaki rats, but greater than the average enlargement in STZ-injected rats in Zucker diabetic fatty rats. Our present studies largely are in line with these findings. Our experiments also add data on four type 2 diabetes/obesity models for which bladder data had not been reported previously. We found a major increase in ZSF1 rats (>200% of control); as ZSF1 rats are a cross between Zucker diabetic fatty and spontaneously hypertensive rats and as Zucker rats were reported to exhibit a major bladder enlargement (Ellenbroek et al., 2018), these data are in line with previous findings. A moderate increase in bladder size was observed in rats injected with STZ at the neonatal stage and in ob/ob mice, whereas IRS2 knock-out mice did not exhibit

bladder enlargement. In conclusion, the present data almost double the number of models of type 2 diabetes for which BW data have been reported. Together with data from previous systematic reviews (Arioglu Inan et al., 2018; Ellenbroek et al., 2018), these findings indicate that all animal models of type 1 diabetes exhibit bladder enlargement, although perhaps to a different extent, whereas BW increases markedly in some models of type 2 diabetes, only moderately in others and not at all in additional models. Apparently, severity of diabetes as assessed by blood glucose levels does not explain the observed heterogeneity of bladder enlargement. While the reasons for this heterogeneity are not fully clear, it is interesting that subgroups of patients with type 2 diabetes exhibiting distinct phenotypes are now also being recognized (Ahlqvist et al., 2020).

Other than in diabetes, bladder enlargement occurs in many conditions in animal models and patients, including bladder outlet obstruction and bladder denervation (Michel and Arioglu-Inan, 2021). It typically is associated with LUTD. Therefore, a better understanding of the pathophysiology underlying diabetes-associated bladder enlargement may help to define innovative treatment strategies to combat frequent LUTD in diabetic patients.

4.3 Differential effects of diets and pharmacological treatments

The present studies are the first to explore effects of drug treatments other than insulin (Ellenbroek et al., 2018) on diabetes-associated bladder enlargement. The four drugs applied in the underlying studies had the expected effects or lack thereof on glucose levels for the model in which they were used but, like the diets, did not affect glucose and BW in the same way in several cases: empagliflozin [a glycosuric drug (Michel et al., 2015)] lowered glucose but, if anything, increased BW; linagliptin (a drug not affecting glucosuria) tested within the same study caused a similar extent of bladder enlargement without affecting glucose levels. Semaglutide lowered glucose without affecting BW, and elafibranor did not affect glucose but reduced BW. These differential effects of diets and drug treatments are not easy to interpret because none of the studies had been designed to compare diet or drug effects on glucose and BW and because CI were wide in several cases. Nonetheless, the divergent effects casted doubt on the assumption that diabetic polyuria is the main reason for bladder enlargement.

4.4 Role of glucose and insulin in bladder enlargement

When blood glucose levels exceed the renal reabsorption threshold, the excreted glucose can act as an osmotic diuretic and cause diabetes-associated polyuria. It had been proposed that such polyuria is the main cause for bladder enlargement in experimental diabetes. Support for this hypothesis largely comes from studies in which feeding with sucrose caused a similar degree of diuresis as STZ injection and a similar degree of bladder enlargement (Kudlacz et al., 1988; Eika et al., 1994; Fukumoto et al., 1994; Tammela et al., 1994; Tammela et al., 1995; Liu and Daneshgari, 2005; Xiao et al., 2013). The polyuria hypothesis mechanistically implies that the degree of enlargement should be correlated with blood glucose levels because glucose levels determine the extent of diabetic polyuria. However, the presence of bladder enlargement segregated only poorly with glucose levels relative to the renal reabsorption threshold in our analyses of 16 studies.

To further test the diabetic polyuria hypothesis, we have previously correlated the reported glucose levels and bladder size alterations at the group level across a total of >100 studies: while we detected a correlation at the group level, it was only of moderate strength, i.e., less than 20% in variability of BW could mathematically be attributed to that of glucose levels (Ellenbroek et al., 2018). A major limitation of that analysis was that we only had access to data at the group level. We performed a similar correlation analysis based on individual animal data for glucose level and BW in a recent pilot study, which also yielded a correlation of only moderate strength (Yesilyurt et al., 2021). Therefore, individual animal-based correlation analyses were performed for the 16 studies reported here as a pre-specified outcome parameter (Table 2). BW was correlated with blood glucose concentration in the three studies with type 1 diabetes models but only in three out of 13 studies in type 2 diabetes/obesity models. Moreover, the strength of correlation varied markedly across models. Thus, a strong correlation was observed in RIP-LCMV mice, a moderate correlation in STZ-injected rats, ZSF1 rats and rats with neonatal STZ injection, but correlations were very weak if existing at all in the other models. To corroborate these findings, we also performed a correlation analysis based on pooled individual animals from the hyperglycaemic/diabetic groups of all 16 studies, which yielded an r^2 of 0.0621 (Figure 2). While a positive correlation does not prove a cause-effect relationship, lack of correlations makes it unlikely that such relationship exists to a biologically meaningful extent. Taken together, these data do not support the hypothesis that polyuria is the main factor to explain diabetes-associated bladder enlargement.

Insulin is not only a hormone but also a growth factor (Ikle and Gloyn, 2021), and fructose-fed rats often exhibit a greater increase in insulin than in glucose levels, possibly reflecting peripheral insulin resistance (Chen et al., 2018). After having noticed a moderate to strong correlation of bladder enlargement with insulin levels in one study with fructose-fed rats (r^2 = 0.5127), we performed a similar post-hoc analysis on the other five studies with available insulin data: all five studies including another study in fructose-fed rats exhibited very

weak, and in one of them and in the pooled analysis of all studies numerically inverse correlations (Figure 3; Table 3). This is not too surprising given that type 1 diabetes is characterized by a reduced presence of insulin; while insulin can be increased in models of type 2 diabetes including those reported here, this effect typically is counterbalanced by a reduced insulin sensitivity.

Thus, our data on diets, drug treatments, blood glucose levels relative to the renal reabsorption threshold and most importantly our correlations between glucose and BW at the individual animal level do not support the diabetic polyuria hypothesis of bladder enlargement in animal models of type 2 diabetes. While this mechanism may play a role in some models such as RIP-LCMV mice, and perhaps a more moderate one in STZ-injected rats, it plays only a very minor if any role in most other models. More generally, our data suggest that animal models of diabetes not only differ in the presence and extent of bladder enlargement, but also in the pathophysiology leading to such enlargement in the models where it occurs. This conclusion is in line with the proposal that human type 2 diabetes is a heterogeneous condition with multiple underlying subgroups (Ahlqvist et al., 2020).

5 Conclusion

Based on an unprecedented number of studies and animal models, we have shown that bladder enlargement is ubiquitous in animal models of type 1 diabetes and common, but not consistently present in those of type 2 diabetes/obesity. This heterogeneity among type 2 diabetes models is not explained by the severity of diabetes/hyperglycaemia, specifically not by glucose levels relative to the renal reabsorption threshold. For the first time, we have explored effects of various diets and drug treatments other than insulin on diabetes-associated bladder enlargement; many of them had differential effects on glucose levels and bladder enlargement. These differential effects together with the generally moderate to absent association of glucose levels with BW do not support the hypothesis that diabetic polyuria is the main cause of diabetes-associated bladder enlargements—at least in most models. Refuting the polyuria hypothesis generates the necessity for additional studies to identify alternative mechanisms leading to bladder enlargement in some experimental models of diabetes. Our analyses highlight the heterogeneity between animal models of diabetes. While type 2 diabetes patients apparently also are a heterogeneous group (Ahlqvist et al., 2020), specific links between such subgroups and specific animal models remain to be established. Finally, our data demonstrate that major research accomplishments can be made without use of extra animals if smart planning is applied.

Data availability statement

The original contributions presented in the study are included in the article/Supplementary Material, further inquiries can be directed to the corresponding author.

Ethics statement

Each of the 16 studies reported here had been reviewed and approved by the applicable committee; details for each study are provided in the Supplementary Material.

Author contributions

ZY: Experimentation for STZ study Ankara; overall data analysis; co-development of primary manuscript draft. JM: Collection of data and supervision of study with ob/ob and IRS2 knock-out mice. EH: Experimentation for RIP-LCMV mouse study. TC: Planning and experimentation for studies in ZSF1 rats and C57BL/6J, C57BL/6N, db/db, ob/ob, and HFD mice. RE: Planning and experimentation in C57BL/6N and HFD mice JB-O: Experimentation for fructose-fed and STZ rat studies. DS-V: Experimentation for neonatal STZ rat study. NX: Data collection and study supervision of the HFD model (Mainz). AK: Planning of studies in in ZSF1 rats and C57BL/6J, C57BL/6N, db/db, ob/ob, and HFD mice. UC: Experimentation for RIP-LCMV mouse study. DC: Supervision of fructose-fed, STZ and neonatal STZ rat studies. HL: Study supervision of the HFD model (Mainz). AP: Conceptualization of overall project. EA-I: Supervision of STZ study Ankara; co-lead of overall project. MM: conceptualization and lead of overall project; supervision of data analysis; co-development of primary manuscript draft. All authors have critical reading of manuscript for important intellectual content and approval of final manuscript.

Funding

This work was funded in part by TÜBITAK 2211/A (to ZY), TÜBITAK-SBAG 118S443 and 119S769 (to EA-I), Landesoffensive zur Entwicklung wissenschaftlich-ökonomischer Exzellenz (LOEWE; LOEWE Center for Translational Medicine and Pharmacology) of the State of Hessen, Germany (to UC), Conacyt Mexico 252702 (to DC), and Deutsche Forschungsgemeinschaft XI 139/2-1 (to NX), LI-1042/5-1 (to HL) and Mi 294/10-1 (to MM). Some underlying studies were performed and/or funded by Sanofi-Aventis (identified as “Hoechst”) for purposes unrelated to this manuscript.

Conflict of interest

TC, RE, and AK are former employees of Sanofi-Aventis.

All other authors declare that the research was conducted in the absence of any commercial or financial relationships that could be construed as a potential conflict of interest.

Publisher's note

All claims expressed in this article are solely those of the authors and do not necessarily represent those of their affiliated organizations, or those of the publisher, the editors and the reviewers. Any product that may be evaluated in this article, or claim that may be made by its manufacturer, is not guaranteed or endorsed by the publisher.

Supplementary material

The Supplementary Material for this article can be found online at: https://www.frontiersin.org/articles/10.3389/fphys.2022.923555/full#supplementary-material

References

Ahlqvist, E., Prasad, R. B., and Groop, L. (2020). Subtypes of type 2 diabetes determined from clinical parameters. *Diabetes* 69, 2086–2093. doi:10.2337/dbi20-0001

Arioglu Inan, E., Ellenbroek, J. H., and Michel, M. C. (2018). A systematic review of urinary bladder hypertrophy in experimental diabetes: part I. Streptozotocin-induced rat models. *Neurourol. Urodyn.* 37, 1212–1219. doi:10.1002/nau.23490

Benner, J. S., Becker, R., Fanning, K., Jumadilova, Z., Bavendam, T., and Brubaker, L. (2009). Bother related to bladder control and health care seeking behavior in adults in the United States. *J. Urol.* 181, 2591–2598. doi:10.1016/j.juro.2009.02.018

Chen, I.-H., Cheng, J.-T., and Tong, Y.-C. (2018). Metabolic syndrome induced bladder cannabinoid receptor changes in the fructose-fed rats. *LUTS Low. Urin. Tract. Symptoms* 10, 198–203. doi:10.1111/luts.12156

Daneshgari, F., and Moore, C. (2006). Diabetic uropathy. *Semin. Nephrol.* 26, 182–185. doi:10.1016/j.semnephrol.2005.09.009

Eika, B., Levin, R. M., and Longhurst, P. A. (1994). Comparison of urinary bladder function in rats with hereditary diabetes insipidus, streptozotocin-induced diabetes mellitus, and nondiabetic osmotic diuresis. *J. Urol.* 151, 496–502. doi:10.1016/s0022-5347(17)35001-2

Ellenbroek, J. H., Arioglu Inan, E., and Michel, M. C. (2018). A systematic review of urinary bladder hypertrophy in experimental diabetes: part 2. Comparison of animal models and functional consequences. *Neurourol. Urodyn.* 37, 2346–2360. doi:10.1002/nau.23786

Fukumoto, Y., Yoshida, M., Weiss, R. M., and Latifpour, J. (1994). Reversability of diabetes- and diuresis-induced alterations in rat bladder dome muscarinic receptors. *Diabetes* 43, 819–826.

Ikle, J. M., and Gloyn, A. L. (2021). 100 years of insulin: a brief history of diabetes genetics: insights for pancreatic beta-cell development and function. *J. Endocrinol.* 250, R23. doi:10.1530/JOE-21-0067

Irwin, D. E., Milsom, I., Kopp, Z., and Abrams, P. (2008). Symptom bother and health care-seeking behavior among individuals with overactive bladder. *Eur. Urol.* 53, 1029–1037. doi:10.1016/j.eururo.2008.01.027

Islam, M. S. (2013). Animal models of diabetic neuropathy: progress since 1960s. *J. Diabetes Res.* 2013, 149452. doi:10.1155/2013/149452

Kannan, H., Radican, L., Turpin, R. S., and Bolge, S. C. (2009). Burden of illness associated with lower urinary tract symptoms including overactive bladder/urinary incontinence. *Urology* 74, 34–38. doi:10.1016/j.urology.2008.12.077

Kilkenny, C., Browne, W., Cuthill, I. C., Emerson, M., and Altman, D. G. (2010). Animal research: reporting *in vivo* experiments: the ARRIVE guidelines. *Br. J. Pharmacol.* 160, 1577–1579. doi:10.1111/j.1476-5381.2010.00872.x

Kudlacz, E. M., Chun, A. L., Skau, K. A., Gerald, M. C., and Wallace, L. J. (1988). Diabetes and diuretic-induced alterations in function of rat urinary bladder. *Diabetes* 37, 949–955. doi:10.2337/diab.37.7.949

Lenzen, S. (2017). Animal models of human type 1 diabetes for evaluating combination therapies and successful translation to the patient with type 1 diabetes. *Diabetes. Metab. Res. Rev.* 33, e2915. doi:10.1002/dmrr.2915

Liu, G., and Daneshgari, F. (2005). Alterations in neurogenically mediated contractile responses of urinary bladder in rats with diabetes. *Am. J. Physiol. Ren. Physiol.* 288, F1220–F1226. doi:10.1152/ajprenal.00449.2004

Mensah, G. A., Wei, G. S., Sorlie, P. D., Fine, L. J., Rosenberg, Y., Kaufmann, P. G., et al. (2017). Decline in cardiovascular mortality: possible causes and implications. *Circ. Res.* 120, 366–380. doi:10.1161/CIRCRESAHA.116.309115

Michel, M. C., and Arioglu-Inan, E. (2021). Function and morphology of the urinary bladder after denervation. *Am. J. Physiol. Regul. Integr. Comp. Physiol.* 320, R833–R834. doi:10.1152/ajpregu.00093.2021

Michel, M. C., Mayoux, E., and Vallon, V. (2015). A comprehensive review of the pharmacodynamics of the SGLT2 inhibitor empagliflozin in animals and humans. *Naunyn. Schmiedeb. Arch. Pharmacol.* 388, 801–816. doi:10.1007/s00210-015-1134-1

Michel, M. C., Murphy, T. J., and Motulsky, H. J. (2020). New author guidelines for displaying data and reporting data analysis and statistical methods in experimental biology. *Mol. Pharmacol.* 97, 49–60. doi:10.1124/mol.119.118927

Mitroupoulos, D., Anastasiou, I., Giannopoulo, C., Nikolopoulos, G., Alamanis, C., and Zervas, A. (2002). Symptomatic benign prostatic hyperplasia: impact on partners' quality of life. *Eur. Urol.* 41, 240–245. doi:10.1016/S0302-2838(02)00041-6

Percie du Sert, N., Hurst, V., Ahluwalia, A., Alam, S., Avey, M. T., Baker, M., et al. (2020). The ARRIVE guidelines 2.0: updated guidelines for reporting animal research. *Br. J. Pharmacol.* 177, 3617–3624. doi:10.1111/bph.15193

Tammela, T. L. J., Briscoe, J. A. K., Levin, R. M., and Longhurst, P. A. (1994). Factors underlying the increased sensitivity to field stimulation of urinary bladder strips from streptozotocin-induced diabetic rats. *Br. J. Pharmacol.* 113, 195–203. doi:10.1111/j.1476-5381.1994.tb16193.x

Tammela, T. L. J., Leggett, R. E., Levin, R. M., and Longhurst, P. A. (1995). Temporal changes in micturition and bladder contractility after sucrose diuresis and streptozotocin-induced diabetes mellitus in rats. *J. Urology* 153, 2014–2021. doi:10.1016/s0022-5347(01)67393-2

Vollert, J., Schenker, E., Macleod, M., Bespalov, A., Wuerbel, H., Michel, M., et al. (2020). Systematic review of guidelines for internal validity in the design, conduct and analysis of preclinical biomedical experiments involving laboratory animals. *BMJ Open Sci.* 4, e100046. doi:10.1136/bmjos-2019-100046

Xiao, N., Wang, Z., Huang, Y., Daneshgari, F., and Liu, G. (2013). Roles of polyuria and hyperglycemia in bladder dysfunction in diabetes. *J. Urol.* 189, 1130–1136. doi:10.1016/j.juro.2012.08.222

Yesilyurt, Z. E., Erdogan, B. R., Karaomerlioglu, I., Müderrisoglu, A. E., Michel, M. C., Arioglu Inan, E., et al. (2019). Urinary bladder weight and function in a rat model of mild hyperglycemia and its treatment with dapagliflozin. *Front. Pharmacol.* 10, 911. doi:10.3389/fphar.2019.00911

Yesilyurt, Z. E., Ertürk, B. M., Erdogan, B. R., Arioglu-Inan, E., and Michel, M. C. (2021). Effects of the sodium-glucose transporter 2 inhibitor empagliflozin on bladder size, contraction and relaxation in a rat model of type 1 diabetes. *Neurourol. Urodyn.* 42 (Suppl 2), S141–S142. doi:10.1002/nau.24746

frontiers | Frontiers in Physiology

TYPE Review
PUBLISHED 12 August 2022
DOI 10.3389/fphys.2022.914963

OPEN ACCESS

EDITED BY
Laurival Antonio De Luca Jr.,
Departamento de Fisiologia e Patologia da Faculdade de Odontologia da Universidade Estadual Paulista, Brazil

REVIEWED BY
Joel Charles Geerling,
University of Iowa Hospitals and Clinics, United States
Matthew Scott Sherwood,
Wright State University, United States

*CORRESPONDENCE
Limin Liao,
lmliao@263.net

†These authors share first authorship

SPECIALTY SECTION
This article was submitted to Integrative Physiology, a section of the journal Frontiers in Physiology

RECEIVED 07 April 2022
ACCEPTED 05 July 2022
PUBLISHED 12 August 2022

CITATION
Pang D, Gao Y and Liao L (2022), Functional brain imaging and central control of the bladder in health and disease.
Front. Physiol. 13:914963.
doi: 10.3389/fphys.2022.914963

Functional brain imaging and central control of the bladder in health and disease

Dongqing Pang[1,2,3†], Yi Gao[1,2,3†] and Limin Liao[1,2,3*]

[1]China Rehabilitation Research Center, School of Rehabilitation, Capital Medical University, Beijing, China, [2]Department of Urology, China Rehabilitation Research Center, Beijing, China, [3]Department of Urology, Capital Medical University, Beijing, China

Central control of the bladder is a complex process. With the development of functional imaging technology and analysis methods, research on brain-bladder control has become more in-depth. Here, we review previous functional imaging studies and combine our latest findings to discuss brain regions related to bladder control, interactions between these regions, and brain networks, as well as changes in brain function in diseases such as urgency urinary incontinence, idiopathic overactive bladder, interstitial cystitis/bladder pain syndrome, urologic chronic pain syndrome, neurogenic overactive bladder, and nocturnal enuresis. Implicated brain regions include the pons, periaqueductal grey, thalamus, insula, prefrontal cortex, cingulate cortex, supplementary motor area, cerebellum, hypothalamus, basal ganglia, amygdala, and hippocampus. Because the brain is a complex information transmission and processing system, these regions do not work in isolation but through functional connections to form a number of subnetworks to achieve bladder control. In summarizing previous studies, we found changes in the brain functional connectivity networks related to bladder control in healthy subjects and patients involving the attentional network, central executive network or frontoparietal network, salience network, interoceptive network, default mode network, sensorimotor network, visual network, basal ganglia network, subcortical network, cerebella, and brainstem. We extend the working model proposed by Griffiths et al. from the brain network level, providing insights for current and future bladder-control research.

KEYWORDS

bladder, urination, functional magnetic resonance imaging, near-infrared spectroscopy, brain mapping

Introduction

Understanding brain-bladder control mechanisms in healthy adults is essential to identifying the central abnormalities in patients with lower urinary tract dysfunction (LUTD). The lower urinary tract has two main functions: urine storage and micturition. Switching between the two phases depends on current bladder capacity, external environment, and volitional control. The supraspinal, spinal, autonomic, and somatic nerve pathways work together to control the balance between these two functions. In

2008, Fowler et al. (2008) proposed the neural circuits that control continence and micturition. Specifically, there are two reflexes: 1) Urine storage reflexes, which occur mainly in the spinal cord and are important in the urine-storage phase. During bladder filling, bladder distention generates low levels of bladder-afferent signals that stimulate the hypogastric and pudendal nerves to contract the bladder outlet, inhibit the contraction of the detrusor, and contract the external urethral sphincter, respectively; and 2) Voiding reflexes, in which the intense afferent signal from the bladder during urination activates the pontine micturition center (PMC), which increases the efferent activity of the parasympathetic nerve and contracts the detrusor muscle, while inhibiting efferent activity of the sympathetic and pudendal nerves to the urethral outlet. Upstream afferent signals from the spinal cord may reach the PMC through the periaqueductal grey (PAG).

People can urinate voluntarily when it is convenient or delay urination when it is inconvenient, which may rely on brain circuits above the PAG. (Fowler et al., 2008). Because previous articles have reviewed PAG and pons in detail, (de Groat et al., 2015), we focused on brain regions above PAG, especially the interaction between brain regions and networks.

Brain regions related to bladder control

The idea that the brain may be involved in bladder control was supported by clinical experience. As early as 1964, Andrew and Nathan found that prefrontal cortex (PFC) lesions caused by issues such as tumors, aneurysms, wounds, and leukotomy, which may lead to an impaired ability to inhibit the voiding reflex, resulting in urinary urgency and incontinence, suggesting that the PFC is crucial for bladder control. (Andrew and Nathan, 1964). In 1996, Sakakibara (Sakakibara et al., 1996) analyzed the cranial computed tomography (CT) or magnetic resonance imaging (MRI) of 72 patients with acute hemispheric stroke and their urodynamic examination results, finding that patients with frontal lobe lesions showed detrusor hyperreflexia and uninhibited sphincter relaxation, leading to lower urinary tract symptoms (LUTS) such as frequency and urgency urinary incontinence (UUI) in stroke patients.

In the past few decades, with the rapid development of functional brain imaging technology, single-photon emission CT (SPECT) and positron emission tomography (PET) technologies have been gradually applied in brain-bladder research. These methods can indirectly reflect local brain neural activity by measuring regional cerebral blood flow (rCBF) changes in brain regions. (Kitta et al., 2015). Fukuyama et al. (1996) first used SPECT in 1996 to search for brain regions with activity potentially correlated to urination control in healthy subjects. In 1997, Blok et al. (1997) first performed a 15O-H2O PET study of healthy men during storage, micturition, and post-micturition. They conducted the same study in 1998 in healthy women, finding the same changes (i.e., significantly increased blood flow in the inferior frontal gyrus, pons, and PAG). They suggested that the micturition may be associated with these brain regions. (Blok et al., 1998). In 2000, Nour et al. (2000) first applied the experimental paradigm of bladder filling by means of bladder perfusion, in which the bladder was filled by perfusing normal saline into the intravesical catheter. They were the first to try a PET scan with simultaneous detrusor pressure monitoring. PET scans were performed during an empty bladder, full bladder (normal desire to void), and micturition.

Subsequently, two other brain functional imaging techniques, namely functional magnetic resonance imaging (fMRI) and functional near-infrared spectroscopy (rs-fNIRS), have been used to study the hypothetical central mechanism of bladder control. fMRI is based on the quantification of paramagnetism of deoxy-Hb and has the advantages of high temporal and spatial resolution. (Kitta et al., 2015). The physiological processes underlying BOLD fMRI imaging are neurovascular coupling mechanisms. (Stackhouse and Mishra, 2021). Specifically, increased synaptic activity leads to the dilation of local arterioles and an increase in cerebral blood flow (CBF) to match enhanced metabolic demands and maintain normal brain function. (Munoz et al., 2015). fNIRS is based on the absorption of near-infrared light by oxyhemoglobin (oxy-Hb) and deoxy-Hb and has the advantages of portability and high temporal resolution. (Jobsis, 1977).

Previous studies have shown that activation of brain regions shows increased rCBF and glucose utilization but little increase in oxygen utilization, resulting in an increase in the amount of oxygen available in the active regions (i.e., oxy-Hb), which explains the blood oxygen level-dependent (BOLD) signal of fMRI and fNIRS, while deactivation shows an opposite pattern of change. (Raichle et al., 2001). Because both excitatory and inhibitory neural activity increase local glucose utilization in animal models, (Ackermann et al., 1984; Batini et al., 1984), deactivation is unlikely to result from increased activity of locally inhibitory neurons. Deactivation, in contrast, may indicate a reduction in nerve cell activity to a level below baseline.

In 2015, Griffiths et al. (2015a) (de Groat et al., 2015) reviewed previous brain functional imaging studies and proposed a working model related to bladder control. Specifically, circuit one includes the thalamus, insula, lateral PFC (LPFC), medial PFC (MPFC), and PAG. Griffiths et al. (2015a) suggested a possible mechanism for maintaining continence in healthy subjects: the sensation of bladder dilation is uploaded to the insula *via* the thalamus, which activates LPFC and in turn reduces MPFC activity through an inhibitory connection, reducing MPFC input to PAG, stabilizing PAG and inhibiting the voiding reflex and, finally, maintaining continence.

Circuit 2 includes the dorsal anterior cingulate cortex (dACC) and supplementary motor area (SMA). The team

suggested that this circuit is a backup used by people with UUI or overactive bladder (OAB) rather than healthy subjects. That is, if there is a threat of urinary incontinence, dACC and SMA seem to respond by producing a sense of urgency and urinary sphincter contraction, enhancing the ability to delay urination. Circuit 3 includes the PAG and parts of the inferior or middle temporal (parahippocampal) cortex, whose role may be to provide unconscious monitoring during low bladder volume/low bladder sensation in healthy subjects.

Urine storage phase

Most previous functional brain imaging studies focused on changes in brain activity during the urine storage phase. These studies achieved a full bladder/desire to void by having participants drink water (Fukuyama et al., 1996; Blok et al., 1997; Gao et al., 2015; Pang et al., 2020; Pang and Liao, 2021) and performing repeated perfusion/withdrawal of saline through the urinary catheter, (Griffiths et al., 2005; Matsumoto et al., 2011; Pang et al., 2021), or repeated spontaneous contraction of pelvic floor muscles (Kuhtz-Buschbeck et al., 2005; Zhang et al., 2005; Seseke et al., 2006) to activate relevant brain regions. Our recent fMRI study (Pang et al., 2021) found that regional homogeneity (ReHo) values in the thalamus, insula, medial frontal gyrus, and bilateral superior frontal gyrus of healthy adults changed significantly when the bladder was full rather than empty, which support the theory of this model. Sakakibara et al. (1996) found that LUTS might be associated with thalamus impairment in stroke patients after the analysis of the lesion site by CT and MRI. Previous studies have shown that bladder filling, leading to a desire to void, may significantly activate the insula in healthy subjects, and activation increases with the degree of bladder filling and desire to void. (Kuhtz-Buschbeck et al., 2005). Moreover, in OAB patients, insula activation was exaggerated during bladder filling, (Griffiths et al., 2005; Tadic et al., 2010), so the insula was considered related to bladder distention and the desire to void. The interoceptive visceral sensation (bladder distention) [27]is uploaded through the spinal cord and then relayed in the thalamus, targeting the insula, the interoceptive afferent cortex. (Blok et al., 1997; Craig, 2003).

The PFC, located in brain regions in front of the primary and premotor cortex, including the superior frontal gyrus, middle frontal gyrus, and inferior frontal gyrus, was shown to be related to bladder control in previous neuroimaging studies. (Nour et al., 2000; Griffiths et al., 2009). Previous studies showed MPFC deactivation (Griffiths et al., 2007; Griffiths et al., 2009) and LPFC activation when the bladder was full during urine storage. (Kuhtz-Buschbeck et al., 2005; Yin et al., 2008; Sakakibara et al., 2010; Matsumoto et al., 2011). The deactivation of MPFC is thought to be related to maintaining urine storage. (Blok et al., 1997; Blok et al., 1998; Griffiths et al., 2007; Griffiths et al., 2009). Andrew and Nathan generalize their idea of a possible center (i.e., the medial, periventricular, mid-frontal region) that might control the function of urination after reviewing a case series that included an abundance of leukotomy patients. They found that permanent urination problems may be associated with large lesions and severe lesions. (Andrew and Nathan, 1964). Deactivation of the MPFC may indicate reduced neural activity of the MPFC to below baseline. (Raichle et al., 2001). MPFC is an important part of the default mode network (DMN), which is characterized by activation of brain areas within the network in the resting state (i.e., eyes closed or simple visual fixation) and deactivation in the presence of external stimuli. (Raichle et al., 2001; Fox and Raichle, 2007). Deactivation of a brain region within DMN indicates that resting activity is suspended while the brain uses its resources to process events that require conscious attention.

But until now, it has not been clear whether the deactivation of MPFC during urine storage phase is the cause of urinary incontinence or the mechanism by which the urination reflex is suppressed and continence is maintained. Griffiths believes the latter is the brain response of people trying to avoid improper bladder contractions. (Griffiths, 2015b). The fear of public incontinence during urinary urgency can cause tension related to social etiquette, with increased heart rate. Previous studies have shown that this increased heart rate caused by social evaluative threat may be mediated by activation of rostral dorsal ACC and deactivation of ventral mPFC. (Wager et al., 2009). Griffiths suggested that the bladder control during urinary urgency may be achieved by using a dorsal ACC-based sympathetic mechanism and MPFC-based parasympathetic mechanism. (Griffiths, 2015a). PFC is involved in human higher cognitive function, and the brain region responsible for executive function is mainly the bilateral dorsolateral prefrontal cortex (DLPFC), including BA9, 10, and 46. Executive functions include organizing input from different sensory modes, maintaining attention, monitoring information in working memory, and coordinating goal-directed behavior. (Teffer and Semendeferi, 2012). Duffau and Capelle (2005) reported two cases of patients with long-term UUI after glioma resection, considering that DLPFC lesions confirmed by structural MRI may result in an inability to delay voiding. Previous studies have shown that the stronger the desire to void, the stronger the activation of bilateral DLPFC, suggesting that DLPFC may be related to the monitoring of interoceptive stimulation and the perception of bladder sensation. (Kuhtz-Buschbeck et al., 2005; Matsumoto et al., 2011).

Micturition phase

Compared with the urine storage stage, relatively few studies have investigated changes in brain activity during micturition, including one SPECT, (Fukuyama et al., 1996),

TABLE 1 Brain areas activated during micturition.

Brain areas activated during micturition	Authors	Subjects	Functional imaging technique
Lateral PFC/inferior frontal gyrus	Fukuyama et al. (1996)	Healthy men	SPECT
	Blok et al. (1997)	Healthy men	PET
	Blok et al. (1998)	Healthy women	PET
	Nour et al. (2000)	Healthy men	PET
	Krhut et al. (2012)	Healthy women	fMRI
Pons/PMC	Fukuyama et al. (1996)	Healthy men	SPECT
	Blok et al. (1997)	Healthy men	PET
	Blok et al. (1998)	Healthy women	PET
	Nour et al. (2000)	Healthy men	PET
	Shy et al. (2014)	Healthy women	fMRI
PAG	Blok et al. (1997)	Healthy men	PET
	Blok et al. (1998)	Healthy women	PET
	Nour et al. (2000)	Healthy men	PET
Hypothalamus	Blok et al. (1997)	Healthy men	PET
	Blok et al. (1998)	Healthy women	PET
	Nour et al. (2000)	Healthy men	PET
Basal ganglia	Blok et al. (1997) (striatum)	Healthy men	PET
	Nour et al. (2000) (globus pallidus)	Healthy men	PET
	Shy et al. (2014) (caudate nucleus and lentiform nucleus)	Healthy women	fMRI
ACC	Blok et al. (1997)	Healthy men	PET
	Krhut et al. (2012)	Healthy women	fMRI
	Shy et al. (2014)	Healthy women	fMRI
Postcentral gyrus	Nour et al. (2000)	Healthy men	PET
	Shy et al. (2014)	Healthy women	fMRI
Thalamus	Nour et al. (2000)	Healthy men	PET
	Shy et al. (2014)	Healthy women	fMRI
Insula	Nour et al. (2000)	Healthy men	PET
	Shy et al. (2014)	Healthy women	fMRI
Superior frontal gyrus/mPFC	Nour et al. (2000)	Healthy men	PET
	Shy et al. (2014)	Healthy women	fMRI
Cerebellar	Nour et al. (2000)	Healthy men	PET
	Shy et al. (2014)	Healthy women	fMRI
SMA	Fukuyama et al. (1996)	Healthy men	SPECT
	Shy et al. (2014)	Healthy women	fMRI

three PET, (Blok et al., 1997; Blok et al., 1998; Nour et al., 2000), and two fMRI studies. (Krhut et al., 2012; Shy et al., 2014). The task paradigm of repeated micturition was first used in 2012. (Krhut et al., 2012). By summarizing information on the brain regions involved in these studies for the first time (Table 1), we found that the frequency of activation of brain regions during micturition was five times for the LPFC/inferior frontal gyrus and pons; three times for PAG, hypothalamus, basal ganglia, and anterior cingulate cortex (ACC); twice for the postcentral gyrus, thalamus, insula, superior frontal gyrus, cerebellar, and SMA. This suggests that these brain regions play an important role in the micturition phase.

Interactions between brain regions and networks

In addition to studying the activation/deactivation of a specific brain region associated with bladder control, some studies over the past 20 years have focused on the communication, collaboration, separation, and integration of brain regions. Functional connectivity (FC) refers to the display of coherent neural activity in anatomically isolated brain regions. The FC of different paired brain regions together constitute brain functional networks. (Ketai et al., 2016; Zuo et al., 2019b). By summarizing these studies, we

TABLE 2 Changes in the brain FC and networks related to bladder control in healthy subjects and patients with LUTD.

Network	Description anatomic areas and function	Activation or FC changes within the network	Authors	Subjects
Attentional network, AN	**Ventral** AN includes the temporoparietal junction (TPJ) and ventral frontal/prefrontal cortex. **Ventral** AN response to unexpected events (bottom-up attention) Vossel et al. (2014)	Bladder distention increased the activation of brain regions within the ventral AN (bilateral TPJ). (task-fMRI)	Jarrahi et al. (2015a)	Healthy women
		The ventral AN (left supramarginal gyrus) were significantly activated in healthy women with a full bladder compared with an empty bladder. (task-fMRI)	Nardos et al. (2014)	Healthy women
		Compared to the baseline before treatment, combined groups showed decreased activation of the left TPJ. (task-fMRI)	Ketai et al. (2021)	UUI women; hypnotherapy VS. pharmacotherapy
		Compared to HC, UUI group showed greater activation within the **ventral** AN (i.e., VLPFC, bilateral middle superior temporal and supramarginal gyrus). (task-fMRI)	Ketai et al. (2016)	UUI women VS. HC
	Dorsal AN includes the bilateral frontal eye field and the intraparietal sulcus	Compared to pharmacotherapy, hypnotherapy participants manifested increased functional connectivity (FC) within **dorsal** AN. (rs-fMRI)	Ketai et al. (2016)	UUI women; hypnotherapy VS. pharmacotherapy
	Dorsal AN response to goal-directed (top-down attention) processing. Vossel et al. (2014)			
		FC within the **dorsal** DAN (i.e., precentral gyrus) was significantly decreased in OAB group compared with HC. (rs-fMRI)	Zuo et al. (2019a)	OAB patients VS. HC
Central executive network (CEN) or frontoparietal network (FPN)	CEN consists of the DLPFC and the lateral posterior parietal cortex. Chan et al. (2016)	Bladder distention increased the activation of brain regions within the CEN (DLPFC and posterior parietal cortices). (task-fMRI)	Jarrahi et al. (2015a)	Healthy women
	CEN is responsible for active maintenance and manipulation of information in working memory, as well as judgment and decision making under goal-directed behavior. Chan et al. (2016)	Compared to HC, OAB group showed increased FC strength in middle frontal gyrus, which is a part of DLPFC. (rs-fMRI)	Zuo et al. (2019b)	OAB patients VS. HC
		FC within the LFPN (i.e., superior frontal gyrus) was significantly decreased in OAB group compared with HC. (rs-fMRI)	Zuo et al. (2019a)	OAB patients VS. healthy controls
		UUI patients had significantly abnormal activation within CEN (i.e., inferior and superior frontal gyrus) compared with HC. (task-fMRI)	Nardos et al. (2016)	UUI women VS. HC
Salience network (SN) or interoceptive network (IN)	SN includes the ACC and the anterior insula. Seeley et al. (2007)	Compared to empty bladder, we found increased ReHo in the brain region (i.e., left insula and bilateral ACC) within SN with a full bladder. (rs-fMRI)	Pang et al. (2021)	Healthy subjects; full bladder VS. empty bladder
	SN is responsible for locating and detecting associated stimuli. Seeley et al. (2007)			
		Bladder distention increased the activation of brain regions within the SN (anterior insula and ACC). (task-fMRI)	Jarrahi et al. (2015a)	Healthy women
		The SN (i.e., left ACC) were significantly activated in healthy women with a full bladder compared with an empty bladder. (task-fMRI)	Nardos et al. (2014)	Healthy women
		Compared to HC, UUI group showed greater activation within the Interoceptive network (i.e., left island and ACC). (task-fMRI)	Ketai et al. (2016)	UUI women VS. HC

(Continued on following page)

TABLE 2 (*Continued*) Changes in the brain FC and networks related to bladder control in healthy subjects and patients with LUTD.

Network	Description anatomic areas and function	Activation or FC changes within the network	Authors	Subjects
Default mode network, DMN	DMN includes the posterior cingulate cortex (PCC), the medial prefrontal cortex (MPFC), the precuneus, the medial temporal lobe, and the **AG**. Fox and Raichle (2007)	Compared to empty bladder, we found increased ReHo in the brain region (i.e., left temporal gyrus and left **AG**) within DMN with a full bladder. (rs-fMRI)	Pang et al. (2021)	Healthy subjects; full bladder VS. empty bladder
	DMN is involved in social or self-referential processing, stimulus-independent thought, manipulation of episodic memories, and semantic knowledge. Chan et al. (2016)	Compared to empty bladder, significantly increased FC within DMN (i.e., superior frontal gyrus, PCG, and AG) when the desire to void was strong. (rs-fMRI)	Pang et al. (2020)	Healthy subjects; strong desire to void VS. empty bladder
		Bladder distention increased the activation of brain regions within the DMN (MPFC, the precuneus/PCC, bilateral parietal lobules, and the inferior temporal gyri). (task-fMRI)	Jarrahi et al. (2015a)	Healthy women
		Compared to HC, OAB group showed decreased FC strength in hubs of the DMN (eg the PCG and the MPFC). (rs-fMRI)	Zuo et al. (2019b)	OAB patients VS. HC
		UUI patients had significantly abnormal activation within DMN (i.e., inferior parietal lobe) compared with HC. (task-fMRI)	Nardos et al. (2016)	UUI women VS. HC
		Compared to HC, UUI group showed greater activation within the posterior DMN (i.e., PCC and precuneus). (task-fMRI)	Ketai et al. (2016)	UUI women VS. HC
		Compared to HC, urologic chronic pain syndrome (UCPPS) group showed that the FC of DMN was significantly reduced to PCC and left precuneus. (rs-fMRI)	Martucci et al. (2015)	women with UCPPS VS. HC
Sensorimotor network, SMN	SMN includes the somatosensory area, the primary motor cortex, the secondary motor cortex, the SMA, and the premotor cortex. Chan et al. (2016)	Compared to empty bladder, strong desire to void group showed an increased nodal efficiency in the SMN (i.e., bilateral postcentral gyrus). (rs-fMRI)	Pang et al. (2020)	Healthy subjects; strong desire to void VS. empty bladder
	SMN has pre-mediated functions that coordinate the functions of multiple brain regions in preparation for motor responses to sensory input. Zuo et al. (2019a)	FC within the SMN (i.e., paracentral lobule) was significantly decreased in OAB group compared with HC. (rs-fMRI)	Zuo et al. (2019a)	OAB women VS. healthy controls
		UUI patients had significantly abnormal activation within SMN (i.e., precentral and postcentral gyrus) compared with HC. (task-fMRI)	Nardos et al. (2016)	UUI women VS. HC
Visual network, VN	VN located in the visual cortex and is divided into dorsal VN and ventral VN.	Compared to empty bladder, strong desire to void group showed an increased nodal efficiency in the VN (i.e., superior occipital gyrus, bilateral middle occipital gyrus, and cuneus). (rs-fMRI)	Pang et al. (2020)	Healthy subjects; strong desire to void VS. empty bladder
	The dorsal VN processes information about the position of objects and adjusts visual controls for skilled movements. Migliaccio et al. (2016)			
		FC within the dorsal VN (i.e., left cuneus) was significantly decreased in OAB group compared with HC. (rs-fMRI)	Zuo et al. (2019a)	OAB patients VS. healthy controls with empty bladder
Basal ganglia network, BGN	BGN includes the striatum, consisting of caudate nucleus and lenticular nucleus (including putamen and globus pallidus), claustrum, amygdala, red nucleus, substantia nigra, and subthalamic nucleus. (Smitha et al., 2017)	Compared to empty bladder, strong desire to void group showed an increased nodal efficiency in the BGN (i.e., caudate nucleus). (rs-fMRI)	Pang et al. (2020)	Healthy subjects; strong desire to void VS. empty bladder
	BGN is responsible for the process of motor areas control, emotion, cognition, etc. They engage in goal-directed behavior that requires movement. (Smitha et al., 2017)	Bladder distention increased the activation of brain regions within the BGN (bilateral striatum and amygdala) and thalamus. (task-fMRI)	Jarrahi et al. (2015a)	Healthy women

(Continued on following page)

TABLE 2 (*Continued*) Changes in the brain FC and networks related to bladder control in healthy subjects and patients with LUTD.

Network	Description anatomic areas and function	Activation or FC changes within the network	Authors	Subjects
		Patients with UUI who responded to pelvic floor muscle therapy (PFMT) had significant differences in FC of BG (caudate nucleus and putamen), thalamus, and dACC compared with before treatment. (rs-fMRI)	Clarkson et al. (2018)	UUI women who responded VS. non-responded to PFMT

found changes in the brain FC and brain network related to bladder control in healthy subjects and patients with LUTD, including the following brain networks (Table 2): Attentional network (AN), central executive network (CEN) or frontoparietal network (FPN), salience network (SN) or interoceptive network (IN), default mode network (DMN), sensorimotor network (SMN), visual network (VN), basal ganglia network (BGN), subcortical network, cerebella, and the brainstem.

Healthy subjects

Some studies on healthy subjects could serve as a basis for explaining brain abnormalities in patients with LUTD. We found that healthy subjects showed increased ReHo in the brain region within DMN (i.e., left superior temporal gyrus and left angular gyrus [AG]) and SN with a full bladder, compared with an empty bladder. (Pang et al., 2021). Moreover, we found significantly increased FC within DMN (i.e., superior frontal gyrus, posterior cingulate cortex [PCC], and AG), and increased nodal efficiency (enodal) in the BGN (i.e., caudate nucleus), DMN (i.e., PCC), SMN (i.e., bilateral postcentral gyrus), and VN (i.e., superior occipital gyrus, bilateral middle occipital gyrus, and cuneus) in healthy subjects when the desire to void was strong versus an empty bladder. (Pang et al., 2020). We suggested that that SN provides bladder sensation and that DMN may provide self-reference, self-refection, and decision-making about whether to void after assessment of the external environment. Moreover, the bladder-control process may be coordinated by multiple subnetworks (e.g., BG, SMN, VN). (Pang et al., 2020; Pang et al., 2021). Nardos et al. (2014) found that the SN (i.e., left ACC), ventral AN (left supramarginal gyrus), and left cerebellum were significantly activated in healthy women with a full bladder compared with an empty bladder. rs-fMRI fixation effect analysis revealed significant changes in FC between a full and empty bladder in DMN (i.e., MPFC, cingulate gyrus, inferior lateral temporal gyrus), SMN (i.e., postcentral gyrus), and BGN (i.e., amygdala and caudate nucleus). They suggested that bladder control during bladder filling depends primarily on the functional integration of distributed brain systems. Jarrahi et al. (2015a) found that subliminal stimulation of bladder filling in healthy women can cause significant changes in FC within and between the SN (insula and ACC), SMN, subcortical network (amygdala, hippocampus, and thalamus), and posterior DMN, BGN, cerebellum, and brainstem networks, suggesting that subliminal sensory input may affect mood, emotion, and behavior.

In another fMRI study, Jarrahi et al. (2015b) performed task fMRI of repeated bladder perfusion/withdrawal of saline in four states in healthy women [i.e., empty bladder (warm), empty bladder (cold), 100 ml (warm), and strong desire to void (warm)]. They found that visceral interoception (i.e., bladder distention) in healthy women caused increased activation of brain regions within the SN (anterior insula and ACC), CEN [DLPFC and posterior parietal cortices (PPC)], DMN (MPFC, precuneus/PCC, bilateral parietal lobules, and the inferior temporal gyri), ventral AN [bilateral temporoparietal junction (TPJ)], BGN (bilateral striatum and bilateral amygdala), subcortical network (thalamus and parahippocampa gyri) and cerebellum/brainstem networks. (Jarrahi et al., 2015b). By analyzing the functional network connectivity (FNC), Jarrahi et al. found that bladder filling in all four states could cause an FC decrease between AN and DMN and an FC increase between the DMN and subcortical network. Furthermore, compared with empty bladder (warm), the FC between aDMN and AN in 100 ml (warm) and strong desire to void (warm) state decreases, while the FC between aDMN and BGN increases, as well as DMN and SN. The team indicated that visceral sensation is a dynamic process in which the components interact closely but are separable. In this system, SN (insula, ACC), CEN (DLPFC and posterior parietal cortex), thalamus, and ventral AN (TPJ) provide visceral status monitoring and significance detection, while the DMN (MPFC and IFG), BGN (striatum, and amygdala), SN (insula and ACC), subcortical network (thalamus, hippocampi, and parahippocampal gyrus) and brainstem are more likely involved in the regulation of arousal, motivation, emotion, and action initiation.

Urgency urinary incontinence

Ketai et al. (2016) found that the activation of some brain regions in the UUI group were greater than in the HC group when the bladder was full, including the interoceptive network

(i.e., left insula, ACC and MCC), VAN (i.e., VLPFC, bilateral middle superior temporal and supramarginal gyrus) and posterior DMN (i.e., PCC and Precuneus). They thought the increased desire to void was associated with greater urgency and incontinence. Even before the bladder is full, the FC between MCC and DAN in the UUI group was abnormally stronger than in the HC group. On the contrary, the FC between MCC and VAN in the HC group was stronger than in UUI group. Ketai et al. (2016) suggested that this increased connection to DAN may indicate top-down attentional support for goal-directed (e.g., maintaining continence) behaviors in UUI patients. This is different from HC in that VAN is used for bottom-up attention support.

Nardos et al. (2016) found that UUI patients had significantly abnormal activation of brain regions within the DMN (i.e., inferior parietal lobe), CEN (i.e., inferior and superior frontal gyrus), and SMN (i.e., precentral and postcentral gyrus) compared with HC. They suggested that LUTS is associated with attention, decision making, and primary motor and sensory dysfunction in patients with UUI. Moreover, six typical FC features could predict the severity of UUI, including the connections linked to SN (i.e., dorsal/ventral ACC) and DMN (i.e., AG and ventral medial frontal regions) to SMN areas, between CEN (i.e., superior frontal gyrus) and cerebellum and between SN (i.e., insula) and SMN (i.e., paracentral lobule). They suggest that UUI patients have atypical functional integration between emotional, cognitive, and motor areas that can help distinguish the presence or absence of UUI and predict the severity of symptoms. Clarkson et al. (2018) found that patients with UUI who responded to pelvic floor muscle therapy (PFMT) had significant differences in FC of BGN (caudate nucleus and putamen) and dACC compared with before treatment. They suggest that this variation in FC indicates that the motor processing mechanism may be related to UUI and can be altered by PFMT. Clarkson et al. (2018) found that responders exhibit significant differences in the FC (i.e., between the MPFC and the precuneus, cingulum and postcentral gyrus) from nonresponders at baseline. They suggest that UUI has two subtypes, one primarily caused by abnormalities in brain control (responders) and the other with little to do with brain function (nonresponders). Ketai et al. (2021) found that successful pharmacological treatment of UUI is associated with reduced activation of VAN (bottom-up attention), which may be caused by the drug's reduction of bladder-afferent impulses. Conversely, the decrease in VAN activation in successful hypnotherapy treatment of UUI may be due to the balancing effect of DAN (top-down attention).

Overactive bladder

Zuo et al. (2019a) found that in OAB patients, the FC strength within the DMN (i.e., MPFC and PCG), ACG, and MCG was significantly decreased, while the FC strength of middle frontal gyrus (MFG), components of CEN, was significantly increased when compared with healthy controls. They suggested that the reduced FC strength of MPFC, ACG, MCG, and PCG result in inhibition of urine storage and promotes voiding reflex in patients with OAB. In another rs-fMRI study, Zuo et al. (2019a) found that the FC within the SMN (i.e., paracentral lobule), ECN (i.e., both supramarginal gyrus), DAN (i.e., precentral gyrus), dVN (i.e., left cuneus), and LFPN(i.e., superior frontal gyrus) was significantly decreased, as well as the FC between the SMN and the anterior DMN, is reduced in OAB group compared with HC. They believe that these brain networks are related to bladder control, which can perform a series of sensory, motor, emotional, and cognitive processing of incoming signals from the bladder, and evaluate and respond to them in the social environment. These intranetwork and internetwork FC anomalies may affect the OAB.

Our recent study (Pang et al., 2022) showed that the activation of left DLPFC was significantly reduced in OAB patients with a strong desire to void compared with HC and that LUTS improved in OAB patients after 2–4 weeks of sacral neuromodulation (SNM), while the activation of the left DLPFC was restored with no significant difference from HC. We suggest that decreased DLPFC activation in OAB patients releases its inhibition of the voiding reflex, leading to classic OAB symptoms.

Interstitial cystitis/painful bladder syndrome or urologic chronic pain syndrome

We investigated the FC within the prefrontal cortex (PFC) of patients with IC/BPS versus healthy subjects using the rs-fNIRS. (Pang and Liao, 2021). FC was significantly decreased within the PFC in the IC/BPS group, whether with an empty bladder or a strong desire to void. Moreover, compared with the empty bladder state (BA9,10, and 46; 18 edges), the FC decreased in a wider range during the strong desire to void (BA9,10,45, and 46; 28 edges). Edge stands for FC between two brain regions. We suggest that the abnormal reduction of FC within the PFC in IC/BPS patients may cause the release of inhibition of the PFC on the voiding reflex, causing LUTS. Kilpatrick et al. (2014) found significant changes in the frequency distribution of visceral sensation (insula), somatosensory (postcentral gyrus), and motor area (anterior paracentral lobule and SMA) in IC/BPS patients compared with HC. They suggest that sensory and motor dysfunction in IC/BPS patients is a pathological mechanism. Kilpatrick et al. (2014) found that the insula and SMA were enhanced with FC in the midbrain (red nucleus) and cerebellum, and they suggested that it is also a manifestation of IC/BPS pathology. Martucci et al. (2015) found that FC of DMN was significantly reduced to the PCC and left precuneus in women with urologic chronic pain syndrome (UCPPS) compared with HC. They suggested that DMN dissociation occurs in UCPPS patients and that pain and emotional

regulation may be related to the self-referential thinking and introspective neural processes responsible for DMN.

Neurogenic overactive bladder

Gao et al. (2021) found that PFC and ACC were activated in neurogenic detrusor overactivity (NDO) patients with tethered cord syndrome compared with the HC group. Moreover, compared with HC, FC analysis showed increased FC between different regions within the PFC and decreased FC between the PFC and other brain regions in NDO patients. They suggest that decreased FC in PFC and other bladder control-related brain regions may be related to reduced PFC decision-making function, which may affect bladder control.

Nocturnal enuresis

Jiang et al. (2018) found that the degree centrality values of posterior cerebellar lobe, ACC, MPFC, and the left superior temporal gyrus in children with nocturnal enuresis (NE) were significantly decreased in HC, suggesting that these brain regions may be associated with NE. Lei et al. (2012) used rs-fMRI to study changes in spontaneous brain activity in children with primary monosymptomatic NE. They found significant differences in amplitude of low frequency fluctuation (ALFF) or ReHo in the left inferior frontal gyrus/LPFC and MPFC (Brodmann area, BA10) compared with HC, suggesting that abnormalities in the inferior frontal gyrus/LPFC and MPFC may affect children's urination decision-making ability.

Discussion

Our review has two novel hypotheses. First, we summarized studies on the activation changes of brain regions during the micturition phase, illuminating possible brain circuits during micturition. Second, we summarized brain FC and brain network studies related to bladder control, providing new information on the existing bladder control model proposed by Griffiths et al. (2015a) (de Groat et al., 2015) in 2015.

Brain circuits associated with micturition

Only six previous brain functional imaging studies on the micturition phase have been conducted, far fewer than those on the storage phase. To better explain brain activity during voiding, we summarized the six studies (Table 1) and found that the frequency of activation of brain regions during micturition was five times more for the LPFC/inferior frontal gyrus and pons; three times more for the PAG, hypothalamus, basal ganglia, and ACC; twice for the postcentral gyrus, thalamus, insula, superior frontal gyrus, cerebellar, and SMA.

In short, the LPFC is activated both during storage and urination, while the MPFC is deactivated during storage but activated during micturition. Pons is activated only during micturition, while the PAG, ACC, insula, thalamus, hypothalamus, basal ganglia, and postcentral gyrus are activated in both phases. We believe that, similar to urine storage, micturition also requires DLPFC activity for executive function (i.e., organization of input from different sensory modes (e.g., bladder sensation and vision), maintaining attention, monitoring information (e.g., surroundings and social etiquette) in working memory, and coordinating goal-directed (voiding) behavior. (Teffer and Semendeferi, 2012).

Given that MPFC activation is critical for the representation of reward- and value-based decisions, (Hiser and Koenigs, 2018), we suggest that decisions about voiding are driven by MPFC activation at the onset of micturition. Manohar et al. (2017) found that LC and MPFC activation in rats occurred synchronously about 20 s before urination, presenting consistent θ oscillations, which they suggested shifted the rats from ongoing behaviors unrelated to urination to initiation of specific urination behaviors in order to urinate in appropriate conditions. Although PAG is activated in both phases, the degree of activation may be different. (Griffiths, 2015a). We considered that the activation of MPFC may further increase the activity of PAG to exceed a certain threshold, activating the pons, which transmits the void impulse to the spinal cord and controls the coordinated movement of detrusor muscle and urethral sphincter to achieve voiding.

The ACC, insula, thalamus, hypothalamus, basal ganglia, and postcentral gyrus have been reported to be activated in both phases, and we believe that these brain regions play a similar role in urine storage and urination. For example, bladder sensation is uploaded to the insula *via* the thalamus, and the insula and ACC, as parts of the SN, are responsible for sensing and encoding the desire to void. The postcentral gyrus may be involved in somatosensory perception as part of the SMN. Yamamoto et al. (2005) analyzed three patients with hypothalamic compression due to pituitary adenoma and found that hypothalamic lesions could lead to DO during urine storage and detrusor insufficiency during urination, suggesting that the hypothalamus plays a role in both phases. The caudate nucleus, a component of basal ganglia (BG), was thought to has an inhibitory effect on micturition reflex. (Seseke et al., 2008; Gao et al., 2015). Electrical stimulation applied to the caudate nucleus can cause inhibition of spontaneous bladder contraction in cats. (Yamamoto et al., 2009).

Brain FC and networks related to bladder control: An extended working model

Most previous studies focused on the activation/inactivation of a specific brain region related to bladder control. Brain regions

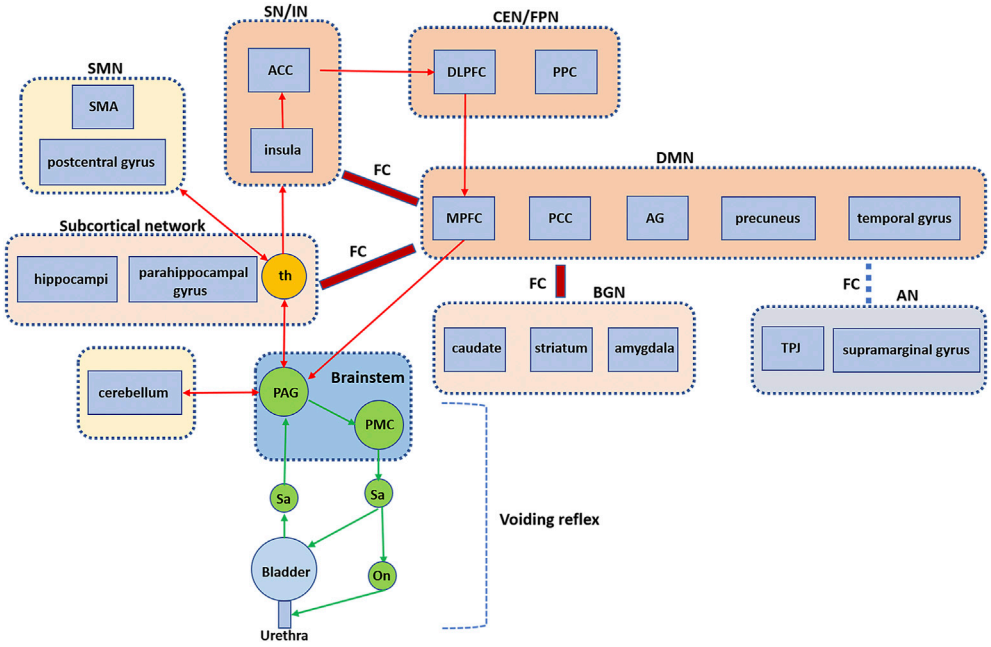

FIGURE 1
Brain FC and networks related to bladder control. An extended working mode showing the voiding reflex and the brain circuits, especially the interaction between brain regions and networks. FC, functional connectivity; PAG, periaqueductal gray; PMC, pontine micturition center; th, thalamus; SMA, supplementary motor area; SMN, sensorimotor network; ACC, anterior cingulate cortex; SN, salience network; IN, interoceptive network; DLPFC, dorsolateral prefrontal cortex; PPC, posterior parietal cortices; CEN, central executive network; FPN, frontoparietal network; MPFC = medial prefrontal cortex; PCC, posterior cingulate cortex; AG, angular gyrus; DMN, default mode network; BGN, basal ganglia network; AN, attentional network; TPJ, temporoparietal junction. (Extended based on working model by de Groat et al., 2015).

do not work independently, and the separation, integration, communication, and cooperation between regions are important mechanisms of brain-bladder control, which depends on the brain FC or network. By summarizing the brain FC network articles related to bladder control over the past 20 years, we found five studies on HC, four on UUI, two on OAB, three on IC/BPS or UCPPS, two on NE, and one on NDO patients with tethered cord syndrome. These studies all explored brain FC network changes during the urine storage phase using fMRI and fNIRS, without observing the micturition phase.

The results of the five studies on HC showed increased activity within certain brain networks during urine storage in healthy patients, including the ventral AN (bilateral TPJ and supramarginal gyrus), CEN/FPN (DLPFC and posterior parietal cortices), SN/IN (insula and ACC), DMN (superior frontal gyrus, PCG, precuneus, parietal lobules, temporal gyrus, and AG), SMN (postcentral gyrus), VN (superior occipital gyrus, middle occipital gyrus, and cuneus), BGN (caudate nucleus, striatum, and amygdala), subcortical network (thalamus, hippocampus, and parahippocampal gyrus), cerebellum, and brainstem. Changes in interactions between networks and bladder distention could cause decreases in FC between AN and DMN and increases in FC between the DMN and the subcortical network. Moreover, the repeated perfusion/withdrawal task with prefilling (100 ml or strong desire to void) can cause a decrease in FC between aDMN and AN and an increase in FC between aDMN and BGN and between DMN and SN, compared with the task with an empty bladder. Based on these results, we extend the working model proposed by Griffiths et al. (Griffiths, 2015a; de Groat et al., 2015) to include the specific brain regions and networks involved in bladder control and the interactions between networks (Figure 1). We performed rs-fMRI imaging of 20 healthy subjects with empty and full bladder. We identified seven known resting state networks using independent component analysis method, including SN, DMN, CEN, dAN, SMN, VN, and cerebellum network (CN), as shown in our previous article. (Pang et al., 2021). This will help us understand the composition of these networks.

Under normal circumstances, the physiological filling of the bladder is a slow process from subthreshold (no sensation) to upper threshold (e.g., first sensation of bladder filling, first desire to void, normal desire to void, strong desire to void, urgency desire to void, and pain). The perception of bladder filling/distention is a type of interoception, which is defined as all sensations produced in the body, (Craig, 2003), including pressure, fullness, and pain of the visceral organs. (Cameron, 2001). The signal of bladder dilation is uploaded to the thalamus via PAG and then relayed to the insula and the interoceptive

afferent cortex, (Blok et al., 1997; Craig, 2003), which encodes the degree of bladder filling and forms the interoceptive awareness of bladder sensation. (Craig, 2003; Griffiths and Tadic, 2008). The ACC and insula are part of the SN, which has extensive coactivation and plays a role in integrating internal and external information. (Torta et al., 2013; Jarrahi et al., 2015b). The SN is responsible for locating and detecting associated stimuli. (Seeley et al., 2007). Previous studies have shown that ACC can initiate autonomic responses and prompt goal-directed behaviors such as withholding urine or void. (Craig, 2003). As the bladder continues to dilate, SN becomes more aware of this interoception, forming a gradually increased desire to void, which may activate another network (i.e., CEN). (Jarrahi et al., 2015a). CEN consists of the DLPFC and the lateral posterior parietal cortex (PCC). (Chan et al., 2016).

Anticipation and attention to visceral sensation and pain depend on DLPFC. (Aziz et al., 2000). DLPFC can maintain attention, organize input from different sensory modes (e.g., bladder sensation), monitor environment and social etiquette in working memory, judge whether it is appropriate to void, and decide on goal-directed (withholding/voiding) behavior. (Teffer and Semendeferi, 2012; Chan et al., 2016). In other words, CEN allows us to make behavioral choices by continually paying attention to salient stimuli, balancing the changing environment against the changing demands of interoception. (Seeley et al., 2007).

MPFC, as part of DMN, is usually reported to be activated during micturition (Nour et al., 2000; Shy et al., 2014) and deactivated during urine storage. (Blok et al., 1997; Blok et al., 1998; Griffiths et al., 2007; Griffiths et al., 2009). In contrast, Jarrahi et al. (Jarrahi et al., 2015a) found activation of brain regions (i.e., MPFC, the precuneus/PCC, bilateral parietal lobules, and the inferior temporal gyri) within the DMN. We found increased ReHo in the brain region within DMN (i.e., left temporal gyrus and left AG) and increased FC within the DMN (i.e., superior frontal gyrus, PCG, and AG) when the desire to void was strong, compared with an empty bladder. These inconsistent results may suggest that DMN activity is isolated or dynamic during urine storage, which is worthy of further exploration. Previous studies have shown that stimulation of PCG can interrupt urination when a cat's bladder is rapidly filled. (Gjone, 1966). AG is responsible for episodic memory, which allows recall of past experiences. (Bonnici et al., 2018). DMN has been reported to be activated at rest (i.e., no significant external stimulus task) (Raichle, 2015) but has also been reported to be active in introverted cognitive activities such as self-reference, self-reflection, social functioning, and physiological processes. (Nardos et al., 2014; Raichle, 2015). The DMN is thought to be involved in physiological processes such as bladder control, possibly through interoception mechanisms or self-reflection. (Nardos et al., 2014). The DMN may be able to support internal psychology by simulating the dynamic psychological changes of past experiences. (Nardos et al., 2016; Bonnici et al., 2018). Animal studies have shown that MPFC is the main source of cortical-PAG projection and that MPFC is involved in autonomic and emotional regulation of external stimuli through direct connection with PAG. (Hardy and Leichnetz, 1981). The deactivation of MPFC may reduce MPFC input to PAG, stabilizing PAG, inhibiting the voiding reflex, and maintaining continence. In addition, mPFC projections to other regions, particularly the hypothalamus and extended amygdala, play an equally plausible role to bladder control. (Pajolla et al., 2001).

Moreover, other networks are involved in bladder control during urinary storage, including the VAN (bilateral TPJ and supramarginal gyrus) response to unexpected events (bottom-up attention). (Vossel et al., 2014). The VAN was reported to be activated when the bladder was full, which is also easy to understand because visceral changes are unexpected events, inside-out processes that can attract bottom-up attention. (Vossel et al., 2014; Jarrahi et al., 2015b). The subcortical network (thalamus, hippocampi, and parahippocampal gyrus), which overlaps with limbic correlates, has been reported to be involved in the intersensory processing of smell, taste, and hunger responses. (Laird et al., 2011). The thalamus is responsible for motor/sensory relay and consciousness regulation. (Smitha et al., 2017). The subcortical network is also similar to neural circuit 3 proposed by Griffiths et al. (2015a) (de Groat et al., 2015). Activation of the subcortical network may be involved in unconscious monitoring of sensory information in the bladder when bladder volume is small, and there is little sensation. (Griffiths, 2015a; de Groat et al., 2015).

The BGN (caudate nucleus, striatum, and amygdala) showed increased activity during urine storage, supporting the hypothesis that BGN inhibits the voiding reflex (Seseke et al., 2008; Gao et al., 2015) and that electrical stimulation of the caudate nucleus results in inhibition of spontaneous bladder contraction in cats. (Yamamoto et al., 2009). Previous studies have shown that the caudate nucleus is involved in motor processing, process learning, and control of motor inhibition, while the putamen is responsible for motor regulation. (Smitha et al., 2017). BGN is responsible for the process of motor area control, emotion, and cognition. BGN engage in goal-directed behavior that requires movement. (Smitha et al., 2017). VN located in the visual cortex and is divided into dorsal VN and ventral VN. The dorsal VN processes information about the position of objects and adjusts visual controls for skilled movements. (Migliaccio et al., 2016). Although significant activation of the occipital lobe (i.e., VN) has been reported many times, (Seseke et al., 2006; Griffiths and Tadic, 2008; Seseke et al., 2008; Ketai et al., 2016; Nardos et al., 2016; Zuo et al., 2019a), its function remains unclear and needs to be elucidated in further studies.

Brain FC network changes in patients with LUTD

According to our review, 12 brain FC/network studies have been conducted in patients with LUTD (four studies on UUI, two

on OAB, three on IC/BPS or UCPPS, two on NE, and one on NDO patients with tethered cord syndrome). A common feature of these disorders is that LUTS are often present in the urinary storage phase (e.g., urinary frequency and urgency, UUI, pain/discomfort of bladder and pelvis).

Compared with HC, UUI patients showed abnormal activation of brain regions within the SN, VAN, DMN, CEN, and SMN. (Ketai et al., 2016; Nardos et al., 2016). The FC between MCC and DAN in the UUI group was stronger than in the HC group. (Ketai et al., 2016). Moreover, six typical FC features could predict the severity of UUI, including the connections between SN and DMN to SMN and between CEN and SN and SMN. (Nardos et al., 2016). Some scholars have explored the central mechanism of effective treatment of UUI, finding that UUI patients who responded to PFMT had significant differences in FC of BGN and dACC compared with before treatment. (Clarkson et al., 2018). UUI successfully treated with pharmacotherapy is associated with reduced activation of VAN, while the decrease in VAN activation in the successful treatment of UUI using hypnotherapy may be due to the balancing effect of DAN. (Ketai et al., 2021). We found that the central mechanism of SNM treatment for OAB may be restoration of the activation of the left DLPFC to a near-normal level. (Pang et al., 2022). Compared with HC patients, OAB patients showed that the FC strength within the DMN, ACG, and MCG was significantly decreased, while the FC strength within the CEN was significantly increased. (Zuo et al., 2019b). The FC within the SMN, DAN, dVN, and LFPN was significantly decreased, as was the FC between the SMN and the anterior DMN. (Zuo et al., 2019a).

Compared with HC, the IC/BPS patients showed significantly decreased FC within the PFC, whether with an empty bladder or a strong desire to void. (Pang and Liao, 2021). IC/BPS patients showed significant changes in the frequency distribution of SN and SMN and enhanced FC between the insula, SMA, midbrain, and cerebellum. (Kilpatrick et al., 2014). The FC of the DMN was significantly reduced to the PCC and left precuneus in women with UCPPS. (Martucci et al., 2015). Compared with HC patients, NDO patients with tethered cord syndrome showed deactivation in the PFC and ACC, increased FC within the PFC, and decreased FC between the PFC and other brain regions. (Gao and Liao, 2021). Compared with HC patients, the NE patients showed a decreased degree centrality of the posterior cerebellar lobe, ACC, MPFC, and left superior temporal gyrus. (Jiang et al., 2018). NE patients showed significant differences in ALFF or ReHo in the left inferior frontal gyrus/LPFC and MPFC (Brodmann area, BA10). (Lei et al., 2012). Problems with collaboration and communication within networks, as well as functional integration between networks, may be the central mechanism of LUTD. Due to differences in experimental paradigms and analytical methods, precise interpretation of these results is difficult.

In summary, bladder control involves complex neural networks, and neural control related to micturition control is still an unstudied area, with many unexplored areas. For example, there have been no studies of the: 1) Brain FC network in healthy subjects and patients (e.g., UAB) during micturition; 2) Dynamic changes of the DMN network during urine storage and micturition in healthy subjects and patients and the relationship and interaction between MPFC and activities of other brain regions within DMN; 3) Dynamic changes and roles of regions such as the VN, SMN, cerebellum, subcortical networks in bladder control; 4) Brain targeted therapy based on abnormal brain activity or FC; and 5) Other methods that can regulate the brain network for LUTD treatment. For instance, Ketai et al. found that the activation of VAN in UUI was abnormally higher than that in HC (Ketai et al., 2016) and improved LUTS in UUI through hypnotherapy. The possible mechanism was to balance the abnormally elevated VAN in UUI patients by upregulating DAN and, ultimately, reduce VAN activity in UUI. (Ketai et al., 2016).

Author contributions

They all made substantial contributions to conception and design, drafting and revising the article critically for important intellectual content, and final approval of the version to be published. DP and YG are joint first authors.

Funding

The study was supported by the National Natural Science Foundation of China (No. 81870523).

Conflict of interest

The authors declare that the research was conducted in the absence of any commercial or financial relationships that could be construed as a potential conflict of interest.

Publisher's note

References

Ackermann, R. F., Finch, D. M., Babb, T. L., and Engel, J., Jr (1984). Increased glucose metabolism during long-duration recurrent inhibition of hippocampal pyramidal cells. *J. Neurosci.* 4, 251–264. doi:10.1523/jneurosci.04-01-00251.1984

Andrew, J., and Nathan, P. W. (1964). Lesions on the anterior frontal lobes and disturbances of micturition and defaecation. *Brain* 87, 233–262. doi:10.1093/brain/87.2.233

Aziz, Q., Thompson, D. G., Ng, V. W., Hamdy, S., Sarkar, S., Brammer, M. J., et al. (2000). Cortical processing of human somatic and visceral sensation. *J. Neurosci.* 20, 2657–2663. doi:10.1523/jneurosci.20-07-02657.2000

Batini, C., Benedetti, F., Buisseret-Delmas, C., Montarolo, P. G., and Strata, P. (1984). Metabolic activity of intracerebellar nuclei in the rat: Effects of inferior olive inactivation. *Exp. Brain Res.* 54, 259–265. doi:10.1007/BF00236225

Blok, B. F., Sturms, L. M., and Holstege, G. (1998). Brain activation during micturition in women. *Brain* 121 (Pt 11), 2033–2042. doi:10.1093/brain/121.11.2033

Blok, B. F., Willemsen, A. T., and Holstege, G. (1997). A PET study on brain control of micturition in humans. *Brain* 120 (Pt 1), 111–121. doi:10.1093/brain/120.1.111

Bonnici, H. M., Cheke, L. G., Green, D. A. E., FitzGerald, T., and Simons, J. S. (2018). Specifying a causal role for angular gyrus in autobiographical memory. *J. Neurosci.* 38, 10438–10443. doi:10.1523/JNEUROSCI.1239-18.2018

Cameron, O. G. (2001). Interoception: The inside story--a model for psychosomatic processes. *Psychosom. Med.* 63, 697–710. doi:10.1097/00006842-200109000-00001

Chan, J. S., Wang, Y., Yan, J. H., and Chen, H. (2016). Developmental implications of children's brain networks and learning. *Rev. Neurosci.* 27, 713–727. doi:10.1515/revneuro-2016-0007

Clarkson, B. D., Karim, H. T., Griffiths, D. J., and Resnick, N. M. (2018). Functional connectivity of the brain in older women with urgency urinary incontinence. *Neurourol. Urodyn.* 37, 2763–2775. doi:10.1002/nau.23766

Craig, A. D. (2003). Interoception: The sense of the physiological condition of the body. *Curr. Opin. Neurobiol.* 13, 500–505. doi:10.1016/s0959-4388(03)00090-4

de Groat, W. C., Griffiths, D., and Yoshimura, N. (2015). Neural control of the lower urinary tract. *Compr. Physiol.* 5, 327–396. doi:10.1002/cphy.c130056

Duffau, H., and Capelle, L. (2005). Incontinence after brain glioma surgery: New insights into the cortical control of micturition and continence. Case report. *J. Neurosurg.* 102, 148–151. doi:10.3171/jns.2005.102.1.0148

Fowler, C. J., Griffiths, D., and de Groat, W. C. (2008). The neural control of micturition. *Nat. Rev. Neurosci.* 9, 453–466. doi:10.1038/nrn2401

Fox, M. D., and Raichle, M. E. (2007). Spontaneous fluctuations in brain activity observed with functional magnetic resonance imaging. *Nat. Rev. Neurosci.* 8, 700–711. doi:10.1038/nrn2201

Fukuyama, H., Matsuzaki, S., Ouchi, Y., YamaucHi, H., Nagahama, Y., Kimura, J., et al. (1996). Neural control of micturition in man examined with single photon emission computed tomography using 99mTc-HMPAO. *Neuroreport* 7, 3009–3012. doi:10.1097/00001756-199611250-00042

Gao, Y., Liao, L., and Blok, B. F. M. (2015). A resting-state functional MRI study on central control of storage: Brain response provoked by strong desire to void. *Int. Urol. Nephrol.* 47, 927–935. doi:10.1007/s11255-015-0978-0

Gao, Y., and Liao, L. (2021). Regional activity and functional connectivity in brain networks associated with urinary bladder filling in patients with tethered cord syndrome. *Int. Urol. Nephrol.* 53, 1805–1812. doi:10.1007/s11255-021-02880-0

Gjone, R. (1966). Excitatory and inhibitory bladder responses to stimulation of 'limbic', diencephalic and mesencephalic structures in the cat. *Acta Physiol. Scand.* 66, 91–102. doi:10.1111/j.1748-1716.1966.tb03171.x

Griffiths, D., Derbyshire, S., Stenger, A., and Resnick, N. (2005). Brain control of normal and overactive bladder. *J. Urol.* 174, 1862–1867. doi:10.1097/01.ju.0000177450.34451.97

Griffiths, D. (2015). Neural control of micturition in humans: A working model. *Nat. Rev. Urol.* 12, 695–705. doi:10.1038/nrurol.2015.266

Griffiths, D. (2015). Functional imaging of structures involved in neural control of the lower urinary tract. *Handb. Clin. Neurol.* 130, 121–133. doi:10.1016/B978-0-444-63247-0.00007-9

Griffiths, D., and Tadic, S. D. (2008). Bladder control, urgency, and urge incontinence: Evidence from functional brain imaging. *Neurourol. Urodyn.* 27, 466–474. doi:10.1002/nau.20549

Griffiths, D., Tadic, S. D., Schaefer, W., and Resnick, N. M. (2007). Cerebral control of the bladder in normal and urge-incontinent women. *Neuroimage* 37, 1–7. doi:10.1016/j.neuroimage.2007.04.061

Griffiths, D. J., Tadic, S. D., Schaefer, W., and Resnick, N. M. (2009). Cerebral control of the lower urinary tract: How age-related changes might predispose to urge incontinence. *Neuroimage* 47, 981–986. doi:10.1016/j.neuroimage.2009.04.087

Hardy, S. G., and Leichnetz, G. R. (1981). Cortical projections to the periaqueductal gray in the monkey: A retrograde and orthograde horseradish peroxidase study. *Neurosci. Lett.* 22, 97–101. doi:10.1016/0304-3940(81)90070-7

Hiser, J., and Koenigs, M. (2018). The multifaceted role of the ventromedial prefrontal cortex in emotion, decision making, social cognition, and psychopathology. *Biol. Psychiatry* 83, 638–647. doi:10.1016/j.biopsych.2017.10.030

Jarrahi, B., Mantini, D., Balsters, J. H., Michels, L., Kessler, T. M., Mehnert, U., et al. (2015a). Differential functional brain network connectivity during visceral interoception as revealed by independent component analysis of fMRI TIME-series. *Hum. Brain Mapp.* 36, 4438–4468. doi:10.1002/hbm.22929

Jarrahi, B., Mantini, D., Mehnert, U., and Kollias, S. (2015b). Exploring influence of subliminal interoception on whole-brain functional network connectivity dynamics. *Annu. Int. Conf. IEEE Eng. Med. Biol. Soc.* 2015, 670–674. doi:10.1109/EMBC.2015.7318451

Jiang, K., Ding, L., Li, H., Shen, H., Zheng, A., Zhao, F., et al. (2018). Degree centrality and voxel-mirrored homotopic connectivity in children with nocturnal enuresis: A functional MRI study. *Neurol. India* 66, 1359–1364. doi:10.4103/0028-3886.241334

Jobsis, F. F. (1977). Noninvasive, infrared monitoring of cerebral and myocardial oxygen sufficiency and circulatory parameters. *Sci. (New York, NY)* 198, 1264–1267. doi:10.1126/science.929199

Ketai, L. H., Komesu, Y. M., Dodd, A. B., Rogers, R. G., Ling, J. M., Mayer, A. R., et al. (2016). Urgency urinary incontinence and the interoceptive network: A functional magnetic resonance imaging study. *Am. J. Obstet. Gynecol.* 215, e441–449. doi:10.1016/j.ajog.2016.04.056

Ketai, L. H., Komesu, Y. M., Schrader, R. M., Rogers, R. G., Sapien, R. E., Dodd, A. B., et al. (2021). Mind-body (hypnotherapy) treatment of women with urgency urinary incontinence: Changes in brain attentional networks. *Am. J. Obstet. Gynecol.* 224, 498.e1–498.e10. doi:10.1016/j.ajog.2020.10.041

Kilpatrick, L. A., Kutch, J. J., Tillisch, K., Naliboff, B. D., Labus, J. S., Jiang, Z., et al. (2014). Alterations in resting state oscillations and connectivity in sensory and motor networks in women with interstitial cystitis/painful bladder syndrome. *J. Urol.* 192, 947–955. doi:10.1016/j.juro.2014.03.093

Kitta, T., Mitsui, T., Kanno, Y., Chiba, H., Moriya, K., Shinohara, N., et al. (2015). Brain-bladder control network: The unsolved 21st century urological mystery. *Int. J. Urol.* 22, 342–348. doi:10.1111/iju.12721

Krhut, J., Tintera, J., Holy, P., Zachoval, R., and Zvara, P. (2012). A preliminary report on the use of functional magnetic resonance imaging with simultaneous urodynamics to record brain activity during micturition. *J. Urol.* 188, 474–479. doi:10.1016/j.juro.2012.04.004

Kuhtz-Buschbeck, J. P., van der Horst, C., Pott, C., Wolff, S., Nabavi, A., Jansen, O., et al. (2005). Cortical representation of the urge to void: A functional magnetic resonance imaging study. *J. Urol.* 174, 1477–1481. doi:10.1097/01.ju.0000173007.84102.7c

Laird, A. R., Fox, P. M., Eickhoff, S. B., Turner, J. A., Ray, K. L., McKay, D. R., et al. (2011). Behavioral interpretations of intrinsic connectivity networks. *J. Cogn. Neurosci.* 23, 4022–4037. doi:10.1162/jocn_a_00077

Lei, D., Ma, J., Du, X., Shen, G., Tian, M., Li, G., et al. (2012). Spontaneous brain activity changes in children with primary monosymptomatic nocturnal enuresis: A resting-state fMRI study. *Neurourol. Urodyn.* 31, 99–104. doi:10.1002/nau.21205

Manohar, A., Curtis, A. L., Zderic, S. A., and Valentino, R. J. (2017). Brainstem network dynamics underlying the encoding of bladder information. *Elife* 6, e29917. doi:10.7554/eLife.29917

Martucci, K. T., Shirer, W. R., Bagarinao, E., Johnson, K. A., Farmer, M. A., Labus, J. S., et al. (2015). The posterior medial cortex in urologic chronic pelvic pain syndrome: Detachment from default mode network-a resting-state study from the MAPP research network. *Pain* 156, 1755–1764. doi:10.1097/j.pain.0000000000000238

Matsumoto, S., Ishikawa, A., Matsumoto, S., and Homma, Y. (2011). Brain response provoked by different bladder volumes: A near infrared spectroscopy study. *Neurourol. Urodyn.* 30, 529–535. doi:10.1002/nau.21016

Migliaccio, R., Gallea, C., Kas, A., Perlbarg, V., Samri, D., Trotta, L., et al. (2016). Functional connectivity of ventral and dorsal visual streams in posterior cortical atrophy. *J. Alzheimers Dis.* 51, 1119–1130. doi:10.3233/JAD-150934

Munoz, M. F., Puebla, M., and Figueroa, X. F. (2015). Control of the neurovascular coupling by nitric oxide-dependent regulation of astrocytic Ca(2+) signaling. *Front. Cell. Neurosci.* 9, 59. doi:10.3389/fncel.2015.00059

Nardos, R., Gregory, W. T., Krisky, C., Newell, A., Nardos, B., Schlaggar, B., et al. (2014). Examining mechanisms of brain control of bladder function with resting state functional connectivity MRI. *Neurourol. Urodyn.* 33, 493–501. doi:10.1002/nau.22458

Nardos, R., Karstens, L., Carpenter, S., Aykes, K., Krisky, C., Stevens, C., et al. (2016). Abnormal functional connectivity in women with urgency urinary incontinence: Can we predict disease presence and severity in individual women using Rs-fcMRI. *Neurourol. Urodyn.* 35, 564–573. doi:10.1002/nau.22767

Nour, S., Svarer, C., Kristensen, J. K., Paulson, O. B., and Law, I. (2000). Cerebral activation during micturition in normal men. *Brain* 123 (Pt 4), 781–789. doi:10.1093/brain/123.4.781

Pajolla, G. P., Crippa, G. E., Corrêa, S. A., Moreira, K. B., Tavares, R. F., Corrêa, F. M., et al. (2001). The lateral hypothalamus is involved in the pathway mediating the hypotensive response to cingulate cortex-cholinergic stimulation. *Cell. Mol. Neurobiol.* 21, 341–356. doi:10.1023/a:1012650021137

Pang, D., Gao, Y., and Liao, L. (2021). Responses of functional brain networks to bladder control in healthy adults: A study using regional homogeneity combined with independent component analysis methods. *Int. Urol. Nephrol.* 53, 883–891. doi:10.1007/s11255-020-02742-1

Pang, D., Gao, Y., Liao, L., and Ying, X. (2020). Brain functional network alterations caused by a strong desire to void in healthy adults: A graph theory analysis study. *Neurourol. Urodyn.* 39, 1966–1976. doi:10.1002/nau.24445

Pang, D., and Liao, L. (2021). Abnormal functional connectivity within the prefrontal cortex in interstitial cystitis/bladder pain syndrome (IC/BPS): A pilot study using resting state functional near-infrared spectroscopy (rs-fNIRS). *Neurourol. Urodyn.* 40, 1634–1642. doi:10.1002/nau.24729

Pang, D., Liao, L., Chen, G., and Wang, Y. (2022). Sacral neuromodulation improves abnormal prefrontal brain activity in patients with overactive bladder: A possible central mechanism. *J. Urol.* 207, 1256–1267.

Raichle, M. E., MacLeod, A. M., Snyder, A. Z., Powers, W. J., Gusnard, D. A., Shulman, G. L., et al. (2001). A default mode of brain function. *Proc. Natl. Acad. Sci. U. S. A.* 98, 676–682. doi:10.1073/pnas.98.2.676

Raichle, M. E. (2015). The brain's default mode network. *Annu. Rev. Neurosci.* 38, 433–447. doi:10.1146/annurev-neuro-071013-014030

Sakakibara, R., Hattori, T., Yasuda, K., and Yamanishi, T. (1996). Micturitional disturbance after acute hemispheric stroke: Analysis of the lesion site by CT and MRI. *J. Neurol. Sci.* 137, 47–56. doi:10.1016/0022-510x(95)00322-s

Sakakibara, R., Tsunoyama, K., Takahashi, O., Sugiyama, M., Kishi, M., Ogawa, E., et al. (2010). Real-time measurement of oxyhemoglobin concentration changes in the frontal micturition area: An fNIRS study. *Neurourol. Urodyn.* 29, 757–764. doi:10.1002/nau.20815

Seeley, W. W., Menon, V., Schatzberg, A. F., Keller, J., Glover, G. H., Kenna, H., et al. (2007). Dissociable intrinsic connectivity networks for salience processing and executive control. *J. Neurosci.* 27, 2349–2356. doi:10.1523/JNEUROSCI.5587-06.2007

Seseke, S., Baudewig, J., Kallenberg, K., Ringert, R. H., Seseke, F., Dechent, P., et al. (2008). Gender differences in voluntary micturition control: An fMRI study. *Neuroimage* 43, 183–191. doi:10.1016/j.neuroimage.2008.07.044

Seseke, S., Baudewig, J., Kallenberg, K., Ringert, R. H., Seseke, F., Dechent, P., et al. (2006). Voluntary pelvic floor muscle control--an fMRI study. *Neuroimage* 31, 1399–1407. doi:10.1016/j.neuroimage.2006.02.012

Shy, M., Fung, S., Boone, T. B., Karmonik, C., Fletcher, S. G., Khavari, R., et al. (2014). Functional magnetic resonance imaging during urodynamic testing identifies brain structures initiating micturition. *J. Urol.* 192, 1149–1154. doi:10.1016/j.juro.2014.04.090

Smitha, K. A., Akhil Raja, K., Arun, K. M., Rajesh, P. G., Thomas, B., Kapilamoorthy, T. R., et al. (2017). Resting state fMRI: A review on methods in resting state connectivity analysis and resting state networks. *Neuroradiol. J.* 30, 305–317. doi:10.1177/1971400917697342

Stackhouse, T. L., and Mishra, A. (2021). Neurovascular coupling in development and disease: Focus on astrocytes. *Front. Cell Dev. Biol.* 9, 702832. doi:10.3389/fcell.2021.702832

Tadic, S. D., Griffiths, D., Schaefer, W., Cheng, C. I., and Resnick, N. M. (2010). Brain activity measured by functional magnetic resonance imaging is related to patient reported urgency urinary incontinence severity. *J. Urol.* 183, 221–228. doi:10.1016/j.juro.2009.08.155

Teffer, K., and Semendeferi, K. (2012). Human prefrontal cortex: Evolution, development, and pathology. *Prog. Brain Res.* 195, 191–218. doi:10.1016/B978-0-444-53860-4.00009-X

Torta, D. M., Costa, T., Duca, S., Fox, P. T., and Cauda, F. (2013). Parcellation of the cingulate cortex at rest and during tasks: A meta-analytic clustering and experimental study. *Front. Hum. Neurosci.* 7, 275. doi:10.3389/fnhum.2013.00275

Vossel, S., Geng, J. J., and Fink, G. R. (2014). Dorsal and ventral attention systems: Distinct neural circuits but collaborative roles. *Neuroscientist* 20, 150–159. doi:10.1177/1073858413494269

Wager, T. D., van Ast, V. A., Hughes, B. L., Davidson, M. L., Lindquist, M. A., Ochsner, K. N., et al. (2009). Brain mediators of cardiovascular responses to social threat, part II: Prefrontal-subcortical pathways and relationship with anxiety. *Neuroimage* 47, 836–851. doi:10.1016/j.neuroimage.2009.05.044

Yamamoto, T., Sakakibara, R., Nakazawa, K., Uchiyama, T., Shimizu, E., Hattori, T., et al. (2009). Effects of electrical stimulation of the striatum on bladder activity in cats. *Neurourol. Urodyn.* 28, 549–554. doi:10.1002/nau.20682

Yamamoto, T., Sakakibara, R., Uchiyama, T., Liu, Z., ITo, T., Yamanishi, T., et al. (2005). Lower urinary tract function in patients with pituitary adenoma compressing hypothalamus. *J. Neurol. Neurosurg. Psychiatry* 76, 390–394. doi:10.1136/jnnp.2004.044644

Yin, Y., Shuke, N., Kaneko, S., Okizaki, A., Sato, J., Aburano, T., et al. (2008). Cerebral control of bladder storage in patients with detrusor overactivity. *Nucl. Med. Commun.* 29, 1081–1085. doi:10.1097/MNM.0b013e328313bc13

Zhang, H., Reitz, A., Kollias, S., Summers, P., Curt, A., Schurch, B., et al. (2005). An fMRI study of the role of suprapontine brain structures in the voluntary voiding control induced by pelvic floor contraction. *Neuroimage* 24, 174–180. doi:10.1016/j.neuroimage.2004.08.027

Zuo, L., Chen, J., Wang, S., Zhou, Y., Wang, B., Gu, H., et al. (2019a). Intra- and inter-resting-state networks abnormalities in overactive bladder syndrome patients: An independent component analysis of resting-state fMRI. *World J. Urol.* 38, 1027–1034. doi:10.1007/s00345-019-02838-z

Zuo, L., Zhou, Y., Wang, S., Wang, B., Gu, H., Chen, J., et al. (2019b). Abnormal brain functional connectivity strength in the overactive bladder syndrome: A resting-state fMRI study. *Urology* 131, 64–70. doi:10.1016/j.urology.2019.05.019

Frontiers in Physiology

Understanding how an organism's components work together to maintain a healthy state

The second most-cited physiology journal, promoting a multidisciplinary approach to the physiology of living systems - from the subcellular and molecular domains to the intact organism and its interaction with the environment.

Discover the latest Research Topics

See more →

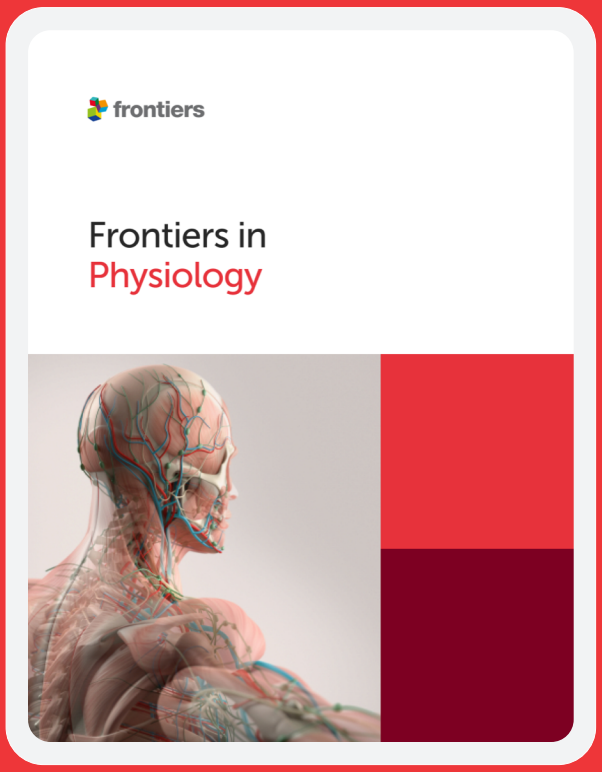

Frontiers

Avenue du Tribunal-Fédéral 34
1005 Lausanne, Switzerland
frontiersin.org

Contact us

+41 (0)21 510 17 00
frontiersin.org/about/contact